CENTRAL CARDIOVASCULAR AND RESPIRATORY CONTROL: NEW TECHNIQUES, NEW DIRECTIONS, NEW HORIZONS

EDITED BY: Vaughan G. Macefield and Geoffrey A. Head

PUBLISHED IN: Frontiers in Physiology and Frontiers in Neuroscience

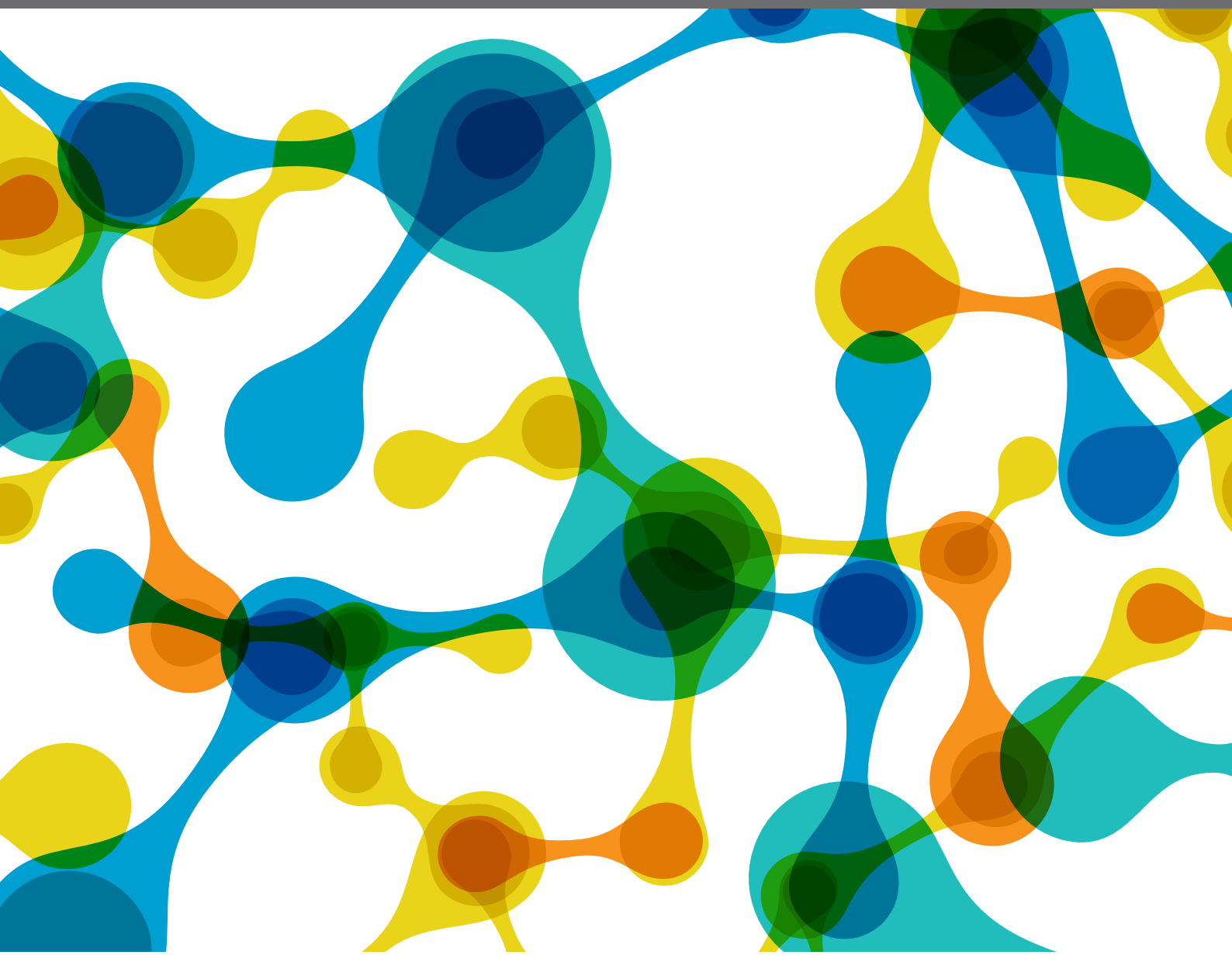

frontiers Research Topics

frontiers

ISSN 1664-8714
ISBN 978-2-88966-353-8
DOI 10.3389/978-2-88966-353-8

About Frontiers

Frontiers is more than just an open-access publisher of scholarly articles: it is a pioneering approach to the world of academia, radically improving the way scholarly research is managed. The grand vision of Frontiers is a world where all people have an equal opportunity to seek, share and generate knowledge. Frontiers provides immediate and permanent online open access to all its publications, but this alone is not enough to realize our grand goals.

Frontiers Journal Series

The Frontiers Journal Series is a multi-tier and interdisciplinary set of open-access, online journals, promising a paradigm shift from the current review, selection and dissemination processes in academic publishing. All Frontiers journals are driven by researchers for researchers; therefore, they constitute a service to the scholarly community. At the same time, the Frontiers Journal Series operates on a revolutionary invention, the tiered publishing system, initially addressing specific communities of scholars, and gradually climbing up to broader public understanding, thus serving the interests of the lay society, too.

Dedication to Quality

Each Frontiers article is a landmark of the highest quality, thanks to genuinely collaborative interactions between authors and review editors, who include some of the world's best academicians. Research must be certified by peers before entering a stream of knowledge that may eventually reach the public - and shape society; therefore, Frontiers only applies the most rigorous and unbiased reviews.
Frontiers revolutionizes research publishing by freely delivering the most outstanding research, evaluated with no bias from both the academic and social point of view. By applying the most advanced information technologies, Frontiers is catapulting scholarly publishing into a new generation.

What are Frontiers Research Topics?

Frontiers Research Topics are very popular trademarks of the Frontiers Journals Series: they are collections of at least ten articles, all centered on a particular subject. With their unique mix of varied contributions from Original Research to Review Articles, Frontiers Research Topics unify the most influential researchers, the latest key findings and historical advances in a hot research area! Find out more on how to host your own Frontiers Research Topic or contribute to one as an author by contacting the Frontiers Editorial Office: researchtopics@frontiersin.org

CENTRAL CARDIOVASCULAR AND RESPIRATORY CONTROL: NEW TECHNIQUES, NEW DIRECTIONS, NEW HORIZONS

Topic Editors:
Vaughan G. Macefield, Baker Heart and Diabetes Institute, Australia
Geoffrey A. Head, Baker Heart and Diabetes Institute, Australia

Citation: Macefield, V. G., Head, G. A., eds. (2021). Central Cardiovascular and Respiratory Control: New Techniques, New Directions, New Horizons. Lausanne: Frontiers Media SA. doi: 10.3389/978-2-88966-353-8

Table of Contents

frontiers in Physiology

EDITORIAL
published: 19 November 2020
doi: 10.3389/fphys.2020.617092

Editorial: Central Cardiovascular and Respiratory Control: New Techniques, New Directions, New Horizons

*Vaughan G. Macefield and Geoffrey A. Head**

Human Autonomic Neurophysiology Laboratory and Neuropharmacology Laboratory, Baker Heart and Diabetes Institute, Melbourne, VIC, Australia

Keywords: sympathetic outflow, connectome, heart failure, hypertension, respiratory regulation, cardiovascular control, respiratory rhythmogenesis

Editorial on the Research Topic

Central Cardiovascular and Respiratory Control: New Techniques, New Directions, New Horizons

INTRODUCTION

How the brain controls blood pressure and respiration has fascinated physiologists for over a century. The cardiovascular and respiratory regulatory systems are tightly coupled, operating within a narrow range to maintain blood pressure, O_2, and CO_2 relatively constant, but with the capacity to operate at different levels according to behavioral or environmental requirements. For a long time, we have known that a decerebrate animal can breathe and maintain its blood pressure with only the brainstem intact. We have learnt much about the circuitry within the medulla required for the beat-to-beat control of blood pressure and heart rate, and the circuitry within the medulla and pons required for the generation of tidal breathing. We have also learnt about the roles of other subcortical structures, such as the hypothalamus and amygdala, in homeostatic regulation of blood pressure and respiration, and the contributions of cortical structures to this control. Much of this knowledge has come through the development of novel techniques, such as viral tracing of pathways, use of the working-heart brainstem preparation and, most recently, optogenetics. New directions that have also changed our focus relate in particular to the genetic and "omics" revolution which has transformed biomedical research in recent years. New models with tissue-specific over-expression, constitutively active receptors and dominant negative genetics have been developed and continue to increase our physiological understanding of these complex systems regulating blood pressure and respiration and how they change during states of disease. There are also new technologies such as CRISPR/Cas9 to enable global, conditional and targeted gene editing. The discoveries of the exquisite detail involved in intracellular signaling, second messengers and biochemical pathways as well as post-transcriptional modulation have markedly enhanced our understanding of regulatory influences and have increased our understanding of physiological processes to a new height.

It is clear that physiologists and pharmacologists will need to be able to integrate a vast array of information to be able to translate preclinical to clinical phases of discovery. Progress continues to be made in identifying the functional connectomes responsible for cardiovascular and respiratory control, and we are now at the stage where some of the work conducted in anesthetized or conscious animals is being pursued in humans through brain imaging. But where does the future lie? What research should we be doing, how should we do it and where will that lead? This Research Topic builds on an annual meeting held in Australia for over

OPEN ACCESS

Edited by:
Nandu Goswami,
Medical University of Graz, Austria

Reviewed by:
Stephane Perrey,
Université de Montpellier, France

***Correspondence:**
Geoffrey A. Head
geoff.head@baker.edu.au

Specialty section:
This article was submitted to Integrative Physiology, a section of the journal Frontiers in Physiology

Received: *14 October 2020*
Accepted: *22 October 2020*
Published: *19 November 2020*

Citation:
Macefield VG and Head GA (2020) Editorial: Central Cardiovascular and Respiratory Control: New Techniques, New Directions, New Horizons. Front. Physiol. 11:617092. doi: 10.3389/fphys.2020.617092

25 years, in which neuroscientists meet to discuss their latest work in central cardiovascular and respiratory control. We have 14 excellent papers in the Research Topic which includes 6 reviews and 8 original articles. Of these, 5 were published in the Frontiers in Neuroscience section while the remaining 9 were published in Frontiers in Physiology and have been viewed over 50,000 times so far. One of the reviews, by Saleeba et al. and Saleeba et al., provides an accessible "how-to guide" to all the approaches that have been used to identify functional networks within the brain. Geared to the student, but also suitable for the avid experimentalist, this article has been hugely popular. Given that it has been viewed >27,000 times it is safe to say that these approaches continue to intrigue and to offer unprecedented access to the networks of the brain. Needless to say, new techniques continue to be developed, and novel applications for their use will continue to allow progress in studying the pathways responsible for cardiovascular and respiratory control.

NEW DIRECTIONS IN HUMAN AUTONOMIC RESEARCH

A number of the contributions highlighted new and sophisticated techniques for analyzing autonomic function in humans. For example, a novel means of assessing sympathetic outflow non-invasively in humans has been proposed by Jendzjowsky et al.. Using optical coherence tomography, a means of imaging the different layers of the retina as well as the overlying blood vessels, the authors show that choroid vascular perfusion density (VPD) correlates very well with muscle sympathetic nerve activity (MSNA), recorded via an intraneural microelectrode: the higher the MSNA the lower the VPD (Jendzjowsky et al.). Interestingly, there was no relationship between MSNA and retinal VPD, suggesting the latter is not under sympathetic control, while choroid VPD decreased during the cold-pressor response and during an apnoea, maneuvers known to increase MSNA. Importantly, this means that imaging the eye allows one to examine sympathetic vasoconstrictor drive and vascular reactivity together and non-invasively. Another human imaging study, in which functional magnetic resonance imaging (fMRI) of the brain is performed at the same time as recording MSNA has revealed the functional location of the human homolog of the rostral ventrolateral medulla (RVLM), which plays a key role in the generation of MSNA (Macefield and Henderson). This combination of imaging and recording sympathetic activity is unique to these investigators and has provided an amazing insight into the pathways and nuclei involved in regulation of sympathetic activity. However, the technology has been further extended so that Macefield and Henderson have been able to show that changes in activity in this nucleus can be measured through brain imaging, revealing excitatory, and inhibitory mechanisms during sympatho-excitatory maneuvers and extending their work on MSNA-coupled fMRI to uncover operation of the human sympathetic connectome. The interesting aspect of this work is the connections from the prefrontal cortex highlight the importance of the cortex and perception of the environment. On that theme (Faull et al.) found the perception of the exertion involved in exercise was influenced by a state of ketoacidosis. Interestingly, the rating of perceived exertion was more influenced by localized perception of breathlessness and discomfort in the exercising legs rather than the presence of acidosis, but overall suggests that there is a complex interplay of humoral signals which may have evolved to cope with exertion under times of extreme metabolic stress. The considerable advancement in precise imaging coupled with neural recording and stimulation technology for studying human physiology are now enabling us to gain a new insight into the complexities of autonomic function.

NEW DIRECTIONS IN PRE-CLINICAL AUTONOMIC RESEARCH

In the area of basic autonomic research, a number of contributions to the topic have included technically sophisticated and cutting-edge technology. Abukar et al. examined a novel micro embolism model of heart failure in sheep to determine the extent of any changes to neural control as well to determine whether this model reflected human heart failure. The technique involves using three sequential embolizations over 3 weeks and to study the animals 12–14 weeks later when heart failure was evident, as indicated by elevated left ventricular end-diastolic pressure (Abukar et al.). Assessment of neural control involved examining the heart rate and blood pressure baroreflex relationship, which was markedly reduced in the heart failure group compared to the control animals. Importantly, these findings and other aspects of the model in generating increased respiratory rate and incidence of apnoea suggests that this large animal model of heart failure replicates the neural and respiratory instabilities seen in the human form of the disease. Zhang et al., using an interesting model of volume overload in rats, tested the influence of the sympathetic nervous system using bilateral stellate ganglionectomy and found significant improvement in cardiac fibrosis associated with decreased cardiac norepinephrine and TGF beta-1 release. Dhingra et al. explore the critical brainstem nuclei involved in respiratory rhythmogenesis, and the contributions of neighboring nuclei in furnishing the normal respiratory pattern through an elegant series of experiments conducted in the working heart-brainstem preparation. They demonstrated that balance of excitation and inhibition exerted onto the central network determines the overall respiratory pattern. In terms of sensory feedback, Driessen presents novel data on the central projections of afferents traveling in the trigeminal, vagus, glossopharyngeal, and spinal nerves, and the role of a hitherto largely unknown nucleus in the lateral medulla, the paratrigeminal nucleus, in multimodal processing of visceral sensory information and its integration for respiratory and cardiovascular control. Continuing on the theme of respiration, and its interaction with cardiovascular control, using the acute intermittent hypoxia (AIH) model, Farnham et al. argue that a specific excitatory amino acid, PACAP, is responsible for the sympatho-excitation resulting from AIH, as shown by direct injection of PACAP into the RVLM. They suggest this may

be involved in the hypertension associated with obstructive sleep apnoea. Dereli et al. identify several brainstem sites in which long-term hypercapnia leads to blunted chemosensitivity, offsetting the increase in ventilation that results from elevated CO_2 levels, with the neuropeptide galanin playing a key role.

There is increasing interest in non-drug therapies for the treatment of hypertension. A quite novel approach has been to use electroacupuncture, which appears to be quite effective in producing a sustained decrease in blood pressure (Li et al., 2015). However, the mechanisms aren't well-understood. Malik et al. examined whether adenosine in the rostral ventrolateral medulla contributes to electroacupuncture modulation of sympatho-excitatory reflexes through an adenosine receptor-opioid mechanism. These elegant studies led to the conclusion that activation of opioid receptors in this region of the medulla inhibits pre-sympathetic activity directly as well through an adenosine related mechanism, resulting in a lowering of blood pressure. Moreover, we now know that the central cardiovascular networks can be affected by inflammatory mediators, with Elsaafien et al. showing central as well as peripheral upregulation of several inflammatory markers in hypertension, arguing that it is the central attraction of these agents to key autonomic nuclei that lead to the increase in sympathetic outflow in high blood pressure.

LATEST CONTRIBUTIONS BY SPECIFIC TOPIC REVIEW

A comprehensive review by Badoer provided an insight into the contribution of the carotid body in cardiovascular and metabolic dysfunction. In particular the concept that overactivity of the carotid body may contribute to both hypertension as well as greater sympathetic activity in metabolic disturbances associated with obesity and insulin resistance. This is an exciting new area since targeting the carotid body for ablation may be a viable treatment for essential as well as obesity- induced hypertension. There is also the possibility of modulating the activity of the carotid body afferents by targeting specific receptors such as P2X3 or ion channels such as TRPM7. To date this treatment has been successful in small clinical studies in drug resistant hypertension and in patients with low ejection fraction heart failure. Importantly the procedure appears to be quite safe to perform (Badoer). Jackson et al. provided an up-to-the-minute examination of the mechanisms responsible for genetic hypertension in the Schlager BPH mouse strain which was developed in the 1970s. This is the first comprehensive review of this strain, which has been used extensively as the mouse equivalent of the spontaneous hypertensive rat (SHR) but there are important differences which relate to the contribution of the sympathetic nervous system in the Schlager strain which appears to be the predominant mechanism driving the hypertension (Jackson et al.). The main evidence for this is that ganglion blockade completely abolishes the difference between normotensive and hypertensive mouse strains but this is not the case in SHR. The review also covers important findings relating to a marked contribution of the medial amygdala to the hypertension in BPH mice as well as the susceptibility to attenuate the hypertension with neurosteroids such as allopregnanolone, which upregulate neuro steroid sensitive extrasynaptic GABA A receptors, particularly in the hypothalamus and amygdala (Jackson et al.). Thus, the Schlager hypertensive mouse provides a relatively pure neurogenic model of hypertension but exactly how this relates to human essential hypertension is not exactly known at this stage.

CONCLUSION

This collection of papers and reviews provides the reader with an overview of the current state-of-the-art in central cardiovascular and respiratory control. We have highlighted some of the findings from the use of the latest technical advances not only in animal models but also in human autonomic neurophysiology, both of which are helping unravel the complexities of the networks governing some of the most important homeostatic regulatory systems. The importance of these systems is such that they are robust with multiple redundant components but nevertheless can be disturbed, leading to disease. Of course, there is much that we still do not know, so the research will continue. We look forward to receiving submissions for the second volume of this Research Topic.

AUTHOR CONTRIBUTIONS

GH and VM contributed to the writing of this editorial. All authors contributed to the article and approved the submitted version.

ACKNOWLEDGMENTS

We would like to acknowledge the excellent submissions that have made this Research Topic so successful.

REFERENCES

Li, P., Tjen-A-Looi, S. C., Cheng, L., Liu, D., Painovich, J., Vinjamury, S., et al. (2015). Long-lasting reduction of blood pressure by electroacupuncture in patients with hypertension: randomized controlled trial. *Med. Acupunct.* 27, 253–66. doi: 10.1089/acu.2015.1106

Conflict of Interest: The authors declare that the research was conducted in the absence of any commercial or financial relationships that could be construed as a potential conflict of interest.

frontiers in Physiology

ORIGINAL RESEARCH
published: 19 March 2019
doi: 10.3389/fphys.2019.00229

Beyond RPE: The Perception of Exercise Under Normal and Ketotic Conditions

Olivia K. Faull[1,2], David J. Dearlove[1], Kieran Clarke[1] and Pete J. Cox[1]*

[1] Department of Physiology, Anatomy and Genetics, University of Oxford, Oxford, United Kingdom, [2] Nuffield Department of Clinical Neurosciences, University of Oxford, Oxford, United Kingdom

Aim: Subjective perceptions of exercising exertion are integral to maintaining homeostasis. Traditional methods have utilized scores of 'rating of perceived exertion' (RPE) to quantify these subjective perceptions, and here we aimed to test whether RPE may encompass identifiable localized perceptions from the lungs (breathlessness) and legs (leg discomfort), as well as their corresponding measures of anxiety. We utilized the intervention of ketoacidosis (via consumption of an exogenous ketone ester drink) to independently perturb exercise-related metabolites and humoral signals, thus allowing us to additionally identify the possible contributing physiological signals to each of these perceptions.

Methods: Twelve trained volunteers underwent two incremental bicycle ergometer tests to exhaustion, following ingestion of either an exogenous ketone ester or a taste-matched placebo drink. Cardiorespiratory measures, blood samples and perceived exertion scales were taken throughout. Firstly, two-way repeated-measures ANOVAs were employed to identify the overall effects of ketoacidosis, followed by generalized linear mixed model regression to isolate physiological predictors contributing to each perception.

Results: Rating of perceived exertion was found to contain contributions from localized perceptions of breathlessness and leg discomfort, with no measurable effect of ketoacidosis on overall exertion. Leg discomfort, anxiety of breathing and anxiety of leg discomfort were increased during ketoacidosis, and correspondingly contained pH within their prediction models. Anxiety of leg discomfort also encompassed additional humoral signals of blood glucose and ketone concentrations.

Conclusion: These results indicate the presence of localized components of RPE in the form of breathlessness and leg discomfort. Furthermore, subjective perceptions of anxiety appear to result from a complex interplay of humoral signals, which may be evolutionarily important when monitoring exertion under times of metabolic stress, such as during starvation.

Keywords: exercise, perception, RPE, ketoacidosis, anxiety

OPEN ACCESS

Edited by:
Geoffrey A. Head, Baker Heart and Diabetes Institute, Australia

Reviewed by:
Alvaro Reischak-Oliveira, Universidade Federal do Rio Grande do Sul (UFRGS), Brazil
Sabrina Skorski, Saarland University, Germany

****Correspondence:***
Olivia K. Faull
faull@biomed.ee.ethz.ch

Specialty section:
This article was submitted to Integrative Physiology, a section of the journal Frontiers in Physiology

Received: *30 October 2018*
Accepted: *21 February 2019*
Published: *19 March 2019*

Citation:
Faull OK, Dearlove DJ, Clarke K and Cox PJ (2019) Beyond RPE: The Perception of Exercise Under Normal and Ketotic Conditions. Front. Physiol. 10:229. doi: 10.3389/fphys.2019.00229

INTRODUCTION

Internal bodily perception of exercising exertion is a vital component in the maintenance of homeostasis. More than simply the sum of our physiology, understanding exercising humans as a psychosomatic whole (Borg, 1982) may lead to valuable insights: from the capacity for physical performance, through to barriers to exercise within population health (Clark, 1999; Cohen-Mansfield et al., 2003). Until now, measuring the subjective perception of exercising exertion has often utilized subjective scores of 'rating of perceived exertion' (RPE), touted as a single indicator of the degree of physical strain (Borg, 1982). RPE is thought to integrate a multitude of ascending and descending signals between the brain and periphery, including feed-forward motor drive as well as neural and humoral feedback (Hampson et al., 2001; Tucker, 2009). However, teasing apart the independent physiological signals contributing to RPE, and possibly the perceptual sub-components of this measure of exertion remain as unsolved challenges.

Whilst RPE can be an informative tool to encompass overall exertion perception, most human experiences are much more complex and nuanced. If we are to better understand subjective perceptions associated with athletic performance, deeper understanding of the potential contributing components to RPE is required. At its simplest level, these components may constitute location of exertion, for example compartmentalized perceptions of the legs or lungs. In light of this, breathlessness and leg fatigue have also previously been quantified during incremental exercise (Borg et al., 2010; Faull et al., 2016), albeit with almost parallel reported growth functions to RPE (Borg et al., 2010). Secondly, beyond localization of exertion, an important (and often overlooked) aspect to our exercise perception is the 'affective' or emotional qualities (Carrieri-Kohlman et al., 1996, 2001, 2009; Faull et al., 2016) such as the anxiety related to a sensation. Due to the salience of anxiety as a symptom, it may be that these affective qualities are powerful contributors to our homeostatic moderation of exercise, in addition to the intensity of a perception. Therefore, whilst fully understanding the host of signals contributing to perceptions of RPE may be beyond our current sensitivity, the aim of this manuscript was to break down exercising perceptions into both location and symptom quality as a first tangible step in understanding how we monitor and modulate perceived exertion during exercise.

Bodily perceptions during exercise may also have an important evolutionary role. During times of famine and starvation we produce ketone bodies, which act as a fuel for the brain and periphery to supplement low carbohydrate stores (Cahill and Owen, 1968; Cahill, 1970, 2006). Additionally, ketones act as a widespread signaling molecule, increasing peripheral fat metabolism and sparing carbohydrate to prolong survival (Robinson and Williamson, 1980). However, ketone bodies are acidic, inducing a mild ketoacidosis even within the physiological limits of controlled ketosis (0.2–7 mM) (Robinson and Williamson, 1980). The perception of acidosis, and furthermore ketoacidosis, may be important in maintaining homeostasis and the trade-off between physical exertion to overcome starvation, and the concomitant physiological strain. Importantly, ketoacidosis can also be induced via consumption of exogenous means, and specific ketone ester drinks have been reported to rapidly invoke blood ketone concentrations of the active D-βHB isoform to levels comparable with several days of starvation (2–5 mM/L) (Clarke et al., 2012a,b; Cox et al., 2016; Shivva et al., 2016; Stubbs et al., 2017). Therefore, using exogenous ketoacidosis to perturb normal exercising metabolism and examining the corresponding perceptual changes, we may be better able to both understand the independent physiological components contributing to exercising exertion, and potentially reveal ketones themselves as possible *perceptual* signaling molecules within the brain.

In this paper, we aimed to understand the simplest formation of potential sub-components that may contribute to the perception of RPE, and the physiological signals that may drive them. To do this, we first investigated the contributions of breathlessness, anxiety of breathing, leg discomfort, and anxiety of leg discomfort toward perceptions of RPE during incremental exercise both under placebo and exogenous ketotic conditions. By employing this tool of exogenous ketosis, we were able to then both separate aspects of physiology that are often tightly linked within exercise, and examine whether the evolutionarily important ketone molecules themselves may act as a homeostatic signal when monitoring bodily sensations.

MATERIALS AND METHODS

Participants

Twelve healthy, athletically trained subjects [nine males, three females; age (mean ± SEM) 28 ± 1.6 years; height 185 ± 3.33 cm; weight 78 ± 3.5 kg; $VO_{2\,max}$ 56.5 ± 3.9 mL/min/kg; W_{max} 382.3 ± 69.8 W] participated in this study. Ethical approval was granted by the Oxfordshire Clinical Research Ethics Committee, and all participants provided written, informed consent.

Protocol

Participants completed two incremental exercise tests to exhaustion on an electronically braked bicycle ergometer (Ergoline, Germany), separated by at least 5 days. Following an overnight fast, participants consumed a drink containing a ketone ester [330 mg/kg body weight of *(R)*-3-hydroxybutyl *(R)*-3-hydroxybutyrate ketone ester] or a calorie-free, taste-matched control drink prior to exercise, in a blinded, randomized and counterbalanced order. The ketone ester drink contained transesterified ethyl *(R)*-3-hydroxybutyrate with *(R)*- 1,3-butanediol, and has previously been shown to be a safe and effective way of elevating blood ketone levels (Clarke et al., 2012a,b; Cox et al., 2016; Shivva et al., 2016; Stubbs et al., 2017). The session order was determined in a randomized, counterbalanced and single-blinded fashion.

For blood measures, participants were inserted with a 22-gauge retrograde indwelling catheter into the dorsal vein of the hand immediately upon arrival. The hand was gently heated prior to blood sampling at rest and during exercise for arterialized blood measures (Forster et al., 1972), and blood

samples were drawn at baseline (prior to drink consumption), immediately prior to exercise, and at exercise intensities of 100, 200, 300 W and maximal intensity prior to exhaustion. For each blood measure, a 1 mL blood sample was first drawn for blood gas measurements, which were immediately analyzed using a benchtop blood gas analyzer (Radiometer, Denmark) for measures of blood gasses, hemoglobin content, oxygen saturation and blood metabolites. Calculations of arterial pH and HCO_3^- from these samples were made using custom MATLAB scripts (MathWorks, Inc., United States) incorporating measured and expected hemoglobin, measured partial pressure of carbon dioxide (PCO_2) and measured oxygen saturations (see **Supplementary Materials and Methods** for equations), and corrected arterial pH values were then transformed into hydrogen concentrations ($[H^+]$) for further analyses (Forster et al., 1972), using a log transformation in Microsoft Excel®.

A second 2 mL blood sample was drawn at each interval for analysis of blood hormone and metabolite concentrations, with D-βHB immediately assayed using a portable analyzer (Abbott Laboratories, Ltd., United Kingdom). Samples were stored on ice, centrifuged (3,600 rpm for 10 min), and subsequently stored at −25°C until further analysis. Glucose, non-esterified fatty acids (NEFAs) and lactate were subsequently assayed using a commercial automated bench-top analyzer (ABX Pentra, France), and insulin assays were performed using an ELISA kit (Mercodia, Sweden).

To collect respiratory gas measures, participants breathed through a facemask (Hans Rudolf, Kansas City, MO, United States) attached to a low-resistance turbine and gas flow analyzer (Cortex Metalyzer 3B, Cranlea Human Performance, Ltd., United Kingdom) to measure the breath-by-breath composition of respiratory gasses and ventilatory parameters (Metasoft Studio Software, Cortex, Version 3.9.9). Respiratory measures were averaged and recorded over approximately 2 min both prior to drink consumption and immediately before exercise. Heart rate was measured and recorded using a chest strap (Polar T31, Polar Electro, Inc., Lake Success, NY, United States) wirelessly connected to the Metasoft Studio.

Incremental exercise to exhaustion was conducted on an electronically braked bicycle ergometer (Ergoline, Germany) for the determination of maximal volume of oxygen consumption ($VO_{2\,max}$) and maximal work (W_{max}) (Cortex Biophysik, Germany). At least one male and one female experimenter were present at both exercise sessions for each participant. Exercise began at 100 W, and increments of either 25 or 50 W were undertaken every 3 min until volitional fatigue. Respiratory measures were averaged and recorded over approximately 30 s within the last minute of each exercise step, and ∼5 mL blood samples were drawn at 100, 200, 300 W and maximal exercise. Subjective scores of RPE ("What is your perceived exertion?"), breathlessness ("How breathless are you?"), leg discomfort ("What is your leg discomfort?"), anxiety of breathing ("How anxious are you about your breathing?") and anxiety of leg discomfort ("How anxious are you about your leg discomfort?") were recorded in a randomized order on a linear scale of 0–10 (from "No [breathlessness/leg discomfort/anxiety of breathing/anxiety of leg discomfort]" = 0 to "Maximal [breathlessness/leg discomfort/anxiety of breathing/anxiety of leg discomfort]" = 10) both immediately prior to exercise and at the end of each incremental step (see **Supplementary Material** for rating scales).

Statistical Analysis

Preliminary statistical analyses were performed using GraphPad Prism (version 7, GraphPad Software, Inc., San Diego, CA, United States). All variables were first analyzed using a two-way analysis of variance (ANOVA) of the intervention (ketone or control) and cycle ergometer power. A p-value of < 0.05 was taken to indicate statistical significance. Self-reported subjective variables (RPE, breathlessness, anxiety of breathing, leg discomfort and anxiety of leg discomfort) were then further explored using generalized linear mixed effects regression models in R (Faraway, 2017) (R version 3.4.1, RStudio version 1.0.143). Mixed-effects regression models allow accountability for repeated measures taken within subjects, such as across an experimental exercise test, without violating residual independence or autocorrelation assumptions of linear regression models.

Following tests for data normality **(Supplementary Material)**, models were fitted to each of the psychological variables using a generalized linear mixed effects model (glmer; Bates et al., 2015), with maximum likelihood (laplace approximation) and a log-normal link function. A subject-specific random effect was included in each model, to allow a different model intercept to be fitted for each subject. Data points where all measured blood, heart rate and respiratory variables were present were used for data modeling, and all variables were centered and scaled prior to inclusion. Two subjects were excluded from modeling analyses due to missing heart rate data.

To firstly test the potential contribution of breathlessness, leg discomfort, anxiety of breathing, and anxiety of leg discomfort toward the perception of RPE, a global model was fitted including covariates for power, heart rate, sex (and their interactions), as well as the four measured psychological components and the interactions between power and both leg discomfort and breathlessness (see **Supplementary Material** for explanation of included variables). A parsimonious model of the key predictor variables was then identified using backward elimination of statistically non-significant terms ($p > 0.05$) until the model contained all significantly contributing variables. This final model was then formally compared to a null model (containing only covariates for power, heart rate, sex and their interactions) using the ANOVA function with type III Wald chisquare tests (R stats package), to assess improvement in fit to the data.

To then test which physiological factors may drive each of the four psychological components, initial global models were fitted containing all hypothesized contributing variables (power, heart rate, sex and their interactions, age, hydrogen ion concentration $[H^+]$, lactate ion concentration $[Lactate^-]$, D-βHB ion concentration $[\beta HB^-]$, glucose concentration [Glucose], ventilation (for breathlessness and anxiety of breathing only), and an interaction term between power and $[H^+]$ (power × $[H^+]$)) (see **Supplementary Material** for included variables). Parsimonious models of the key predictor

variables were then identified using backward elimination of statistically non-significant terms ($p > 0.05$), until each model model contained all significantly contributing variables. Some non-significant variables were retained if their interaction with another variable was significant, to preserve a hierarchical, well-formulated model (Morrell et al., 1997). These reduced models were tested against the initial global models using the ANOVA function in R and type II (no interaction terms) or III (interaction terms present) Wald chisquare tests, to confirm that the reduced set of variables did not impair the quality of the model fit. A p-value of < 0.05 was taken to indicate statistical significance of an independent effect of each parameter, accounting for all other parameters in the model. Finally, full model R^2 and fixed effect R^2-values for each global and reduced model were calculated using the r2beta function within the r2glmm package, using the standardized generalized variance approach (Jaeger et al., 2016), and the predicted data was plotted against the measured data for visualization of model accuracy (**Figure 4**).

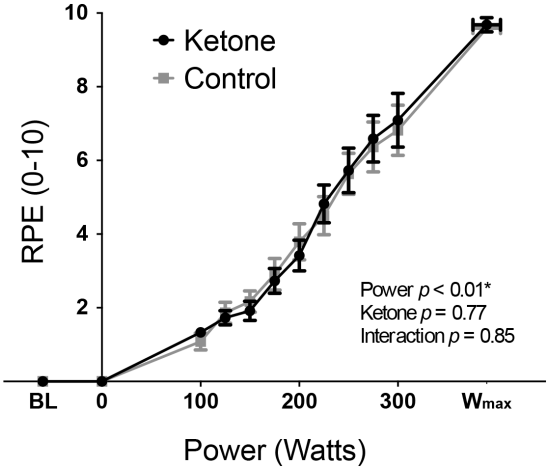

FIGURE 1 | Rate of perceived exertion (RPE: mean ± SEM) plotted against power during incremental exercise under ketosis or placebo control conditions. p-values represent analysis of variance (ANOVA) results for power, ketone ester intervention and an interaction effect. Statistical significance (denoted by *) was taken at $p < 0.05$. BL = baseline.

RESULTS

Intervention Effects of Exogenous Ketosis

Exercise performance (W_{max}) was not significantly different between KE (mean ± SEM: 393 ± 22 W) and control (389 ± 20 W) conditions ($T = 1.07$, $p = 0.31$). Overnight fasted D-βHB levels were 0.2 ± 0.0 mM/L in both conditions at baseline, while D-βHB increased significantly to 3.7 ± 0.3 mM/L following KE consumption prior to exercise. The main effect of a KE on all other physiological variables are presented elsewhere (Dearlove et al., in press). To address the aims of this manuscript, the significance of the contributions of both the KE intervention and cycle ergometer power (both fixed effect measures, determined by the study protocol design) toward the measured perceptual quantities were firstly assessed via two-way repeated measures ANOVA analyses. For both RPE (**Figure 1**) and breathlessness (**Figure 2**), power was the only significantly contributing variable, while leg discomfort demonstrated a significant effect of power, KE intervention and an interaction effect (**Figure 2**). Anxieties of breathing and leg discomfort both showed a significant effect of both power and KE intervention (**Figure 2**), with no interaction effect. Full ANOVA results are provided in the **Supplementary Material**.

RPE Model

The parsimonious generalized linear mixed effects RPE model contained significant contributions from both breathlessness and leg discomfort, but neither anxiety score (**Figure 3**). In addition, a negative interaction between power and breathlessness was also retained within this model, indicating that the increases in breathlessness with power 'tail off' toward maximal exertion. The modeling of RPE scores was improved in comparison to the null model, which contained only physiological variables [ANOVA comparison: Null model: $R^2 = 0.96$, Residual Degrees of freedom (RDoF) = 80, Akaike's Information Criterion (AIC) = 254.1, Bayesian Information Criterion (BIC) = 276.5; vs. Final model: $R^2 = 0.97$, RDoF = 80, AIC = 195.2, BIC = 217.6; Comparison Chi-squared = 58.9, $p < 0.001$]. Positive, significant effects of both breathlessness ($T = 7.5$, $p < 0.001$) and leg discomfort ($T = 3.0$, $p < 0.001$) were found to contribute to RPE score, explaining 31 and 8% of the RPE variance respectively (see **Supplementary Table 2** for full results). A negative effect of the interaction between power and breathlessness ($T = -10.7$, $p < 0.001$) was also observed, explaining 58% of the RPE variance. No significant, independent contribution of anxiety of either breathing or leg discomfort toward RPE score was demonstrated.

Compartmentalized Perceptual Models

Breathlessness

Results of the full model fit for breathlessness are presented in **Table 1**, demonstrating a significant, positive, independent effect of power, and negative effects of sex (male) and glucose (**Table 1**). The reduced, parsimonious model of breathlessness demonstrated significant, driving positive effects of power and heart rate, with a negative effect of sex (male), and a model R^2-value of 0.93 (**Figure 4** and **Supplementary Table 3**).

Anxiety of Breathing

Results of the full model fit demonstrated a positive effect of $[H^+]$, and a negative interaction between power and $[H^+]$ (**Table 1**). The reduced model also demonstrated significant, positive effects of power and $[H^+]$, with a negative interaction between power and $[H^+]$, and a model R^2-value of 0.74 (**Figure 4** and **Supplementary Table 3**).

Leg Discomfort

Results of the full model fit for leg discomfort also demonstrated a positive effect of $[H^+]$, and a negative interaction between power and $[H^+]$ (**Table 1**). The reduced model of leg

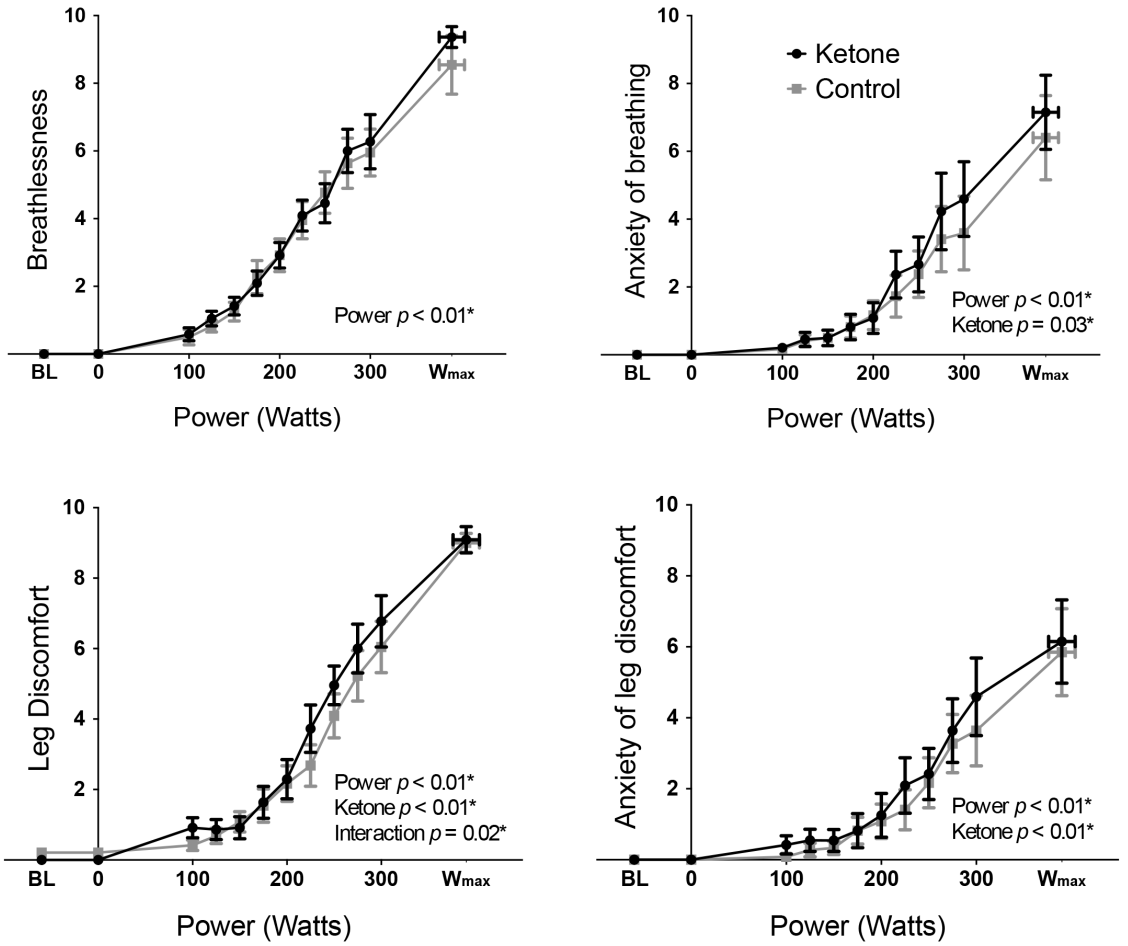

FIGURE 2 | Mean (± SEM) perceptions of breathlessness, anxiety of breathing, leg discomfort, and anxiety of leg discomfort plotted against power during incremental exercise, under ketosis or placebo control conditions. *p*-values represent analysis of variance (ANOVA) results for power, ketone ester intervention, and interaction effects for each perception. $^{*}p < 0.05$. BL = baseline.

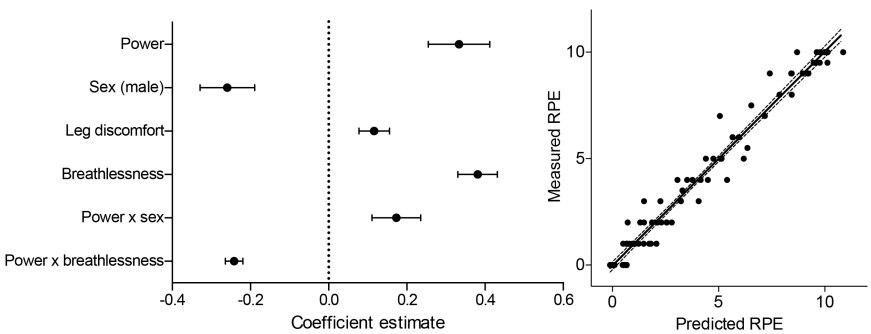

FIGURE 3 | Summary of the model coefficients (left) and predicted vs. measured outcomes for the generalized linear mixed effects regression model (glmer) of RPE (RPE). Glmer was fitted using a log-normal link function to a gaussian distribution. All predictor variables were centered and standardized before inclusion into the model, and are represented as mean estimates (± standard deviations).

discomfort also demonstrated significant, positive effects of power, heart rate and $[H^+]$, with a negative interaction between power and $[H^+]$, and a model R^2-value of 0.90 (**Figure 4** and **Supplementary Table 3**).

Anxiety of Leg Discomfort

Results of the full model fit demonstrated positive effects of heart rate, $[H^+]$, $[Lactate^-]$, and an interaction between power and sex (male) (**Table 1**). Negative effects were shown for

TABLE 1 | Model summaries and coefficients for global model fits to each of the compartmentalized perceptions of breathlessness, leg discomfort, anxiety of breathing (breath anxiety), and anxiety of leg discomfort (leg anxiety).

	Breathlessness			**Breath anxiety**			**Leg discomfort**			**Leg anxiety**		
Fixed effects	***Coefficient***	***T***	***p***	***Coefficient***	***T***	***p***	***Coefficient***	***T***	***p***	***Coefficient***	***T***	***p***
Intercept	1.91	7.95	<0.01*	0.48	0.81	0.42	1.39	4.67	<0.01*	0.17	0.31	0.76
Power	1.10	2.95	<0.01*	0.36	0.43	0.67	0.73	1.65	0.10	−0.89	−1.83	0.07
Heart rate	0.09	0.32	0.75	0.22	0.27	0.79	0.48	1.08	0.28	2.13	3.61	<0.01*
Sex (male)	−0.36	−2.50	0.01*	−0.03	−0.08	0.94	0.03	0.11	0.92	0.88	1.51	0.13
$[H^+]$	−0.01	−0.21	0.84	0.37	2.90	<0.01*	0.14	1.96	0.05*	0.30	4.66	<0.01*
$[Lactate^-]$	0.07	1.05	0.30	−0.02	−0.19	0.85	0.03	0.49	0.63	0.23	3.41	<0.01*
Ventilation	−0.04	−0.39	0.70	0.34	1.53	0.13	–	–	–	–	–	–
$[\beta HB^-]$	−0.04	−1.91	0.06	−0.04	−0.98	0.33	−0.01	−0.40	0.69	−0.04	−1.42	0.15
[Glucose]	−0.08	−2.08	0.04*	0.08	1.09	0.27	−0.04	−1.41	0.16	−0.05	−2.02	0.04*
Power × HR	−0.10	−0.96	0.34	−0.16	−0.62	0.53	−0.03	−0.28	0.78	−0.24	−1.68	0.09
Power × Sex	−0.69	−1.85	0.06	−0.33	−0.38	0.70	−0.09	−0.18	0.85	1.75	3.27	<0.01*
HR × Sex	0.51	1.56	0.12	0.30	0.35	0.73	−0.23	−0.46	0.65	−2.01	−3.10	<0.01*
Power × $[H^+]$	0.02	0.36	0.72	−0.23	−2.06	0.04*	−0.15	−2.40	0.02*	−0.35	−5.57	<0.01*
Random effects	***Intercept***		***Residual***	***Intercept***		***Residual***	***Intercept***		***Residual***	***Intercept***		***Residual***
Subject intercept	0.007		0.860	0.181		1.678	0.052		1.100	0.282		0.624
Model R^2	0.93			0.74			0.90			0.81		

*Indicates $p < 0.05$.

[Glucose], an interaction between heart rate and sex, and an interaction between power and $[H^+]$ (**Table 1**). The reduced model demonstrated significant, positive effects of heart rate, sex (male), $[H^+]$, $[Lactate^-]$, and an interaction between power and sex (male) (**Figure 4** and **Supplementary Table 3**), with negative effects of power, $[\beta HB^-]$ and [Glucose], and negative interactions between heart rate and sex, and between power and $[H^+]$. This reduced model had an R^2-value of 0.81 (**Figure 4**).

DISCUSSION

In this study, we aimed to investigate the subcomponents of RPE and their driving physiological factors. We quantified subjective measures of breathlessness and leg discomfort as contributing components toward RPE, and observed no change in RPE during ketoacidosis despite widespread changes in peripheral exercising physiology. For the isolated perceptual components measured, breathlessness intensity was the only perception unaltered by ketoacidosis, and simultaneously the only perception that was not predicted by changes in blood pH. Whilst anxiety of breathing and intensity of leg discomfort contained pH (hydrogen ion concentration) as a humoral predictor, anxiety of leg discomfort was also associated with a number of other humoral signals, including the concentration of blood βHB ions.

The relationship between perceptions of exertion and physical work was first investigated by Borg and Dahlström in the 1950s (Borg and Dahlström, 1960). Within this early work, it was noted that power functions (with an exponent of approximately 1.6) best described the psychophysical relationship between perceptual changes and exercise intensity (Borg, 1982). These observations led Borg to conclude that RPE may encompass both more linear afferent factors, such as heart rate, and non-linear peripheral factors, such as lactate (exponent of approximately 2) (Borg, 1973, 1982). Therefore, Borg went on to develop the 15-point 'Borg scale' as a singular measure of perceived exertion (Borg, 1970, 1982, 1998), designed to increase linearly and reduce inter-subject variability by using carefully placed word anchors on the scale. In this manuscript, we aimed to decompose the RPE measure into perceptual components during incremental exercise, and assess how the underlying physiological signals contribute to these compartmentalized perceptions. Furthermore, we also incorporated measures of psychological affect (anxiety) toward these intensity perceptions. To model these perceptions and capture all signaling components in their native state, we used linear perception scales (0–10) and generalized linear mixed model regression, to account for inter-subject variability and non-normally distributed data (Faraway, 2017).

Rating of Perceived Exertion

In extension of the seminal work by Borg and Dahlström (1960) and Borg (1962), modern models of RPE have theorized it to be more than simple modulation of afferent feedback (Ulmer, 1996; Hampson et al., 2001; Tucker, 2009). Subjective scores of RPE are thought to also encompass feedforward anticipation of exercise demands, allowing appropriate pacing strategies to be selected under a variety of physiological circumstances (Hampson et al., 2001; Noakes, 2004; Tucker, 2009). Furthermore, the more holistic measure of exercise 'exertion' is now also thought to be distinct from perception of exercising 'effort' (Abbiss et al., 2015). This idea addresses the breakdown of the relationship between RPE and exercise intensity under conditions of hypnosis (Morgan et al., 2008,

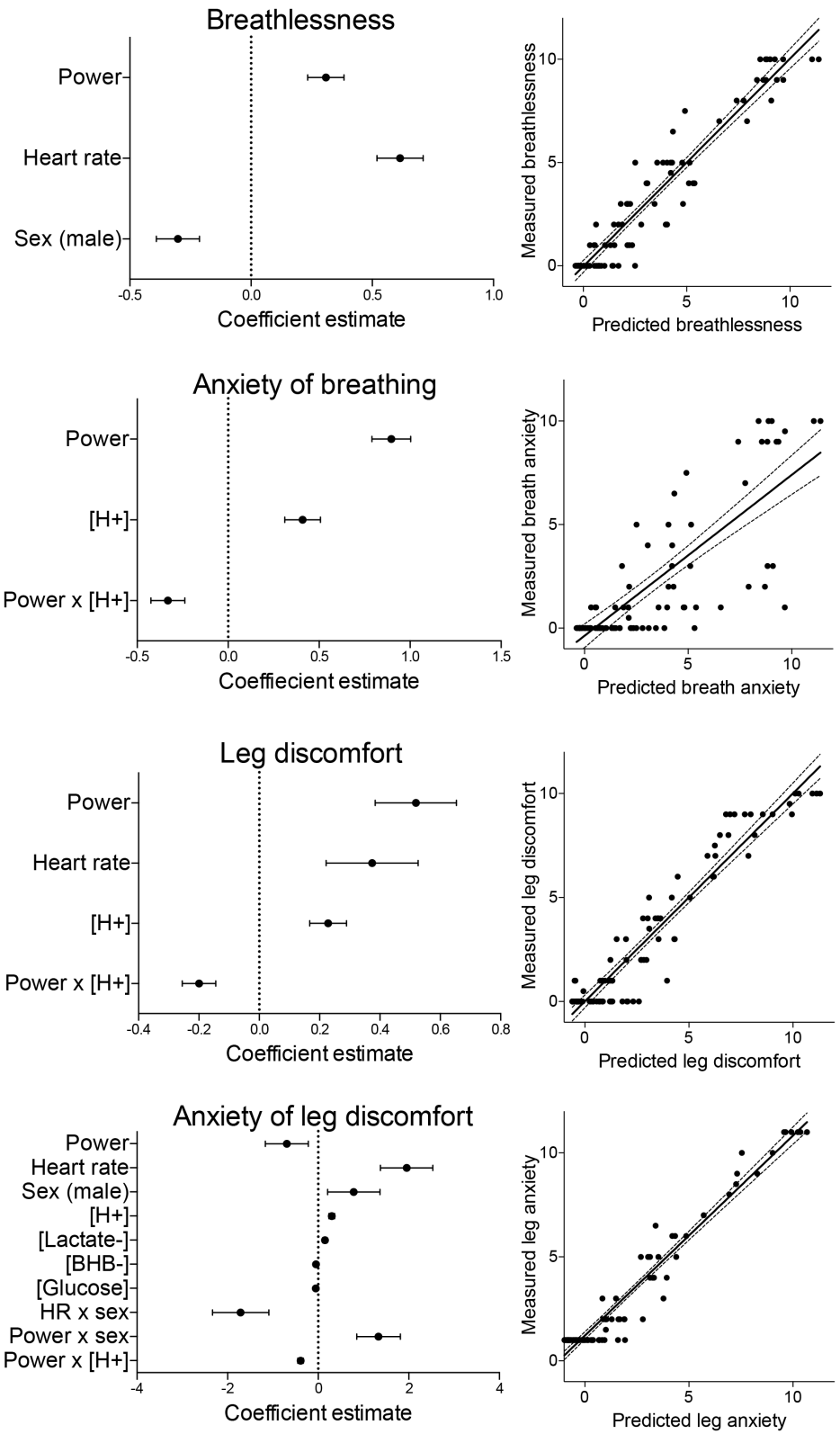

FIGURE 4 | Summary of the model coefficients (left) and predicted vs. measured outcomes for the generalized linear mixed effects regression models (glmer). Models were fitted for ratings of breathlessness, anxiety of breathing, leg discomfort and anxiety of leg discomfort, and each glmer was fitted using a lognormal link function to a gaussian distribution. All predictor variables were centered and standardized before inclusion into the model, and are represented as mean estimates (± standard deviations).

2011), or when key physiological signals are perturbed, such as heart rate via blocking agents (Ekblom and Golobarg, 1971), or in glycogen-deplete states (Baldwin et al., 2003; Noakes, 2004). Therefore, we created a null model of RPE encompassing power, heart rate, and sex (and their interactions), to account for linear and potential anticipatory effort perceptions with increasing power, as well as a measure of cardiac sympathetic drive via changes in heart rate, and any differences according to sex. Whilst this model demonstrated a tight fit to the RPE measures, positive, independent components of breathlessness, leg discomfort and the interaction between breathlessness and power were then shown to also independently contribute and improve this model, indicating each to be a significant component of RPE. Breaking down RPE into localized components may deepen our understanding of the independent contributions of afferent feedback from different bodily sensations, and thus equip us with better tools to explore how this may change across sporting modalities and/or contexts.

Whilst RPE had also originally been theorized to be influenced by psychological affect (Borg, 1998), previous work has also been unable to substantiate this relationship (Hardy and Rejeski, 1989). Therefore, it is possible that measuring RPE alone when investigating exercising perceptions may miss the influence of heavily valent affective emotions such as anxiety, which may also influence performance (Leupoldt von and Dahme, 2005; Banzett et al., 2008; Faull et al., 2016). Here we found no influence of breathlessness anxiety nor anxiety of leg discomfort toward RPE, although it must be noted that the relatively small sample size may hinder our ability to detect potentially small contributions from these variables. These preliminary data thus appear to indicate that perceptual anxiety does not positively contribute to subjective perceptions of RPE. However, as adapted linear scales were employed in this study (allowing for generalized linear models to be applied within the analysis) and the specific wording proposed by Borg to describe RPE ("how laborious it feels to work"; Borg, 1962) were not used in the description of the ratings to participants, care must be taken in the application of these results to other studies employing measures of RPE.

Lastly, RPE was not measurably altered during ketosis, despite widespread changes in physiology. These results further support a dominant component of anticipatory feedforward contributions to perceived exertion (Hampson et al., 2001; Tucker, 2009), even in the face of ketoacidosis. Therefore, whilst measures of RPE are able to garner enormous insight into man as a psychosomatic whole during exercise (Borg, 1982), these results highlights the need for additional, more interrogative measures of psychological affect to be simultaneously adopted. It would appear evolutionarily unlikely that either the presence of vital molecules such as βHB within the brain (Owen et al., 1967; Cahill and Owen, 1968; Cahill et al., 1970; Mikkelsen et al., 2015), or the concurrent changes in blood acidosis would not elicit any changes in perception of exercising exertion.

Localized Perceptions of Exertion

Results of our RPE model revealed positive, independent contributions of breathlessness and leg discomfort perceptions toward overall exertion (RPE) during cycle ergometer exercise. Furthermore, these isolated perceptual intensity components were found to be driven by different physiological signals, where breathlessness contained only power and heart rate, while leg discomfort also contained pH as an integral predictor. In accordance with these modeling results, ketoacidosis did not affect breathlessness perception, while leg discomfort was increased compared to the control condition. Interestingly, leg discomfort was altered in a non-uniform fashion across exercising intensities with ketosis (**Figure 2**). It appears that the effect of pH on leg discomfort also depends on the intensity of the exercise, as demonstrated by the negative interaction effect between power and $[H^+]$. Lower and moderate intensities of exercise were more susceptible to increased leg perception with acidosis, as this may create a peripheral mismatch when monitoring blood pH against what is expected for these exercise intensities (Paulus and Stein, 2006).

Anxiety of Exercising Perceptions

The anxiety associated with interoceptive perception is an important, highly valent driver in the maintenance of homeostasis (Craig, 2003; Paulus and Stein, 2006). Contrary to intensity perceptions, anxiety of *both* breathlessness and leg discomfort were increased throughout ketoacidosis, and contained blood pH as a predictor of perception. Therefore, it is possible that anxiety perception measures are more broadly sensitive to potentially harmful peripheral changes in metabolism, and our homeostatic monitoring of these signals manifest more strongly within the affective perceptual domain. Furthermore, anxiety of leg discomfort appears to be a more complex measure that incorporates further humoral signals, including glucose and βHB. Both glucose and βHB cross the blood–brain barrier (Mikkelsen et al., 2015) and are important signals denoting metabolic stress. The combination of blood glucose and ketone ion concentrations represent two important components of cerebral fuel availability (Owen et al., 1967; Cahill and Owen, 1968; Cahill et al., 1970; Mikkelsen et al., 2015), and if exercise compromises that fuel it may heighten anxiety of leg discomfort. Therefore, perception of exercising limb anxiety may be a homeostatic warning signal whilst exercising under compromised metabolic conditions, such as during starvation. However, further modeling would be required to reproduce and thoroughly investigate these results in the future, incorporating larger datasets for more nuanced and generalisable statistical analyses.

CONCLUSION

In this manuscript, we have conducted a preliminary investigation into the potential localized lung and leg perceptual components that contribute to RPE, and the importance of simultaneous affective anxiety perceptions. While the metabolic state of ketoacidosis does not appear to alter RPE, we reported concomitant increases in leg discomfort and affective perceptions of anxiety. In comparison, breathlessness appears to be unaffected by ketoacidosis.

Finally, we have revealed that anxiety of leg discomfort may be a complex measure that incorporates humoral signals such as glucose and ketone concentrations, and thus potentially an evolutionarily important perception to help moderate exercise during times of metabolic stress. Whilst this data has yielded interesting preliminary modeling results of these perceptions, large scale datasets (with a more equal gender balance and a diverse study population) would be required for greater understanding and further statistical support regarding definitive sub-components of RPE and the physiological signal contributions to exercising perceptions.

DATA AVAILABILITY

The datasets generated for this study are available on request to the corresponding author.

AUTHOR CONTRIBUTIONS

OF, DD, and PC collected the data for this study. PC and KC supervised the project. OF completed the data analysis and wrote the initial manuscript. All authors contributed intellectual ideas towards the final manuscript.

FUNDING

This study was funded by TdeltaS, a spin out company of the University of Oxford, of which KC was the director. This study was also supported by the Royal Commission for the Exhibition of 1851.

ACKNOWLEDGMENTS

The authors would like to thank Dr. Edward Stace for his assistance throughout data collection and Dr. Jack Miller for his assistance with data analysis.

SUPPLEMENTARY MATERIAL

The Supplementary Material for this article can be found online at: https://www.frontiersin.org/articles/10.3389/fphys.2019.00229/full#supplementary-material

REFERENCES

Abbiss, C. R., Peiffer, J. J., Meeusen, R., and Skorski, S. (2015). Role of ratings of perceived exertion during self-paced exercise: what are we actually measuring? *Sports Med.* 2015, 1235–1243. doi: 10.1007/s40279-015-0344-5

Baldwin, J., Snow, R. J., Gibala, M. J., Garnham, A., Howarth, K., and Febbraio, M. A. (2003). Glycogen availability does not affect the TCA cycle or TAN pools during prolonged, fatiguing exercise. *J. Appl. Physiol.* 94, 2181–2187. doi: 10.1152/japplphysiol.00866.2002

Banzett, R. B., Pedersen, S. H., Schwartzstein, R. M., and Lansing, R. W. (2008). The affective dimension of laboratory dyspnea. *Am. J. Respir. Crit. Care Med.* 177, 1384–1390. doi: 10.1164/rccm.200711-1675OC

Bates, D., Maechler, M., Bolker, B. M., and Walker, S. C. (2015). Fitting linear mixed-effects models using lme4. *J. Stat. Softw.* 67, 1–48. doi: 10.18637/jss.v067.i01

Borg, E., Borg, G., Larsson, K., Letzter, M., and Sundblad, B. M. (2010). An index for breathlessness and leg fatigue. *Scand. J. Med. Sci. Sports* 20, 644–650. doi: 10.1111/j.1600-0838.2009.00985.x

Borg, G. (1970). Perceived exertion as an indicator of somatic stress. *Scan. J. Rehabil. Med.* 2, 92–98.

Borg, G. (1998). *Borg's Perceived Exertion and Pain Scales*. Champaign, IL: Human Kinetics.

Borg, G., and Dahlström, H. (1960). *The Perception of Muscular Work*. Umeå: Publications of the Umea Research Library.

Borg, G. A. (1962). *Physical Performance and Perceived Exertion*. Oxford: University Lund.

Borg, G. A. (1973). Perceived exertion: a note on history and methods. *Med. Sci. Sports* 5, 90–93. doi: 10.1249/00005768-197300520-00017

Borg, G. A. (1982). Psychophysical bases of perceived exertion. *Med. Sci. Sports Exerc.* 14, 377–381. doi: 10.1249/00005768-198205000-00012

Cahill, G., Felig, P., Owen, O., and Wahren, J. (1970). Metabolic adaptation to prolonged starvation in man. *Nord. Med.* 83:89.

Cahill, G. F. Jr. (2006). Fuel metabolism in starvation. *Ann. Rev. Nutr.* 26, 1–22. doi: 10.1146/annurev.nutr.26.061505.111258

Cahill, G. F. (1970). Starvation in man. *N. Engl. J. Med.* 282, 668–675. doi: 10.1056/NEJM197003192821209

Cahill, G. F., and Owen, O. E. (1968). Starvation and survival. *Trans. Am. Clin. Climatol. Assoc.* 79, 13–20.

Carrieri-Kohlman, V., Donesky-Cuenco, D., Park, S. K., Mackin, L., Nguyen, H. Q., and Paul, S. M. (2009). Additional evidence for the affective dimension of dyspnea in patients with COPD. *Res. Nurs. Health* 33, 4–19. doi: 10.1002/nur.20359

Carrieri-Kohlman, V., Gormley, J. M., Douglas, M. K., Paul, S. M., and Stulbarg, M. S. (1996). Exercise training decreases dyspnea and the distress and anxiety associated with it: monitoring alone may be as effective as coaching. *Chest J.* 110, 1526–1535. doi: 10.1378/chest.110.6.1526

Carrieri-Kohlman, V., Gormley, J. M., Eiser, S., Demir-Deviren, S., Nguyen, H., Paul, S. M., et al. (2001). Dyspnea and the affective response during exercise training in obstructive pulmonary disease. *Nurs. Res.* 50, 136–146. doi: 10.1097/00006199-200105000-00002

Clark, D. O. (1999). Identifying psychological, physiological, and environmental barriers and facilitators to exercise among older low income adults. *J. Clin. Geropsychol.* 5, 51–62. doi: 10.1023/A:1022942913555

Clarke, K., Tchabanenko, K., Pawlosky, R., Carter, E., Knight, N. S., Murray, A. J., et al. (2012a). Oral 28-day and developmental toxicity studies of (R)-3-hydroxybutyl (R)-3-hydroxybutyrate. *Regul. Toxicol. Pharmacol.* 63, 196–208. doi: 10.1016/j.yrtph.2012.04.001

Clarke, K., Tchabanenko, K., Pawlosky, R., Carter, E., Todd King, M., Musa-Veloso, K., et al. (2012b). Kinetics, safety and tolerability of (R)-3-hydroxybutyl (R)-3-hydroxybutyrate in healthy adult subjects. *Regul. Toxicol. Pharmacol.* 63, 401–408. doi: 10.1016/j.yrtph.2012.04.008

Cohen-Mansfield, J., Marx, M. S., and Guralnik, J. M. (2003). Motivators and barriers to exercise in an older community-dwelling population. *J. Aging Phys. Activ.* 11, 242–253. doi: 10.1123/japa.11.2.242

Cox, P. J., Kirk, T., Ashmore, T., Willerton, K., Evans, R., Smith, A., et al. (2016). Nutritional ketosis alters fuel preference and thereby endurance performance in athletes. *Cell Metab.* 24, 256–268. doi: 10.1016/j.cmet.2016.07.010

Craig, B. A. D. (2003). Interoception: the sense of the physiological condition of the body. *Curr. Opin. Neurobiol.* 13, 500–505. doi: 10.1016/S0959-4388(03)00090-4

Dearlove, D. J., Faull, O. K., Rolls, E., Stace, E., Clarke, K. and Cox, P. J. (in press). The human physiological response to ketoacidosis during exercise. *Front. Physiol. Exercise Physiol.*

Ekblom, B., and Golobarg, A. N. (1971). The influence of physical training and other factors on the subjective rating of perceived exertion. *Acta Physiol.* 83, 399–406. doi: 10.1111/j.1748-1716.1971.tb05093.x

Faraway, J. J. (2017). *Extending the Linear Model with R*. Boca Raton, FL: CRC Press.

Faull, O. K., Cox, P. J., and Pattinson, K. T. S. (2016). Psychophysical differences in ventilatory awareness and breathlessness between athletes and sedentary individuals. *Front. Physiol.* 7:231. doi: 10.3389/fphys.2016.00231

Forster, H. V., Dempsey, J. A., Thomson, J., Vidruk, E., and DoPico, G. A. (1972). Estimation of arterial PO2, PCO2, pH, and lactate from arterialized venous blood. *J. Appl. Physiol.* 32, 134–137. doi: 10.1152/jappl.1972.32.1.134

Hampson, D. B., Clair Gibson, A. S., Lambert, M. I., and Noakes, T. D. (2001). The influence of sensory cues on the perception of exertion during exercise and central regulation of exercise performance. *Sports Med.* 31, 935–952. doi: 10.2165/00007256-200131130-00004

Hardy, C. J., and Rejeski, W. J. (1989). Not what, but how one feels: the measurement of affect during exercise. *J. Sport Exerc. Psychol.* 11, 304–317. doi: 10.1123/jsep.11.3.304

Jaeger, B. C., Edwards, L. J., Das, K., and Sen, P. K. (2016). An R2 statistic for fixed effects in the generalized linear mixed model. *J. Appl. Stat.* 44, 1086–1105. doi: 10.1080/02664763.2016.1193725

Leupoldt von, A., and Dahme, B. (2005). Differentiation between the sensory and affective dimension of dyspnea during resistive load breathing in normal subjects. *Chest* 128, 3345–3349. doi: 10.1378/chest.128.5.3345

Mikkelsen, K. H., Seifert, T., Secher, N. H., Grøndal, T., and van Hall, G. (2015). Systemic, cerebral and skeletal muscle ketone body and energy metabolism during acute hyper-D-β-hydroxybutyratemia in post-absorptive healthy males. *J. Clin. Endocrinol. Metab.* 100, 636–643. doi: 10.1210/jc.2014-2608

Morgan, W. P., Hirta, K., Weitz, G. A., and Balke, B. (2011). Hypnotic perturbation of perceived exertion: ventilatory consequences. *Am. J. Clin. Hypnosis* 18, 182–190. doi: 10.1080/00029157.1976.10403796

Morgan, W. P., Raven, P. B., Drinkwater, B. L., and Horvath, S. M. (2008). Perceptual and metabolic responsivity to standard bicycle ergometry following various hypnotic suggestions. *Int. J. Clin. Exp. Hypnosis* 21, 86–101. doi: 10.1080/00207147308409309

Morrell, C. H., Pearson, J. D., and Brant, L. J. (1997). Linear transformations of linear mixed-effects models. *Am. Stat.* 51, 338–343. doi: 10.1080/00031305.1997.10474409

Noakes, T. D. (2004). Linear relationship between the perception of effort and the duration of constant load exercise that remains. *J. Appl. Physiol.* 96, 1571–1573. doi: 10.1152/japplphysiol.01124.2003

Owen, O. E., Morgan, A. P., Kemp, H. G., Sullivan, J. M., Herrera, M. G., and Cahill, G. F. (1967). Brain metabolism during fasting. *J. Clin. Invest.* 46, 1589–1595. doi: 10.1172/JCI105650

Paulus, M. P., and Stein, M. B. (2006). An insular view of anxiety. *Biol. Psychiatry* 60, 383–387. doi: 10.1016/j.biopsych.2006.03.042

Robinson, A. M., and Williamson, D. H. (1980). Physiological roles of ketone-bodies as substrates and signals in mammalian-tissues. *Physiol. Rev.* 60, 143–187. doi: 10.1152/physrev.1980.60.1.143

Shivva, V., Cox, P. J., Clarke, K., Veech, R. L., Tucker, I. G., and Duffull, S. B. (2016). The population pharmacokinetics of d-β-hydroxybutyrate following administration of (R)-3-hydroxybutyl (R)-3-hydroxybutyrate. *AAPS J.* 18, 678–688. doi: 10.1208/s12248-016-9879-0

Stubbs, B. J., Cox, P. J., Evans, R. D., Santer, P., Miller, J. J., Faull, O. K., et al. (2017). On the metabolism of exogenous ketones in humans. *Front. Physiol.* 8:848. doi: 10.3389/fphys.2017.00848

Tucker, R. (2009). The anticipatory regulation of performance: the physiological basis for pacing strategies and the development of a perception-based model for exercise performance. *Br. J. Sports Med.* 43, 392–400. doi: 10.1136/bjsm.2008.050799

Ulmer, H. V. (1996). Concept of an extracellular regulation of muscular metabolic rate during heavy exercise in humans by psychophysiological feedback. *Experientia* 52, 416–420. doi: 10.1007/BF01919309

Conflict of Interest Statement: The intellectual property and patents covering the uses of ketone bodies and esters are owned by BTG, Ltd., University of Oxford, the NIH and TdeltaS, Ltd. Should royalties ever accrue from these patents, KC and PC as named inventors may receive a share of royalties as determined by the terms of the respective institutions. KC is director of TdeltaS, a spin out company of the University of Oxford, to develop and commercialize products based on the ketone ester. OF was an employee of TdeltaS, Ltd. during the data collection and analysis for this manuscript, and DD is a current employee of TdeltaS, Ltd.

frontiers in Physiology

ORIGINAL RESEARCH
published: 23 July 2019
doi: 10.3389/fphys.2019.00887

Increasing Local Excitability of Brainstem Respiratory Nuclei Reveals a Distributed Network Underlying Respiratory Motor Pattern Formation

Rishi R. Dhingra[1], Werner I. Furuya[1], Tara G. Bautista[1], Thomas E. Dick[2], Roberto F. Galán[3] and Mathias Dutschmann[1]**

[1]Division of Systems Neurophysiology, The Florey Institute of Neuroscience and Mental Health, Parkville, VIC, Australia, [2]Division of Pulmonary, Critical Care and Sleep, Department of Medicine, Case Western Reserve University, Cleveland, OH, United States, [3]Department of Electrical Engineering and Computer Science, Case Western Reserve University, Cleveland, OH, United States

OPEN ACCESS

Edited by:
Vaughan G. Macefield,
Baker Heart and Diabetes Institute, Australia

Reviewed by:
Thiago S. Moreira,
University of São Paulo, Brazil
Simon McMullan,
Macquarie University, Australia

***Correspondence:**
Rishi R. Dhingra
rishi.dhingra@florey.edu.au
Mathias Dutschmann
mathias.dutschmann@florey.edu.au

Specialty section:
This article was submitted to Autonomic Neuroscience, a section of the journal Frontiers in Physiology

Received: 18 January 2019
Accepted: 26 June 2019
Published: 23 July 2019

Citation:
Dhingra RR, Furuya WI, Bautista TG, Dick TE, Galán RF and Dutschmann M (2019) Increasing Local Excitability of Brainstem Respiratory Nuclei Reveals a Distributed Network Underlying Respiratory Motor Pattern Formation. Front. Physiol. 10:887. doi: 10.3389/fphys.2019.00887

The core circuit of the respiratory central pattern generator (rCPG) is located in the ventrolateral medulla, especially in the pre-Bötzinger complex (pre-BötC) and the neighboring Bötzinger complex (BötC). To test the hypothesis that this core circuit is embedded within an anatomically distributed pattern-generating network, we investigated whether local disinhibition of the nucleus tractus solitarius (NTS), the Kölliker-Fuse nuclei (KFn), or the midbrain periaqueductal gray area (PAG) can similarly affect the respiratory pattern compared to disinhibition of the pre-BötC/BötC core. In arterially-perfused brainstem preparations of rats, we recorded the three-phase respiratory pattern (inspiration, post-inspiration and late-expiration) from phrenic and vagal nerves before and after bilateral microinjections of the GABA(A)R antagonist bicuculline (50 nl, 10 mM). Local disinhibition of either NTS, pre-BötC/BötC, or KFn, but not PAG, triggered qualitatively similar disruptions of the respiratory pattern resulting in a highly significant increase in the variability of the respiratory cycle length, including inspiratory and expiratory phase durations. To quantitatively analyze these motor pattern perturbations, we measured the strength of phase synchronization between phrenic and vagal motor outputs. This analysis showed that local disinhibition of all brainstem target nuclei, but not the midbrain PAG, significantly decreased the strength of phase synchronization. The convergent perturbations of the respiratory pattern suggest that the rCPG expands rostrally and dorsally from the designated core but does not include higher mid-brain structures. Our data also suggest that excitation-inhibition balance of respiratory network synaptic interactions critically determines the network dynamics that underlie vital respiratory rhythm and pattern formation.

Keywords: respiratory pattern formation, ataxic breathing, excitation-inhibition balance, respiratory microcircuit, synchronization, oscillator

INTRODUCTION

The concept of central pattern generator (CPG) networks that produce rhythmic physiologic motor activities emerged from studies concerned with invertebrate flight, swimming, feeding, and locomotion (Marder and Calabrese, 1996). The CPG concept is also applied for the generation of rhythmic vertebrate motor activities including locomotion (Grillner and Wallén, 1985; McCrea and Rybak, 2008; Kiehn, 2016), chewing (Yamada and Yamamura, 1996), swallowing (Jean, 2001), sniffing (Deschênes et al., 2012), and breathing (Richter, 1982; von Euler, 1983; Feldman, 1986). The concept of CPGs as a substrate of complex neural network dynamics was extended to the rhythmic neural activity of the cortex (Yuste et al., 2005). Thus, until today, the CPG concept is central to the understanding of neural circuits.

The respiratory CPG (rCPG) of vertebrates is the only motor network whose motor pattern is generated continuously throughout life to serve the vital function of oxygen uptake and carbon dioxide excretion. In contrast, all other motor CPG networks are episodic and require higher commands or sensory stimulation for their activation. The contemporary view on the structure and function of the rCPG implicates a respiratory rhythm generator called the pre-Bötzinger complex (pre-BötC; Smith et al., 1991; Feldman and Del Negro, 2006) that drives a pattern formation circuit located nearby within the Bötzinger complex (BötC). This anatomically localized core of the rCPG generates a sequential three-phase motor pattern of inspiration, post-inspiration and late-expiration (see Smith et al., 2009; Richter and Smith, 2014; Del Negro et al., 2018). Currently, several models for the generation of the three-phase respiratory motor rhythm and pattern are debated. A popular model depends on interconnected excitatory neurons with distinct bursting properties in the pre-BötC (see Rybak et al., 2014) that initiates inspiratory bursts. The rhythmogenic pre-BötC core also contains inspiratory GABAergic and glycinergic neurons that are thought to provide inhibition to expiratory neuron populations in the neighboring BötC and thereby inter-nuclear connectivity is thought to form an inhibitory ring of mutual inhibition between inspiratory, post-inspiratory and late-expiratory neurons (Richter, 1982; Rybak et al., 2004; Smith et al., 2007, 2009; Ausborn et al., 2018). This rhythm- and pattern-generating core is embedded into a larger anatomically functionally compartmentalized lateral respiratory column spanning from the caudal medulla to dorsal pons (Alheid et al., 2004; Rybak et al., 2004; Smith et al., 2007; Alheid and McCrimmon, 2008; Dutschmann and Dick, 2012). The respiratory areas outside of the core circuit, such as the pontine respiratory group (see Dutschmann and Dick, 2012) or the caudal ventral respiratory group of the medulla oblongata are thought to provide tonic modulatory inputs to the core or to relay the phasic respiratory activity to spinal (e.g., phrenic, intercostal, or abdominal motor neurons) or cranial (e.g., vagal-laryngeal, hypoglossal motor neurons) respiratory motor pools.

The recent discovery of an oscillator for post-inspiration, the so-called post-inspiratory complex (PiCo, Anderson et al., 2016), located rostro-medially to the pre-BötC/BötC respiratory core gave rise to an alternative model called the triple oscillator hypothesis (Ramirez and Baertsch, 2018). In this hypothesis, anatomically distinct independent oscillators for inspiration (pre-BötC), post-inspiration (PiCo), and late-expiration (RTN/pFRG) are mutually coupled via inhibitory and excitatory synaptic interactions to generate the three-phase motor pattern of respiration. While the triple oscillator hypothesis is an intriguing new concept for the generation of multi-patterned breathing activity, it requires further experimental and computational verification and validation. Thus, the common view of a layered CPG architecture (see McCrea and Rybak, 2008) that includes a separate rhythm generator (pre-BötC), which is connected to a downstream motor pattern formation network, currently prevails.

A recent publication from our laboratory tested the hypothesis of network degeneracy and redundancy by using *in situ* brainstem perfused brainstem preparations in which brainstem circuits were isolated by transection before re-perfusion at three distinct levels (caudal to the pre-BötC, just rostral to the pre-BötC or just rostral to the RTN/pFRG) (Jones and Dutschmann, 2016). The results confirmed the essential role of the pre-BötC for respiratory rhythm generation but failed to verify the anatomical location of the pattern formation circuit within the medulla alone. Specifically, preparations that maintained the anatomical integrity of all designated key nuclei for the generation of the respiratory rhythm and pattern, including the pre-BötC, BötC, RTN/pFRG, and PiCo, failed to produce a sequential three-phase motor pattern and instead produced a monophasic respiratory motor output that was synchronously expressed in functionally distinct respiratory motor nerves such as inspiratory phrenic, inspiratory/post-inspiratory vagal, and expiratory iliohypogastric nerves. We concluded that respiratory pattern formation requires essential ponto-medullary synaptic interactions to generate a physiologic three-phase respiratory motor pattern. Indeed, anatomically, the rCPG is classically defined as bilaterally organized neuronal columns stretching from the pontine Kölliker-Fuse nuclei through the caudal ventral respiratory group (Alheid et al., 2004; Rybak et al., 2004; Smith et al., 2007, 2009; Alheid and McCrimmon, 2008; Dutschmann and Dick, 2012). Therefore, ponto-medullary synaptic interactions within the rCPG are still considered to be the key mechanism underlying respiratory pattern formation.

As introduced above, the core circuit for respiratory rhythm and pattern generation is commonly anatomically localized to the pre-BötC and the neighboring Bötzinger complex BötC. In the present study, in addition to the pre-BötC/BötC core circuit, we investigated the role of the following nuclei in respiratory rhythm and pattern formation in the perfused brainstem preparation: (1) The nucleus of the solitary tract (NTS) is a major relay for peripheral respiratory sensory inputs (Kubin et al., 2006; Zoccal et al., 2014). In addition, our recent work indicates that the NTS might also be an integral part of the pattern formation network as a component of the dorsal respiratory group (DRG) (Bautista and Dutschmann, 2014b; Jones et al., 2016; Dhingra et al., 2017). (2) The pontine Kölliker-Fuse nuclei (KFn) is a critical area within the pontine respiratory group that controls the centrally mediated inspiratory off-switch (Cohen and Shaw, 2004; Ezure and Tanaka, 2006; Dutschmann and Dick, 2012) and gates post-inspiratory laryngeal adductor activity (Dutschmann and Herbert, 2006) and inspiratory hypoglossal nerve activity (Bautista and Dutschmann, 2014a) in the perfused brainstem preparation. (3) The periaqueductal gray is a midbrain

area that relays and integrates limbic and cortical respiratory commands into brainstem respiratory circuits (Faull et al., 2019). In the perfused brainstem preparation, it was shown that chemical stimulation of PAG compartments triggered pronounced respiratory modulation, whereas pharmacological lesion of the PAG had no effect on the generation of the stationary respiratory motor pattern in the perfused brainstem preparation (Farmer et al., 2014).

To test the hypothesis that the pre-BötC/BötC core circuit is embedded within an anatomically distributed pattern generating network, we locally increased neuronal excitability by locally disinhibiting these anatomically and functionally distinct respiratory nuclei of the brainstem and midbrain via microinjection of the GABA(A) receptor antagonist bicuculline. We used the perfused brainstem preparation (Paton, 1996) for our experiments because it generates a three-phase respiratory motor pattern in the absence of sensory feedback (the lungs are removed; there are no respiratory movements; and there is no effect of carotid sinus nerve transection; see Farmer et al., 2016) and thereby allows for the investigation of the respiratory network's CPG mechanisms. While local pharmacologic disinhibition will not reveal whether an area is active at baseline and likely activates nearby silent neurons, analysis of the effects of local disinhibition on the respiratory motor pattern offers a method to functionally assess the net connectivity of a given area with the whole of the respiratory network. Our data demonstrate that local disinhibition of any target nuclei, except the PAG, severely disrupts the respiratory motor pattern and significantly decreases the strength of synchronization between inspiratory and post-inspiratory motor outputs. Therefore, our data indicate that, contrary to contemporary models, the central generation of the breathing movements depends on synaptic interactions across a distributed neural circuit, rather than consisting of an anatomically localized core circuit.

MATERIALS AND METHODS

Experimental protocols were approved and conducted with strict adherence to the guidelines established by the Animal Ethics Committee of The Florey Institute of Neuroscience and Mental Health, Melbourne, Australia.

Perfused Brainstem Preparation

Experiments were performed in juvenile Sprague-Dawley rats of either sex (N = 37 rats, 17–30 days post-natal) using the arterially perfused *in situ* brainstem-spinal cord preparation as described previously (Paton, 1996; Dutschmann et al., 2000; Dhingra et al., 2017). Briefly, rats were anesthetized by inhalation of isoflurane (2%) until they reached a surgical plane of anesthesia. The rats were then transected below the diaphragm and transferred to an ice-cold bath of artificial cerebrospinal fluid (aCSF, in mM: 125 NaCl, 3 KCl, 1.25 KH_2PO_4, 2.5 $CaCl_2$, 1.25 $MgSO_4$, 25 $NaHCO_3$, 10 D-glucose) for pre-collicular decerebration. After decerebration, the lungs and heart were removed. Next, the descending aorta, phrenic, vagal, and hypoglossal nerves were dissected for subsequent cannulation or recording. Note that analysis of hypoglossal nerve activity was not included in the present study. However, an analysis of the effect of local disinhibition of brainstem target areas on the generation of the inspiratory motor pattern is presented in Dhingra et al. (2019). The preparation was then transferred into the recording chamber. The descending aorta was cannulated with a double-lumen catheter for perfusion and measurement of perfusion pressure. The preparation was perfused with aCSF containing sucrose (4.5×10^{-3} g/ml) for oncotic pressure, warmed to 31°C using a peristaltic pump, recirculating water bath and heat exchanger (ELMI, TW-2.02). The perfusion circuit also contained two bubble traps and a nylon filter (Millipore, 100 μm pore size) to prevent embolism. The perfusate was continually bubbled with carbogen (95% O_2/5% CO_2) to maintain constant chemosensory drive. Phrenic and vagal nerves were mounted in suction electrodes to measure respiratory motor output. Nerve potentials were amplified (10,000×, Warner Instruments, DP-311), filtered (0.01–10 kHz), digitized (AD Instruments, PowerLab 16/35), and stored on a computer using LabChart software (AD Instruments).

Experimental Protocol

After the initial stabilization of the eupneic three-phase respiratory rhythm, we first recorded 10 min of the baseline respiratory motor pattern. In the present work, we targeted the NTS (N = 9 preparations), pre-BötC/BötC (N = 11 preparations), KFn (N = 10 preparations), and PAG (N = 7 preparations) as potential components of the respiratory pattern formation circuit. To functionally identify the target site coordinates, using a triple barreled pipette, we first mapped the target site with glutamate microinjections (50 nl, 10 mM). Glutamate microinjections within the BötC, NTS, and KFn evoked a bradypnea, whereas glutamate microinjections within the pre-BötC and PAG evoked a tachypnea. Once appropriate functionally identified injection site coordinates were identified, we microinjected bicuculline (50 nl, 10 mM), a GABA(A) receptor antagonist, to locally disinhibit and consequently locally increase the excitability of the target site. Next, we microinjected pontamine sky blue (50 nl, 2% w/v in aCSF) for *post hoc* histologic verification of injection site locations. This procedure was then repeated on the contralateral side. Note that after functional and histologic confirmation of injection site coordinates in an initial cohort, in subsequent experiments, we locally microinjected bicuculline and pontamine sky blue according to the established site coordinates without functional identification of target sites. After local disinhibition of the target site, we recorded 10 min of the respiratory motor pattern for measurement of respiratory phase durations, respiratory rhythm variability, and phase synchronization properties.

At the conclusion of the experiment, brainstems were removed, post-fixed in paraformaldehyde (4% w/v in PBS), cryo-protected in sucrose (20% w/v in PBS), cryo-sectioned (50 μm thickness), and counter-stained with neutral red to verify microinjection sites (**Figure 1**).

Data Analysis

Respiratory phase durations and respiratory rhythm variability were assessed from PNA. PNA was first high-pass filtered to remove DC fluctuations with a zero-phase FIR filter (300 Hz), and then integrated (100 ms time constant) and normalized to have zero mean and unit variance. Breaths were detected using a threshold-crossing algorithm to determine the onset and offset times of PNA. Events were manually inspected to ensure that

no false-positive breaths were included in subsequent analyses. From these event times, we measured the mean respiratory period (T_{TOT}), inspiratory (T_I) and expiratory (T_E) phase durations, and their coefficient of variation (CV). To qualitatively compare the respiratory rhythm variability evoked by local disinhibition of the target areas, we generated Poincaré plots of $T_{TOT}(n)$ versus $T_{TOT}(n+1)$ using the entire T_{TOT} time series. Points in such Poincaré plots provide information about the relationship between one respiratory period and its successor (Fishman et al., 2012).

Motif Occurrence

To qualitatively assess the similarities and differences between local disinhibition of the different target sites, we scored the occurrence of eight representative motor pattern motifs during 3-min epochs recorded after bicuculline microinjection. To compare the relative frequencies of motif occurrence across experiments, we normalized the raw counts to the total number of motifs in each epoch, thereby yielding the probability of motif occurrence.

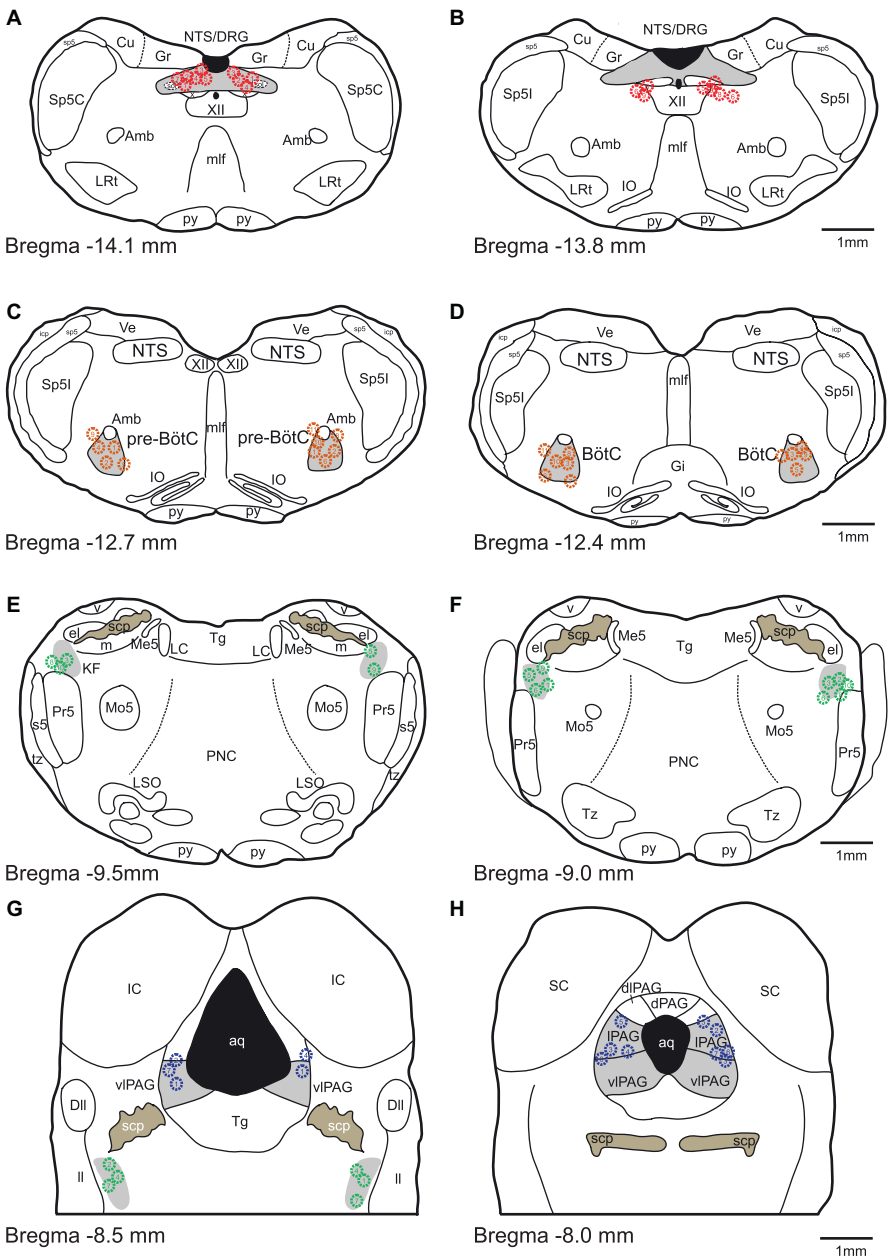

FIGURE 1 | Histologic verification of injection sites. **(A-H)** Schematic drawings indicate the locations of bicuculline microinjections are presented from caudal to rostral. All microinjections were histologically identified within the designated target areas. Red, orange, green and blue symbols indicate NTS, pre-BötC/BötC, KFn and PAG injection sites, respectively.

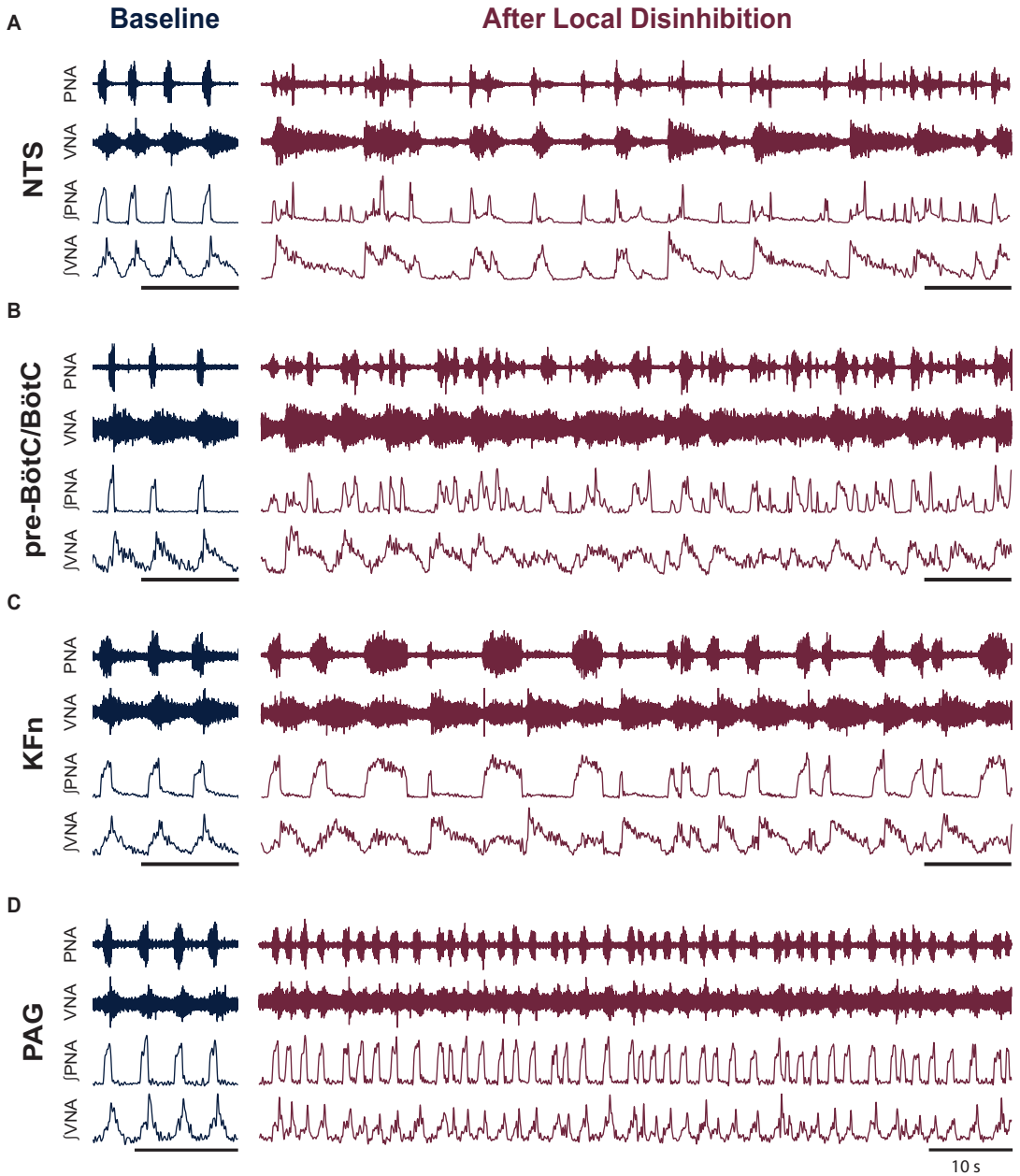

FIGURE 2 | Local disinhibition of anatomically distributed brainstem-, but not midbrain-, respiratory areas disrupts the eupneic three-phase respiratory motor pattern. To test the hypothesis that the pre-BötC/BötC core circuit is embedded within an anatomically distributed respiratory motor pattern generating network, we locally disinhibited the nucleus of the solitary tract (NTS), the pre-Bötzinger complex/Bötzinger complex area (pre-BötC/BötC), the Kölliker-Fuse nuclei (KFn) or the periaqueductal gray (PAG)—brainstem and midbrain areas known to be involved in the generation or modulation of the respiratory rhythm and pattern—by microinjecting the GABA(A)R antagonist bicuculline (50 nl, 10 mM). **(A–D)** Representative traces are shown at baseline and after local disinhibition of the NTS **(A)**, pre-BötC/BötC **(B)**, KFn **(C)**, or PAG **(D)**. The eupneic three-phase motor pattern observed at baseline was disrupted by local disinhibition of any brainstem target site **(A–C)**. In contrast, local disinhibition of the PAG evoked a modulation of the respiratory motor pattern that spared the eupneic three-phase motor pattern **(D)**. The PAG disinhibition-evoked modulation of the respiratory pattern consisted of stationary eupneic breathing intermingled with tachypneic events that were reminiscent of physiologic modulations of the respiratory pattern like sniffing. PNA: phrenic nerve activity; VNA: vagal nerve activity. *Scale bars: 10 s.*

Phase Synchronization Analysis

Because local disinhibition often disrupted the three-phase respiratory rhythm (see **Figure 2**), we developed a quantitative description of the respiratory pattern. We reasoned that the eupneic three-phase respiratory motor pattern could be quantified by the strength of synchronization between the coupled oscillatory respiratory motor outputs (e.g., PNA and VNA).

Because the activity of the phrenic and vagal nerves span the majority of the respiratory cycle, and because their signal-to-noise ratios permit the estimation of their instantaneous

phases via the Hilbert transform method (Kralemann et al., 2008; Zhu et al., 2013), we chose to use the phase synchronization between PNA and VNA to define the respiratory motor pattern at baseline and after local disinhibition of a target site.

In essence, this approach allows us to model the respiratory motor activities under consideration as a system of coupled oscillators. We first confirmed that their activity was periodic by computing their power spectral densities using the Welch method. Next, we band-pass filtered the integrated signals around the respiratory frequency. Instantaneous protophases were then extracted by applying the Hilbert transform. Instantaneous phases were then determined by applying the transformation defined in Kralemann et al. (2008).

To quantify the strength of the phase synchronization interaction between PNA and VNA and to determine the significance of the phase synchronization interaction, we computed the mutual information of the instantaneous phases (Zhu et al., 2013; Dhingra et al., 2017). Mutual information, a measure of the statistical dependence between two variables, was computed from the joint-probability histogram according to the following equation:

$$I(\varphi_{PNA};\varphi_{VNA}) = -\int_0^{2\pi}\int_0^{2\pi} P(\varphi_{PNA},\varphi_{VNA}) \cdot \ln\frac{P(\varphi_{PNA},\varphi_{VNA})}{P(\varphi_{PNA})P(\varphi_{VNA})} d\varphi_{PNA} d\varphi_{VNA}$$

where $P(\varphi_{PNA}, \varphi_{VNA})$ is the joint probability distribution of the instantaneous phases, and $P(\varphi_{PNA})$ and $P(\varphi_{VNA})$ are the marginal probability distributions of either variable. For all measurements of mutual information of the instantaneous phases, we used a fixed bin width of 0.03 rad to discretize the probability distributions. Because we use the natural logarithm in computing mutual information, reported mutual information values are presented in the corresponding unit of nats. Values of mutual information near zero indicate that the variables are independent and have no coupling, whereas high values of mutual information are associated with high dependence between the instantaneous phase variables, and thereby associated with a high synchronization strength between the pair of motor outputs.

To assess whether a given trial had a statistically significant interaction between the input and the output, we bootstrapped the distribution to represent the null hypothesis that the two instantaneous phases were independent by randomly shuffling the inter-event intervals and re-computing the instantaneous phases and their mutual information. The bootstrapping procedure was iterated 100 times to estimate the distribution that represented the null hypothesis. If a forcing trial had mutual information greater than the 99% confidence interval of the bootstrap distribution, it was considered significant.

All analyses were performed using custom routines implemented in MATLAB. Statistical analyses were performed in R. All measurements are reported as the mean ± standard deviation. Unless stated otherwise, statistical comparisons were made by applying a one-way or two-way ANOVA. The Tukey HSD *post hoc* test was used to identify specific differences.

RESULTS

To investigate the distributed organization of the brainstem network regulating the respiratory motor pattern, we locally disinhibited the nucleus of the solitary tract (NTS), pre-Bötzinger complex/Bötzinger complex area (pre-BötC/BötC), the Kölliker-Fuse nuclei (KFn), or the periaqueductal gray (PAG). Representative traces before and after local disinhibition are shown in **Figure 2**. At baseline, all preparations generated a sequential eupneic three-phase respiratory motor pattern that consisted of inspiration, post-inspiration, and late-expiration (**Figures 2A–D**, left panels). Eupneic phrenic nerve activity (PNA) began abruptly at the onset of inspiration and increased in amplitude in a ramp-like fashion until the onset of post-inspiration. The eupneic pattern of vagal nerve activity (VNA) began at the onset of inspiration and increased logarithmically until the onset of post-inspiration. The onset of post-inspiration was denoted by a peak in vagal nerve discharge that decayed exponentially until the onset of late-expiration, at which point, VNA ceased until the beginning of the next inspiratory phase.

Local disinhibition of the NTS, pre-BötC/BötC or KFn, but not the PAG, disrupted the sequential eupneic three-phase respiratory motor pattern (**Figures 2A–D**, *right panels*). Local disinhibition of the NTS enhanced VNA bursting but disrupted the coordination of PNA with VNA. Local disinhibition of the pre-BötC/BötC enhanced the frequency of PNA and VNA but also disrupted their eupneic coordination. Local disinhibition of the KFn enhanced VNA bursting, modulated the duration of inspiration, but did not change the frequency of the respiratory rhythm. Interestingly, despite the enhancement of VNA, local disinhibition of the KFn resulted in a pattern of PNA that alternated between short- and long-bursts. In contrast, local disinhibition of the PAG perturbed the respiratory motor pattern but remained eupneic. PAG-disinhibited respiratory motor patterns also contained brief tachypneic perturbations that maintained a three-phase respiratory motor pattern. Compared qualitatively to the motor pattern disruptions evoked by local disinhibition of ponto-medullary target sites (compare **Figure 2D** with **Figures 2A–C**), local disinhibition of the PAG appeared to evoke physiologic modulations of the respiratory motor pattern, akin to sniffing, rather than evoking the ataxic respiratory patterns observed after local disinhibition of brainstem respiratory areas.

Initially, to assess the effect of local disinhibition of a target site on the respiratory rhythm, we measured the respiratory phase durations and their variability using PNA as an index of the respiratory rhythm. Note that local disinhibition of brainstem-, but not midbrain-, respiratory areas disrupted the respiratory pattern to an extent such that the definition of the three-phase rhythm no longer applied. As such, the following analysis should be interpreted to reflect properties of the respiratory rhythm as expressed in PNA.

Group data of the effect of local disinhibition on respiratory phase durations are presented in **Figure 3A**. Local disinhibition of the NTS significantly reduced the respiratory period (T_{TOT}, from 5.5 ± 2.3 to 1.8 ± 0.6 s, $p < 0.001$, $N = 9$), and the duration of expiration (T_E, from 4.7 ± 2.3 to 1.4 ± 0.5 s,

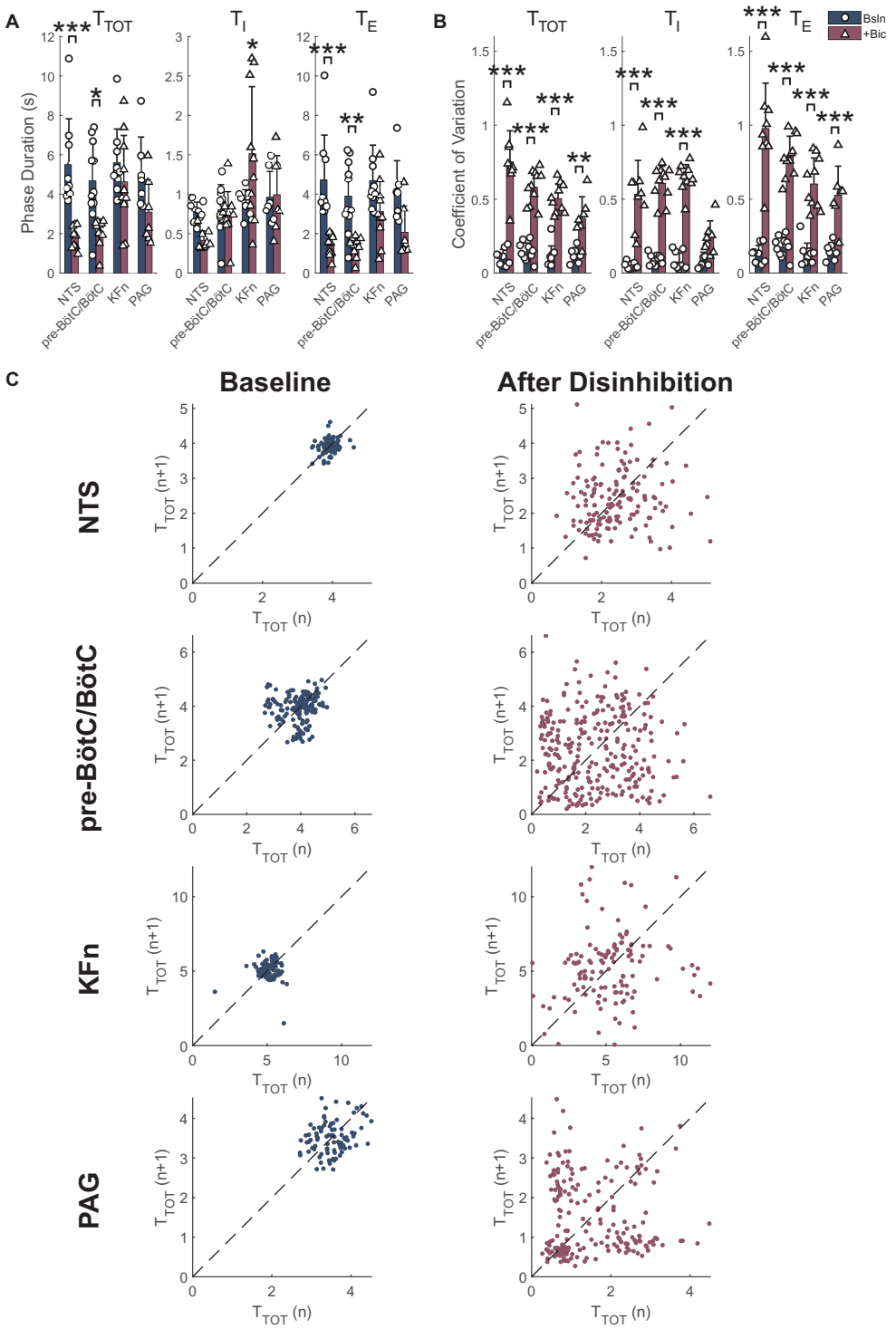

FIGURE 3 | Local disinhibition of brainstem respiratory areas increases stochastic respiratory rhythm variability, whereas local disinhibition of the midbrain PAG increases deterministic respiratory rhythm variability. **(A)** The mean respiratory period (T_{TOT}), inspiratory (T_I), and expiratory (T_E) durations were measured from PNA at baseline (*navy-colored bars*) and after local disinhibition (*wine-colored bars*) of the NTS, pre-BötC/BötC, KFn or PAG. Note that due to the disruption of the three-phase motor pattern evoked by disinhibition of brainstem respiratory target areas, these data should be interpreted to reflect the properties of the respiratory rhythm as expressed in PNA. Local disinhibition of the NTS significantly reduced the respiratory period due to a reduction in expiratory duration. Similarly, local disinhibition of the pre-BötC/BötC significantly decreased the respiratory period, and expiratory phase duration. Finally, local disinhibition of the KFn significantly increased the duration of inspiration but did not change the respiratory period. **(B)** Local disinhibition of any target site evoked a significant increase in the coefficient of variation

(*Continued*)

FIGURE 3 | (CV) of the respiratory period and expiratory phase durations. The CV of T_I was significantly increased after local disinhibition of the NTS, pre-BötC/BötC and KFn, and tended to increase after local disinhibition of the PAG. **(C)** Representative Poincaré plots of the instantaneous respiratory period (T_{TOT}) are shown at baseline (*left*) and after local disinhibition (*right*) of the NTS, pre-BötC/BötC, KFn or PAG. At baseline, all preparations had limited variability that appeared stochastic since the point clouds were clustered around the line of identity (*dashed lines*). After local disinhibition of the NTS, pre-BötC/BötC or KFn, the variability of the respiratory rhythm (width of the point cloud) increased, but still appeared stochastic. In contrast, after local disinhibition of the PAG, the tachypneic events that occurred regularly (see **Figure 2D**) were reflected by additional point clouds offset from the line of identity. This observation suggests that increasing the excitability of the PAG introduced a deterministic source of respiratory rhythm variability. $^*p < 0.05$; $^{**}p < 0.01$; $^{***}p < 0.001$.

$p < 0.001$, $N = 9$), but not the duration of inspiration (T_I). Local disinhibition of the pre-BötC/BötC significantly reduced T_{TOT} (from 4.7 ± 2.0 to 2.1 ± 0.7 s, $p < 0.05$, $N = 11$), and T_E (from 3.9 ± 1.8 to 1.3 ± 0.5 s, $p < 0.01$, $N = 11$), but not T_I. Local disinhibition of the KFn did not change T_{TOT} or T_E, but significantly increased T_I (from 0.9 ± 0.2 to 1.5 ± 0.9 s, $p < 0.05$, $N = 10$). Finally, local disinhibition of the PAG tended to decrease T_{TOT} (from 5.0 ± 1.9 to 3.1 ± 1.7 s, $N = 7$) via a reduction in T_E, but neither change was significant for the group. Together, these data show that local disinhibition of the NTS, pre-BötC/BötC, or KFn had a greater influence on the respiratory rhythm compared to local disinhibition of the PAG.

Group data of the effect of local disinhibition on the variability of the PNA rhythm are shown in **Figure 3B**. Local disinhibition of the NTS significantly increased the coefficient of variation of T_{TOT} [CV(T_{TOT}) (from 0.11 ± 0.05 to 0.75 ± 0.21, $p < 0.001$, $N = 9$), CV(T_I) (from 0.05 ± 0.02 to 0.53 ± 0.23, $p < 0.001$, $N = 9$), and CV(T_E) (from 0.13 ± 0.06 to 0.98 ± 0.31, $p < 0.001$, $N = 9$)]. Similarly, local disinhibition of the pre-BötC/BötC significantly increased CV(T_{TOT}) (from 0.14 ± 0.06 to 0.58 ± 0.11, $p < 0.001$, $N = 11$), CV(T_I) (from 0.09 ± 0.03 to 0.61 ± 0.12, $p < 0.001$, $N = 11$) and CV(T_E) (from 0.17 ± 0.07 to 0.79 ± 0.14, $p < 0.001$, $N = 11$). Local disinhibition of the KFn significantly increased CV(T_{TOT}) (from 0.11 ± 0.07 to 0.50 ± 0.10, $p < 0.001$, $N = 10$), CV(T_I) (from 0.08 ± 0.06 to 0.64 ± 0.09, $p < 0.001$, $N = 10$) and CV(T_E) (from 0.13 ± 0.08 to 0.60 ± 0.18, $p < 0.001$, $N = 10$). Finally, local disinhibition of the PAG significantly increased CV(T_{TOT}) (from 0.12 ± 0.05 to 0.37 ± 0.15, $p < 0.01$, $N = 7$) and CV(T_E) (from 0.15 ± 0.06 to 0.53 ± 0.20, $p < 0.001$, $N = 7$), but not CV(T_I). Together, these data suggest that local disinhibition of any target site increases the variability of the respiratory rhythm and expiratory intervals. However, whereas local disinhibition of brainstem respiratory areas increased the variability of inspiration, local disinhibition of the PAG did not modulate the variability of inspiration.

Representative Poincaré plots of the instantaneous respiratory period (T_{TOT}) highlight the qualitative difference in the respiratory rhythm variability evoked by local disinhibition of brainstem respiratory areas versus the PAG (**Figure 3C**). At baseline, all preparations had a consistent respiratory rhythm with limited stochastic variability which was centered around the line-of-identity. In some cases, like the baseline condition before pre-BötC/BötC and PAG disinhibition, the variability of the respiratory rhythm in the perfused preparation can show some deterministic structure that may indicate the presence of consistent breath-to-breath sequences of respiratory cycle durations in the underlying time series. After local disinhibition of the NTS, pre-BötC/BötC, or KFn, all preparations showed a marked increase in the variability of T_{TOT} that was reflected by an increase in the size of the point cloud. The variability of the respiratory rhythm evoked by local disinhibition of any of these brainstem respiratory areas appeared random. In contrast, local disinhibition of the PAG was associated with a modulation of the respiratory pattern such that brief (two to four cycles) tachypneic events were intermingled with stationary breathing. In the Poincaré plot after local disinhibition of the PAG, this structured variability was reflected by the presence of clouds of points offset from the line of identity. This qualitative analysis suggests that local disinhibition of brainstem-respiratory areas increased the stochastic variability of the respiratory rhythm, whereas local disinhibition of the PAG introduced a deterministic source of variability into the respiratory rhythm.

To further analyze the motor patterns expressed after local disinhibition of respiratory areas, we scored the occurrence of eight representative motor pattern motifs during a 3-min epoch after local disinhibition (**Figure 4**). Representative traces for each of these motor pattern motifs are shown in **Figure 4**. To compare motif occurrence after local disinhibition of the NTS, pre-BötC/BötC, KFn, or PAG, we normalized the motif counts in each epoch to the total number of events to determine the probability of motif occurrence within each epoch.

The eupnea motif (**Figure 4A**) is defined by inspiratory activity on PNA, and by a bi-phasic VNA discharge that begins during inspiration, peaks at the onset of post-inspiration, and decays exponentially until the onset of the late-expiratory phase. The eupnea motif was almost never observed after local disinhibition of brainstem target sites but was preserved after PAG disinhibition. For the group, the probability of eupnea motif occurrence after PAG disinhibition was significantly greater compared to local disinhibition of the NTS, pre-BötC/BötC, or KFn ($p < 0.05$).

The staccato PNA motif (**Figure 4B**) was defined by repeated, short bursts of PNA associated with inspiratory-like discharges on VNA. The probability of staccato PNA motif occurrence was equally likely after NTS-, pre-BötC/BötC-, or KFn-disinhibition. After local disinhibition of the PAG, this motif never occurred and was significantly less likely to occur compared to local disinhibition of brainstem areas ($p < 0.05$).

The sub-threshold PNA motif was defined by the sub-threshold tonic discharge on PNA (compare black- versus wine-colored arrowheads in **Figure 4C**). Note that in the representative example shown, the tonic sub-threshold PNA was also associated with additional full amplitude PNA bursts during the period of tonic discharge. Sub-threshold PNA motifs were observed after NTS-, pre-BötC/BötC-, or

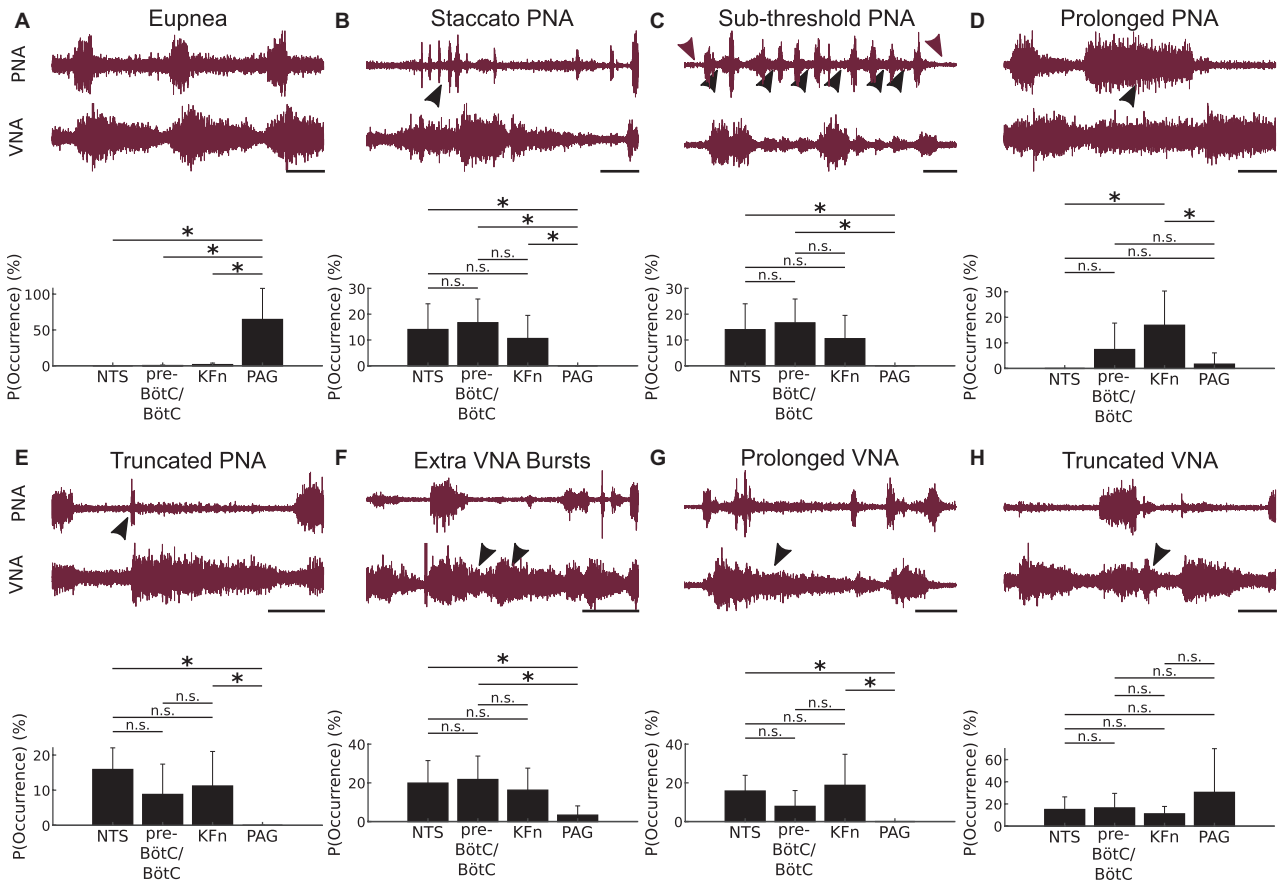

FIGURE 4 | Local disinhibition of brainstem-, but not midbrain-, respiratory areas evokes ataxic respiratory motor patterns composed of a similar set of motifs. To qualitatively analyze the ataxic respiratory motor patterns expressed after local disinhibition of the NTS, pre-BötC/BötC, KFn or PAG, we scored the occurrence of eight representative respiratory motor pattern motifs during 3-min epochs recorded after bicuculline microinjection. The representative traces shown in this figure depict the definitions of the motor pattern motifs scored after local disinhibition of each target compartment. Below each set of raw traces, we plot the probability (or relative frequency) of observing a given respiratory motor pattern motif after local disinhibition of each target respiratory area. **(A)** *Eupnea*: The eupneic motif is defined by inspiratory activity on PNA, and by a bi-phasic VNA discharge that begins during inspiration, peaks at the onset of post-inspiration, and decays abruptly at the onset of the late-expiratory phase. As noted in **Figure 2**, the eupneic respiratory motor pattern motif was disrupted after local disinhibition of brainstem respiratory areas, but was spared after local disinhibition of the midbrain PAG. Further, the probability of observing eupneic fictive breaths was significantly greater after local disinhibition of the PAG compared to local disinhibition of either of the three brainstem respiratory areas. **(B)** *Staccato PNA*: This motif was defined by repeated, short bursts of PNA (*arrowhead*) associated with inspiratory-like discharges on VNA. There was no significant difference between the probability of occurrence of staccato PNA motifs after local disinhibition of brainstem respiratory areas. However, this motif was observed significantly less frequently after local disinhibition of the PAG. **(C)** *Sub-threshold PNA*: This motif was defined by the sub-threshold tonic discharge on PNA (*sub-threshold activity indicated by black- versus DC-level of noise indicated by wine-colored arrowheads, respectively*). This motif occurred significantly less frequently after PAG-disinhibition compared to disinhibition of brainstem respiratory areas. **(D)** *Prolonged PNA*: This motif was defined by apneustic bursts (*arrowhead*) reminiscent of those evoked by KFn lesions. This apneustic motif occurred significantly more frequently after KFn-disinhibition compared to after NTS-, or PAG-disinhibition. There was no significant difference in the probability of prolonged PNA motif occurrence after NTS-, pre-BötC/BötC- or PAG-disinhibition. **(E)** *Truncated PNA*: In this motif, we observed a short burst of PNA (*arrowhead*) that was quickly terminated by an exaggerated post-inspiratory discharge of VNA. This motif occurred significantly less frequently after PAG-disinhibition compared to after disinhibition of the NTS or KFn. Further, there was no significant difference in the probability of observing truncated PNA motifs after NTS-, pre-BötC/BötC- or KFn-disinhibition. **(F)** *Extra VNA Bursts*: This motif was characterized by the presence of one or more additional bursts or peaks of VNA discharge (*arrowheads*) after the initial VNA burst at the onset of post-inspiration. This motif occurred significantly less frequently after PAG-disinhibition compared to after NTS- or pre-BötC/BötC-disinhibition. There was no significant difference in the probability of observing extra VNA burst motifs after local disinhibition of brainstem respiratory areas. **(G)** *Prolonged VNA*: This motif was characterized by an exaggerated and sustained VNA (*arrowhead*) that continued through multiple cycles of PNA. This motif occurred significantly more frequently after NTS- or KFn-disinhibition compared to after PAG-disinhibition. There was no significant difference in the probability of observing this motif after local disinhibition of brainstem respiratory areas. **(H)** *Truncated VNA*: This motif was characterized by a rapidly decaying post-inspiratory discharge of VNA (*arrowhead*) that was very short compared to baseline post-inspiratory VNA. There was no significant difference in the probability of occurrence of this motif after local disinhibition of any respiratory area. *Scale bars: 2 s; n.s.: not significant; *p < 0.05.*

KFn-disinhibition but not after PAG-disinhibition. The probability of sub-threshold PNA motif occurrence was equally likely after local disinhibition of brainstem areas. The probability of sub-threshold PNA motif occurrence was significantly less after local disinhibition of the PAG compared to after local disinhibition of the NTS or pre-BötC/BötC ($p < 0.05$).

The prolonged PNA motif (**Figure 4D**) was defined by apneustic bursts reminiscent of those evoked by KFn

lesions. Less severe apneustic PNA bursts were also observed after pre-BötC/BötC- or PAG-disinhibitions. For the group, the probability of prolonged PNA motif occurrence was equally likely after NTS-, pre-BötC/BötC-, or PAG-disinhibition. After local disinhibition of the KFn, the probability of prolonged PNA motif occurrence was significantly greater compared to after NTS- or PAG-disinhibition ($p < 0.05$).

In the truncated PNA motif (**Figure 4E**), we observed a burst of PNA that is quickly terminated by an exaggerated post-inspiratory discharge of VNA. This motif was observed after local disinhibition of the NTS, pre-BötC/BötC, or KFn, but not the PAG. The probability of truncated PNA motif occurrence was equally likely after NTS-, pre-BötC/BötC-, or KFn-disinhibition. The probability of this motif occurring was significantly less after local disinhibition of the PAG compared to local disinhibition of the NTS or KFn ($p < 0.05$).

The extra VNA bursts motif (**Figure 4F**) was characterized by the presence of one or more additional bursts or peaks of VNA discharge after the initial VNA burst at the onset of post-inspiration. This motif was observed after local disinhibition of any respiratory area. The probability of extra VNA burst occurrence was equally likely after local disinhibition of the NTS, pre-BötC/BötC, or KFn. After local disinhibition of the PAG, the probability of this motif occurring was significantly less compared to after local disinhibition of the NTS or pre-BötC/BötC ($p < 0.05$).

The prolonged VNA motif (**Figure 4G**) was characterized by an exaggerated and sustained VNA that continued through multiple cycles of PNA. This motif was observed after local disinhibition of the NTS, pre-BötC/BötC, or KFn but never after PAG disinhibition. The probability of prolonged VNA motif occurrence was equally likely after NTS-, pre-BötC/BötC-, or KFn-disinhibition. The probability of this motif occurring was significantly greater after NTS- or KFn-disinhibition compared to after PAG-disinhibition ($p < 0.05$).

Finally, the truncated VNA motif (**Figure 4H**) was characterized by a rapidly decaying post-inspiratory discharge of VNA that was very short compared to baseline post-inspiratory VNA. For the group, the probability of truncated VNA motif occurrence was equally likely after local disinhibition of any site.

In general, the distributions of motif occurrence probabilities after local disinhibition of the NTS, pre-BötC/BötC and KFn clustered together, whereas the set of motifs occurring after local disinhibition of the PAG was in most cases significantly different from brainstem respiratory areas. Taken together, this analysis suggests that local disinhibition of the NTS, pre-BötC/BötC or KFn areas evokes a convergent set of respiratory motor pattern motifs, especially when compared to the breathing patterns evoked by local disinhibition of the PAG.

Because the previous qualitative analyses were prone to variability due to their subjective nature (e.g., manual scoring of phase durations and motif occurrence), we next sought to apply a more quantitative method to compare the effect of disinhibition of the NTS, pre-BötC/BötC, KFn, or PAG on the respiratory motor pattern. We assumed that the deviations from the eupneic three-phase respiratory rhythm could be quantified via changes in the strength of synchronization between respiratory motor outputs. Because PNA and VNA remained periodic after local disinhibition of any target site, and because the instantaneous phases of PNA and VNA could be determined in an un-biased fashion using the Hilbert transform method, we measured the phase synchronization between PNA and VNA to quantitatively analyze the disruption of the respiratory motor pattern after local disinhibition of target sites.

Representative joint probability distributions of the instantaneous phases of PNA and VNA are shown before and after local disinhibition in **Figure 5**. In these plots, diagonal banding patterns appear when the instantaneous phases of PNA and VNA maintain a constant relative phase difference consistently for many cycles. Thus, the presence of such banding patterns indicates a potential phase synchronization interaction between PNA and VNA. As expected, at baseline (**Figure 5**, left panels), PNA and VNA were tightly synchronized. After local disinhibition of any target site (**Figure 5**, right panels), the non-eupneic respiratory motor pattern motifs were reflected as trajectories that deviated from the synchronized path around the torus. Nonetheless, for many respiratory cycles, PNA and VNA remained partially synchronized.

The mutual information of the instantaneous phases of PNA and VNA quantifies the strength of phase synchronization between these two respiratory motor outputs. Group data regarding the mutual information statistic are shown before and after local disinhibition in **Figure 6A**. For the group, local disinhibition of the NTS significantly reduced the mutual information of PNA and VNA (from 2.19 ± 0.28 to 0.88 ± 0.13 nats, $p < 0.001$, $N = 9$). Similarly, local disinhibition of the pre-BötC/BötC significantly reduced the mutual information of PNA and VNA (from 1.58 ± 0.35 to 0.71 ± 0.24 nats, $p < 0.001$, $N = 11$). Local disinhibition of the KFn also significantly reduced the mutual information of PNA and VNA (from 2.04 ± 0.29 to 1.07 ± 0.24 nats, $p < 0.001$, $N = 10$). Finally, local disinhibition of the PAG tended to increase the mutual information of PNA and VNA (from 1.69 ± 0.32 to 1.86 ± 0.39 nats, $N = 7$), but this change was not significant. Importantly, the mutual information of PNA and VNA after local disinhibition of the PAG was significantly greater than that evoked by local disinhibition of the NTS, pre-BötC/BötC, and KFn ($p < 0.001$).

To assess whether the presence of phase synchronization between PNA and VNA in each epoch was not simply due to chance, for each analyzed epoch, we generated a surrogate dataset by shuffling whole cycles of the instantaneous phases of PNA and VNA to determine the 99% confidence interval for the mutual information statistic. The original values of the mutual information of PNA and VNA (stars) and the upper-bound of the 99% confidence interval of the surrogate dataset (solid bars) are shown in **Figure 6B**. As expected, at baseline, all preparations showed a significant phase synchronization interaction between PNA and VNA, i.e., the original mutual information of the instantaneous phases was greater than the upper-bound of the 99% confidence interval of the surrogate

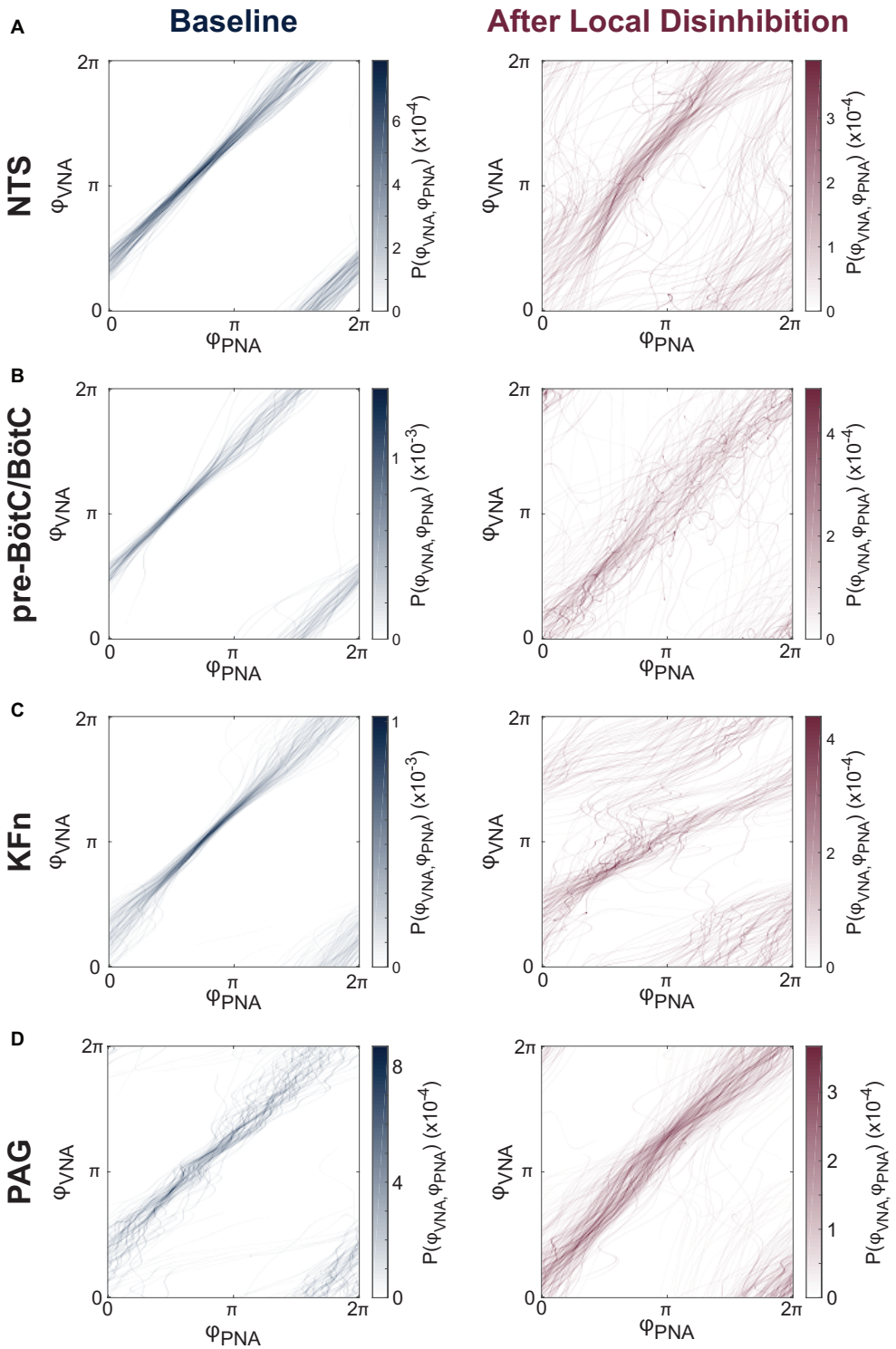

FIGURE 5 | Local disinhibition of brainstem-, but not midbrain-, respiratory circuit compartments reduces the strength of PNA-VNA synchrony. **(A–D)** We assumed that the eupneic three-phase respiratory rhythm could be quantified via the synchrony between respiratory motor outputs. Because PNA and VNA remained periodic after local disinhibition of any target site, and because the instantaneous phases of PNA and VNA could be determined in an un-biased fashion by applying the Hilbert transform, we characterized the phase synchronization between PNA and VNA to quantitatively analyze the disruption of the respiratory motor pattern after local disinhibition of target sites. Representative joint probability distributions of the instantaneous phase of PNA (φ_{PNA}) and VNA (φ_{VNA}) are shown at baseline (*left*) and after local disinhibition (*right*) of the NTS **(A)**, pre-BötC/BötC **(B)**, KFn **(C)** or PAG **(D)**. The joint probability histograms are representative examples

(*Continued*)

FIGURE 5 | from single experiments that reflect all respiratory cycles in a given epoch. Banding patterns in these histograms reflect the presence of a phase synchronization interaction between PNA and VNA. As expected, at baseline, all preparations showed strong phase synchronization between PNA and VNA. After local disinhibition of any brainstem target site **(A–C)**, many trajectories around this toroidal phase space deviated from the strongly synchronized trajectory observed at baseline. However, an interaction (banding pattern) remained between the instantaneous phases of PNA and VNA, suggesting that some component of the physiologic inspiration-to-post-inspiration transition remained after local disinhibition of any target compartment. In contrast, after local disinhibition of the PAG, the trajectories around the toroidal phase space remained clustered suggesting that local disinhibition of the PAG spared the eupneic phase synchronization interaction between PNA and VNA **(D)**.

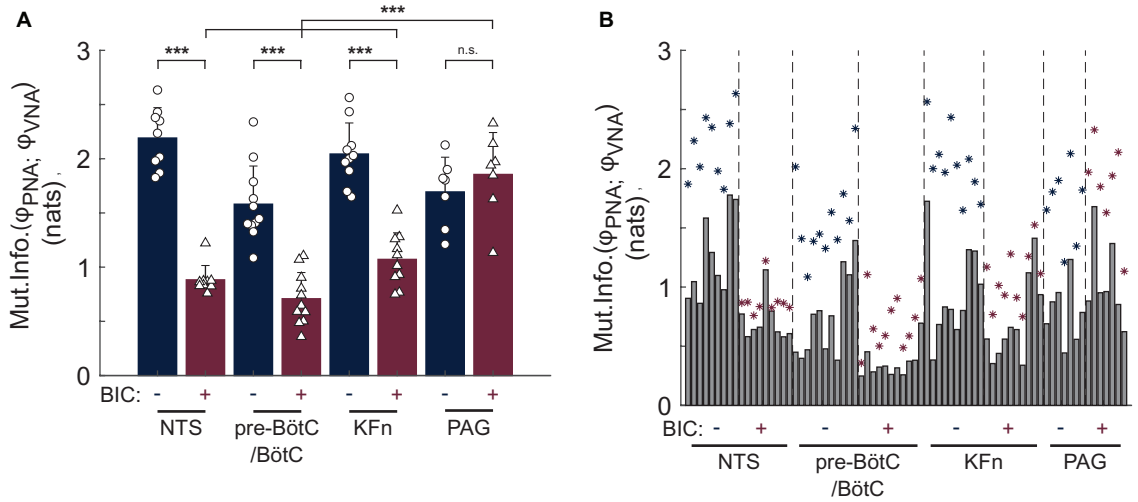

FIGURE 6 | Group data reveal a quantitative difference in the effect of local disinhibition of brainstem-versus midbrain-respiratory areas on the strength of PNA-VNA synchrony. The mutual information of the instantaneous phases of PNA and VNA quantifies the strength of the phase synchronization between these two respiratory motor outputs. **(A)** After local disinhibition of any brainstem-, but not midbrain-, target site, the strength of the phase synchronization between PNA and VNA was significantly reduced. Further, the mutual information of the instantaneous phases of PNA and VNA after local disinhibition of the PAG was significantly greater than that after local disinhibition of the NTS, pre-BötC/BötC or KFn. **(B)** To assess the statistical significance of the phase synchronization interaction, we compared the mutual information of the original dataset with that of a surrogate distribution which was generated by shuffling whole cycles of the instantaneous phases. This plot shows the observed mutual information (*navy- or wine-colored stars*) and the upper-bound of the 99% confidence interval of the surrogate distributions (*gray bars*). Both before and after local disinhibition of target sites, the original mutual information of the instantaneous phases was greater than that of the respective surrogate distribution indicating the presence of a significant phase synchronization interaction between PNA and VNA. Taken together, the measurement of phase synchronization before and after local disinhibition of brainstem target sites suggests that a significant, but weaker, phase synchronization interaction persisted after local disinhibition of the NTS, pre-BötC/BötC or KFn. In contrast, the synchronization of PNA and VNA was preserved after local disinhibition of the PAG. ****p < 0.001; n.s.: not significant.*

dataset. Interestingly, after local disinhibition of the NTS, pre-BötC/BötC, KFn, the phase synchronization between PNA and VNA remained significant despite the change in the mutual information of the instantaneous phases. Taken together, these data demonstrate that a significant, but weaker, phase synchronization interaction persists after local disinhibition of the NTS, pre-BötC/BötC, or KFn.

DISCUSSION

The present study shows that local disinhibition of the NTS, pre-BötC/BötC, or KFn—respiratory nuclei which are distributed along the rostro-caudal and dorso-ventral axes of the ponto-medullary brainstem—evokes convergent disruptions of the respiratory motor pattern. In contrast, disinhibition of the midbrain PAG, which is known to potently modulate respiration, does not perturb the eupneic respiratory motor pattern. Our data support the conclusion that the circuit underlying respiratory pattern formation is anatomically distributed across the ponto-medullary brainstem, rather than being localized solely within a core circuit in the ventrolateral medulla.

Local Disinhibition of Anatomically Distinct Nuclei in the Ponto-Medullary Brainstem, but Not Midbrain, Evokes Convergent Disruptions of the Respiratory Motor Pattern

The present study qualitatively and quantitatively demonstrates convergence between the highly disturbed respiratory motor patterns evoked by locally increasing excitability within either the NTS, the pre-BötC/BötC, or the KFn areas, especially when compared to the effect of local disinhibition of the midbrain PAG.

Locally increasing excitability of a respiratory area via pharmacologic disinhibition enables the functional measurement (via respiratory motor outputs) of the net connectivity of the target area with the remainder of the respiratory network. We postulate that if there are few connections from the target

to the network, we would expect that the respiratory motor pattern would be minimally impacted by the disinhibition. If there is dense connectivity from the target area to the network, we would expect the respiratory pattern to be strongly modulated by the disinhibition. In addition, the effect of a local disinhibition may also depend on the pattern of connections from a target to the rest of the network. If projections from the target to the network influence many types of respiratory neurons (inspiratory, post-inspiratory, late-expiratory, phase spanning, etc.), we would expect the disinhibition to disrupt the respiratory pattern because these pathways would not be coherently activated by the disinhibition, i.e., we would introduce a strong source of stochastic variability in the network. Alternatively, if the projections from the target to the network are themselves coherent, e.g., neurons in the target area project to one or a few cooperative respiratory neuron types, we would expect that local disinhibition of the target would modulate the respiratory pattern since these synergistic projections would be coherently activated despite the noisy pharmacologic activation of the target.

In our results, all tested areas had a strong influence on the respiratory motor pattern, as predicted by previous work (Wasserman et al., 2002; Dutschmann and Herbert, 2006; Smith et al., 2007; Zhang et al., 2009; Bautista and Dutschmann, 2014b; Dhingra et al., 2017). However, the data also suggested a difference between local disinhibition of brainstem- versus midbrain-respiratory areas. Local disinhibition of brainstem respiratory areas (NTS, pre-BötC/BötC, or KFn) evoked ataxic respiratory motor patterns that could be described as respiratory motor pattern disruptions, whereas local disinhibition of the midbrain PAG evoked coherent modulations of the respiratory motor pattern that spared the eupneic three-phase respiratory motor pattern. We speculate that the latter was likely due to the presence of coherently organized projections from the PAG to select expiratory components of the respiratory network.

While previous studies have also used local disinhibition as a perturbation of physiologic respiratory network dynamics *in vivo* (Wasserman et al., 2002; Zhang et al., 2009; Bongianni et al., 2010; Janczewski et al., 2013), the most relevant study in the context of the present results is that of Marchenko et al. who microinjected a cocktail of GABAergic and glycinergic antagonists into the pre-BötC or BötC in the perfused preparation of rats (Marchenko et al., 2016). Consistent with the results of the present study, these authors observed a disruption of the respiratory pattern after local disinhibition of either the pre-BötC or BötC. Our results extend their findings by characterizing the specific disruptions of the respiratory motor pattern and by comparing the local disinhibition of the pre-BötC/BötC core circuit with the local disinhibition of other brainstem- and midbrain-respiratory nuclei.

Local microinjection of bicuculline into brainstem target areas triggered the emergence of generally similar sets of ataxic respiratory motor pattern motifs, especially when compared to local disinhibition of the PAG. While subtle differences in the expression of respiratory motor pattern motifs were observed, in most cases, we showed that probability of respiratory motor pattern motif occurrence was equivalent after local disinhibition of brainstem respiratory areas, whereas the respiratory pattern evoked by local disinhibition of the PAG consisted largely of eupneic breaths.

We further analyzed the effect of local disinhibition of respiratory areas with an unbiased quantitative approach based on measuring the phase synchronization between the motor outputs of the respiratory network. This analysis revealed that the strength of the synchronization between phrenic and vagal motor activities was significantly reduced after all three perturbations of brainstem respiratory areas, whereas local disinhibition of the PAG spared the phase synchronization interaction between phrenic and vagal motor pools. Importantly, local disinhibition and the resultant increased excitability of any brainstem target respiratory area resulted in a similar decrease in the synchronization strength between phrenic and vagal motor activities. If one specific brainstem area would have shown a significantly different reduction in the coupling strength compared to the other brainstem areas, it would have been considered to play a more significant role in respiratory pattern formation. However, since such a difference between the magnitudes of the reduction in phase synchronization strength after disinhibition of brainstem target sites was not observed, our data imply that the functional rCPG network is distributed across ventral and dorsal brainstem areas.

In contrast, we have shown that local disinhibition of the midbrain PAG evoked a qualitatively different modulation of the respiratory rhythm, but not pattern, compared to the local disinhibition of brainstem target nuclei. Neuronal cell columns within the PAG have long been known to project to various ponto-medullary respiratory nuclei to modulate respiration and are thought to relay and integrate limbic and cortical respiratory commands into respiratory brainstem circuits (Faull et al., 2019). Thus far, it has been shown that the respiratory effects of PAG stimulation depend on the activities of the parabrachial nuclei (located dorso-medially to the KFn) and the NTS (Huang et al., 2000; Hayward et al., 2004). While these projections overlap with the brainstem target nuclei considered in the present study, it is also clear that local disinhibition of the PAG did not evoke the ataxic respiratory motor pattern motifs observed after NTS-, pre-BötC/BötC-, or KFn-disinhibition. This observation suggests that the descending connectivity of the PAG may not be sufficient to enable the PAG to have direct control of respiratory pattern formation (Farmer et al., 2014).

Excitation-Inhibition Balance Is a Mechanism Underlying Respiratory Pattern Formation

An important observation of the present study is that locally increasing excitability within a node of the distributed rCPG network was sufficient to disrupt respiratory pattern formation suggesting that the balance between excitation and inhibition (E-I balance) may serve as a mechanism that underlies the physiologic generation of the eupneic three-phase respiratory motor pattern. In cortical circuits, both during spontaneous and sensory-evoked activities, excitation is accompanied by a lagging inhibition (Borg-Graham et al., 1996; Wehr and Zador, 2003; Mariño et al., 2005; Haider et al., 2006). E-I balance is thought to keep cortical circuits in a state of criticality that may enhance information transfer (Shew and Plenz, 2013).

In general, inhibitory neurons have been shown to be intermingled with excitatory neurons in in the NTS, pre-BötC/BötC area, and KFn (Guthmann et al., 1998; Fong et al., 2005; Winter et al., 2009). In the present study, we observed that locally increasing the excitability of only one anatomically-distinct brainstem target area was sufficient to completely disrupt the eupneic three-phase respiratory motor pattern. Thus, the present results are in accordance with a role for E-I balance in determining the respiratory pattern.

Considering the bicuculline microinjections in the context of E-I balance also helps to understand the paradoxical appearance of apneustic respiratory motor pattern motifs, especially after local disinhibition of the KFn. Importantly, all three target areas within the ponto-medullary brainstem were previously shown to be key elements for the mediation of the inspiratory off-switch because local pharmacological inhibition (lesion) of either the NTS, BötC, or KFn reportedly triggers apneusis (prolonged PNA motif, see **Figure 4D**; Cohen and Shaw, 2004; Dutschmann and Herbert, 2006; Burke et al., 2010; Bautista and Dutschmann, 2014a; Dhingra et al., 2017). Apneusis is a pathological prolongation of inspiration, and typically reflects a delay in the inspiratory off-switch mechanisms. While the evidence that pharmacologic inhibition of the KFn triggers apneusis supports a hypothesis that increasing the excitability of the KFn should inhibit inspiration and enhance post-inspiratory motor outputs, in the present study, we observed that increasing the excitability of the KFn paradoxically also triggers apneusis. It is important to note, however, that the apneusis triggered by disinhibition of the KFn was qualitatively different from the previously reported apneusis triggered by KFn inhibition (Dutschmann and Herbert, 2006; Dhingra et al., 2017). Previous studies have shown that KFn- (or NTS- or BötC-) inhibition evokes a stationary apneustic respiratory motor pattern in which every respiratory cycle contains a prolonged inspiratory effort without the expression of post-inspiratory VNA. In contrast, in the present study, we observed a highly variable apneustic respiratory motor pattern after disinhibition of the KFn. More specifically, as can be observed in the raw traces shown in **Figure 2**, local disinhibition of the KFn did not cause every respiratory cycle to be apneustic. Instead, we observed both severely apneustic respiratory cycles associated with a prolonged inspiratory effort and no post-inspiratory VNA, and truncated PNA motifs wherein inspiratory motor output in PNA was quickly terminated by a prolonged VNA motif. A similarly variable pattern of PNA was previously reported after local disinhibition of the BötC with bicuculline in anesthetized rabbits (Bongianni et al., 2010). Therefore, the results of the present study suggest that a mixture of excitatory and inhibitory inputs (from either local or long-range projections) to the KFn determines the timing of the inspiratory off-switch and highlight E-I balance as a mechanism underlying eupneic respiratory pattern formation. Consequently, the perturbation of E-I balance in any given brainstem node of the pattern generating circuit was sufficient to perturb the global respiratory network dynamics underlying the formation of the respiratory pattern.

Pathological changes in E-I balance are also known to underlie pathologic breathing patterns in Rett syndrome. Initially, excitability-related synaptic dysfunction was identified functionally in the NTS, KFn, locus coeruleus, and ventrolateral medulla (Stettner et al., 2007; Medrihan et al., 2008; Taneja et al., 2009; Kline et al., 2010; Abdala et al., 2016). However, from these studies alone, it was difficult to determine the causal source of pathologic breathing patterns in Rett syndrome. The findings of the present study show that disruption of E-I balance within any of these brainstem areas could potentially underlie Rett syndrome pathology. Consistent with this interpretation, later Fos-expression studies in MeCP2-deficient mice demonstrated that forebrain circuits are subject to widespread hypo-excitability, whereas brainstem networks are hyperexcitable (Kron et al., 2012). While E-I imbalance in the brainstem respiratory network will trigger neurogenic breathing disorders, the findings of the present study also suggest that a specific pathologic motor pattern may not necessarily be predictive of the anatomic location of the E-I imbalance. Thus, the findings of the present study extend a growing body of literature supporting the hypothesis that eupneic respiratory pattern formation depends on E-I balance within brainstem respiratory circuits.

Technical Considerations

Bicuculline is classified as a competitive GABA(A) receptor antagonist. However, the aim of the present study was not to investigate the role of GABAergic inhibition within localized brainstem or midbrain nuclei. Instead, we used bicuculline microinjections as a pharmacologic tool to locally increase neuronal excitability. Thus, bicuculline-related side-effects, including the blockade of calcium-activated potassium conductances or GABA reuptake (Olsen et al., 1976; Heyer et al., 1981; Johnson and Seutin, 1997; Johansson et al., 2001), do not interfere with our conclusions. First, blocking GABA reuptake should have a marginal effect on neuronal excitability when local GABA(A) receptors are also blocked. Second, the apamin-like activity of bicuculline that blocks calcium-dependent potassium conductances should also increase neuronal excitability. Thus, potential off-target effects of bicuculline should further enhance local hyperexcitability.

CONCLUSIONS AND FUTURE DIRECTIONS

While effects of the network perturbation following bicuculline-evoked increases in excitability on the generation of the respiratory pattern (Bautista and Dutschmann, 2014b; Abdala et al., 2016) or reflex mediation (Dutschmann and Herbert, 1998) were previously reported, this is the first publication that qualitatively and quantitatively compared such effects of a local disinhibition. The role of the KFn as a key area for the control of respiration has been appreciated for many years (see Marckwald, 1887). The interaction between the KFn and pre-BötC/BötC core circuit is also considered in many

computational and conceptual models (Rybak et al., 2004; Smith et al., 2007, 2009; Mörschel and Dutschmann, 2009; Dutschmann and Dick, 2012; Ausborn et al., 2018). Consequently, the anatomical location of the rCPG is commonly depicted as continuous bilateral respiratory columns that stretch from the ventral caudal medulla to the dorsolateral pons (see Alheid et al., 2004; Alheid and McCrimmon, 2008). However, the role of the NTS and adjacent dorsal brain structures of the medulla oblongata, as a dorsal respiratory group and integral part of the rCPG, was just recently re-discovered in experiments using the perfused brainstem preparation (Bautista and Dutschmann, 2014b; Jones et al., 2016) and further supported by the findings of the present study.

Overall, the data of the present study strongly suggest that the rCPG cannot be associated with a compact and continuous cell column that only extends rostrocaudally and instead needs to also be functionally and anatomically extended to dorsal brainstem area(s). Therefore, future investigations exploring the dynamical mechanisms underlying respiratory control should look broadly across respiratory neuronal populations to unravel the fundamental neurophysiologic principles controlling the breath. Our observations also highlight the need to implement modern experimental tools, like population imaging and multi-electrode array recording, in preparations that maintain the functional and anatomic integrity of the rCPG to optimally capture brainstem-wide respiratory circuit dynamics.

ETHICS STATEMENT

Experimental protocols were approved by and conducted with strict adherence to the guidelines established by the Animal Ethics Committee of The Florey Institute of Neuroscience and Mental Health, Melbourne, Australia.

AUTHOR CONTRIBUTIONS

MD and RD designed and conceived the study. RD, WF, and TB conducted the experiments. RD, WF, and MD analyzed the data. RD, WF, TD, RG, and MD interpreted the data and wrote the manuscript.

FUNDING

This study was supported by an ARC Future Fellowship to MD and an ARC Discovery grant (DP170104861).

REFERENCES

Abdala, A. P., Toward, M. A., Dutschmann, M., Bissonnette, J. M., and Paton, J. F. R. (2016). Deficiency of GABAergic synaptic inhibition in the Kölliker–fuse area underlies respiratory dysrhythmia in a mouse model of Rett syndrome. *J. Physiol.* 594, 223–237. doi: 10.1113/JP270966

Alheid, G. F., and McCrimmon, D. R. (2008). The chemical neuroanatomy of breathing. *Respir. Physiol. Neurobiol.* 164, 3–11. doi: 10.1016/j.resp.2008.07.014

Alheid, G. F., Milsom, W. K., and McCrimmon, D. R. (2004). Pontine influences on breathing: an overview. *Respir. Physiol. Neurobiol.* 143, 105–114. doi: 10.1016/j.resp.2004.06.016

Anderson, T. M., Garcia, A. J., Baertsch, N. A., Pollak, J., Bloom, J. C., Wei, A. D., et al. (2016). A novel excitatory network for the control of breathing. *Nature* 536, 76–80. doi: 10.1038/nature18944

Ausborn, J., Koizumi, H., Barnett, W. H., John, T. T., Zhang, R., Molkov, Y. I., et al. (2018). Organization of the core respiratory network: insights from optogenetic and modeling studies. *PLoS Comput. Biol.* 14:e1006148. doi: 10.1371/journal.pcbi.1006148

Bautista, T. G., and Dutschmann, M. (2014a). Inhibition of the pontine Kölliker-fuse nucleus abolishes eupneic inspiratory hypoglossal motor discharge in rat. *Neuroscience* 267, 22–29. doi: 10.1016/j.neuroscience.2014.02.027

Bautista, T. G., and Dutschmann, M. (2014b). Ponto-medullary nuclei involved in the generation of sequential pharyngeal swallowing and concomitant protective laryngeal adduction in situ. *J. Physiol.* 592, 2605–2623. doi: 10.1113/jphysiol.2014.272468

Bongianni, F., Mutolo, D., Cinelli, E., and Pantaleo, T. (2010). Respiratory responses induced by blockades of GABA and glycine receptors within the Bötzinger complex and the pre-Bötzinger complex of the rabbit. *Brain Res.* 1344, 134–147. doi: 10.1016/j.brainres.2010.05.032

Borg-Graham, L., Monier, C., and Frégnac, Y. (1996). Voltage-clamp measurement of visually-evoked conductances with whole-cell patch recordings in primary visual cortex. *J. Physiol.* 90, 185–188. doi: 10.1016/S0928-4257(97)81421-0

Burke, P. G. R., Abbott, S. B. G., McMullan, S., Goodchild, A. K., and Pilowsky, P. M. (2010). Somatostatin selectively ablates post-inspiratory activity after injection into the Bötzinger complex. *Neuroscience* 167, 528–539. doi: 10.1016/j.neuroscience.2010.01.065

Cohen, M. I., and Shaw, C.-F. (2004). Role in the inspiratory off-switch of vagal inputs to rostral pontine inspiratory-modulated neurons. *Respir. Physiol. Neurobiol.* 143, 127–140. doi: 10.1016/j.resp.2004.07.017

Del Negro, C. A., Funk, G. D., and Feldman, J. L. (2018). Breathing matters. *Nat. Rev. Neurosci.* 19:351. doi: 10.1038/s41583-018-0003-6

Deschênes, M., Moore, J., and Kleinfeld, D. (2012). Sniffing and whisking in rodents. *Curr. Opin. Neurobiol.* 22, 243–250. doi: 10.1016/j.conb.2011.11.013

Dhingra, R. R., Dutschmann, M., Galán, R. F., and Dick, T. E. (2017). Kölliker-fuse nuclei regulate respiratory rhythm variability *via* a gain-control mechanism. *Am. J. Physiol. Regul. Integr. Comp. Physiol.* 312, R172–R188. doi: 10.1152/ajpregu.00238.2016

Dhingra, R. R., Furuya, W. I., Galán, R. F., and Dutschmann, M. (2019). Excitation-inhibition balance regulates the patterning of spinal and cranial inspiratory motor outputs in rats in situ. *Respir. Physiol. Neurobiol.* 266, 95–102. doi: 10.1016/j.resp.2019.05.001

Dutschmann, M., and Dick, T. E. (2012). Pontine mechanisms of respiratory control. *Compr. Physiol.* 2, 2443–2469. doi: 10.1002/cphy.c100015

Dutschmann, M., and Herbert, H. (1998). NMDA and GABAA receptors in the rat Kölliker-fuse area control cardiorespiratory responses evoked by trigeminal ethmoidal nerve stimulation. *J. Physiol.* 510, 793–804. doi: 10.1111/j.1469-7793.1998.793bj.x

Dutschmann, M., and Herbert, H. (2006). The Kölliker-fuse nucleus gates the postinspiratory phase of the respiratory cycle to control inspiratory off-switch and upper airway resistance in rat. *Eur. J. Neurosci.* 24, 1071–1084. doi: 10.1111/j.1460-9568.2006.04981.x

Dutschmann, M., Wilson, R. J. A., and Paton, J. F. R. (2000). Respiratory activity in neonatal rats. *Auton. Neurosci.* 84, 19–29. doi: 10.1016/S1566-0702(00)00177-6

Ezure, K., and Tanaka, I. (2006). Distribution and medullary projection of respiratory neurons in the dorsolateral pons of the rat. *Neuroscience* 141, 1011–1023. doi: 10.1016/j.neuroscience.2006.04.020

Farmer, D. G. S., Bautista, T. G., Jones, S. E., Stanic, D., and Dutschmann, M. (2014). The midbrain periaqueductal grey has no role in the generation of the respiratory motor pattern, but provides command function for the modulation of respiratory activity. *Respir. Physiol. Neurobiol.* 204, 14–20. doi: 10.1016/j.resp.2014.07.011

Farmer, D. G. S., Dutschmann, M., Paton, J. F. R., Pickering, A. E., and McAllen, R. M. (2016). Brainstem sources of cardiac vagal tone and respiratory sinus arrhythmia. *J. Physiol.* 594, 7249–7265. doi: 10.1113/JP273164

Faull, O. K., Subramanian, H. H., Ezra, M., and Pattinson, K. T. S. (2019). The midbrain periaqueductal gray as an integrative and interoceptive neural structure for breathing. *Neurosci. Biobehav. Rev.* 98, 135–144. doi: 10.1016/j.neubiorev.2018.12.020

Feldman, J. L. (1986). Neurophysiology of breathing in mammals. handbook of physiology. The nervous system. Intrinsic regulatory system in the brain. *Am. Physiol. Soc. Sect.* 1, 463–524. doi: 10.1002/cphy.cp010409

Feldman, J. L., and Del Negro, C. A. (2006). Looking for inspiration: new perspectives on respiratory rhythm. *Nat. Rev. Neurosci.* 7, 232–241. doi: 10.1038/nrn1871

Fishman, M., Jacono, F. J., Park, S., Jamasebi, R., Thungtong, A., Loparo, K. A., et al. (2012). A method for analyzing temporal patterns of variability of a time series from Poincaré plots. *J. Appl. Physiol.* 113, 297–306. doi: 10.1152/japplphysiol.01377.2010

Fong, A. Y., Stornetta, R. L., Foley, C. M., and Potts, J. T. (2005). Immunohistochemical localization of GAD67-expressing neurons and processes in the rat brainstem: subregional distribution in the nucleus tractus solitarius. *J. Comp. Neurol.* 493, 274–290. doi: 10.1002/cne.20758

Grillner, S., and Wallén, P. (1985). Central pattern generators for locomotion, with special reference to vertebrates. *Annu. Rev. Neurosci.* 8, 233–261. doi: 10.1146/annurev.ne.08.030185.001313

Guthmann, A., Fritschy, J.-M., Ottersen, O. P., Torp, R., and Herbert, H. (1998). GABA, GABA transporters, GABAAreceptor subunits, and GAD mRNAs in the rat parabrachial and Kölliker-fuse nuclei. *J. Comp. Neurol.* 400, 229–243. doi: 10.1002/(SICI)1096-9861(19981019)400:2<229::AID-CNE5>3.0.CO;2-B

Haider, B., Duque, A., Hasenstaub, A. R., and McCormick, D. A. (2006). Neocortical network activity *in vivo* is generated through a dynamic balance of excitation and inhibition. *J. Neurosci.* 26, 4535–4545. doi: 10.1523/JNEUROSCI.5297-05.2006

Hayward, L. F., Castellanos, M., and Davenport, P. W. (2004). Parabrachial neurons mediate dorsal periaqueductal gray evoked respiratory responses in the rat. *J. Appl. Physiol.* 96, 1146–1154. doi: 10.1152/japplphysiol.00903.2003

Heyer, E. J., Nowak, L. M., and Macdonald, R. L. (1981). Bicuculline: a convulsant with synaptic and nonsynaptic actions. *Neurology* 31, 1381–1390. doi: 10.1212/WNL.31.11.1381

Huang, Z.-G., Subramanian, S. H., Balnave, R. J., Turman, A. B., and Moi Chow, C. (2000). Roles of periaqueductal gray and nucleus tractus solitarius in cardiorespiratory function in the rat brainstem. *Respir. Physiol.* 120, 185–195. doi: 10.1016/S0034-5687(00)00107-9

Janczewski, W. A., Tashima, A., Hsu, P., Cui, Y., and Feldman, J. L. (2013). Role of inhibition in respiratory pattern generation. *J. Neurosci.* 33, 5454–5465. doi: 10.1523/JNEUROSCI.1595-12.2013

Jean, A. (2001). Brain stem control of swallowing: neuronal network and cellular mechanisms. *Physiol. Rev.* 81, 929–969. doi: 10.1152/physrev.2001.81.2.929

Johansson, S., Druzin, M., Haage, D., and Wang, M.-D. (2001). The functional role of a bicuculline-sensitive Ca2+–activated K+ current in rat medial preoptic neurons. *J. Physiol.* 532, 625–635. doi: 10.1111/j.1469-7793.2001.0625e.x

Johnson, S. W., and Seutin, V. (1997). Bicuculline methiodide potentiates NMDA-dependent burst firing in rat dopamine neurons by blocking apamin-sensitive Ca2+–activated K+ currents. *Neurosci. Lett.* 231, 13–16. doi: 10.1016/S0304-3940(97)00508-9

Jones, S. E., and Dutschmann, M. (2016). Testing the hypothesis of neurodegeneracy in respiratory network function with *a priori* transected arterially perfused brain stem preparation of rat. *J. Neurophysiol.* 115, 2593–2607. doi: 10.1152/jn.01073.2015

Jones, S. E., Stanić, D., and Dutschmann, M. (2016). Dorsal and ventral aspects of the most caudal medullary reticular formation have differential roles in modulation and formation of the respiratory motor pattern in rat. *Brain Struct. Funct.* 221, 4353–4368. doi: 10.1007/s00429-015-1165-x

Kiehn, O. (2016). Decoding the organization of spinal circuits that control locomotion. *Nat. Rev. Neurosci.* 17, 224–238. doi: 10.1038/nrn.2016.9

Kline, D. D., Ogier, M., Kunze, D. L., and Katz, D. M. (2010). Exogenous brain-derived neurotrophic factor rescues synaptic dysfunction in Mecp2-null mice. *J. Neurosci.* 30, 5303–5310. doi: 10.1523/JNEUROSCI.5503-09.2010

Kralemann, B., Cimponeriu, L., Rosenblum, M., Pikovsky, A., and Mrowka, R. (2008). Phase dynamics of coupled oscillators reconstructed from data. *Phys. Rev. E* 77:066205. doi: 10.1103/PhysRevE.77.066205

Kron, M., Howell, C. J., Adams, I. T., Ransbottom, M., Christian, D., Ogier, M., et al. (2012). Brain activity mapping in Mecp2 mutant mice reveals functional deficits in forebrain circuits, including key nodes in the default mode network, that are reversed with ketamine treatment. *J. Neurosci.* 32, 13860–13872. doi: 10.1523/JNEUROSCI.2159-12.2012

Kubin, L., Alheid, G. F., Zuperku, E. J., and McCrimmon, D. R. (2006). Central pathways of pulmonary and lower airway vagal afferents. *J. Appl. Physiol.* 101, 618–627. doi: 10.1152/japplphysiol.00252.2006

Marchenko, V., Koizumi, H., Mosher, B., Koshiya, N., Tariq, M. F., Bezdudnaya, T. G., et al. (2016). Perturbations of respiratory rhythm and pattern by disrupting synaptic inhibition within pre-Bötzinger and Bötzinger complexes. *eNeuro* 3:ENEURO.0011-16.2016. doi: 10.1523/ENEURO.0011-16.2016

Marckwald, M. (1887). Die Athembewegungen und deren Innervation beim Kaninchen. *Z. Biol.* 23, 149–283.

Marder, E., and Calabrese, R. L. (1996). Principles of rhythmic motor pattern generation. *Physiol. Rev.* 76, 687–717. doi: 10.1152/physrev.1996.76.3.687

Mariño, J., Schummers, J., Lyon, D. C., Schwabe, L., Beck, O., Wiesing, P., et al. (2005). Invariant computations in local cortical networks with balanced excitation and inhibition. *Nat. Neurosci.* 8, 194–201. doi: 10.1038/nn1391

McCrea, D. A., and Rybak, I. A. (2008). Organization of mammalian locomotor rhythm and pattern generation. *Brain Res. Rev.* 57, 134–146. doi: 10.1016/j.brainresrev.2007.08.006

Medrihan, L., Tantalaki, E., Aramuni, G., Sargsyan, V., Dudanova, I., Missler, M., et al. (2008). Early defects of GABAergic synapses in the brain stem of a MeCP2 mouse model of Rett syndrome. *J. Neurophysiol.* 99, 112–121. doi: 10.1152/jn.00826.2007

Mörschel, M., and Dutschmann, M. (2009). Pontine respiratory activity involved in inspiratory/expiratory phase transition. *Philos. Trans. R. Soc. B Biol. Sci.* 364, 2517–2526. doi: 10.1098/rstb.2009.0074

Olsen, R. W., Ban, M., and Miller, T. (1976). Studies on the neuropharmacological activity of bicuculline and related compounds. *Brain Res.* 102, 283–299. doi: 10.1016/0006-8993(76)90883-0

Paton, J. F. R. (1996). A working heart-brainstem preparation of the mouse. *J. Neurosci. Methods* 65, 63–68. doi: 10.1016/0165-0270(95)00147-6

Ramirez, J.-M., and Baertsch, N. A. (2018). Defining the rhythmogenic elements of mammalian breathing. *Physiol.* 33, 302–316.

Richter, D. W. (1982). Generation and maintenance of the respiratory rhythm. *J. Exp. Biol.* 100, 93–107.

Richter, D. W., and Smith, J. C. (2014). Respiratory rhythm generation *in vivo*. *Physiology* 29, 58–71. doi: 10.1152/physiol.00035.2013

Rybak, I. A., Molkov, Y. I., Jasinski, P. E., Shevtsova, N. A., and Smith, J. C. (2014). "Chapter 1–rhythmic bursting in the pre-bötzinger complex: mechanisms and models" in *Progress in brain research. The central nervous system control of respiration*. eds. G. Holstege, C. M. Beers and H. H. Subramanian (Elsevier), 209, 1–23. doi: 10.1016/B978-0-444-63274-6.00001-1

Rybak, I. A., Shevtsova, N. A., Paton, J. F. R., Dick, T. E., St.-John, W. M., Mörschel, M., et al., (2004). Modeling the ponto-medullary respiratory network. *Respir. Physiol. Neurobiol.* 143, 307–319. doi: 10.1016/j.resp.2004.03.020

Shew, W. L., and Plenz, D. (2013). The functional benefits of criticality in the cortex. *Neuroscientist* 19, 88–100. doi: 10.1177/1073858412445487

Smith, J. C., Abdala, A. P. L., Koizumi, H., Rybak, I. A., and Paton, J. F. R. (2007). Spatial and functional architecture of the mammalian brain stem respiratory network: a hierarchy of three oscillatory mechanisms. *J. Neurophysiol.* 98, 3370–3387. doi: 10.1152/jn.00985.2007

Smith, J. C., Abdala, A. P. L., Rybak, I. A., and Paton, J. F. R. (2009). Structural and functional architecture of respiratory networks in the mammalian brainstem. *Philos. Trans. Biol. Sci.* 364, 2577–2587. doi: 10.1098/rstb.2009.0081

Smith, J. C., Ellenberger, H. H., Ballanyi, K., Richter, D. W., and Feldman, J. L. (1991). Pre-Botzinger complex: a brainstem region that may generate respiratory rhythm in mammals. *Science* 254, 726–729. doi: 10.1126/science.1683005

Stettner, G. M., Huppke, P., Brendel, C., Richter, D. W., Gärtner, J., and Dutschmann, M. (2007). Breathing dysfunctions associated with impaired control of postinspiratory activity in Mecp2–/y knockout mice. *J. Physiol.* 579, 863–876. doi: 10.1113/jphysiol.2006.119966

Taneja, P., Ogier, M., Brooks-Harris, G., Schmid, D. A., Katz, D. M., and Nelson, S. B. (2009). Pathophysiology of locus ceruleus neurons in a mouse

model of Rett syndrome. *J. Neurosci.* 29, 12187–12195. doi: 10.1523/JNEUROSCI.3156-09.2009

von Euler, C. (1983). On the central pattern generator for the basic breathing rhythmicity. *J. Appl. Physiol.* 55, 1647–1659. doi: 10.1152/jappl.1983.55.6.1647

Wasserman, A. M., Ferreira, M., Sahibzada, N., Hernandez, Y. M., and Gillis, R. A. (2002). GABA-mediated neurotransmission in the ventrolateral NTS plays a role in respiratory regulation in the rat. *Am. J. Physiol. Regul. Integr. Comp. Physiol.* 283, R1423–R1441. doi: 10.1152/ajpregu.00488.2001

Wehr, M., and Zador, A. M. (2003). Balanced inhibition underlies tuning and sharpens spike timing in auditory cortex. *Nature* 426, 442–446. doi: 10.1038/nature02116

Winter, S. M., Fresemann, J., Schnell, C., Oku, Y., Hirrlinger, J., and Hülsmann, S. (2009). Glycinergic interneurons are functionally integrated into the inspiratory network of mouse medullary slices. *Pflüg. Arch.* 458, 459–469. doi: 10.1007/s00424-009-0647-1

Yamada, Y., and Yamamura, K. (1996). Possible factors which may affect phase durations in the natural chewing rhythm. *Brain Res.* 706, 237–242. doi: 10.1016/0006-8993(95)01061-0

Yuste, R., MacLean, J. N., Smith, J., and Lansner, A. (2005). The cortex as a central pattern generator. *Nat. Rev. Neurosci.* 6, 477–483. doi: 10.1038/nrn1686

Zhang, W., Hayward, L. F., and Davenport, P. W. (2009). Influence of dorsal periaqueductal gray activation on respiratory occlusion reflexes in rats. *Auton. Neurosci.* 150, 62–69. doi: 10.1016/j.autneu.2009.04.008

Zhu, Y., Hsieh, Y.-H., Dhingra, R. R., Dick, T. E., Jacono, F. J., and Galán, R. F. (2013). Quantifying interactions between real oscillators with information theory and phase models: application to cardiorespiratory coupling. *Phys. Rev. E* 87:022709. doi: 10.1103/PhysRevE.87.022709

Zoccal, D. B., Furuya, W. I., Bassi, M., Colombari, D. S. A., and Colombari, E. (2014). The nucleus of the solitary tract and the coordination of respiratory and sympathetic activities. *Front. Physiol.* 5:238. doi: 10.3389/fphys.2014.00238

Conflict of Interest Statement: The authors declare that the research was conducted in the absence of any commercial or financial relationships that could be construed as a potential conflict of interest.

frontiers in Physiology

MINI REVIEW
published: 02 August 2019
doi: 10.3389/fphys.2019.00984

Chemoattraction and Recruitment of Activated Immune Cells, Central Autonomic Control, and Blood Pressure Regulation

*Khalid Elsaafien[1], Willian S. Korim[1], Anthony Setiadi[1], Clive N. May[1] and Song T. Yao[1,2]**

[1]Discovery Science, Florey Institute of Neuroscience and Mental Health, Parkville, VIC, Australia, [2]Florey Department of Neuroscience and Mental Health, The University of Melbourne, Parkville, VIC, Australia

Inflammatory mediators play a critical role in the regulation of sympathetic outflow to cardiovascular organs in hypertension. Emerging evidence highlights the involvement of immune cells in the regulation of blood pressure. However, it is still unclear how these immune cells are activated and recruited to key autonomic brain regions to regulate sympathetic outflow to cardiovascular organs. Chemokines such as C-C motif chemokine ligand 2 (CCL2), and pro-inflammatory cytokines such as tumor necrosis factor alpha (TNF-α) and interleukin 1 beta (IL-1β), are upregulated both peripherally and centrally in hypertension. More specifically, they are upregulated in key autonomic brain regions that control sympathetic activity and blood pressure such as the paraventricular nucleus of the hypothalamus and the rostral ventrolateral medulla. Furthermore, this upregulation of inflammatory mediators is associated with the infiltration of immune cells to these brain areas. Thus, expression of pro-inflammatory chemokines and cytokines is a potential mechanism promoting invasion of immune cells into key autonomic brain regions. In pathophysiological conditions, this can result in abnormal activation of brain circuits that control sympathetic nerve activity to cardiovascular organs and ultimately in increases in blood pressure. In this review, we discuss emerging evidence that helps explain how immune cells are chemoattracted to autonomic nuclei and contribute to changes in sympathetic outflow and blood pressure.

Keywords: neuroinflammation, chemoattraction, immune system, autonomic nervous system, hypertension

OPEN ACCESS

Edited by:
Vaughan G. Macefield, Baker Heart and Diabetes Institute, Australia

Reviewed by:
J. Thomas Cunningham, University of North Texas Health Science Center, United States
Melissa Mary Jean Farnham, Heart Research Institute, Australia

***Correspondence:**
Song T. Yao
song.yao@florey.edu.au

Specialty section:
This article was submitted to Integrative Physiology, a section of the journal Frontiers in Physiology

Received: *31 May 2019*
Accepted: *15 July 2019*
Published: *02 August 2019*

Citation:
Elsaafien K, Korim WS, Setiadi A, May CN and Yao ST (2019) Chemoattraction and Recruitment of Activated Immune Cells, Central Autonomic Control, and Blood Pressure Regulation. Front. Physiol. 10:984. doi: 10.3389/fphys.2019.00984

INTRODUCTION

The autonomic nervous system plays a major role in blood pressure regulation whereby dysfunction can lead to hypertension. Brain regions lacking a functional blood-brain barrier (BBB), known as circumventricular organs (CVOs), can sense and respond to circulating factors such as blood-borne hormones, like angiotensin II. This can lead to elevated sympathetic discharge and blood pressure (BP) (Nunes and Braga, 2011; Zubcevic et al., 2017). CVOs, such as the subfornical organ (SFO) and the area postrema (AP), regulate sympathetic outflow by changing the activity of neurons in the paraventricular nucleus of the hypothalamus (PVN) and the rostral ventrolateral medulla in the brainstem (RVLM) (van der Kooy and Koda, 1983; Dampney et al., 1987; Braga et al., 2011). Both the PVN and the RVLM are implicated in

the regulation of sympathetic outflow to cardiovascular organs *via* direct projections to sympathetic preganglionic neurons (SPNs) located in the spinal cord (Strack et al., 1989a,b; Schramm et al., 1993). Thus, these brain regions play an important role in regulating homeostatic levels of sympathetic outflow to the cardiovascular organs such that activation of the AP, by inflammatory mediators such as tumor necrosis factor alpha (TNF-α), for example, can lead to increases in both cardiac and renal sympathetic nerve activity (Korim et al., 2018).

The upregulation of pro-inflammatory mediators is associated with human hypertension (Chrysohoou et al., 2004; Antonelli et al., 2012). Studies in experimental rodent models of hypertension confirm this finding. Moreover, they further show that upregulation of a wide range of pro-inflammatory mediators occurs in key brain regions known to regulate sympathetic outflow to cardiovascular organs (Shen et al., 2015). These pro-inflammatory cytokines include TNF-α, interleukin 1 beta (IL-1β), interleukin 6 (IL-6), and pro-inflammatory chemokines such as C-C motif chemokine ligand 2 (CCL2). These mediators are upregulated in the PVN and RVLM, in models of both primary and secondary hypertension (Li et al., 2014; Song et al., 2014). Selective blockade of these inflammatory mediators in the central nervous system reduces BP in animal models of hypertension (Li et al., 2014; Song et al., 2014). These studies indicate that upregulation of pro-inflammatory mediators in brain regions that control cardiovascular function contributes to sustained BP increase in hypertension. However, the factors leading to upregulation of these mediators in critical brain areas in the context of cardiovascular control remain unclear.

Recently, focus has shifted to the role of immune cells in the development of hypertension (Bomfim et al., 2018; Caillon et al., 2018; Carnagarin et al., 2018). Resident immune cells in the central nervous system (microglia) are responsible for local inflammatory processes in the brain (Shen et al., 2015). In fact, chronic central infusion of minocycline, an anti-inflammatory antibiotic that reduces microglia activation, reduces central inflammation and BP in hypertension (Shi et al., 2010). There is also evidence that peripheral bone marrow immune cells are involved in inducing brain inflammation, leading to a hypertensive phenotype (Santisteban et al., 2015). Interestingly, when the bone marrow of spontaneously hypertensive rats (SHRs) is ablated and replaced with bone marrow from normotensive Wistar Kyoto rats (WKYs), central inflammation is attenuated, leading to BP reduction (Santisteban et al., 2015). This evidence suggests that peripheral immune cells play an important role in central inflammation and the development of hypertension.

Infiltrating immune cells are activated and recruited by pro-inflammatory chemokines, such as CCL2 (Deshmane et al., 2009). Interestingly, CCL2 is upregulated in the PVN of hypertensive rodents. This upregulation of CCL2 was linked to the presence of infiltrating immune cells in the PVN of these animals (Wang et al., 2018). Moreover, there is a clear gradient of CCL2 levels in hypertensive animals, whereby the lowest levels are detected in bone marrow and the highest levels are detected in the cerebrospinal fluid (CSF) of rodents (Santisteban et al., 2015). Hence, this forms a distinct chemotactic gradient, such that immune cells are recruited to specialized cardiovascular control regions of the brain. Once there, they initiate an inflammatory cascade, which impairs sympathetic control and mediates sustained increases in BP.

In this review, we discuss the evidence supporting brain chemoattraction and the involvement of immune cells in regulating sympathetic outflow to cardiovascular organs. We will focus on the effects of chemoattraction of immune cells to induce inflammatory cascades in key autonomic brain centers that control cardiovascular function, and the potential role of these changes in the development of hypertension.

UPREGULATION OF BRAIN PRO-INFLAMMATORY CYTOKINES AND CHEMOATTRACTION OF IMMUNE CELLS ON THE REGULATION OF BLOOD PRESSURE

Upregulation of Brain Pro-inflammatory Cytokines in Hypertension

Increases in BP in rodent models of hypertension are associated with the upregulation of pro-inflammatory mediators, both peripherally and centrally. Recent studies demonstrate that a number of pro-inflammatory mediators are elevated in different rodent models of hypertension (Jia et al., 2014; Song et al., 2014; Yu et al., 2015; Li et al., 2016). For example, there are significantly higher levels of TNF-α, IL-1β, IL-6, and CCL2 in the PVN of SHRs, a model of primary hypertension, compared with normotensive WKYs. Similarly, in a model of secondary hypertension (renovascular; two kidney-one clip, 2 K-1C), the levels of TNF-α, IL-1β, IL-6, and CCL2 are elevated in the RVLM (Li et al., 2014). Furthermore, the levels of these pro-inflammatory mediators are also elevated in the PVN of angiotensin II-induced hypertensive rat models (Kang et al., 2009, 2014; Sriramula et al., 2013; Su et al., 2014), as well as in high salt diet-induced hypertension (Gao et al., 2016; Wang et al., 2018). The downstream effect of this increased inflammation is thought to contribute to altered neuronal signaling caused by imbalances in neurotransmitter and neuromodulator levels in key autonomic brain centers. For instance, glutamate and norepinephrine are upregulated whereas GABA was downregulated within both the PVN and the RVLM of hypertensive animals (Jia et al., 2014; Song et al., 2014; Yu et al., 2015; Li et al., 2016). Thus, changes in the activity of neurons in key autonomic brain nuclei may contribute to elevated sympathetic nerve activity (SNA) and increases in BP.

Blockade of receptors for pro-inflammatory mediators within cardiovascular brain regions reduces BP in rodent models of hypertension. Recently, we showed that blockade of TNF-α receptors (TNFR1) in the AP reduces BP in the 2 K-1C model of hypertension (Korim et al., 2018). Others have also demonstrated that non-selective blockade of TNF-α receptors (Sriramula et al., 2013; Song et al., 2014), IL-1β receptors (Lu et al., 2017), and the downstream secondary messenger of pro-inflammatory cytokines NF-κB (Yu et al., 2015) in the PVN of hypertensive rats reduced BP. Interestingly, antagonism of pro-inflammatory

cytokine receptors within the central nervous system not only reduced SNA and BP in hypertension, but also appeared to restore the neurotransmitter imbalances and excessive activation of cardiovascular brain regions (Sriramula et al., 2013; Song et al., 2014; Lu et al., 2017). Thus, the dysregulation of pro-inflammatory mediator levels within key autonomic centers appears to be associated with the development of hypertension.

Exogenous application of pro-inflammatory cytokines into specific central cardiovascular control centers of normotensive animals increases SNA and BP. For example, microinjections of TNF-α and IL-1β into the SFO (Wei et al., 2015) and in the PVN (Shi et al., 2011) increased renal SNA and BP. Furthermore, our group has recently shown that the microinjection of TNF-α into the AP increases both renal and cardiac SNA and BP (Korim et al., 2018). Interestingly, we found receptors for TNF-α to be expressed on AP neurons projecting to the RVLM – a cardiovascular brain region known for containing neurons directly projecting to SPNs (Strack et al., 1989a,b; Schramm et al., 1993). These neurons appear to be chronically activated in hypertensive animals and are also active following microinjection of TNF-α into the AP (Korim et al., 2018). These studies provide a direct causal relationship whereby activation of neurons by pro-inflammatory mediators, within important central cardiovascular control regions such as the AP, increases the sympathetic outflow and BP. Indeed, we have also previously demonstrated that the AP is critical in driving the increased cardiac SNA in an ovine model of heart failure (Abukar et al., 2018). Taken together, these studies provide compelling evidence to support a link between increases in brain pro-inflammatory mediators and the dysregulation of SNA and BP in hypertension.

C-C Motif Chemokine Ligand 2 and the Chemoattraction of Immune Cells in Hypertension

Chemokines are pro-inflammatory mediators and chemotactic cytokines, whose main function is to regulate cell trafficking (Rollins, 1997; Deshmane et al., 2009; Zlotnik and Yoshie, 2012). These proteins create a concentration gradient and activate immune cells, causing them to move up this chemotactic gradient (Zlotnik and Yoshie, 2012). The chemokine CCL2 (also known as monocyte chemoattractant protein-1 or MCP-1), and its cognate receptor C-C Chemokine receptor type 2 (CCR2), is one of the most extensively studied chemokines. While CCL2 can be secreted by a variety of cell types, including endothelial cells and vascular smooth muscle cells (Bartoli et al., 2001), the main source of CCL2 is believed to be monocytes/macrophages (Yoshimura et al., 1989a,b). CCL2 is secreted in response to injury, oxidative stress, growth factors, and expression of other pro-inflammatory cytokines – where CCL2 secretion forms a gradient toward these stimuli. This process is termed chemotaxis, where CCL2 recruits circulating monocytes/macrophages to the respective chemical stimulus in the inflamed tissue or site of injury (Ajuebor et al., 1998). Evidence that CCL2 plays a vital role in the process of monocyte recruitment and cytokine expression is demonstrated by the finding that these are abnormal in CCL2 knockout mice (Lu et al., 1998). Interestingly, both CCL2 and its receptor, CCR2, are expressed and produced in the brain, specifically in central autonomic control centers such as the PVN and the RVLM (Wittendorp et al., 2004; Banisadr et al., 2005; Hinojosa et al., 2011; Morioka et al., 2013). However, the extent to which CCL2 and the chemoattraction of immune cells contribute to increased SNA and BP in the development of hypertension is still unknown and requires further investigation.

There is some evidence suggesting the involvement of increased chemoattraction of immune cells by CCL2 into cardiovascular brain centers during the development of hypertension. For example, selective antagonism of CCR2 receptors reduces BP in rodent models of hypertension (Aiyar et al., 1999; Elmarakby et al., 2007; Chan et al., 2012; Chang et al., 2014; Wang et al., 2015). Furthermore, studies in models of both primary and secondary hypertension reveal upregulation of CCL2 both peripherally and centrally (Sriramula et al., 2013; Li et al., 2014; Song et al., 2014), with a 3-fold elevation in the levels of CCL2 within the PVN of hypertensive animals (Sriramula et al., 2013; Li et al., 2014; Song et al., 2014). Upregulation of CCL2 occurs in the bone marrow, serum, and cerebrospinal fluid of SHRs compared with normotensive WKYs (Santisteban et al., 2015). Interestingly, the increase in CCL2 levels in SHRs forms a gradient from the bone marrow (lowest concentrations) toward the cerebrospinal fluid (highest concentrations) (Santisteban et al., 2015), possibly forming a chemotactic gradient toward the central nervous system. Thus, it seems that CCL2 chemoattracts immune cells and triggers an inflammatory cascade within the brain, leading to increases in BP.

THE NEURO-IMMUNE-INFLAMMATORY MODEL OF HYPERTENSION

In hypertension, increased circulating levels of angiotensin II is a potential cause for increased levels of brain CCL2 (Matsuda et al., 2015). A hallmark of hypertension is the upregulation of renin-angiotensin system and increased levels of angiotensin II (Goldblatt et al., 1934; Crowley et al., 2006, 2010). While not all human essential hypertension is angiotensin II mediated, the serum levels of CCL2 are increased in hypertensive patients (Antonelli et al., 2012). Interestingly, treating these patients with angiotensin II receptor blockers, which reduces blood pressure, also reduces plasma levels of CCL2 (Marketou et al., 2011), suggesting a link between angiotensin II and increased levels of CCL2. Similarly, in a rodent renovascular model of hypertension, peripheral blockade of receptors for angiotensin II attenuates peripheral CCL2 production (Xie et al., 2006). Moreover, *in vitro* studies show that angiotensin II can directly stimulate the production of CCL2 from monocytes and vascular smooth muscle cells (Chen et al., 1998; Tsou et al., 2007). In addition, systemic angiotensin II infusion increases CCR2 receptor expression in circulating monocytes – which is blunted by blocking angiotensin II receptors (Ishibashi et al., 2004). Recent studies further show that application of angiotensin II to primary hypothalamic neurons induces increased CCL2 mRNA and CCL2 protein levels in the cell culture media (Santisteban et al., 2015).

As such, the stimulation of receptors for angiotensin II on peripheral circulating monocytes, vascular smooth muscle cells, and even on neurons induces the production of CCL2 in these cells.

Increased levels of CCL2 lead to the disruption of the BBB and facilitate immune cell infiltration into the brain tissue. While the BBB prevents immune cells from entering the brain, we have previously suggested that this structure is disrupted in hypertension (Setiadi et al., 2018). The regulation of BBB permeability involves tight junction proteins expressed on endothelial cells (Begley and Brightman, 2003). CCL2 is known to disrupt the BBB, through dysregulation of tight junction proteins such as ZO-1, ZO-2, occludin, and claudin-5 (Stamatovic et al., 2009; Roberts et al., 2012). *In vitro* studies have demonstrated that the application of CCL2 to primary mouse brain endothelial cell cultures reorganizes and redistributes tight junction proteins, increasing the permeability of the BBB (Stamatovic et al., 2003, 2009). Hence, CCL2 can directly disrupt the BBB by regulating the distribution of tight junction proteins. In SHRs, increased BBB permeability in the PVN and RVLM facilitates the entry of circulating angiotensin II into these brain structures (Biancardi et al., 2013). Interestingly, *in vitro* studies using primary human brain endothelial cells corroborate *in vitro* animal studies by showing that CCL2 can disrupt tight junction proteins expressed on endothelial cells cultured from human brains (Roberts et al., 2012). Furthermore, the application of CCL2 to primary human brain endothelial cell cultures induces the expression of cell adhesion molecules, such as PECAM-1 on the surface membrane of endothelial cells, which is required for facilitating transmigration of immune cells through endothelial cells (Muller et al., 1993; Roberts

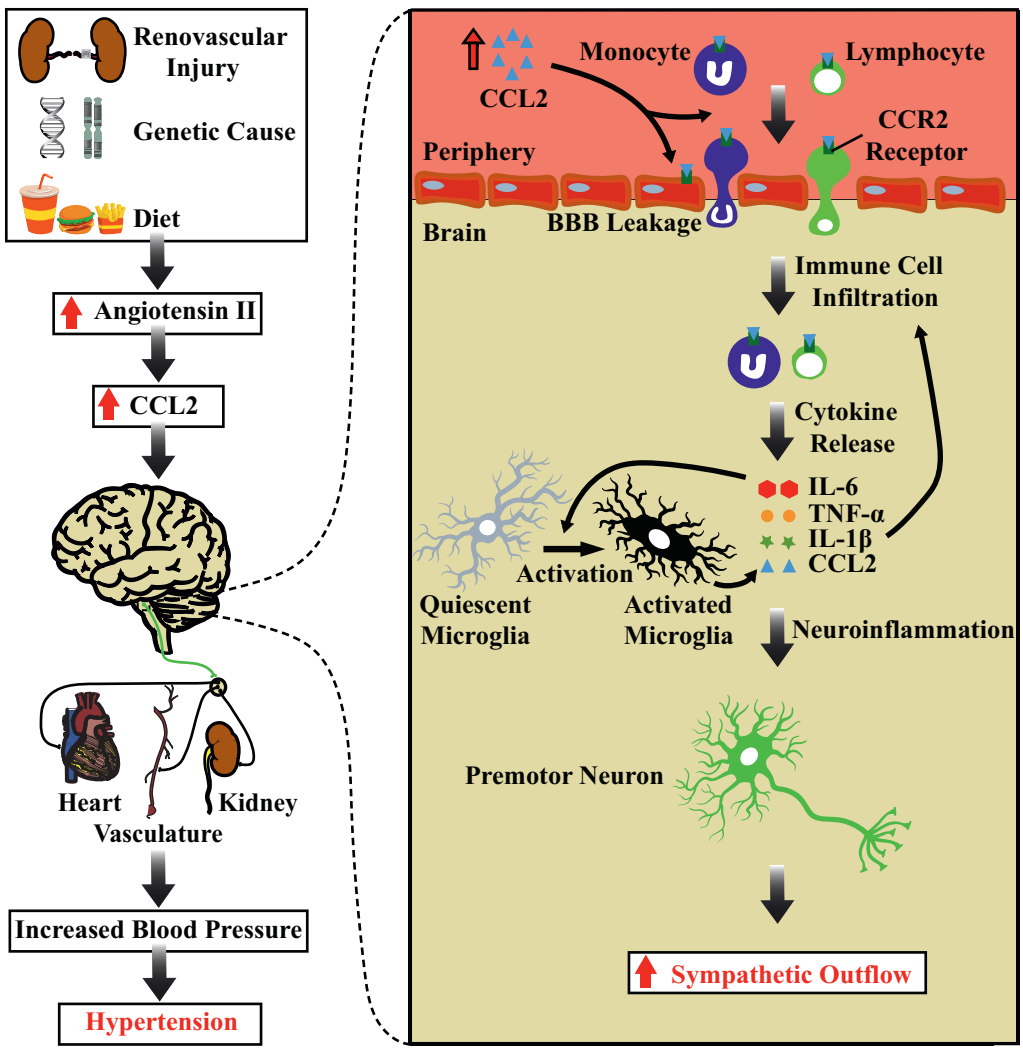

FIGURE 1 | Chemoattraction of immune cells in the brain, autonomic dysfunction, and hypertension. Schematic diagram showing the potential role of chemoattraction of immune cells and their components in determining increases in sympathetic nerve activity and blood pressure. Increased circulating levels of angiotensin II leads to production of the chemokine CCL2. CCL2 can act directly on the BBB, increasing the permeability of endothelial cells and recruiting immune cells to the brain tissue. The resulting overexpression of pro-inflammatory cytokines produces sustained activation of cardiovascular sympathetic neurons and increases blood pressure. Abbreviations: BBB, blood brain barrier; CCL2, C-C motif chemokine ligand 2; CCR2, C-C Chemokine receptor type 2; IL-1β, interleukin 1 beta; IL-6, interleukin 6; TNF-α, tumor necrosis factor alpha.

et al., 2012). Thus, not only can CCL2 reorganize the distribution of tight junction proteins expressed on endothelial cells to increase BBB permeability, it can also induce the expression of cell adhesion molecules on the surface membrane of endothelial cells to facilitate immune cell entry into brain tissue (**Figure 1**).

The recruitment and infiltration of immune cells into distinct brain regions can induce an inflammatory cascade resulting in the local upregulation of pro-inflammatory cytokines. The recruitment of activated immune cells into brain areas, including the PVN, results in the production and the upregulation of pro-inflammatory cytokines such as TNF-α, IL-1β, and IL-6 (Santisteban et al., 2015; Zubcevic et al., 2017; Sharma et al., 2019). These pro-inflammatory cytokines are capable of directly activating neurons and increasing sympathetic outflow and BP (Shi et al., 2011; Wei et al., 2015; Korim et al., 2018). Furthermore, the upregulation of pro-inflammatory cytokines and chemoattraction of activated immune cells also leads to activation of microglial cells (Santisteban et al., 2015; Zubcevic et al., 2017; Sharma et al., 2019). As microglia are the resident immune cells of the brain, activation of microglia leads to further release of pro-inflammatory mediators (Shi et al., 2010; Shen et al., 2015), therefore establishing an inflammatory state and escalating the inflammatory process centrally. Such a chronic inflammatory state results in further activation of immune cells, further neuroinflammation, and further rises in BP, leading to severe hypertension (Marvar et al., 2010). Whereas the blockade of receptors for pro-inflammatory cytokines in the brain (Sriramula et al., 2013; Song et al., 2014; Lu et al., 2017) prevents the activation of microglia (Shi et al., 2010), the recruitment of peripheral macrophages to the brain (Santisteban et al., 2015) and completely reverses the increased levels of peripheral and central pro-inflammatory cytokines and chemokines, leading to a reduced BP in hypertensive rats.

In summary, we propose a possible mechanism by which an inflammatory state in brain areas that control cardiovascular function is established, resulting in impaired BP control and hypertension. We propose that the increased levels of angiotensin II in the circulation results in the production and release of CCL2. This chemokine produces a chemotactic gradient that recruits immune cells toward the central nervous system. In addition, CCL2 increases BBB permeability and promotes the recruitment of activated immune cells. These immune cells initiate an inflammatory cascade where several pro-inflammatory mediators are released locally. Pro-inflammatory mediators activate neurons directly or indirectly by involving microglial transmission, which relays excitatory synapses to cardiovascular sympathetic premotor neurons in the ventrolateral medulla (Brown and Guyenet, 1985). The excitation of these neuronal subsets increases SNA and BP. These findings suggest that sustained activation of autonomic circuits contributes to the development of increased SNA and BP in neurogenic hypertension. Hence, chronic chemoattraction and recruitment of immune cells into key cardiovascular control regions might be a potential pathophysiological mechanism responsible for impaired BP control and hypertension (**Figure 1**).

CONCLUSION

In this review, we discussed recent findings that support our proposal of a potential mechanism to explain the contribution of neuroinflammation and chemoattraction mediated by CCL2, in brain regions that control cardiovascular function, as a cause of the sustained increase in sympathetic tone and BP in hypertension. This mechanism likely involves the recruitment and the infiltration of immune cells by chemokines to key autonomic brain areas. In future, targeting brain immune cells or the chemoattraction of immune cells may serve as a new avenue for developing antihypertensive treatments. In fact, in the pre-clinical setting, blockade of receptors for CCL2 or preventing immune cells from being activated reduces BP, in addition to slowing the development of atherosclerosis and vascular hypertrophy (Aiyar et al., 1999; Bush et al., 2000; Elmarakby et al., 2007; Chan et al., 2012; Chang et al., 2014; Santisteban et al., 2015; Wang et al., 2015). However, more thorough investigations are required to determine the mechanism by which chemoattraction and immune cells interact with the central nervous system, during the development and maintenance of hypertension.

AUTHOR CONTRIBUTIONS

KE drafted the manuscript and Figure. WK, AS, CM, and SY critically revised the intellectual content. All authors conceived and discussed the content of the manuscript, approved the final version of the manuscript, and agreed to be accountable for all aspects of the work.

FUNDING

This work was supported by the National Health and Medical Research Council of Australia (GNT 1079680 to SY; GNT 1128108 to CM and SY), the High Blood Pressure Research Council of Australia, the Rebecca L Cooper Medical Foundation (WK), and the Victorian Government through the Operational Infrastructure Scheme. KE and AS are supported by the Australian Government Research Training Program Scholarships. SY is supported by an Australian Research Council Future Fellowship (FT170100363).

REFERENCES

Abukar, Y., Ramchandra, R., Hood, S. G., McKinley, M. J., Booth, L. C., Yao, S. T., et al. (2018). Increased cardiac sympathetic nerve activity in ovine heart failure is reduced by lesion of the area postrema, but not lamina terminalis. *Basic Res. Cardiol.* 113:35. doi: 10.1007/s00395-018-0695-9

Aiyar, N., Disa, J., Stadel, J. M., and Lysko, P. G. (1999). Calcitonin gene-related peptide receptor independently stimulates 3′,5′-cyclic adenosine monophosphate and Ca2+ signaling pathways. *Mol. Cell. Biochem.* 197, 179–185.

Ajuebor, M. N., Flower, R. J., Hannon, R., Christie, M., Bowers, K., Verity, A., et al. (1998). Endogenous monocyte chemoattractant protein-1 recruits monocytes in the zymosan peritonitis model. *J. Leukoc. Biol.* 63, 108–116. doi: 10.1002/jlb.63.1.108

Antonelli, A., Fallahi, P., Ferrari, S., Ghiadoni, L., Virdis, A., Mancusi, C., et al. (2012). High serum levels of CXC (CXCL10) and CC (CCL2) chemokines in untreated essential hypertension. *Int. J. Immunopathol. Pharmacol.* 25, 387–395. doi: 10.1177/039463201202500208

Banisadr, G., Gosselin, R. D., Mechighel, P., Kitabgi, P., Rosene, W., and Parsadaniantz, S. P. M. (2005). Highly regionalized neuronal expression of monocyte chemoattractant protein-1 (MCP-1/CCL2) in rat brain: evidence for its colocalization with neurotransmitters and neuropeptides. *J. Comp. Neurol.* 489, 275–292. doi: 10.1002/cne.20598

Bartoli, C., Civatte, M., Pellissier, J., and Figarella-Branger, D. (2001). CCR2A and CCR2B, the two isoforms of the monocyte chemoattractant protein-1 receptor are up-regulated and expressed by different cell subsets in idiopathic inflammatory myopathies. *Acta Neuropathol.* 102, 385–392. doi: 10.1007/s004010100394

Begley, D. J., and Brightman, M. W. (2003). "Structural and functional aspects of the blood-brain barrier" in *Peptide transport and delivery into the central nervous system* (Birkhäuser, Basel: Springer), 39–78.

Biancardi, V. C., Son, S. J., Ahmadi, S., Filosa, J. A., and Stern, J. E. (2013). Circulating angiotensin II gains access to the hypothalamus and brain stem during hypertension via breakdown of the blood–brain barrier. *Hypertension* 63, 572–579. doi: 10.1161/HYPERTENSIONAHA.113.01743

Bomfim, G. F., Cau, S. B. A., Bruno, A. S., Fedoce, A. G., and Carneiro, F. S. (2018). Hypertension: a new treatment for an old disease? Targeting the immune system. *Br. J. Pharmacol.* 176, 2028–2048. doi: 10.1111/bph.14436

Braga, V. A., Medeiros, I. A., Ribeiro, T. P., Franca-Silva, M. S., Botelho-Ono, M. S., and Guimaraes, D. D. (2011). Angiotensin-II-induced reactive oxygen species along the SFO-PVN-RVLM pathway: implications in neurogenic hypertension. *Braz. J. Med. Biol. Res.* 44, 871–876. doi: 10.1590/s0100-879x2011007500088

Brown, D., and Guyenet, P. G. (1985). Electrophysiological study of cardiovascular neurons in the rostral ventrolateral medulla in rats. *Circ. Res.* 56, 359–369.

Bush, E., Maeda, N., Kuziel, W. A., Dawson, T. C., Wilcox, J. N., DeLeon, H., et al. (2000). CC chemokine receptor 2 is required for macrophage infiltration and vascular hypertrophy in angiotensin II–induced hypertension. *Hypertension* 36, 360–363. doi: 10.1161/01.HYP.36.3.360

Caillon, A., Paradis, P., and Schiffrin, E. L. (2018). Role of immune cells in hypertension. *Br. J. Pharmacol.* 176, 1818–1828. doi: 10.1111/bph.14427

Carnagarin, R., Matthews, V., Zaldivia, M. T., Peter, K., and Schlaich, M. P. (2018). The bidirectional interaction between the sympathetic nervous system and immune mechanisms in the pathogenesis of hypertension. *Br. J. Pharmacol.* 176, 1839–1852. doi: 10.1111/bph.14481

Chan, C. T., Moore, J. P., Budzyn, K., Guida, E., Diep, H., Vinh, A., et al. (2012). Reversal of vascular macrophage accumulation and hypertension by a CCR2 antagonist in deoxycorticosterone/salt-treated mice. *Hypertension* 60, 1207–1212. doi: 10.1161/HYPERTENSIONAHA.112.201251

Chang, A. Y., Li, F. C., Huang, C.-W., Wu, J. C., Dai, K.-Y., Chen, C.-H., et al. (2014). Interplay between brain stem angiotensins and monocyte chemoattractant protein-1 as a novel mechanism for pressor response after ischemic stroke. *Neurobiol. Dis.* 71, 292–304. doi: 10.1016/j.nbd.2014.08.005

Chen, X.-L., Tummala, P. E., Olbrych, M. T., Alexander, R. W., and Medford, R. M. (1998). Angiotensin II induces monocyte chemoattractant protein-1 gene expression in rat vascular smooth muscle cells. *Circ. Res.* 83, 952–959. doi: 10.1161/01.RES.83.9.952

Chrysohoou, C., Pitsavos, C., Panagiotakos, D. B., Skoumas, J., and Stefanadis, C. (2004). Association between prehypertension status and inflammatory markers related to atherosclerotic disease* The ATTICA Study. *Am. J. Hypertens.* 17, 568–573. doi: 10.1016/j.amjhyper.2004.03.675

Crowley, S. D., Gurley, S. B., Herrera, M. J., Ruiz, P., Griffiths, R., Kumar, A. P., et al. (2006). Angiotensin II causes hypertension and cardiac hypertrophy through its receptors in the kidney. *Proc. Natl. Acad. Sci. USA* 103, 17985–17990. doi: 10.1073/pnas.0605545103

Crowley, S. D., Song, Y.-S., Sprung, G., Griffiths, R., Sparks, M., Yan, M., et al. (2010). A role for angiotensin II type 1 receptors on bone marrow-derived cells in the pathogenesis of angiotensin II–dependent hypertension. *Hypertension* 55, 99–108. doi: 10.1161/HYPERTENSIONAHA.109.144964

Dampney, R. A., Czachurski, J., Dembowsky, K., Goodchild, A. K., and Seller, H. (1987). Afferent connections and spinal projections of the pressor region in the rostral ventrolateral medulla of the cat. *J. Auton. Nerv. Syst.* 20, 73–86.

Deshmane, S. L., Kremlev, S., Amini, S., and Sawaya, B. E. (2009). Monocyte chemoattractant protein-1 (MCP-1): an overview. *J. Interf. Cytokine Res.* 29, 313–326. doi: 10.1089/jir.2008.0027

Elmarakby, A. A., Quigley, J. E., Olearczyk, J. J., Sridhar, A., Cook, A. K., Inscho, E. W., et al. (2007). Chemokine receptor 2b inhibition provides renal protection in angiotensin II–salt hypertension. *Hypertension* 50, 1069–1076. doi: 10.1161/HYPERTENSIONAHA.107.098806

Gao, H.-L., Yu, X.-J., Qi, J., Yi, Q.-Y., Jing, W.-H., Sun, W.-Y., et al. (2016). Oral CoQ10 attenuates high salt-induced hypertension by restoring neurotransmitters and cytokines in the hypothalamic paraventricular nucleus. *Sci. Rep.* 6:30301. doi: 10.1038/srep30301

Goldblatt, H., Lynch, J., Hanzal, R. F., and Summerville, W. W. (1934). Studies on experimental hypertension I. The production of persistent elevation of systolic blood pressure by means of renal ischemia. *J. Exp. Med.* 59, 347–379.

Hinojosa, A. E., Garcia-Bueno, B., Leza, J. C., and Madrigal, J. L. (2011). Regulation of CCL2/MCP-1 production in astrocytes by desipramine and atomoxetine: involvement of alpha2 adrenergic receptors. *Brain Res. Bull.* 86, 326–333. doi: 10.1016/j.brainresbull.2011.09.014

Ishibashi, M., Hiasa, K.-I., Zhao, Q., Inoue, S., Ohtani, K., Kitamoto, S., et al. (2004). Critical role of monocyte chemoattractant protein-1 receptor CCR2 on monocytes in hypertension-induced vascular inflammation and remodeling. *Circ. Res.* 94, 1203–1210. doi: 10.1161/01.RES.0000126924.23467.A3

Jia, L. L., Kang, Y. M., Wang, F. X., Li, H. B., Zhang, Y., Yu, X. J., et al. (2014). Exercise training attenuates hypertension and cardiac hypertrophy by modulating neurotransmitters and cytokines in hypothalamic paraventricular nucleus. *PLoS One* 9:e85481. doi: 10.1371/journal.pone.0085481

Kang, Y.-M., Ma, Y., Zheng, J.-P., Elks, C., Sriramula, S., Yang, Z.-M., et al. (2009). Brain nuclear factor-kappa B activation contributes to neurohumoral excitation in angiotensin II-induced hypertension. *Cardiovasc. Res.* 82, 503–512. doi: 10.1093/cvr/cvp073

Kang, Y.-M., Zhang, D.-M., Yu, X.-J., Yang, Q., Qi, J., Su, Q., et al. (2014). Chronic infusion of enalaprilat into hypothalamic paraventricular nucleus attenuates angiotensin II-induced hypertension and cardiac hypertrophy by restoring neurotransmitters and cytokines. *Toxicol. Appl. Pharmacol.* 274, 436–444. doi: 10.1016/j.taap.2013.12.001

Korim, W. S., Elsaafien, K., Basser, J. R., Setiadi, A., May, C. N., and Yao, S. T. (2018). In renovascular hypertension, TNF-α type-1 receptors in the area postrema mediate increases in cardiac and renal sympathetic nerve activity and blood pressure. *Cardiovasc. Res.* 115, 1092–1101. doi: 10.1093/cvr/cvy268

Li, H.-B., Li, X., Huo, C.-J., Su, Q., Guo, J., Yuan, Z.-Y., et al. (2016). TLR4/MyD88/NF-κB signaling and PPAR-γ within the paraventricular nucleus are involved in the effects of telmisartan in hypertension. *Toxicol. Appl. Pharmacol.* 305, 93–102. doi: 10.1016/j.taap.2016.06.014

Li, H.-B., Qin, D.-N., Ma, L., Miao, Y.-W., Zhang, D.-M., Lu, Y., et al. (2014). Chronic infusion of lisinopril into hypothalamic paraventricular nucleus modulates cytokines and attenuates oxidative stress in rostral ventrolateral medulla in hypertension. *Toxicol. Appl. Pharmacol.* 279, 141–149. doi: 10.1016/j.taap.2014.06.004

Lu, P., Jiang, S.-J., Pan, H., Xu, A.-L., Wang, G.-H., Ma, C.-L., et al. (2017). Short hairpin RNA interference targeting interleukin 1 receptor type I in the paraventricular nucleus attenuates hypertension in rats. *Pflugers Arch.* 470, 1–10. doi: 10.1007/500424-017-2081-0

Lu, B., Rutledge, B. J., Gu, L., Fiorillo, J., Lukacs, N. W., Kunkel, S. L., et al. (1998). Abnormalities in monocyte recruitment and cytokine expression in monocyte chemoattractant protein 1–deficient mice. *J. Exp. Med.* 187, 601–608. doi: 10.1084/jem.187.4.601

Marketou, M. E., Kontaraki, J. E., Tsakountakis, N. A., Zacharis, E. A., Kochiadakis, G. E., Arfanakis, D. A., et al. (2011). Differential effect of telmisartan and amlodipine on monocyte chemoattractant protein-1 and peroxisome proliferator-activated receptor-gamma gene expression in peripheral monocytes in patients with essential hypertension. *Am. J. Cardiol.* 107, 59–63. doi: 10.1016/j.amjcard.2010.08.048

Marvar, P. J., Thabet, S. R., Guzik, T. J., Lob, H. E., McCann, L. A., Weyand, C., et al. (2010). Central and peripheral mechanisms of T-lymphocyte activation and vascular inflammation produced by angiotensin II–induced hypertension. *Circ. Res.* 107, 263–270. doi: 10.1161/CIRCRESAHA.110.217299

Matsuda, S., Umemoto, S., Yoshimura, K., Itoh, S., Murata, T., Fukai, T., et al. (2015). Angiotensin II Activates MCP-1 and induces cardiac hypertrophy

and dysfunction via toll-like receptor 4. *J. Atheroscler. Thromb.* 22, 833–844. doi: 10.5551/jat.27292

Morioka, N., Tokuhara, M., Harano, S., Nakamura, Y., Hisaoka-Nakashima, K., and Nakata, Y. (2013). The activation of P2Y6 receptor in cultured spinal microglia induces the production of CCL2 through the MAP kinases-NF-kappaB pathway. *Neuropharmacology* 75, 116–125. doi: 10.1016/j.neuropharm.2013.07.017

Muller, W. A., Weigl, S. A., Deng, X., and Phillips, D. M. (1993). PECAM-1 is required for transendothelial migration of leukocytes. *J. Exp. Med.* 178, 449–460.

Nunes, F. C., and Braga, V. A. (2011). Chronic angiotensin II infusion modulates angiotensin II type I receptor expression in the subfornical organ and the rostral ventrolateral medulla in hypertensive rats. *J. Renin-Angiotensin-Aldosterone Syst.* 12, 440–445. doi: 10.1177/1470320310394891

Roberts, T. K., Eugenin, E. A., Lopez, L., Romero, I. A., Weksler, B. B., Couraud, P.-O., et al. (2012). CCL2 disrupts the adherens junction: implications for neuroinflammation. *Lab. Investig.* 92, 1213–1233. doi: 10.1038/labinvest.2012.80

Rollins, B. J. (1997). Chemokines. *Blood* 90, 909–928.

Santisteban, M. M., Ahmari, N., Carvajal, J. M., Zingler, M. B., Qi, Y., Kim, S., et al. (2015). Involvement of bone marrow cells and neuroinflammation in hypertension. *Circ. Res.* 117, 178–191. doi: 10.1161/CIRCRESAHA.117.305853

Schramm, L. P., Strack, A. M., Platt, K. B., and Loewy, A. D. (1993). Peripheral and central pathways regulating the kidney: a study using pseudorabies virus. *Brain Res.* 616, 251–262.

Setiadi, A., Korim, W. S., Elsaafien, K., and Yao, S. T. (2018). The role of the blood–brain barrier in hypertension. *Exp. Physiol.* 103, 337–342. doi: 10.1113/EP086434

Sharma, R. K., Yang, T., Oliveira, A. C., Lobaton, G. O., Aquino, V., Kim, S., et al. (2019). Microglial cells impact gut microbiota and gut pathology in angiotensin II-induced hypertension. *Circ. Res.* 124, 727–736. doi: 10.1161/CIRCRESAHA.118.313882

Shen, X. Z., Li, Y., Li, L., Shah, K. H., Bernstein, K. E., Lyden, P., et al. (2015). Microglia participate in neurogenic regulation of hypertension. *Hypertension* 66, 309–316. doi: 10.1161/HYPERTENSIONAHA.115.05333

Shi, P., Diez-Freire, C., Jun, J. Y., Qi, Y., Katovich, M. J., Li, Q., et al. (2010). Brain microglial cytokines in neurogenic hypertension. *Hypertension* 56, 297–303. doi: 10.1161/HYPERTENSIONAHA.110.150409

Shi, Z., Gan, X. B., Fan, Z. D., Zhang, F., Zhou, Y. B., Gao, X. Y., et al. (2011). Inflammatory cytokines in paraventricular nucleus modulate sympathetic activity and cardiac sympathetic afferent reflex in rats. *Acta Physiol.* 203, 289–297. doi: 10.1111/j.1748-1716.2011.02313.x

Song, X.-A., Jia, L.-L., Cui, W., Zhang, M., Chen, W., Yuan, Z.-Y., et al. (2014). Inhibition of TNF-α in hypothalamic paraventricular nucleus attenuates hypertension and cardiac hypertrophy by inhibiting neurohormonal excitation in spontaneously hypertensive rats. *Toxicol. Appl. Pharmacol.* 281, 101–108. doi: 10.1016/j.taap.2014.09.004

Sriramula, S., Cardinale, J. P., and Francis, J. (2013). Inhibition of TNF in the brain reverses alterations in RAS components and attenuates angiotensin II-induced hypertension. *PLoS One* 8:e63847. doi: 10.1371/journal.pone.0063847

Stamatovic, S. M., Keep, R. F., Kunkel, S. L., and Andjelkovic, A. V. (2003). Potential role of MCP-1 in endothelial cell tight junctionopening': signaling via Rho and Rho kinase. *J. Cell Sci.* 116, 4615–4628. doi: 10.1242/jcs.00755

Stamatovic, S. M., Keep, R. F., Wang, M. M., Jankovic, I., and Andjelkovic, A. V. (2009). Caveolae-mediated internalization of occludin and claudin-5 during CCL2-induced tight junction remodeling in brain endothelial cells. *J. Biol. Chem.* 284, 19053–19066. doi: 10.1074/jbc.M109.000521

Strack, A., Sawyer, W., Hughes, J., Platt, K., and Loewy, A. (1989a). A general pattern of CNS innervation of the sympathetic outflow demonstrated by transneuronal pseudorabies viral infections. *Brain Res.* 491, 156–162.

Strack, A. M., Sawyer, W. B., Platt, K. B., and Loewy, A. D. (1989b). CNS cell groups regulating the sympathetic outflow to adrenal gland as revealed by transneuronal cell body labeling with pseudorabies virus. *Brain Res.* 491, 274–296.

Su, Q., Qin, D.-N., Wang, F.-X., Ren, J., Li, H.-B., Zhang, M., et al. (2014). Inhibition of reactive oxygen species in hypothalamic paraventricular nucleus attenuates the renin–angiotensin system and proinflammatory cytokines in hypertension. *Toxicol. Appl. Pharmacol.* 276, 115–120. doi: 10.1016/j.taap.2014.02.002

Tsou, C.-L., Peters, W., Si, Y., Slaymaker, S., Aslanian, A. M., Weisberg, S. P., et al. (2007). Critical roles for CCR2 and MCP-3 in monocyte mobilization from bone marrow and recruitment to inflammatory sites. *J. Clin. Invest.* 117, 902–909. doi: 10.1172/JCI29919

van der Kooy, D., and Koda, L. Y. (1983). Organization of the projections of a circumventricular organ: the area postrema in the rat. *J. Comp. Neurol.* 219, 328–338.

Wang, M.-L., Kang, Y.-M., Li, X.-G., Su, Q., Li, H.-B., Liu, K.-L., et al. (2018). Central blockade of NLRP3 reduces blood pressure via regulating inflammation microenvironment and neurohormonal excitation in salt-induced prehypertensive rats. *J. Neuroinflammation* 15:95. doi: 10.1186/s12974-018-1131-7

Wang, Y., Zhu, M., Xu, H., Cui, L., Liu, W., Wang, X., et al. (2015). Role of the monocyte chemoattractant protein-1/CC chemokine receptor 2 signaling pathway in transient receptor potential vanilloid type 1 ablation-induced renal injury in salt-sensitive hypertension. *Exp. Biol. Med.* 240, 1223–1234. doi: 10.1177/1535370214565970

Wei, S.-G., Yu, Y., Zhang, Z.-H., and Felder, R. B. (2015). Proinflammatory cytokines upregulate sympathoexcitatory mechanisms in the subfornical organ of the rat. *Hypertension* 65, 1126–1133. doi: 10.1161/HYPERTENSIONAHA.114.05112

Wittendorp, M. C., Boddeke, H. W. G. M., and Biber, K. (2004). Adenosine A(3) receptor-induced CCL2 synthesis in cultured mouse astrocytes. *Glia* 46, 410–418. doi: 10.1002/glia.20016

Xie, Q.-Y., Sun, M., Yang, T.-L., and Sun, Z.-L. (2006). Losartan reduces monocyte chemoattractant protein-1 expression in aortic tissues of 2K1C hypertensive rats. *Int. J. Cardiol.* 110, 60–66. doi: 10.1016/j.ijcard.2005.07.046

Yoshimura, T., Robinson, E., Tanaka, S., Appella, E., and Leonard, E. (1989a). Purification and amino acid analysis of two human monocyte chemoattractants produced by phytohemagglutinin-stimulated human blood mononuclear leukocytes. *J. Immunol.* 142, 1956–1962.

Yoshimura, T., Yuhki, N., Moore, S. K., Appella, E., Lerman, M. I., and Leonard, E. J. (1989b). Human monocyte chemoattractant protein-1 (MCP-1) full-length cDNA cloning, expression in mitogen-stimulated blood mononuclear leukocytes, and sequence similarity to mouse competence gene JE. *FEBS Lett.* 244, 487–493.

Yu, X.-J., Zhang, D.-M., Jia, L.-L., Qi, J., Song, X.-A., Tan, H., et al. (2015). Inhibition of NF-κB activity in the hypothalamic paraventricular nucleus attenuates hypertension and cardiac hypertrophy by modulating cytokines and attenuating oxidative stress. *Toxicol. Appl. Pharmacol.* 284, 315–322. doi: 10.1016/j.taap.2015.02.023

Zlotnik, A., and Yoshie, O. (2012). The chemokine superfamily revisited. *Immunity* 36, 705–716. doi: 10.1016/j.immuni.2012.05.008

Zubcevic, J., Santisteban, M. M., Perez, P. D., Arocha, R., Hiller, H., Malphurs, W. L., et al. (2017). A single angiotensin II hypertensive stimulus is associated with prolonged neuronal and immune system activation in Wistar-Kyoto rats. *Front. Physiol.* 8:592. doi: 10.3389/fphys.2017.00592

Conflict of Interest Statement: The authors declare that the research was conducted in the absence of any commercial or financial relationships that could be construed as a potential conflict of interest.

frontiers in Neuroscience

ORIGINAL RESEARCH
published: 21 August 2019
doi: 10.3389/fnins.2019.00881

PACAP-PAC1 Receptor Activation Is Necessary for the Sympathetic Response to Acute Intermittent Hypoxia

Melissa M. J. Farnham[1,2,3], Vikram J. Tallapragada[2], Edward T. O'Connor[4], Polina E. Nedoboy[1,3], Bowen Dempsey[2], Suja Mohammed[1,2,3], Angelina Y. Fong[2,5], Mandy S. Y. Lung[2], Fatemeh Derakhshan[4], Richard J. A. Wilson[4] and Paul M. Pilowsky[1,3]*

[1] The Heart Research Institute, Newtown, NSW, Australia, [2] Faculty of Medicine, Macquarie University, North Ryde, NSW, Australia, [3] Department of Physiology, Faculty of Medicine, University of Sydney, Sydney, NSW, Australia, [4] Department of Physiology and Pharmacology, Hotchkiss Brain Institute and Alberta Children's Hospital Research Institute, University of Calgary, Calgary, AB, Canada, [5] Department of Physiology, Faculty of Medicine, Dentistry and Health Sciences, University of Melbourne, Melbourne, VIC, Australia

OPEN ACCESS

Edited by:
Vaughan G. Macefield, Baker Heart and Diabetes Institute, Australia

Reviewed by:
David Vaudry, Institut National de la Santé et de la Recherche Médicale (INSERM), France
Norihito Shintani, Osaka University, Japan

***Correspondence:**
Melissa M. J. Farnham
melissa.farnham@hri.org.au

Specialty section:
This article was submitted to Autonomic Neuroscience, a section of the journal Frontiers in Neuroscience

Received: *28 May 2019*
Accepted: *05 August 2019*
Published: *21 August 2019*

Citation:
Farnham MMJ, Tallapragada VJ, O'Connor ET, Nedoboy PE, Dempsey B, Mohammed S, Fong AY, Lung MSY, Derakhshan F, Wilson RJA and Pilowsky PM (2019) PACAP-PAC1 Receptor Activation Is Necessary for the Sympathetic Response to Acute Intermittent Hypoxia. Front. Neurosci. 13:881. doi: 10.3389/fnins.2019.00881

Repetitive hypoxia is a key feature of obstructive sleep apnoea (OSA), a condition characterized by intermittent airways obstruction. Patients with OSA present with persistent increases in sympathetic activity and commonly develop hypertension. The objectives of this study were to determine if the persistent increases in sympathetic nerve activity, known to be induced by acute intermittent hypoxia (AIH), are mediated through activation of the pituitary adenylate cyclase activating polypeptide (PACAP) signaling system. Here, we show that the excitatory neuropeptide PACAP, acting in the spinal cord, is important for generating the sympathetic response seen following AIH. Using PACAP receptor knockout mice, and pharmacological agents in Sprague Dawley rats, we measured blood pressure, heart rate, pH, $PaCO_2$, and splanchnic sympathetic nerve activity, under anaesthesia, to demonstrate that the sympathetic response to AIH is mediated via the PAC1 receptor, in a cAMP-dependent manner. We also report that both intermittent microinjection of glutamate into the rostroventrolateral medulla (RVLM) and intermittent infusion of a sub-threshold dose of PACAP into the subarachnoid space can mimic the sympathetic response to AIH. All the sympathetic responses are independent of blood pressure, pH or $PaCO_2$ changes. Our results show that in AIH, PACAP signaling in the spinal cord helps drive persistent increases in sympathetic nerve activity. This mechanism may be a precursor to the development of hypertension in conditions of chronic intermittent hypoxia, such as OSA.

Keywords: Sprague-Dawley rat, mice, anaesthetized, PACAP, sympathetic, intermittent hypoxia, intrathecal

INTRODUCTION

Obstructive sleep apnoea (OSA) is characterized by collapse of the upper airway, resulting in frequent intermittent episodes of hypoxemia and hypercapnia. OSA affects approximately 10% of the population and is strongly associated with major cardiovascular diseases, including hypertension, stroke and heart failure; in these disorders, the prevalence of sleep apnoea is close

to 50% (Bradley and Floras, 2009). The hypoxemic/hypercapnic events cause large sympathetic surges including increases in heart rate, blood pressure and frequent arousal from sleep, leading to persistently elevated sympathetic nerve activity (SNA), i.e., sympathoexcitation (Leung et al., 2012). While sympathoexcitation may be critical for survival in diseases characterized by high risk of acute crisis such as sudden infant death syndrome (SIDS), marked sympathoexcitation is a key feature of hypertension which, in turn, causes target organ damage, atherosclerosis, renal failure, heart failure and stroke. Common to both OSA and hypertension, elevated SNA is evident before the development of hypertension.

To study the physiological effects of sleep apnoea in animals, investigators use acute intermittent hypoxia (AIH; minutes to hour of exposure), AIH with concurrent hypercapnia, or chronic intermittent hypoxia (CIH; weeks of exposure) (Fletcher, 2001). Despite the temporal pattern and magnitude of hypoxia varying considerably between these models, they all result in persistent sympathoexcitation (Kumar et al., 2006; Dick et al., 2007; Coleman et al., 2010; Iturriaga et al., 2010; Xing and Pilowsky, 2010; Roy et al., 2018), which is important since OSA is a hugely variable condition. The longer the period of sympathoexcitation the more likely it will lead to hypertension (Dick et al., 2007; Xing and Pilowsky, 2010). However, the mechanism of this persistent sympathoexcitation is not understood.

As pituitary adenylate cyclase activating polypeptide (PACAP) is essential for normal cardiorespiratory stress responses including apneas in neonates (Cummings et al., 2004; Ferguson et al., 2013; Barrett et al., 2017), we propose that PACAP plays an important role in intermittent hypoxia induced sympathoexcitation in adults. PACAP is an excitatory neurotransmitter present in all parts of the sympathetic pathway from sensors to efferents, including the carotid body, the rostroventrolateral medulla (RVLM), sympathetic preganglionic neurons (SPN), and the adrenal medulla (Lai et al., 1997; Mazzocchi et al., 2002; Farnham et al., 2008, 2011, 2012; Inglott et al., 2011; Roy et al., 2013). Intrathecal infusion of 1 mM PACAP-38 causes large, long lasting sympathoexcitation without any change in blood pressure (Farnham et al., 2008), similar to that seen after AIH. PACAP acts at 3 receptors, PAC1, VPAC1, and VPAC2, and can differentially regulate blood pressure by activating either PAC1 or VPAC receptors in the spinal cord (Inglott et al., 2012). PACAP is closely associated with catecholaminergic regions and is rate-limiting for the release of catecholamines from the adrenal medulla during prolonged stress (Stroth et al., 2013). Neonatal PACAP knockout mice also have reduced brainstem expression of tyrosine hydroxylase (TH) (Arata et al., 2013), the rate limiting enzyme for catecholamine synthesis. Thus, enhanced PACAP neurotransmission in cardiorespiratory pathways may be the underlying cause of the persistent sympathetic efferent activity seen following periods of sleep-disordered breathing, involving intermittent hypoxia, in sleep apnoea patients (Bradley and Floras, 2009). We therefore hypothesized that much of the persistent increase in sympathoexcitation seen following an episode of intermittent hypoxia, is due to PACAP acting at the PAC1 receptor that exerts long-term plastic effects on post-synaptic sympathetic neurons.

It should be noted, however, that the relative importance of central immune cells such as microglia, in mediating sympathoexcitation is unknown. Microglia in the sympathetic nervous system possess receptors for virtually all neurotransmitters, including PACAP (Kapoor et al., 2016), but ascertaining their function is challenging. In conditions of CIH, it is proposed that microglia may be activated by intermittent hypoxia either directly or indirectly, or by a combination of both mechanisms (Kiernan et al., 2016). Whether microglia directly, or indirectly contribute to intermittent hypoxia-induced sympathoexcitation, remains to be investigated.

Here we report that AIH causes persistent sympathoexcitation and increased expression of phosphorylated TH (serine 40) in PACAP-containing C1 cardiovascular neurons in the RVLM. This sympathoexcitation can be blocked with intrathecal administration of the PACAP antagonist, PACAP(6–38) and does not occur in mice lacking the PAC1 receptor. Using intermittent intrathecal application of PACAP or intermittent glutamate stimulation of the RVLM, we show that PACAP signaling within the spinal cord is an important cause of the long-term facilitation of sympathetic activity. These PACAP effects are mediated by the PACAP preferring receptor, PAC1, in a cAMP-dependent manner.

MATERIALS AND METHODS

Animals

Procedures and protocols were approved by the Animal Care and Ethics Committees of Macquarie University, Sydney Local Area Health District, and the University of Calgary and conducted in accordance with the Australian and Canadian codes of practice for the care and use of animals for scientific purposes. Rats are used as the experiments described involve an integrative approach and no artificial models of these systems currently exist. Mice are used as conventional models for investigating the effects of knocking out genes of interest.

Experiments were conducted on adult male Sprague-Dawley (SD) rats (350–500 g; Animal Resource Centre, Perth, Australia) and adult male and female mice (20–70 g; C57BL/J6 background; University of Calgary, Canada) that were PAC1R$^{+/+}$, PAC1R$^{+/-}$ PAC1R$^{-/-}$, VPAC2R$^{+/+}$ or VPAC2$^{-/-}$. The PAC1 receptor mouse colony (Jamen et al., 2000) was provided by Dr. L. Journot (Hannibal et al., 2001). The VPAC2 receptor mouse colony (Harmar et al., 2002) was provided by Dr. A. Harmar (deceased).

Surgical Preparation

Sprague Dawley (SD; male; n = 104) rats, and mice (male and female; n = 6 PAC1$^{+/+}$; 5 PAC1$^{+/-}$; 3 PAC1$^{-/-}$; 8 VPAC2$^{+/+}$; 6 VPAC2$^{-/-}$) were anaesthetized with urethane. For the Fos study n = 8 SD rats were anaesthetized with sodium pentobarbitone. Complete details of surgical preparation and data acquisition methods are as described elsewhere (Farnham et al., 2008, 2015).

Briefly, the core temperature of all animals was maintained at 37 ± 0.5°C. The right carotid artery and jugular vein were cannulated for measurement of arterial blood pressure and administration of drugs and fluids, respectively. The

trachea was cannulated to permit artificial ventilation. The left greater splanchnic sympathetic nerve was isolated and activity recorded. All animals were bilaterally vagotomized (cervical), ventilated with oxygen-enriched room air and paralyzed (rats – pancuronium bromide 0.8 mg/kg i.v., followed by an infusion of 0.8 mg/kg/hr of pancuronium in 0.9% saline at a rate of 2 ml/h; Astra Zeneca, Australia; mice – rocuronium bromide 0.02 ml/h, i.p., 10 mg/ml; Sandoz, Melbourne). In rats, arterial blood was withdrawn and respiratory blood gas (O_2 and CO_2) and pH analysis (electrolyte and blood gas analyzer; IDEXX Laboratories, United States) conducted 10 min before any treatment, and during the recording periods. In some groups, an occipital craniotomy was performed, a needle was inserted into the RVLM with tip location confirmed with a rise in blood pressure > 30 mmHg (Gaede and Pilowsky, 2013) in response to a 50 nl injection of glutamate (100 mM; Sigma). For full details of the *in vivo* mouse preparation see Farnham et al. (2015). All recordings were maintained for 60 min following the final stimulus. Blood gas sampling was not possible in mouse as the volume required proved fatal.

Single Intrathecal Administration of Drugs

For intrathecal administration of drugs (rats), a catheter was inserted into the intrathecal space and advanced caudally from the cisterna magna to the level of vertebra T5/T6. The drugs in **Table 1** were administered in a 10 μl infusion and washed in with 6 μl phosphate buffered saline (PBS). Injections were made over a 30–45 s period, as previously described (Farnham et al., 2008). Responses were recorded for 10 min before performing the AIH protocol.

Acute Intermittent Hypoxia

In the rat, the AIH protocol consisted of 10, 45 s, episodes of 10% O_2 in N_2, each separated by a 5 min recovery period (Xing and Pilowsky, 2010).

In mouse, the AIH protocol consisted of 10 episodes of 25–30 s of removal of O_2 supplementation (i.e., ventilation with room air alone), separated by 2.5 min recovery periods (Farnham et al., 2015).

Intermittent, Intrathecal, and RVLM Drug Administration

In rat, the intermittent intrathecal drug infusion protocol consisted of 10 infusions of 10 μl, each conducted over 30–45 s, separated by 5 min. The RVLM microinjections consisted of 10 microinjections of 50 nl, separated by 5 min. The drugs used in this series of experiments are described in **Table 2**.

In vivo Data Acquisition and Analysis

Data were acquired using a CED 1401 ADC system and Spike 2 acquisition and analysis software (v. 7.12; Cambridge, United Kingdom). Recordings of splanchnic SNA (sSNA) were filtered (10–1000 Hz) and amplified (×2000), then rectified, smoothed (τ 1 s), and normalized by subtracting the residual activity after death. The transformed sSNA was used to calculate changes in sympathetic nerve activity following treatment by obtaining the % change in sSNA from baseline (1 min average of sSNA prior to intermittent stimulation). Mean arterial pressure (MAP), heart rate (HR), and sSNA, were analyzed from 1 min blocs taken 10 and 1 min prior to, and 60 min, after intermittent stimuli. Statistical analysis was conducted with GraphPad Prism software (v 7).

The responses at 60 min after AIH or intermittent drug administrations between strains were compared using a one-way ANOVA with *post hoc t*-tests, and Holm-Šidák correction, or unpaired *t*-tests. Statistical tests are described in section Results.

Perfusion and Tissue Harvest

Rats that underwent an AIH or intermittent infusion protocol and were to be used for the anatomical Fos, PACAP, TH, and pSer40TH study, were perfused transcardially with ice-cold, RNase-free PBS. Brains that were to be used for qPCR were then extracted, the RVLM excised bilaterally from a 1 mm coronal section under sterile and RNase free conditions. The procedure was carried out in cold conditions to avoid thawing of the samples. The RVLM samples were combined and transferred immediately after excision to 1.5 ml Eppendorf tube, snap-frozen in dry-ice-ethanol slurry and stored immediately at −80°C. Animals used for combined *in situ* hybridization and immunohistochemistry and were additionally perfused with 4%

TABLE 1 | Drug information for bolus intrathecal administration.

Drug	Action	Concentration	Dose	Company
Phosphate buffered 0.9% saline (PBS)	Vehicle control	10 mM	100 nmol	Sigma
PACAP-38	Agonist for PAC1, VPAC1 and VPAC2 receptors	300 μM	3 nmol	Auspep Pty. Ltd., Australia
PACAP(6–38)	PAC1 antagonist with some actions at VPAC2	1 mM	10 nmol	Auspep Pty. Ltd., Australia
Rp-Diastereomer of Adenosine 3′,5-Cyclic Monophosphorothioate (Rp-cAMP)	PKA inhibitor	100 mM	1 μmol	Sigma
Brefeldin A (BFA)	EPAC inhibitor	1 mM	10 nmol	Sigma
4-(N-Ethyl-N-phenylamino)-1,2 dimethyl-6-(methylamino)pyrimidium chloride (ZD-7288)	HCN channel blocker	3 mM	30 nmol	Sigma

PFA, the brains removed and post-fixed for 24 h in 4% PFA. Following post-fixation, brains were sectioned coronally at 40 μm and cryoprotected until use.

Combined *in situ* Hybridization (ISH) Fluorescence Immunohistochemistry

The combined protocol for free-floating *in situ* hybridization (PACAP-ISH forward: 5′-GGATCCATTTAGGTGACACTATAGAAGTTACGATCAGGACGGAAACC-3′; PACAP-ISH reverse: 5′-GAATTCTAATACGACTCACTATAGGGAGATGC-ACGCTTATGAATTGCTC-3′) and immunohistochemistry was performed as previously described (Li et al., 2005; Farnham et al., 2008). The PACAP probe was used at a final concentration of 100 ng/ml and sections were incubated shaking at 58°C overnight. Digoxigenin-labeled probe was detected using an alkaline phosphatase labeled sheep anti-digoxigenin antibody (1:1000, Roche, Switzerland). TH was detected using a mouse anti-TH (1:2000; Sigma–Aldrich Cat# T1299) primary antibody and a Cy3-conjugated donkey anti-mouse (1:500; Jackson ImmunoResearch Labs Cat# 715-167-003 RRID:AB_2340818) secondary antibody. Fos was detected with a rabbit anti-Fos (1:2000; Thermo Fisher Cat#SCZSC-253) primary antibody and a DyLite488-conjugated donkey anti-rabbit (1:500; Jackson ImmunoResearch Labs Cat# 711-485-152 RRID:AB_2492289) secondary antibody. A colorimetric reaction using nitroblue tetrazolium (NBT) (Roche) and 5-bromo-4-chloro-3-indolyl phosphate (BCIP) salts (Roche) in buffer (0.1 M NaCl, 0.1 M Tris.HCl, pH9.5, 0.1 M $MgCl_2$, 0.1% Tween-20, 2 mM levamisole) revealed digoxigenin-labeled neurons as somata containing dark purple precipitants. Immunohistochemistry for pSer40TH was performed as previously described (Nedoboy et al., 2016).

Quantitative PCR (qPCR) for PACAP and NMDA Receptors

RNA extractions were carried out using Direct-zol Miniprep (Zymoresearch, R2050) kit according to recommendations. Only RNA samples with an optical densiometry 260–280 nm absorption ratio higher than 1.95 were used. Total RNA (50 ng) was reverse transcribed into cDNA in a 40 μl reaction. The resulting reverse transcription products were used in subsequent real-time qPCR experiments for the quantification of mRNA expression of PACAP and NMDA receptors. The reference gene was hypoxanthine guanine phosphoribosyl transferase (HPRT) which is reliably expressed under hypoxic conditions (Yao et al., 2012). Primers for PAC1, vasoactive intestinal peptide receptor types 1 and 2 (VPAC1, and VPAC2, respectively) were used previously (Farnham et al., 2012). All primers were designed using Primer 3 software based on published gene sequences. The sequences and properties of each primer pair are shown in **Table 3**.

Real-time qPCR. Each reaction for real-time qPCR experiments contained 2 μl of reverse transcription product, 400 nM of each primer, and 12.5 μl of the 2× Platinum SYBR Green qPCR Master Mix (Qiagen), made up to 26.5 μl with sterile Milli-Q water. After a 95°C denaturation for 10 min, the reactions were cycled 40 times with a 95°C denaturation step for 30 s and 55°C combined annealing and extension step for 1 min with a single fluorescence measurement. A dissociation curve cycle (95°C -1 min, 55°C -30 s, 95°C -30 s) was conducted after the final cycle to verify that only the specific product was amplified.

All qPCR experiments were set up using the relative standard curve method. Samples from six animals from each group were run in duplicate. Results were obtained, normalized and analyzed as described by us previously (Farnham et al., 2012).

Imaging and Analysis

Sections of the brainstem extending from the caudal pole of the facial nucleus (Bregma -11.6 mm) to the caudal C1/A1 region were examined under both bright-field and fluorescence conditions (AxioImager Z1, Zeiss, Germany). Cells were counted within the RVLM bilaterally on five sections spaced 200 μm apart, extending from Bregma -11.6 mm caudally to Bregma -12.7 mm by operators blinded to the treatment conditions. The RVLM was defined as a triangular area ventral to the nucleus ambiguus, medial to the spinal trigeminal tract and lateral to the inferior olive or the pyramidal tracts. Once all counts were completed and verified, the conditions were unblinded, and the results were plotted as the mean ± SEM at 200 μm intervals. Counts were made for $PACAP^+$, TH-ir, pSer40TH-ir, and Fos-ir neurons as well as all double- and triple- labeling combinations.

TABLE 2 | Drug information for intermittent administration.

Drug	Concentration	Dose	Site of delivery	Company
Glutamate	100 mM	5 nmol	RVLM	Sigma
PBS	10 mM	100 nmol 500 pmol	Intrathecal RVLM	Sigma
PACAP-38	10 μM	100 pmol	Intrathecal	Auspep Pty. Ltd., Australia
Vasoactive intestinal polypeptide (VIP)	10 μM	1 nmol	Intrathecal	Auspep Pty. Ltd., Australia

TABLE 3 | Sequences and properties of gene-specific real-time qPCR primers.

Gene	Genebank accession no.	Sequence (5′–3′)	Amplicon size (bp)
HPRT 1	NM_012583	(+) GCTTTCCTTGGTCAAGCAGT (-) TCCAACAAAGTCTGGCCTG	103
PAC1	NM_133511	(+) TCTTGAATGGGGAGGTACAGG (-) TCTTGCTCAGGATGGACAGC	150
VPAC1	NM_012685	(+) CAGCAAGATGTGGGACAACC (-) TGCTGCTCATCCAGACTCG	216
VPAC2	NM_017238	(+) CCGAGGATGAGAGTAAGATCACG (-) AGATGGCTCTCAGCATGAAGG	183
NR1a	NM_017010	(+) ACGGGAGTCCAAGGCAGAGA (-) TCGCTTGCAGAAAGGATGAT	117

Images were captured in grayscale with an Axiocam MR3 digital camera. Pseudocoloring was applied to the fluorescence images. The images were adjusted individually for brightness and contrast with Axiovision 4.5 software to best reflect the appearance of the original images.

RESULTS

PACAP Acting at PAC1 Receptors at the Level of the Spinal Cord Is Necessary for the Sympathetic Response to AIH

To determine the physiological relevance of PACAP signaling during AIH, a sub-threshold dose (3 nmol) of PACAP (Farnham et al., 2011) 10 min prior to AIH was administered intrathecally. PACAP pre-treatment nearly doubled the sympathetic response 60 min after the 10th hypoxic challenge (n = 13; Δ62.3 ± 7.2%; ANOVA with Holm- Šidák correction P = 0.02; **Figures 1A,B**), compared to AIH alone (Δ37.2 ± 8.0%). PACAP was necessary for the AIH-induced sympathoexcitation, since the PACAP antagonist, PACAP(6–38) (10 nmol) completely abrogated this response (Δ3.2 ± 2.7%; ANOVA with Holm- Šidák correction P = 0.003; **Figures 1A,B**). PACAP(6–38) acts primarily at PAC1, does not act at VPAC1, but can have some antagonist effects at VPAC2 receptors (Dickinson et al., 1997).

To further clarify which receptor was responsible for mediating this response, the AIH protocol was conducted in PAC1 and VPAC2 receptor knockout mice and their wildtype littermate controls (Farnham et al., 2015). Strikingly, AIH did not cause an elevation of sympathetic activity in PAC1$^{-/-}$ mice (n = 3; Δ-19.0 ± 12.9%; ANOVA with Holm-Šidák correction P = 0.047 compared to wild-type; **Figures 1C,D**). A limitation should be noted here that due to the difficulty in breeding PAC1$^{-/-}$ mice only 3 mice were available for this study. However, the sympathetic response to AIH of heterozygous PAC1$^{+/-}$ mice (n = 5; Δ35.3 ± 9.3%; **Figures 1C,D**) was indistinguishable from that of the wildtype mice (PAC1$^{+/+}$: n = 6; Δ33.8 ± 13.3%; ANOVA with Holm- Šidák correction P = 0.93), and the rat model described in **Figures 1A,B**. In contrast, deletion of the VPAC2 receptor (VPAC2 $^{-/-}$) did not affect AIH-induced sympathoexcitation (n = 6; Δ48.3 ± 3.7%; **Figure 1C**), which was comparable to the wildtype (VPAC2$^{+/+}$: n = 8; Δ35.6 ± 10.6%; ANOVA with Holm- Šidák correction P = 0.63; **Figure 1C**). Taken together, these rat and mouse results suggest that the sympathetic long term facilitation (LTF) response to AIH is caused by activation of the PAC1 receptor.

Intermittent PACAP Acting at PAC1 Receptors in the Spinal Cord, Is Sufficient to Cause LTF in the Absence of AIH

Next, we determined if intermittent PACAP can elicit a sympathetic response qualitatively similar to that seen following AIH. First, determined if PACAP was sufficient to cause sympathoexcitation by administering 10 intermittent doses (100 pmol) of PACAP (to a total dose of 1 nmol that was well below threshold for a sympathetic response when delivered as a bolus (Farnham et al., 2011). Each 10 μl infusion was delivered at a 5 min interval (n = 9). This protocol evoked sympathoexcitation (Δ35.8 ± 6.2%; **Figures 1E,F**) to a level that was similar to that observed following AIH. The results demonstrate that intermittent administration of PACAP alone, at a sub-threshold dose at the level of the spinal cord, is sufficient to cause marked sympathoexcitation. Importantly, pre-treatment with the PACAP antagonist [10 nmol PACAP(6–38)] prior to intermittent PACAP significantly reduced (n = 6; Δ14.9 ± 3.2%; ANOVA with Holm-Šidák correction P = 0.04 **Figures 1E,F**) the sympathoexcitatory response to intermittent PACAP. On the other hand, intermittent application of VIP (1 nmol; a VPAC1/2 agonist) did not affect sympathetic activity (n = 7; Δ1.3 ± 5.9%; **Figures 1E,F**) and was equivalent to intermittent infusion of PBS (vehicle control; n = 8; Δ7.7 ± 2.2%; ANOVA with Holm- Šidák correction P = 0.90; **Figures 1E,F**). These data demonstrate that PACAP, acting at the PAC1 receptor, mediates the sympathoexcitatory response.

Fos, PACAP and NMDA1a Receptor Expression, in Rat RVLM, Is Unaltered by AIH, but pSer40TH Expression Is Elevated

Previously we showed that the 80% of spinally projecting, TH neurons contain PACAP mRNA (Farnham et al., 2008) suggesting that the source of the AIH-induced PACAP in the spinal cord is from the presympathetic RVLM neurons. To determine which neurons in the RVLM are activated during AIH, we subjected sodium pentobarbitone anaesthetized rats, to the AIH protocol (n = 4). Sodium pentobarbitone was used because urethane is well known to cause substantial Fos expression in the absence of any challenge. Control rats (n = 4) were prepared in the same way but did not undergo the AIH protocol. After the experiment, rats were perfused, and the brains removed. Sections were processed for PACAP mRNA *in situ* hybridization, TH-immunoreactivity (ir) and Fos-ir. Somewhat surprisingly, AIH did not cause an increase in the numbers of neurons expressing Fos in the RVLM (304 ± 41 vs. 265 ± 24; Unpaired t-test P = 0.45) but this was also reported by another group (Herr et al., 2013). There was also no change in Fos expression within the TH population (41 ± 10 vs. 43 ± 6; Unpaired t-test P = 085; **Figure 2A**) or the PACAP population (81 ± 18 vs. 100 ± 6; Unpaired t-test P = 0.36). There was also no change in PACAP receptor mRNA or NMDA1a receptor mRNA collected from RVLM punches of rats that had undergone AIH (n = 6), intrathecal PACAP prior to AIH (n = 6), intrathecal PACAP antagonist prior to AIH (n = 6), intrathecal intermittent PACAP (n = 6) and intrathecal intermittent PBS (n = 6); quantitative real-time PCR (qPCR), data not shown.

To approach the question of neuronal activation from a different angle we used an antibody that we developed against TH that was phosphorylated at Serine 40 and showed a spatial expression pattern, different to TH, after 2 h of hypotension (Nedoboy et al., 2016), suggesting that it may be an alternative marker of activation of catecholaminergic

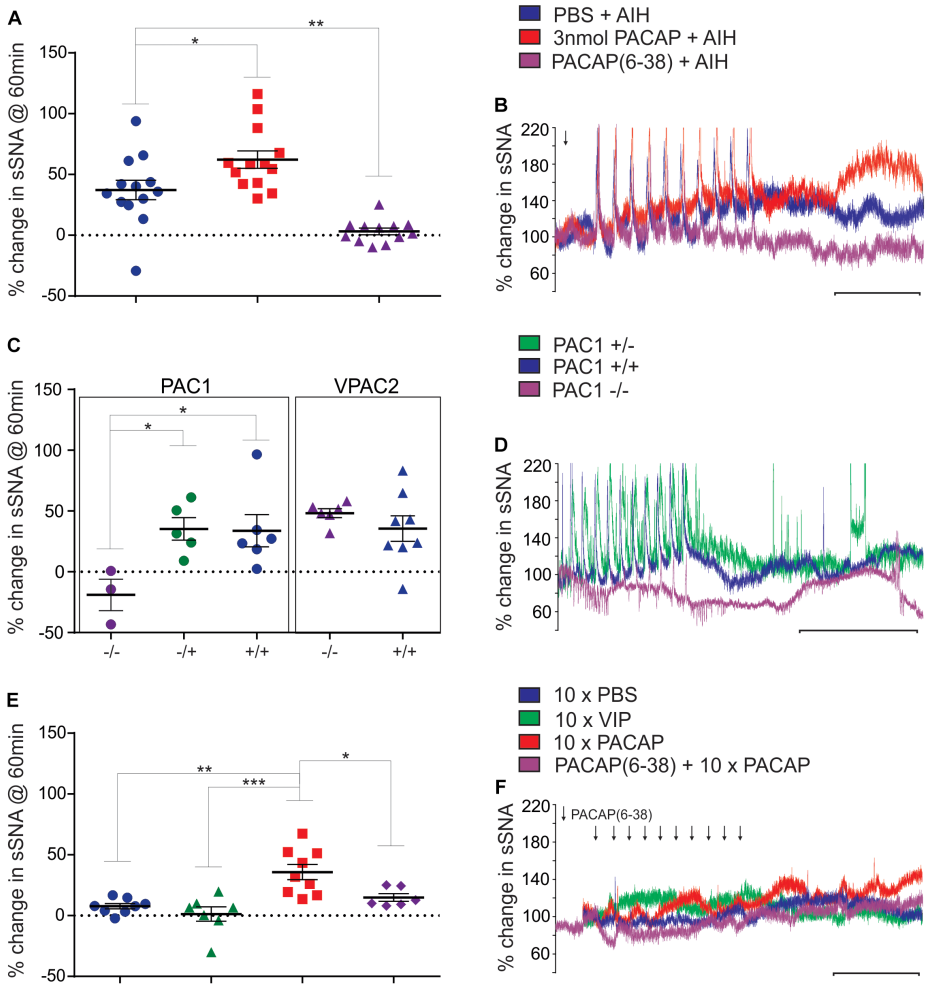

FIGURE 1 | Acute intermittent hypoxia and PAC1 receptor activation causes persistent sympathoexcitation. **(A)** Grouped data (rat) showing the sympathetic response 60 min following AIH treatments after either: intrathecal infusion of PBS (vehicle), 3 nmol PACAP or 10 nmol PACAP(6–38). PACAP (3 nmol) nearly doubles the response to AIH, while the antagonist abolishes the response to AIH. **(B)** Integrated traces of splanchnic nerve recordings (rat) showing the effect of intrathecal infusion of PBS (vehicle), 3 nmol PACAP or 10 nmol PACAP(6–38) and AIH on sympathetic nerve activity. Arrow indicates time of intrathecal infusion. **(C)** Grouped data showing the sympathetic response 60 min following AIH treatment in PAC1 and VPAC2 mouse strains. The PAC1 knockout mouse does not have a sympathetic response to AIH, whereas the PAC1 heterozygous and wild-type strains show a normal response to AIH, as do the VPAC2 strains. **(D)** Splanchnic nerve recordings (mouse) showing the effect of AIH. **(E)** Grouped data (rat) showing the sympathetic response 60 min following intermittent treatments of PBS (vehicle), 1 nmol VIP, 100 pmol PACAP or 10 nmol PACAP(6–38) + intermittent 100 pmol PACAP. Intermittent PACAP, but not VIP, causes a persistent sympathetic response, similar to that seen following AIH. The response to intermittent PACAP is significantly reduced by prior administration of the PACAP antagonist. **(F)** Integrated traces of splanchnic nerve recordings (rat) showing the effect of intermittent intrathecal infusion of PBS (vehicle), 1 nmol VIP, 100 pmol PACAP or 10 nmol PACAP(6–38) + intermittent 100 pmol PACAP on sympathetic nerve activity. In **(B,D,F)** the scale bar represents 30 min and arrows indicate time of intrathecal infusion. $^{*}P < 0.05$, $^{**}P < 0.01$, $^{***}P < 0.001$.

neurons. Since expression of phosphorylated TH is unaffected by urethane anaesthesia, and to match the anatomy with the experimental condition used for the physiological results, we performed the AIH protocol (n = 3) and compared it with control (n = 3) on another set of urethane-anaesthetized rats for immunoreactivity to TH and pSer40TH (**Figure 2C**). In the control state we found that 28% of TH neurons in the RVLM were phosphorylated (serine40) as described previously (Nedoboy et al., 2016). AIH had no effect on the overall number of TH or PACAP positive neurons but increased the number of phosphorylated TH (pSer40TH) neurons (of which 41% are PACAP expressing) by 93% (48 ± 9 vs. 92 ± 10 neurons; Unpaired t-test P = 0.005; **Figure 2B**). When focused on the TH and pSer40TH populations we found that 27% of TH neurons expressed pSer40TH in the control condition and this doubled to 58% following AIH (unpaired t-test P < 0.0001; **Figure 2C**). Likewise, 11% of TH neurons contained both pSer40TH and PACAP mRNA under control conditions, which doubled to 22% following AIH (Unpaired t-test P = 0.009; **Figures 2C,D**) indicating that the PACAP neurons in the RVLM may be being activated.

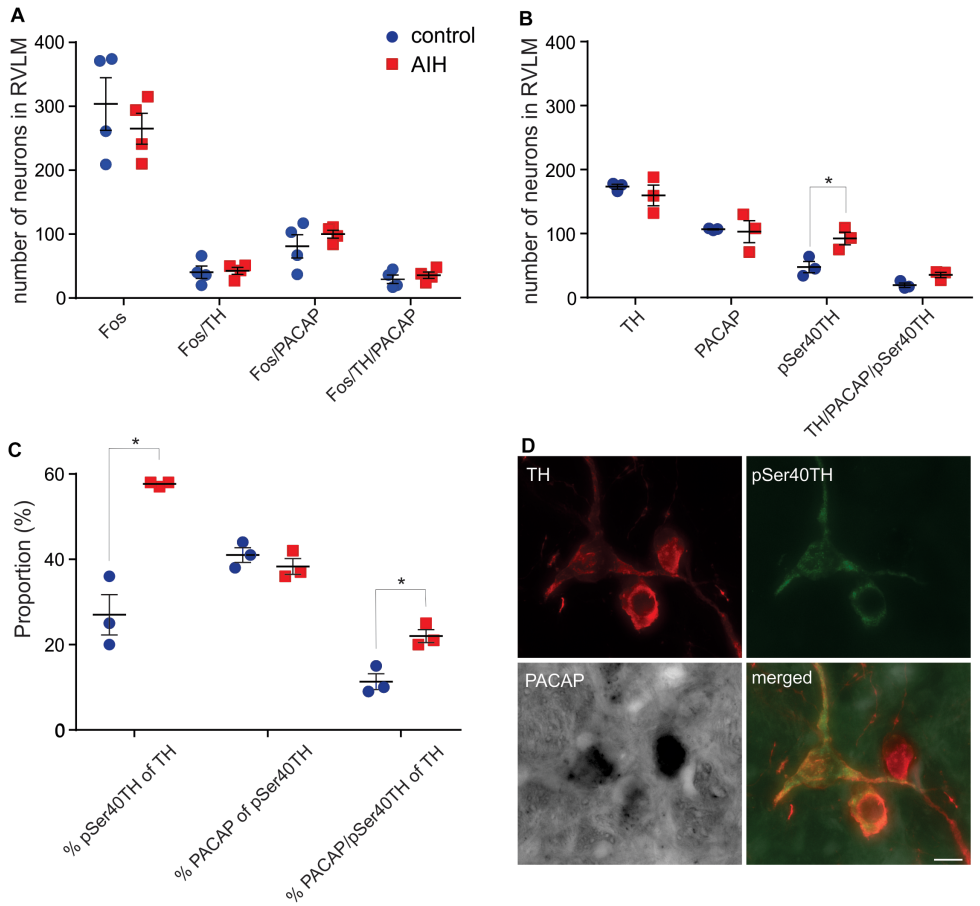

FIGURE 2 | C1 neurons in rat RVLM are activated by AIH. **(A)** Mean ± SEM number of neurons in RVLM stained for Fos, TH and PACAP mRNA 60 min after control (n = 4) or AIH (n = 4). There are no differences in Fos staining, in any population, between the two treatment groups. **(B)** Neurons in RVLM (mean ± SEM) stained for pSer40TH, TH and PACAP mRNA 60 min after control (n = 3) or AIH (n = 3). Number of neurons expressing pSer40TH doubled in the AIH treated group compared to control. **(C)** The data from **(B)** is expressed as proportion of TH or pSer40TH populations. AIH caused a doubling in the proportion of TH neurons that also expressed pSer40TH (27 ± 5% vs. 58 ± 0.3%) and a doubling in the proportion of TH neurons that also contained pSer40TH and PACAP mRNA. **(D)** Micrographs with 3 neurons, from an AIH treated rat, stained for TH, pSer40TH and PACAP mRNA, and a merged image. All 3 TH neurons are positive for PACAP mRNA but only 2 are pSer40TH positive. RVLM – rostral ventrolateral medulla. Scale bar represents 10 μm. *P < 0.05.

Intermittent Activation of RVLM Neurons Is Sufficient to Cause Sympathoexcitation in the Absence of AIH and Is Dependent on PACAP Release in the Spinal Cord

We next determined if neurons in the RVLM, including C1 neurons that project to the spinal cord, are responsible for the PACAP-mediated effects described above. Since TH in C1 neurons was phosphorylated in response to AIH, demonstrating an increase in activation, we aimed to determine if the sympathetic response to AIH was due specifically to the effects of hypoxia, or more generally due to intermittent stimulation of sympathoexcitatory pathways. We found that intermittent microinjection of glutamate (5 nmol) into the RVLM caused persistent sympathoexcitation (n = 5; Δ64.1 ± 11.5%; ANOVA with Holm- Šidák correction P = 0.005; **Figure 3A**), compared to intermittent microinjection of PBS (n = 4; Δ-3.0 ± 2.5%; **Figure 3A**) as described previously (Kakall et al., 2018). This sympathetic response was qualitatively similar to that induced by AIH. Significantly, the RVLM-glutamate induced sympathoexcitation was abolished by prior intrathecal infusion of the PACAP antagonist (10 nmol; n = 4; Δ7.7 ± 15.1%; ANOVA with Holm- Šidák correction P = 0.01; **Figure 3A**). In summary, the findings suggest that the persistent sympathoexcitation induced by AIH is due to intermittent activation of PACAP-containing bulbospinal sympathoexcitatory cardiovascular pathways and does not require direct effects of hypoxia on sympathetic neurons.

Sympathoexcitation Following AIH Is Mediated by cAMP

Finally, we determined if the sympathoexcitation following AIH is mediated through cAMP signaling pathway as the PAC1 receptor is primarily coupled to cAMP via Gαs

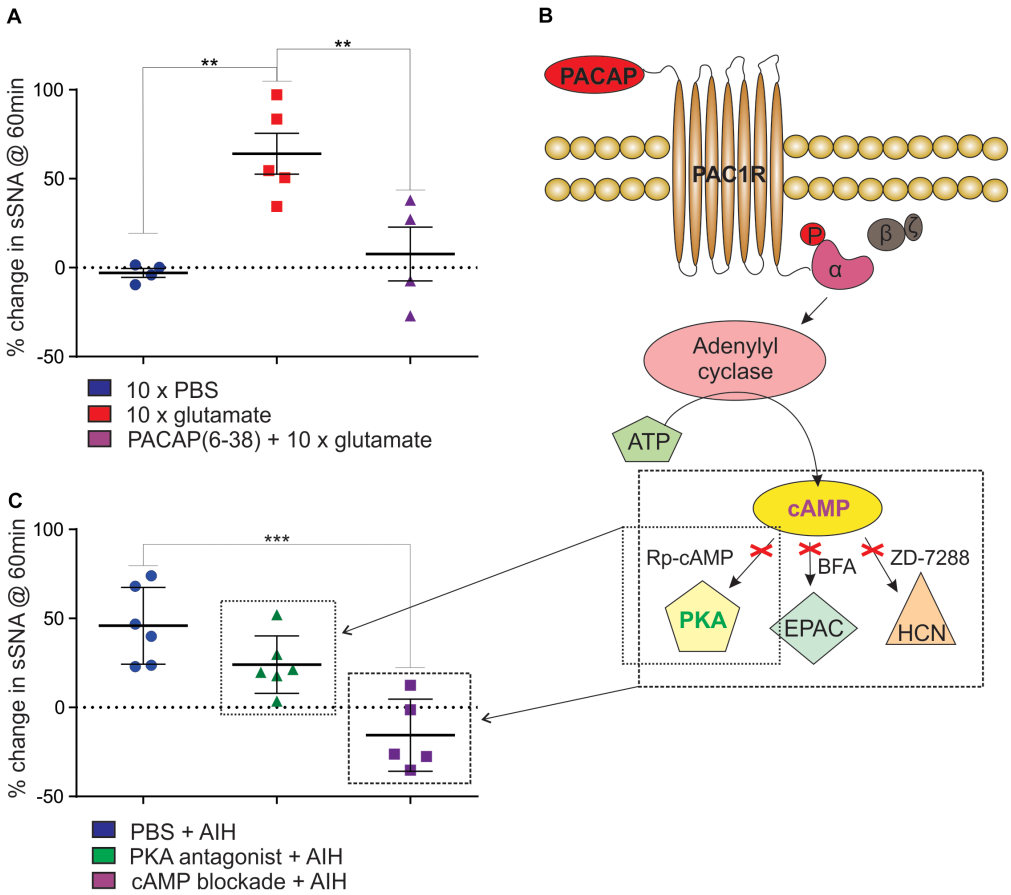

FIGURE 3 | Intermittent activation of rat RVLM mimics AIH, mediated by PACAP in a cAMP-dependent manner. **(A)** Intermittent injections of 5 nmol glutamate in the RVLM cause a persistent increase in sympathetic nerve activity, which does not occur after intermittent injection of the vehicle control, PBS. The sympathetic response following intermittent glutamate injections is abolished by prior intrathecal infusion of the PACAP antagonist, 10 nmol PACAP(6–38). **(B)** An illustration of the intracellular signaling pathway used by PACAP. When PACAP binds to the PAC1 G-protein coupled receptor, the α-subunit of the G-protein is phosphorylated ("P"), adenylyl cyclase is then activated causing the conversion of ATP into cAMP. cAMP acts at 3 downstream effector proteins, Protein Kinase A (PKA), Exchange Protein Activated by cAMP (EPAC) and hyperpolarization-activated cyclic nucleotide-gated (HCN) channels. The activity of cAMP can be blocked by using a cocktail of 1μmol Rp-Diastereomer of Adenosine 3′,5-Cyclic Monophosphorothioate (Rp-cAMP), 10 nmol Brefeldin A (BFA) and 30 nmol 4-(N-Ethyl-N-phenylamino)-1,2 dimethyl-6-(methylamino)pyrimidium chloride (ZD-7288) to block the three downstream effector proteins. **(C)** When PKA alone is blocked using 1 μmol Rp-cAMP (small box in **B**) there is no significant reduction in the response to AIH. When cAMP is blocked with 1 μmol Rp-cAMP, 10 nmol BFA and 30 nmol ZD-7288 (large box in **B**), the sympathetic response to AIH is abolished. $^{**}P < 0.01$, $^{***}P < 0.001$.

(Vaudry et al., 2000). As there is no single pharmacological blocker of cAMP we intrathecally administered a combination of antagonists to the downstream effector proteins of cAMP – PKA, EPAC, and HCN channels at previously described concentrations (Tallapragada et al., 2016). Administration of the antagonists had no effect on resting sympathetic tone prior to AIH and had no effect on the responses to each hypoxic bout. We found that blocking the cAMP pathway (1 μmol Rp-cAMP + 10 nmol BFA + 30 nmol ZD-7288; **Table 1** and **Figure 3B**) abolished the sympathetic response to AIH ($n = 5$; Δ-15.6 ± 9.0%; ANOVA with Holm- Šidák correction $P = 0.0003$; **Figure 3C**) compared to AIH alone. As PKA is the primary effector of cAMP we also administered the PKA blocker (1 μmol Rp-cAMP) on its own prior to AIH ($n = 6$), but did not find any significant change in the sympathetic response to AIH (Δ24.0 ± 6.6%; ANOVA with Holm- Šidák correction $P = 0.14$; **Figure 3C**), suggesting that although the response requires cAMP, it is not solely dependent on the PKA pathway.

All Increases in Sympathetic Activity Following Intermittent Stimulation of Cardiovascular Areas Occur in the Absence of Any Changes in Blood Pressure, pH or $PaCO_2$

A short duration of intermittent hypoxia (i.e., AIH) is known to cause increased sympathetic activity without any change in mean arterial pressure (Dick et al., 2007; Xing and Pilowsky, 2010) a result confirmed here (**Table 4**). Changes in pH and $PaCO_2$ can also affect sympathetic nerve activity and confound the results. Blood gases were monitored throughout the experiments (except for the mice, as the blood volume is too small) to

ensure that the increases in sympathetic nerve activity observed following AIH were not due to the stimulatory effects of CO_2. **Table 4** shows that $PaCO_2$ and pH were within the physiological range at the end of the recording period for all treatment groups.

DISCUSSION

We report here for the first time that the sympathoexcitation caused by AIH is likely mediated, at least in part, by central neuroplasticity involving PACAP acting on PAC1 receptors in the spinal cord. Our results support that of Xing and Pilowsky (2010), with the increase in SNA occurring without any significant change in MAP, $PaCO_2$, or pH. Mimicking the response seen after AIH, sub-threshold intermittent intrathecal PACAP alone is sufficient to generate a prolonged sympathetic response, as is intermittent activation of the RVLM with glutamate (Kakall et al., 2018). Using pharmacological agents and PACAP receptor knockout mice, we demonstrate that the sympathetic response to AIH is mediated via spinal PAC1 receptors and dependent on cAMP.

Sustained hypertension is a serious disorder with devastating individual and community consequences that include: vascular disease, heart failure and stroke. Hypertension is usually associated with elevated sympathetic nerve activity (SNA) and increased activity of presympathetic neurons in the RVLM (Chan et al., 1991; Minson et al., 1996). An outstanding question in this field is, how do sympathetic pathways and their neurotransmitter systems cause this persistent change? One hypothesis lies in the pattern of neurotransmitter signaling.

Intermittent activation of neuronal pathways is more potent in enhancing neuronal activity and having long term consequences than continuous activation (Fuller et al., 2003; Kumar et al., 2006; Peng et al., 2009; Roy et al., 2018); phenomena that are the basis for memory formation and are well-known at the behavioral (gambling) and cellular (long-term potentiation) levels, but relatively uncharacterized in cardiovascular control. Yet, repetitive, intermittent hypoxic events are the hallmark of OSA which is characterized by persistent sympathoexcitation and now regarded as the leading cause of secondary hypertension (Pedrosa et al., 2011).

While the pathophysiology of sympathoexcitation and hypertension in OSA are not completely understood, current evidence suggests there are multiple sites contributing to the persistent effects of intermittent hypoxia. For example, intermittent hypoxia with concurrent hypercapnia acts at the carotid body to cause robust increases in afferent activity to the brain which is also reflected in the long-lasting sympathetic output (Roy et al., 2018). This activity is dependent on TRPV1 and P2X receptors. Other long term effects of intermittent hypoxia appear to involve reactive oxygen species (Prabhakar et al., 2012), angiotensin (Kim et al., 2018), and serotonin (Ling et al., 2001) to name a few. Intermittent stimulation of the RVLM also causes a persistent sympathoexcitation (Kakall et al., 2018), but what has remained elusive is the identity of the final central output driving the increase in sympathetic activity.

TABLE 4 | MAP and metabolic parameters were unchanged 60 min after intermittent stimulation.

Treatment group	N (animals)	Baseline MAP (mean ± SEM)	Change in MAP (mean ± SEM) @ 60 min	pH @ 60 min	$PaCO_2$ @ 60 min
RAT SPINAL CORD STUDIES					
PBS + AIH	13	88 ± 5	6 ± 2	7.42 ± 0.01	39 ± 2
3 nmol PACAP + AIH	13	95 ± 4	3 ± 3	7.42 ± 0.01	40 ± 1
PACAP(6–38) + AIH	12	97 ± 4	−5 ± 5	7.41 ± 0.01	40 ± 1
10 × PBS	8	95 ± 3	−2 ± 3	7.41 ± 0.01	40 ± 2
10 × PACAP	9	95 ± 6	0 ± 4	7.40 ± 0.01	40 ± 2
10 × VIP	7	98 ± 3	−4 ± 4	7.41 ± 0.01	41 ± 2
PACAP(6–38) + 10 × PACAP	6	104 ± 2	−5 ± 3	7.45 ± 0.03	37 ± 2
RAT RVLM STUDY					
10 × PBS	4	118 ± 8	−18 ± 6	7.41 ± 0.01	43 ± 1
10 × glutamate	4	101 ± 4	−3 ± 3	7.44 ± 0.002	41 ± 1
PACAP(6–38)+10 × glutamate	4	106 ± 9	−11 ± 5	7.44 ± 0.01	42 ± 2
RAT CAMP STUDY					
PBS + AIH	6	101 ± 4	0 ± 8	7.41 ± 0.01	42 ± 1
cAMP block + AIH	5	103 ± 6	0 ± 5	7.45 ± 0.01	38 ± 2
PKA block + AIH	6	110 ± 8	2 ± 5	7.42 ± 0.04	40 ± 1
MOUSE STUDY					
PAC1 +/+	5	58 ± 5	−2 ± 3	–	–
PAC1 l'	5	61 ± 5	−11 ± 4	–	–
PAC1 -/-	3	45 ± 5	−5 ± 3	–	–
VPAC2 +/+	7	70 ± 6	−15 ± 4	–	–
VPAC2 -/-	5	57 ± 2	−7 ± 4	–	–

PACAP is found almost unchanged in every vertebrate species examined (Hannibal, 2002; Vaudry et al., 2009) and is generally excitatory. PACAP binds to three G-protein coupled receptors, PAC1, VPAC1, and VPAC2 (all of which have many splice variants). The PACAP receptors are primarily coupled to either Gαs or Gαq and activate the cAMP pathway to exert short- and long- term changes in neuronal activity and gene expression (Farnham and Pilowsky, 2010; Harmar et al., 2012). The presence of PACAP and its receptors throughout the cardiorespiratory sympathetic circuit, from the carotid body (Roy et al., 2013) and RVLM, to sympathetic post-ganglionic neurons and the adrenal medulla in the periphery, indicates that this peptide plays an important role in blood pressure regulation (Farnham and Pilowsky, 2010). Consistent with a role in blood pressure regulation, activation of PACAP receptors regulate catecholamine gene expression (Hong et al., 1998; Choi et al., 1999; Park et al., 1999; Borba et al., 2005), TH activity which is rate limiting for noradrenaline (and adrenaline) synthesis (Tonshoff et al., 1997; Hamelink et al., 2002; Bobrovskaya et al., 2007), and release of acetylcholine at neuronal nicotinic synapses (Pugh et al., 2010). Our finding that AIH increased the number of phosphorylated TH neurons in the RVLM is consistent with this literature and may explain why antagonism of RVLM PACAP receptors blocked the intermittent glutamate-induced sympathoexcitation (Kakall et al., 2018). Interestingly, while AIH increased the number of phosphorylated TH neurons in the RVLM within 60 min, the number of Fos positive neurons over the same time window was unchanged. This indicates that pSer40TH may be a more precocious, sensitive and/or persistent marker of neuronal activation in the C1 population than Fos.

Notwithstanding a role for PACAP signaling in the RVLM, the results herein suggest that the sympathoexcitation observed following AIH is due, at least in part, to PACAP triggering additional plastic changes via spinal PAC1 receptors. Specifically, our data demonstrate that persistent sympathoexcitation can be induced by AIH *and* intermittent stimulation of the RVLM in the absence of hypoxic events; and in both cases, sympathoexcitation is dependent upon activation of PAC1 receptors in the spinal cord. Moreover, the similarity of the time-course of action of PACAP on SNA when administered intermittently into the spinal cord with the time-course of the response to AIH, and the finding that blocking spinal PACAP receptors abolishes this response, highlights the likely importance of spinal PACAP signaling in this physiological condition. Accordingly, PACAP-mediated plasticity in the spinal cord might further exacerbate and prolong neuronal excitability caused by plasticity in the carotid body and RVLM, giving rise to long term sympathoexcitation which, in turn, may contribute significantly to the hypertension that accompanies OSA.

Indeed, PACAP may be an important mediator of the hypertensive response observed in OSA. Whereas AIH causes sympathoexcitation without any change in blood pressure, experimental CIH – a well-established model for sleep apnoea – causes hypertension which is accompanied by increased noradrenaline release from the adrenal medulla (Kumar et al., 2006). In this respect, we note that a high dose of intrathecal PACAP can elevate blood pressure directly by activating PAC1 receptors on SPN innervating noradrenaline-secreting adrenal medulla chromaffin cells (Inglott et al., 2012) and that PACAP knockout mice, a proposed model of Sudden Infant Death Syndrome (SIDS) with blunted cardiorespiratory responses to hypoxia (Cummings et al., 2004), also have reduced TH expression (Arata et al., 2013).

Neurons or Glia?

PACAP receptors are present on blood vessels, microglia, astrocytes, and neurons, and therefore the question arises, which of these cell types mediates the reported effects? The cerebral and pial vasculature primarily expresses VPAC1 receptors (Fahrenkrug et al., 2000) which are unaffected by PACAP(6–38), and are therefore unlikely to contribute to the PACAP-mediated sympathetic responses to AIH. Microglia are also unlikely to contribute for several reasons: (1) Activation of microglial VPAC1 and PAC1 receptors *reduce* the severe cardiovascular consequences of acute kainic acid-induced seizure (Delgado et al., 2002; Bhandare et al., 2015; Bhandare et al., 2016). This contrasts with PACAP-mediated *prolongation* of the milder cardiovascular consequences of AIH. (2) Only a fraction of microglia (1–20%) respond to neuropeptides, even when in an activated state (Pannell et al., 2014). (3) Even in chronic conditions of intermittent hypoxia the activation state and function of microglia is unclear (Kiernan et al., 2016). Therefore, the effects we see in our AIH model following activation or blockade of PAC1 receptors are unlikely due to activation of microglia.

Astrocytes may have a role in PACAP-mediated sympathetic responses to AIH because they are important for maintaining long lasting PACAP-induced dorsal horn-mediated neuropathic pain (Yokai et al., 2016). However, only a few astrocytes express PAC1 receptors (Yokai et al., 2016). Thus, while astrocytes may have an indirect role, PACAP receptors on neurons remain the most likely mediators of long-term sympathetic responses to AIH.

Technical Considerations

Our electrophysiological data are drawn from an anesthetized and vagotomized preparation used widely to study sympathetic activity. Indeed, there were good reasons for each of these conditions. Urethane was used to ensure the preparation stability required to maintain long term (>2 h) splanchnic nerve recordings; vagotomy prevented sensory information from lung stretch receptors caused by mechanical ventilation; and we cut the splanchnic nerve distal to the recording electrode to ensure only efferent (sympathetic) activity was monitored. Nonetheless, each of these maneuvers may have caused unforeseen effects on sympathetic activity, such as accentuating the short or long-term effects of hypoxia. The effects of the surgical preparation may also have affected Fos expression, thereby masking any AIH-induced changes.

Another important caveat is that infusion of solutions into the intrathecal space creates the risk of diffusion of the solution back up the spinal cord, to the RVLM. To minimize this risk, we used small injection volumes, positioned the animals with their heads elevated in relation to the thoracic spinal cord and, in previous studies, used dye and spinal cord transections to confirm that

diffusion to the brainstem does not occur (Inglott et al., 2011). In addition, as PACAP is rapidly broken down by dipeptidyl peptidase IV (DPP-IV) with a half-life ∼ 2 min (Zhu et al., 2003) and DPP-IV is expressed in the CSF (Kato et al., 1979), we judge the possibility of intrathecal PACAP diffusing to, and activating, the RVLM as being highly unlikely.

CONCLUSION

The PACAP signaling system may be a useful therapeutic target, not only for sleep apnoea sufferers, but in other conditions of repetitive insults, as persistent sympathoexcitation was generated in the absence of intermittent hypoxia. Little is known about neuroplasticity in the cardiovascular system and further information is vital if we are to understand disorders such as sleep apnoea, that cause hypertension leading to target organ damage, heart failure, vascular disease, renal failure and stroke. A better understanding of how different neurotransmitters operate in central cardiorespiratory pathways will lead to precision-targeted and effective treatments for many autonomic disorders including sleep-apnoea-induced hypertension.

DATA AVAILABILITY

The raw data supporting the conclusions of this manuscript will be made available by the authors, without undue reservation, to any qualified researcher.

ETHICS STATEMENT

Animal Subjects: The animal study was reviewed and approved by the Sydney Local Area Health District Animal Care and Ethics Committee, Macquarie University Animal Care and Ethics Committee, and University of Calgary Animal Care and Ethics Committee.

AUTHOR CONTRIBUTIONS

MF, PP, and RW designed the experiments, interpreted the results, and prepared the manuscript. MF, AF, and ML performed the Fos study. BD acquired all the microscopic images for the Fos study and performed the initial count, which was verified by VT and analyzed by MF. MF and VT performed and analyzed the AIH and intermittent drug experiments in rat. SM performed, analyzed, and interpreted the quantitative real-time PCR experiments, and designed and constructed the PACAP riboprobes for *in situ* hybridization. MF and EO'C performed and analyzed the AIH experiments in mice. MF and PN performed and analyzed the TH/pSer40TH data and, with FD, the intermittent glutamate data. MF and PN prepared the figures. All authors critically reviewed and commented on the manuscript.

FUNDING

Work performed in the authors laboratories was supported by the ARC (DECRA; DE120100992), Heart Foundation (G 11S 5957), NHMRC (1082215, 1065485, 1024489, and 457080), Macquarie University, the Heart Research Institute, CIHR, and AIHS.

ACKNOWLEDGMENTS

We thank Dr. L. Journot for providing the PAC1 receptor mice and Dr. A. Harmar (deceased) for providing the VPAC2 receptor mice.

REFERENCES

Arata, S., Nakamachi, T., Onimaru, H., Hashimoto, H., and Shioda, S. (2013). Impaired response to hypoxia in the respiratory center is a major cause of neonatal death of the PACAP-knockout mouse. *Eur. J. Neurosci.* 37, 407–416. doi: 10.1111/ejn.12054

Barrett, K. T., Daubenspeck, J. A., and Wilson, R. J. A. (2017). Pituitary adenylate cyclase-activating polypeptide drives cardiorespiratory responses to heat stress in neonatal mice. *Am. J. Physiol.* 313, R385–R394. doi: 10.1152/ajpregu.00118.2017

Bhandare, A. M., Kapoor, K., Pilowsky, P. M., and Farnham, M. M. (2016). Seizure-induced sympathoexcitation is caused by activation of glutamatergic receptors in RVLM that also causes proarrhythmogenic changes mediated by PACAP and microglia in rats. *J. Neurosci.* 36, 506–517. doi: 10.1523/JNEUROSCI.2584-15.2016

Bhandare, A. M., Mohammed, S., Pilowsky, P. M., and Farnham, M. M. (2015). Antagonism of PACAP or microglia function worsens the cardiovascular consequences of kainic-acid-induced seizures in rats. *J. Neurosci.* 35, 2191–2199. doi: 10.1523/JNEUROSCI.4058-14.2015

Bobrovskaya, L., Gelain, D. P., Gilligan, C., Dickson, P. W., and Dunkley, P. R. (2007). PACAP stimulates the sustained phosphorylation of tyrosine hydroxylase at serine 40. *Cell. Signal.* 19, 1141–1149. doi: 10.1016/j.cellsig.2006.12.006

Borba, J. C., Henze, I. P., Silveira, M. S., Kubrusly, R. C., Gardino, P. F., de Mello, M. C., et al. (2005). Pituitary adenylate cyclase-activating polypeptide (PACAP) can act as determinant of the tyrosine hydroxylase phenotype of dopaminergic cells during retina development. *Brain Res. Dev. Brain Res.* 156, 193–201. doi: 10.1016/j.devbrainres.2005.02.016

Bradley, T. D., and Floras, J. S. (2009). Obstructive sleep apnoea and its cardiovascular consequences. *Lancet* 373, 82–93. doi: 10.1016/s0140-6736(08)61622-0

Chan, R. K., Chan, Y. S., and Wong, T. M. (1991). Electrophysiological properties of neurons in the rostral ventrolateral medulla of normotensive and spontaneously hypertensive rats. *Brain Res.* 549, 118–126. doi: 10.1016/0006-8993(91)90607-w

Choi, H. J., Park, S. Y., and Hwang, O. (1999). Differential involvement of PKA and PKC in regulation of catecholamine enzyme genes by PACAP. *Peptides* 20, 817–822. doi: 10.1016/s0196-9781(99)00067-4

Coleman, C. G., Wang, G., Park, L., Anrather, J., Delagrammatikas, G. J., Chan, J., et al. (2010). Chronic intermittent hypoxia induces NMDA receptor-dependent plasticity and suppresses nitric oxide signaling in the mouse hypothalamic paraventricular nucleus. *J. Neurosci.* 30, 12103–12112. doi: 10.1523/JNEUROSCI.3367-10.2010

Cummings, K. J., Pendlebury, J. D., Sherwood, N. M., and Wilson, R. J. (2004). Sudden neonatal death in PACAP-deficient mice is associated with reduced respiratory chemoresponse and susceptibility to apnoea. *J. Physiol.* 555(Pt 1), 15–26. doi: 10.1113/jphysiol.2003.052514

Delgado, M., Jonakait, G. M., and Ganea, D. (2002). Vasoactive intestinal peptide and pituitary adenylate cyclase-activating polypeptide inhibit chemokine production in activated microglia. *Glia* 39, 148–161. doi: 10.1002/glia.10098

Dick, T. E., Hsieh, Y. H., Wang, N., and Prabhakar, N. (2007). Acute intermittent hypoxia increases both phrenic and sympathetic nerve activities in the rat. *Exp. Physiol.* 92, 87–97. doi: 10.1113/expphysiol.2006.035758

Dickinson, T., Fleetwood-Walker, S. M., Mitchell, R., and Lutz, E. M. (1997). Evidence for roles of vasoactive intestinal polypeptide (VIP) and pituitary adenylate cyclase activating polypeptide (PACAP) receptors in modulating the responses of rat dorsal horn neurons to sensory inputs. *Neuropeptides* 31, 175–185. doi: 10.1016/s0143-4179(97)90087-1

Fahrenkrug, J., Hannibal, J., Tams, J., and Georg, B. (2000). Immunohistochemical localization of the VIP1 receptor (VPAC(1)R) in rat cerebral blood vessels: relation to PACAP and VIP containing nerves. *J. Cereb. Blood Flow Metab.* 20, 1205–1214. doi: 10.1097/00004647-200008000-00006

Farnham, M. M., Inglott, M. A., and Pilowsky, P. M. (2011). Intrathecal PACAP-38 causes increases in sympathetic nerve activity and heart rate but not blood pressure in the spontaneously hypertensive rat. *Am. J. Physiol.* 300, H214–H222. doi: 10.1152/ajpheart.00662.2010

Farnham, M. M., Li, Q., Goodchild, A. K., and Pilowsky, P. M. (2008). PACAP is expressed in sympathoexcitatory bulbospinal C1 neurons of the brain stem and increases sympathetic nerve activity in vivo. *Am. J. Physiol.* 294, R1304–R1311. doi: 10.1152/ajpregu.00753.2007

Farnham, M. M., Lung, M. S., Tallapragada, V. J., and Pilowsky, P. M. (2012). PACAP causes PAC1/VPAC2 receptor mediated hypertension and sympathoexcitation in normal and hypertensive rats. *Am. J. Physiol.* 303, H910–H917. doi: 10.1152/ajpheart.00464.2012

Farnham, M. M., O'Connor, E. T., Wilson, R. J., and Pilowsky, P. M. (2015). Surgical preparation of mice for recording cardiorespiratory parameters in vivo. *J. Neurosci. Methods* 248, 41–45. doi: 10.1016/j.jneumeth.2015.03.038

Farnham, M. M., and Pilowsky, P. M. (2010). The role of PACAP in central cardiorespiratory regulation. *Respir. Physiol. Neurobiol.* 174, 65–75. doi: 10.1016/j.resp.2010.05.004

Ferguson, E. V., Roy, A., Ciechanski, P., and Wilson, R. J. (2013). Stress peptide PACAP stimulates and stabilizes neonatal breathing through distinct mechanisms. *Respir. Physiol. Neurobiol.* 187, 217–223. doi: 10.1016/j.resp.2013.04.009

Fletcher, E. C. (2001). Physiological and genomic consequences of intermittent hypoxia - Invited Review: physiological consequences of intermittent hypoxia: systemic blood pressure. *J. Appl. Physiol.* 90, 1600–1605. doi: 10.1152/jappl.2001.90.4.1600

Fuller, D. D., Johnson, S. M., Olson, E. B., and Mitchell, G. S. (2003). Synaptic pathways to phrenic motoneurons are enhanced by chronic intermittent hypoxia after cervical spinal cord injury. *J. Neurosci.* 23, 2993–3000. doi: 10.1523/jneurosci.23-07-02993.2003

Gaede, A. H., and Pilowsky, P. M. (2013). "Excitatory responses to microinjection of glutamate depend on dose not volume: a meta-analysis of studies in rat RVLM", in *Stimulation and Inhibition of Neurons. Neuromethods*, Vol.78 eds P. Pilowsky, M. Farnham, and A. Fong (Totowa, NJ: Humana Press), 141–150.

Hamelink, C., Tjurmina, O., Damadzic, R., Young, W. S., Weihe, E., Lee, H. W., et al. (2002). Pituitary adenylate cyclase-activating polypeptide is a sympathoadrenal neurotransmitter involved in catecholamine regulation and glucohomeostasis. *Proc. Natl. Acad. Sci. U.S.A.* 99, 461–466. doi: 10.1073/pnas.012608999

Hannibal, J. (2002). Pituitary adenylate cyclase-activating peptide in the rat central nervous system: an immunohistochemical and in situ hybridization study. *J. Comp. Neurol.* 453, 389–417. doi: 10.1002/cne.10418

Hannibal, J., Jamen, F., Nielsen, H. S., Journot, L., Brabet, P., and Fahrenkrug, J. (2001). Dissociation between light-induced phase shift of the circadian rhythm and clock gene expression in mice lacking the pituitary adenylate cyclase activating polypeptide type 1 receptor. *J. Neurosci.* 21, 4883–4890. doi: 10.1523/jneurosci.21-13-04883.2001

Harmar, A. J., Fahrenkrug, J., Gozes, I., Laburthe, M., May, V., Pisegna, J. R., et al. (2012). Pharmacology and functions of receptors for vasoactive intestinal peptide and pituitary adenylate cyclase-activating polypeptide: IUPHAR review 1. *Br. J. Pharmacol.* 166, 4–17. doi: 10.1111/j.1476-5381.2012.01871.x

Harmar, A. J., Marston, H. M., Shen, S. B., Spratt, C., West, K. M., Sheward, W. J., et al. (2002). The VPAC(2) receptor is essential for circadian function in the mouse suprachiasmatic nuclei. *Cell* 109, 497–508. doi: 10.1016/s0092-8674(02)00736-5

Herr, K. B., Stettner, G. M., and Kubin, L. (2013). Reduced c-Fos expression in medullary catecholaminergic neurons in rats 20 h after exposure to chronic intermittent hypoxia. *Am. J. Physiol.* 304, R514–R522. doi: 10.1152/ajpregu.00542.2012

Hong, M., Yon, L., Fournier, A., Vaudry, H., and Pelletier, G. (1998). Effect of pituitary adenylate cyclase-activating polypeptide (PACAP) on tyrosine hydroxylase gene expression in the rat adrenal medulla. *Ann. N. Y. Acad. Sci.* 865, 478–481. doi: 10.1111/j.1749-6632.1998.tb11220.x

Inglott, M. A., Farnham, M. M., and Pilowsky, P. M. (2011). Intrathecal PACAP-38 causes prolonged widespread sympathoexcitation via a spinally mediated mechanism and increases in basal metabolic rate in anesthetized rat. *Am. J. Physiol.* 300, H2300–H2307. doi: 10.1152/ajpheart.01052.2010

Inglott, M. A., Lerner, E. A., Pilowsky, P. M., and Farnham, M. M. (2012). Activation of PAC(1) and VPAC receptor subtypes elicits differential physiological responses from sympathetic preganglionic neurons in the anaesthetized rat. *Br. J. Pharmacol.* 167, 1089–1098. doi: 10.1111/j.1476-5381.2012.02045.x

Iturriaga, R., Moya, E. A., and Del Rio, R. (2010). Cardiorespiratory alterations induced by intermittent hypoxia in a rat model of sleep apnea. *Adv. Exp. Med. Biol.* 669, 271–274. doi: 10.1007/978-1-4419-5692-7_55

Jamen, F., Persson, K., Bertrand, G., Rodriguez-Henche, N., Puech, R., Bockaert, J., et al. (2000). PAC1 receptor-deficient mice display impaired insulinotropic response to glucose and reduced glucose tolerance. *J. Clin. Invest.* 105, 1307–1315. doi: 10.1172/jci9387

Kakall, Z. M., Pilowsky, P. M., and Farnham, M. M. J. (2018). PACAP-(6-38) or kynurenate microinjections in the RVLM prevent the development of sympathetic long-term facilitation after acute intermittent hypoxia. *Am. J. Physiol.* 314, H563–H572. doi: 10.1152/ajpheart.00596.2017

Kapoor, K., Bhandare, A. M., Farnham, M. M., and Pilowsky, P. M. (2016). Alerted microglia and the sympathetic nervous system: a novel form of microglia in the development of hypertension. *Respir. Physiol. Neurobiol.* 226, 51–62. doi: 10.1016/j.resp.2015.11.015

Kato, T., Iwase, K., Nagatsu, T., Sakakibara, S., and Fujita, K. (1979). Comparison of X-prolyl dipeptidyl-aminopeptidase activity in human cerebrospinal fluid with that in serum. *Experientia* 35, 20–21. doi: 10.1007/bf01917849

Kiernan, E. A., Smith, S. M., Mitchell, G. S., and Watters, J. J. (2016). Mechanisms of microglial activation in models of inflammation and hypoxia: implications for chronic intermittent hypoxia. *J. Physiol.* 594, 1563–1577. doi: 10.1113/JP271502

Kim, S. J., Fong, A. Y., Pilowsky, P. M., and Abbott, S. B. G. (2018). Sympathoexcitation following intermittent hypoxia in rat is mediated by circulating angiotensin II acting at the carotid body and subfornical organ. *J. Physiol.* 596, 3217–3232. doi: 10.1113/JP275804

Kumar, G. K., Rai, V., Sharma, S. D., Ramakrishnan, D. P., Peng, Y. J., Souvannakitti, D., et al. (2006). Chronic intermittent hypoxia induces hypoxia-evoked catecholamine efflux in adult rat adrenal medulla via oxidative stress. *J. Physiol.* 575(Pt 1), 229–239. doi: 10.1113/jphysiol.2006.112524

Lai, C. C., Wu, S. Y., Lin, H. H., and Dun, N. J. (1997). Excitatory action of pituitary adenylate cyclase activating polypeptide on rat sympathetic preganglionic neurons in vivo and in vitro. *Brain Res.* 748, 189–194. doi: 10.1016/s0006-8993(96)01297-8

Leung, R. S., Comondore, V. R., Ryan, C. M., and Stevens, D. (2012). Mechanisms of sleep-disordered breathing: causes and consequences. *Pflugers. Arch.* 463, 213–230. doi: 10.1007/s00424-011-1055-x

Li, Q., Goodchild, A. K., Seyedabadi, M., and Pilowsky, P. M. (2005). Pre-protachykinin A mRNA is colocalized with tyrosine hydroxylase-immunoreactivity in bulbospinal neurons. *Neuroscience* 136, 205–216. doi: 10.1016/j.neuroscience.2005.07.057

Ling, L., Fuller, D. D., Bach, K. B., Kinkead, R., Olson, E. B., and Mitchell, G. S. (2001). Chronic intermittent hypoxia elicits serotonin-dependent plasticity in the central neural control of breathing. *J. Neurosci.* 21, 5381–5388. doi: 10.1523/jneurosci.21-14-05381.2001

Mazzocchi, G., Malendowicz, L. K., Neri, G., Andreis, P. G., Ziolkowska, A., Gottardo, L., et al. (2002). Pituitary adenylate cyclase-activating polypeptide and PACAP receptor expression and function in the rat adrenal gland. *Int. J. Mol. Med.* 9, 233–243.

Minson, J., Arnolda, L., Llewellyn-Smith, I., Pilowsky, P., and Chalmers, J. (1996). Altered c-fos in rostral medulla and spinal cord of spontaneously hypertensive rats. *Hypertension* 27(3 Pt 1), 433–441. doi: 10.1161/01.hyp.27.3.433

Nedoboy, P. E., Mohammed, S., Kapoor, K., Bhandare, A. M., Farnham, M. M., and Pilowsky, P. M. (2016). pSer40 tyrosine hydroxylase immunohistochemistry identifies the anatomical location of C1 neurons in rat RVLM that are activated by hypotension. *Neuroscience* 317, 162–172. doi: 10.1016/j.neuroscience.2016.01.012

Pannell, M., Szulzewsky, F., Matyash, V., Wolf, S. A., and Kettenmann, H. (2014). The subpopulation of microglia sensitive to neurotransmitters/neurohormones is modulated by stimulation with LPS, interferon-gamma, and IL-4. *Glia* 62, 667–679. doi: 10.1002/glia.22633

Park, S. Y., Choi, H. J., and Hwang, O. (1999). Regulation of basal expression of catecholamine-synthesizing enzyme genes by PACAP. *Mol. Cells* 9, 146–151.

Pedrosa, R. P., Drager, L. F., Gonzaga, C. C., Sousa, M. G., de Paula, L. K., Amaro, A. C., et al. (2011). Obstructive sleep apnea: the most common secondary cause of hypertension associated with resistant hypertension. *Hypertension* 58, 811–817. doi: 10.1161/HYPERTENSIONAHA.111.179788

Peng, Y. J., Nanduri, J., Yuan, G., Wang, N., Deneris, E., Pendyala, S., et al. (2009). NADPH oxidase is required for the sensory plasticity of the carotid body by chronic intermittent hypoxia. *J. Neurosci.* 29, 4903–4910. doi: 10.1523/JNEUROSCI.4768-08.2009

Prabhakar, N. R., Kumar, G. K., and Peng, Y. J. (2012). Sympatho-adrenal activation by chronic intermittent hypoxia. *J. Appl. Physiol.* 113, 1304–1310. doi: 10.1152/japplphysiol.00444.2012

Pugh, P. C., Jayakar, S. S., and Margiotta, J. F. (2010). PACAP/PAC1R signaling modulates acetylcholine release at neuronal nicotinic synapses. *Mol. Cell. Neurosci.* 43, 244–257. doi: 10.1016/j.mcn.2009.11.007

Roy, A., Derakhshan, F., and Wilson, R. J. (2013). Stress peptide PACAP engages multiple signaling pathways within the carotid body to initiate excitatory responses in respiratory and sympathetic chemosensory afferents. *Am. J. Physiol.* 304, R1070–R1084. doi: 10.1152/ajpregu.00465.2012

Roy, A., Farnham, M. M. J., Derakhshan, F., Pilowsky, P. M., and Wilson, R. J. A. (2018). Acute intermittent hypoxia with concurrent hypercapnia evokes P2X and TRPV1 receptor-dependent sensory long-term facilitation in naive carotid bodies. *J. Physiol.* 596, 3149–3169. doi: 10.1113/JP275001

Stroth, N., Kuri, B. A., Mustafa, T., Chan, S. A., Smith, C. B., and Eiden, L. E. (2013). PACAP controls adrenomedullary catecholamine secretion and expression of catecholamine biosynthetic enzymes at high splanchnic nerve firing rates characteristic of stress transduction in male mice. *Endocrinology* 154, 330–339. doi: 10.1210/en.2012-1829

Tallapragada, V. J., Hildreth, C. M., Burke, P. G., Raley, D. A., Hassan, S. F., McMullan, S., et al. (2016). Tonically active cAMP-dependent signaling in the ventrolateral medulla regulates sympathetic and cardiac vagal outflows. *J. Pharmacol. Exp. Ther.* 356, 424–433. doi: 10.1124/jpet.115.227488

Tonshoff, C., Hemmick, L., and Evinger, M. J. (1997). Pituitary adenylate cyclase activating polypeptide (PACAP) regulates expression of catecholamine biosynthetic enzyme genes in bovine adrenal chromaffin cells. *J. Mol. Neurosci.* 9, 127–140. doi: 10.1007/bf02736856

Vaudry, D., Falluel-Morel, A., Bourgault, S., Basille, M., Burel, D., Wurtz, O., et al. (2009). Pituitary adenylate cyclase-activating polypeptide and its receptors: 20 years after the discovery. *Pharmacol. Rev.* 61, 283–357. doi: 10.1124/pr.109.001370

Vaudry, D., Gonzalez, B. J., Basille, M., Yon, L., Fournier, A., and Vaudry, H. (2000). Pituitary adenylate cyclase-activating polypeptide and its receptors: from structure to functions. *Pharmacol. Rev.* 52, 269–324.

Xing, T., and Pilowsky, P. M. (2010). Acute intermittent hypoxia in rat in vivo elicits a robust increase in tonic sympathetic nerve activity that is independent of respiratory drive. *J. Physiol.* 588, 3075–3088. doi: 10.1113/jphysiol.2010.190454

Yao, L., Chen, X., Tian, Y., Lu, H., Zhang, P., Shi, Q., et al. (2012). Selection of housekeeping genes for normalization of RT-PCR in hypoxic neural stem cells of rat in vitro. *Mol. Biol. Rep.* 39, 569–576. doi: 10.1007/s11033-011-0772-8

Yokai, M., Kurihara, T., and Miyata, A. (2016). Spinal astrocytic activation contributes to both induction and maintenance of pituitary adenylate cyclase-activating polypeptide type 1 receptor-induced long-lasting mechanical allodynia in mice. *Mol. Pain* 12:1744806916646383. doi: 10.1177/1744806916646383

Zhu, L., Tamvakopoulos, C., Xie, D., Dragovic, J., Shen, X., Fenyk-Melody, J. E., et al. (2003). The role of dipeptidyl peptidase IV in the cleavage of glucagon family peptides: in vivo metabolism of pituitary adenylate cyclase activating polypeptide-(1-38). *J. Biol. Chem.* 278, 22418–22423. doi: 10.1074/jbc.m212355200

Conflict of Interest Statement: The authors declare that the research was conducted in the absence of any commercial or financial relationships that could be construed as a potential conflict of interest.

frontiers in Neuroscience

REVIEW
published: 27 August 2019
doi: 10.3389/fnins.2019.00897

A Student's Guide to Neural Circuit Tracing

Christine Saleeba[1,2†], Bowen Dempsey[3†], Sheng Le[1], Ann Goodchild[1] and Simon McMullan[1]*

[1] Neurobiology of Vital Systems Node, Faculty of Medicine and Health Sciences, Macquarie University, Sydney, NSW, Australia, [2] The School of Physiology, Pharmacology and Neuroscience, University of Bristol, Bristol, United Kingdom, [3] CNRS, Hindbrain Integrative Neurobiology Laboratory, Neuroscience Paris-Saclay Institute (Neuro-PSI), Université Paris-Saclay, Gif-sur-Yvette, France

The mammalian nervous system is comprised of a seemingly infinitely complex network of specialized synaptic connections that coordinate the flow of information through it. The field of connectomics seeks to map the structure that underlies brain function at resolutions that range from the ultrastructural, which examines the organization of individual synapses that impinge upon a neuron, to the macroscopic, which examines gross connectivity between large brain regions. At the mesoscopic level, distant and local connections between neuronal populations are identified, providing insights into circuit-level architecture. Although neural tract tracing techniques have been available to experimental neuroscientists for many decades, considerable methodological advances have been made in the last 20 years due to synergies between the fields of molecular biology, virology, microscopy, computer science and genetics. As a consequence, investigators now enjoy an unprecedented toolbox of reagents that can be directed against selected subpopulations of neurons to identify their efferent and afferent connectomes. Unfortunately, the intersectional nature of this progress presents newcomers to the field with a daunting array of technologies that have emerged from disciplines they may not be familiar with. This review outlines the current state of mesoscale connectomic approaches, from data collection to analysis, written for the novice to this field. A brief history of neuroanatomy is followed by an assessment of the techniques used by contemporary neuroscientists to resolve mesoscale organization, such as conventional and viral tracers, and methods of selecting for sub-populations of neurons. We consider some weaknesses and bottlenecks of the most widely used approaches for the analysis and dissemination of tracing data and explore the trajectories that rapidly developing neuroanatomy technologies are likely to take.

Keywords: neuroanatomy, viral tracers, anterograde tracer, retrograde tracers, synaptic contacts, connectome analysis

OPEN ACCESS

Edited by:
Vaughan G. Macefield, Baker Heart and Diabetes Institute, Australia

Reviewed by:
Patrice G. Guyenet, University of Virginia, United States
Eberhard Weihe, University of Marburg, Germany
Alice McGovern, The University of Melbourne, Australia

***Correspondence:**
Simon McMullan
simon.mcmullan@mq.edu.au

[†]These authors have contributed equally to this work

Specialty section:
This article was submitted to Autonomic Neuroscience, a section of the journal Frontiers in Neuroscience

Received: *31 May 2019*
Accepted: *12 August 2019*
Published: *27 August 2019*

Citation:
Saleeba C, Dempsey B, Le S, Goodchild A and McMullan S (2019) A Student's Guide to Neural Circuit Tracing. Front. Neurosci. 13:897. doi: 10.3389/fnins.2019.00897

INTRODUCTION

The relationship between structure and function is a central theme in the field of biology. In the same way that deciphering the crystal structure of DNA propelled research toward the mechanics of inheritance in the 20th century (Watson and Crick, 1953), it is widely believed that elucidation of the structural architecture of the brain will fundamentally alter neuroscience in the 21st

(Rubinov and Bullmore, 2013; Lerner et al., 2016; Mikula, 2016). Here, we review the approaches used by contemporary neuroscientists to identify connectivity patterns between components of neural circuits, the trajectories that rapidly developing neuroanatomy technologies are likely to take, and some bottlenecks that may hinder this mission.

It is unknown at what point in history the brain was first recognized as the control center for the body. Although sometimes attributed to Hippocrates and Galen around 2,000 years ago, the association between traumatic brain injury and distinct functional deficits was clearly understood by Egyptian physicians 30 centuries before that (Stiefel et al., 2006), and archeological evidence indicates widespread neurosurgical practice in diverse cultures since time immemorial (Andrushko and Verano, 2008, reviewed by Kshettry et al., 2007; Moghaddam et al., 2015). What is clear is that the association between brain structure and function is a relatively recent realization: this consensus was only reached in the late 1800s after nearly 100 years of disagreement between those who, like influential French physiologist and child prodigy Marie-Jean-Pierre Flourens, believed that the brain, like the mind, was indivisible (Pearce, 2009), and those like Frantz Joseph Gall who proposed that the brain is composed of distinct functional compartments, and that the relative contribution of each is to some extent independent from the others [see Ferrier (1884) for contemporaneous review].[1]

At the same time that Broca and others were cementing the idea of cerebral localization at a macroscopic scale, the first histologists were using the microscope to discover the delicate structure of neural tissue and developing theories about the cellular basis of brain function. The "neuron theory" developed by Ramon y Cajal, Waldeyer-Hartz and others argued that a particular cell type, the neuron, was the functional unit of the nervous system, from which axons grew and relied upon for nutrition; that neurons were discontinuous and formed physical contacts at which communication occurred; and that information flowed across neurons in one direction, from the dendrite toward the axonal terminals (reviewed by Fishman, 1994; Llinas, 2003; Guillery, 2005; Lopez-Munoz et al., 2006). These central tenets are now universally accepted, with caveats (Guillery, 2005), but spawned an acrimonious and dogmatic battle between "reticularists" and "neuronists" that persisted from the late 1870s until the invention of the electron microscope and subsequent visualization of mammalian synapses in the 1950s.[2]

[1]Ironically, despite having already been discredited as a serious science by then, phrenology contributed to the general acceptance of this view by fostering the notion that individual variation in discrete brain functions are reflected by skull topography (summarized by Gross, 2009).

[2]Opponents to the neuronist school have been characterized as subscribing to a chaotic and somewhat absurd view of the brain. Guillery (2005) makes a compelling case for reassessment of this historical debate, highlighting discoveries that were made after the description of the physical structure of the synapse (e.g., gap junctions, axo-axonic contacts) that fundamentally undermine some tenets of the neuron theory. Guillery argues that both models were ultimately wrong, and that a less dogmatic post-neuronist view is more appropriate.

THE FIELD OF CONNECTOMICS

Since then, generations of neuroscientists have used progressively more selective labeling techniques and more powerful microscopes to reveal the patterns of synaptic connectivity that are thought to underlie the functional properties of neural circuits. This effort has given rise to the field of "connectomics," a now standalone sub-discipline of neuroscience with the stated aim of understanding the "*structural architecture of nervous system connectivity in all animals at all resolutions*" (reviewed by Hagmann, 2005; Sporns et al., 2005; Swanson and Bota, 2010; Catani et al., 2013). Connectomics generates simplified circuit diagrams at macroscopic (brain-wide), mesoscopic (circuit level) or nanoscopic (synapse level) resolutions that classify neurons in terms of their connectivity to each other (**Figure 1**: discussed by Branco and Staras, 2009). However, these efforts have been hampered by both the technical complexity involved in accurately identifying synaptic connections and the sheer magnitude of the task: full connectomic reconstruction of the human brain would require the mapping of approximately 86 billion neurons (Azevedo et al., 2009; Herculano-Houzel, 2009) and the identification of the thousands of inputs and outputs that connect each one (Nimchinsky et al., 2002).

As a result of this complexity, the only entire connectomes thus far cataloged belong to tiny animals: the first (nearly) complete map of the entire nervous system of an individual species was made by White et al. (1986) from reconstructed serial electron micrographs of the roundworm *Caenorhabditis elegans* (later completed by Varshney et al., 2011), and more recently larval and adult *Drosophila melanogaster* (Ohyama et al., 2015; Zheng et al., 2018) and the larval sea-squirt *Ciona intestinalis* (Ryan et al., 2016). The "nanoscale" approach used to map these connectomes offers comprehensive knowledge of every neuronal connection, and is well-suited to components of relatively small local circuits such as in the retina, in which the inputs and outputs are understood (Briggman et al., 2011; Denk et al., 2012).

However, ultrastructural strategies are poorly suited to the interrogation of large or dispersed circuits because of the enormous investments of time and infrastructure required to acquire and handle the data (Lichtman and Denk, 2011; Wanner et al., 2015). These technical limitations seem unlikely to be resolved in the foreseeable future; despite recent innovations such as the development of serial block-face and Focused Ion Beam electron microscopy, which have reduced the acquisition time for a cubic millimeter of tissue from ∼18 to ∼1.5 years (Wanner et al., 2015; Xu et al., 2017), obstacles to the analysis and even the storage of high resolution microscopy data remain. For example, the raw dataset for a single human brain would require ∼175 exabytes of storage space, costing 2–8 billion Euros (Mikula, 2016). By comparison, the entire storage capacity of the planet in 2011 was ∼295 exabytes (Hilbert and Lopez, 2011).

These limitations have provided a stimulus for the development of genetically modified viral tracers that can be used to identify components of a given neuronal circuit without requiring direct visualization of synaptic contacts. The major advantages of this approach are its compatibility with light microscopy, greatly reducing the imaging, analysis and storage

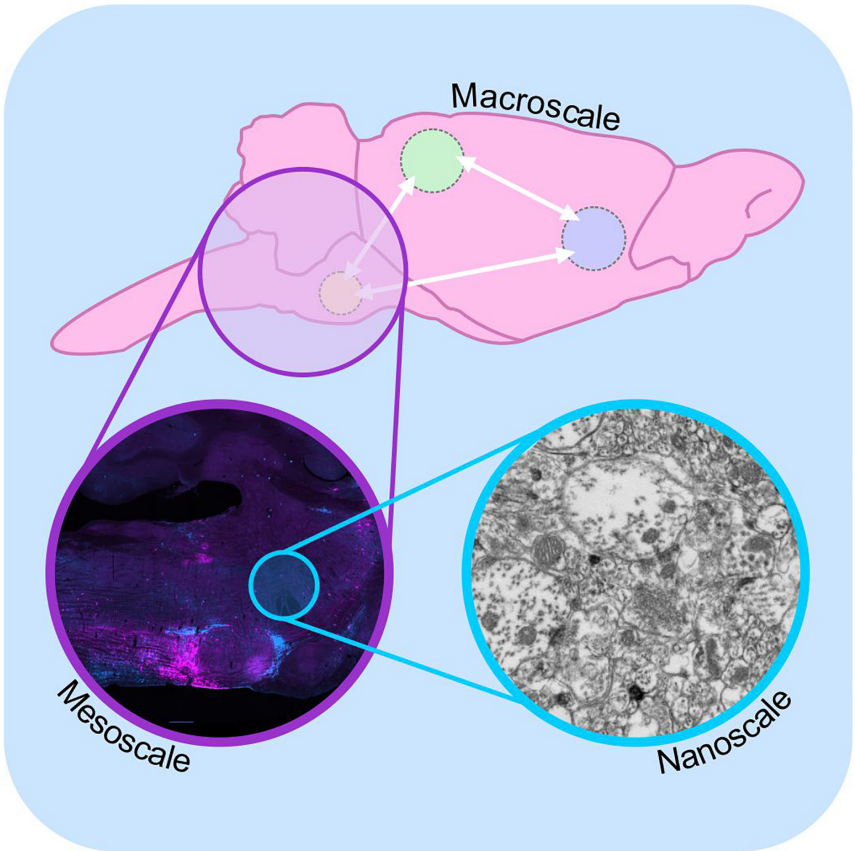

FIGURE 1 | Macro-, meso-, and microscale connectomics. Schematic diagram illustrating connectome analysis at macroscale (top), mesoscale (purple inset), and nanoscale resolutions (blue inset). Macroscale approaches (top) examine communication between regions of the brain on a global level, using approaches such as diffusion-weighted magnetic resonance imaging. Mesoscale connectomics interrogates neural circuitry at the cellular level, employing light microscopy to map the distribution of synaptically linked neurons, in this case monosynaptic inputs to putative sympathetic premotor neurons (see Menuet et al., 2017, modified with permission). Nanoscale connectomics assesses individual synaptic contacts using electron microscopy. Nanoscale image shows electron micrograph of synapses and polysialyic acid immunoreactivity: see Bokiniec et al. (2017).

burden inherent to ultrastructural analysis, and its applicability to mapping networks that are dispersed throughout the brain.

ANTEROGRADE AND RETROGRADE TRACERS

Early tracing approaches involved the physical or electrical lesion of a region of interest, which rendered the degenerating axons differentially susceptible to impregnation with metallic silver (Hoff, 1932). Although crude, this approach was eventually refined to the point where terminal boutons could be resolved (Glees, 1946; Nauta, 1952; Fink and Heimer, 1967). Visualization of Wallerian degeneration was replaced by approaches that did not require destructive lesions, relying instead on the axonal transport of injected/applied materials from the site of injection to either the cell body (retrograde tracers) or axonal processes (anterograde tracers; **Figure 2**). The earliest of these tracers were radiolabeled amino acids such as tritiated leucine and proline that were injected into neural tissue then incorporated into polypeptides in the soma and transported to axons and terminal processes where they were identified by autoradiography (Grafstein, 1967; Cowan et al., 1972). These tracers were soon surpassed by materials that could be detected with conventional light microscopy via histological or immunohistochemical (IHC) processing, intrinsic fluorescence, or conjugation with a fluorophore or enzymatically active probe. This variety of tracer constitutes what are now referred to as "conventional tracers" (in contrast to viral tracers). The variety and utility of conventional tracing techniques are broad and have been extensively reviewed elsewhere (Köbbert et al., 2000; Vercelli et al., 2000; Lanciego and Wouterlood, 2011): here, we provide a simple overview of some of the most popular conventional tracers for comparison with the viral tracers discussed in upcoming sections.

Conventional (Mainly) Retrograde Tracers

The glycoprotein and enzyme horse radish peroxidase (HRP) was found in the early 1970s to be an effective retrograde tracer,

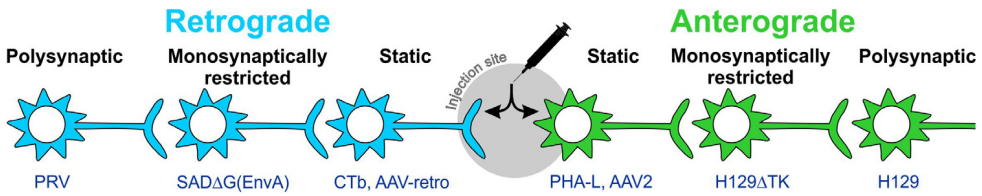

FIGURE 2 | Anterograde and retrograde labeling with static and trans-synaptic tracers. Tracers are categorized as anterograde or retrograde based on their direction of travel within neurons. Anterograde tracers (green) are taken up by neuronal cell bodies at the injection site and travel down the axon to terminal processes. Retrograde tracers (blue) are taken up by terminals and travel back to the cell body. Static tracers remain within the first neurons they enter, while other tracers can spread trans-synaptically and may or may not be monosynaptically restricted. CTb: cholera toxin B subunit; H129ΔTK: tyrosine kinase-deleted H129 herpes; PHA-L: *Phaseolus vulgaris*-leucoagglutinin; PRV: pseudorabies virus; SADΔG(EnvA): glycoprotein-deleted EnvA-pseudotyped rabies.

having been taken up into neurons non-selectively by passive endocytosis (Kristensson and Olsson, 1971; LaVail and LaVail, 1972; Köbbert et al., 2000; Vercelli et al., 2000). HRP is visualized as it catalyzes, together with hydrogen peroxide, the oxidation of chromogenic substrates such as 3,3′-diaminobenzidine and tetramethylbenzidine. The resultant staining is limited to the cell soma and primary dendrites (Köbbert et al., 2000) and, on its own, HRP demonstrates a relatively low sensitivity due to inefficient uptake by neurons at the injection site. However, conjugation of HRP to the plant lectin wheat germ agglutinin (WGA), itself a neuronal tracer, significantly improved both uptake and transport within neurons (Staines et al., 1980; Köbbert et al., 2000). WGA binds to *N*-acetylglucosamine and the plasma membrane-bound sugar sialic acid, and is rapidly actively transported in both the anterograde and retrograde directions, providing more extensive (but not complete) labeling of the neuron compared to HRP (Schwab et al., 1978; Dumas et al., 1979; Levy et al., 2017). WGA-HRP conjugates are also capable of limited trans-synaptic travel (Goshgarian and Buttry, 2014; Sillitoe, 2016), introducing some ambiguity to the interpretation of data. WGA is now available in a fluorophore-conjugated preparation, eliminating the need for immunohistochemical processing for visualization.

Cholera toxin subunit B (CTb) was introduced as a retrograde tracer in 1977 (Stoeckel et al., 1977; Vercelli et al., 2000). Trojanowski et al. (1981, 1982) then sought to improve the sensitivity of HRP using CTb-HRP conjugates, and found that when the number and detail of labeled neurons was compared, CTb-HRP significantly out-performed free HRP. They attributed this to the GM1 ganglioside (sugar) mediated uptake of CTb in comparison to the non-specific endocytosis of HRP (Trojanowski et al., 1981; Trojanowski et al., 1982; Lanciego and Wouterlood, 2011). Unconjugated CTb can be detected via immunohistochemistry, however, the development of CTb-conjugated fluorophores (Conte et al., 2009a,b) or even magnetically opaque labels visible to MRI (Wu et al., 2011) has extended the scope of CTb. The signal strength of fluorescently conjugated CTb, its rapid transport (2–7 days), low toxicity, and ease of use also makes it suitable for identification of neurons for subsequent electrophysiological recordings *in vitro* (Korim et al., 2014; Bou Farah et al., 2016) or *in vivo* (Yamashita and Petersen, 2016), and has elevated fluorescently conjugated CTb variants as a go-to retrograde tracer for many researchers (Parker et al., 2015; Zhao et al., 2017), although it should be noted that, like most conventional tracers, CTb transport is to some extent bidirectional (Noseda et al., 2010). In our experience, CTb-conjugated fluorophores can suffer quenching when used in conjunction with *in situ* hybridization, and as the fluorophore prevents binding of anti-CTb antibodies, quenched signal cannot be boosted with anti-CTb IHC, so for dual labeling of mRNA and CTb the unconjugated form is preferable.

A number of inorganic tracers are also widely used. Hydroxystilbamidine (FluoroGold^{TM}) is a fluorescent inorganic compound directly visible with fluorescence microscopy. Following uptake into nerve terminals by fluid phase endocytosis, FluoroGold^{TM} is transported retrogradely to cell bodies in vesicles and accumulates in the cytoplasm, where it remains detectable for months (Köbbert et al., 2000; Lanciego and Wouterlood, 2011). The intense, bleach-resistant labeling achieved using FluoroGold^{TM}, and the availability of anti-FluoroGold^{TM} antibodies for further amplification, has resulted in it becoming the "gold-standard" tracer in rodents, against which newly developed tracers are compared (Lanciego and Wouterlood, 2011; Tervo et al., 2016).

Other noteworthy inorganic fluorescent tracers are Fast Blue, Diamidino Yellow, True Blue and the carbocyanines DiI and DiO (Bentivoglio et al., 1980; Bonhoeffer and Huf, 1980; Kuypers et al., 1980; Puigdellivol-Sanchez et al., 1998; Schofield, 2008; Yu et al., 2015). Although no longer widely used for tracing projections in the central nervous system, they (along with organic tracers such as CTb, WGA, etc.) remain popular choices for the identification of autonomic, motor or sensory innervation of peripheral targets, into which they can be injected in relatively large volumes (Furukawa et al., 2008; Zele et al., 2010; Yu et al., 2015; Pidsudko et al., 2019; Rytel et al., 2019). Interestingly, because they are not dependent on active transport, inorganic dyes may also be used for identification of projections in fixed tissue *post mortem*. Typically applied as crystals to the surface of formalin-fixed tissue blocks, highly lipophilic dyes such as DiI (red) and DiO (green) move evenly throughout cells in both anterograde and retrograde directions via the lipid portion of neuronal membranes, resulting in complete labeling of the soma and dendritic tree (Thanos et al., 1991, 1992; Köbbert et al., 2000; Boon et al., 2019; Trivino-Paredes et al., 2019). However, the lipophilic nature of carbocyanine dyes makes them difficult to use in conjunction with standard IHC protocols that use

lipid-solubilizing detergents to facilitate antibody penetration (Elberger and Honig, 1990; Matsubayashi et al., 2008).

Fluorescent latex microspheres 30–90 nm in diameter (Retrobeads^{TM}) were recognized as retrograde tracers in the mid-1980s (Katz et al., 1984; Katz and Iarovici, 1990) and, like FluoroGold^{TM}, are highly resistant to fading and offer long-term labeling. Although somewhat difficult to use, based on their tendency to clump in the injection pipette, latex beads offer stable fluorescence with minimal diffusion from the injection site, exclusive retrograde travel with minimal entry to undamaged fibers of passage, and are non-toxic to neurons so can be used in long duration experiments (Köbbert et al., 2000; Vercelli et al., 2000; Lanciego and Wouterlood, 2011). Their distinctive bright punctate appearance makes them easy to distinguish, meaning they can be mixed with an anterograde tracer of the same color [e.g., to simultaneously identify retro- and anterograde projections from a single brain region (Turner et al., 2013)].

Conventional (Mainly) Anterograde Tracers

Phaseolus vulgaris-leucoagglutinin (PHA-L) is one of the earliest and most widely used anterograde tracers (Gerfen and Sawchenko, 1984; Köbbert et al., 2000) and, like WGA, PHA-L binds to membrane bound carbohydrates to gain cell entry (in this case *N*-acetyl D-glucosamine and mannose). PHA-L is detected using IHC, revealing detailed cell morphology, including axon terminal branches to the level of terminal boutons (Lanciego and Wouterlood, 2011; Wouterlood et al., 2014). PHA-L requires longer post-injection survival times to achieve transport compared other conventional tracers, typically 10 to 20 days (Vercelli et al., 2000).

Emerging in the mid-1980s, dextran-amines (DAs) were rapidly adopted and remain widely used as conventional axonal tracers (Gimlich and Braun, 1985; Glover et al., 1986; Brandt and Apkarian, 1992; Veenman et al., 1992; Wouterlood et al., 2014). DAs enter injured neurons at the injection site and spread evenly throughout the entire neuron via diffusion, resulting in a Golgi-like level of staining detail (Glover et al., 1986; Fritzsch, 1993; Glover, 1995; Köbbert et al., 2000; Lanciego and Wouterlood, 2011; Wouterlood et al., 2014).

Despite the common perception that DAs are preferential anterograde tracers, many studies indicate bidirectional travel (Schmued et al., 1990; Fritzsch, 1993; Glover, 1995; Zhang et al., 2017), including the original description of their axonal transport by Glover et al. (1986). Their retrograde capabilities have been exploited both for conventional tracing (Sivertsen et al., 2014, 2016; Lunde et al., 2019) and for delivery of calcium-sensitive indicators for optical recording of neurons selected by axonal trajectory (O'Donovan et al., 1993; McPherson et al., 1997).

There is a perception that the molecular weight of DA-conjugates contributes to their directional selectivity, with smaller molecules exhibiting superior performance as a retrograde tracer (Reiner et al., 2000; Lanciego and Wouterlood, 2011). However, the influence, if any, of molecular weight on directional specificity is probably overstated, and may instead reflect differences in speed of transport, which is distinctly faster for smaller compounds (Fritzsch, 1993), combined with differences in volume of synaptic terminals compared to cell bodies (Glover, personal communication).

Like CTb, fluorophore-labeled dextran amine variants are now widely used instead of or in addition to biotinylated versions that require histological processing for visualization, and we and others have used tetramethylrhodamine-conjugated dextran for juxtacellular labeling during electrophysiological recordings (Noseda et al., 2010; Dempsey et al., 2015).

Limitations of Conventional Tracers

Despite their ongoing popularity, the major limitations of conventional tracers are worthy of consideration:

(1) Conventional tracers can be taken up by fibers of passage (Dado et al., 1990; Chen and Aston-Jones, 1995; Conte et al., 2009a), which can lead to incorrect identification of projections. [Notably, canine adenovirus (CAV) can also be taken up by fibers of passage (Schwarz et al., 2015)].

(2) The spread of many conventional tracers around the injection site results in intense and diffuse labeling that may reflect deposition in the extracellular matrix or take-up by neurons or glia. Such non-specific labeling makes it difficult to reliably identify labeled neurons within ∼1 mm of the injection site. Thus the historical use of conventional tracers has probably overemphasized the relative significance of distant inputs/outputs compared to those originating from local interneurons; contemporary connectomic studies indicate that long-distance projections are relatively rare compared to short-distance connections (Oh et al., 2014; Henriksen et al., 2016; van den Heuvel et al., 2016; Dempsey et al., 2017).

(3) Tracer uptake relies predominantly on sugars that are located on the glycocalyx of most, if not all neurons, or on common mechanisms such as endocytosis. Consequently, restricted uptake by functionally or neurochemically/genetically homogeneous neuronal populations is not possible.

(4) The direction of axonal transport is rarely exclusive, which complicates circuit analysis; the archetypal retrograde and anterograde tracers, CTb and BDA respectively, both label axons traveling in the "wrong" direction (Luppi et al., 1987; Schmued et al., 1990; Fritzsch, 1993; Glover, 1995; Angelucci et al., 1996; Noseda et al., 2010; Zhang et al., 2017).

VIRAL TRACERS

Recombinant viral vectors that drive the expression of fluorescent "reporter" proteins in transduced neurons have been widely adopted by neuroscientists because of their directional specificity, the high (in most cases permanent) levels of reporter expression obtained, and the absence of transduction of fibers of passage (comprehensively reviewed by Callaway, 2005; Luo et al., 2008; Betley and Sternson, 2011; Nassi et al., 2015). Here, we will examine some widely used variants and consider the extent to which they address the limitations of conventional tracers.

Viral tracers may be divided into two distinct classes: static vectors that remain locked within the targeted cell population and essentially function like conventional tracers, which are usually replication-deficient, and vectors that spread through linked circuits via trans-synaptic travel, which are almost always replication-competent. Each class contains vectors that can be used to label selectively in an antero- or retrograde direction.

Static Viral Tracers

Recombinant vectors derived from human immunodeficiency virus (HIV), herpes simplex virus type 1 (HSV-1), human and canine adenoviridae (Ad), adeno-associated virus (AAV), semliki forest virus, sindbis virus (SIN), and rabies have all been developed as alternatives to conventional chemical tracers (Chamberlin et al., 1998; Furuta et al., 2001; Wickersham et al., 2007a; Junyent and Kremer, 2015; Lerner et al., 2016; Jia et al., 2017; Farmer et al., 2019). A detailed review of the biology of each is beyond the scope of the current article; the following resources provide useful overviews of the most commonly used replication deficient viral vectors (Ad: Akli et al., 1993, AAV: Kuo et al., 1995; Drouin and Agbandje-McKenna, 2013; Junyent and Kremer, 2015, HIV: Lundberg et al., 2008; Murlidharan et al., 2014, HSV-1: Neve, 2012). HIV, HSV, Ad, SIN, and AAV vectors differ in their maximum genetic payload, whether transgenes are integrated into the host genome, and the onset and duration of gene expression, but share common features: the wild-type virus is modified to remove genes required for viral replication and replaced with a genetic sequence that encodes a reporter protein under the control of a ubiquitous (e.g., cytomegalovirus, CaMKII), pan-neuronal (e.g., neuron-specific enolase, synapsin) or cell-type specific (e.g., PRSx8, GAD1) promoter or, if used in transgenic animals (reviewed by Wang et al., 2011), genetically restricted expression systems such as Cre-LoxP or FLP-FRT (Blomer et al., 1997; Hwang et al., 2001; Jakobsson et al., 2003; Schnutgen et al., 2003; Gofflot et al., 2011; Liu et al., 2013; Fenno et al., 2014; Luo et al., 2018). In contrast, glycoprotein-deleted rabies is a static retrograde vector that retains its capacity for replication, but has been modified so that it can no longer spread trans-synaptically (Larsen et al., 2007; Wickersham et al., 2007a). This has the advantage of self-amplification, resulting in very high levels of reporter expression, but results in cytotoxicity within a few weeks of infection and, as transcription is not promoter-dependent, cannot be targeted to particular cell types without further genomic alterations (discussed below). Furthermore, as the rabies genome is RNA based, strategies for selective recombination within subpopulations of infected neurons (e.g., Cre-LoxP) are not possible.

The mode of use of static viral tracers is similar to conventional tracers; vectors are injected in small volumes into the region or organ of interest under anesthesia, and experimental animals are allowed to recover with appropriate post-operative care. Following a period sufficient for transgene translation, the animal is euthanized and perfused with fixative, and the CNS removed for histological processing, which may include IHC amplification of reporter signal, followed by imaging. The major differences compared to conventional tracers lie in the duration of recovery (although reporter expression is visible within 12 h of HSV or rabies injections, protein transcription is typically optimal 10–20 days after transduction by AAV and lentiviral vectors), the volume of injectate, which is typically larger for conventional tracers (300–1000 nl vs. 20–100 nl for CNS injections, 1–5 μl for peripheral injections into target organs), and the level of biological containment required. When injected into the periphery, a further consideration is the age of the animal; in our experience peripheral injections of rabies and HSV-1 vectors do not result in detectable neuronal labeling when administered to mice older than post-natal day 7, perhaps reflecting the immaturity of the innate and adaptive immune responses in the early post-natal period.

Like conventional tracers, cell entry is mediated via interactions between glycans or proteins expressed on the cell membrane and components of the viral vector (Lykken et al., 2018). The tendency of a given vector to label in an anterograde or retrograde direction therefore reflects the cellular distribution of cognate receptors to its particular surface proteins; binding with receptors expressed on the soma results in anterograde labeling (e.g., AAV serotype 2, 5, 7, 8, and rh.10, human adenovirus), whereas binding with receptors preferentially expressed at the axon terminal results in retrograde labeling (e.g., HSV-1, rabies and canine adenovirus) (Frampton et al., 2005; Berges et al., 2007; Salinas et al., 2009; Penrod et al., 2015; Castle et al., 2016; Hirschberg et al., 2017; Sathiyamoorthy et al., 2017; Farmer et al., 2019). Note that viral titer may also play a role in the direction of travel; human adenovirus becomes a retrograde tracer at high titers as the recruited immune response limits their efficacy (Howorth et al., 2009). Perhaps unsurprisingly, variation of viral surface proteins by natural selection or human manipulation can alter their affinity for cellular binding partners, changing the tropism for different cell types (e.g., neuronal versus non-neuronal) or different neuronal compartments (e.g., pre-synaptic versus post-synaptic) (Kanaan et al., 2017; Lykken et al., 2018). The diverse capsid sequences found in the dozen or so naturally occurring primate AAVs that have been developed as vectors for gene transfer exhibit dramatically different tropisms for different cell types (reviewed by Drouin and Agbandje-McKenna, 2013; Castle et al., 2016) and hosts (Watakabe et al., 2015). When injected into the rodent central nervous system, most result in anterograde labeling, but the AAV1, 5 and 9 serotypes exhibit both anterograde and retrograde transport, with the degree of retrograde tropism varying according to the region studied and construct used (Rothermel et al., 2013; Castle et al., 2016). Altered directional tropism can also be conferred by pseudotyping viral vectors with chimeric envelope proteins from other viruses; this approach has been used with success to switch between anterograde and retrograde tropism in HIV-1 and vesicular stomatitis virus vectors, and to generate rabies variants that can gain cellular access at the soma instead of the axon terminal (Blomer et al., 1997; Wickersham et al., 2007b; Kato et al., 2011; Beier et al., 2011, 2013).

Many different viruses have been developed as potential vehicles for gene delivery, but in recent years AAV vectors have emerged as front-runners (Kanaan et al., 2017). Although the maximum size of the AAV payload is limited compared to

lentiviral, adenoviral and HSV vectors, they are easy to work with, have low toxicity and immunogenicity, and result in rapid (∼14 days) and permanent transgene expression in post-mitotic cells such as neurons (reviewed by Chamberlin et al., 1998; Betley and Sternson, 2011; Sun and Schaffer, 2018). These properties have made AAV vectors attractive candidates in gene therapy for cancer, metabolic, and neurological diseases (Weinberg et al., 2013; O'Connor and Boulis, 2015; Santiago-Ortiz and Schaffer, 2016; Grimm and Buning, 2017), stimulating investment in AAV production and targeting technologies that are likely to further accelerate their development. AAV capsids have been manipulated to improve their transduction ability for both gene therapy and neuroanatomical applications (Tervo et al., 2016; Chan et al., 2017). Of particular relevance to the neuroscientist is the recent development of a synthetic AAV capsid that drives retrograde transduction with particularly high efficiency and selectivity (Tervo et al., 2016). This capsid, known as AAV-retro, results in transduction profiles that closely resemble conventional retrograde tracers such as FluoroGold^{TM} (Tervo et al., 2016), is compatible with small injection volumes, and is not associated with significant toxicity (Sun et al., 2019). These features, and the fact that it can be made in any viral production facility that produces conventional AAV vectors, indicate that the popularity of AAVs will continue to increase.

The AAV-retro variant, and other synthetic AAV capsids, were made using *in vivo* directed evolution, a process in which error-prone PCR is used to introduce mutations to the *cap* gene (Drouin and Agbandje-McKenna, 2013). Mutant viral particles are then injected into organoids or animal models and the tissue of interest is harvested, from which AAV variants are isolated and sequenced to identify mutations with the desired tropism (Kotterman and Schaffer, 2014; Sun and Schaffer, 2018). In producing AAV-retro, AAV variants with different *cap* mutations were injected into either the substantia nigra or the cerebellar cortex and harvested from the striatum or inferior olive, respectively, revealing candidate capsid sequences with high selectivity for retrograde transport (Tervo et al., 2016). Given the many dozens of unstudied capsid subtypes that lie within the 13 major groups of primate AAV (Gao et al., 2004), the many thousands of potential capsids that lie within putative ancestral primate AAV libraries (Santiago-Ortiz et al., 2015), and the perhaps millions of capsid variants yet to be isolated and characterized from non-primate AAVs (Smith et al., 2016), it seems likely that AAV capsids with useful tropisms will continue to be discovered and developed for neuroscience applications. This may even lead to development of capsid variants with selectivity for particular neuronal cell types, bypassing the need for recombinase-driving transgenic animals or cell-type specific promoters, the Achilles' heel of AAV due to its small payload size (although the selectivity of synthetic AAV promoters is also rapidly improving: see Jüttner et al., 2019), with obvious benefits to both research and gene therapy applications.

Identification of Synaptic Contacts

Irrespective of whether anterograde labeling is achieved by conventional tracers or vector-mediated reporter expression, the identification of terminal appositions under light microscopy remains a challenge because of their small size (Burette et al., 2015). The development of vectors that selectively label presynaptic terminals (e.g., synaptophysin-GFP or synaptophysin-mRuby) makes disambiguation of terminals from axons and fibers easier (Li et al., 2010; Oh et al., 2014; Beier et al., 2015; Lerner et al., 2015), but the fact remains that <50% of "close appositions" constitute functional synapses (Pilowsky et al., 1992; Descarries and Mechawar, 2000; da Costa and Martin, 2011), and so their presence needs to be interpreted with caution. In recent years a number of elegant approaches have been developed to circumvent this limitation, the ultimate of which is GRASP (GFP Reconstitution Across Synaptic Partners), a dual vector system where each vector drives the expression of one half of a GFP-derived dimer that only becomes fluorescent when both halves bind. When presynaptic neurons are targeted with one and post-synaptic neurons with the other, the only place at which the two components can become physically close enough to bind is the synaptic cleft, and so GFP fluorescence denotes synaptic contact (Feinberg et al., 2008; Kim et al., 2011). The interested reader is directed to recent reviews that considers alternative methods for synaptic complementation (Wickersham and Feinberg, 2012; Luo et al., 2018).

TRANS-SYNAPTIC CIRCUIT TRACING

Replication-deficient viral vectors that drive reporter expression are ideal anterograde tracers, because they can target genetically restricted cells in circumscribed brain regions and result in unambiguous labeling of the entire neuron and/or its synaptic terminals. However, for the reasons outlined above, such fine detail is not easy to extract across whole brains and, moreover, anterograde labeling experiments are generally conducted in an effort to determine the post-synaptic targets of a given population of neurons, not to map the distribution or number of synaptic contacts arising from them. For the purposes of identifying post-synaptic targets, a better solution would be a tracer that labels the entire post-synaptic cell, which can be unambiguously and rapidly detected using light microscopy under relatively low magnification instead of the high-resolution methods required to reliably detect individual synapses. One approach that can achieve this exploits the trans-synaptic trafficking of Cre recombinase that occurs when expressed at high levels by *replication-deficient* viral vectors. Zingg et al. (2017) found that AAV-mediated Cre recombinase expressed in presynaptic neurons could drive Cre-dependent transgene expression in post-synaptic neurons, and that the degree of post-synaptic transgene expression, which presumably reflects the degree of Cre recombinase trafficking, varies depending on AAV serotype. This provides a useful tool for identification and manipulation of post-synaptic neurons, although the approach is somewhat confounded by the partial retrograde tropism of the AAV1 and AAV9 serotypes (Rothermel et al., 2013; Castle et al., 2016), which coincidentally produced the highest Cre recombinase trafficking (Zingg et al., 2017), leading to ambiguity over whether tagged neurons represent post- or pre-synaptic network components.

Another strategy that avoids having to identify individual synapses is to infect target populations with a *replication-competent* neurotrophic virus and to trace circuit components via the trans-synaptic infection of viral progeny (comprehensively reviewed by Nassi et al., 2015). This approach, initially developed using wild-type viruses that exhibit selectively retrograde (rabies, pseudorabies) or anterograde tropism (HSV-1 strain H129) (Strack et al., 1989b; Zemanick et al., 1991; Card and Enquist, 1995; Ugolini, 1995; Aston-Jones and Card, 2000; Kelly and Strick, 2000), represents a significant advance over static tracers in the sense that labeling can be safely interpreted as indicating synaptic contact. However, tracing using intact replication-competent viruses suffers two major drawbacks: first, it is never clear whether connections are mono- or polysynaptic, because the replicating virus continues to propagate along the synaptic hierarchy. Second, wild-type replication-competent viruses cannot be used to selectively target groups of neurons embedded in the CNS; direct injection of these vectors gives rise to non-selective infection, and so their use is best restricted to circuits that begin (i.e., sensory) or end (i.e., motor) in the periphery.

Anterograde Trans-Synaptic Tracing via HSV-1 Strain H129

Investigators have attempted to sidestep the drawbacks listed above by modifying viral constructs to alter their tropisms (so that target populations of neurons can be selectively infected following central injection), by comparing the results of viral and conventional tracing studies (to gain insight into which projections are likely to represent monosynaptic connections), and by performing detailed time-course studies to map the likely hierarchy of neuronal connections. All of these approaches have been performed with H129, a strain of HSV-1 that was originally isolated from a patient who died from acute necrotizing encephalitis (Dix et al., 1983) and is notable for its predominantly anterograde direction of trans-synaptic travel (Archin and Atherton, 2002; Wojaczynski et al., 2015). H129 has been used for the mapping of neural circuits for over 20 years (Sun et al., 1996; Garner and LaVail, 1999; Labetoulle et al., 2000); it exhibits rapid replication and spread, with reporter-driving variants producing detectable fluorescence at the site of primary infection within 24 h of innoculation. In our hands, H129 produces detectable trans-synaptic labeling of visual pathways within 48 h of intraocular injection, and the progression of labeling suggests another synapse is "jumped" every 48 h thereafter, although signal strength is variable and benefits from IHC amplification.

As infection progresses, H129 causes cytopathic changes in cell morphology and, if left unchecked, eventual death of the animal, imposing ethical and practical constraints on the duration of experiments (Lo and Anderson, 2011; McGovern et al., 2012b, Wojaczynski et al., 2015). Inoculated rodents begin to show signs of neurological disease that may include hemiparesis, ataxia and drastic weight loss, which varies in its onset time, severity, and prevalence depending on the site of initial infection (Archin and Atherton, 2002; Rinaman and Schwartz, 2004; McGovern et al., 2012a). Interestingly, a significant proportion of rodents inoculated with H129 never develop any detectable infection: in our hands intraocular infection fails to "take" in almost half of cases, similar to the 36% failure rate reported by Lo and Anderson (2011), who also found a surprisingly high failure rate following direct brain injection (18%). The transient nature of the primary viral infection and host defense mechanisms may contribute to variability in uptake and differences in reported strength of labeling.

The specificity of H129 for tracing subpopulations of neurons has been improved by modification of the viral genome: Lo and Anderson (2011) produced a H129 strain dependent on Cre recombinase for replication and transcription of a red reporter. This was achieved by the insertion of a floxed STOP cassette upstream of the tdTomato and TK genes (the TK gene being necessary for replication). Infection of Cre-containing neurons therefore results in permanent removal of the STOP cassette, restoration of viral replication and transcription of the reporter gene, whereas initial infection is unable to take hold in neurons that do not synthesize Cre recombinase. Reporter expression therefore indicates that a neuron either contains Cre recombinase or lies downstream from a Cre-containing neuron, allowing the identification of post-synaptic circuit components. A similar strategy was devised by McGovern et al. (2015b), in which the H129 genome was modified to encode a floxed GFP lying upstream of a red reporter gene (H129-HCMV-loxP-EGFP-HCMVpA-loxP-tdTomato-SV40pA, **Figure 3**). In this case the GFP gene is expressed in naïve neurons but is excised by Cre, resulting in a switch in reporter color in Cre-synthesizing neurons and their (polysynaptic) downstream partners. These modifications allow H129 to be targeted to subpopulations of central neurons, allowing identification of connected circuits, but these variants are still compromised by ambiguity regarding the number of synapses that link labeled neurons to the originally targeted population and the systemic illness that results from unrestricted central infection. These limitations have been recently overcome by deletion of a gene required for viral replication, tyrosine kinase (*TK*), which arrests the spread of H129. When supplied by a helper vector *in trans*, *TK* transiently restores the ability of H129 to replicate and to spread into monosynaptically connected neurons. As these do not contain *TK*, the H129 becomes trapped and so viral reporter expression can be safely interpreted as denoting monosynaptic spread (Zeng et al., 2017; Li et al., 2018).

Retrograde Poly-Synaptic Viral Tracers

Rabies and pseudorabies virus (PRV, a member of the alphaherpes virus family) were developed as retrograde trans-synaptic tracers in the latter decades of the 20th century (Strack et al., 1989a; Ugolini, 1995). PRV, HSV-1 and other alphaherpes viridae rely on interactions between the viral envelope glycoprotein complex and cell surface receptors to gain intracellular access (reviewed by Frampton et al., 2005; Sathiyamoorthy et al., 2017); in neuronal tissue, nectin-1, a synaptic adhesion molecule that is predominantly expressed on the presynaptic membrane and colocalizes well with synaptophysin, is the primary mediator of cell entry and infection, without which little neuronal infection

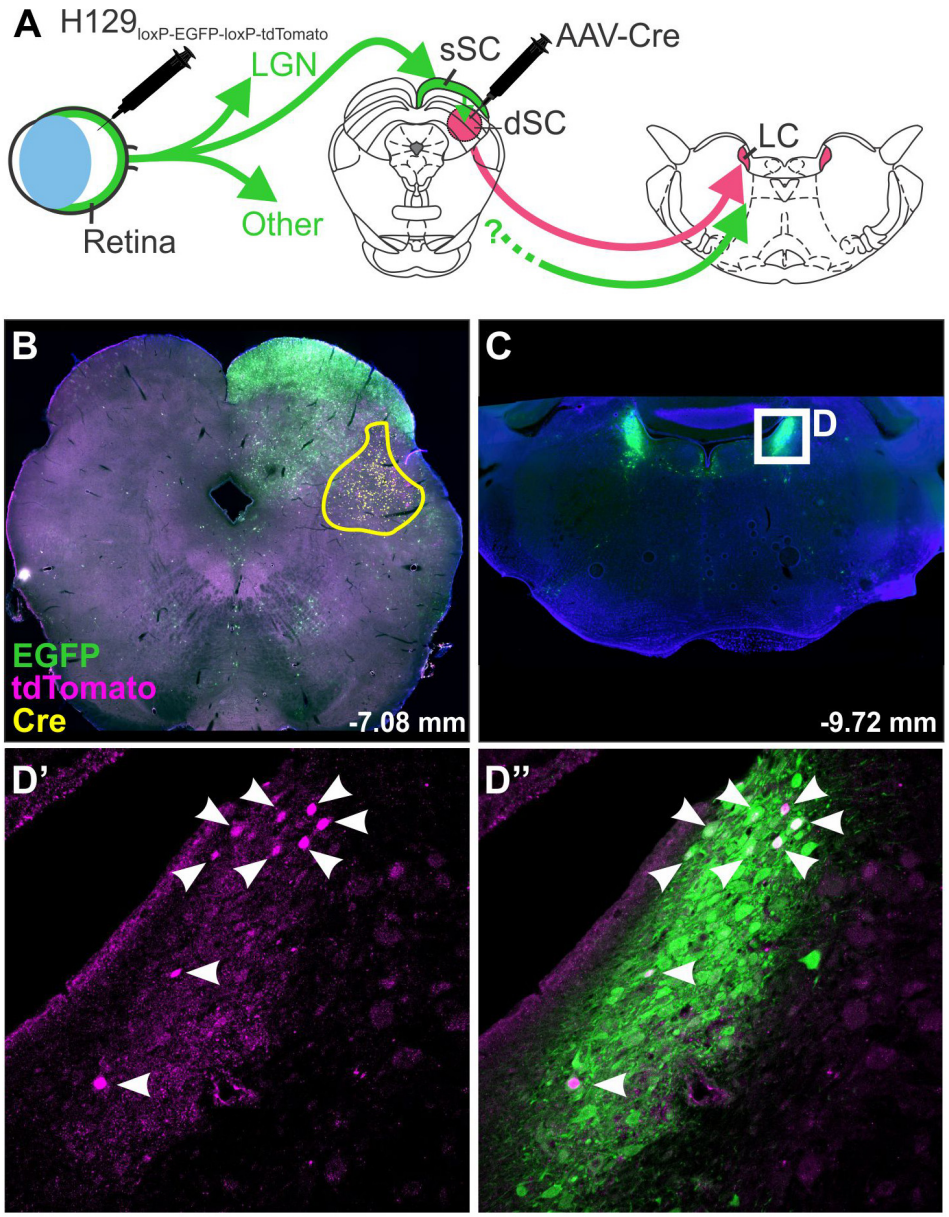

FIGURE 3 | H129 tracing of a polysynaptic pathway. Demonstration of H129 infection of a polysynaptic pathway from the retina, through the deep superior colliculus (dSC), to the locus coeruleus (LC). **(A)** Intravitreal injections of H129-HCMV-loxP-EGFP-HCMVpA-loxP-tdTomato-SV40pA initially infected retinal ganglion cells, driving EGFP expression in retinorecipient nuclei and downstream neurons. When AAV-Cre was injected into the dSC prior to H129 infection (yellow boundary in **B**) the genomes of H129 virions passing through the dSC were cleaved, resulting in tdTomato expression in post-synaptic neurons. Red neurons in downstream regions, such as LC (Low power micrograph in **C**, magnified view in **D'**), can therefore be interpreted as being part of a pathway passing through the dSC. Co-expression of tdTomato and EGFP was common (see merged image, **D"**) and may indicate incomplete H129 cleavage or multiple pathways converging on the same region. LGN: lateral geniculate nucleus; sSC: superficial layer of the superior colliculus.

occurs (Geraghty et al., 1998; Campadelli-Fiume et al., 2000; Mizoguchi et al., 2002; Takai et al., 2008). In addition to the nectin-1- pathway, it is understood that direct cell-to-cell transfer can occur via non-synaptic mechanisms, and that direction of transport may be bi-directional, particularly in wild-type PRV strains, although this confound is reduced in the PRV-Bartha laboratory strain (Card et al., 1998, 1990, 1991, 1999; Pickard et al., 2002; Ugolini, 2011). As a result, PRV experiments are often limited to short incubations and low viral doses in an attempt to reduce the incidence of non-synaptic release of viral particles via cytotoxic cell death.

PRV spreads rapidly, causing observable transgene expression within 6 h *in vitro*, 1 day *in vivo*, and demonstrating trans-synaptic travel within 2 days *in vivo* (Card et al., 1990;

Kobiler et al., 2010). The speed and directional selectivity of PRV has made it the historical tracer of choice for both peripheral and central tracing studies (Martin and Dolivo, 1983; Strack et al., 1989a; Jansen et al., 1995; Smith et al., 1998; DeFalco et al., 2001) although, due to its polysynaptic nature, PRV poses the same challenge as H129 – the differentiation of mono- and polysynaptic connections. As with H129, time-course analyses have sought to address this issue, as well as co-injection of PRV with conventional tracers to identify regions sequentially labeled along polysynaptic pathways (Card et al., 1990; Smith et al., 1998; Kim et al., 1999; Aston-Jones and Card, 2000; DeFalco et al., 2001; Card and Enquist, 2014). Replicating PRV viruses cause neuronal damage and ultimately death of the animal within 5 to 6 days following peripheral injections and 4 days following intracerebral injections (Ugolini et al., 1987; Card et al., 1990, 1992; Card and Enquist, 2014; Oyibo et al., 2014). A less virulent strain has been developed in which the only immediate early gene of PRV, IE80, has been deleted ("IE80-null PRV," Oyibo et al., 2014). Neurons infected with IE80-null PRV have been reported to maintain physiological properties similar to non-infected neurons up to 6 months post infection, with injected mice surviving the same period of time, demonstrating a promising reduction in toxicity.

As with H129 (McGovern et al., 2015a), strains of PRV encoding different transgenes have been used in dual-tracing experiments in which the aim is to assess whether two populations of neurons receive input from a common, third region (Jansen et al., 1995; Banfield et al., 2003). For example, Jansen et al. (1995) used two strains of PRV-Bartha encoding different viral antigens, one encoding the viral glycoprotein gC, and the other encoding β-galactosidase. One strain was injected into the stellate ganglion, while the second was injected into the adrenal gland and IHC used to identify single- and double-labeled neurons. While dual tracing studies appear deceptively simple, a number of important factors must be taken into consideration when selecting the viral vectors to use. The core issue is "superinfection inhibition"; the limited capacity of a single neuron to be infected by more than one virus (Kobiler et al., 2010; Card and Enquist, 2014). Alterations to the viral genome, including the transgene expressed and the location of its insertion, influence the virulence and efficiency of expression, which may place a vector at a disadvantage compared to a "fitter" strain (Kobiler et al., 2010; Card and Enquist, 2014), and so isogenic strains of viruses should be used to minimize these differences (Smith et al., 2000; Banfield et al., 2003). The speed of travel and therefore time of arrival of a virus to the population of interest is also critical; Banfield et al. (2003) compared the dual-infection of rat dorsal root ganglion neurons *in vitro* by PRV152 and PRV614 introduced asynchronously. They found that when the vectors were added simultaneously, almost all neurons were double-labeled, but that a delay of 2 h between injections reduced double-labeling by ∼70%, and that a 4-h delay resulted in almost none. Furthermore, there is a limit to the number of copies of a transgene that a neuron can produce: Kobiler et al. (2010) injected three isogenic strains of PRV that expressed the "Brainbow" cassette and, based on the combinations of fluorophores expressed, estimated that no more than seven genomes could be expressed in each cell. Therefore, vectors should be chosen that are as closely matched as possible for genomic sequence, virulence, speed of transduction and transgene expression, and should arrive at the common region of interest at as close a timepoint as possible.

Retrograde Trans-Synaptic Tracing via Glycoprotein-Deleted Rabies

The evolution of the TK-deleted H129 virus parallels the development of glycoprotein-deleted rabies, the first virus to be developed as a genetically restricted monosynaptic tracer (reviewed by Luo et al., 2008, 2018; Callaway and Luo, 2015). It was developed from the Street Alabama, Dufferin B19 (SADB19) strain of rabies, a virus isolated from a symptomatic dog in the 1930s and maintained on cultured rodent tissue for decades thereafter, over which time it became rodent-specific, attenuated, and incapable of horizontal or vertical transmission (Vos et al., 1999; Beckert et al., 2009). These features make recombinant SADB19 not only a safer option as a research tool, but also led to its development as a live oral vaccine for wild foxes across central Europe, with over 50 million doses airdropped since the 1980s (Geue et al., 2008).

Genetically modified SADB19 has provided a new generation of tracing tools that avoid the shortcomings of classic replication-competent neurotrophic viruses. At the heart of this technology is the key role the rabies glycoprotein plays in the infection and exclusively retrograde trans-synaptic spread of rabies, which occurs through still-undefined mechanisms (Lentz et al., 1982; Mebatsion et al., 1996; Etessami et al., 2000; Schnell et al., 2010; Ugolini, 2010). Deletion of the glycoprotein gene renders the virus, so-called SADΔG, incapable of spreading from one neuron to another but does not affect its capacity for replication (Mebatsion et al., 1996; Etessami et al., 2000; Wickersham et al., 2007a), meaning that SADΔG variants becomes trapped inside infected neurons.

The key insight made by Wickersham et al. (2007b) is that SADΔG's ability to trans-synaptically migrate can be transiently restored by expression of the rabies glycoprotein in infected neurons *in trans* (Marshel et al., 2010). For example, when motoneurons are induced to express rabies glycoprotein using an AAV vector, subsequent infection of those neurons by intramuscular injection of SADΔG results in retrograde infection of monosynaptic input neurons in the spinal cord and brainstem (Esposito et al., 2014).

This approach was further refined by restricting initial access of SADΔG to targeted populations of neurons by pseudotyping glycoprotein-deleted rabies with the envelope protein of a virus that is unable to infect naïve mammalian neurons, avian sarcoma and leukosis virus (EnvA). Infection by pseudotyped SADΔG, notated as SADΔG(EnvA), can be controlled by selective expression of its cognate receptor, TVA, on target neurons (Wickersham et al., 2007b; Marshel et al., 2010). The starting point for monosynaptic retrograde tracing strategies that use SADΔG(EnvA) can be defined by co-expression of the genes that encode TVA and the rabies glycoprotein in target neurons, often referred to as "seed" or "starter" neurons. Direct CNS injection of SADΔG(EnvA) selectively infects seed neurons at the injection

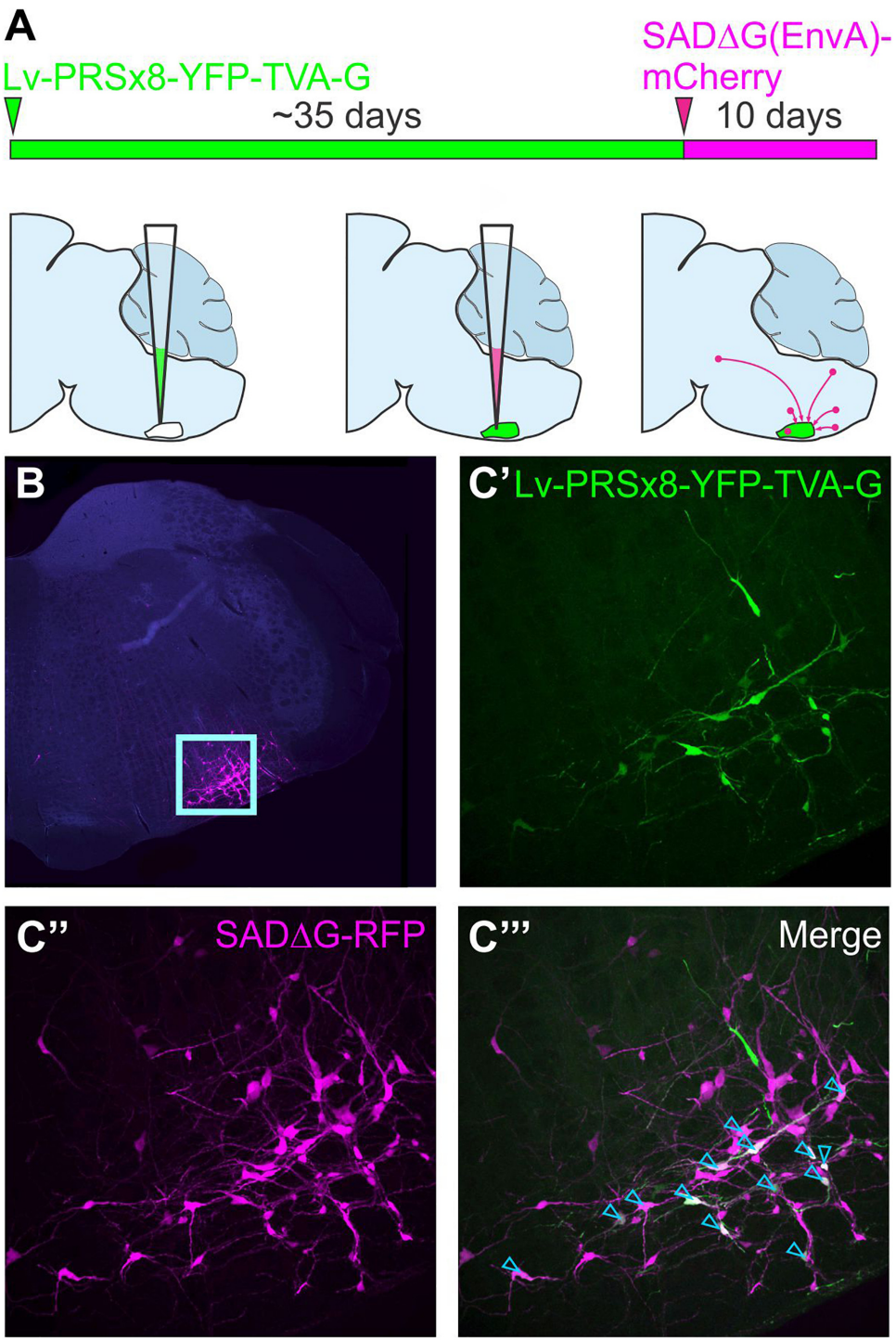

FIGURE 4 | Monosynaptically restricted retrograde tracing using glycoprotein-deleted rabies. **(A)** Experimental strategy: the starting point is co-expression of genes that encode TVA and the rabies glycoprotein in target neurons, in this case delivered by a lentiviral vector that targets putative sympathetic premotor neurons in the ventrolateral medulla (Lv-PRSx8-YFP-TVA-G). Subsequent infection of TVA/G-expressing neurons by SADΔG(EnvA) microinjection leads to trans-synaptic infection of pre-synaptic ("input") neurons. Panel **(B)** shows low power micrograph with infected neurons concentrated in the ventrolateral medulla (boxed region, enlarged in C) "Seed" neurons may be distinguished from "input" neurons by co-expression of the reporters contained in the lentiviral **(C')** and rabies constructs **(C")**, which appear white in the merged image (**C"'**, denoted by blue arrowheads). Modified with permission from Menuet et al. (2017).

site, wherein virions replicate, incorporate the glycoprotein, and spread to monosynaptically connected pre-synaptic ("input") neurons. To distinguish input neurons from seed neurons, a reporter that differs in color from that contained in the SADΔG genome is by convention included within the TVA/glycoprotein cassette (**Figure 4**).

In theory, this approach could be used to identify monosynaptic inputs to any population in which it is possible to selectively drive TVA and the rabies glycoprotein. Investigators from diverse branches of neuroscience have used innovative approaches to limit seeding to their populations of interest, using transgenic mice (Takatoh et al., 2013), lentiviral, AAV or HSV-1 viral vectors (Brennand et al., 2011; Liu et al., 2013; Yonehara et al., 2013; Dempsey et al., 2017; Menuet et al., 2017), and even *in vivo* transfection of single functionally identified neurons (Rancz et al., 2011; Velez-Fort et al., 2014; Wertz et al., 2015).

SADΔG(EnvA) represents a current state-of-the-art technique for interrogation of circuit structure; its promise is reflected by its rapid adoption by diverse branches of neuroscience, high citation rates of studies that use it, and the continued investment in its refinement. However, it is not without its limitations: first, the proportion of monosynaptic input neurons labeled by SADΔG(EnvA) is low and subject to variability, with the ratio of input neurons per starter neuron ranging from less than 10 to several hundred (Rancz et al., 2011; Velez-Fort et al., 2014; Stornetta et al., 2016). Although some of this variability reflects actual differences in the numbers of afferent neurons that converge upon different cell types (Velez-Fort et al., 2014), as discussed at length by Callaway and Luo (2015), the strength of glycoprotein/TVA expression on the target neuron, the titer of SADΔG(EnvA) (and therefore initial number of replicating virions within starter cells), and the duration of the experiment also interact to determine labeling efficiency. Efforts to improve labeling efficiency have focussed on modification of the rabies glycoprotein, resulting in a codon-optimized chimera of the SADB19 and Pasteur G glycoproteins known as "oG" (Kim et al., 2016), or generation of glycoprotein-deleted variants of other rabies strains (Reardon et al., 2016), both of which have improved the efficiency of the original system.

A second caveat to the use of glycoprotein-deleted rabies variants lies in uncertainty regarding potential biases in its tropism. Although validation of trans-synaptic infection of excitatory and inhibitory neurons was included in the initial description of this system (Wickersham et al., 2007b), the potential for differential selectivity according to proximity or phenotype has been raised by a number of investigators (Callaway and Luo, 2015; Reardon et al., 2016). Recent work by Sun et al. (2019) has confirmed these concerns, showing differential labeling of neurons by AAV-retro, SADΔG and conventional tracers, as well as by polysynaptic strains of rabies and pseudorabies, which they speculate reflects variable expression of cognate receptors to viral proteins in different neuronal populations.

A third weakness of the SADΔG system is its neurotoxicity, which is low compared to H129 but nonetheless results in microglial infiltration, gene dysregulation, and cell death within a few weeks of infection (Wickersham et al., 2007a; Sun et al., 2019), and is a major barrier to its integration with functional tools. Again, the development of glycoprotein-deleted versions of other rabies strains has been reported to reduce toxicity (Reardon et al., 2016), and much has been made of a self-inactivating form that clears infected neurons of histotoxic elements shortly after infection (Ciabatti et al., 2017), although a recent early report by Wickersham et al. throws the validity of this approach into doubt (preprint by Matsuyama et al., 2019). Perhaps more promising is the development of so-called "double-deletion rabies" variants (SADΔGL), in which the "L" gene responsible for transcription and replication of the viral genome is deleted in addition to that of the glycoprotein, resulting in a virus with negligible gene transcription and toxicity but which can nonetheless drive expression of recombinase proteins at levels sufficient to drive site-specific recombination in transgenic animals (Chatterjee et al., 2018). Although the recent work by Chatterjee et al. (2018) supports the suitability of SADΔGL as an alternative to AAV-retro, the applicability of this system as a monosynaptically restricted tracer is still unknown.

Finally, in contrast to PRV and H129, the cellular mechanisms responsible for the transmission of rabies are yet to be comprehensively delineated, resulting in some skepticism regarding its supposed retrograde trans-synaptic exclusivity (eloquently summarized in a recent blog by Svoboda, 2019). The strongest evidence in favor of the exclusivity of this mechanism is broad coherence between the results of rabies tracing, ultrastructural, and electrophysiology studies (considered extensively by Ugolini, 2011), and in particular the absence of rabies virions from the extracellular space (which would indicate non-synaptic transmission). However, as pointed out by Svoboda, without a complete understanding of the rabies life cycle it remains difficult to account for discrepancies in connectivity schemes suggested by the results of viral tracing and electrophysiological mapping studies, and so some caution should be exercised in the interpretation of these data.

IMAGING, ANALYSIS AND PRESENTATION OF CONNECTOMIC DATA

The repurposing of viral vectors as instruments for scientific research has transformed the field of neuroanatomy in less than 20 years. The mass production of viral vectors by commercial "vector cores" has lowered economic barriers to their adoption by researchers, while the development of technologies that permit high-throughput manipulation of viral genomes and selection of useful traits, such as directed evolution and genetic barcoding, has made it easier than ever for vector biologists to prototype new viral tools. These factors, coupled with the scientific merit of the approach, will drive innovation in this space for the foreseeable future.

It is therefore surprising that the technologies used by researchers to capture, analyze and present anatomical data have changed so little over the same period: with few exceptions, researchers continue to present their data in terms of the numbers

of labeled neurons that lie within each region of the brain, averaged across replicates and estimated by comparing images of histological sections to plates from a 2-D reference atlas. As we have argued before (Dempsey et al., 2017), expressing rich datasets in such crude terms precludes their independent analysis by other researchers, while potential future reclassification of brain taxonomy threatens the shelf-life of the data. Moreover, it is a laborious and error-prone process, because accuracy is contingent on cutting histological sections in perfect alignment with the reference atlas while maintaining correct ordering and orientation. This task sounds straightforward but is hard to achieve in reality – it took George Paxinos over 50 attempts to get a perfect example for the original Paxinos and Watson rat brain atlas (G. Paxinos, personal communication) – and small deviations from the orthogonal make correct alignment with the reference atlas impossible; for example, if a section through the widest part of the rat brain is cut at 5° mediolateral from true coronal alignment, the lateral border of the cortex on one side of the brain will lie 1.4 mm rostral to the other.

How should this problem be addressed? In our view, it will not be resolved by improving imaging technologies *per se* – if one's objective is to simply map populations of labeled neurons, then improvements in optical resolution are unlikely to help much (although the lowered cost, improved speed and spectral sensitivity of modern microscopes present benefits of their own). Nor are recently developed tissue processing techniques that permit continuous imaging of thick volumes of brain likely to provide a simple solution (Chung et al., 2013; Renier et al., 2014; Tomer et al., 2014): although useful for imaging small volumes of brain, they are slow, labor- and resource-intensive, and inherently difficult to align to a reference atlas. Instead, a new generation of tools is required that can automate and standardize the analysis of tracing data by automatically registering histological tissue into 3-d volumetric brain atlases, extracting the locations of labeled neurons and expressing them in Cartesian co-ordinates as well as identifying the regions in which they reside. This development would simplify analysis, reduce variability, and permit the sharing and independent analysis of connectivity data. Although a number of investigators have highlighted the importance of this mission (Osten and Margrie, 2013; Renier et al., 2016; Furth et al., 2018; Puchades et al., 2019), to date the tools available are hard to use and far from intuitive.

CONCLUSION

Connectomic data will not, by itself, explain how brains work: connectivity is but one parameter in an overlapping spectrum of classifications used by neuroscientists to bracket neurons. However, when combined with electrophysiological properties, synaptic strength, neurotransmitter content, receptor expression and developmental lineage, connectivity data may provide clues to the processes that underlie the function of specific brain circuits and provide insights into the general rules that underlie brain circuit formation, growth and plasticity (Rockland, 2015).

Nevertheless, controversy about the utility of extensive connectomic data remains unresolved (Carandini, 2012; Denk et al., 2012; Rockland, 2015; Jonas and Kording, 2017) (interested readers are also encouraged to watch the debates between Anthony Movshon and Sebastian Seung hosted by Neuwrite at Columbia University in 2012[3] and between Anthony Movshon and Moritz Helmstaedter, held as part of the Cognitive Neuroscience Society annual meeting in 2016[4]). Similar skepticism characterized the early years of the Human Genome Project: the scientific value of sequencing the whole human genome, the exploratory nature of the Project, the seemingly insurmountable technical challenges and high cost projections were a cause for concern for scientists, politicians and tax-payers alike (reviewed by Gannett, 2016). However, the completion of the Human Genome Project not only dramatically advanced sequencing techniques (e.g., personal genealogical genotyping is now commercially viable), but also accelerated the incorporation of genetic technologies to biology at large and spawned gene therapy (Lander, 2011). Whether the discoveries that emerge from the contemporary neuroscience equivalents of the Human Genome Project will lead to analogous translational technologies remains to be seen, but the connectomic movement has already transformed neuroscience.

AUTHOR CONTRIBUTIONS

All authors contributed to the planning, discussion, and drafting of the manuscript.

FUNDING

This research was generously supported by the Hillcrest Foundation (IPAP2019/0933) and by the National Health and Medical Research Council of Australia (APP1127817). CS is a Macquarie University and University of Bristol Ph.D. scholar.

ACKNOWLEDGMENTS

H129 virus was kindly shared by Stuart Mazzone and Alice McGovern, The University of Melbourne. We thank Professor Anthony Pickering for his helpful suggestions and comments.

[3] https://youtu.be/fRHzkRqGf-g

[4] https://youtu.be/uSbNRyY2QH0

REFERENCES

Akli, S., Caillaud, C., Vigne, E., Stratford-Perricaudet, L. D., Poenaru, L., Perricaudet, M., et al. (1993). Transfer of a foreign gene into the brain using adenovirus vectors. *Nat. Genet.* 3, 224–228. doi: 10.1038/ng0393-224

Andrushko, V. A., and Verano, J. W. (2008). Prehistoric trepanation in the Cuzco region of Peru: a view into an ancient Andean practice. *Am. J. Phys. Anthropol.* 137, 4–13. doi: 10.1002/ajpa.20836

Angelucci, A., Clascá, F., and Sur, M. (1996). Anterograde axonal tracing with the subunit B of cholera toxin: a highly sensitive immunohistochemical protocol

for revealing fine axonal morphology in adult and neonatal brains. *J. Neurosci. Methods* 65, 101–112. doi: 10.1016/0165-0270(95)00155-7

Archin, N. M., and Atherton, S. S. (2002). Rapid spread of a neurovirulent strain of HSV-1 through the CNS of BALB/c mice following anterior chamber inoculation. *J. Neurovirol.* 8, 122–135. doi: 10.1080/13550280290049570

Aston-Jones, G., and Card, J. P. (2000). Use of pseudorabies virus to delineate multisynaptic circuits in brain: opportunities and limitations. *J. Neurosci. Methods* 103, 51–61. doi: 10.1016/s0165-0270(00)00295-8

Azevedo, F. A., Carvalho, L. R., Grinberg, L. T., Farfel, J. M., Ferretti, R. E., Leite, R. E., et al. (2009). Equal numbers of neuronal and nonneuronal cells make the human brain an isometrically scaled-up primate brain. *J. Comp. Neurol.* 513, 532–541. doi: 10.1002/cne.21974

Banfield, B. W., Kaufman, J. D., Randall, J. A., and Pickard, G. E. (2003). Development of pseudorabies virus strains expressing red fluorescent proteins: new tools for multisynaptic labeling applications. *J. Virol.* 77, 10106–10112. doi: 10.1128/jvi.77.18.10106-10112.2003

Beckert, A., Geue, L., Vos, A., Neubert, A., Freuling, C., and Muller, T. (2009). Genetic stability (in vivo) of the attenuated oral rabies virus vaccine SAD B19. *Microbiol. Immunol.* 53, 16–21. doi: 10.1111/j.1348-0421.2008.00085.x

Beier, K. T., Saunders, A., Oldenburg, I. A., Miyamichi, K., Akhtar, N., Luo, L., et al. (2011). Anterograde or retrograde transsynaptic labeling of CNS neurons with vesicular stomatitis virus vectors. *Proc. Natl. Acad. Sci. U.S.A.* 108, 15414–15419. doi: 10.1073/pnas.1110854108

Beier, K. T., Saunders, A. B., Oldenburg, I. A., Sabatini, B. L., and Cepko, C. L. (2013). Vesicular stomatitis virus with the rabies virus glycoprotein directs retrograde transsynaptic transport among neurons *in vivo*. *Front. Neural Circ.* 7:11. doi: 10.3389/fncir.2013.00011

Beier, K. T., Steinberg, E. E., DeLoach, K. E., Xie, S., Miyamichi, K., Schwarz, L., et al. (2015). Circuit architecture of VTA dopamine neurons revealed by systematic input-output mapping. *Cell* 162, 622–634. doi: 10.1016/j.cell.2015.07.015

Bentivoglio, M., Kuypers, H. G., Catsman-Berrevoets, C. E., Loewe, H., and Dann, O. (1980). Two new fluorescent retrograde neruonal tracers which are transported over long distances. *Neurosci. Lett.* 18, 25–30. doi: 10.1016/0304-3940(80)90208-6

Berges, B. K., Wolfe, J. H., and Fraser, N. W. (2007). Transduction of brain by herpes simplex virus vectors. *Mol. Ther.* 15, 20–29. doi: 10.1038/sj.mt.6300018

Betley, J. N., and Sternson, S. M. (2011). Adeno-associated viral vectors for mapping, monitoring, and manipulating neural circuits. *Hum. Gene Ther.* 22, 669–677. doi: 10.1089/hum.2010.204

Blomer, U., Naldini, L., Kafri, T., Trono, D., Verma, I. M., and Gage, F. H. (1997). Highly efficient and sustained gene transfer in adult neurons with a lentivirus vector. *J. Virol.* 71, 6641–6649.

Bokiniec, P., Shahbazian, S., McDougall, S. J., Berning, B. A., Cheng, D., Llewellyn-Smith, I. J., et al. (2017). Polysialic acid regulates sympathetic outflow by facilitating information transfer within the nucleus of the solitary tract. *J. Neurosci.* 37, 6558–6574. doi: 10.1523/JNEUROSCI.0200-17.2017

Bonhoeffer, F., and Huf, J. (1980). Position-dependent propoerties of retinal axons and their growth-cones. *J. Neurosci. Methods* 45, 35–40.

Boon, J., Clarke, E., Kessaris, N., Goffinet, A., Molnar, Z., and Hoerder-Suabedissen, A. (2019). Long-range projections from sparse populations of GABAergic neurons in murine subplate. *J. Comp. Neurol.* 527, 1610–1620. doi: 10.1002/cne.24592

Bou Farah, L., Bowman, B. R., Bokiniec, P., Karim, S., Le, S., Goodchild, A. K., et al. (2016). Somatostatin in the rat rostral ventrolateral medulla: origins and mechanism of action. *J. Comp. Neurol.* 524, 323–342. doi: 10.1002/cne.23846

Branco, T., and Staras, K. (2009). The probability of neurotransmitter release: variability and feedback control at single synapses. *Nat. Rev. Neurosci.* 10, 373–383. doi: 10.1038/nrn2634

Brandt, H. M., and Apkarian, A. V. (1992). Biotin-dextran: a sensitive anterograde tracer for neuroanatomic studies in rat and monkey. *J. Neurosci. Methods* 45, 35–40. doi: 10.1016/0165-0270(92)90041-b

Brennand, K. J., Simone, A., Jou, J., Gelboin-Burkhart, C., Tran, N., Sangar, S., et al. (2011). Modelling schizophrenia using human induced pluripotent stem cells. *Nature* 473, 221–225. doi: 10.1038/nature09915

Briggman, K. L., Helmstaedter, M., and Denk, W. (2011). Wiring specificity in the direction-selectivity circuit of the retina. *Nature* 471, 183–188. doi: 10.1038/nature09818

Burette, A., Collman, F., Micheva, K. D., Smith, S. J., and Weinberg, R. J. (2015). Knowing a synapse when you see one. *Front. Neuroanat.* 9:100. doi: 10.3389/fnana.2015.00100

Callaway, E. M. (2005). A molecular and genetic arsenal for systems neuroscience. *Trends Neurosci.* 28, 196–201. doi: 10.1016/j.tins.2005.01.007

Callaway, E. M., and Luo, L. (2015). monosynaptic circuit tracing with glycoprotein-deleted rabies viruses. *J. Neurosci.* 35, 8979–8985. doi: 10.1523/jneurosci.0409-15.2015

Campadelli-Fiume, G., Cocchi, F., Menotti, L., and Lopez, M. (2000). The novel receptors that mediate the entry of herpes simplex viruses and animal alphaherpesviruses into cells. *Rev. Med. Virol.* 10, 305–309.

Carandini, M. (2012). From circuits to behavior: a bridge too far? *Nat. Neurosci.* 15, 507–509. doi: 10.1038/nn.3043

Card, J. P., and Enquist, L. W. (1995). Neurovirulence of pseudorabies virus. *Crit. Rev. Neurobiol.* 9, 137–162.

Card, J. P., and Enquist, L. W. (2014). Transneuronal circuit analysis with pseudorabies viruses. *Curr. Protoc. Neurosci.* 68, 1.5.1–1.5.39. doi: 10.1002/0471142301.ns0105s68

Card, J. P., Enquist, L. W., and Moore, R. Y. (1999). Neuroinvasiveness of pseudorabies virus injected intracerebrally is dependent on viral conventration and terminal field density. *J. Comp. Neurol.* 407, 438–452. doi: 10.1002/(sici)1096-9861(19990510)407:3<438::aid-cne11>3.0.co;2-2

Card, J. P., Levitt, P., and Enquist, L. W. (1998). Different patterns of neuronal infection after intracerebral injections of two strains of pseudorabies virus. *J. Virol.* 72, 4434–4441.

Card, J. P., Rinaman, L., Schwaber, J. S., Miselis, R. R., Whealy, M. E., Robbins, A. K., et al. (1990). Neurotropic properties of pseudorabies virus: uptake and transneuronal passage in the rat central nervous system. *J. Neurosci.* 10, 1974–1994. doi: 10.1523/jneurosci.10-06-01974.1990

Card, J. P., Whealy, M. E., Robbins, A. K., and Enquist, L. W. (1992). Pseudorabies virus envelope glycoprotein gI influences both neurotropism and virulence during infection of the rat visual system. *J. Virol.* 66, 3032–3041.

Card, J. P., Whealy, M. E., Robbins, A. K., Moore, J. P., and Enquist, L. W. (1991). Two ?-herpesvirus strains are transported differentially in the rodent visual system. *Neuron* 6, 957–969. doi: 10.1016/0896-6273(91)90236-s

Castle, M. J., Turunen, H. T., Vandenberghe, L. H., and Wolfe, J. H. (2016). Controlling AAV tropism in the nervous system with natural and engineered capsids. *Methods Mol. Biol.* 1382, 133–149. doi: 10.1007/978-1-4939-3271-9_10

Catani, M., Thiebaut de Schotten, M., Slater, D., and Dell'Acqua, F. (2013). Connectomic approaches before the connectome. *Neuroimage* 80, 2–13. doi: 10.1016/j.neuroimage.2013.05.109

Chamberlin, N. L., Du, B., de Lacalle, S., and Saper, C. B. (1998). Recombinant adeno-associated virus vector: use for transgene expression and anterograde tract tracing in the CNS. *Brain Res.* 793, 169–175. doi: 10.1016/s0006-8993(98)00169-3

Chan, K. Y., Jang, M. J., Yoo, B. B., Greenbaum, A., Ravi, N., Wu, W. L., et al. (2017). Engineered AAVs for efficient noninvasive gene delivery to the central and peripheral nervous systems. *Nat. Neurosci.* 20, 1172–1179. doi: 10.1038/nn.4593

Chatterjee, S., Sullivan, H. A., MacLennan, B. J., Xu, R., Hou, Y., Lavin, T. K., et al. (2018). Nontoxic, double-deletion-mutant rabies viral vectors for retrograde targeting of projection neurons. *Nat. Neurosci.* 21, 638–646. doi: 10.1038/s41593-018-0091-7

Chen, S., and Aston-Jones, G. (1995). Evidence that cholera toxin B subunit (CTb) can be avidly taken up and transported by fibers of passage. *Brain Res.* 674, 107–111. doi: 10.1016/0006-8993(95)00020-q

Chung, K., Wallace, J., Kim, S. Y., Kalyanasundaram, S., Andalman, A. S., Davidson, T. J., et al. (2013). Structural and molecular interrogation of intact biological systems. *Nature* 497, 332–337. doi: 10.1038/nature12107

Ciabatti, E., González-Rueda, A., Mariotti, L., Morgese, F., and Tripodi, M. (2017). Life-long genetic and functional access to neural circuits using self-inactivating rabies virus. *Cell* 170, 382–392. doi: 10.1016/j.cell.2017.06.014

Conte, W. L., Kamishina, H., and Reep, R. L. (2009a). Multiple neuroanatomical tract-tracing using fluorescent Alexa Fluor conjugates of cholera toxin subunit B in rats. *Nat. Protoc.* 4, 1157–1166. doi: 10.1038/nprot.2009.93

Conte, W. L., Kamishina, H., and Reep, R. L. (2009b). The efficacy of the fluorescent conjugates of cholera toxin subunit B for multiple retrograde tract tracing in the central nervous system. *Brain Struct. Funct.* 213, 367–373. doi: 10.1007/s00429-009-0212-x

Cowan, W. M., Gottlieb, D. I., Hendrickson, A. E., Price, J. L., and Woolsey, T. A. (1972). The autoradiographic demonstration of axonal connections in the central nervous system. *Brain Res.* 37, 21–51. doi: 10.1016/0006-8993(72)90344-7

da Costa, N. M., and Martin, K. A. (2011). How thalamus connects to spiny stellate cells in the cat's visual cortex. *J. Neurosci.* 31, 2925–2937. doi: 10.1523/JNEUROSCI.5961-10.2011

Dado, R. J., Burstein, R., Cliffer, K. D., and Giesler, G. J. Jr. (1990). Evidence that fluoro-gold can be transported avidly through fibers of passage. *Brain Res.* 533, 329–333. doi: 10.1016/0006-8993(90)91358-n

DeFalco, J., Tomishima, M., Liu, H., Zhao, C., Cai, X., Marth, J. D., et al. (2001). Virus-assisted mapping of neural inputs to a feeding center in the hypothalamus. *Science* 291, 2608–2613. doi: 10.1126/science.1056602

Dempsey, B., Le, S., Turner, A., Bokiniec, P., Ramadas, R., Bjaalie, J. G., et al. (2017). Mapping and analysis of the connectome of sympathetic premotor neurons in the rostral ventrolateral medulla of the rat using a volumetric brain atlas. *Front. Neural Circ.* 11:9. doi: 10.3389/fncir.2017.00009

Dempsey, B., Turner, A. J., Le, S., Sun, Q. J., Bou Farah, L., Allen, A. M., et al. (2015). Recording, labeling, and transfection of single neurons in deep brain structures. *Physiol. Rep.* 3:e12246. doi: 10.14814/phy2.12246

Denk, W., Briggman, K. L., and Helmstaedter, M. (2012). Structural neurobiology: missing link to a mechanistic understanding of neural computation. *Nat. Rev. Neurosci.* 13, 351–358. doi: 10.1038/nrn3169

Descarries, L., and Mechawar, N. (2000). Ultrastructural evidence for diffuse transmission by monoamine and acetylcholine neurons of the central nervous system. *Prog. Brain Res.* 125, 27–47. doi: 10.1016/s0079-6123(00)25005-x

Dix, R. D., McKendall, R. R., and Baringer, R. (1983). Comparitive neurovirulence of herpes simplex virus type 1 strains after peripheral or intracerebral inoculation of BALB/c mice. *Infect. Immun.* 40, 103–112.

Drouin, L. M., and Agbandje-McKenna, M. (2013). Adeno-associated virus structural biology as a tool in vector development. *Future Virol.* 8, 1183–1199. doi: 10.2217/fvl.13.112

Dumas, M., Schwab, M. E., and Thoenen, H. (1979). Retrograde axonal transport of specific macromolecules as a tool for characterizing nerve terminal membranes. *J. Neurobiol.* 10, 179–197. doi: 10.1002/neu.480100207

Elberger, A. J., and Honig, M. G. (1990). Double-labeling of tissue containing the carbocyanine dye DiI for immunocytochemistry. *J. Histochem. Cytochem.* 38, 735–739. doi: 10.1177/38.5.2110209

Esposito, M. S., Capelli, P., and Arber, S. (2014). Brainstem nucleus MdV mediates skilled forelimb motor tasks. *Nature* 508, 351–356. doi: 10.1038/nature13023

Etessami, R., Conzelmann, K. K., Fadai-Ghotbi, B., Natelson, B., Tsiang, H., and Ceccaldi, P. E. (2000). Spread and pathogenic characteristics of a G-deficient rabies virus recombinant: an in vitro and in vivo study. *J. Gen. Virol.* 81, 2147–2153. doi: 10.1099/0022-1317-81-9-2147

Farmer, D. G. S., Pracejus, N., Dempsey, B., Turner, A., Bokiniec, P., Paton, J. F. R., et al. (2019). On the presence and functional significance of sympathetic premotor neurons with collateralized spinal axons in the rat. *J. Physiol.* 597, 3407–3423. doi: 10.1113/JP277661

Feinberg, E. H., Vanhoven, M. K., Bendesky, A., Wang, G., Fetter, R. D., Shen, K., et al. (2008). GFP reconstitution across synaptic partners (GRASP) defines cell contacts and synapses in living nervous systems. *Neuron* 57, 353–363. doi: 10.1016/j.neuron.2007.11.030

Fenno, L. E., Mattis, J., Ramakrishnan, C., Hyun, M., Lee, S. Y., He, M., et al. (2014). Targeting cells with single vectors using multiple-feature Boolean logic. *Nat. Methods* 11, 763–772. doi: 10.1038/nmeth.2996

Ferrier, D. (1884). Cerebral localisation. a review and forecast. being the marshall hall prize oration. *Med. Chir. Trans.* 67, 33–49. doi: 10.1177/095952878406700103

Fink, R. P., and Heimer, L. (1967). Two methods for selective silver impregnation of degenerating axons and their synaptic endings in the central nervous system. *Brain Res.* 4, 369–374. doi: 10.1016/0006-8993(67)90166-7

Fishman, R. A. (1994). Origins of neuroscience: a history of explorations into brain function.By Stanley Finger, New York, Oxford University Press, 1994, 462 pp, illustrated, $75.00. *Ann. Neurol.* 36:807. doi: 10.1002/ana.410360532

Frampton, A. R. Jr., Goins, W. F., Nakano, K., Burton, E. A., and Glorioso, J. C. (2005). HSV trafficking and development of gene therapy vectors with applications in the nervous system. *Gene Ther.* 12, 891–901. doi: 10.1038/sj.gt.3302545

Fritzsch, B. (1993). Fast axonal diffusion of 3000 molecular weight dextran amines. *J. Neurosci. Methods* 50, 95–103. doi: 10.1016/0165-0270(93)90060-5

Furth, D., Vaissiere, T., Tzortzi, O., Xuan, Y., Martin, A., Lazaridis, I., et al. (2018). An interactive framework for whole-brain maps at cellular resolution. *Nat. Neurosci.* 21, 139–149. doi: 10.1038/s41593-017-0027-7

Furukawa, H., Saito, A., Mol, W., Sekido, M., Sasaki, S., and Yamamoto, Y. (2008). Double innervation occurs in the facial mimetic muscles after facial-hypoglossal end-to-side neural repair: rat model for neural supercharge concept. *J. Plast. Reconstr. Aesthet. Surg.* 61, 257–264. doi: 10.1016/j.bjps.2007.01.075

Furuta, T., Tomioka, R., Taki, K., Nakamura, K., Tamamaki, N., and Kaneko, T. (2001). In vivo transduction of central neurons using recombinant Sindbis virus: golgi-like labeling of dendrites and axons with membrane-targeted fluorescent proteins. *J. Histochem. Cytochem.* 49, 1497–1508.

Gannett, L. (2016). "The human genome project," in *The Stanford Encyclopedia of Philosophy*, ed. E. N. Zalta, (Stanford, CA: Metaphysics Research Lab, Stanford University).

Gao, G., Vandenberghe, L. H., Alvira, M. R., Lu, Y., Calcedo, R., Zhou, X., et al. (2004). Clades of Adeno-associated viruses are widely disseminated in human tissues. *J. Virol.* 78, 6381–6388. doi: 10.1128/jvi.78.12.6381-6388.2004

Garner, J. A., and LaVail, J. H. (1999). Differential anterograde transport of HSV type 1 viral strains in the murine optic pathway. *J. Neurovirol.* 5, 140–150. doi: 10.3109/13550289909021996

Geraghty, R. J., Krummenacher, C., Cohen, G. H., Eisenberg, R. J., and Spear, P. G. (1998). Entry of alphaherpesviruses mediated by poliovirus receptor-related protein 1 and poliovirus receptor. *Science* 280, 1618–1620. doi: 10.1126/science.280.5369.1618

Gerfen, C. R., and Sawchenko, P. E. (1984). An anterograde neuroanatomical tracing method that shows the detailed morphology of neurons, their axons and terminals: immunohistochemical localization of an axonally transported plant lectin,Phaseolus vulgaris leucoagglutinin (PHA-L). *Brain Res.* 290, 219–238. doi: 10.1016/0006-8993(84)90940-5

Geue, L., Schares, S., Schnick, C., Kliemt, J., Beckert, A., Freuling, C., et al. (2008). Genetic characterisation of attenuated SAD rabies virus strains used for oral vaccination of wildlife. *Vaccine* 26, 3227–3235. doi: 10.1016/j.vaccine.2008.04.007

Gimlich, R. L., and Braun, J. (1985). Improved fluorescent compounds for tracing cell lineage. *Dev. Biol.* 109, 509–514. doi: 10.1016/0012-1606(85)90476-2

Glees, P. (1946). Terminal degeneration within the central nervous system as studied by a new silver method. *J. Neuropathol. Exp. Neurol.* 5, 54–59. doi: 10.1097/00005072-194601000-00005

Glover, J. C. (1995). Retrograde and anterograde axonal tracing with fluorescent dextrans in the embryonic nervous system. *Neurosci. Protoc.* 95, 1–13.

Glover, J. C., Petursdottir, G., and Jansen, J. K. S. (1986). Fluorescent dextran amines used as axonal tracers in the nervous system of chicken embryo. *J. Neurosci. Methods* 18, 243–254. doi: 10.1016/0165-0270(86)90011-7

Gofflot, F., Wendling, O., Chartoire, N., Birling, M. C., Warot, X., and Auwerx, J. (2011). Characterization and validation of cre-driver mouse lines. *Curr. Protoc. Mouse Biol.* 1, 1–15. doi: 10.1002/9780470942390.mo100103

Goshgarian, H. G., and Buttry, J. L. (2014). The pattern and extent of retrograde transsynaptic transport of WGA-Alexa 488 in the phrenic motor system is dependent upon the site of application. *J. Neurosci. Methods* 222, 156–164. doi: 10.1016/j.jneumeth.2013.11.003

Grafstein, B. (1967). Transport of protein by goldfish optic nerve fibers. *Science* 157, 196–198. doi: 10.1126/science.157.3785.196

Grimm, D., and Buning, H. (2017). Small but increasingly mighty: latest advances in AAV vector research, design, and evolution. *Hum. Gene Ther.* 28, 1075–1086. doi: 10.1089/hum.2017.172

Gross, C. G. (2009). "Phrenology," in *Encyclopedia of Neuroscience*, ed. L. R. Squire, (Oxford: Academic Press), 701–705.

Guillery, R. W. (2005). Observations of synaptic structures: origins of the neuron doctrine and its current status. *Philos. Trans. R.*

Soc. Lond. B Biol. Sci. 360, 1281–1307. doi: 10.1098/rstb.2003.1459

Hagmann, P. (2005). *From Diffusion MRI to Brain Connectomics*. Ph.D thesis, Ecole Polytechnique Fédérale de Lausanne, Lausanne.

Henriksen, S., Pang, R., and Wronkiewicz, M. (2016). A simple generative model of the mouse mesoscale connectome. *eLife* 5:e12366. doi: 10.7554/eLife.12366

Herculano-Houzel, S. (2009). The human brain in numbers: a linearly scaled-up primate brain. *Front. Hum. Neurosci.* 3:31. doi: 10.3389/neuro.09.031.2009

Hilbert, M., and Lopez, P. (2011). The world's technological capacity to store, communicate, and compute information. *Science* 332, 60–65. doi: 10.1126/science.1200970

Hirschberg, S., Li, Y., Randall, A., Kremer, E. J., and Pickering, A. E. (2017). Functional dichotomy in spinal-vs prefrontal-projecting locus coeruleus modules splits descending noradrenergic analgesia from ascending aversion and anxiety in rats. *eLife* 6:e29808. doi: 10.7554/eLife.29808

Hoff, E. C. (1932). Central nerve terminals in the mammalian spinal cord and their examination by experimental degeneration. *Proc. R. Soc. Lond. Ser. BContain. Pap. Biol.* 111, 175–188. doi: 10.1098/rspb.1932.0049

Howorth, P. W., Thornton, S. R., O'Brien, V., Smith, W. D., Nikiforova, N., Teschemacher, A. G., et al. (2009). Retrograde viral vector-mediated inhibition of pontospinal noradrenergic neurons causes hyperalgesia in rats. *J. Neurosci.* 29, 12855–12864. doi: 10.1523/JNEUROSCI.1699-09.2009

Hwang, D. Y., Carlezon, W. A. Jr., Isacson, O., and Kim, K. S. (2001). A high-efficiency synthetic promoter that drives transgene expression selectively in noradrenergic neurons. *Hum. Gene Ther.* 12, 1731–1740. doi: 10.1089/104303401750476230

Jakobsson, J., Ericson, C., Jansson, M., Bjork, E., and Lundberg, C. (2003). Targeted transgene expression in rat brain using lentiviral vectors. *J. Neurosci. Res.* 73, 876–885. doi: 10.1002/jnr.10719

Jansen, A. S. P., Van Nguyen, X., Karpitskiy, X., Mettenleiter, T. C., and Loewy, A. D. (1995). Central command neurons of the sympathetic nervous system: basis of the fight-or-flight response. *Science* 270, 253–260.

Jia, F., Miao, H., Zhu, X., and Xu, F. (2017). Pseudo-typed semliki forest virus delivers EGFP into neurons. *J. Neurovirol.* 23, 205–215. doi: 10.1007/s13365-016-0486-8

Jonas, E., and Kording, K. P. (2017). Could a neuroscientist understand a microprocessor? *PLoS Comput. Biol.* 13:e1005268. doi: 10.1371/journal.pcbi.1005268

Junyent, F., and Kremer, E. J. (2015). CAV-2–why a canine virus is a neurobiologist's best friend. *Curr. Opin. Pharmacol.* 24, 86–93. doi: 10.1016/j.coph.2015.08.004

Jüttner, J., Szabo, A., Gross-Scherf, B., Morikawa, R. K., Rompani, S. B., Hantz, P., et al. (2019). Targeting neuronal and glial cell types with synthetic promoter AAVs in mice, non-human primates and humans. *Nat. Neurosci.* 22, 1345–1356. doi: 10.1038/s41593-019-0431-2

Kanaan, N. M., Sellnow, R. C., Boye, S. L., Coberly, B., Bennett, A., Agbandje-McKenna, M., et al. (2017). Rationally engineered AAV capsids improve transduction and volumetric spread in the CNS. *Mol. Ther. Nucleic Acids* 8, 184–197. doi: 10.1016/j.omtn.2017.06.011

Kato, S., Kobayashi, K., Inoue, K., Kuramochi, M., Okada, T., Yaginuma, H., et al. (2011). A lentiviral strategy for highly efficient retrograde gene transfer by pseudotyping with fusion envelope glycoprotein. *Hum. Gene Ther.* 22, 197–206. doi: 10.1089/hum.2009.179

Katz, L. C., Burkhalter, A., and Dreyer, W. J. (1984). Fluorescent latex microspheres as a retrograde neuronal marker for in vivo and in vitro studies of visual cortex. *Nature* 310, 498–500. doi: 10.1038/310498a0

Katz, L. C., and Iarovici, D. M. (1990). Green fluorescent latex microspheres: a new retrograde tracer. *Neuroscience* 34, 511–520. doi: 10.1016/0306-4522(90)90159-2

Kelly, R. M., and Strick, P. L. (2000). Rabies as a transneuronal tracer of circuits in the central nervous system. *J. Neurosci. Methods* 103, 63–71. doi: 10.1016/s0165-0270(00)00296-x

Kim, E. J., Jacobs, M. W., Ito-Cole, T., and Callaway, E. M. (2016). Improved monosynaptic neural circuit tracing using engineered rabies virus glycoproteins. *Cell Rep.* 15, 692–699. doi: 10.1016/j.celrep.2016.03.067

Kim, J., Zhao, T., Petralia, R. S., Yu, Y., Peng, H., Myers, E., et al. (2011). mGRASP enables mapping mammalian synaptic connectivity with light microscopy. *Nat. Methods* 9, 96–102. doi: 10.1038/nmeth.1784

Kim, J. S., Moore, R. Y., Enquist, L. W., and Card, J. P. (1999). Circuit-specific co-infection of the neurons in the rat central nervous system with two pseudorabies virus recombinants. *J. Virol.* 75, 9521–9531.

Köbbert, C., Apps, R., Bechmann, I., Lanciego, J. L., Mey, J., and Thanos, S. (2000). Current concepts in neuroanatomical tracing. *Prog. Neurobiol.* 62, 327–351. doi: 10.1016/s0301-0082(00)00019-8

Kobiler, O., Lipman, Y., Therkelsen, K., Daubechies, I., and Enquist, L. W. (2010). Herpesviruses carrying a Brainbow cassette reveal replication and expression of limited numbers of incoming genomes. *Nat. Commun.* 1:146. doi: 10.1038/ncomms1145

Korim, W. S., Bou Farah, L., McMullan, S., and Verberne, A. J. (2014). Orexinergic activation of medullary premotor neurons modulates the adrenal sympathoexcitation to hypothalamic glucoprivation. *Diabetes Metab. Res. Rev.* 63, 1895–1906. doi: 10.2337/db13-1073

Kotterman, M. A., and Schaffer, D. V. (2014). Engineering adeno-associated viruses for clinical gene therapy. *Nat. Rev. Genet.* 15, 445–451. doi: 10.1038/nrg3742

Kristensson, K., and Olsson, Y. (1971). Retrograde axonal transport of protein. *Brain Res.* 29, 363–365. doi: 10.1016/0006-8993(71)90044-8

Kshettry, V. R., Mindea, S. A., and Batjer, H. H. (2007). The management of cranial injuries in antiquity and beyond. *Neurosurg. Focus* 23:E8.

Kuo, H., Ingram, D. K., Crystal, R. G., and Mastrangeli, A. (1995). Retrograde transfer of replication deficient recombinant adenovirus vector in the central nervous system for tracing studies. *Brain Res.* 705, 31–38. doi: 10.1016/0006-8993(95)01065-3

Kuypers, H. G., Bentivoglio, M., Castman-Berreveoets, C. E., and Bharos, A. T. (1980). Double retrograde neuronal labeling through divergent axon collaterals, using two fluorescent tracers with the same excitation wavelength which label different features of the cell. *Exp. Brain Res.* 40, 383–392.

Labetoulle, M., Kucera, P., Ugolini, G., Lafay, F., Frau, E., Offret, H., et al. (2000). Neuronal pathways for the propagation of herpes simplex virus type 1 from one retina to the other in a murine model. *J. Gen. Virol.* 81, 1201–1210. doi: 10.1099/0022-1317-81-5-1201

Lanciego, J. L., and Wouterlood, F. G. (2011). A half century of experimental neuroanatomical tracing. *J. Chem. Neuroanat.* 42, 157–183. doi: 10.1016/j.jchemneu.2011.07.001

Lander, E. S. (2011). Initial impact of the sequencing of the human genome. *Nature* 470, 187–197. doi: 10.1038/nature09792

Larsen, D. D., Wickersham, I. R., and Callaway, E. M. (2007). Retrograde tracing with recombinant rabies virus reveals correlations between projection targets and dendritic architecture in layer 5 of mouse barrel cortex. *Front. Neural Circ.* 1:5. doi: 10.3389/neuro.04.005.2007

LaVail, J. H., and LaVail, M. M. (1972). Retrograde axonal transport in the central nervous system. *Science* 176, 1416–1417. doi: 10.1126/science.176.4042.1416

Lentz, T. L., Burrage, T. G., Smith, A. L., Crick, J., and Tignor, G. H. (1982). Is the acetylcholine receptor a rabies virus receptor? *Science* 215, 182–184. doi: 10.1126/science.7053569

Lerner, T. N., Shilyansky, C., Davidson Thomas, J., Evans Kathryn, E., Beier Kevin, T., Zalocusky Kelly, A., et al. (2015). Intact-Brain analyses reveal distinct information carried by SNc dopamine subcircuits. *Cell* 162, 635–647. doi: 10.1016/j.cell.2015.07.014

Lerner, T. N., Ye, L., and Deisseroth, K. (2016). Communication in neural circuits: tools. *Oppor. Chall. Cell* 164, 1136–1150. doi: 10.1016/j.cell.2016.02.027

Levy, S. L., White, J. J., Lackey, E. P., Schwartz, L., and Sillitoe, R. V. (2017). WGA-Alexa conjugates for axonal tracing. *Curr. Protoc. Neurosci.* 79, 12821–212824. doi: 10.1002/cpns.28

Li, L., Tasic, B., Micheva, K. D., Ivanov, V. M., Spletter, M. L., Smith, S. J., et al. (2010). Visualizing the distribution of synapses from individual neurons in the mouse brain. *PLoS One* 5:e11503. doi: 10.1371/journal.pone.0011503

Li, X., Chen, W., Pan, K., Li, H., Pang, P., Guo, Y., et al. (2018). Serotonin receptor 2c-expressing cells in the ventral CA1 control attention via innervation of the Edinger-Westphal nucleus. *Nat. Neurosci.* 21, 1239–1250. doi: 10.1038/s41593-018-0207-0

Lichtman, J. W., and Denk, W. (2011). The big and the small: challenges of imaging the brain's circuits. *Science* 334, 618–623. doi: 10.1126/science.1209168

Liu, Y.-J., Ehrengruber Markus, U., Negwer, M., Shao, H.-J., Cetin Ali, H., and Lyon David, C. (2013). Tracing inputs to inhibitory or excitatory neurons of mouse and cat visual cortex with a targeted rabies virus. *Curr. Biol.* 23, 1746–1755. doi: 10.1016/j.cub.2013.07.033

Llinas, R. R. (2003). The contribution of santiago ramon y cajal to functional neuroscience. *Nat. Rev. Neurosci.* 4, 77–80. doi: 10.1038/nrn1011

Lo, L., and Anderson, D. J. (2011). A Cre-dependent, anterograde transsynaptic viral tracer for mapping output pathways of genetically marked neurons. *Neuron* 72, 938–950. doi: 10.1016/j.neuron.2011.12.002

Lopez-Munoz, F., Boya, J., and Alamo, C. (2006). Neuron theory, the cornerstone of neuroscience, on the centenary of the Nobel Prize award to Santiago Ramon y Cajal. *Brain Res. Bull.* 70, 391–405. doi: 10.1016/j.brainresbull.2006.07.010

Lundberg, C., Bjorklund, T., Carlsson, T., Jakobsson, J., Hantraye, P., Deglon, N., et al. (2008). Applications of lentiviral vectors for biology and gene therapy of neurological disorders. *Curr. Gene Ther.* 8, 461–473. doi: 10.2174/156652308786847996

Lunde, A., Okaty, B. W., Dymecki, S. M., and Glover, J. C. (2019). Molecular profiling defines evolutionarily conserved transcription factor signatures of major vestibulospinal neuron groups. *eNeuro* 6:e0475-0418.2019. doi: 10.1523/ENEURO.0475-18.2019

Luo, L., Callaway, E. M., and Svoboda, K. (2008). Genetic dissection of neural circuits. *Neuron* 57, 634–660. doi: 10.1016/j.neuron.2008.01.002

Luo, L., Callaway, E. M., and Svoboda, K. (2018). Genetic dissection of neural circuits: a decade of progress. *Neuron* 98, 256–281. doi: 10.1016/j.neuron.2018.03.040

Luppi, P. H., Sakai, K., Salvert, D., Fort, P., and Jouvet, M. (1987). Peptidergic hypothalamic afferents to the cat nucleus raphe pallidus as revealed by a double immunostaining technique using unconjugated cholera toxin as a retrograde tracer. *Brain Res.* 402, 339–345. doi: 10.1016/0006-8993(87)90041-2

Lykken, E. A., Shyng, C., Edwards, R. J., Rozenberg, A., and Gray, S. J. (2018). Recent progress and considerations for AAV gene therapies targeting the central nervous system. *J. Neurodev. Disord.* 10:16. doi: 10.1186/s11689-018-9234-0

Marshel, J. H., Mori, T., Nielsen, K. J., and Callaway, E. M. (2010). Targeting single neuronal networks for gene expression and cell labeling *In Vivo*. *Neuron* 67, 562–574. doi: 10.1016/j.neuron.2010.08.001

Martin, X., and Dolivo, M. (1983). Neuronal and transneuronal tracing in the trigeminal system of the rat using the herpes virus suis. *Brain Res.* 273, 253–276. doi: 10.1016/0006-8993(83)90850-8

Matsubayashi, Y., Iwai, L., and Kawasaki, H. (2008). Fluorescent double-labeling with carbocyanine neuronal tracing and immunohistochemistry using a cholesterol-specific detergent digitonin. *J. Neurosci. Methods* 174, 71–81. doi: 10.1016/j.jneumeth.2008.07.003

Matsuyama, M., Jin, L., Lavin, T. K., Sullivan, H. A., Hou, Y., Lea, N. E., et al. (2019). *"Self-inactivating" Rabies Viruses are Just First-Generation, ΔG Rabies Viruses*. Available at: https://www.biorxiv.org/content/10.1101/550640v1 (accessed July 24, 2019).

McGovern, A. E., Davis-Poynter, N., Farrell, M. J., and Mazzone, S. B. (2012a). Transneural tracing of airways-related sensory circuitry using herpes simplex virus 1, strain H129. *Neuroscience* 207, 148–166. doi: 10.1016/j.neuroscience.2012.01.029

McGovern, A. E., Davis-Poynter, N., Rokoczy, J., Phipps, A., Simmons, D. G., and Mazzone, S. B. (2012b). Anterograde neuronal circuit tracing using a genetically modified herpes simplex virus expressing EGFP. *J. Neurosci. Methods* 209, 158–167. doi: 10.1016/j.jneumeth.2012.05.035

McGovern, A. E., Davis-Poynter, N., Yang, S. K., Simmons, D. G., Farrell, M. J., and Mazzone, S. B. (2015a). Evidence for multiple sensory circuits in the brain arising from the respiratory system: an anterograde viral tract tracing study in rodents. *Brain Struct. Funct.* 220, 3683–3699. doi: 10.1007/s00429-014-0883-9

McGovern, A. E., Driessen, A. K., Simmons, D. G., Powell, J., Davis-Poynter, N., Farrell, M. J., et al. (2015b). Distinct brainstem and forebrain circuits receiving tracheal sensory neuron inputs revealed using a novel conditional anterograde transsynaptic viral tracing system. *J. Neurosci.* 35, 7041–7055. doi: 10.1523/JNEUROSCI.5128-14.2015

McPherson, D. R., McClellan, A. D., and O'Donovan, M. J. (1997). Optical imaging of neuronal activity in tissue labeled by retrograde transport of Calcium Green Dextran. *Brain Res. Brain Res. Protoc.* 1, 157–164. doi: 10.1016/S1385-299X(96)00024-4

Mebatsion, T., Konig, M., and Conzelmann, K. K. (1996). Budding of rabies virus particles in the absence of the spike glycoprotein. *Cell* 84, 941–951. doi: 10.1016/s0092-8674(00)81072-7

Menuet, C., Le, S., Dempsey, B., Connelly, A. A., Kamar, J. L., Jancovski, N., et al. (2017). Excessive respiratory modulation of blood pressure triggers hypertension. *Cell Metab.* 25, 1–10. doi: 10.1016/j.cmet.2017.01.019

Mikula, S. (2016). Progress towards mammalian whole-brain cellular connectomics. *Front. Neuroanat.* 10:62. doi: 10.3389/fnana.2016.00062

Mizoguchi, A., Nakanishi, H., Kimura, K., Matsubara, K., Ozaki-Kuroda, K., Katata, T., et al. (2002). Nectin: an adhesion molecule involved in formation of synapses. *J. Cell Biol.* 156, 555–565. doi: 10.1083/jcb.200103113

Moghaddam, N., Mailler-Burch, S., Kara, L., Kanz, F., Jackowski, C., and Lösch, S. (2015). Survival after trepanation—Early cranial surgery from Late Iron Age Switzerland. *Int. J. Paleopathol.* 11, 56–65. doi: 10.1016/j.ijpp.2015.08.002

Murlidharan, G., Samulski, R. J., and Asokan, A. (2014). Biology of adeno-associated viral vectors in the central nervous system. *Front. Mol. Neurosci.* 7:76. doi: 10.3389/fnmol.2014.00076

Nassi, J. J., Cepko, C. L., Born, R. T., and Beier, K. T. (2015). Neuroanatomy goes viral! *Front. Neuroanat.* 9:80. doi: 10.3389/fnana.2015.00080

Nauta, W. J. (1952). Selective silver impregnation of degenerating axons in the central nervous system. *Stain Technol.* 27, 175–179. doi: 10.3109/10520295209105080

Neve, R. L. (2012). Overview of gene delivery into cells using HSV-1-based vectors. *Curr. Protoc. Neurosci.* Chapter 4:Unit 4.12. doi: 10.1002/0471142301.ns0412s61

Nimchinsky, E. A., Sabatini, B. L., and Svoboda, K. (2002). Structure and function of dendritic spines. *Annu. Rev. Physiol.* 64, 313–353.

Noseda, R., Kainz, V., Jakubowski, M., Gooley, J. J., Saper, C. B., Digre, K., et al. (2010). A neural mechanism for exacerbation of headache by light. *Nat. Neurosci.* 13, 239–245. doi: 10.1038/nn.2475

O'Connor, D. M., and Boulis, N. M. (2015). Gene therapy for neurodegenerative diseases. *Trends Mol. Med.* 21, 504–512. doi: 10.1016/j.molmed.2015.06.001

O'Donovan, M. J., Ho, S., Sholomenko, G., and Yee, W. (1993). Real-time imaging of neurons retrogradely and anterogradely labelled with calcium-sensitive dyes. *J. Neurosci. Methods* 46, 91–106. doi: 10.1016/0165-0270(93)90145-H

Oh, S. W., Harris, J. A., Ng, L., Winslow, B., Cain, N., Mihalas, S., et al. (2014). A mesoscale connectome of the mouse brain. *Nature* 508, 207–214. doi: 10.1038/nature13186

Ohyama, T., Schneider-Mizell, C. M., Fetter, R. D., Aleman, J. V., Franconville, R., Rivera-Alba, M., et al. (2015). A multilevel multimodal circuit enhances action selection in Drosophila. *Nature* 520, 633–639. doi: 10.1038/nature14297

Osten, P., and Margrie, T. W. (2013). Mapping brain circuitry with a light microscope. *Nat. Methods* 10, 515–523. doi: 10.1038/nmeth.2477

Oyibo, H. K., Znamenskiy, P., Oviedo, H. V., Enquist, L. W., and Zador, A. M. (2014). Long-term Cre-mediated retrograde tagging of neurons using a novel recombinant pseudorabies virus. *Front. Neuroanat.* 8:86. doi: 10.3389/fnana.2014.00086

Parker, L. M., Kumar, N. N., Lonergan, T., McMullan, S., and Goodchild, A. K. (2015). Distribution and neurochemical characterization of neurons in the rat ventrolateral medulla activated by glucoprivation. *Brain Struct. Funct.* 220, 117–134. doi: 10.1007/s00429-013-0642-3

Pearce, J. M. (2009). Marie-Jean-Pierre Flourens (1794-1867) and cortical localization. *Eur. Neurol.* 61, 311–314. doi: 10.1159/000206858

Penrod, R. D., Wells, A. M., Carlezon, W. A. Jr., and Cowan, C. W. (2015). Use of adeno-associated and herpes simplex viral vectors for *In Vivo* neuronal expression in mice. *Curr. Protoc. Neurosci.* 73, 4.37.1–4.37.31. doi: 10.1002/0471142301.ns0437s73

Pickard, G. E., Smeraski, C. A., Tomlinson, C. C., Banfield, B. W., Kaufman, J., Wilcox, C. L., et al. (2002). Intravitreal injection of the attenuated pseudorabies virus PRV-Bartha results in infection of the hamster suprachiasmatic nucleus only by retrograde transsynaptic transport via autonomic circuits. *J. Neurosci.* 22, 2701–2710. doi: 10.1523/jneurosci.22-07-02701.2002

Pidsudko, Z., Listowska, Z., Franke-Radowiecka, A., Klimczuk, M., Zalecki, M., and Kaleczyc, J. (2019). Distribution and chemical coding of urinary bladder apex-projecting neurons in aorticorenal and testicular ganglia of the male pig. *Pol. J. Vet. Sci.* 22, 427–430. doi: 10.24425/pjvs.2019.129227

Pilowsky, P., Llewellyn-Smith, I. J., Lipski, J., and Chalmers, J. (1992). Substance P immunoreactive boutons form synapses with feline sympathetic preganglionic neurons. *J. Comp. Neurol.* 320, 121–135. doi: 10.1002/cne.903200109

Puchades, M. A., Csucs, G., Ledergerber, D., Leergaard, T. B., and Bjaalie, J. G. (2019). Spatial registration of serial microscopic brain images to three-dimensional reference atlases with the QuickNII tool. *PLoS One* 14:e0216796. doi: 10.1371/journal.pone.0216796

Puigdellivol-Sanchez, A., Prats-Galino, A., Ruano-Gil, D., and Molander, C. (1998). Efficacy of the fluorescent dyes Fast Blue, Fluoro-Gold, and diamidino yellow for retrograde tracing to dorsal root ganglia after subcutaneous injection. *J. Neurosci. Methods* 86, 7–16. doi: 10.1016/s0165-0270(98)00137-x

Rancz, E. A., Franks, K. M., Schwarz, M. K., Pichler, B., Schaefer, A. T., and Margrie, T. W. (2011). Transfection via whole-cell recording in vivo: bridging single-cell physiology, genetics and connectomics. *Nat. Neurosci.* 14, 527–532. doi: 10.1038/nn.2765

Reardon, T. R., Murray, A. J., Turi, G. F., Wirblich, C., Croce, K. R., Schnell, M. J., et al. (2016). Rabies virus CVS-N2c(DeltaG) strain enhances retrograde synaptic transfer and neuronal viability. *Neuron* 89, 711–724. doi: 10.1016/j.neuron.2016.01.004

Reiner, A., Veenman, C. L., Medina, L., Jiao, Y., Del Mar, N., and Honig, M. G. (2000). Pathway tracing using biotinylated dextran amines. *J. Neurosci. Methods* 103, 23–37. doi: 10.1016/s0165-0270(00)00293-4

Renier, N., Adams, E. L., Kirst, C., Wu, Z., Azevedo, R., Kohl, J., et al. (2016). Mapping of brain activity by automated volume analysis of immediate early genes. *Cell* 165, 1789–1802. doi: 10.1016/j.cell.2016.05.007

Renier, N., Wu, Z., Simon, D. J., Yang, J., Ariel, P., and Tessier-Lavigne, M. (2014). iDISCO: a simple, rapid method to immunolabel large tissue samples for volume imaging. *Cell* 159, 896–910. doi: 10.1016/j.cell.2014.10.010

Rinaman, L., and Schwartz, G. (2004). Anterograde transneuronal viral tracing of central viscerosensory pathways in rats. *J. Neurosci.* 24, 2782–2786. doi: 10.1523/jneurosci.5329-03.2004

Rockland, K. S. (2015). About connections. *Front. Neuroanat.* 9:61. doi: 10.3389/fnana.2015.00061

Rothermel, M., Brunert, D., Zabawa, C., Díaz-Quesada, M., and Wachowiak, M. (2013). Transgene expression in target-defined neuron populations mediated by retrograde infection with adeno-associated viral vectors. *J. Neurosci.* 33, 15195–15206. doi: 10.1523/JNEUROSCI.1618-13.2013

Rubinov, M., and Bullmore, E. T. (2013). Fledgline pathoconnectomics of psychiatric disorders. *Trends Cogn. Sci.* 17, 641–647. doi: 10.1016/j.tics.2013.10.007

Ryan, K., Lu, Z., and Meinertzhagen, I. A. (2016). The CNS connectome of a tadpole larva of *Ciona intestinalis* (L.) highlights sidedness in the brain of a chordate sibling. *eLife* 5:e16962. doi: 10.7554/eLife.16962

Rytel, L., Snarska, A., Gonkowski, S., Wojtkiewicz, J., Szenci, O., and Sobiech, P. (2019). Identification of neuropeptide y in superior cervical ganglion neurons that project to the oesophagus - A combined immunohistochemical labelling and retrograde tracing study in pigs. *Acta Vet. Hung.* 67, 98–105. doi: 10.1556/004.2019.011

Salinas, S., Bilsland, L. G., Henaff, D., Weston, A. E., Keriel, A., Schiavo, G., et al. (2009). CAR-associated vesicular transport of an adenovirus in motor neuron axons. *PLoS Pathog.* 5:e1000442. doi: 10.1371/journal.ppat.1000442

Santiago-Ortiz, J., Ojala, D. S., Westesson, O., Weinstein, J. R., Wong, S. Y., Steinsapir, A., et al. (2015). AAV ancestral reconstruction library enables selection of broadly infectious viral variants. *Gene Ther.* 22, 934–946. doi: 10.1038/gt.2015.74

Santiago-Ortiz, J. L., and Schaffer, D. V. (2016). Adeno-associated virus (AAV) vectors in cancer gene therapy. *J. Control. Release* 240, 287–301. doi: 10.1016/j.jconrel.2016.01.001

Sathiyamoorthy, K., Chen, J., Longnecker, R., and Jardetzky, T. S. (2017). The COMPLEXity in herpesvirus entry. *Curr. Opin. Virol.* 24, 97–104. doi: 10.1016/j.coviro.2017.04.006

Schmued, L., Kyriakidis, K., and Heimer, L. (1990). *In vivo* anterograde and retrograde axonal transport of the fluorescent rhodamine-dextran-amine, Fluoro-Ruby, within the CNS. *Brain Res.* 526, 127–134. doi: 10.1016/0006-8993(90)90258-D

Schnell, M. J., McGettigan, J. P., Wirblich, C., and Papaneri, A. (2010). The cell biology of rabies virus: using stealth to reach the brain. *Nat. Rev. Microbiol.* 8, 51–61. doi: 10.1038/nrmicro2260

Schnutgen, F., Doerflinger, N., Calleja, C., Wendling, O., Chambon, P., and Ghyselinck, N. B. (2003). A directional strategy for monitoring Cre-mediated recombination at the cellular level in the mouse. *Nat. Biotechnol.* 21, 562–565. doi: 10.1038/nbt811

Schofield, B. R. (2008). Retrograde axonal tracing with fluorescent markers. *Curr. Protoc. Neurosci.* Chapter 1:Unit1.17. doi: 10.1002/0471142301.ns0117s43

Schwab, M. E., Javoy-Agid, F., and Agid, Y. (1978). Labeled wheat germ agglutinin (WGA) as a new, highly sensitive retrograde tracer in the rat brain hippocampal system. *Brain Res.* 152, 145–150. doi: 10.1016/0006-8993(78)90140-3

Schwarz, L. A., Miyamichi, K., Gao, X. J., Beier, K. T., Weissbourd, B., DeLoach, K. E., et al. (2015). Viral-genetic tracing of the input-output organization of a central noradrenaline circuit. *Nature* 524, 88–92. doi: 10.1038/nature14600

Sillitoe, R. V. (2016). Mossy fibers terminate directly within purkinje cell zones during mouse development. *Cerebellum* 15, 14–17. doi: 10.1007/s12311-015-0712-6

Sivertsen, M. S., Glover, J. C., and Perreault, M. C. (2014). Organization of pontine reticulospinal inputs to motoneurons controlling axial and limb muscles in the neonatal mouse. *J. Neurophysiol.* 112, 1628–1643. doi: 10.1152/jn.00820.2013

Sivertsen, M. S., Perreault, M. C., and Glover, J. C. (2016). Pontine reticulospinal projections in the neonatal mouse: internal organization and axon trajectories. *J. Comp. Neurol.* 524, 1270–1291. doi: 10.1002/cne.23904

Smith, B. N., Banfield, B. W., Smeraski, C. A., Wilcox, C. L., Dudek, F. E., Enquist, L. W., et al. (2000). Pseudorabies virus expressing enhanved green fluorescent protein: a tool for *in vitro* electrophysiological analysis of transsynaptically labeled neurons in identified central nervous system circuits. *Proc. Natl. Acad. Sci. U.S.A.* 97, 9264–9269. doi: 10.1073/pnas.97.16.9264

Smith, J. E., Jansen, A. S., Gilbey, M. P., and Loewy, A. D. (1998). CNS cell groups projecting to sympathetic outflow of tail artery: neural circuits involved in heat loss in the rat. *Brain Res.* 786, 153–164. doi: 10.1016/s0006-8993(97)01437-6

Smith, R. H., Hallwirth, C. V., Westerman, M., Hetherington, N. A., Tseng, Y.-S., Cecchini, S., et al. (2016). Germline viral "fossils" guide in silico reconstruction of a mid-Cenozoic era marsupial adeno-associated virus. *Sci. Rep.* 6:28965. doi: 10.1038/srep28965

Sporns, O., Tononi, G., and Kotter, R. (2005). The human connectome: a structural description of the human brain. *PLoS Comput. Biol.* 1:e42. doi: 10.1371/journal.pcbi.0010042

Staines, W. A., Kimura, H., Fibiger, H. C., and McGeer, E. G. (1980). Peroxidase-labeled lectin as a neuroanatomical tracer: evaluation in a CNS pathway. *Brain Res.* 197, 485–490. doi: 10.1016/0006-8993(80)91133-6

Stiefel, M., Shaner, A., and Schaefer, S. D. (2006). The edwin smith papyrus: the birth of analytical thinking in medicine and otolaryngology. *Laryngoscope* 116, 182–188. doi: 10.1097/01.mlg.0000191461.08542.a3

Stoeckel, K., Schwab, M., and Thoenen, H. (1977). Role of gangliosides in the uptake and retrograde axonal transport of cholera and tetanus toxin as compared to nerve growth factor and wheat germ agglutinin. *Brain Res.* 132, 273–285. doi: 10.1016/0006-8993(77)90421-8

Stornetta, R. L., Inglis, M. A., Viar, K. E., and Guyenet, P. G. (2016). Afferent and efferent connections of C1 cells with spinal cord or hypothalamic projections in mice. *Brain Struct. Funct.* 221, 4027–4044. doi: 10.1007/s00429-015-1143-3

Strack, A. M., Sawyer, W. B., Hughes, J. H., Platt, K. B., and Loewy, A. D. (1989a). A general pattern of CNS innervation of the sympathetic outflow demonstrated by transneuronal pseudorabies viral infections. *Brain Res.* 491, 156–162. doi: 10.1016/0006-8993(89)90098-x

Strack, A. M., Sawyer, W. B., Platt, K. B., and Loewy, A. D. (1989b). CNS cell groups regulating the sympathetic outflow to adrenal gland as revealed by transneuronal cell body labeling with pseudorabies virus. *Brain Res.* 491, 274–296. doi: 10.1016/0006-8993(89)90063-2

Sun, L., Tang, Y., Yan, K., Yu, J., Zou, Y., Xu, W., et al. (2019). Differences in neurotropism and neurotoxicity among retrograde viral tracers. *Mol. Neurodegener.* 14:8. doi: 10.1186/s13024-019-0308-6

Sun, N., Cassell, M. D., and Perlman, S. (1996). Anterograde transneuonal transport of herpes simplex virus type 1 strain H129 in the murine visual system. *J. Virol.* 70, 5405–5413.

Sun, S., and Schaffer, D. V. (2018). Engineered viral vectors for functional interrogation, deconvolution, and manipulation of neural circuits. *Curr. Opin. Neurobiol.* 50, 163–170. doi: 10.1016/j.conb.2017.12.011

Svoboda, K. (2019). "Using rabies virus for tracing neural connections: caveats and limitations exposed by studies of barrel cortex circuits," in *Spikesphotons*, Wordpress.com. Available at: https://spikesphotons.blog/2019/05/13/

using-rabies-virus-for-tracing-neural-connections-caveats-and-limitations-exposed-by-studies-of-barrel-cortex-circuits/ (accessed July 24, 2019).

Swanson, L. W., and Bota, M. (2010). Foundational model of structural connectivity in the nervous system with a schema for wiring diagrams, connectome, and basic plan architecture. *Proc. Natl. Acad. Sci. U.S.A.* 107, 20610–20617. doi: 10.1073/pnas.1015128107

Takai, Y., Miyoshi, J., Ikeda, W., and Ogita, H. (2008). Nectins and nectin-like molecules: roles in contact inhibition of cell movement and proliferation. *Nat. Rev. Mol. Cell Biol.* 9, 603–615. doi: 10.1038/nrm2457

Takatoh, J., Nelson, A., Zhou, X., Bolton, M. M., Ehlers, M. D., Arenkiel, B. R., et al. (2013). New modules are added to vibrissal premotor circuitry with the emergence of exploratory whisking. *Neuron* 77, 346–360. doi: 10.1016/j.neuron.2012.11.010

Tervo, D. G., Hwang, B. Y., Viswanathan, S., Gaj, T., Lavzin, M., Ritola, K. D., et al. (2016). A designer AAV variant permits efficient retrograde access to projection neurons. *Neuron* 92, 372–382. doi: 10.1016/j.neuron.2016.09.021

Thanos, S., Rohrbach, J. M., and Thiel, H. J. (1991). Postmortem preservation of ganglion cells in the human retina. A morphometric investigation with the carbocyanine dye DiI. *Retina* 11, 318–327. doi: 10.1097/00006982-199111030-00009

Thanos, S., Vanselow, J., and Mey, J. (1992). Ganglion cells in the juvenile chick retina and their ability to regenerate axons *in vito*. *Exp. Eye Res.* 54, 377–391. doi: 10.1016/0014-4835(92)90050-3

Tomer, R., Ye, L., Hsueh, B., and Deisseroth, K. (2014). Advanced CLARITY for rapid and high-resolution imaging of intact tissues. *Nat. Protoc.* 9, 1682–1697. doi: 10.1038/nprot.2014.123

Trivino-Paredes, J. S., Nahirney, P. C., Pinar, C., Grandes, P., and Christie, B. R. (2019). Acute slice preparation for electrophysiology increases spine numbers equivalently in the male and female juvenile hippocampus: a DiI labeling study. *J. Neurophysiol.* doi: 10.1152/jn.00332.2019 [Epub ahead of print].

Trojanowski, J. Q., Gonatas, J. O., and Gonatas, N. K. (1981). Conjugates of horseradish peroxidase (HRP) with cholera toxin and wheat germ agglutinin are superior to free HRP as orthogradely transported markers. *Brain Res.* 223, 381–385. doi: 10.1016/0006-8993(81)91151-3

Trojanowski, J. Q., Gonatas, J. O., and Gonatas, N. K. (1982). Horseradish peroxidase (HRP) conjugates of cholera toxin and lectins are more sensitive retrogradely transported markers than free HRP. *Brain Res.* 231, 33–50. doi: 10.1016/0006-8993(82)90005-1

Turner, A., Kumar, N., Farnham, M., Lung, M., Pilowsky, P., and McMullan, S. (2013). Rostroventrolateral medulla neurons with commissural projections provide input to sympathetic premotor neurons: anatomical and functional evidence. *Eur. J. Neurosci.* 38, 2504–2515. doi: 10.1111/ejn.12232

Ugolini, G. (1995). Specificity of rabies virus as a transneuronal tracer of motor networks: transfer from hypoglossal motoneurons to connected second-order and higher order central nervous system cell groups. *J. Comp. Neurol.* 356, 457–480. doi: 10.1002/cne.903560312

Ugolini, G. (2010). Advances in viral transneuronal tracing. *J. Neurosci. Methods* 194, 2–20. doi: 10.1016/j.jneumeth.2009.12.001

Ugolini, G. (2011). Rabies virus as a transneuronal tracer of neuronal connections. *Adv. Virus Res.* 79, 165–202. doi: 10.1016/B978-0-12-387040-7.00010-X

Ugolini, G., Kuypers, H. G. J. M., and Simmons, A. (1987). Retrograde transneuronal transfer of Herpes simplex virus type 1 (HSV 1) from motoneurons. *Brain Res.* 422, 242–256. doi: 10.1016/0006-8993(87)90931-0

van den Heuvel, M. P., Bullmore, E. T., and Sporns, O. (2016). Comparative connectomics. *Trends Cogn. Sci.* 20, 345–361. doi: 10.1016/j.tics.2016.03.001

Varshney, L. R., Chen, B. L., Paniagua, E., Hall, D. H., and Chklovskii, D. B. (2011). Structural properties of the Caenorhabditis elegans neuronal network. *PLoS Comput. Biol.* 7:e1001066. doi: 10.1371/journal.pcbi.1001066

Veenman, C. L., Reiner, A., and Honig, M. G. (1992). Biotinylated dextran amine as an anterograde tracer for single- and double-labeling studies. *J. Neurosci. Methods* 41, 239–254. doi: 10.1016/0165-0270(92)90089-v

Velez-Fort, M., Rousseau, C. V., Niedworok, C. J., Wickersham, I. R., Rancz, E. A., Brown, A. P., et al. (2014). The stimulus selectivity and connectivity of layer six principal cells reveals cortical microcircuits underlying visual processing. *Neuron* 83, 1431–1443. doi: 10.1016/j.neuron.2014.08.001

Vercelli, A., Repici, M., Garbossa, D., and Grimaldi, A. (2000). Recent techniques for tracing pathways in the central nervous system of developing and adult mammals. *Brain Res. Bull.* 51, 11–28. doi: 10.1016/s0361-9230(99)00229-4

Vos, A., Neubert, A., Aylan, O., Schuster, P., Pommerening, E., Muller, T., et al. (1999). An update on safety studies of SAD B19 rabies virus vaccine in target and non-target species. *Epidemiol. Infect.* 123, 165–175. doi: 10.1017/s0950268899002666

Wang, Y., Yau, Y.-Y., Perkins-Balding, D., and Thomson, J. G. (2011). Recombinase technology: applications and possibilities. *Plant Cell Rep.* 30, 267–285. doi: 10.1007/s00299-010-0938-1

Wanner, A. A., Kirschmann, M. A., and Genoud, C. (2015). Challenges of microtome-based serial block-face scanning electron microscopy in neuroscience. *J. Microsc.* 259, 137–142. doi: 10.1111/jmi.12244

Watakabe, A., Ohtsuka, M., Kinoshita, M., Takaji, M., Isa, K., Mizukami, H., et al. (2015). Comparative analyses of adeno-associated viral vector serotypes 1, 2, 5, 8 and 9 in marmoset, mouse and macaque cerebral cortex. *Neurosci. Res.* 93, 144–157. doi: 10.1016/j.neures.2014.09.002

Watson, J. D., and Crick, F. H. (1953). Molecular structure of nucleic acids; a structure for deoxyribose nucleic acid. *Nature* 171, 737–738.

Weinberg, M. S., Samulski, R. J., and McCown, T. J. (2013). Adeno-associated virus (AAV) gene therapy for neurological disease. *Neuropharmacology* 69, 82–88. doi: 10.1016/j.neuropharm.2012.03.004

Wertz, A., Trenholm, S., Yonehara, K., Hillier, D., Raics, Z., Leinweber, M., et al. (2015). PRESYNAPTIC NETWORKS. Single-cell-initiated monosynaptic tracing reveals layer-specific cortical network modules. *Science* 349, 70–74. doi: 10.1126/science.aab1687

White, J. G., Southgate, E., Thomson, J. N., and Brenner, S. (1986). The structure of the nervous system of the nematode Caenorhabditis elegans. *Philos. Trans. R. Soc. Lond. B Biol. Sci.* 314, 1–340.

Wickersham, I. R., and Feinberg, E. H. (2012). New technologies for imaging synaptic partners. *Curr. Opin. Neurobiol.* 22, 121–127. doi: 10.1016/j.conb.2011.12.001

Wickersham, I. R., Finke, S., Conzelmann, K. K., and Callaway, E. M. (2007a). Retrograde neuronal tracing with a deletion-mutant rabies virus. *Nat. Methods* 4, 47–49. doi: 10.1038/nmeth999

Wickersham, I. R., Lyon, D. C., Barnard, R. J., Mori, T., Finke, S., Conzelmann, K. K., et al. (2007b). Monosynaptic restriction of transsynaptic tracing from single, genetically targeted neurons. *Neuron* 53, 639–647. doi: 10.1016/j.neuron.2007.01.033

Wojaczynski, G. J., Engel, E. A., Steren, K. E., Enquist, L. W., and Patrick Card, J. (2015). The neuroinvasive profiles of H129 (herpes simplex virus type 1) recombinants with putative anterograde-only transneuronal spread properties. *Brain Struct. Funct.* 220, 1395–1420. doi: 10.1007/s00429-014-0733-9

Wouterlood, F. G., Bloem, B., Mansvelder, H. D., Luchicchi, A., and Deisseroth, K. (2014). A fourth generation of neuroanatomical tracing techniques: exploiting the offspring of genetic engineering. *J. Neurosci. Methods* 235, 331–348. doi: 10.1016/j.jneumeth.2014.07.021

Wu, C. W., Vasalatiy, O., Liu, N., Wu, H., Cheal, S., Chen, D. Y., et al. (2011). Development of a MR-visible compound for tracing neuroanatomical connections in vivo. *Neuron* 70, 229–243. doi: 10.1016/j.neuron.2011.03.010

Xu, C. S., Hayworth, K. J., Lu, Z., Grob, P., Hassan, A. M., García-Cerdán, J. G., et al. (2017). Enhanced FIB-SEM systems for large-volume 3D imaging. *eLife* 6:e25916. doi: 10.7554/eLife.25916

Yamashita, T., and Petersen, C. (2016). Target-specific membrane potential dynamics of neocortical projection neurons during goal-directed behavior. *eLife* 5:e15798. doi: 10.7554/eLife.15798

Yonehara, K., Farrow, K., Ghanem, A., Hillier, D., Balint, K., Teixeira, M., et al. (2013). The first stage of cardinal direction selectivity is localized to the dendrites of retinal ganglion cells. *Neuron* 79, 1078–1085. doi: 10.1016/j.neuron.2013.08.005

Yu, Y.-L., Li, H.-Y., Zhang, P.-X., Yin, X.-F., Han, N., Kou, Y.-H., et al. (2015). Comparison of commonly used retrograde tracers in rat spinal motor neurons. *Neural Regen. Res.* 10, 1700–1705. doi: 10.4103/1673-5374.167772

Zele, T., Sketelj, J., and Bajrovic, F. F. (2010). Efficacy of fluorescent tracers in retrograde labeling of cutaneous afferent neurons in the rat. *J. Neurosci. Methods* 191, 208–214. doi: 10.1016/j.jneumeth.2010.06.021

Zemanick, M. C., Strick, P. L., and Dix, R. D. (1991). Direction of transneuronal transport of herpes simplex virus 1 in the primate motor system is strain-dependent. *Proc. Natl. Acad. Sci. U.S.A.* 88, 8048–8051. doi: 10.1073/pnas.88.18.8048

Zeng, W.-B., Jiang, H.-F., Gang, Y.-D., Song, Y.-G., Shen, Z.-Z., Yang, H., et al. (2017). Anterograde monosynaptic transneuronal tracers derived from herpes

simplex virus 1 strain H129. *Mol. Neurodegener.* 12:38. doi: 10.1186/s13024-017-0179-7

Zhang, W. J., Xu, D. S., Cui, J. J., Jing, X. H., Xu, N. G., Liu, J. H., et al. (2017). Anterograde and retrograde tracing with high molecular weight biotinylated dextran amine through thalamocortical and corticothalamic pathways. *Microsc. Res. Tech.* 80, 260–266. doi: 10.1002/jemt.22797

Zhao, Z., Wang, L., Gao, W., Hu, F., Zhang, J., Ren, Y., et al. (2017). A central catecholaminergic circuit controls blood glucose levels during stress. *Neuron* 95, 138–152.e5. doi: 10.1016/j.neuron.2017.05.031

Zheng, Z., Lauritzen, J. S., Perlman, E., Robinson, C. G., Nichols, M., Milkie, D., et al. (2018). A complete electron microscopy volume of the brain of adult *Drosophila melanogaster*. *Cell* 174, 730–743.e22. doi: 10.1016/j.cell.2018.06.019

Zingg, B., Chou, X. L., Zhang, Z. G., Mesik, L., Liang, F., Tao, H. W., et al. (2017). AAV-mediated anterograde transsynaptic tagging: mapping corticocollicular input-defined neural pathways for defense behaviors. *Neuron* 93, 33–47. doi: 10.1016/j.neuron.2016.11.045

Conflict of Interest Statement: SL was a Ph.D. student at the time of writing. He is now an employee of the Olympus Australia. He has approved the submission of the manuscript but has not provided any material input since becoming an Olympus Australia employee.

The remaining authors declare that the research was conducted in the absence of any commercial or financial relationships that could be construed as a potential conflict of interest.

frontiers in Neuroscience

CORRECTION
published: 10 March 2020
doi: 10.3389/fnins.2020.00177

Corrigendum: A Student's Guide to Neural Circuit Tracing

Christine Saleeba[1,2†], *Bowen Dempsey*[3†], *Sheng Le*[1], *Ann Goodchild*[1] and *Simon McMullan*[1*]

[1] Neurobiology of Vital Systems Node, Faculty of Medicine and Health Sciences, Macquarie University, Sydney, NSW, Australia, [2] The School of Physiology, Pharmacology and Neuroscience, University of Bristol, Bristol, United Kingdom, [3] CNRS, Hindbrain Integrative Neurobiology Laboratory, Neuroscience Paris-Saclay Institute (Neuro-PSI), Université Paris-Saclay, Gif-sur-Yvette, France

Keywords: neuroanatomy, viral tracers, anterograde tracer, retrograde tracers, synaptic contacts, connectome analysis

A Corrigendum on

A Student's Guide to Neural Circuit Tracing
by Saleeba, C., Dempsey, B., Le, S., Goodchild, A., and McMullan, S. (2019). Front. Neurosci. 13:897. doi: 10.3389/fnins.2019.00897

In the original article, there was an error: one section of our review considers reagents traditionally considered to be anterograde tracers (i.e., fluorescent or antigenic substances that are taken up by neuronal cell bodies at the site of application and transported to the synaptic terminals). The original text read:

Emerging in the mid-1980s, dextran-based tracers, particularly biotinylated dextran amine (BDA), were rapidly adopted and remain one of the most widely used conventional anterograde tracers (Glover et al., 1986; Brandt and Apkarian, 1992; Veenman et al., 1992; Wouterlood et al., 2014). BDA enters injured neurons at the injection site, undergoes rapid anterograde transport and spreads evenly throughout the entire neuron, resulting in a Golgi-like level of staining detail (Köbbert et al., 2000; Lanciego and Wouterlood, 2011; Wouterlood et al., 2014). Interestingly, while 10 kDa BDA travels mostly anterogradely, the 3 kDa form is a retrograde tracer (Reiner et al., 2000; Lanciego and Wouterlood, 2011). Like CTb, fluorophore-labeled dextran amine variants are now widely used instead of biotinylated versions that require histological processing for visualization, and a number of authors have used tetramethylrhodamine-conjugated dextran for juxtacellular labeling during electrophysiological recordings (Noseda et al., 2010; Dempsey et al., 2015).

Limitations of Conventional Tracers

Despite their ongoing popularity, the major limitations of conventional tracers are worthy of consideration:

(1) Conventional tracers are taken up by fibers of passage (Dado et al., 1990; Chen and Aston-Jones, 1995; Conte et al., 2009), which can lead to incorrect identification of projections. [Notably, canine adenovirus (CAV) can also be taken up by fibers of passage (Schwarz et al., 2015)].
(2) The spread of many conventional tracers around the injection site results in intense and diffuse labeling that may reflect deposition in the extracellular matrix or take-up by neurons or glia. Such non-specific labeling makes it difficult to reliably identify labeled neurons within ∼1 mm of the injection site. Thus the historical use of conventional tracers has probably overemphasized the relative significance of distant inputs/outputs compared to those originating from local interneurons; contemporary connectomic studies indicate that long-distance projections are relatively rare compared to short-distance connections (Oh et al., 2014; Henriksen et al., 2016; van den Heuvel et al., 2016; Dempsey et al., 2017).

OPEN ACCESS

Edited and reviewed by:
Vaughan G. Macefield, Baker Heart and Diabetes Institute, Australia

***Correspondence:**
Simon McMullan
simon.mcmullan@mq.edu.au

[†] *These authors have contributed equally to this work*

Specialty section:
This article was submitted to Autonomic Neuroscience, a section of the journal Frontiers in Neuroscience

Received: *04 February 2020*
Accepted: *17 February 2020*
Published: *10 March 2020*

Citation:
Saleeba C, Dempsey B, Le S, Goodchild A and McMullan S (2020) Corrigendum: A Student's Guide to Neural Circuit Tracing. Front. Neurosci. 14:177. doi: 10.3389/fnins.2020.00177

(3) Tracer uptake relies predominantly on sugars that are located on the glycocalyx of most, if not all neurons, or on common mechanisms such as endocytosis. Consequently, restricted uptake by functionally or neurochemically/genetically homogeneous neuronal populations is not possible.
(4) The direction of axonal transport is often not exclusive, which complicates circuit analysis; for example, CTb, perhaps the mostly widely used "retrograde" tracer, is also an efficient anterograde tracer (Luppi et al., 1987; Angelucci et al., 1996; Noseda et al., 2010).

The authors were contacted by Professor Joel Glover, who first described the use of dextran amines as neuronal tracers in the 1980s and expressed concern that we had inadvertently perpetuated a myth regarding the directional sensitivity of these tracers.

The amendment to the article clarifies the bidirectional nature of dextran amine transport.

A correction has been made to the Anterograde and Retrograde Tracers section, subsection Conventional (Mainly) Anterograde Tracers;

"Emerging in the mid-1980s, dextran-amines (DAs) were rapidly adopted and remain widely used as conventional axonal tracers (Gimlich and Braun, 1985; Glover et al., 1986; Brandt and Apkarian, 1992; Veenman et al., 1992; Wouterlood et al., 2014). DAs enter injured neurons at the injection site and spread evenly throughout the entire neuron via diffusion, resulting in a Golgi-like level of staining detail (Glover et al., 1986; Fritzsch, 1993; Glover, 1995; Köbbert et al., 2000; Lanciego and Wouterlood, 2011; Wouterlood et al., 2014).

Despite the common perception that DAs are preferential anterograde tracers, many studies indicate bidirectional travel (Schmued et al., 1990; Fritzsch, 1993; Glover, 1995; Zhang et al., 2017), including the original description of their axonal transport by Glover et al. (1986). Their retrograde capabilities have been exploited both for conventional tracing (Sivertsen et al., 2014, 2016; Lunde et al., 2019) and for delivery of calcium-sensitive indicators for optical recording of neurons selected by axonal trajectory (O'Donovan et al., 1993; McPherson et al., 1997).

There is a perception that the molecular weight of DA-conjugates contributes to their directional selectivity, with smaller molecules exhibiting superior performance as a retrograde tracer (Reiner et al., 2000; Lanciego and Wouterlood, 2011). However, the influence, if any, of molecular weight on directional specificity is probably overstated, and may instead reflect differences in speed of transport, which is distinctly faster for smaller compounds (Fritzsch, 1993), combined with differences in volume of synaptic terminals compared to cell bodies (Joel C Glover, personal communication).

Like CTb, fluorophore-labeled dextran amine variants are now widely used instead of or in addition to biotinylated versions that require histological processing for visualization, and we and others have used tetramethylrhodamine-conjugated dextran for juxtacellular labeling during electrophysiological recordings (Noseda et al., 2010; Dempsey et al., 2015).

Limitations of Conventional Tracers

Despite their ongoing popularity, the major limitations of conventional tracers are worthy of consideration:

1. Conventional tracers can be taken up by fibers of passage (Dado et al., 1990; Chen and Aston-Jones, 1995; Conte et al., 2009), which can lead to incorrect identification of projections. [Notably, canine adenovirus (CAV) can also be taken up by fibers of passage (Schwarz et al., 2015)].
2. The spread of many conventional tracers around the injection site results in intense and diffuse labeling that may reflect deposition in the extracellular matrix or take-up by neurons or glia. Such non-specific labeling makes it difficult to reliably identify labeled neurons within ∼1 mm of the injection site. Thus the historical use of conventional tracers has probably overemphasized the relative significance of distant inputs/outputs compared to those originating from local interneurons; contemporary connectomic studies indicate that long-distance projections are relatively rare compared to short-distance connections (Oh et al., 2014; Henriksen et al., 2016; van den Heuvel et al., 2016; Dempsey et al., 2017).
3. Tracer uptake relies predominantly on sugars that are located on the glycocalyx of most, if not all neurons, or on common mechanisms such as endocytosis. Consequently, restricted uptake by functionally or neurochemically/genetically homogeneous neuronal populations is not possible.
4. The direction of axonal transport is rarely exclusive, which complicates circuit analysis; the archetypal retrograde and anterograde tracers, CTb and BDA respectively, both label axons traveling in the "wrong" direction (Luppi et al., 1987; Schmued et al., 1990; Fritzsch, 1993; Glover, 1995; Angelucci et al., 1996; Noseda et al., 2010; Zhang et al., 2017)."

The authors apologize for this error and state that this does not change the scientific conclusions of the article in any way. The original article has been updated.

REFERENCES

Angelucci, A., Clascá, F., and Sur, M. (1996). Anterograde axonal tracing with the subunit B of cholera toxin: a highly sensitive immunohistochemical protocol for revealing fine axonal morphology in adult and neonatal brains. *J. Neurosci. Methods* 65, 101–112. doi: 10.1016/0165-0270(95)00155-7

Brandt, H. M., and Apkarian, A. V. (1992). Biotin-dextran: a sensitive anterograde tracer for neuroanatomic studies in rat and monkey. *J. Neurosci. Methods* 45, 35–40. doi: 10.1016/0165-0270(92)90041-b

Chen, S., and Aston-Jones, G. (1995). Evidence that cholera toxin B subunit (CTb) can be avidly taken up and transported by fibers of passage. *Brain Res.* 674, 107–111. doi: 10.1016/0006-8993(95)00020-q

Conte, W. L., Kamishina, H., and Reep, R. L. (2009). Multiple neuroanatomical tract-tracing using fluorescent Alexa Fluor conjugates of cholera toxin subunit B in rats. *Nat. Protoc.* 4, 1157–1166. doi: 10.1038/nprot.2009.93

Dado, R. J., Burstein, R., Cliffer, K. D., and Giesler, G. J. Jr. (1990). Evidence that fluoro-gold can be transported avidly through fibers of passage. *Brain Res.* 533, 329–333. doi: 10.1016/0006-8993(90)91358-n

Dempsey, B., Le, S., Turner, A., Bokiniec, P., Ramadas, R., Bjaalie, J. G., et al. (2017). Mapping and analysis of the connectome of sympathetic premotor neurons in the rostral ventrolateral medulla of the rat using a volumetric brain atlas. *Front. Neural Circ.* 11:9. doi: 10.3389/fncir.2017.00009

Dempsey, B., Turner, A. J., Le, S., Sun, Q. J., Bou Farah, L., Allen, A. M., et al. (2015). Recording, labeling, and transfection of single neurons in deep brain structures. *Physiol. Rep.* 3:e12246. doi: 10.14814/phy2.12246

Fritzsch, B. (1993). Fast axonal diffusion of 3000 molecular weight dextran amines. *J. Neurosci. Methods* 50, 95–103.

Gimlich, R. L., and Braun, J. (1985). Improved fluorescent compounds for tracing cell lineage. *Dev. Biol.* 109, 509–514.

Glover, J. C. (1995). Retrograde and anterograde axonal tracing with fluorescent dextran-amines in the embryonic nervous system. *Neurosci. Protoc.* 95, 1–13.

Glover, J. C., Petursdottir, G., and Jansen, J. K. S. (1986). Fluorescent dextran amines used as axonal tracers in the nervous system of chicken embryo. J. Neurosci. Methods 18, 243–254. doi: 10.1016/0165-0270(86)90011-7

Henriksen, S., Pang, R., and Wronkiewicz, M. (2016). A simple generative model of the mouse mesoscale connectome. *eLife* 5:e12366. doi: 10.7554/eLife.12366

Köbbert, C., Apps, R., Bechmann, I., Lanciego, J. L., Mey, J., and Thanos, S. (2000). Current concepts in neuroanatomical tracing. *Prog. Neurobiol.* 62, 327–351. doi: 10.1016/s0301-0082(00)00019-8

Lanciego, J. L., and Wouterlood, F. G. (2011). A half century of experimental neuroanatomical tracing. *J. Chem. Neuroanat.* 42, 157–183. doi: 10.1016/j.jchemneu.2011.07.001

Lunde, A., Okaty, B. W., Dymecki, S. M., and Glover, J. C. (2019). Molecular profiling defines evolutionarily conserved transcription factor signatures of major vestibulospinal neuron groups. *eNeuro* 6:e0475-0418.2019. doi: 10.1523/ENEURO.0475-18.2019

Luppi, P. H., Sakai, K., Salvert, D., Fort, P., and Jouvet, M. (1987). Peptidergic hypothalamic afferents to the cat nucleus raphe pallidus as revealed by a double immunostaining technique using unconjugated cholera toxin as a retrograde tracer. *Brain Res.* 402, 339–345. doi: 10.1016/0006-8993(87)90041-2

McPherson, D. R., McClellan, A. D., and O'Donovan, M. J. (1997). Optical imaging of neuronal activity in tissue labeled by retrograde transport of Calcium Green Dextran. *Brain Res. Brain Res. Protoc.* 1, 157–164. doi: 10.1016/S1385-299X(96)00024-4

Noseda, R., Kainz, V., Jakubowski, M., Gooley, J. J., Saper, C. B., Digre, K., et al. (2010). A neural mechanism for exacerbation of headache by light. *Nat. Neurosci.* 13, 239–245. doi: 10.1038/nn.2475

O'Donovan, M. J., Ho, S., Sholomenko, G., and Yee, W. (1993). Real-time imaging of neurons retrogradely and anterogradely labelled with calcium-sensitive dyes. *J. Neurosci. Methods* 46, 91–106. doi: 10.1016/0165-0270(93)90145-H

Oh, S. W., Harris, J. A., Ng, L., Winslow, B., Cain, N., Mihalas, S., et al. (2014). A mesoscale connectome of the mouse brain. *Nature* 508, 207–214. doi: 10.1038/nature13186

Reiner, A., Veenman, C. L., Medina, L., Jiao, Y., Del Mar, N., and Honig, M. G. (2000). Pathway tracing using biotinylated dextran amines. *J. Neurosci. Methods* 103, 23–37. doi: 10.1016/s0165-0270(00)00293-4

Schmued, L., Kyriakidis, K., and Heimer, L. (1990). *In vivo* anterograde and retrograde axonal transport of the fluorescent rhodamine-dextran-amine, Fluoro-Ruby, within the CNS. *Brain Res.* 526, 127–134. doi: 10.1016/0006-8993(90)90258-D

Schwarz, L. A., Miyamichi, K., Gao, X. J., Beier, K. T., Weissbourd, B., DeLoach, K. E., et al. (2015). Viral-genetic tracing of the input-output organization of a central noradrenaline circuit. *Nature* 524, 88–92. doi: 10.1038/nature14600

Sivertsen, M. S., Glover, J. C., and Perreault, M. C. (2014). Organization of pontine reticulospinal inputs to motoneurons controlling axial and limb muscles in the neonatal mouse. *J. Neurophysiol.* 112, 1628–1643. doi: 10.1152/jn.00820.2013

Sivertsen, M. S., Perreault, M. C., and Glover, J. C. (2016). Pontine reticulospinal projections in the neonatal mouse: Internal organization and axon trajectories. *J. Comp. Neurol.* 524, 1270–1291. doi: 10.1002/cne.23904

van den Heuvel, M. P., Bullmore, E. T., and Sporns, O. (2016). Comparative connectomics. *Trends Cogn. Sci.* 20, 345–361. doi: 10.1016/j.tics.2016.03.001

Veenman, C. L., Reiner, A., and Honig, M. G. (1992). Biotinylated dextran amine as an anterograde tracer for single- and double-labeling studies. *J. Neurosci. Methods* 41, 239–254. doi: 10.1016/0165-0270(92)90089-v

Wouterlood, F. G., Bloem, B., Mansvelder, H. D., Luchicchi, A., and Deisseroth, K. (2014). A fourth generation of neuroanatomical tracing techniques: exploiting the offspring of genetic engineering. *J. Neurosci. Methods* 235, 331–348. doi: 10.1016/j.jneumeth.2014.07.021

Zhang, W. J., Xu, D. S., Cui, J. J., Jing, X. H., Xu, N. G., Liu, J. H., et al. (2017). Anterograde and retrograde tracing with high molecular weight biotinylated dextran amine through thalamocortical and corticothalamic pathways. *Microsc. Res. Tech.* 80, 260–266. doi: 10.1002/jemt.22797

frontiers in Physiology

REVIEW
published: 28 August 2019
doi: 10.3389/fphys.2019.01110

Vagal Afferent Processing by the Paratrigeminal Nucleus

*Alexandria K. Driessen**

School of Biomedical Science, Department of Anatomy and Neuroscience, University of Melbourne, Parkville, VIC, Australia

The paratrigeminal nucleus is an obscure region in the dorsal lateral medulla, which has been best characterized as a collection of interstitial cells located in the dorsal tip of the spinal trigeminal tract. The paratrigeminal nucleus receives afferent input from the vagus, trigeminal, spinal, and glossopharyngeal nerves, which contribute to its long-known roles in the baroreceptor reflex and nociceptive processing. More recently, studies have shown that this region is also involved in the processing of airway-derived sensory information. Notably, these studies highlight an underappreciated complexity in the neuronal content and circuit connectivity of the paratrigeminal nucleus. However, much remains to be understood about how paratrigeminal processing of vagal afferents is altered in disease. The aim of the present review is to provide an update of the current understanding of vagal afferent processing in the paratrigeminal nucleus and to explore how dysregulation at this site may contribute to vagal sensory neural dysfunction during disease.

Keywords: respiratory, nociception, jugular ganglia, paratrigeminal connectome, cough

OPEN ACCESS

Edited by:
Vaughan G. Macefield,
Baker Heart and Diabetes Institute, Australia

Reviewed by:
Winfried Neuhuber,
University of Erlangen Nuremberg, Germany
Simon McMullan,
Macquarie University, Australia

***Correspondence:**
Alexandria K. Driessen
ally.driessen@monash.edu

Specialty section:
This article was submitted to Integrative Physiology, a section of the journal Frontiers in Physiology

Received: *30 May 2019*
Accepted: *12 August 2019*
Published: *28 August 2019*

Citation:
Driessen AK (2019) Vagal Afferent Processing by the Paratrigeminal Nucleus.
Front. Physiol. 10:1110.
doi: 10.3389/fphys.2019.01110

INTRODUCTION

Vagal afferents innervating visceral tissues are well described to terminate in the medullary nucleus of the solitary tract (Cajal, 1909; Donoghue et al., 1982; Kubin et al., 1985; Mutoh et al., 2000; McGovern et al., 2012). However, it has also long been known that there are additional brainstem termination sites for vagal afferent fibers in the dorsal lateral medulla, including a region known as the paratrigeminal nucleus (Cajal, 1909; Altschuler et al., 1989; McGovern et al., 2012). Recent studies using viral circuit tracing of the airway sensory nervous system demonstrated that only a specific subset of vagal afferents project to the paratrigeminal nucleus (McGovern et al., 2015a) and since this observation there has been significant progress made toward understanding the role of the paratrigeminal nucleus in airway defense (Driessen et al., 2015, 2018). This brief review aims to bring together anatomical and functional investigations of the paratrigeminal nucleus to present a case for why this nucleus should be acknowledged as a second key processing site for vagal afferent inputs to the central nervous system.

NEUROANATOMICAL STUDIES OF THE PARATRIGEMINAL NUCLEUS AND ITS CONNECTOME

Anatomically Defining the Paratrigeminal Nucleus

The paratrigeminal nucleus is an obscure medullary region that was first characterized in the 1960s by Albert Rhoton. He defined this nucleus, in the monkey, as a collection of interstitial neurons located within the dorsal segment of the spinal trigeminal tract that is located in the lateral aspect of the medulla (Rhoton et al., 1966). Neurons in this region receive a

diverse range of sensory inputs arising from trigeminal, glossopharyngeal, vagal sensory, and upper cervical dorsal root sensory ganglia (Ciriello et al., 1981; Panneton and Burton, 1981; Nomura and Mizuno, 1984; Altschuler et al., 1989; McGovern et al., 2012; Mahadi et al., 2019). Subsequent studies have identified comparable interstitial cells in the rat, guinea pig, cat, and human (Chan-Palay, 1978; Nasution and Shigenaga, 1987; Phelan and Falls, 1989; Pinto et al., 2006; Driessen et al., 2015; McGovern et al., 2015a). Phelan and Falls (1989) were the first to investigate the rostro-caudal extent of the paratrigeminal nucleus in the rat, showing that presumptive paratrigeminal neurons extend rostrally for approximately 1.5–2 mm from caudal to obex. Similarly, in the guinea pig, the paratrigeminal nucleus spreads 1.5 mm with the highest density of neurons located in the caudal (−0.4 mm to obex) and central (at the level of obex) aspects of this nucleus (Driessen et al., 2018).

Investigations of the cellular composition of the paratrigeminal nucleus have shown it to contain morphologically distinct subpopulations of neurons, as well as pronounced numbers of glia and astrocytes in its most superficial layers (Chan-Palay, 1978; Phelan and Falls, 1989; Saxon and Hopkins, 2006). The paratrigeminal nucleus is also enriched with a peptidergic neuropil, predominately expressing the neuropeptides calcitonin gene-related peptide and substance P that presumably represent the central terminal processes of the sensory neural inputs (Saxon and Hopkins, 2006; Caous et al., 2012; Driessen et al., 2015). Recent immunohistochemical characterization of the paratrigeminal nucleus in the guinea pig has demonstrated at least two distinct paratrigeminal neuron subtypes based on their immunoreactivity for either calbindin or the neurokinin 1 receptor (Driessen et al., 2018), analogous with the dorsal horn nociceptive system that contains phenotypically comparable neurons in receipt of nociceptive inputs (Li et al., 1999). However, this is unlikely a complete representation of the neuron subtypes that exist in the paratrigeminal nucleus and further neuronal heterogeneity may exist, like that in the dorsal horn (Hu et al., 2016; Li et al., 2016; Jurcakova et al., 2018). It seems reasonable to speculate that this under-appreciated complexity of the paratrigeminal nucleus likely confers functional significance with respect to the integration and processing capabilities of this nucleus.

Vagal Afferent Terminations in the Paratrigeminal Nucleus

Vagal afferents have their cell bodies located in either the jugular (superior) or nodose (inferior) vagal ganglia (Canning et al., 2004; Undem et al., 2004; McGovern et al., 2012). These two ganglia are derived from different embryological origins (D'Autréaux et al., 2011; Nomaksteinsky et al., 2013) and this confers significant differences in the physiology, pharmacology, and neuroanatomy of the neurons originating in each (Kwong et al., 2008; Chang et al., 2015; McGovern et al., 2015a,b; Nonomura et al., 2017; Kupari et al., 2019). Studies of airway projecting vagal sensory neurons in the mouse and guinea pig indicate that the visceral placodal nodose-derived neurons are characteristically non-peptidergic consisting of myelinated Aδ- or Aβ- fibers and unmyelinated C-fibers (Riccio et al., 1996; Undem et al., 2004; Mazzone and Undem, 2016) that can be selectively activated by serotonin 5-HT3 receptor agonists and adenosine 5′-triphosphate (ATP) as they uniquely express the purinergic receptors P2X2 and P2X3 (Kwong et al., 2008; Potenzieri et al., 2012). On the other hand, airway somatic neural crest-derived jugular neurons are classically characterized as non-peptidergic Aδ-fibers or peptidergic C-fibers unresponsive to both 5-HT and ATP due to lack of expression of 5HT3 and P2X2 receptors (Riccio et al., 1996; Canning et al., 2004; Undem et al., 2004; Potenzieri et al., 2012). Recent single-cell RNA sequencing of unidentified nodose and jugular afferent neurons in the mouse reveal comparable phenotypic differences, with jugular neurons demonstrating more similarities to neurons of the dorsal root ganglia, which is underpinned by their developmental origin (Kupari et al., 2019).

In the guinea pig, viral tract tracing using an adeno-associated virus encoding green fluorescent protein (AAV2/8-eGFP) microinjected into the vagal sensory ganglia revealed that vagal afferents predictably project to the nucleus of the solitary tract, and additionally to the caudal and central regions of the paratrigeminal nucleus, which are the medullary levels that align with the highest density of postsynaptic neurons (Driessen et al., 2018). Similarly, tracing in the rat of vagally innervated viscera, the pharynx and larynx show bilateral afferent projections to both the nucleus of the solitary tract and the paratrigeminal nucleus (Saxon and Hopkins, 2006). Furthermore, direct electrical stimulation of the vagus nerve (Rutherfurd et al., 1992) or larynx (Wang et al., 2015) results in neuronal activation of paratrigeminal neurons. These data raise the question of whether paratrigeminal projecting vagal afferents represent a distinct population of neurons from the nodose or jugular vagal ganglia. McGovern et al. (2015b) addressed this by performing tracing studies of the afferents innervating different levels of the respiratory tree. In doing so, they showed that the lungs are predominately innervated by afferents from the nodose ganglia, while the upper airways (larynx, trachea, and mainstem bronchi) are innervated by the neurons derived from the jugular ganglia (McGovern et al., 2015b). Subsequent dual retrograde neural tracing studies in rats and guinea pigs confirmed the existence of differential vagal inputs to brainstem processing sites demonstrating that nodose vagal afferents project exclusively to the nucleus of the solitary tract, while the jugular vagal ganglia afferents project almost entirely to the paratrigeminal nucleus (**Figure 1A**; Driessen et al., 2015; McGovern et al., 2015a). These studies suggest that two parallel vagal sensory circuits exist, broadly classified as either a nodose-nucleus of the solitary tract processing pathway or jugular-paratrigeminal processing pathway.

Paratrigeminal Nucleus Output Connectivity

Neuronal tracing studies in both rat and guinea pig have shown output projections from paratrigeminal neurons to bulbar nuclei integral to autonomic and nociceptive processing,

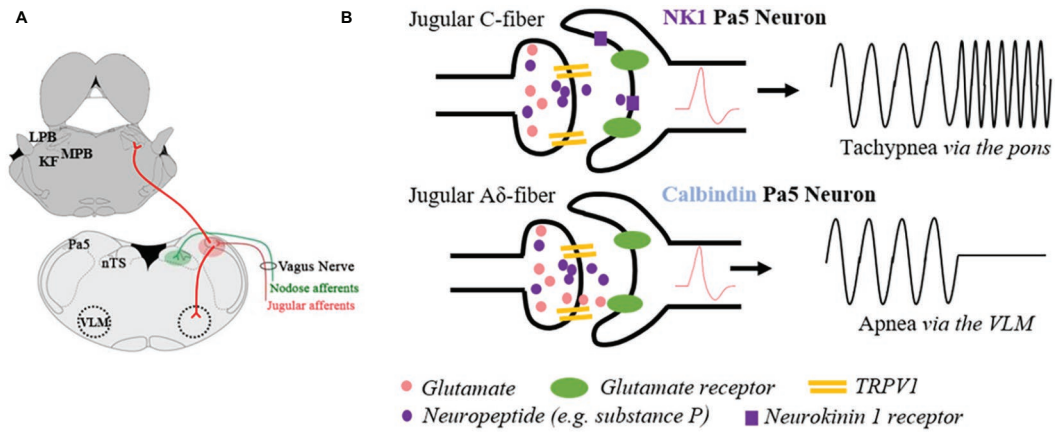

FIGURE 1 | Schematic representation of the anatomical and functional specificity of the paratrigeminal nucleus (Pa5). **(A)** Illustration of jugular vagal afferents (red) specifically terminating in the Pa5, located in the dorsal-lateral medulla. Conversely, the nodose vagal afferents (green) exclusively project to the nucleus of the solitary tract (nTS). Jugular vagal afferent inputs are first synaptically integrated with Pa5 neurons, which differentially project to additional bulbar nuclei involved in cardiorespiratory control. Depicted are a subset of Pa5 neurons projecting to the ventrolateral medulla (VLM), and a separate population ascending to the pontine nuclei that collectively include the Kölliker Fuse (KF) nucleus and lateral (LPB) and medial (MPB) parabrachial nuclei. **(B)** Stylized diagram depicting a hypothesis for how the neuroanatomical organization of the Pa5 underpins functional specificity at this site based on studies of laryngeal-evoked reflexes in guinea pigs (Driessen et al., 2018). Non-peptidergic jugular A-fibers expressing the transient receptor potential vanilloid 1 (TRPV1) appear to mediate the abrupt cessation in breathing (apnea) observed when the larynx is electrically or chemically stimulated. Synaptically, this response is dependent on fast ionotropic glutamatergic neurotransmission in the Pa5, and it is hypothesized that calbindin expressing Pa5 neurons projecting to cardiorespiratory cells of the ventrolateral medulla are principally involved. Peptidergic (e.g., substance P containing fibers) inputs to the Pa5 are likely responsible for increased respiratory drive (i.e., tachypnea). Physiological or pathophysiological conditions that allow for neuropeptide release will activate NK1 receptor expressing Pa5 neurons, which possibly ascend the neuraxis and terminate diffusely in the pons. This pathway may contribute to respiratory and autonomic processing *via* these pontine circuits or excite bulbar-circuits involved in sensory discrimination.

including the nucleus of the solitary tract, spinal trigeminal nuclei, rostral ventrolateral medulla, nucleus ambiguus, reticular nuclei, parabrachial nuclei, Kölliker-Fuse nucleus, and principal sensory trigeminal nucleus (Feil and Herbert, 1995; Saxon and Hopkins, 1998; Caous et al., 2001; de Sousa Buck et al., 2001; Pinto et al., 2006; McGovern et al., 2015b; Driessen et al., 2018). While no monosynaptic projections were observed above the level of the pons in the guinea pig (Driessen et al., 2018), ascending projections directly to the somatosensory thalamus (ventroposterior medial thalamus) have been observed in rats (Saxon and Hopkins, 1998; Pinto et al., 2006; McGovern et al., 2015a). Interestingly, dual cholera-toxin retrograde tracing studies have shown different projection patterns of subpopulations of paratrigeminal neurons (Saxon and Hopkins, 1998; Pinto et al., 2006; Driessen et al., 2018). For example, Pinto et al. (2006) showed topography of pontine projections could be mapped across the rostro-caudal extent of the paratrigeminal nucleus, indicative of selective pontomedullary connectivity. Additionally, in the rat, separate paratrigeminal neurons project to the parabrachial nuclei compared to the ventroposterior medial thalamus (Saxon and Hopkins, 1998), while in the guinea pig there are distinct neurons that project to the parabrachial nuclei compared to the ventrolateral medulla (**Figure 1A**; Driessen et al., 2018). Given that at least two populations of phenotypically different paratrigeminal neurons exist (expressing neurokinin 1 receptors or calbindin; Driessen et al., 2018), it will be important to investigate whether these populations preserve a level of connectivity specificity.

THE PHYSIOLOGICAL ROLE OF THE PARATRIGEMINAL NUCLEUS IN VAGAL AFFERENT REGULATION OF CARDIORESPIRATORY CONTROL

Vagal afferent inputs from aortic baroreceptors to the brainstem play an essential role in the regulation of blood pressure *via* circuits involving the ventrolateral medulla (Bonham and Jeske, 1989; Ruggiero et al., 1996; Choong et al., 2013; Koganezawa and Paton, 2014; Tallapragada et al., 2016; Ghali, 2017). Although many baroreceptive afferents terminate centrally in the nucleus of the solitary tract, neurons in the paratrigeminal nucleus also demonstrate baroreceptor-related activity (Caous et al., 2001; de Sousa Buck et al., 2001). In the rat, up to 72% of paratrigeminal neurons are barosensitive and of these almost all show rhythmic activity with the cardiac cycle (Balan Júnior et al., 2004; Sousa and Lindsey, 2009). Importantly, baroreceptor reflex evoked changes in cardiovascular activity is modulated by altering synaptic processing in the paratrigeminal nucleus. Thus, microinjection of bradykinin into the paratrigeminal nucleus results in increased arterial pressure, while lesioning this nucleus increases resting arterial pressure and heart rate and impairs baroreceptor reflex sensitivity (Lindsey et al., 1997; Sousa and Lindsey, 2009). Although not proven, these effects are presumably mediated by paratrigeminal neuronal connectivity with the ventrolateral medulla. However, some entrainment of barosensitive neural activity in the paratrigeminal nucleus and the nucleus of the solitary tract suggests functional interconnectivity between these vagal sensory processing sites (Balan Júnior et al., 2004).

Vagal afferents are essential for maintaining appropriate airway patency and adequate respiration. In anesthetized animals, nodose vagal stimulation results in apnea *via* slowly adapting lung stretch receptors (Knowlton and Larrabee, 1946; Backman et al., 1984; Kubin et al., 1985; Widdicombe, 2001; Nonomura et al., 2017), tachypnea *via* rapidly adapting mechanoreceptors or C-fibers (Chou et al., 2008), or cough *via* the activation of the specialized mechanically sensitive nodose Aδ-fibers (the cough receptor) in the upper airways (Canning et al., 2004, 2006; Mazzone et al., 2009). A full description of nodose-evoked responses is beyond the scope of this review.

Conversely, only a few studies have specifically investigated the effects of jugular vagal stimulation on respiration. In guinea pigs, jugular vagal afferents evoke an apnea in anesthetized animals when stimulated and mediate coughing in response to inhaled noxious chemicals in conscious animals (Chou et al., 2008, 2018; Driessen et al., 2015, 2018). The apneic response, readily induced from the guinea pig larynx (Driessen et al., 2015, 2018), is perhaps consistent with the reported role of the paratrigeminal nucleus in the diving reflex whereby stimulation of trigeminal afferents in the nose promotes breath holding (Panneton et al., 2000; McCulloch et al., 2018). Indeed, the jugular vagal innervation to the larynx is particularly dense an either electrical stimulation or topically applied capsaicin evokes a profound withdrawal of respiratory drive. This reflex response to laryngeal stimulation is abolished by generalized inhibition of the paratrigeminal nucleus, but not the nucleus of the solitary tract, using microinjections of the GABA receptor antagonist muscimol (Driessen et al., 2015). Furthermore, laryngeal-evoked reductions in breathing are predominately dependent upon glutamatergic neurotransmission in the paratrigeminal nucleus, while neuropeptides appear to play a neuromodulatory role (**Figure 1B**; Driessen et al., 2018). Consistent with this, apneas can also be induced by activation of neurons in the paratrigeminal nucleus by direct microinjection of glutamate (Driessen et al., 2018). Together, these functional data support the role of jugular vagal afferents in suppressing respiratory drive.

Intriguingly, when the central terminals of afferents in the paratrigeminal nucleus are activated using microinjection of capsaicin, a slowly developing but long-lasting tachypnea is observed, distinctly opposite to the abrupt apneas described above. This tachypneic response is unaffected by glutamate antagonism but abolished in the presence of substance P receptor antagonists (Driessen et al., 2018). Whether this effect is mediated by vagal afferent nerve fibers is not known. However, these data suggest that at least two distinct neural circuits arise from the paratrigeminal nucleus and display opposing effects on respiration.

The potential role of the paratrigeminal nucleus in cough has not been investigated but is predicted based on the known role of jugular vagal afferents in evoking coughing (Hewitt et al., 2016; Chou et al., 2018). In conscious guinea pigs, inhaled chemical stimuli that activate both nodose and jugular nociceptors (e.g., capsaicin, bradykinin, citric acid) reliably evoke cough, whereas selective stimuli of nodose nociceptors (ATP, adenosine and 5HT) do not evoke coughing (Chou et al., 2018). Furthermore, nicotine selective for jugular afferents (Gu et al., 2008; Tao et al., 2019) readily induces cough (Forsberg et al., 1988; Lee et al., 2007), as does Arnold's reflex involving stimulation of the auricular branch of the vagus nerve (Ryan et al., 2014; Dicpinigaitis et al., 2019) whose fibers are derived from the jugular vagal ganglia (DuBois and Folley, 1937). A hypersensitive Arnold's reflex has now been shown to be a biomarker that defines chronic cough (Dicpinigaitis et al., 2019) and in turn could be a promising therapeutic target given that transcutaneous vagal stimulation at this site has been shown to be important for a variety of cardiovascular conditions (Murrary et al., 2016). How jugular afferent inputs are integrated in the paratrigeminal nucleus to coordinate cough and other changes to respiration has not been studied.

THE PARATRIGEMINAL NUCLEUS AND CONSCIOUS PERCEPTION OF VAGAL AFFERENTS

The ascending circuits from the paratrigeminal nucleus largely involve somatosensory processing regions of the thalamus and cortex (Ralston, 2005; McGovern et al., 2015a) and this may implicate the jugular-paratrigeminal pathway in the conscious perception of jugular vagal inputs to the brain. Indeed, the paratrigeminal nucleus has been shown to be involved in processing pain (Ma et al., 2005; Koepp et al., 2006). With respect to the vagal system, this has been best studied for airway jugular nociceptors. In guinea pigs and rats, jugular vagal afferents are most concentrated in the large proximal airways (McGovern et al., 2015b; Driessen et al., 2018), which are the structures most commonly associated with perceivable sensations (Ando et al., 2014; Hilton et al., 2015). In this regard, it is interesting that previous studies have shown that jugular vagal afferents are important for the induction of coughing evoked by noxious chemical stimuli in conscious but not anesthetized animals (Mazzone et al., 2005), where conscious perception is presumably absent. In humans, stimulation of upper airway structures innervated by jugular afferents evokes a sensory experience known as the urge-to-cough (Mazzone et al., 2011) that while in healthy individuals is relieved by coughing; in disease, these irritations persist contributing to chronic cough and increased morbidity associated with respiratory disease (Chung, 2011; Morice, 2013). A hypothesis is that the urge-to-cough and associated cough is dependent upon jugular C-fibers synapsing with neurokinin 1 receptor expressing paratrigeminal neurons. In the medullary dorsal horn, neurokinin 1 receptor expressing neurons are excitatory and project to higher order circuits that are important for discriminative and emotive processing associated with orofacial pain (Cameron et al., 2015; Li et al., 2017). Furthermore, with respect to cough, neurokinin 1 receptor antagonists have shown to be antitussive in both animal and human studies (Amadesi et al., 2001; Chapman et al., 2004; El-Hashim et al., 2004; Grobman and Reinero, 2016). Therefore, future studies aiming to define the organization of the jugular-neurokinin 1 receptor paratrigeminal circuitry in cough will improve our understanding of the airway sensory nervous system and in turn generate new and improved treatment options for sufferers of respiratory disease.

CONCLUSION: SIGNIFICANCE AND FUTURE DIRECTIONS

The paratrigeminal nucleus has an undeniable role in the processing of vagal afferent inputs. It has roles in both autonomic and nociceptive processing acting akin to the nucleus of the solitary tract and dorsal horn respectively in a context specific manner. However, the extent of this involvement has largely remained unstudied, perhaps reflecting the technical difficulties associated with studying jugular vagal afferents and this small region of the brainstem. Consequently, many questions remain about the mechanistic processing of different sensory modalities and their integration in the paratrigeminal nucleus. To this end, it will be interesting to determine the relative contributions of jugular A- and C-fiber sensory neural inputs into different paratrigeminal circuits (**Figure 1B**) and to define the physiological circumstance under which neuropeptides are released. Indeed recent advancements in molecular phenotyping of vagal sensory neurons (Kupari et al., 2019), the development of new viral vector systems and advances in imaging technologies may lead to novel approaches for investigating this neuronal circuitry.

However, it is also important to recognize that our current understanding of this topic is derived predominately from studies in healthy animals. Therefore, we likely have an under-appreciation of the importance of this nucleus in aberrant vagal afferent processing, which is well known to accompany the symptoms of disease. As such, it will be intriguing to investigate the potential plasticity in afferent processing that occurs in the paratrigeminal nucleus in a disease context, as this may provide new insights into the manifestation of heightened sensitivity and exaggerated reflexes that are characteristic of many visceral conditions. The trigeminal system (including the paratrigeminal area) has been implicated as a key region in chronic pain arising from the face (Imbe and Ren, 1999; Yamazaki et al., 2008). Under these conditions, the neurons of the trigeminal sensory nuclei have increased excitability that is likely underpinned by increased neuropeptide production and altered neuron-glial cross talk (Devesa et al., 2014; Romero-Reyes et al., 2015; Yang et al., 2016; Chen et al., 2017). In addition, changes in higher order circuitry have been described (Hayes et al., 2017). Similar sensory plasticity in the paratrigeminal nucleus may occur in visceral diseases and this could be especially relevant in conditions of vagal hypersensitivities, in which altered neurochemistry of jugular-paratrigeminal afferent processing may be an underlying feature of the associated sensory disturbances. This should be a matter of interest because sensory hypersensitivities accompanying visceral disease have proven difficult to treat and the paratrigeminal nucleus may represent a novel alternate target for therapeutic intervention.

AUTHOR CONTRIBUTIONS

The author confirms being the sole contributor of this work and has approved it for publication.

ACKNOWLEDGMENTS

The author would like to acknowledge and thank the support of the Picchi Brothers Foundation.

REFERENCES

Altschuler, S. M., Bao, X. M., Bieger, D., Hopkins, D. A., and Miselis, R. R. (1989). Viscerotopic representation of the upper alimentary tract in the rat: sensory ganglia and nuclei of the solitary and spinal trigeminal tracts. *J. Comp. Neurol.* 283, 248–268. doi: 10.1002/cne.902830207

Amadesi, S., Moreau, J., Tognetto, M., Springer, J., Trevisani, M., Naline, E., et al. (2001). NK1 receptor stimulation causes contraction and inositol phopsphate increase in medium size human isolated bronchi. *Am. J. Respir. Crit. Care Med.* 163, 1206–1211. doi: 10.1164/ajrccm.163.5.2002079

Ando, A., Farrell, M. J., and Mazzone, S. B. (2014). Cough-related neural processing in the brain: a roadmap for cough dysfunction? *Neurosci. Biobehav. Rev.* 47, 457–468. doi: 10.1016/j.neubiorev.2014.09.018

Backman, S. B., Anders, C., Ballantyne, D., Röhrig, N., Camerer, H., Mifflin, S., et al. (1984). Evidence for a monosynaptic connection between slowly adapting pulmonary stretch receptor afferents and inspiratory beta neurones. *Pflugers Arch.* 402, 129–136. doi: 10.1007/BF00583324

Balan Júnior, A., Caous, C. A., Yu, Y. G., and Lindsey, C. J. (2004). Barosensitive neurons in the rat tractus solitarius and paratrigeminal nucleus: a new model for medullary, cardiovascular reflex regulation. *J. Physiol. Pharmacol.* 82, 474–484. doi: 10.1139/y04-054

Bonham, A. C., and Jeske, I. (1989). Cardiorespiratory effects of DL-Homocysteic acid in caudal centrolateral medulla. *Am. J. Phys.* 256, H688–H696. doi: 10.1152/ajpheart.1989.256.3.H688

Cajal, S. R. (1909). *Histologie du système nerveaux de l'homme et des vertébrés*. (Paris: Maloine).

Cameron, D., Polgár, E., Gutierrez-Mecinas, M., Gomez-Lima, M., Watanabe, M., and Todd, A. J. (2015). The organisation of spinoparabrachial neurons in the mouse. *Pain* 156, 2061–2071. doi: 10.1097/j.pain.0000000000000270

Canning, B. J., Mazzone, S. B., Meeker, S. N., Mori, N., Reynolds, S. M., and Undem, B. J. (2004). Identification of the tracheal and laryngeal afferent neurones mediating cough in anaesthetized Guinea-pigs. *J. Physiol.* 557, 543–558. doi: 10.1113/jphysiol.2003.057885

Canning, B. J., Mori, N., and Mazzone, S. B. (2006). Vagal afferent nerves regulating the cough reflex. *Respir. Physiol. Neurobiol.* 152, 223–242. doi: 10.1016/j.resp.2006.03.001

Caous, C. A., de Sousa Buck, H., and Lindsey, C. J. (2001). Neuronal connections of the paratrigeminal nucleus: a topographic analysis of neurons projecting to bulbar, pontine and thalamic nuclei related to cardiovascular, respiratory and sensory functions. *Auton. Neurosci.* 94, 14–24. doi: 10.1016/S1566-0702(01)00338-1

Caous, C. A., Smith, R. L., Haapalainen, E. F., and Lindsey, C. J. (2012). Ultrstructural transneuronal degeneration study of axonal elements within the paratrigeminal nucleus in sinoaortic deafferented rats. *Einstein* 10, 145–150. doi: 10.1590/S1679-45082012000200006

Chang, R. B., Strochlic, D. E., Williams, E. K., Umans, B. D., and Liberles, S. D. (2015). Vagal sensory neuron subtypes that differentially control breathing. *Cell* 161, 622–633. doi: 10.1016/j.cell.2015.03.022

Chan-Palay, V. (1978). The paratrigeminal nucleus. II. Identification and interrelations of catecholamine axons, indoleamine axons and substance P immunoreactive cells in the neuropil. *J. Neurocytol.* 7, 419–412. doi: 10.1007/BF01173989

Chapman, R. W., House, A., Liu, F., Celly, C., Mei, H., and Hey, J. A. (2004). Antitussive activity of the tachykinin NK1 receptor antagonist, CP-99994, in dogs. *Eur. J. Pharmacol.* 485, 329–332. doi: 10.1016/j.ejphar.2003.11.048

Chen, S. P., Qin, T., Seidel, J. L., Zheng, Y., Eikermann, M., Ferrari, M. D., et al. (2017). Inhibition of the P2X7-PANX1 complex suppresses spreading depolarisation and neuroinflammation. *Brain* 140, 1643–1656. doi: 10.1093/brain/awx085

Choong, Y. T., Menuet, C., Jancovski, N., and Allen, A. M. (2013). Baroreceptor reflex control of heart rate in angiotensin type 1A receptor knockout mice. *Phys. Rep.* 1:e00171. doi: 10.1002/phy2.171

Chou, Y. L., Mori, N., and Canning, B. J. (2018). Opposing effects of bronchopulmonary C-fiber subtypes on cough in Guinea-pigs. *Am. J. Phys. Regul. Integr. Comp. Phys.* 314, R489–R498. doi: 10.1152/ajpregu.00313.2017

Chou, Y. L., Scarupa, M. D., Mori, N., and Canning, B. J. (2008). Differential effects of airway afferent nerve subtypes on cough and respiration in anesthetized Guinea pigs. *Am. J. Phys. Regul. Integr. Comp. Phys.* 295, R1572–R1584. doi: 10.1152/ajpregu.90382.2008

Chung, K. F. (2011). Chronic 'cough hypersensitivty syndrome': a more precise label for chronic cough. *Pulm. Pharmacol. Ther.* 24, 267–271. doi: 10.1016/j.pupt.2011.01.012

Ciriello, J., Hrycyshyn, A. W., and Calaresu, F. R. (1981). Glossopharyngeal and vagal afferent projections to the brain stem of the cat: a horseradish peroxidase study. *J. Auton. Nerv. Syst.* 4, 63–79.

D'Autréaux, F., Coppola, E., Hirsch, M. R., Birchmeier, C., and Brunet, J. F. (2011). Homeoprotein Phox2b commands a somatic-to-visceral switch in cranial sensory pathways. *Proc. Natl. Acad. Sci. USA* 108, 20018–20023. doi: 10.1073/pnas.1110416108

de Sousa Buck, H., Caous, C. A., and Lindsey, C. J. (2001). Projections of the paratrigeminal nucleus to the ambiguus, rostroventrolateral and lateral reticular nuclei, and the solitary tract. *Auton. Neurosci.* 87, 187–200. doi: 10.1016/S1566-0702(00)00259-9

Devesa, I., Ferrándiz-Huertas, C., Mathivanan, S., Wolf, C., Luján, R., Changeux, J. P., et al. (2014). αCGRP is essential for algesic exocytotic mobilisation of TRPV1 channels in peptidergic nociceptors. *Proc. Natl. Acad. Sci. U. S. A.* 111, 18345–18350. doi: 10.1073/pnas.1420252111

Dicpinigaitis, P. V., Enilari, O., and Cleven, K. L. (2019). Prevelance of Arnold nerve reflex in subjects with and without chronic cough: relevance to cough hypersensitivity syndrome. *Pulm. Pharmacol. Ther.* 54, 22–24. doi: 10.1016/j.pupt.2018.11.003

Donoghue, S., Garcia, M., Jordan, D., and Spyer, K. M. (1982). The brain-stem projections of pulmonary stretch afferent neurons in cats and rabbits. *J. Physiol.* 322, 353–363. doi: 10.1113/jphysiol.1982.sp014041

Driessen, A. K., Farrell, M. J., Dutschmann, M., Stanic, D., McGovern, A. E., and Mazzone, S. B. (2018). Reflex regulation of breathing by the paratrigeminal nucleus via multiple bulbar circuits. *Brain Struct. Funct.* 223, 4005–4022. doi: 10.1007/s00429-018-1732-z

Driessen, A. K., Farrell, M. J., Mazzone, S. B., and McGovern, A. E. (2015). The role of the paratrigeminal nucleus in vagal afferent evoked respiratory reflexes: a neuroanatomical and functional study in Guinea pigs. *Front. Physiol.* 6:378. doi: 10.3389/fphys.2015.00378

DuBois, F. S., and Folley, J. O. (1937). Quantitiative studies of the vagus nerve in the cat. II. The ratio of jugular to nodose fibers. *J. Comp. Neurol.* 67, 69–87.

El-Hashim, A. Z., Wyss, D., and Lewis, C. (2004). Effect of a novel NK1 receptor selective antagonist (NKP608) on citric acid induced cough and airway obstruction. *Pulm. Pharmacol. Ther.* 17, 11–18. doi: 10.1016/j.pupt.2003.08.002

Feil, K., and Herbert, H. (1995). Topographic organization of spinal and trigeminal somatosensory pathways to the rat parabrachial and Kolliker-fuse nuclei. *J. Comp. Neurol.* 353, 506–528. doi: 10.1002/cne.903530404

Forsberg, K., Karlsson, J. A., Theodorsson, E., Lundberg, J. M., and Persson, C. G. (1988). Cough and bronchoconstriction mediatted by capsaicin-sensitive sensory neurons in the Guinea pig. *Pulm. Pharmacol.* 1, 33–39. doi: 10.1016/0952-0600(88)90008-7

Ghali, M. G. Z. (2017). The brainstem network controlling blood pressure: an important role for pressor sites in the caudal medulla and cervical spinal cord. *J. Hypertens.* 35, 1938–1947. doi: 10.1097/HJH.0000000000001427

Grobman, M., and Reinero, C. (2016). Investigation of neurokinin-1 receptor antagonism as a novel treatment for chronic bronchitis in dogs. *J. Vet. Intern. Med.* 30, 847–852. doi: 10.1111/jvim.13935

Gu, Q., Ni, D., and Lee, L. Y. (2008). Expression of neuronal nicotinic acetylcholine receptors in rat vagal pulmonary sensory neurons. *Respir. Physiol. Neurobiol.* 161, 87–91. doi: 10.1016/j.resp.2007.11.006

Hayes, D. J., Chen, D. Q., Zhong, J., Lin, A., Behan, B., Walker, M., et al. (2017). Affective circuitry alterations in patients with trigeminal neuralgia. *Front. Neuroanat.* 11:73. doi: 10.3389/fnana.2017.00073

Hewitt, M. M., Adams, G. Jr., Mazzone, S. B., Mori, N., Yu, L., Canning, B. J., et al. (2016). Pharmacology of bradykinin-evoked coughing in guinea pigs. *J. Pharmacol. Exp. Ther.* 357, 620–628.

Hilton, E., Marsden, P., Thurston, A., Kennedy, S., Decalmer, S., and Smith, J. A. (2015). Clinical features of the urge-to-cough in patients with chronic cough. *Respir. Med.* 109, 701–707. doi: 10.1016/j.rmed.2015.03.011

Hu, G., Huang, K., Hu, Y., Du, G., Xue, Z., Zhu, X., et al. (2016). Single-cell RNA-seq reveals distinct injury responses in different types of DRG sensory neurons. *Sci. Rep.* 6:31851. doi: 10.1038/srep31851

Imbe, H., and Ren, K. (1999). Orofacial deep and cutaneous tissue inflammation differentially upregulates preprodynorphin mRNA in the trigeminal and paratrigeminal nuclei of the rat. *Brain Res. Mol. Brain Res.* 67, 87–97. doi: 10.1016/S0169-328X(99)00040-6

Jurcakova, D., Ru, F., Kollarik, M., Sun, H., Krajewski, J., and Undem, B. J. (2018). Voltage-gated sodium channels regulating action potential generation in itch-, nociceptive-, and low threshold mechanosensitive cutaneous C-fibres. *Mol. Pharmacol.* 94, 1047–1056. doi: 10.1124/mol.118.112839

Knowlton, G. C., and Larrabee, M. G. (1946). A unitary analysis of pulmonary volume receptors. *Am. J. Phys.* 147, 100–114.

Koepp, J., Lindsey, C. J., Motta, E. M., and Rae, G. A. (2006). Role of the paratrigeminal nucleus in nocifensive responses of rats to chemical, thermal and mechanical stimuli applied to the hind paw. *Pain* 122, 235–244. doi: 10.1016/j.pain.2006.01.038

Koganezawa, T., and Paton, J. F. (2014). Intrinsic chemosensitivity of rostral ventrolateral medullary sympathetic premotor neurons in the in situ arterially perfused preparation of rats. *Exp. Physiol.* 99, 1453–1466. doi: 10.1113/expphysiol.2014.080069

Kubin, L., Alheid, G. F., Zuperku, E. J., and McCrimmon, D. R. (1985). Central pathways of pulmonary and lower airway vagal afferents. *J. Appl. Physiol.* 101, 618–627.

Kupari, J., Häring, M., Agirre, E., Castelo-Branco, G., and Ernfors, P. (2019). An atlas of vagal sensory neurons and their molecular specialization. *Cell Rep.* 27, 2508–2523. doi: 10.1016/j.celrep.2019.04.096

Kwong, K., Kollarik, M., Nassenstein, C., Ru, F., and Undem, B. J. (2008). P2X2 receptors differentiate placodal vs. neural crest C-fiber phenotypes innervating Guinea pig lungs and esophagus. *Am. J. Phys. Lung Cell. Mol. Phys.* 295, L858–L865. doi: 10.1152/ajplung.90360.2008

Lee, L. Y., Burki, N. K., Gerhardstein, D. C., Gu, Q., Kou, Y. R., and Xu, J. (2007). Airway irritation and cough evoked by inhlaed cigarette smoke: role of neuronal nicotinic acetylcholine receptors. *Pulm. Pharmacol. Ther.* 20, 355–364. doi: 10.1016/j.pupt.2006.10.007

Li, C. L., Li, K. C., Wu, D., Chen, Y., Luo, H., Zhao, J. R., et al. (2016). Somatosensory neuron types identified by high-coverage single-cell RNA-sequencing and functional heterogenity. *Cell Res.* 26:967. doi: 10.1038/cr.2016.90

Li, J. L., Li, Y. Q., Li, J. S., Kaneko, T., and Mizuno, N. (1999). Calcium-binding protein-immunoreactive projection neurons in the caudal subnucleus of the spinal trigeminal nucleus of the rat. *Neurosci. Res.* 35, 225–240. doi: 10.1016/S0168-0102(99)00086-3

Li, X., Ge, S. N., Li, Y., and Wang, H. T. (2017). Neurokinin-1 receptor-immunopositive neurons in the medullary dorsal horn provide collateral axons to both the thalamus and parabrachial nucleus in rats. *Neurochem. Res.* 42, 375–388. doi: 10.1007/s11064-016-2080-0

Lindsey, C. J., Buck, H. S., Fior-Chadi, D. R., and Lapa, R. C. (1997). Pressor effect mediated by bradykinin in the paratrigeminal nucleus of the rat. *J. Physiol.* 502, 119–129. doi: 10.1111/j.1469-7793.1997.119bl.x

Mahadi, K. M., Lall, V. K., Deuchars, S. A., and Deuchars, J. (2019). Cardiovascular autonomic effects of transcutanoues auricular nerve stimulation via the tragus in the rat involve spinal cervical sensory afferent pathways. *Brain Stimul.* 12, 1151–1158. doi: 10.1016/j.brs.2019.05.002

Ma, W. L., Zhang, W. B., Feng, G., and Cai, Y. L. (2005). Calbindin D28k-containing neurons in the paratrigeminal nucleus receive convergent nociceptive information and project to nucleus of the solitary tract in rat. *Brain Res.* 1038, 132–140. doi: 10.1016/j.brainres.2005.01.021

Mazzone, S. B., Cole, L. J., Ando, A., Egan, G. F., and Farrell, M. J. (2011). Investigation of the neural control of cough and cough suppression in humans using functional brain imaging. *J. Neurosci.* 31, 2948–2958. doi: 10.1523/JNEUROSCI.4597-10.2011

Mazzone, S. B., Mori, N., and Canning, B. J. (2005). Synergistic interactions between airway afferent nerve subtypes regulating the cough reflex in Guinea-pigs. *J. Physiol.* 569, 559–573. doi: 10.1113/jphysiol.2005.093153

Mazzone, S. B., Reynolds, S. M., Mori, N., Kollarik, M., Farmer, D. G., Myers, A. C., et al. (2009). Selective expression of a sodium pump isozyme by cough receptors and evidence for its essential role in regulating cough. *J. Neurosci.* 29, 13662–13671. doi: 10.1523/JNEUROSCI.4354-08.2009

Mazzone, S. B., and Undem, B. J. (2016). Vagal afferent innervation of the airways in health and disease. *Physiol. Rev.* 96, 975–1024. doi: 10.1152/physrev.00039.2015

McCulloch, P. F., Lahrman, K. A., DelPrete, B., and DiNovo, K. M. (2018). Innervation of the nose and nasal region of the rat: implication for initiating the mammalian diving response. *Front. Neuroanat.* 12:85. doi: 10.3389/fnana.2018.00085

McGovern, A. E., Davis-Poynter, N., Farrell, M. J., and Mazzone, S. B. (2012). Transneuronal tracing of airways-related sensory circuitry using herpes simplex virus 1, strain H129. *Neuroscience* 207, 148–166. doi: 10.1016/j.neuroscience.2012.01.029

McGovern, A. E., Driessen, A. K., Simmons, D. G., Powell, J., Davis-Poynter, N., Farrell, M. J., et al. (2015a). Distinct brainstem and forebrain circuits receiving tracheal sensory neuron inputs revealed using a novel conditional anterograde transsynaptic viral tracing system. *J. Neurosci.* 35, 7041–7055. doi: 10.1523/JNEUROSCI.5128-14.2015

McGovern, A. E., Davis-Poynter, N., Yang, S. K., Simmons, D. G., Farrell, M. J., and Mazzone, S. B. (2015b). Evidence for multiple sensory circuits in the brain arising from the respiratory system: an anterograde viral tract tracing study in rodents. *Brain Struct. Funct.* 220, 3683–3699. doi: 10.1007/s00429-014-0883-9

Morice, A. H. (2013). Chronic cough hypersensitivity syndrome. *Cough* 9, 14–18. doi: 10.1186/1745-9974-9-14

Murrary, A. R., Atkinson, L., Mahadi, M., Deuchars, S., and Deuchars, J. (2016). The strange case of the ear and the heart: the auricular vagus nerve and its influence on cardiac control. *Auton. Neurosci.* 199, 48–53. doi: 10.1016/j.autneu.2016.06.004

Mutoh, T., Bonham, A. C., and Joad, J. P. (2000). Substance P in the nucleus of the solitary tract augments bronchopulmonary C fibre reflex output. *Am. J. Phys. Regul. Integr. Comp. Phys.* 279, R1215–R1223. doi: 10.1152/ajpregu.2000.279.4.R1215

Nasution, I. D., and Shigenaga, Y. (1987). Ascending and descending internuclear projections within the trigeminal sensory nuclear complex. *Brain Res.* 425, 234–247. doi: 10.1016/0006-8993(87)90506-3

Nomaksteinsky, M., Kassabov, S., Chettouh, Z., Stoeklé, H. C., Bonnaud, L., Fortin, G., et al. (2013). Ancient origin of somatic and visceral neurons. *BMC Biol.* 11:53. doi: 10.1186/1741-7007-11-53

Nomura, S., and Mizuno, N. (1984). Central distribution of primary afferent fibers in the Arnold's nerve (the auricular branch of the vagus nerve): a transganglionic HRP study in the cat. *Brain Res.* 292, 199–205. doi: 10.1016/0006-8993(84)90756-X

Nonomura, K., Woo, S. H., Chang, R. B., Gillich, A., Qiu, Z., Francisco, A. G., et al. (2017). Piezo2 sense airway stretch and mediates lung inflation-induced apnoea. *Nature* 541, 176–181. doi: 10.1038/nature20793

Panneton, W. M., and Burton, H. (1981). Corneal and periocular representation within the trigeminal sensory complex in the cat studied with transganglionic transport of horseradish peroxidase. *J. Comp. Neurol.* 199, 327–344. doi: 10.1002/cne.901990303

Panneton, W. M., McCulloch, P. F., and Sun, W. (2000). Trigemino-autonomic connections in the muskrat: the neural substrate for the diving response. *Brain Res.* 874, 48–65. doi: 10.1016/S0006-8993(00)02549-X

Phelan, K. D., and Falls, W. M. (1989). The interstitial system of the spinal trigeminal tract in the rat: anatomical evidence for morphological and functional heterogeneity. *Somatosens. Mot. Res.* 6, 367–399.

Pinto, M. L., de Cássia Machado, R., Schoorlemmer, G. H., Colombari, E., and de Cássia Ribeiro da Silva Lapa, R. (2006). Topographic organization of the projections from the interstitial system of the spinal trigeminal tract to the parabrachial nucleus in the rat. *Brain Res.* 1113, 137–145. doi: 10.1016/j.brainres.2006.07.028

Potenzieri, C., Meeker, S., and Undem, B. J. (2012). Activation of mosue bronchopulmonary C-fibres by serotonin and allergen-ovalbumin challenge. *J. Physiol.* 590, 5449–5559. doi: 10.1113/jphysiol.2012.237115

Ralston, H. J. 3rd (2005). Pain and the primate thalamus. *Prog. Brain Res.* 149, 1–10. doi: 10.1016/S0079-6123(05)49001-9

Rhoton, A. L. Jr., O'leary, J. L., and Ferguson, J. P. (1966). The trigeminal, facial, vagal and glossopharyngeal nerves in the monkey. Afferent connections. *Arch. Neurol.* 14, 530–540.

Riccio, M. M., Kummer, W., Biglari, B., Myers, A. C., and Undem, B. J. (1996). Interganglionic segregation of distinct vagal afferent fibre phenotypes in Guinea-pig airways. *J. Physiol.* 496, 521–530. doi: 10.1113/jphysiol.1996.sp021703

Romero-Reyes, M., Pardi, V., and Akerman, S. (2015). A potent and selective calcitonin gene-related peptide (CGRP) receptor anatongist, MK-8825, inhibits responses to nociceptive trigeminal activation: a role of CGRP in orofacial pain. *Exp. Neurol.* 271, 95–103. doi: 10.1016/j.expneurol.2015.05.005

Ruggiero, D. A., Tong, S., Anwar, M., Gootman, N., and Gootman, P. M. (1996). Hypotension-induced expression of the c-fos gene in the medulla oblongata of piglets. *Brain Res.* 706, 199–209. doi: 10.1016/0006-8993(95)01173-0

Rutherfurd, S. D., Widdop, R. E., Sannajust, F., Louis, W. J., and Gundlach, A. L. (1992). Expression of c-fos and NGFI-A messenger RNA in the medulla oblongata of the anaesthetized rat following stimulation of vagal and cardiovascualr afferents. *Brain Res. Mol. Brain Res.* 13, 301–312. doi: 10.1016/0169-328X(92)90213-U

Ryan, N. M., Gibson, P. G., and Birring, S. S. (2014). Arnold's nerve cough reflex: evidence for chronic cough as a sensory vagal neuropathy. *J. Thorac. Dis.* 6, S748–S752. doi: 10.3978/j.issn.2072-1439.2014.04.22

Saxon, D. W., and Hopkins, D. A. (1998). Efferent and collateral organization of paratrigeminal nucleus projections: an anterograde and retrograde fluorescent tracer study in the rat. *J. Comp. Neurol.* 402, 93–110. doi: 10.1002/(SICI)1096-9861(19981207)402:1<93::AID-CNE7>3.0.CO;2-A

Saxon, D. W., and Hopkins, D. A. (2006). Ultrastructure and synaptology of the paratrigeminal nucleus in the rat: primary pharyngeal and laryngeal afferent projections. *Synapse* 59, 220–234. doi: 10.1002/syn.20233

Sousa, L. O., and Lindsey, C. J. (2009). Discharge rate profiles of paratrigeminal nucleus neurons throughout a pressor event in non-anaesthetised rats. *Auton. Neurosci.* 147, 20–26. doi: 10.1016/j.autneu.2008.12.012

Tallapragada, V. J., Hildreth, C. M., Burke, P. G., Raley, D. A., Hassan, S. F., McMullan, S., et al. (2016). Tonically active cAMP-dependent signalling in the ventrolateral medulla regulates sympathetic and cardiac vagal outflows. *J. Pharmacol. Exp. Ther.* 356, 424–433. doi: 10.1124/jpet.115.227488

Tao, M., Liu, Q., Miyazaki, Y., and Canning, B. J. (2019). Nicotinic receptor dependent regulation of cough and other airway defensive reflexes. *Pulm. Pharmacol. Ther.* 58:101810. doi: 10.1016/j.pupt.2019.101810

Undem, B. J., Chuaychoo, B., Lee, M. G., Weinreich, D., Myers, A. C., and Kollarik, M. (2004). Subtypes of vagal afferent C-fibres in Guinea-pig lungs. *J. Physiol.* 556, 905–917. doi: 10.1113/jphysiol.2003.060079

Wang, X., Guo, R., and Zhao, W. (2015). Distribution of Fos-like immunoreactivity catecholaminergic and serotinergic neurons activated by the laryngeal chemoreflex in the medulla oblongata of rats. *PLoS One* 10:e0130822. doi: 10.1371/journal.pone.0130822

Widdicombe, J. (2001). Airway receptors. *Respir. Physiol.* 125, 3–15. doi: 10.1016/S0034-5687(00)00201-2

Yamazaki, Y., Ren, K., Shimada, M., and Iwata, K. (2008). Modulation of paratrigeminal nociceptive neurons following temporomandibular joint inflammation in rats. *Exp. Neurol.* 214, 209–218. doi: 10.1016/j.expneurol.2008.08.005

Yang, Y. J., Hu, L., Xia, Y. P., Jiang, C. Y., Miao, C., Yang, C. Q., et al. (2016). Resveratrol suppresses glial activation and alleviates trigeminal neuralgia via activation of AMPK. *J. Neuroinflammation* 13, 84–95. doi: 10.1186/s12974-016-0550-6

Conflict of Interest Statement: The author declares that the research was conducted in the absence of any commercial or financial relationships that could be construed as a potential conflict of interest.

frontiers in Physiology

ORIGINAL RESEARCH
published: 12 September 2019
doi: 10.3389/fphys.2019.01146

Functional-Optical Coherence Tomography: A Non-invasive Approach to Assess the Sympathetic Nervous System and Intrinsic Vascular Regulation

*Nicholas G. Jendzjowsky[1], Craig D. Steinback[2], Robert J. Herman[3], Willis H. Tsai[3,4], Fiona E. Costello[3,5,6] and Richard J. A. Wilson[1]**

[1] Department of Physiology and Pharmacology, Cumming School of Medicine, University of Calgary, Calgary, AB, Canada, [2] Program for Pregnancy and Postpartum Health, Physical Activity and Diabetes Laboratory, Faculty of Kinesiology, Sport and Recreation, University of Alberta, Edmonton, AB, Canada, [3] Department of Medicine, Cumming School of Medicine, University of Calgary, Calgary, AB, Canada, [4] Department of Community Health Sciences, Cumming School of Medicine, University of Calgary, Calgary, AB, Canada, [5] Department of Clinical Neuroscience, Cumming School of Medicine, University of Calgary, Calgary, AB, Canada, [6] Department of Surgery, Cumming School of Medicine, University of Calgary, Calgary, AB, Canada

OPEN ACCESS

Edited by:
Vaughan G. Macefield, Baker Heart and Diabetes Institute, Australia

Reviewed by:
Gavin W. Lambert, Swinburne University of Technology, Australia
Olaf Grisk, University of Greifswald, Germany

***Correspondence:**
Richard J. A. Wilson
wilsonr@ucalgary.ca

Specialty section:
This article was submitted to Integrative Physiology, a section of the journal Frontiers in Physiology

Received: *07 July 2019*
Accepted: *22 August 2019*
Published: *12 September 2019*

Citation:
Jendzjowsky NG, Steinback CD, Herman RJ, Tsai WH, Costello FE and Wilson RJA (2019) Functional-Optical Coherence Tomography: A Non-invasive Approach to Assess the Sympathetic Nervous System and Intrinsic Vascular Regulation. Front. Physiol. 10:1146. doi: 10.3389/fphys.2019.01146

Sympathetic nervous system dysregulation and vascular impairment in neuronal tissue beds are hallmarks of prominent cardiorespiratory diseases. However, an accurate and convenient method of assessing SNA and local vascular regulation is lacking, hindering routine clinical and research assessments. To address this, we investigated whether spectral domain optical coherence tomography (OCT), that allows investigation of retina and choroid vascular responsiveness, reflects sympathetic activity in order to develop a quick, easy and non-invasive sympathetic index. Here, we compare choroid and retina vascular perfusion density (VPD) acquired with OCT and heart rate variability (HRV) to microneurography. We recruited 6 healthy males (26 ± 3 years) and 5 healthy females (23 ± 1 year) and instrumented them for respiratory parameters, ECG, blood pressure and muscle sympathetic nerve microneurography. Choroid VPD decreases with the cold pressor test, inhaled hypoxia and breath-hold, and increases with hyperoxia and hyperpnea suggesting that sympathetic activity dominates choroid responses. In contrast, retina VPD was unaffected by the cold pressor test, increased with hypoxia and breath hold and decreases with hyperoxia and hyperpnea, suggesting metabolic vascular regulation dominates the retina. With regards to integrated muscle sympathetic nerve activity, HRV had low predictive power whereas choroid VPD was strongly (inversely) correlated with integrated muscle sympathetic nerve activity ($R = -0.76$; $p < 0.0001$). These data suggest that Functional-OCT may provide a novel approach to assess sympathetic activity and intrinsic vascular responsiveness

(i.e., autoregulation). Given that sympathetic nervous system activity is the main determinant of autonomic function, sympathetic excitation is associated with severe cardiovascular/cardiorespiratory diseases and autoregulation is critical for brain health, we suggest that the use of our new Functional-OCT technique will be of broad interest to clinicians and researchers.

Keywords: sympathetic nervous system, autoregulation, microvascular, vascular, choroid

INTRODUCTION

Abnormal sympathetic nervous system activity damages local vascular regulation, including the ability of the microvasculature to resist associated changes in blood pressure (i.e., myogenic autoregulation) and respond appropriately to local metabolic demands. Concurrently, impaired local microvascular regulation reduces tissue perfusion within vital organs, causing tissue damage and organ dysfunction, triggering sympathetic excitation. Consequently, abnormal sympathetic nervous system activity and impoverished microvascular regulation are associated with, and causal to a host of common cardiovascular, cardiorespiratory and metabolic diseases including sleep apnea, hypertension, metabolic diseases, stroke, heart failure and dementia (Mancia et al., 1999; Barretto et al., 2009; Grassi et al., 2009; Agemy et al., 2015; Gutterman et al., 2016; Doustar et al., 2017; Nelis et al., 2018).

Available methods to measure sympathetic responses suffer from poor time resolution (i.e., norepinephrine spillover), multiple neuronal inputs (i.e., skin temperature, heart rate variability), are invasive (i.e., microneurography) and/or do not completely reflect sympathetic activity (i.e., heart rate variability) (Mancia et al., 1998; Notarius et al., 1999; Jänig and Häbler, 2003; Baumert et al., 2009; Martelli et al., 2014). Methods to measure microvascular responses – especially in relation to cerebral vascular beds – are limited to techniques which suffer from poor cost effectiveness (i.e., MRI), spatial resolution (i.e., trans-cranial doppler) and/or temporal resolution (i.e., MRI/CT), or require some degree of invasiveness (i.e., dye tracer techniques) (Provenzale et al., 2008; Willie et al., 2014; Blair et al., 2016). Our inability to measure these properties efficiently and non-invasively limits early diagnosis, treatment and research of cardiovascular and cardiorespiratory diseases (Mancia et al., 1999; Grassi et al., 2009; Padilla et al., 2014; Gutterman et al., 2016). To solve this issue, we have developed a new approach to measure blood vessel physiology in humans using spectral domain optical coherence tomography (OCT) imaging of ophthalmic vascular beds.

The posterior segment of the eye is an extension of the brain, but with two distinct vascular beds. The vascular beds of the retina and choroid differ in their local vascular responses and sympathetic innervation (Delaey and Van De Voorde, 2000; Nickla and Wallman, 2010). Specifically, blood vessels of the retina appear to be controlled almost exclusively by myogenic and metabolic mechanisms triggered in response to their local environment (Delaey and Van De Voorde, 2000; Nickla and Wallman, 2010); thus, they behave similarly to blood vessels in the brain (Willie et al., 2012, 2014). In contrast, blood vessels of the choroid express an abundance of α-adrenergic receptors and constrict in response to global sympathetic activation (Bill and Sperber, 1990; Delaey and Van De Voorde, 2000; McDougal and Gamlin, 2015). Accordingly, the vascular compartments of the retina and choroid respond differently to conditions which change global sympathetic activity or reflect local metabolic demands (Delaey and Van De Voorde, 2000; Nickla and Wallman, 2010) and therefore reflect differences in vascular regulation.

Modern OCT devices can easily image both the retina and choroid (Fujimoto et al., 2000; Poddar et al., 2014). Optical coherence tomography is a non-invasive, fast, high-resolution and relatively affordable ophthalmic imaging technology used routinely to detect anatomical abnormalities associated with retinopathies in ophthalmic clinics. Near-infrared lasers and sophisticated image reconstruction algorithms allow visualization deep within the tissue with a spatial resolution of ∼4 μm, 3–4 orders of magnitude greater than magnetic resonance imaging (Fujimoto et al., 2000; Poddar et al., 2014). Ophthalmic OCT imaging of the retina has been used to identify late-stage microvascular anatomic markers for several vascular diseases including diabetes and dementia (Agemy et al., 2015; Doustar et al., 2017; Nelis et al., 2018). However, optimization of diagnostic criteria should include microvascular physiology as changes in functional responses likely occur before anatomic abnormalities are detectable. Given the capabilities of OCT to measure the microvasculature and the differential vascular regulation of the retina and choroid, we hypothesized that Functional-OCT imaging of the eye can be used to assess sympathetic and neurovascular reactivity to physiological perturbations.

To test our hypothesis, we used OCT to compare the microvascular responses of the choroid and retina to different conditions (inspiratory challenges and cold pressor test) designed to disentangle sympathetic and local metabolic vascular control mechanisms. The inspiratory challenges were chosen to stimulate the central and peripheral chemoreflexes reflective of reflex stimulation and mimic sympathetic activation encountered with cardiorespiratory diseases; the cold pressor causes sympathetic activation independent of changes to blood gases. Experiments were performed in 11 healthy human participants while recording ventilation, blood pressure, heart rate and direct measures of sympathetic nerve activity using microneurography, the only method to record from the sympathetic nervous system in directly.

MATERIALS AND METHODS

Participants

The study was approved by the Conjoint Health Research Ethics Board at the University of Calgary and University of Alberta and conformed to institutional guidelines and the standards set by the latest revision of the Declaration of Helsinki. Seventeen healthy volunteers (11 male) 18–36 years of age were recruited from the University of Calgary community. All participants were normotensive, non-smokers and free of respiratory, cardiovascular, neurological diseases, and provided written informed consent prior to study. Data from 11 participants (6 male, 5 female) were analyzed; 6 (5 male, 1 female) participants did not complete the protocol because of difficulty locating and maintaining stable sympathetic recordings and/or, the onset of vasovagal reflexes (n = 2) associated with microneurography in the seated position as assessed by cardiovascular indices of pre-syncope (Meah et al., 2019).

Optical Coherence Tomography

Left eyes were scanned with a Cirrus HD 4000 spectral domain optical coherence tomography system (OCT, Zeiss optics, Toronto, ON, Canada). The Cirrus HD 4000 uses near-infrared laser interferometry, enabling an optical reconstruction of a 6 mm^3 cube of the eye. All OCT scans were acquired by the same operator (RH) with the Cirrus OCT device (software version 6.5.0772). Image acquisition of the Cirrus OCT system, averages 1024 scans within ∼3 s using active eye-tracking features and centred around the fovea, thus standardizing each image to the anatomical characteristics of each individual eye, to produce a single image set. For each participant, the baseline scan was used to establish a slice which encased the large vessels of the choroid as identified by visual inspection. Once anatomical parameters for the slice were established from the baseline scan, the same parameters were maintained for scans from all subsequent perturbations for that subject. The average slice thickness across subjects was 86 ± 3 μm (the inner and outer surfaces of the slice were located 85 ± 6 μm and 171 ± 9 μm, respectively, from the outer portion of the hyper-reflective line corresponding to the retina pigment epithelium). The retina circulation was measured from images obtained from the 3D visualization mode by capturing the aggregate of the retina vessels on a 2D "flattened" image. Retina thickness was measured using the automatic segmentation values of the Cirrus HD OCT software. Two images were collected during each stimulus. A single image chosen from paired scans was selected for each intervention from each participant. Image selection and image analysis were performed independently by different team members (RH, RW, and, NJ, respectively).

Instrumentation

Peripheral muscle SNA (MSNA) was assessed using microneurography. Briefly, a tungsten recording electrode with an uninsulated 1–5 μm diameter tip was inserted transcutaneously into the peroneal nerve at or distal to the fibular head. A reference electrode was inserted subcutaneously 1–3 cm from the recording site. The recording electrode was manipulated into position within a sympathetic nerve fascicle, which produced pulse-synchronous bursts of activity characteristic of sympathetic vasoconstrictor neurons innervating skeletal muscle. The sympathetic signal was verified by an increase in firing frequency during voluntary apnoea and lack of responsiveness during arousal to a loud noise. The raw sympathetic signal was amplified by a preamplifier (1000×) and secondary isolated amplifier (gain: 10 K; model 662C-3; Iowa University Bioengineering, IA), band-pass–filtered (700–2000 Hz), rectified and integrated (time constant: 0.1 s) as per standardized methods (Hart et al., 2017). All recordings were performed by a trained microneurographer (CS).

Heart rate was measured using a 3-lead ECG. Respiratory flow was monitored by a pneumotachometer (ParvoMedics/Hans Rudolph, UT, United States) and end-tidal gas concentrations were measured via an oxygen and carbon dioxide analyzer (Powerlab, AD Instruments, CO, United States). Blood pressure was measured continuously using finger photoplethysmography (Finometer; Finapres Medical Systems, Amsterdam, Netherlands) and calibrated to baseline blood pressure values obtained using manual sphygmomanometry. Manual blood pressures were assessed at the brachial artery just proximal to the elbow (arm straight or in mild elbow flexion) using a mercury sphygmomanometer and a medium-sized blood pressure cuff performed by a clinician (RH). Calibrated pressure waveforms were analyzed to determine beat-by-beat MAP and systolic and diastolic blood pressures. Blood oxygen saturation was measured with a pulse oximeter (Nellcor N-395 Medtronic, Brampton, ON, Canada).

Protocol

Participants were instructed to refrain from caffeine (12 h), exercise (24 h), and alcohol (24 h), and ingest their last meal at least 3 h prior to the laboratory visit. All female participants were tested during the midluteal phase (21 ± 2 days) of their menstrual cycle where minimal effects of the menstrual cycle on sympathetic activity have been demonstrated (Usselman et al., 2015); 4/5 were prescribed oral contraceptives.

After arriving at the laboratory, the study protocol was reviewed with the participants, who were then allowed to acclimatize to the environment prior to being instrumented for the study. Once instrumentation was complete, participants rested for 10 min in a seated position during instrumentation and remained seated throughout the entire protocol. Familiarization to the OCT device entailed 2–4 practice scans which were followed by baseline hemodynamic and neurographic recordings for >15 min. Subsequently, respiratory gas challenges of hypoxia (12% O_2, balance N_2, 3 min), hyperoxia (100% O_2, 3 min), hyperoxic-hypercapnia (5% CO_2, balance O_2, 3 min), hyperpnea (participants were instructed to breathe "hard and fast"-not paced, 3 min), voluntary end-expiratory sub maximal breath hold (∼10 s) and cold pressor test (hand immersed up to the wrist in ∼1°C ice water, 3 min). The hypoxic challenge was always performed last due to the long lasting hemodynamic and sympathetic changes associated with hypoxia (Xie et al., 2001) while all other interventions were administered in random order.

Each challenge was interspersed with ≥10 min of rest to allow baseline cardiovascular and neurographic values to return. The cold pressor test was included to augment sympathetic activation without marked blood gas changes to minimize changes in local vascular regulation.

Data Analysis

Vascular perfusion density (VPD) defined as a static index of perfusion within the image, was calculated for the choroid and retina of each image for each participant within each condition. The resulting images were analyzed offline using Image J software (NIH, Bethesda, MD, United States). Choroid images were obtained from the RPEFIT mode. All images were subject to the same analysis involving the Iterative Self- Organizing Data Analysis Technique Algorithm (ISODATA). This algorithm provides unsupervised determination of a threshold to classify background and objects (Ridler and Calvard, 1978). Images of the retina were obtained from the 3D visualization mode and a 2D flattened image was selected in order to obtain the aggregate vasculature of the retina circulation. All images were processed the same way using a macro written in Image J (RW). The macro filtered out artifacts and used the moment auto-thresholding approach to obtain vessel density values, reflecting retina VPD.

All hemodynamic and neurographic data were stored for offline data analysis (PowerLab/16SP with LabChart 8; AD Instruments, Colorado Springs, CO, United States). Heart rate variability was assessed by utilizing 3-min bins (time of each perturbation) and analyzed with built-in heart rate variability software (LabChart8; AD Instruments, Colorado Springs, CO, United States). Hemodynamic and neurographic responses to gas challenges and cold pressor test were averaged over 2 min (Notay et al., 2016) while the OCT scan occurred during the middle portion of the 2 min segment. Sympathetic activity was analyzed by a custom written semi-automated peak detection software written in VEE (RW) and confirmed by a trained observer (NJ). Burst amplitude and total activity were analyzed after removal of extraneous noise from the recordings based on statistical parameters derived from the signal itself. The software assigns a threshold cut-off for the noise (four standard deviations from the mean) and calculates the area under all spikes above the cut-off; it then derives total neural activity using all spikes within the field of interest. In this way, the amplitude and total activity is normalized within each participant. For all hemodynamic and sympathetic outcomes, relative responses to sympathetic provocations were normalized to baseline. These methods align with established criteria (Hart et al., 2017) and, importantly, remove observer bias.

Statistics

Differences between sexes were tested with independent *t*-test. Differences between sympathetic provocations were tested with the Friedman's non-parametric one-way repeated measures ANOVA using raw values (data are presented as percent change from baseline). When significant F-ratios were found, Student Newman Keuls *post hoc* test was used to discern differences from the baseline condition. Relationships between indices were assessed with Pearson product correlation; and select relationships were analyzed with partial correlation in order to account for gender. Multiple regression analysis was performed when more than one index was used to relate to sympathetic nervous activity. Assessment of inter-measurement agreement was completed using Bland-Altman analysis. A p-value < 0.05 was considered statistically significant. All data are expressed as mean ± SEM.

RESULTS

Figure 1 shows OCT images of the retina and choroid, with associated processed images and muscle sympathetic nerve activity (MSNA), from one participant during baseline and the six conditions designed to disentangle sympathetic from local metabolic and myogenic mechanisms of vascular regulation. Once the participant was appropriately instrumented and seated, each OCT scan took ∼3 s acquiring 1024 scans of 5 μm resolution from a 6 mm^3 block of tissue. As blood absorbs near-infrared light, blood appears dark in OCT images; to assist in comparisons, the raw images are false colored such that tissues which have high vascular perfusion appear blue whereas tissues with low vasculature perfusion appear red. In the choroid, conditions that result in low sympathetic activity (baseline, hyperoxia and voluntary hyperpnea) tend to increase vascular perfusion (appearing bluer), whereas conditions expected to activate the sympathetic nervous system (voluntary breath hold, hypoxia, hypercapnia and cold pressor test) reduce vascular perfusion (appearing greener). Note that the choroid has far greater vascular perfusion (blue-green) than the retina (yellow-red). Although the effects of the different conditions on the retina are subtler, hypoxia resulted in higher vascular perfusion compared to hyperoxia (during which less perfusion is anticipated). As expected this effect was predominantly demonstrated in distal portions of arteriolar branches (i.e., distal segments dilate or constrict according to the condition).

To use OCT for quantitative assessment of changes in microvascular perfusion, we adopted a measure of vascular perfusion density (VPD) based on pixel intensities in the processed images (Agemy et al., 2015), applied to both the retina and choroid vascular beds. Baseline choroid VPD was identical between sexes; however, baseline retina VPD was greater in females (**Table 1**). No other sex differences in cardiovascular, ophthalmic or MSNA indices were found within our dataset and, given that burst frequency and total MSNA were similar between males and females during the midluteal phase of the ovarian cycle as previously demonstrated (Usselman et al., 2015), data from males and females were pooled for analysis.

Retina VPD, choroid VPD, MSNA and cardiorespiratory parameter responses to the six test conditions in 11 participants are illustrated in **Figure 2**. Hyperpnea increased MSNA mildly (**Figure 2H**) but had no decisive effect on retina (**Figure 2B**) or choroid VPD (**Figure 2C**). The cold pressor test, which caused a substantial increase in MSNA (**Figure 2H**) without changing blood gases (**Figures 2J,K**), decreased choroid VPD (**Figure 2C**). Choroid VPD also decreased with the two respiratory conditions (**Figure 2C**) which increased MSNA the most (hypoxia and

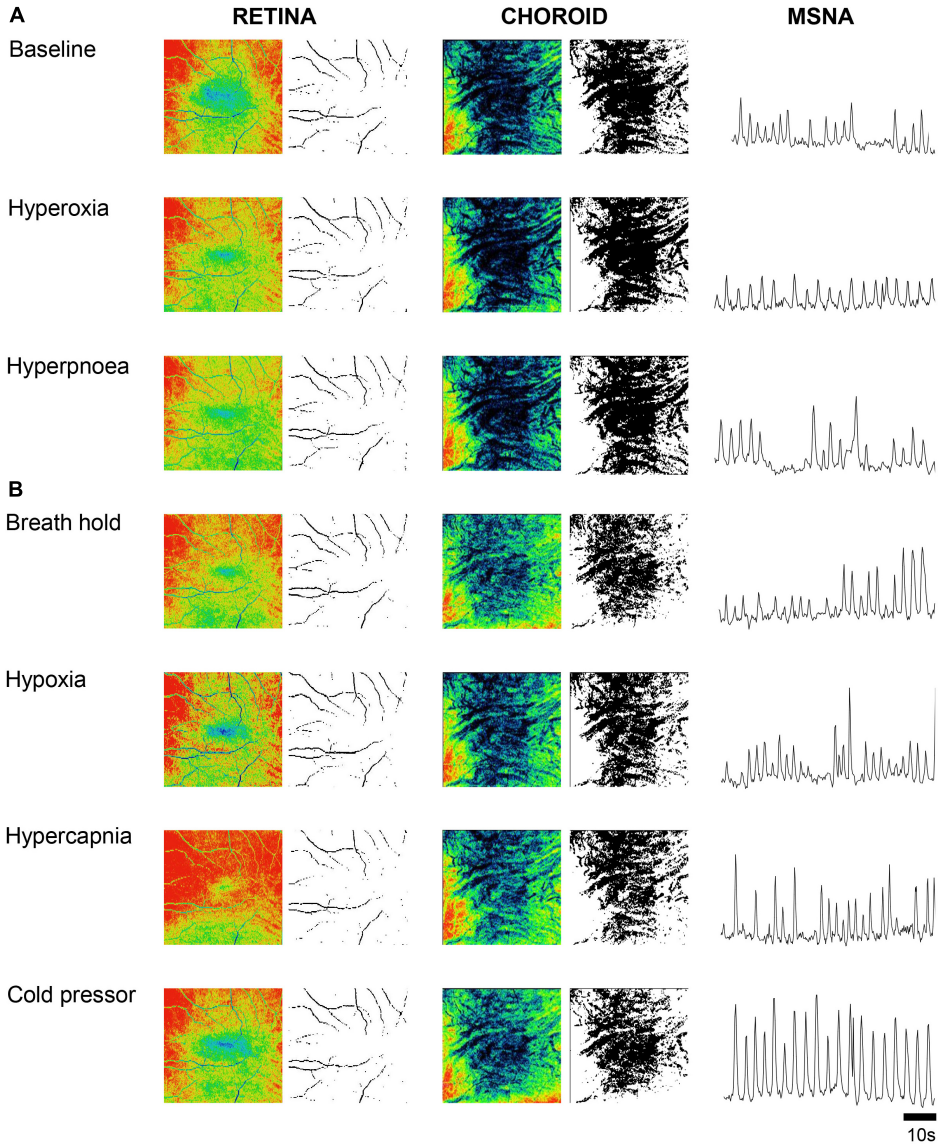

FIGURE 1 | Ophthalmic coherence tomography images demonstrating retina and choroid vascular perfusion and accompanying sympathetic nerve activity from one participant. Raw and processed images from a single participant of the retina (left two columns) and choroid (center two columns) during baseline and various cardiorespiratory challenges. Vascular perfusion is false colored in the raw images; blue and red represents high and low vascular perfusion, respectively. Retina and choroid VPD is demarcated by black pixels in the processed black and white images. Sympathetic activity was recorded from the peroneal nerve using microneurography and is rectified and integrated (right column). When sympathetic activity is low, perfusion in the choroid is high **(A)**; when sympathetic activity is high, perfusion in the choroid is low **(B)**. Note that the retina VPD remains relatively constant in comparison to the choroid.

voluntary breath hold). Hypercapnia increased MSNA only mildly (**Figure 2H**); at best, it caused a slight decrease in choroid VPD (p = 0.083, **Figure 2C**). In contrast, hyperoxia which reduced MSNA (**Figure 2H**), significantly increased choroid VPD (**Figure 2C**). Together, these data suggest that choroid VPD is inversely related to SNA: as sympathetic activity increases, vascular perfusion of the choroid decreases and vice versa.

With regards to the retina, hypoxia significantly increased retina VPD compared to baseline (**Figure 2B**); despite the concurrent increase in sympathetic activation (**Figure 2H**), blood vessels in the retina vasodilate in response to hypoxia (Eperon et al., 1975; Peeters et al., 1980; Milley et al., 1984; Roff et al., 1999; Ahmed et al., 2001; Wang et al., 2008). Conversely, despite the reduction in sympathetic activity (**Figure 2H**), hyperoxia reduced retina VPD (**Figure 2B**) consistent with previous investigations (Eperon et al., 1975; Milley et al., 1984; Nair et al., 2011; Pechauer et al., 2015). Importantly, the cold pressor test which increased sympathetic activity substantially (**Figure 2H**) without changing blood gases (**Figures 2J,K**) did not affect retina VPD (**Figure 2B**). These data confirm that the blood vessels within the retina have dearth sympathetic innervation, are governed primarily by local mechanisms

TABLE 1 | Baseline ophthalmic indices, hemodynamics and sympathetic nerve activity.

Parameter	Male (n = 6)	Female (n = 5)
Age (years)	26 ± 3	23 ± 1
Height (cm)	177 ± 3	168 ± 6
Mass (kg)	77 ± 4	69 ± 3
HR (beats · min^{-1})	73 ± 9	72 ± 5
SBP (mmHg)	126 ± 5	120 ± 5
DBP (mmHg)	72 ± 4	69 ± 4
MAP (mmHg)	89 ± 3	82 ± 4
SaO_2 (%)	98 ± 1	99 ± 1
End-Tidal O_2 (mmHg)	100 ± 2	102 ± 5
End-Tidal CO_2 (mmHg)	35 ± 1	33 ± 1
VE (L · min^{-1})	7.9 ± 0.4	6.5 ± 0.9
RMSSD (ms)	85.70 ± 25.37	47.81 ± 11.26
LF (Hz)	2655.92 ± 1266.57	1503.36 ± 975.34
LF/HF (a.u.)	1.30 ± 0.33	0.44 ± 0.48
SD1 (ms)	55.84 ± 18.33	34.00 ± 7.97
SD2 (ms)	105.28 ± 26.70	43.66 ± 17.26
SNA Burst Frequency (burst · min^{-1})	20.8 ± 2.9	23.5 ± 3.8
SNA Burst Incidence (burst · 100 heart beat^{-1})	34.5 ± 4.4	34.4 ± 5.2
SNA (Amplitude, a.u.)	12 ± 2	17 ± 3
SNA (Bursts, a.u.)	108 ± 8	123 ± 17
Retina thickness (μm)	294 ± 7	289 ± 9
Retina VPD (a.u.)	4.0 ± 0.19	5.2 ± 0.45*
Choroid VPD (a.u.)	34.69 ± 3.81	38.08 ± 2.95

*Heart rate variability parameters include: RMSSD, root mean square of successive R–R interval differences (represents parasympathetic mediated changes in heart rate). LF, relative power of the low frequency band of R–R interval Fourier analysis (putative index of sympathetic activity). LF/HF, low frequency to high frequency ratio of Fourier power analysis the R–R interval (putative index of sympathetic: parasympathetic balance). SD1, Poincare plot standard deviation perpendicular line of identity (putative sympathetic index). SD2, Poincare plot standard deviation along the line of identity (putative sympathetic index) (Shaffer and Ginsberg, 2017). *demonstrates a significant difference between males and females (p = 0.013).*

(Nickla and Wallman, 2010; McDougal and Gamlin, 2015) and, suggest that retina vessels reflect cerebral vascular responsiveness (Willie et al., 2012, 2014).

Images were also used to measure the retina thickness; no differences between sexes were identified at baseline (**Table 1**). Retina thickness changed minimally (<2%) in response to the six conditions; retina thickness was reduced significantly during hyperoxia (consistent with a decrease in retina perfusion volume) and increased with hypoxia (consistent with an increase in retina perfusion volume **Figure 2A**).

To further examine the linear correlation between changes in VPD and sympathetic activity, we plotted choroid VPD and retina VPD against MSNA for individual and mean data across all conditions (**Figure 3**). As shown in **Figure 3A** with individual data across all conditions, sympathetic activity and choroid VPD had a significant inverse relationship ($R = -0.76$, $p < 0.0001$). Even when accounting for gender with a partial correlation, the relationship between choroid VPD and MSNA remains unchanged ($R = -0.76$, $p < 0.0001$). This relationship was even stronger when mean data for each condition was used (**Figure 3B**; $R = -0.92$, $p = 0.003$). The predictive capability of choroid VPD is further exemplified by a tight agreement with Bland-Altman analysis for both absolute (**Figure 4A**) and percentage change values (**Figure 4B**). For comparison, the relationship between sympathetic activity and MAP in our nominally healthy participants, across all conditions, were $R = 0.54$ ($p < 0.00001$) for all individual and $R = 0.93$ ($p = 0.007$) for mean data. Thus, for individuals, choroid VPD is a better predictor of MSNA than blood pressure. This is further supported by the fact that, though choroid VPD has an inverse relationship with both MSNA and MAP, the relationship between choroid VPD and MSNA is stronger for both individual (**Figures 3A** vs. **3C**) and mean data (**Figures 3B** vs. **3D**). Similarly, within each condition the relationship between choroid VPD and MSNA was stronger than that between choroid VPD and MAP (e.g., hypoxia: $R = -0.90$, $p = 0.0002$ vs. $R = 0.61$, $p = 0.06$; hyperoxia: $R = -0.65$, $p = 0.03$ vs. $R = 0.23$, $p = 0.53$; cold pressor test: $R = -0.66$, $p = 0.03$ vs. $R = 0.18$, $p = 0.63$; voluntary breath hold: $R = -0.66$, $p = 0.03$ vs. $R = 0.28$, $p = 0.44$). Notwithstanding that choroid VPD is a better predictor of MSNA than MAP, combining MAP and choroid VPD responses in a multiple regression analysis improved the power to predict sympathetic responses, compared with using choroid VPD responses alone (individual: $R = 0.81$, $p < 0.001$; mean: $R = 0.98$, $p < 0.001$).

In contrast, the relationships between retina VPD and MSNA or MAP, were weaker when individual data from all six conditions were pooled. This was because across all participants, retina VPD was not responsive to voluntary hyperpnea, hypercapnia, breath hold or the cold pressor test (**Figures 3E,G**; red stats); controlling for gender with partial correlation, did not alter this relationship ($R = 0.13$, $p = 0.28$). When the cold pressor data were removed (predominant sympathetic stimulus, no metabolic component), a weak positive relationship between retina VPD and MSNA was indicated (**Figure 3E**, $R = 0.25$, $p = 0.06$ and was not improved with a partial correlation controlling for gender $R = 0.26$, $p = 0.05$); this relationship was improved, but not significantly so, when mean data were used (**Figure 3F**; excluding cold pressor test, $R = 0.80$, $p = 0.11$). Use of mean data did not reveal a correlation between retina VPD and MAP (**Figure 3H**). These data suggest that retina VPD is a measure of metabolically driven vascular regulation – primarily vasodilation caused by hypoxia and/or hyperoxia – but not sympathetic activation.

The divergent vascular regulation between the choroid and the retina in response to changes in inspired oxygen is also demonstrated in **Figure 5**. Comparing between participants, we found that the greater the increase in MSNA (with hypoxia), the greater the reduction in choroid VPD; and the greater the decrease in MSNA (with hyperoxia), the greater the increase in choroid VPD. Overall, with data from only the hypoxic and hyperoxic conditions, the inverse relationship between MSNA and choroid VPD was extremely strong (**Figure 5A**, $R = -0.93$, $p < 0.0001$). Generally, retina VPD increased with hypoxia and decreased with hyperoxia, but the correlation to MSNA was lesser (**Figure 5B**, $R = 0.63$, $p = 0.002$). As expected for two vascular beds differentially controlled by sympathetic inputs and local vascular control mechanisms, the VPD of the choroid and retina

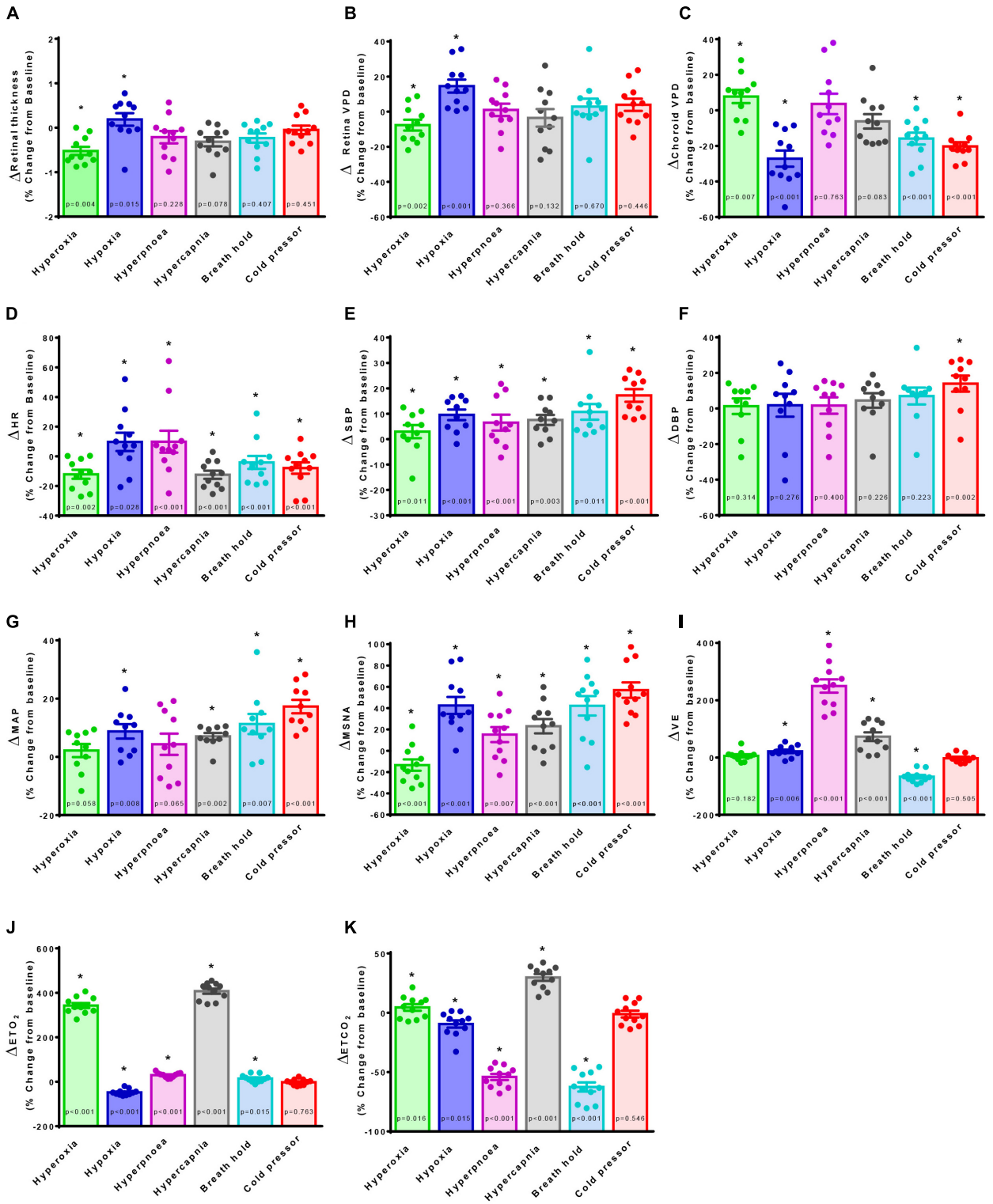

FIGURE 2 | The effect of sympatho-modulation on ophthalmic, cardiorespiratory and sympathetic parameters. Retina thickness **(A)**, retina vascular perfusion density (Retina VPD, **B**), choroid vascular perfusion density (Choroid VPD, **C**), heart rate (HR, **D**), systolic blood pressure (SBP, **E**), diastolic blood pressure (DBP, **F**), mean arterial pressure (MAP, **G**), muscle sympathetic nervous activity (MSNA, **H**), minute ventilation (VE, **I**), end-tidal oxygen content (ETO_2, **J**), end-tidal carbon dioxide content ($ETCO_2$, **K**) in response to hyperoxia (green), hypoxia (blue), hyperpnea (magenta), hypercapnia (gray), breath hold (cyan) or cold pressor test (red). All data are presented as a percentage change from baseline. Absolute data were analyzed with Friedman's non-parametric repeated measures ANOVA where (*) denotes a significant difference from baseline measures as assessed with Student Newman Keuls *post hoc* test; *p*-values are indicated within each bar.

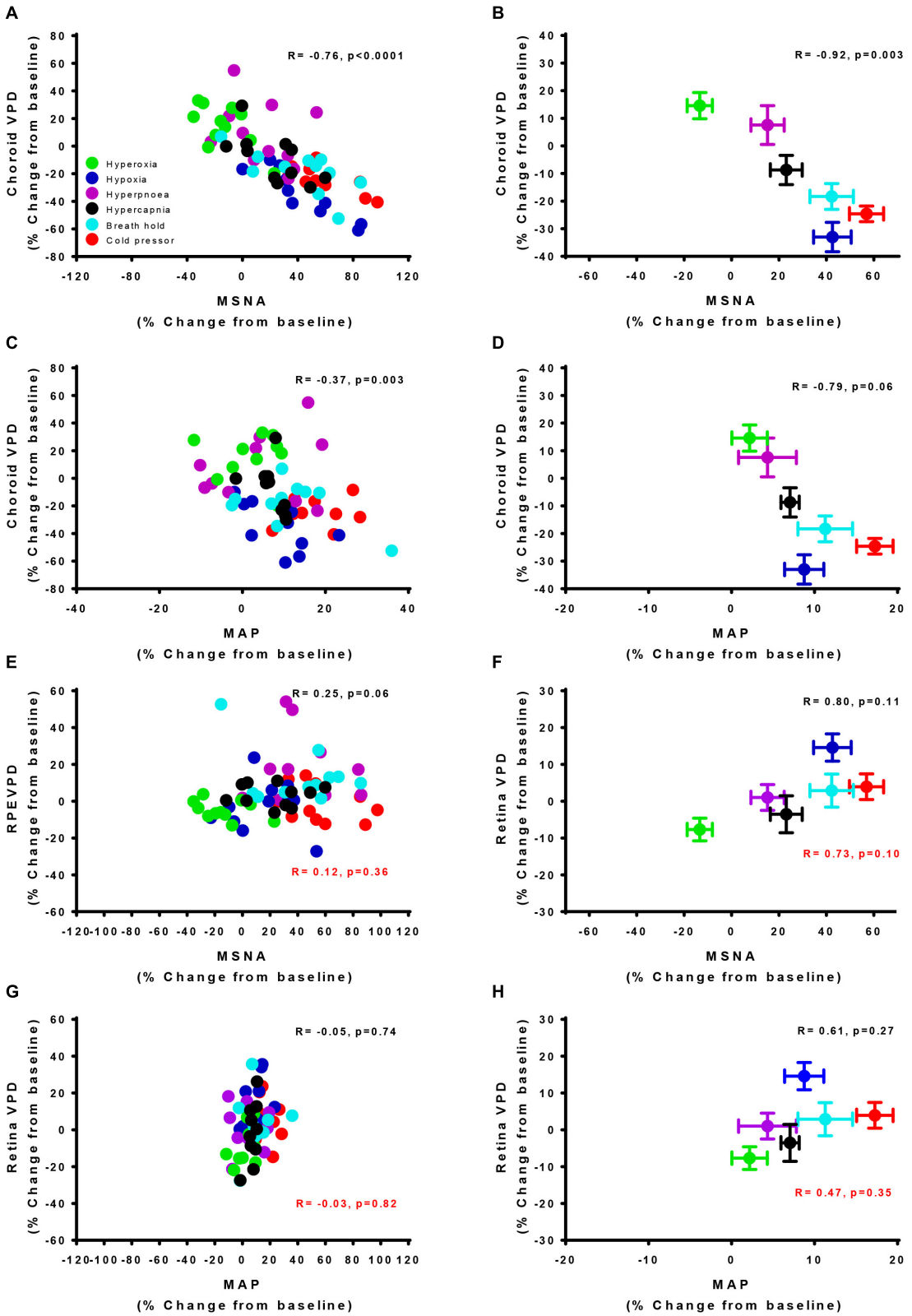

FIGURE 3 | Vascular perfusion density relationships with sympathetic nervous activity and mean arterial pressure for individual and mean data. The relationship of choroid vascular perfusion density (Choroid VPD) to muscle sympathetic nervous activity (MSNA) for individual **(A)** and mean data **(B)** in response to sympathetic

(Continued)

FIGURE 3 | Continued
provocations. The relationship of Choroid VPD to mean arterial pressure (MAP) for individual **(C)** and mean data **(D)** in response to sympathetic provocations. The relationship of retina vascular perfusion density (Retina VPD) to muscle sympathetic nervous activity (MSNA) for individual **(E)** and mean data **(F)** in response to sympathetic provocations. The relationship of retina VPD to mean arterial pressure (MAP) for individual **(G)** and mean data **(H)** in response to sympathetic provocations. All data are expressed as a percentage change from the initial baseline condition in response to hyperoxia (green), hypoxia (blue), hyperpnea (magenta), hypercapnia (gray), breath hold (cyan), or cold pressor test (red). Pearson R correlation coefficient with accompanying *p*-values are indicated within each panel. For relationships involving the retina, values in red text are inclusive of cold pressor test, values in solid text exclude cold pressor test.

were inversely related when interrogated with inspired oxygen (**Figure 5C**, $R = -0.66$, $p = 0.001$).

Finally, the relationship between choroid VPD and MSNA was far stronger than common indices of HRV widely used as non-invasive, though increasingly controversial (Notarius et al., 1999; Baumert et al., 2009; Goldstein et al., 2011; Heathers, 2014; Martelli et al., 2014), measures of SNA (Individual data- RMSSD: $R = -0.34$, $p = 0.005$; LF: $R = -0.01$, $p = 0.96$; LF/HF: $R = 0.08$, $p = 0.51$; SD1: $R = -0.34$, $p = 0.005$; SD2: $R = -0.27$, $p = 0.03$; Mean data- RMSSD: $R = -0.25$, $p = 0.63$; LF: $R = -0.37$, $p = 0.48$; LF/HF: $R = 0.15$, $p = 0.77$; SD1: $R = -0.31$, $p = 0.55$; SD2: $R = -0.09$, $p = 0.87$).

DISCUSSION

This study confirms the divergent behavior of the choroid and retina in response to sympathetic stimuli and strongly suggests that ophthalmic Functional-OCT can be used to measure the divergent effects of sympathetic and local regulation of microvascular physiology within neuronal tissue in conscious humans. Our data suggest that the relationship between MSNA and OCT-derived choroid VPD far surpasses that between MSNA and HRV. This illustrates the potential for Functional-OCT as a novel non-invasive method to monitor sympathetic responsiveness in clinical and research settings that are often ill-suited for microneurography and suggests this technique as a new method to assess overall microvascular health.

The data herein where obtained by combining MSNA recording and ophthalmic OCT imaging which raised several technical challenges. MSNA recording and OCT imaging required participants to remain stationary in a seated position while breathing gas mixtures through a mouth piece. The seated position and mouth piece likely increased participant discomfort and compounding the difficulty of making stable MSNA recordings. However, that we found no evidence to suggest that scanning with the OCT device caused additional stress (see "Limitations"). In addition, while requiring MSNA recording, two of our participants experienced vasovagal reflexes that were rapidly resolved by placing in a horizontal position (Meah et al., 2019); this ended the protocol as our participants were required to remain seated. Consequently, we limited our participant pool to $n = 17$, of which we were only able to obtain stable recordings sufficient to complete the protocol in 6 females and 5 males (65%).

The protocol produced alterations in SNA by employing perturbations that primarily stimulate peripheral carotid body chemoreceptor activity (hypoxia), central brainstem chemoreceptor activity with carotid bodies inactivated (hypercapnia with hyperoxic background), combined chemoreceptor activity (voluntary breath hold, i.e., reduced PaO_2 and increased $PaCO_2$; voluntary hyperpnea, i.e., increased PaO_2 and decreased $PaCO_2$), or thermal afferent stimulation (sympathetic stimulation independent of chemoreceptors). MSNA responses to these perturbations were consistent between males and females and with previous human studies measuring MSNA with microneurography during similar sympathetic stressors (Victor et al., 1987; Steinback et al., 2009). Thus, we conclude that our sample size, while limited, is likely sufficient to generalize sympathetic responses to a larger healthy young population.

Across the majority of sympathetic perturbations, changes in choroid VPD of individual participants that completed the protocol were strongly (and inversely) associated with their MSNA responses, consistent with robust choroid vascular

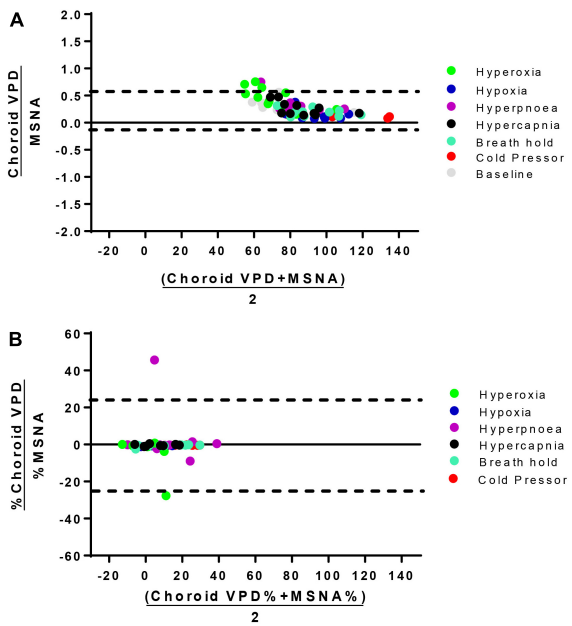

FIGURE 4 | Bland-Altman analysis of choroid VPD versus MSNA. The agreement between absolute choroid vascular perfusion density (Choroid VPD) and absolute muscle sympathetic nerve activity (MSNA, **A**), and percentage change of choroid VPD and percentage change of MSNA **(B)**. Bland Altman analyses are expressed as the ratio of the two measures versus the average of the two measures. Dotted lines represent the lower and upper standard deviation. Absolute choroid VPD and MSNA Bias = 0.27, *SD* = 0.16; Percentage change choroid VPD and MSNA Bias = −4.30, *SD* = 24.48. Hyperoxia (green), hypoxia (blue), hyperpnea (magenta), hypercapnia (gray), breath hold (cyan), cold pressor test (red), baseline (gray).

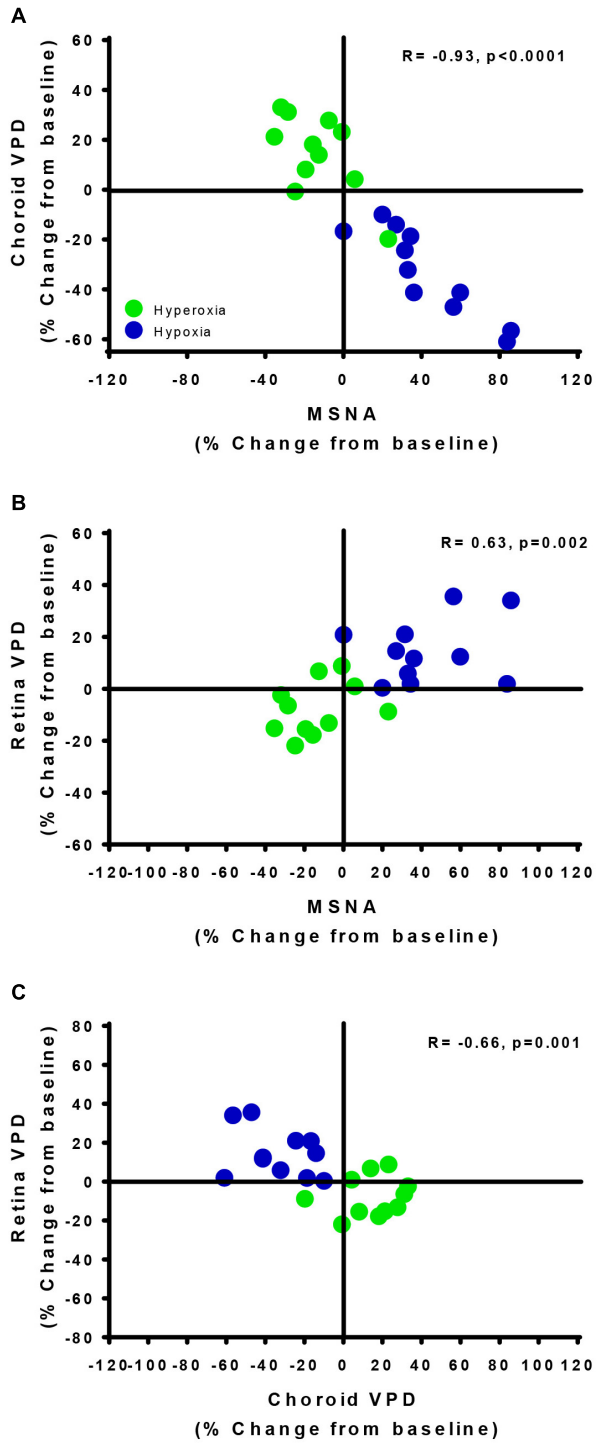

FIGURE 5 | Vascular regulatory mechanisms of autoregulation and sympathetic regulation are revealed by the retina and choroid. The relationships of choroid vascular perfusion density (Choroid VPD, **A**), retina vascular perfusion density (Retina VPD, **B**) to muscle sympathetic nervous activity (MSNA) in response to hypoxia (green) and hyperoxia (blue). The relationships of choroid VPD to retina VPD **(C)**. Each data point represents each participant's response to hyperoxia (green) and hypoxia (blue) as a percentage change from baseline. Pearson R correlation coefficient with accompanying *p*-values are indicated within each panel.

sympathetic regulation. This is in accordance with human (Matsuo and Cynader, 1992) and animal (Milley et al., 1984; Riva et al., 1994; Kawarai and Koss, 1998; Steinle et al., 2000; Wikberg-Matsson et al., 2000; Suzuki et al., 2002; Muir and Duong, 2011) investigations demonstrating that the choroid expresses α_1- and α_2-adrenergic receptors (Matsuo and Cynader, 1992; Kawarai and Koss, 1998; Steinle et al., 2000; Wikberg-Matsson et al., 2000; Suzuki et al., 2002), and choroid perfusion is reduced with hypoxia (Milley et al., 1984; Muir and Duong, 2011) and increased with hyperoxia (Milley et al., 1984; Riva et al., 1994) in anesthetized animals. Indeed, we found that hyperoxia and hypoxia caused an increase and decrease in choroid VPD, respectively. Moreover, and confirming the utility of the choroid VPD to gauge sympathetic activity, the cold pressor test had little effect on respiratory parameters yet caused a robust MSNA response which was met by an equally robust decrease in choroid VPD. However, the authors note that sympathetic activity is regionalized and further comparisons to other sympathetically innervated tissues may provide further insight into the regulation of global sympathetic activity.

Previous studies suggest that sympathetic outputs to muscle (peroneal), heart and renal vascular beds are differentially regulated (Park et al., 2007; Kuroki et al., 2012; Frithiof et al., 2014). This regulation may be highly variable between different organs and individuals and be a source of disease susceptibility (Simms et al., 2007; Subramanian and Mueller, 2016). Choroid VPD is highly correlated and predictive of MSNA as assessed by linear correlation and Bland Altman analysis. However, unlike microneurography, choroid VPD provides a measure – albeit a surrogate – of sympathetic activity to a neuronal tissue within the central nervous system, not muscle.

With regards to differential regulation between different limbs of the sympathetic nervous system, we note that while overall choroid VPD was inversely proportional to MSNA and strongly correlated, some of our more complex challenges caused disengagement between these variables. For example, hypercapnia on a hyperoxic background (5% CO_2, 95% O_2) and voluntary hyperpnea both increased MSNA, yet neither had a significant effect on choroid VPD. Some previous studies also reported no change (Wang et al., 2008; Nair et al., 2011) or an increase (Milley et al., 1984; Geiser et al., 2000; Hétu et al., 2013) in choroid perfusion with increased inspired CO_2 whereas others reported both increases or decreases (Strang et al., 1974). Previous studies have also reported no difference or a slight decrease in choroid perfusion with hyperpnea/reduced CO_2 (Strang et al., 1974; Wang et al., 2008). These findings likely reflect the complex systemic effects of these stimuli on central (CO_2; Wilson and Teppema, 2016), peripheral (O2; Wilson and Teppema, 2016) and metabotropic chemoreceptors (ventilatory work; St Croix et al., 2000), and their differential effects on different limbs of the sympathetic system. In addition to the sympathetic innervation from the superior cervical ganglion, the choroid receives parasympathetic innervation predominantly from the pterygopalatine ganglion (Nilsson, 2000; Steinle et al., 2000; Nickla and Wallman, 2010), but also from the trigeminal ganglion (Nakanome et al., 1995; Nickla and Wallman, 2010) and, the ciliary ganglion (a mixed parasympathetic and sympathetic

ganglion; Shih et al., 1999; Nickla and Wallman, 2010; McDougal and Gamlin, 2015). Thus, parasympathetic innervation may have been an additional source of variability in response to the imposed ventilatory stimuli. However, the stimuli employed produced significant increases in MSNA with no change in HRV, some parameters of which are highly suggestive of parasympathetic activity. Therefore, we suggest that the choroid VPD is largely dominated by changes in sympathetic activity.

Comparing choroid VPD and MAP data, we found MSNA responses of individuals to be more strongly associated with changes in choroid VPD than changes in MAP. This suggest that choroid vascular regulation and sympathetic activity is partially uncoupled from systemic arterial pressure. Indeed, partial uncoupling of sympathetic activity from systemic arterial pressure is congruent with one of the primary roles of sympathetic activity in healthy humans: adjusting peripheral vascular resistance to maintain systemic blood pressure, and thus ensuring a constant supply of blood to the brain and other vital organs (Charkoudian et al., 2005).

In contrast to the choroid, retina VPD was not directly correlated with MSNA in individuals, as evidenced by no change in retina VPD with the cold pressor test. That retina VPD and MSNA co-varied in response to some respiratory challenges (hypoxia and hyperoxia) – but not the cold pressor test – suggest that retina vessels are solely governed by local metabolic control mechanisms. For example, during hypoxia the retina blood vessels dilate in response to a metabolic stimulus to increase the supply of oxygen to the surrounding tissue, whereas the converse occurs when the metabolic stimulus is reduced during hyperoxia (Delaey and Van De Voorde, 2000). The retina microvascular responses reported here, mirror cerebrovascular regulation as the large middle cerebral artery reduces blood flow in response to hyperoxia and hypocapnia and increases blood flow to hypoxia and hypercapnia (Willie et al., 2012, 2014). The lack of direct sympathetic regulation in the retina and the poor association in individuals between retina VPD with MAP suggest that Functional-OCT may be used to deliver a quick and relatively low-cost method for assessing the local microcirculatory control mechanisms in a neuronal vascular bed. The response of the retina circulation to metabolic signals is consistent with a recent OCT study in mice demonstrating that retina vessels respond to stimulus−evoked neural activity (Son et al., 2018). As OCT technologies improve so will the accuracy and utility of these measurements.

OCT – Comparison to Other Technologies

Choroid VPD provides distinct advantages and disadvantages in comparison to other methods of assessing sympathetic activity in humans such as galvanic skin responses, pupil diameter, catecholamine measurements in blood, HRV or microneurography (Mancia et al., 1998; Grassi and Esler, 1999; Jänig and Häbler, 2003; Hart et al., 2017). Distinguishing it from these other techniques and opening new avenues for research, drug discovery and clinical use, choroid VPD provides information about sympathetic control of a vascular bed within the central nervous system. Having the ability to measure from multiple branches of the sympathetic nervous system in humans is likely to be important for research, given animal studies demonstrating differential regulation of different sympathetic outflows (Park et al., 2007; Kuroki et al., 2012; Frithiof et al., 2014; Subramanian and Mueller, 2016). Moreover, as regulation of cerebral blood flow plays a critical role in chronic diseases such as sleep apnea, hypertension and cognitive decline (Willie et al., 2014), having a method to measure sympathetic (and local microvascular) control mechanisms of cerebral vascular bed is likely to provide important indices of cerebral microvascular function (Willie et al., 2012, 2014). Another distinct advantage of OCT for sympathetic assessment is that the retina, lacking sympathetic innervation, can provide a convenient internal control.

On a practical level, unlike catecholamine measurements in blood, OCT is non-invasive and provides a temporal resolution better than or equal to fast blood sampling (∼3 s), but OCT does not allow continuous sampling like microneurography and HRV. Although microneurography provides a direct measurement of SNA and is the only method to directly record sympathetic activity directly and in real-time in humans, its invasive nature and other operational limitations (e.g., inability to determine electrode proximity to nerve fascicle and therefore calculate accurate burst amplitude, and difficulty obtaining a stable signal) minimize its use in research and clinical settings. Galvanic skin responses and pupil diameter appear to be associated with autonomic activity but may suffer from sensory, emotional and higher cortical influences (Bradley et al., 2008; Smith and Johnson, 2016). Heart rate variability, another non-invasive technique available for inferring sympathetic activity is limited by the inherent challenge of parsing out sympathetic from competing parasympathetic signals, effects of respiration and, intrinsic regulatory mechanisms that contribute to heart rate. This diminishes the accuracy of HRV as a simple index of sympathetic activity (Notarius et al., 1999; Baumert et al., 2009; Goldstein et al., 2011; Heathers, 2014; Martelli et al., 2014), as is exemplified in our comparison between measures of HRV and MSNA. In summary, the use of multiple measurements of sympathetic activity is necessary as no single method is likely to reveal complete information regarding the status of autonomic activity in humans.

Current methods to image/assess microcirculatory function are insufficient to resolve microvascular morphometry and, MRI and CT machines are too costly to use broadly (Neeman and Dafni, 2003). Other methods which rely on near-infrared light hemo-absorption do not accurately reflect differences between vascular branches, and the amount and depth of tissue penetration is unknown, compromising repeatability. The image depth and resolution of OCT, as well as the ability to differentiate sympathetic (choroid) and local/metabolic vascular control (retina) mechanisms, allow for a largely independent microcirculatory assessment.

Limitations

The use of the Functional-OCT provides many advantages over other techniques as listed above. However, the technique has

several potential limitations which require consideration. (1) This technique requires the head to be fixed in relation to the OCT machine. Modern OCT devices include eye tracking software that allow movement of the rest of the body, which minimize such distortions. (2) Although OCT is used clinically, the scan itself may impose stress. To gain a bearing on this possibility, we compared our MSNA data (a measure of stress response) before and during OCT scans whilst breathing room air (normal baseline condition). The change in MSNA between the scan vs. no scan condition was $-2.7 \pm 4.6\%$ and not different between conditions (analyzed with paired two-sided t-test, $p = 0.34$). (3) Another potential issue is that shadowing from large diameter vessels in the retina may obscure the signal used to measure choroid responses. In the current study, we circumvented this issue by assessing each choroid image for shadow of retinal vessels. In the few cases where this was a factor, we excluded the regions affected from the choroid analysis. (4) Changes to perfusion in one vascular bed may affect the perfusion in the other vascular bed. Sympathetic activation of the choroid does not affect retina VPD, as the cold pressor test had an independent effect on the choroid. We cannot exclude the converse possibility that changes in retina VPD affect choroid VPD. Nonetheless, we note that responses of the choroid and retina to hypoxia and hyperoxia are diametrically opposed, thus any effect on the choroid of microcirculatory changes in the retina in response to metabolic stimuli must be limited to magnitude.

CONCLUSION

The data herein demonstrate the ability of OCT to assess the divergent behavior of ophthalmic vascular beds to provocations designed to disentangle sympathetic from local vascular control mechanisms. Thus, Functional-OCT may provide a novel, fast, non-invasive and relatively affordable imaging solution to assess sympathetic activity and microvascular function, supplementing currently available autonomic measurements. Given dysregulation of the sympathetic nervous system and metabolic/myogenic vascular control are linked to, and often precede clinical identification of serious cardiorespiratory disease (Mancia et al., 1999; Triantafyllou et al., 2015), we suggest Functional-OCT will be of broad interest to clinicians and researchers alike.

DATA AVAILABILITY

The datasets generated for this study are available on request to the corresponding author.

ETHICS STATEMENT

The studies involving human participants were reviewed and approved by the University of Calgary Conjoint Health Research Ethics Board. The patients/participants provided their written informed consent to participate in this study.

AUTHOR CONTRIBUTIONS

NJ, RH, WT, FC, and RW were responsible for research conception and edited and approved the final version of the manuscript. NJ, RH, CS, and RW designed and performed the experiments. NJ, RH, and RW analyzed the data and interpreted the results of the experiments. NJ and RW prepared the figures and drafted the manuscript.

FUNDING

This study was supported by the Canadian Institutes of Health Research (RW and WT). RW is an Alberta Innovates Health Solutions Senior Scholar. NJ received postdoctoral salary and/or travel support for aspects of this project from the T. Chen Fong Foundation, Campus Alberta Neuroscience and BRAIN CREATE (NSERC).

REFERENCES

Agemy, S. A., Scripsema, N. K., Shah, C. M., Chui, T., Garcia, P. M., Lee, J. G., et al. (2015). Retinal vascular perfusion density mapping using optical coherence tomography angiography in normals and diabetic retinopathy patients. *Retina* 35, 2353–2363. doi: 10.1097/IAE.0000000000000862

Ahmed, J., Pulfer, M. K., and Linsenmeier, R. A. (2001). Measurement of blood flow through the retinal circulation of the cat during normoxia and hypoxemia using fluorescent microspheres. *Microvasc. Res.* 62, 143–153. doi: 10.1006/mvre.2001.2321

Barretto, A. C. P., Santos, A. C., Munhoz, R., Rondon, M. U. P. B., Franco, F. G., Trombetta, I. C., et al. (2009). Increased muscle sympathetic nerve activity predicts mortality in heart failure patients. *Int. J. Cardiol.* 135, 302–307. doi: 10.1016/j.ijcard.2008.03.056

Baumert, M., Lambert, G. W., Dawood, T., Lambert, E. A., Esler, M. D., McGrane, M., et al. (2009). Short-term heart rate variability and cardiac norepinephrine spillover in patients with depression and panic disorder. *Am. J. Physiol. Heart Circ. Physiol.* 297, H674–H679. doi: 10.1152/ajpheart.00236.2009

Bill, A., and Sperber, G. O. (1990). Control of retinal and choroidal blood flow. *Eye Lond. Engl.* 4(Pt 2), 319–325. doi: 10.1038/eye.1990.43

Blair, G. W., Doubal, F. N., Thrippleton, M. J., Marshall, I., and Wardlaw, J. M. (2016). Magnetic resonance imaging for assessment of cerebrovascular reactivity in cerebral small vessel disease: a systematic review. *J. Cereb. Blood Flow Metab.* 36, 833–841. doi: 10.1177/0271678X16631756

Bradley, M. M., Miccoli, L., Escrig, M. A., and Lang, P. J. (2008). The pupil as a measure of emotional arousal and autonomic activation. *Psychophysiology* 45, 602–607. doi: 10.1111/j.1469-8986.2008.00654.x

Charkoudian, N., Joyner, M., Johnson, C., Eisenach, J., Dietz, N., and Wallin, B. (2005). Balance between cardiac output and sympathetic nerve activity in resting humans: role in arterial pressure regulation. *J. Physiol.* 568, 315–321. doi: 10.1113/jphysiol.2005.090076

Delaey, C., and Van De Voorde, J. (2000). Regulatory mechanisms in the retinal and choroidal circulation. *Ophthalmic Res.* 32, 249–256. doi: 10.1159/000055622

Doustar, J., Torbati, T., Black, K. L., Koronyo, Y., and Koronyo-Hamaoui, M. (2017). Optical coherence tomography in alzheimer's disease and other neurodegenerative diseases. *Front. Neurol.* 8:701. doi: 10.3389/fneur.2017.00701

Eperon, G., Johnson, M., and David, N. J. (1975). The effect of arterial PO2 on relative retinal blood flow in monkeys. *Invest. Ophthalmol.* 14, 342–352.

Frithiof, R., Xing, T., McKinley, M. J., May, C. N., and Ramchandra, R. (2014). Intracarotid hypertonic sodium chloride differentially modulates sympathetic nerve activity to the heart and kidney. *Am. J. Physiol. Regul. Integr. Comp. Physiol.* 306, R567–R575. doi: 10.1152/ajpregu.00460.2013

Fujimoto, J. G., Pitris, C., Boppart, S. A., and Brezinski, M. E. (2000). Optical coherence tomography: an emerging technology for biomedical imaging and optical biopsy. *Neoplasia* 2, 9–25. doi: 10.1038/sj.neo.7900071

Geiser, M. H., Riva, C. E., Dorner, G. T., Diermann, U., Luksch, A., and Schmetterer, L. (2000). Response of choroidal blood flow in the foveal region to hyperoxia and hyperoxia-hypercapnia. *Curr. Eye Res.* 21, 669–676. doi: 10.1076/0271-3683(200008)21:2;1-v;ft669

Goldstein, D. S., Bentho, O., Park, M.-Y., and Sharabi, Y. (2011). Low-frequency power of heart rate variability is not a measure of cardiac sympathetic tone but may be a measure of modulation of cardiac autonomic outflows by baroreflexes. *Exp. Physiol.* 96, 1255–1261. doi: 10.1113/expphysiol.2010.056259

Grassi, G., Arenare, F., Pieruzzi, F., Brambilla, G., and Mancia, G. (2009). Sympathetic activation in cardiovascular and renal disease. *J. Nephrol.* 22, 190–195.

Grassi, G., and Esler, M. (1999). How to assess sympathetic activity in humans. *J. Hypertens.* 17, 719–734. doi: 10.1097/00004872-199917060-00001

Gutterman, D. D., Chabowski, D. S., Kadlec, A. O., Durand, M. J., Freed, J. K., Ait-Aissa, K., et al. (2016). The human microcirculation: regulation of flow and beyond. *Circ. Res.* 118, 157–172. doi: 10.1161/CIRCRESAHA.115.305364

Hart, E. C., Head, G. A., Carter, J. R., Wallin, B. G., May, C. N., Hamza, S. M., et al. (2017). Recording sympathetic nerve activity in conscious humans and other mammals: guidelines and the road to standardization. *Am. J. Physiol. Heart Circ. Physiol.* 312, H1031–H1051. doi: 10.1152/ajpheart.00703.2016

Heathers, J. A. J. (2014). Everything hertz: methodological issues in short-term frequency-domain HRV. *Front. Physiol.* 5:177. doi: 10.3389/fphys.2014.00177

Hétu, S., Pouliot, M., Cordahi, G., Couture, R., and Vaucher, E. (2013). Assessment of retinal and choroidal blood flow changes using laser doppler flowmetry in rats. *Curr. Eye Res.* 38, 158–167. doi: 10.3109/02713683.2012.723296

Jänig, W., and Häbler, H.-J. (2003). Neurophysiological analysis of target-related sympathetic pathways – from animal to human: similarities and differences*. *Acta Physiol. Scand.* 177, 255–274. doi: 10.1046/j.1365-201X.2003.01088.x

Kawarai, M., and Koss, M. C. (1998). Sympathetic vasoconstriction in the rat anterior choroid is mediated by alpha(1)-adrenoceptors. *Eur. J. Pharmacol.* 363, 35–40. doi: 10.1016/S0014-2999(98)00790-0

Kuroki, M. T., Guzman, P. A., Fink, G. D., and Osborn, J. W. (2012). Time-dependent changes in autonomic control of splanchnic vascular resistance and heart rate in ANG II-salt hypertension. *Am. J. Physiol. Heart Circ. Physiol.* 302, H763–H769. doi: 10.1152/ajpheart.00930.2011

Mancia, G., Daffonchio, A., Di Rienzo, M., Ferrari, A. U., and Grassi, G. (1998). Methods to quantify sympathetic cardiovascular influences. *Eur. Heart J.* 19(Suppl. F), F7–F13.

Mancia, G., Grassi, G., Giannattasio, C., and Seravalle, G. (1999). Sympathetic activation in the pathogenesis of hypertension and progression of organ damage. *Hypertension* 34, 724–728. doi: 10.1161/01.HYP.34.4.724

Martelli, D., Silvani, A., McAllen, R. M., May, C. N., and Ramchandra, R. (2014). The low frequency power of heart rate variability is neither a measure of cardiac sympathetic tone nor of baroreflex sensitivity. *Am. J. Physiol. Heart Circ. Physiol.* 307, H1005–H1012. doi: 10.1152/ajpheart.00361.2014

Matsuo, T., and Cynader, M. (1992). Localization of Alpha-2 adrenergic-receptors in the human eye. *Ophthalmic Res.* 24, 213–219. doi: 10.1159/000267170

McDougal, D. H., and Gamlin, P. D. (2015). Autonomic control of the eye. *Compr. Physiol.* 5, 439–473. doi: 10.1002/cphy.c140014

Meah, V. L., Busch, S. A., Jones, K. E., Davenport, M. H., and Steinback, C. D. (2019). A review of acute responses, after-effects and chronic complications related to microneurography. *Clin. Neurophysiol.* 130, 1781–1788. doi: 10.1016/j.clinph.2019.06.228

Milley, J. R., Rosenberg, A. A., and Jones, M. D. Jr. (1984). Retinal and choroidal blood flows in hypoxic and hypercarbic newborn lambs. *Pediatr. Res.* 18, 410–414. doi: 10.1203/00006450-198405000-00003

Muir, E. R., and Duong, T. Q. (2011). Layer-specific functional and anatomical MRI of the retina with passband balanced SSFP. *Magn. Reson. Med.* 66, 1416–1421. doi: 10.1002/mrm.22935

Nair, G., Tanaka, Y., Kim, M., Olson, D. E., Thule, P. M., Pardue, M. T., et al. (2011). MRI reveals differential regulation of retinal and choroidal blood volumes in rat retina. *Neuroimage* 54, 1063–1069. doi: 10.1016/j.neuroimage.2010.09.020

Nakanome, Y., Karita, K., Izumi, H., and Tamai, M. (1995). Two types of vasodilatation in cat choroid elicited by electrical stimulation of the short ciliary nerve. *Exp. Eye Res.* 60, 37–42. doi: 10.1016/s0014-4835(05)80081-8

Neeman, M., and Dafni, H. (2003). Structural, functional, and molecular MR imaging of the microvasculature. *Annu. Rev. Biomed. Eng.* 5, 29–56. doi: 10.1146/annurev.bioeng.5.040202.121606

Nelis, P., Kleffner, I., Burg, M. C., Clemens, C. R., Alnawaiseh, M., Motte, J., et al. (2018). OCT-angiography reveals reduced vessel density in the deep retinal plexus of CADASIL patients. *Sci. Rep.* 8:8148. doi: 10.1038/s41598-018-26475-5

Nickla, D. L., and Wallman, J. (2010). The multifunctional choroid. *Prog. Retin. Eye Res.* 29, 144–168. doi: 10.1016/j.preteyeres.2009.12.002

Nilsson, S. F. E. (2000). The significance of nitric oxide for parasympathetic vasodilation in the eye and other orbital tissues in the cat. *Exp. Eye Res.* 70, 61–72. doi: 10.1006/exer.1999.0752

Notarius, C. F., Butler, G. C., Ando, S., Pollard, M. J., Senn, B. L., and Floras, J. S. (1999). Dissociation between microneurographic and heart rate variability estimates of sympathetic tone in normal subjects and patients with heart failure. *Clin. Sci. Lond. Engl.* 96, 557–565. doi: 10.1042/cs0960557

Notay, K., Seed, J. D., Incognito, A. V., Doherty, C. J., Nardone, M., Burns, M. J., et al. (2016). Validity and reliability of measuring resting muscle sympathetic nerve activity using short sampling durations in healthy humans. *J. Appl. Physiol.* 121, 1065–1073. doi: 10.1152/japplphysiol.00736.2016

Padilla, J., Jenkins, N. T., Laughlin, M. H., and Fadel, P. J. (2014). Blood pressure regulation VIII: resistance vessel tone and implications for a pro-atherogenic conduit artery endothelial cell phenotype. *Eur. J. Appl. Physiol.* 114, 531–544. doi: 10.1007/s00421-013-2684-x

Park, J., Galligan, J. J., Fink, G. D., and Swain, G. M. (2007). Differences in sympathetic neuroeffector transmission to rat mesenteric arteries and veins as probed by in vitro continuous amperometry and video imaging. *J. Physiol.* 584, 819–834. doi: 10.1113/jphysiol.2007.134338

Pechauer, A. D., Jia, Y., Liu, L., Gao, S. S., Jiang, C., and Huang, D. (2015). Optical coherence tomography angiography of peripapillary retinal blood flow response to hyperoxia. *Invest. Ophthalmol. Vis. Sci.* 56, 3287–3291. doi: 10.1167/iovs.15-16655

Peeters, L. L., Sheldon, R. E., Jones, M. D., and Battaglia, F. C. (1980). Retinal and choroidal blood flow in unstressed fetal and neonatal lambs. *Pediatr. Res.* 14, 1047–1052. doi: 10.1203/00006450-198009000-6

Poddar, R., Kim, D. Y., Werner, J. S., and Zawadzki, R. J. (2014). In vivo imaging of human vasculature in the chorioretinal complex using phase-variance contrast method with phase-stabilized 1-mum swept-source optical coherence tomography. *J. Biomed. Opt.* 19:126010. doi: 10.1117/1.JBO.19.12.126010

Provenzale, J. M., Shah, K., Patel, U., and McCrory, D. C. (2008). Systematic review of CT and MR perfusion imaging for assessment of acute cerebrovascular disease. *AJNR Am. J. Neuroradiol.* 29, 1476–1482. doi: 10.3174/ajnr.A1161

Ridler, T., and Calvard, S. (1978). Picture thresholding using an iterative selection method. *IEEE Trans. Syst. Man Cybern.* 8, 630–632. doi: 10.1109/tsmc.1978.4310039

Riva, C. E., Cranstoun, S. D., Mann, R. M., and Barnes, G. E. (1994). Local choroidal blood flow in the cat by laser doppler flowmetry. *Invest. Ophthalmol. Vis. Sci.* 35, 608–618.

Roff, E. J., Harris, A., Chung, H. S., Hosking, S. L., Morrison, A. M., Halter, P. J., et al. (1999). Comprehensive assessment of retinal, choroidal and retrobulbar haemodynamics during blood gas perturbation. *Graefes Arch. Clin. Exp. Ophthalmol.* 237, 984–990. doi: 10.1007/s004170050334

Shaffer, F., and Ginsberg, J. P. (2017). An overview of heart rate variability metrics and norms. *Front. Public Health* 5:258. doi: 10.3389/fpubh.2017.00258

Shih, Y. F., Fitzgerald, M. E., Cuthbertson, S. L., and Reiner, A. (1999). Influence of ophthalmic nerve fibers on choroidal blood flow and myopic eye growth in chicks. *Exp. Eye Res.* 69, 9–20. doi: 10.1006/exer.1999.0692

Simms, A. E., Paton, J. F. R., and Pickering, A. E. (2007). Hierarchical recruitment of the sympathetic and parasympathetic limbs of the baroreflex in normotensive and spontaneously hypertensive rats. *J. Physiol.* 579, 473–486. doi: 10.1113/jphysiol.2006.124396

Smith, C. J., and Johnson, J. M. (2016). Responses to hyperthermia. Optimizing heat dissipation by convection and evaporation: neural control of skin blood flow and sweating in humans. *Auton. Neurosci. Basic Clin.* 196, 25–36. doi: 10.1016/j.autneu.2016.01.002

Son, T., Alam, M., Toslak, D., Wang, B., Lu, Y., and Yao, X. (2018). Functional optical coherence tomography of neurovascular coupling interactions in the retina. *J. Biophotonics* 11:e201800089. doi: 10.1002/jbio.201800089

St Croix, C. M., Morgan, B. J., Wetter, T. J., and Dempsey, J. A. (2000). Fatiguing inspiratory muscle work causes reflex sympathetic activation in humans. *J. Physiol.* 529, 493–504. doi: 10.1111/j.1469-7793.2000.00493.x

Steinback, C. D., Salzer, D., Medeiros, P. J., Kowalchuk, J., and Shoemaker, J. K. (2009). Hypercapnic vs. hypoxic control of cardiovascular, cardiovagal, and sympathetic function. *Am. J. Physiol. Regul. Integr. Comp. Physiol.* 296, R402–R410. doi: 10.1152/ajpregu.90772.2008

Steinle, J. J., Krizsan-Agbas, D., and Smith, P. G. (2000). Regional regulation of choroidal blood flow by autonomic innervation in the rat. *Am. J. Physiol. Regul. Integr. Comp. Physiol.* 279, R202–R209.

Strang, R., Wilson, T. M., and Johnson, N. F. (1974). The effect of alterations in arterial carbon dioxide tensions on choroidal blood flow in rabbits. *Exp. Eye Res.* 18, 153–156. doi: 10.1016/0014-4835(74)90101-8

Subramanian, M., and Mueller, P. J. (2016). Altered differential control of sympathetic outflow following sedentary conditions: role of subregional neuroplasticity in the RVLM. *Front. Physiol.* 7:290. doi: 10.3389/fphys.2016.00290

Suzuki, F., Taniguchi, T., Nakamura, S., Akagi, Y., Kubota, C., Satoh, M., et al. (2002). Distribution of alpha-1 adrenoceptor subtypes in RNA and protein in rabbit eyes. *Br. J. Pharmacol.* 135, 600–608. doi: 10.1038/sj.bjp.0704503

Triantafyllou, A., Anyfanti, P., Pyrpasopoulou, A., Triantafyllou, G., Aslanidis, S., and Douma, S. (2015). Capillary rarefaction as an index for the microvascular assessment of hypertensive patients. *Curr. Hypertens. Rep.* 17:33. doi: 10.1007/s11906-015-0543-3

Usselman, C. W., Gimon, T. I., Nielson, C. A., Luchyshyn, T. A., Coverdale, N. S., Uum, S. H. M. V., et al. (2015). Menstrual cycle and sex effects on sympathetic responses to acute chemoreflex stress. *Am. J. Physiol. Heart Circ. Physiol.* 308, H664–H671. doi: 10.1152/ajpheart.00345.2014

Victor, R. G., Leimbach, W. N., Seals, D. R., Wallin, B. G., and Mark, A. L. (1987). Effects of the cold pressor test on muscle sympathetic nerve activity in humans. *Hypertension* 9, 429–436. doi: 10.1161/01.HYP.9.5.429

Wang, L., Grant, C., Fortune, B., and Cioffi, G. A. (2008). Retinal and choroidal vasoreactivity to altered PaCO2 in rat measured with a modified microsphere technique. *Exp. Eye Res.* 86, 908–913. doi: 10.1016/j.exer.2008.03.005

Wikberg-Matsson, A., Uhlen, S., and Wikberg, J. E. S. (2000). Characterization of alpha(1)-adrenoceptor subtypes in the eye. *Exp. Eye Res.* 70, 51–60. doi: 10.1006/exer.1999.0753

Willie, C. K., Macleod, D. B., Shaw, A. D., Smith, K. J., Tzeng, Y. C., Eves, N. D., et al. (2012). Regional brain blood flow in man during acute changes in arterial blood gases. *J. Physiol. Lond.* 590, 3261–3275. doi: 10.1113/jphysiol.2012.228551

Willie, C. K., Tzeng, Y.-C., Fisher, J. A., and Ainslie, P. N. (2014). Integrative regulation of human brain blood flow. *J. Physiol. Lond.* 592, 841–859. doi: 10.1113/jphysiol.2013.268953

Wilson, R. J. A., and Teppema, L. J. (2016). Integration of central and peripheral respiratory chemoreflexes. *Compr. Physiol.* 6, 1005–1041. doi: 10.1002/cphy.c140040

Xie, A., Skatrud, J. B., Puleo, D. S., and Morgan, B. J. (2001). Exposure to hypoxia produces long-lasting sympathetic activation in humans. *J. Appl. Physiol.* 91, 1555–1562. doi: 10.1152/jappl.2001.91.4.1555

Conflict of Interest Statement: NJ, CS, RH, WT, FC, and RW have submitted a patent application for the use of optical coherence tomography as a method to interrogate cardiorespiratory function.

frontiers in Neuroscience

ORIGINAL RESEARCH
published: 04 October 2019
doi: 10.3389/fnins.2019.01049

Adenosine Receptor A_{2a}, but Not A_1 in the rVLM Participates Along With Opioids in Acupuncture-Mediated Inhibition of Excitatory Cardiovascular Reflexes

Shaista Malik, Tracy Samaniego and Zhi-Ling Guo**

Department of Medicine, Susan Samueli Integrative Health Institute, University of California, Irvine, Irvine, CA, United States

Electroacupuncture (EA) can be used to lower high blood pressure (BP) in clinical practice. However, precise mechanisms underlying its effects on elevated BP remain unclear. Our previous studies have shown that EA at the P5-6 acupoints, overlying the median nerve, attenuates elevated BP induced by gastric distension (GD) through influence on rostral ventrolateral medulla (rVLM). Although adenosine is released during neuronal activation in the rVLM, its role in acupuncture-cardiovascular regulation is unknown. The purinergic system is involved in cardiovascular pressor and depressor responses, including via selective activation of A_1 and A_{2a} rVLM receptors, respectively. The action of A_{2a} receptor stimulation in the central nervous system may be further regulated through an endogenous opioid mechanism. However, it is uncertain whether this putative action occurs in the rVLM. We hypothesized that adenosine in the rVLM contributes to EA modulation of sympathoexcitatory reflexes through an A_{2a} but not an A_1 adenosine receptor-opioid mechanism. EA or sham-EA was applied at the P5-6 acupoints in Sprague-Dawley male rats subjected to repeated GD under anesthesia. We found that EA ($n = 6$) but not sham-EA ($n = 5$) at P5-6 significantly ($P < 0.05$) attenuated GD-induced elevations in BP. EA modulation of sympathoexcitatory cardiovascular reflexes was reversed significantly after rVLM microinjection (50 nl) of 8-SPT (10 mM; non-selective adenosine receptor antagonist; $n = 7$) or SCH 58261 (1 mM; A_{2a} receptor antagonist; $n = 8$; both $P < 0.05$), but not by DPCPX (3 mM; A_1 receptor antagonist; $n = 6$) or the vehicle (5% dimethylsulfoxide; $n = 6$). Moreover, microinjection of an A_{2a} receptor agonist, CGS-21680 (0.4 mM; $n = 8$) into the rVLM attenuated GD-induced pressor responses without EA, which mimicked EA's inhibitory effects ($P < 0.05$). After blockade of opioid receptors with naloxone (1 mM) in the rVLM, SCH 58261's reversal of EA's effect on GD-induced pressor responses was blunted, and CGS-21680-mediated inhibitory effect on pressor responses was not observed. Furthermore, neurons labeled with adenosine A_{2a} receptors were anatomically co-localized with neurons stained with enkephalin in the rVLM. These data suggest that the involvement of rVLM adenosine A_{2a} receptors in EA modulation of GD-induced pressor reflexes is, at least in part, dependent on the presence of endogenous opioids.

Keywords: blood pressure, adenosine, opioids, brain stem, acupuncture

OPEN ACCESS

Edited by:
Geoffrey A. Head, Baker Heart and Diabetes Institute, Australia

Reviewed by:
Ahmed Ayedur Rahman, Victoria University, Australia
Yang-kai Wang, Second Military Medical University, China

****Correspondence:***
Shaista Malik
smalik@uci.edu
Zhi-Ling Guo
zguo@uci.edu

Specialty section:
This article was submitted to Autonomic Neuroscience, a section of the journal Frontiers in Neuroscience

Received: *20 July 2019*
Accepted: *19 September 2019*
Published: *04 October 2019*

Citation:
Malik S, Samaniego T and Guo Z-L (2019) Adenosine Receptor A_{2a}, but Not A_1 in the rVLM Participates Along With Opioids in Acupuncture-Mediated Inhibition of Excitatory Cardiovascular Reflexes. Front. Neurosci. 13:1049. doi: 10.3389/fnins.2019.01049

INTRODUCTION

Acupuncture has been practiced for at least three millennia in Asia, and it increasingly is accepted as a potential therapy for many disorders in the Western world, including hypertension (Andersson, 1993; Li and Longhurst, 2010; Li et al., 2015). In this respect, acupuncture offers a non-pharmacological as well as an adjunctive approach to reduce high BP with fewer adverse effects compared to anti-hypertensive drugs. However, specific mechanisms underlying the physiological effects of acupuncture remain unclear, and the postulated actions of acupuncture have not been examined by rigorous scientific studies.

There is clear evidence that the CNS plays a critical role in the development and maintenance of hypertension. Increase in the activity of the sympathetic nervous system contributes to high BP. Our previous studies have shown that EA attenuates reflex elevation in BP induced by visceral stimulation, like GD (Li et al., 2002). The rVLM is a brain nucleus that critically controls sympathetic outflow and cardiovascular function (Dampney, 1994). Several modulatory neurotransmitters, including endogenous opioids and GABA in the rVLM, contribute to central processing of somatic afferent nerve stimulation induced by EA, resulting in improvement of elevated BP (Tjen-A-Looi et al., 2007; Zhou et al., 2007). However, inhibiting the action of any single neurotransmitter in the rVLM does not reverse EA's hypotensive effect completely, implying the involvement of other neuromodulators during EA. In this regard, adenosine, which is released during neuronal activation (Spyer et al., 1997; Ribeiro et al., 2002), is another potential neuromodulator of EA's effect on elevated BP. The purinergic system primarily modulates neuronal function through P1 (subclassified into adenosine A_1, A_{2a}, A_{2b}, and A_3) receptors (Ribeiro et al., 2002; Borea et al., 2018). Selective activation of A_1 or A_{2a} receptors in the rVLM induces pressor or depressor responses, respectively (Nassar and bdel-Rahman, 2008, 2009; Jiang et al., 2011) and this is consistent with adenosine A_1 and A_{2a} receptors generally having opposing actions at cellular and neuronal levels (Ribeiro et al., 2002; Borea et al., 2018). It is unknown if A_{2a} or A_1 receptors in the rVLM contribute to EA's modulation of sympathoexcitatory reflexes.

The action of A_{2a} receptors in the CNS may be regulated, at least in part, through an opioid mechanism (Ribeiro et al., 2002; By et al., 2011). Our previous studies have shown that EA lowers reflex elevations in BP through an opioid mechanism, modulating rVLM activity (Tjen-A-Looi et al., 2007). It remains unknown if opioid peptides are involved in adenosine regulation of BP, especially during EA. In this study, we evaluated the role of A_1 or A_{2a} receptors in the rVLM in modulating EA's action in lowering elevated BP as well as its potential relevance to endogenous opioids. We hypothesized that A_{2a} but not A_1 adenosine receptors in the rVLM contributes to EA modulation of sympathoexcitatory reflexes, and the action of A_{2a} adenosine receptors is associated with the presence of opioids in the rVLM.

Abbreviations: BP, blood pressure; CNS, central nervous system; DMSO, dimethyl sulfoxide; EA, electroacupuncture; GD, gastric distension; MAP, mean arterial blood pressure; rVLM, rostral ventrolateral medulla.

MATERIALS AND METHODS

Anesthesia and Surgical Preparations

Studies were performed on adult Sprague-Dawley male rats (450–500 g) following an overnight fast. All experimental protocols and preparations were reviewed and approved by the Animal Care and Use Committee of the University of California at Irvine. Also, the study conformed to the American Physiological Society's Guiding Principles for Research Involving Animals.

Anesthesia was induced with ketamine (100 mg/kg, im) and maintained with α-chloralose (50–60 mg/kg, iv). Additional doses of α-chloralose (25–30 mg/kg, iv) were given as necessary to maintain an adequate depth of anesthesia by observing the absence of conjunctival reflex response. The femoral vein was cannulated for the administration of fluids, and the femoral artery was cannulated and connected to a pressure transducer (Statham P23 ID, Gould) to monitor systemic BP. Heart rate was derived from the pulsatile pressure waveform signal. The trachea was intubated and respiration was maintained with a ventilator (model 661, Harvard Apparatus, Holliston, MA, United States). Arterial blood gases and pH were measured periodically with a blood-gas analyzer (model ABL5, Radiometer, Copenhagen, Denmark) and were kept within normal physiological limits (pH 7.35 – 7.43, PO2 > 100 mmHg and PCO2 30–40 mmHg) by adjusting the ventilation rate or volume, enriching the inspired oxygen supply and infusion of a solution of 8% sodium bicarbonate at a rate of 0.1 ml/min. Body temperature was monitored with a rectal thermometer (model 44TD) and maintained between 36.0 and 37.5°C with a heating pad and lamp.

Induction of Pressor Reflexes

Consistent reflex increases in BP were induced by GD, as we described in detail previously (Li et al., 2002; Zhou et al., 2005a; Guo et al., 2018). Briefly, an unstressed 2-cm diameter latex balloon (catalog no.: 391766)[1] was attached to a polyurethane tube (3-mm diameter) and inserted into the stomach through the mouth and esophagus. Transmural pressure was determined by measuring the pressure required to inflate the balloon with various volumes of air before it was inserted into the stomach (Li et al., 2002). The balloon was palpated manually from the surface of the body during insertion, as it was passed through the esophagus into the stomach to confirm the positioning of the balloon inside the stomach. A syringe was attached to the cannula to inflate and deflate the balloon with air, while a manometer through a T-connection was used to monitor balloon pressure. Distention pressures were selected to fall within the range that a rat normally experiences during ingestion of food and fluids in a single meal (Li et al., 2002; Guo et al., 2018). To induce increases in BP, the balloon was inflated inside the stomach. Increases in BP were observed within 30 s of inflation. The balloon was deflated within 30 s after reaching the maximal rise in BP. We did not include animals in the study when the balloon was verified post mortem to be in the esophagus. This animal model has been used in several previous studies to assess acupuncture's

[1] www.Amscan.com

sympatholytic action (Li et al., 2002, 2013; Crisostomo et al., 2005; Guo et al., 2018).

Acupuncture Application

P5 and P6 acupoints are located on forelimbs correspondingly 2.5 and 4.0 mm above the flexor crease in the paw (**Figure 1**), between the tendons of the palmaris longus and flexor carpi radialis muscles overlying the median nerve (Hua, 1994). Acupuncture needles (40 gauge stainless steel; diameter, 0.16 mm) were inserted (through the skin) into P5-6 acupoints bilaterally at a depth of ∼3 mm. Stimulation of these acupoints has been shown to lower BP during sympathoexcitatory reflexes (Li et al., 2002; Guo et al., 2018) and in chronic hypertension (Li et al., 2015). The needles were connected to a photoelectric stimulus isolation unit and the stimulator (model no. S88, Grass, West Warwick, RI, United States). Each set of electrodes was stimulated separately as a positive and negative pole, so that current did not flow from one location to the contralateral forelimb. Correct placement of the needles at the P5-P6 acupoints was confirmed by observing slight repetitive paw twitches at or near motor threshold during EA. The twitches were important observations to confirm the stimulation of motor fibers in the median nerve. Gallamine triethiodide (4 mg/kg) was administered intravenously before application of 30 min EA (2 Hz, 0.5 ms, 0.3–0.5 mA) to avoid muscle movement during stimulation of the median nerve. We typically lowered current during electrical stimulation to a level just below the motor threshold. The frequency (2 Hz) for EA was used to modulate reflex-induced elevations in BP as we have demonstrated previously (Li et al., 2002, 2013; Guo et al., 2018). During sham-EA, needles were inserted into the same acupoints without subsequent electrical stimulation, which was an appropriate control of the acupuncture study (Li et al., 2002, 2013; Tjen-A-Looi et al., 2004; Guo et al., 2018).

Microinjection Into the rVLM

Animals were placed in a stereotaxic head frame to position their heads with the floor of the fourth ventricle in a horizontal position. A partial craniotomy was performed to expose the medulla to allow access to the rVLM. We performed microinjections using a modified CMA microdialysis probe that was 14 mm long (tip diameter 0.24 mm; CMA Microdialysis, Stockholm, Sweden) and lacked the microdialysis membrane. After being positioned by a micromanipulator (Kopf Instruments), the probe was inserted unilaterally (side chosen randomly) into the medulla with visual approximation at a 90° angle relative to the dorsal surface of the medulla, 1.8 – 2.3 mm lateral from the midline, 1.1 – 1.6 mm rostral to the obex, and advanced 3.0 – 3.3 mm from dorsal toward the ventral surface. These coordinates provide access to a region in the rVLM that has been found to contain premotor sympathoexcitatory cells (Li et al., 2002, 2013). Proper positioning of probes in the rVLM was confirmed by noting a 5–10 mmHg elevation in BP following the probe insertion as well as microinjection of glutamate (2 nmol in 50 nl) (Guo et al., 2009). The correct location of the rVLM was confirmed further by histological examination of stain from 0.5% pontamine sky blue, which was injected along with the chemicals tested after each experiment (Guo et al., 2009). The probe was connected to a microsyringe fastened to microdialysis pump (CMA/102, North Chelmsford, MA, United States) through a fluorinated ethylene propylene tubing (0.12-mm inner diameter) and tubing adaptors. The injection of the low possible volume of 50 nl was carried out at a rate of 0.6 μl/min over a 5-s period. Of note, we have demonstrated significant blockade of EA's actions following unilateral administration of drugs, which allows maintaining optimal physiological state to study EA-modulation of cardiovascular responses. This simplified approach of unilateral microinjection has been proven to be successful (Li et al., 2002; Crisostomo et al., 2005; Tjen-A-Looi et al., 2007). Microinjection of the vehicle into the rVLM and drug into surrounding regions provided chemical and anatomical controls. We allowed any small transient changes in basal BP induced by injecting drugs to recover before conducting an experiment (Li et al., 2002, 2013; Tjen-A-Looi et al., 2007).

Drugs

The following drugs were used: a non-selective opioid receptor antagonist, naloxone (1 mM) (Li et al., 2002); adenosine A_{2a} receptor agonist, CGS-21680 (0.4 mM) (Ichinose et al., 2009); adenosine receptor antagonists: non-selective 8-(*p*-sulfophenyl)theophylline (8-SPT, 10 mM) (Ichinose et al., 2009); A_1 selective, 1,3-Dipropyl-8-cyclopentylxanthine (DPCPX, 3 mM) (Collis et al., 1989; Nassar and bdel-Rahman, 2009); A_{2a} selective, SCH 58261 (1 mM) (Jiang et al., 2011). The vehicles for these drugs are normal saline or 5% dimethylsulfoxide (DMSO). All chemicals were purchased from Sigma Aldrich (St. Louis, MO, United States). Affinities, specificities, and dosages of the drugs are documented in the previous studies, as indicated by cited references for each individual one mentioned above. The solution of each drug or vehicle contained 0.5% pontamine sky blue for histological examination of the injection site after the experiment.

Experimental Protocols

Role of Adenosine Receptors in Acupuncture Inhibition of Reflex Elevations in BP

A 30-min stabilization period was allowed after the surgical procedure. Rats were subjected to 11-repeated GDs every 10 min, and BPs were recorded and measured before and after each GD, as described in the methods section. Ten-minute intervals between GDs prevented tachyphylaxis of the cardiovascular responses (Li et al., 2002; Guo et al., 2018). In each experiment, after recording two repeatable elevations in BP in response to GDs, EA started right after the 2nd time of GD and ended after the 5th time of GD. EA was conducted for 30 min during which three GDs (e.g., 3rd – 5th times of GD) were performed. We applied EA at P5-P6 bilaterally at a frequency of 2 Hz (0.3–0.5 mA, 0.5-ms duration). A non-selective adenosine receptor antagonist, 8-PST or its vehicle (5% DMSO) was microinjected into the rVLM 5 min before the 5th time of GD and the termination of EA. Afterward, six times of GDs were conducted. In rats treated with sham-EA, the same procedure was carried out as that performed in the EA-treated animal, except for that the acupuncture needles

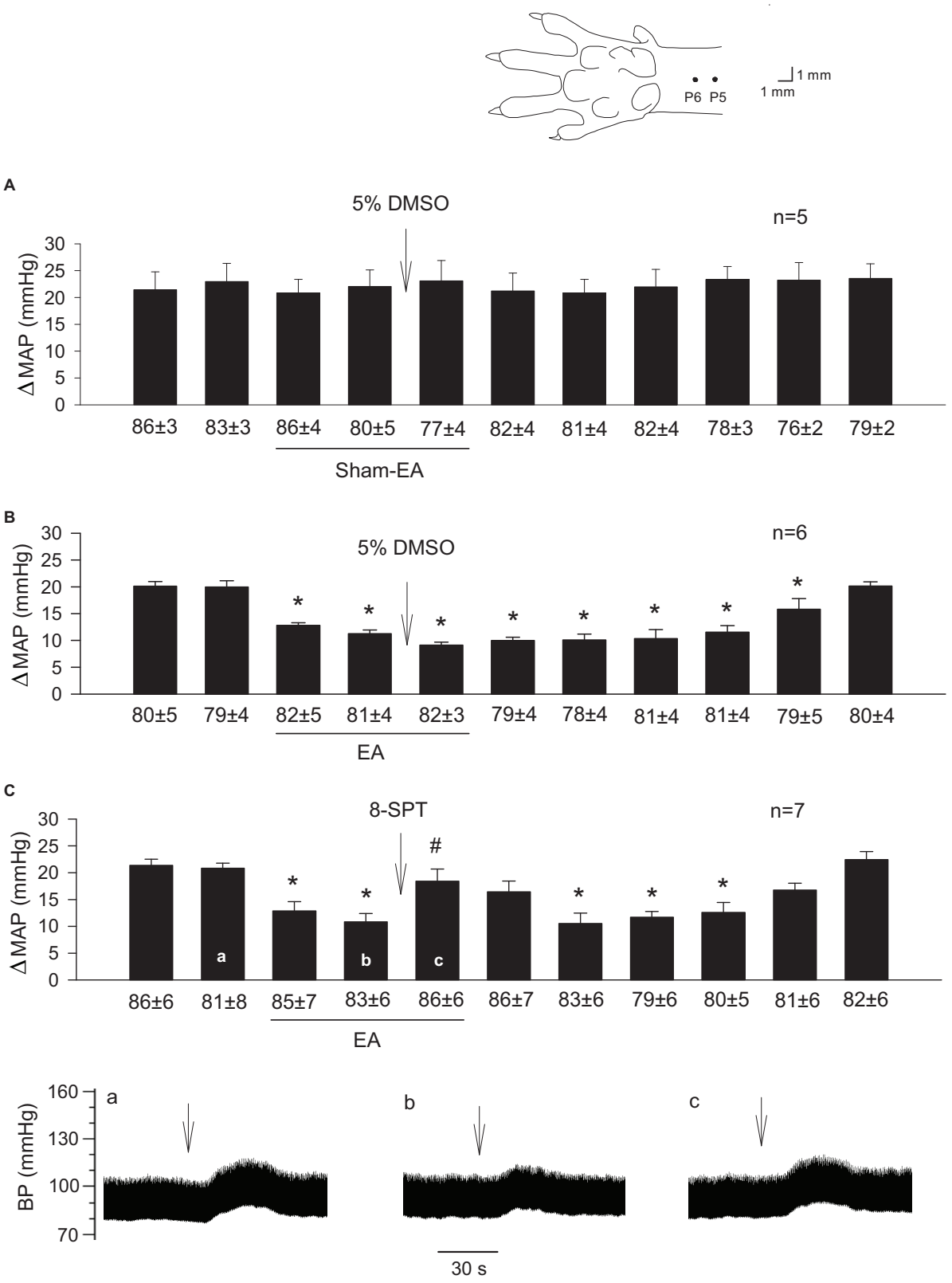

FIGURE 1 | Continued

FIGURE 1 | Influence of blockade of adenosine receptors in the rVLM on EA modulation of GD-induced pressor reflexes. The diagram above bar graphs displays the sites of the P5 and P6 acupoints (Hua, 1994). Bars represent increases in mean arterial blood pressure (MAP) following GD. Values below each bar indicate the baseline MAP (means ± SE) before GD. **(A,B)** 5% DMSO (50 nl) was injected into the rVLM as sham-EA **(A)** or EA **(B)** was conducted at P5-6; **(C)** microinjection of 8-SPT (10 mM in 50 nl; a non-selective adenosine receptor antagonist) into the rVLM with EA treatment. $^{*}P < 0.05$, a decrease of GD response after the onset of EA; $^{\#}P < 0.05$, after vs. before microinjection into the rVLM. Labels a-c in **(C)** indicate examples of the original BP tracings of a rat; ↓, time of GD application. These data suggest that adenosine in the rVLM is involved in EA modulation of GD-induced pressor reflexes.

were inserted bilaterally into P5-6 acupoints without electrical stimulation. The 5% DMSO was microinjected into the rVLM 5 min before the end of 30 min of sham-EA.

Specificity of Adenosine A_1 and A_{2a} Receptors in Acupuncture Inhibition of Reflex Elevations in BP

Similar to the protocol used to examine the effect of 8-PST on EA's action in the rVLM described above, SCH 58261 (1 mM, A_{2a} receptor-selective antagonist) or DPCPX (3 mM, A_1 receptor-selective antagonist) were microinjected unilaterally into the rVLM 5 min before termination of 30 min of EA. BP responses to GD in the rat were measured every 10 min before, during, and for 60 min after EA. The vehicle for both drugs was 5% DMSO, similar to that for the 8-PST.

Influence of Activation or Inhibition of A_{2a} Receptors in the rVLM on Pressor Reflexes

In separate animals without treatment with EA or sham-EA, six-repeated GDs were carried out every 10 min. Five min after the establishment of two consistent pressor responses to GD, we performed unilateral microinjection (50 nl) of 5% DMSO, SCH 58261 (1 mM; adenosine A_{2a} receptor-specific antagonist) or CGS-21680 (0.4 mM; adenosine A_{2a} receptor-specific agonist) into the rVLM. Five min later, repeated GDs were conducted for four times, lasting for 40 min.

Contribution of Endogenous Opioids to Adenosine A_{2a} Receptor-Mediated Acupuncture Modulation of Pressor Responses

In separate rats that underwent EA treatment, we measured BP responses to 11-repeated GDs every 10 min. EA at P5-P6 was employed for 30 min following two repeatable responses to GDs, similar to the protocol described above. Differently, in this protocol, 5 min before termination of EA or the 5th time of GD, naloxone (1 mM; a non-selective opioid receptor antagonist), or 0.9% normal saline (the vehicle for naloxone) were administered (50 nl) unilaterally into the rVLM. Five min after the end of EA or the 6th time of GD, we microinjected (50 nl) SCH 58261 (1 mM, adenosine A_{2a} receptor-specific antagonist), CGS-21680 (0.4 mM, adenosine A_{2a} receptor-specific agonist) or 5% DMSO into the same site of the rVLM. Afterward, GDs were conducted repeatedly for five times.

Histology

Rats were euthanized under deep anesthesia with additional α-chloralose, followed by saturated potassium chloride (1 M) at the end of each experiment. The stomach was exposed to confirm the placement of the balloon. The medulla oblongata was removed and submerged in 4% paraformaldehyde for at least 72 h. Frozen 60-μm coronal sections were cut with a cryostat microtome (Leica CM1850 Heidelberger Strasse, Nussloch, Germany) to confirm the microinjection sites histologically. Blue dye spots were identified with a microscope. Using the atlas of Paxinos and Watson as a guide (Paxinos and Watson, 2005), places of microinjections in the medulla were plotted with Corel Presentation software on reconstructed coronal sections (Li et al., 2002, 2013).

Immunohistochemistry

Adult male Sprague-Dawley rats were anesthetized with a large dose of ketamine/xylazine (0.6–1.0 ml, im). Transcardial perfusion was performed using 300 ml of 0.9% saline solution followed by 300 ml of 4% paraformaldehyde in 0.1 M phosphate buffer (pH 7.4). Medulla oblongata was harvested and sliced into 30 μm sections using a cryostat microtome (Leica CM1850). Medullary sections were collected serially.

Free-floating sections were used for immunohistochemical staining. Briefly, after washing for 30 min (10 min × 3 times) using phosphate-buffered saline containing 0.3% Triton X-100 (PBST; pH = 7.4), brain sections were treated for 1 h with 1% normal donkey serum (Jackson Immunoresearch Laboratories, West Grove, PA, United States). The sections were incubated with a primary rabbit anti-adenosine A_{2a} receptor antibody (1:200; Abcam, Cambridge, MA, United States) and a mouse anti-enkephalin antibody (1:200; EMD Millipore Corporation, Temecula, CA, United States) at 4°C for 48 h. The tissues subsequently were rinsed three times (10 min for each rinse) in PBST and incubated with a fluorescein-conjugated donkey anti-rabbit and a rhodamine-conjugated donkey anti-mouse (1:200 dilution; Jackson Immunoresearch Laboratories) for 24 h at 4°C. These secondary antibodies raised in the donkey are made for multiple labels. They have minimal cross-reactivity to other non-specific species (2010 catalog specializing in secondary antibodies; Jackson Immunoresearch Laboratories). Brain sections on the slide were air-dried. The slides were coverslipped using a mounting medium (Vector Laboratories, Burlingame, CA, United States). In immunohistochemical control studies, no labeling was detected when the primary or secondary antibody was omitted.

Image data analysis: Brain sections were scanned and examined with a standard fluorescent microscope (Nikon, E400, Melville, NY, United States). Two epifluorescence filters (B-2A, or G-2A) equipped in a fluorescent microscope were used to identify single stains appearing as green (fluorescein) or red (rhodamine) in brain sections. Immunoreactive neurons

labeled with adenosine A_{2a} receptors and enkephalin appeared as bright green and red colors, respectively (**Figure 6**). Selected sections were evaluated further using a Zeiss (LSM 780) laser scanning confocal microscope (Zeiss LSM 710, Meta system; Zeiss, Thornwood, NY, United States). This apparatus was equipped with HeNe and Argon lasers and allowed operation of multiple channels. Lasers of 488- and 543-nm wavelengths were used to excite fluorescein and rhodamine. Each confocal section analyzed was limited to a 0.5-μm thickness in the Z-plane. Digital images of the labels were captured and analyzed with software (Zeiss LSM) provided with this microscope. Images in two colors in the same plane were merged to reveal the relationship between two labels. Single- and double-labeled neurons were evaluated.

Statistical Analyses

Reflex responses are expressed as the difference in MAP comparing steady-state baseline BP and pressure at peak response. Changes in MAP are presented as bar histograms. Data are presented as means ± SE. The increases in BPs before and after delivery of experimental drug or vehicle were compared by a one-way repeated-measures ANOVA followed *post hoc* by the Student–Newman–Keuls test. Data are plotted and analyzed with the Kolmogorov–Smirnov test for normal data distribution and normalized when necessary with SigmaPlot (Jandel Scientific Software, San Rafael, CA, United States). All statistical analyses were performed with SigmaPlot/Stat (Jandel Scientific). Values were considered to be significantly different when $P < 0.05$.

RESULTS

The Action of Adenosine Receptors in EA Inhibition of Reflex Elevations in BP

BP responses to GD were consistent in a group of rats subjected to sham-EA at P5-6 (**Figure 1A**; $n = 5$). Heart rate was not affected by GD consistently. In contrast, EA applied at P5-6 significantly attenuated GD-induced pressor responses (**Figure 1B**; $P < 0.05$, $n = 6$). The vehicle (5% DMSO) administered into the rVLM did not influence BP responses to GD during sham-EA or EA (**Figures 1A,B**). However, EA-modulation of GD-induced pressor reflex responses was significantly reversed following administration of 8-SPT (a non-selective adenosine receptor antagonist) into the rVLM (**Figure 1C**; $P < 0.05$, $n = 7$).

Specificity of Adenosine A_1 and A_{2a} Receptors in EA Inhibition of Reflex Elevations in BP

We observed that EA modulation of GD-induced pressor reflexes was not altered by DPCPX (an A_1 receptor-specific inhibitor; **Figure 2A**, $n = 6$). However, it was reversed by rVLM microinjection of SCH 58261 (an adenosine A_{2a} receptor-specific antagonist; **Figure 2B**, $n = 8$). The administration of the vehicle for both chemicals (5% DMSO) into the rVLM did not influence EA inhibitory effects on GD-induced elevations in BP, as demonstrated in **Figure 1B**.

Changes in Pressor Reflexes After Activation or Inhibition of rVLM A_{2a} Receptors in the Absence of EA Treatment

In the absence of EA, we observed consistent pressor responses to GD (**Figure 3A**). Further, we noted that GD-induced elevations in BP were unaltered by rVLM microinjection of 5% DMSO (the vehicle; **Figure 3A**; $n = 5$) or SCH 58261 (adenosine A_{2a} receptor-selective antagonist; **Figure 3B**; $n = 6$). In contrast, microinjection of CGS-21680 (A_{2a} receptor-selective agonist) into the rVLM significantly attenuated GD-induced pressor responses (**Figure 3C**; $P < 0.05$, $n = 8$), mimicking the EA's inhibitory effect on pressor responses (**Figure 1B**).

Involvement of Endogenous Opioids in Adenosine A_{2a} Receptor-Mediated EA Modulation of Pressor Responses

Similar to the prior experiments in which rats underwent EA treatment (**Figure 1B**), we observed that 11-repeated GDs every 10 min induced consistent pressor responses despite two subsequent microinjections of 0.9% normal saline and 5% DMSO (the vehicles) into the rVLM (**Figure 4A**; $n = 5$). Microinjection of naloxone (a non-selective blocker of opioid receptors) into the rVLM significantly reversed EA inhibitory effects on GD-induced pressor responses (**Figures 4B–D**; all $P < 0.05$), lasting at least for 25 min. The naloxone-induced reversion of EA-modulated pressor responses was unchanged following subsequent administration of 5% DMSO (**Figure 4B**; $n = 7$), SCH 58261 (**Figure 4C**; $n = 7$) or CGS-21680 (**Figure 4D**; $n = 8$) into the same site of the rVLM, where the naloxone was employed.

Histological Confirmation of Microinjection Sites

We examined brain slices of rats subjected to the microinjection into the rVLM and included animals in which the injections were verified to be located within the rVLM, as described above and shown in **Figure 5**. Microinjection sites were identified 1.8–2.3 mm lateral to the midline, 1.1–1.6 mm rostral to the obex, and 0.5–1.0 mm from the ventral surface. This region was consistent with the location of the rVLM, according to the atlas of Paxinos and Watson (2005).

Co-localization of Adenosine A_{2a} Receptors and Enkephalin in the rVLM

In the rVLM of all four rats, we found perikarya and neural fibers labeled with adenosine A_{2a} receptors, and many neural fibers and some cell bodies stained with enkephalin. More importantly, we noted co-localization of adenosine A_{2a} receptors with neurons containing enkephalin in these rats. Approximately

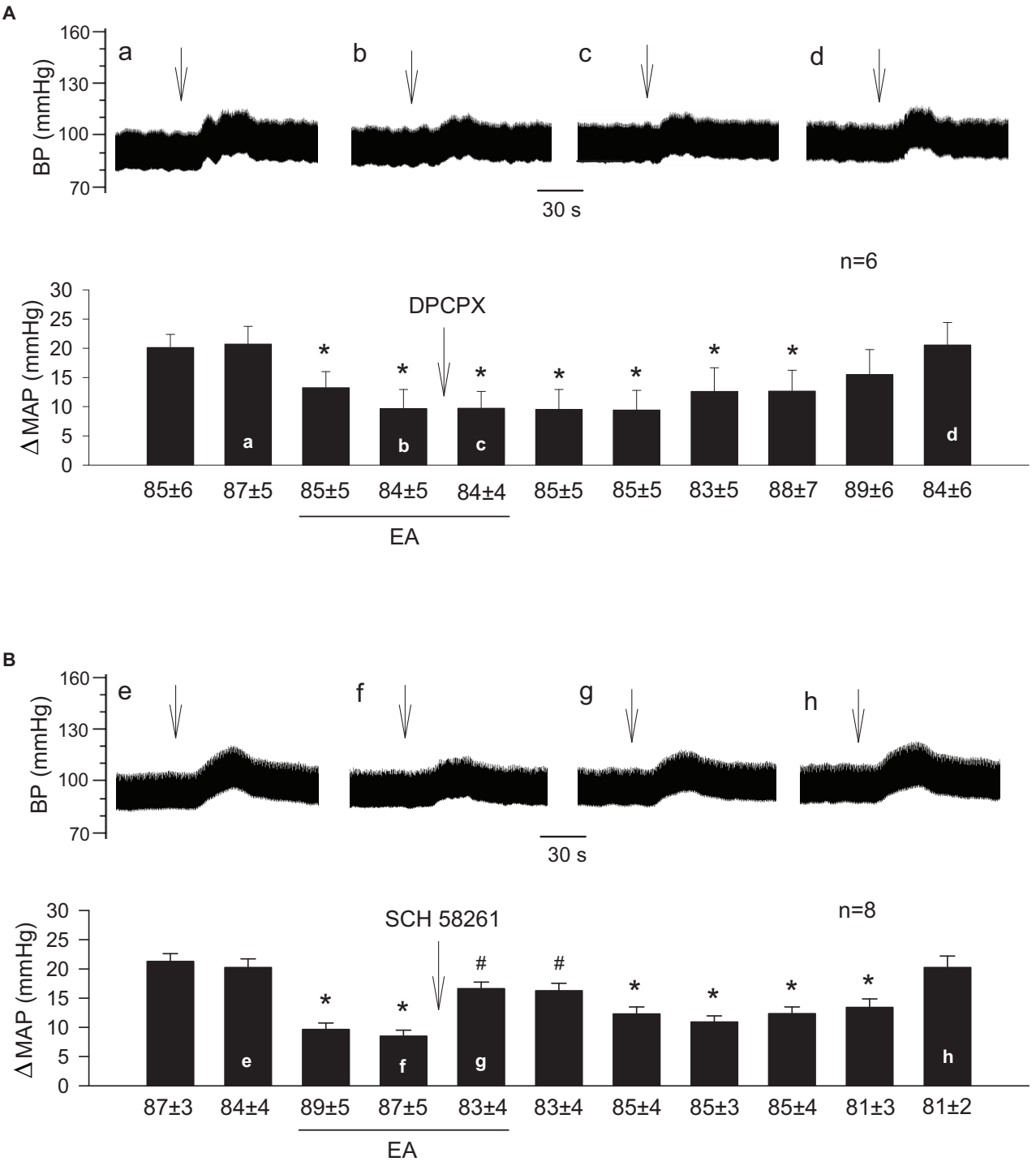

FIGURE 2 | Influence of specific blockade of A_1 or A_{2a} receptors in the rVLM on EA modulation of GD-induced pressor reflexes. Bars represent increases in mean arterial blood pressure (MAP) following GD. Values below each bar indicate the baseline MAP (means ± SE) before GD. **(A,B)** Microinjection of DPCPX (3 mM in 50 nl; an A_1 receptor antagonist; **A**) or SCH 58261 (1 mM in 50 nl; an A_{2a} receptor antagonist; **B**) into the rVLM with EA treatment. $^*P < 0.05$, a decrease of GD response after the onset of EA; $^{\#}P < 0.05$, after vs. before microinjection into the rVLM. Labels a–d in **(A)** and e–h in **(B)** indicate examples of original BP tracings of a rat from each group; ↓, time of GD application. These data suggest that adenosine A_{2a}, but not A_1 receptors in the rVLM contribute to EA modulation of GD-induced pressor reflexes.

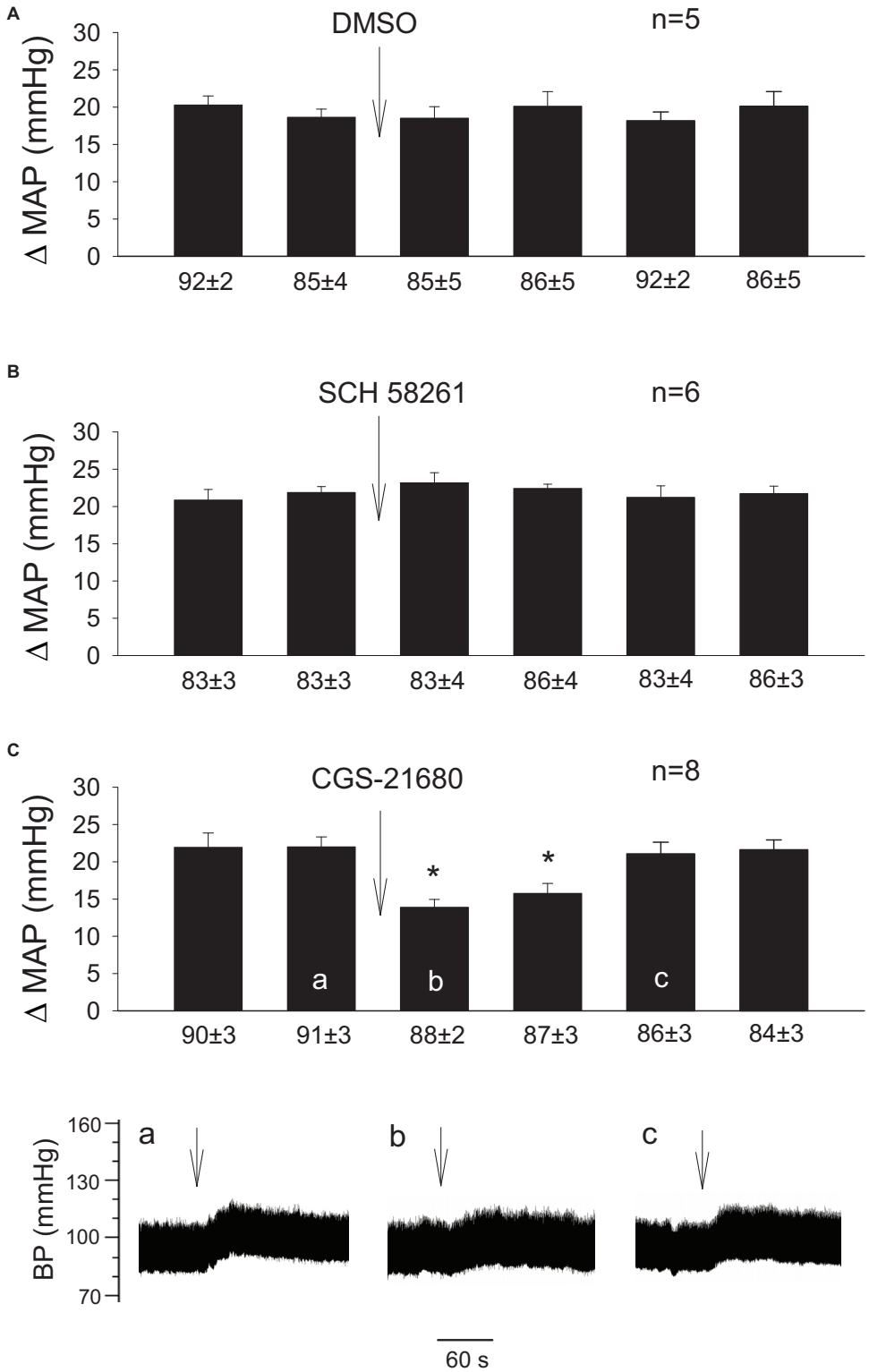

FIGURE 3 | Influence of activation of A_{2a} receptors in the rVLM on GD-induced pressor reflexes. Bars represent increases in mean arterial blood pressure (MAP) following GD. Values below each bar indicate the baseline MAP (means ± SE) before GD. **(A–C)** Microinjection of 5% DMSO (50 nl; **A**), SCH 58261 (1 mM in 50 nl; an A_{2a} receptor antagonist; **B**) or CGS-21680 (0.4 mM in 50 nl; an A_{2a} receptor agonist; **C**) into the rVLM without EA treatment. $^*P < 0.05$, after vs. before microinjection into the rVLM. Labels a–c in **(C)** indicate examples of the original BP tracings of a rat from this group; ↓, time of GD application. These data suggest that the activation of adenosine A_{2a} receptors in the rVLM contributes to inhibition of GD-induced pressor reflexes.

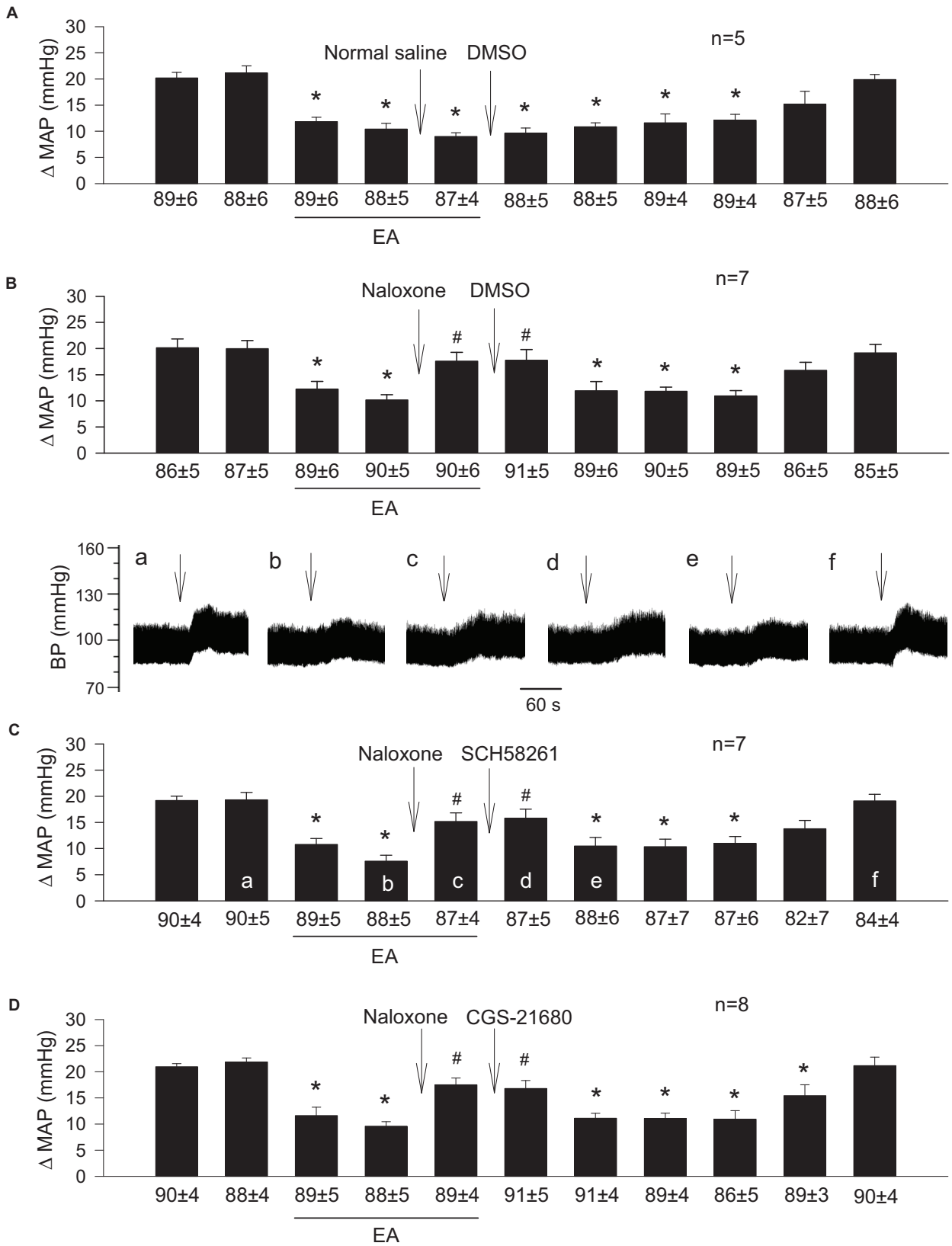

FIGURE 4 | Continued

FIGURE 4 | Importance of opioids in adenosine-mediated EA inhibition of GD-induced pressor reflexes through A_{2a} receptors in the rVLM. Bars represent increases in mean arterial blood pressure (MAP) following GD. Values below each bar indicate the baseline MAP (means ± SE) before GD. **(A)** Sequential microinjections of normal saline and 5% DMSO (both 50 nl) into the rVLM, which are vehicles for naloxone (a non-selective opioid receptor antagonist) and SCH 58261 & CGS-21680 (an A_{2a} receptor antagonist and agonist, correspondingly), respectively; **(B–D)** following microinjection of naloxone (1 mM in 50 nl) into the rVLM with EA treatment, 5% DMSO (the vehicle; **B**), SCH 58261 (1 mM in 50 nl; **C**) or CGS-21680 (0.4 mM in 50 nl; **D**) were administered into the same site of the rVLM. $^{*}P < 0.05$, a decrease of GD response after the onset of EA; $^{\#}P < 0.05$, after vs. before microinjection of naloxone into the rVLM. Labels a–f in **(C)** indicate examples of the original BP tracings of a rat from this group; ↓, time of GD application. Blockade or activation of A_{2a} receptors did not alter EA's action in attenuating GD-evoked sympathoexcitatory cardiovascular reflexes after inhibition of opioid receptors in the rVLM. These data suggest that the involvement of rVLM adenosine A_{2a} receptors in EA modulation of GD-induced pressor reflexes is dependent on the presence of opioids.

26 adenosine A_{2a} receptor-containing neurons were identified in each section of the rat's rVLM. Eighteen of these neurons were co-labeled with enkephalin. Thus, ∼70% of adenosine A_{2a} receptor-containing neurons were enkephalinergic neurons. **Figure 6** demonstrates confocal images showing the neuron double-labeled with adenosine A_{2a} receptors and enkephalin in the rVLM of a rat.

DISCUSSION

Our findings show that underlying EA's modulation of elevated BP is a complex mechanism involving both the purinergic and endogenous opioid systems in the rVLM. Blockade of adenosine receptors, specifically A_{2a}, but not A_1 in the rVLM reversed EA modulation of GD-induced pressor responses. In the absence of EA, inhibition of adenosine A_{2a} receptors in the rVLM did not alter pressor reflexes evoked by GD. However, the activation of these receptors attenuated the reflexes, mimicking EA's inhibitory effect. Blockade of opioid receptors in the rVLM reversed EA's action in inhibiting GD-induced pressor responses and blunted the contribution of A_{2a} receptors to the mediation of the EA effect on reflexive responses as well. Moreover, neurons labeled with adenosine A_{2a} receptors were co-localized with neurons stained with enkephalin in the rVLM. These data support our working hypothesis that adenosine, through rVLM A_{2a}, but not A_1, receptor stimulation, contributes to the processing of EA-associated sympathoinhibition via an endogenous opioid mechanism.

We have previously shown that EA lowers elevated BP in experimental hypertensive models and patients with hypertension (Longhurst and Tjen-A-Looi, 2013; Li et al., 2015, 2016). Mechanical and chemical stimulation of visceral spinal afferents commonly causes reflex increases in BP due to enhanced sympathetic nerve activity (Li et al., 2002; Zhou et al., 2005b; Tjen-A-Looi et al., 2007) and the CNS is critically involved in the development of hypertension (Dampney, 1994). Our previous studies have demonstrated that EA at P5-6 attenuates reflex elevations in BP induced by visceral stimulation, like GD and chemical stimulation of gall bladder, compared to sham-EA without electrical stimulation and EA applied at non-acupoints. Our results indicate that the function of EA depends on both electrical activation and specific acupoints (Tjen-A-Looi et al., 2004, 2007; Zhou et al., 2005a; Guo et al., 2018). EA at P5-6 inhibits visceral sympathoexcitatory pressor responses through influence on multiple brain regions like arcuate nuclei, periaquductal gray, among others, which finally affect the rVLM and modulate hypertensive responses (Li and Longhurst, 2010). The rVLM is a crucial brain area that controls sympathetic outflow and integrates cardiovascular reflexes (Dampney, 1994). It also appears to serve as an essential area for processing the inhibitory effect of EA on sustained hypertension and pressor responses (Tjen-A-Looi et al., 2007; Li and Longhurst, 2010; Li et al., 2016). Visceral afferents including those located in the stomach pass through the splanchnic nerve to the brain regions, including the rVLM (Li et al., 2002; Zhou et al., 2005b; Li and Longhurst, 2010). Since EA at P5-6 inhibits evoked-activity of rVLM pre-sympathetic neurons during stimulation of the splanchnic nerve (Zhou et al., 2005b; Tjen-A-Looi et al., 2007), excitatory cardiovascular responses induced by splanchnic inputs to the rVLM likely are inhibited by EA through stimulation of somatic afferents.

We observed previously that EA modulates pressor cardiovascular responses induced by visceral stimulation through several neurotransmitters or neuromodulators, including opioids, GABA, nociception, and serotonin in the rVLM (Tjen-A-Looi et al., 2007; Moazzami et al., 2010). However, inhibition of any one of these neural substances in the rVLM only partially eliminates EA's hypotensive effect, implying the contribution of other modulators during EA. In this regard, adenosine is released during neuronal activation (Spyer et al., 1997; St Lambert et al., 1997; Burnstock, 2007) and primarily modulates neuronal function through P1 receptors (Spyer et al., 1997; Burnstock, 2007). Adenosine receptors are distributed in various regions in CNS, including the rVLM (Thomas and Spyer, 1999; Nassar and bdel-Rahman, 2008, 2009; Jiang et al., 2011). Moreover, there is evidence showing that adenosine modulates rVLM activity (Thomas and Spyer, 1999). Although adenosine likely serves a peripheral local role in acupuncture antinociception (Goldman et al., 2010), its contribution to modulatory action of acupuncture in the brain, particularly in the rVLM, is uncertain. In the present study, we found that non-selective inhibition of adenosine receptors in the rVLM reversed the EA-inhibitory effect on GD-induced pressor responses, implying involvement of adenosine and its receptors in processing EA's action in the rVLM.

Adenosine P1 receptors are sub-classified into four G protein-coupled receptors: A_1, A_{2a}, A_{2b}, and A_3. The expression of patterns of these receptors varies among cell types, and adenosine induces a multitude of physiological effects, including neuronal activity in the body. While all four adenosine receptor subtypes are present in CNS, the adenosine A_1 and A_{2a} receptors are predominantly expressed in the brain (Ribeiro et al., 2002; Borea et al., 2018). Previous studies showed that selective

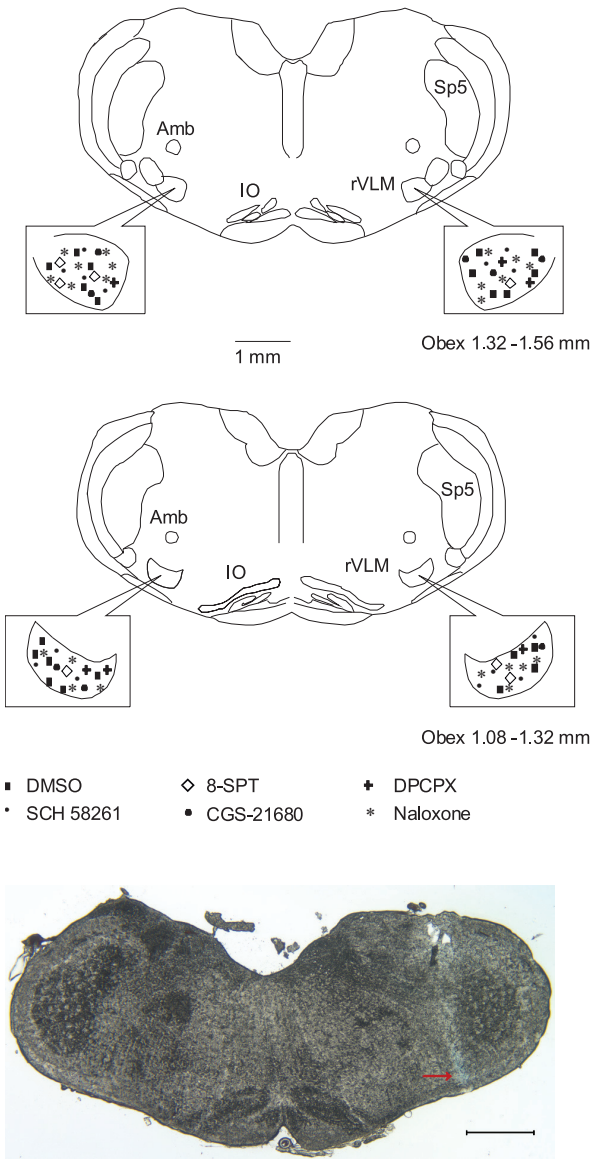

FIGURE 5 | Anatomic locations of microinjection sites in the rat. **(Top two panels)** Composite maps displaying histologically verified sites of microinjections in the rVLM of rats. The box indicates the magnified area of the rVLM in these panels. Brain section shows the composite of planes of brain stem rostral to the obex (Paxinos and Watson's atlas) (Paxinos and Watson, 2005). Symbols represent microinjection of 5% DMSO with and without normal saline (■), 8-SPT (◇), DPCPX (+), SCH 58261 only (▲), CGS-21680 only (●), and naloxone (★). All the injections were unilateral (side chosen randomly). Sections are 1.08 – 1.32 and 1.32 – 1.56 mm rostral to the obex. Amb, nucleus ambiguous; IO, inferior olive; rVLM, rostral ventrolateral medulla; Sp5, spinal trigeminal nucleus. **(Bottom panel)** An original slide of the medulla oblongata (1.32 mm rostral to the obex) shows the blue-dyed track of a modified microdialysis probe insertion used for injection. Ventral aspect of blue dye represents the site of microinjection in the rVLM as indicated by an arrow. A scale bar represents 1 mm.

pharmacological activation of A_1 or A_{2a} receptors in the rVLM induces pressor or depressor responses, respectively (Nassar and bdel-Rahman, 2008, 2009; Jiang et al., 2011). Based on these previous studies, we hypothesized that adenosine receptors A_{2a} rather than A_1 are involved in EA's inhibitory effect on excitatory cardiovascular responses. Data from the present study support our working hypothesis, which demonstrated that specific inhibition of A_{2a}, but not A_1 receptors in the rVLM reversed EA modulation of GD-induced pressor reflexes. Furthermore, the application of the specific A_{2a} receptor agonist into the rVLM reduces GD-induced pressor responses without EA treatment, which mimics EA's effect. Blockade of A_{2a} receptors in the rVLM did not alter GD-induced pressor reflexes in the absence of EA, which implies no involvement of this type of adenosine receptors in primary GD-induced excitatory cardiovascular responses. Our results support the notion about the role of adenosine via A_{2a} receptors in the rVLM in processing EA's modulatory action on visceral sympathoexcitatory reflexes. Goldman and colleagues showed that adenosine A_1 receptors participate in antinociceptive effects of manual acupuncture in peripheral tissues (Goldman et al., 2010), but they unlikely contribute to EA modulation of cardiovascular pressor responses in the rVLM as A_{2a} receptors do. As such, we suggest that adenosine may contribute to the effect of acupuncture through different types of adenosine receptors in CNS versus peripheral tissues. Also, different kinds of adenosine receptors may be involved in acupuncture's action in various physiological and pathophysiological statuses as well as during the application of varying acupuncture stimulation (e.g., EA vs. manual acupuncture). Addressing these issues requires further investigations.

In general, adenosine A_1 receptors are coupled to $G_{i/o}$ and A_{2a} receptors to G_s protein. Thus, adenosine triggers opposite effects on adenylate cyclase and its associated cAMP intracellular pathway, leading to inhibition and excitation of cells through adenosine A_1 and A_{2a} receptors respectively (Ribeiro et al., 2002; Borea et al., 2018). Excitation of pre-sympathetic premotor neurons in the rVLM usually leads to an increase in BP, while inhibition of them causes a decrease in BP (Dampney, 1994). It seems to be reasonable to assume that activation of A_1 and A_{2a} receptors in the rVLM premotor neurons contributes to reduction and elevation in BP, accordingly. However, several lines of evidence show that selective pharmacological excitation of adenosine A_1 or A_{2a} receptors in the rVLM leads to increase or decrease in BP, respectively (Nassar and bdel-Rahman, 2008, 2009; Jiang et al., 2011), which disagree with the assumption aforementioned. These reports imply that adenosine unlikely influences post-synaptic premotor neurons in rVLM through A_1 or A_{2a} receptors directly. In this respect, it is possible that adenosine may, through these subtypes, modulate the release of neurotransmitters or modulators from pre-synaptic neurons, which then affect rVLM premotor neurons and BP. Previous studies in the brain support this possibility, demonstrating that A_1 and A_{2a} receptors are involved in inhibition and enhancement of pre-synaptic release of neurotransmitters (Cunha and Ribeiro, 2000; Ribeiro et al., 2002; Scislo and O'Leary, 2006). In particular, adenosine reduces GABA release through pre-synaptic A_1 receptors in the rVLM, which contributes to increasing the rVLM activity and elevated BP during stimulation of the hypothalamic defense area (Thomas and Spyer, 1996, 1999; St Lambert et al., 1996; Han et al., 2011).

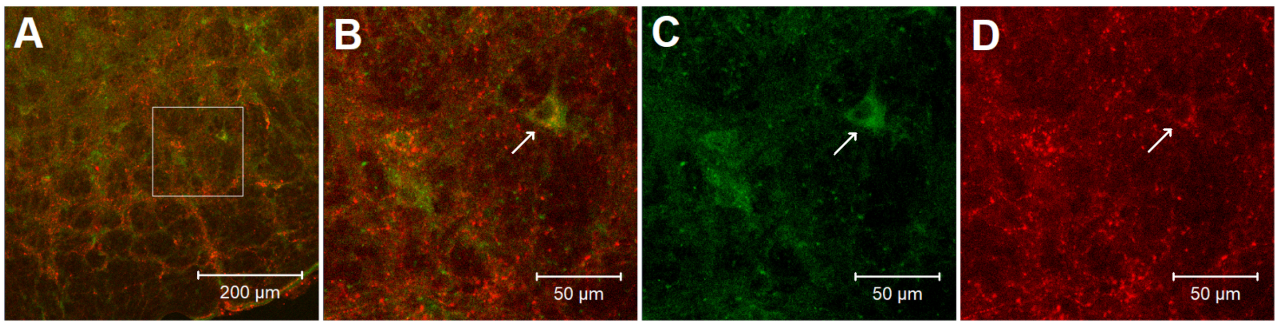

FIGURE 6 | Confocal microscopic images show double-fluorescent labeling of adenosine A_{2a} receptors and enkephalin in the rVLM of a rat. **(A)** Low-power photomicrograph (1.44 mm rostral to the obex). **(B)** Magnified region displayed within the box in **(A)**. **(B)** Is a merged image from **(C,D)**. Arrows in **(B–D)** indicate a neuron co-labeled with adenosine A_{2a} receptors and enkephalin (yellow), adenosine A_{2a} receptors (green) and enkephalin (red), respectively. Scale bars in **(A,B–D)** represent 200 and 50 μm, correspondingly.

Given our previous findings of EA's inhibitory effects on pressor cardiovascular responses through GABA, opioids, and nociceptin in the rVLM (Crisostomo et al., 2005; Tjen-A-Looi et al., 2007), we speculate that EA likely enhances these neurotransmitters or modulators through adenosine-mediated A_{2a} receptor mechanisms in the rVLM and lowers elevated BP during cardiovascular pressor responses.

A body of evidence shows interactions between the adenosine and opioid systems in CNS (Ribeiro et al., 2002; Borea et al., 2018). In this regard, a previous study notably demonstrated that antinociceptive effects of intracerebroventricular administration of A_{2a} receptor agonist are regulated, at least in part, through an opioid mechanism (By et al., 2011). Opioids play a role in EA regulation of cardiovascular responses (Tjen-A-Looi et al., 2007; Li and Longhurst, 2010). In this respect, EA reduces rVLM pre-sympathetic activity and reflex-induced elevations in BP through an opioid mechanism involving enkephalins (via δ- and μ-receptors) and endorphins (μ-receptors), but not dynorphins (κ-receptors) (Li et al., 2001, 2002; Tjen-A-Looi et al., 2007). Moreover, administering one of δ- and μ-receptor agonists into the rVLM attenuates pressor responses caused by visceral stimulation, including GD (Li et al., 2002, 2013; Crisostomo et al., 2005; Tjen-A-Looi et al., 2007), which mimics EA's effect. Enkephalins are synthesized in EA-activated rVLM neurons (Guo et al., 2004), while endorphins are produced in the hypothalamic arcuate nucleus and then transported to the rVLM (Li et al., 2009). Preproenkephalin mRNA in the rVLM is increased following single and repetitive EA in normotensive models (Li et al., 2010, 2012). It is unknown if opioids are involved in adenosine regulation of elevated BP during EA. In the present study, we observed that non-selective blockade of opioid receptors in the rVLM partially reverses EA inhibitory effects on GD-induced pressor responses, which are consistent with our previous findings of the importance of opioids in the EA's impact, as aforementioned (Li et al., 2002, 2013). More interestingly, we noted that neither inhibition nor activation of A_{2a} receptors in the rVLM cause any changes in GD-induced elevation in BP following blockade of opioid receptors in animals subjected to EA. These observations suggest that the involvement of rVLM adenosine A_{2a} receptors in EA modulation of GD-induced pressor reflexes is, at least in part, specifically dependent on the presence of endogenous opioids. Furthermore, our anatomical data demonstrate that A_{2a} receptors in the rVLM co-localize with enkephalin-containing neurons, indicating an influence of adenosine on these enkephalinergic neurons through A_{2a} receptors in the rVLM. With our previous and current findings taken together, we think that EA likely excites rVLM enkephalin-containing neurons, at least in part, through adenosine via A_{2a} receptors and promotes enkephalin release, leading to modulation of the pre-sympathetic activity of rVLM neurons and elevated BP evoked by GD (**Figure 7**).

Adenosine A_{2a} receptors also are present in the post-synaptic neurons, including rVLM premotor neurons (Thomas and Spyer, 1999; Ribeiro et al., 2002; Borea et al., 2018). Thus, we cannot exclude a possibility that A_{2a} receptors in these neurons are activated during EA. However, the potential excitatory effect of activation of A_{2a} receptors on the post-synaptic neurons might be counteracted by the inhibitory action, resulting from activation of adenosine A_1 receptors as well as receptors associated with other neurotransmitters or neuromodulators like opioids, GABA, and among others. In this respect, particularly, there is evidence showing that δ-receptor agonists inhibit A_{2a} receptor-mediated activation of adenylyl cyclase, leading to a reduction in cAMP-regulated phosphorylation of neurons in the striatum and caudate putamen of rats (Noble and Cox, 1995; By et al., 2011). Further studies are needed to examine this possibility (**Figure 7**).

One limitation of the present study is that we cannot identify directly the source of EA-activated neurons that generate adenosine due to technical restrictions. However, as we demonstrated previously, EA activates neurons in multiple brain regions like the paraventricular nucleus, arcuate nucleus, nucleus tractus solilatrii, caudal ventrolateral medulla, and raphe nucleus, which project to the rVLM directly with mono-synaptic axons (Li et al., 2009; Moazzami et al., 2010; Tjen-A-Looi et al., 2013, 2016; Guo and Malik, 2019). As such, it is reasonable to suggest that neurons generating adenosine during EA may be present

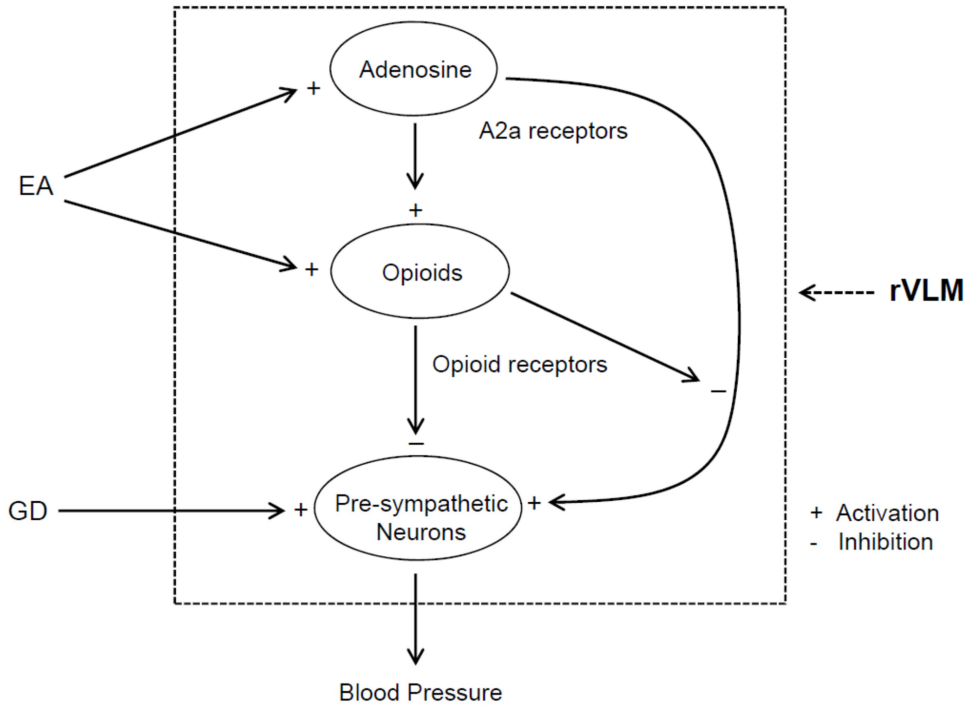

FIGURE 7 | Potential neural pathways associated with the action of adenosine A_{2a} receptor-opioids in the rVLM in EA regulation of sympathetic outflow and cardiovascular pressor responses during visceral stimulation. +, indicates activation or enhancement of the system; –, indicates inhibition of the system; EA, electroacupuncture; GD, gastric distension. EA likely activates adenosine A_{2a} receptors in the rVLM, which promotes opioid generation. The activation of opioid receptors causes inhibition of the pre-sympathetic activity of rVLM neurons directly as well as through suppression of A_{2a} receptor-mediated excitation of these neurons, leading to a reduction in blood pressure.

in the rVLM as well as in other brain areas that have direct connections with the rVLM.

Perspective and Significance Elevated BP during sympathoexcitatory responses frequently increase morbidity and mortality of patients with cardiovascular diseases (Guo et al., 2009; Li and Longhurst, 2010). Acupuncture's effects on reflex-induced elevations in BP provide important clues to clinical treatment of acute pressor responses and essential hypertension (Li and Longhurst, 2010; Longhurst and Tjen-A-Looi, 2013). In this respect, using modalities of stimulation proven to reduce elevated BP in reflex animal models effectively, we have found in patients with essential hypertension that repetitive EA lowers BP for weeks following therapy (Li and Longhurst, 2010; Li et al., 2015). The acute reflex studies in anesthetized animals have allowed in-depth mechanistic investigation of EA-related alterations in CNS processing of autonomic outflow to complement studies in sustained hypertension. The present study identified adenosine's role in the rVLM through opioids during EA modulation of reflex-induced elevations in BP. Our results thus expand the understanding of neural mechanisms underlying EA inhibition of elevated BP and suggest conducting further studies to elucidate these mechanisms further. With this respect, we may examine if adenosine receptors in other brain regions participate in EA modulation of cardiovascular responses. Also, it will be interesting to test if adenosine via specific receptors interacts with neurotransmitters or neuromodulators other than opioids in the brain areas during EA's effects on elevated BP, including through adenosine receptor heteromers. These proposed studies will further explore central mechanisms underlying the specific contribution of adenosine to EA's action in regulating cardiovascular responses.

Caffeine is a non-specific antagonist for adenosine receptors (Ribeiro et al., 2002). In light of our new results, patients with hypertension and other cardiovascular diseases may need to avoid consuming high levels of caffeine, when they undergo acupuncture treatment to achieve the full benefits of this therapy. These stimulants may reduce the activity of adenosine A_{2a} receptors and thus the beneficial effects of acupuncture. On the other hand, our result also suggests that an agonist drug, like deoxycoformycin (Pentostatin) that can increase adenosine may act through the adenosine A_{2a} receptors to enhance the clinical benefits of acupuncture, particularly, in management of cardiovascular disorders.

CONCLUSION

In conclusion, the results from the present study demonstrate that A_{2a} adenosine receptors in the rVLM play a role in central processing EA's action in modulating reflex excitatory

cardiovascular responses. The participation of rVLM adenosine A_{2a} receptors in EA modulation of GD-induced pressor reflexes is, at least in part, dependent on the presence of opioids. These new findings extend our knowledge regarding central neural mechanisms underlying acupuncture's influence on cardiovascular function and provide hints at possible ways to enhance the clinical response of acupuncture therapy.

DATA AVAILABILITY STATEMENT

The datasets generated for this study are available on request to the corresponding author.

ETHICS STATEMENT

The animal study was reviewed and approved by the Animal Care and Use Committee of the University of California, Irvine.

AUTHOR CONTRIBUTIONS

Z-LG and SM responsible for the conception and design of research, and wrote the manuscript. Z-LG and TS performed the experiments. All authors analyzed and interpreted the results of the experimental data, and edited, revised, and approved the final version of the manuscript. Z-LG prepared the figures.

FUNDING

This work was supported by the National Center for Complementary and Integrative Health, R01 grant AT009347 and diversity supplement award to this grant, United States.

ACKNOWLEDGMENTS

The authors gratefully acknowledge the technical assistance of Andrew Phillip Ramirez.

REFERENCES

Andersson, S. (1993). The functional background in acupuncture effects. *Scand. J. Rehabil. Med. Suppl.* 29, 31–60.

Borea, P. A., Gessi, S., Merighi, S., Vincenzi, F., and Varani, K. (2018). Pharmacology of adenosine receptors: the state of the art. *Physiol. Rev.* 98, 1591–1625. doi: 10.1152/physrev.00049.2017

Burnstock, G. (2007). Physiology and pathophysiology of purinergic neurotransmission. *Physiol. Rev.* 87, 659–797. doi: 10.1152/physrev.00043.2006

By, Y., Condo, J., Durand-Gorde, J. M., Lejeune, P. J., Mallet, B., Guieu, R., et al. (2011). Intracerebroventricular injection of an agonist-like monoclonal antibody to adenosine A(2A) receptor has antinociceptive effects in mice. *J. Neuroimmunol.* 230, 178–182. doi: 10.1016/j.jneuroim.2010.07.025

Collis, M. G., Stoggall, S. M., and Martin, F. M. (1989). Apparent affinity of 1,3-dipropyl-8-cyclopentylxanthine for adenosine A1 and A2 receptors in isolated tissues from guinea-pigs. *Br. J. Pharmacol.* 27, 1274–1278. doi: 10.1111/j.1476-5381.1989.tb12589.x

Crisostomo, M., Li, P., Tjen-A-Looi, S. C., and Longhurst, J. C. (2005). Nociceptin in rVLM mediates electroacupuncture inhibition of cardiovascular reflex excitatory response in rats. *J. Appl. Physiol.* 98, 2056–2063. doi: 10.1152/japplphysiol.01282.2004

Cunha, R. A., and Ribeiro, J. A. (2000). Purinergic modulation of [(3)H]GABA release from rat hippocampal nerve terminals. *Neuropharmacology* 39, 1156–1167. doi: 10.1016/s0028-3908(99)00237-3

Dampney, R. A. L. (1994). Functional organization of central pathways regulating the cardiovascular system. *Physiol. Rev.* 74, 323–364. doi: 10.1152/physrev.1994.74.2.323

Goldman, N., Chen, M., Fujita, T., Xu, Q., Peng, W., Liu, W., et al. (2010). Adenosine A1 receptors mediate local anti-nociceptive effects of acupuncture. *Nat. Neurosci.* 13, 883–888. doi: 10.1038/nn.2562

Guo, Z. L., Fu, L. W., Su, H. F., Tjen-A-Looi, S. C., and Longhurst, J. C. (2018). Role of TRPV1 in acupuncture modulation of reflex excitatory cardiovascular responses. *Am. J. Physiol. Regul. Integr. Comp. Physiol.* 314, R655–R666. doi: 10.1152/ajpregu.00405.2017

Guo, Z. L., and Malik, S. (2019). Acupuncture activates a direct pathway from the nucleus tractus solitarii to the rostral ventrolateral medulla. *Brain Res.* 1708, 69–77. doi: 10.1016/j.brainres.2018.12.009

Guo, Z.-L., Moazzami, A. R., and Longhurst, J. C. (2004). Electroacupuncture induces c-Fos expression in the rostral ventrolateral medulla and periaqueductal gray in cats: relation to opioid containing neurons. *Brain Res.* 1030, 103–115. doi: 10.1016/j.brainres.2004.09.059

Guo, Z.-L., Tjen-A-Looi, S. C., Fu, L. W., and Longhurst, J. C. (2009). Nitric oxide in rostral ventrolateral medulla regulates cardiac-sympathetic reflex: role of synthase isoforms. *Am. J. Physiol.* 297, H1479–H1486. doi: 10.1152/ajpheart.00209.2009

Han, T. H., Jang, S. H., Lee, S. Y., and Ryu, P. D. (2011). Adenosine reduces GABAergic IPSC frequency via presynaptic A(1) receptors in hypothalamic paraventricular neurons projecting to rostral ventrolateral medulla. *Neurosci. Lett.* 490, 63–67. doi: 10.1016/j.neulet.2010.12.026

Hua, X. B. (1994). *Acupuncture Manual for Small Animals Experimental Acupuncture* (Shanghai: Shanghai Science and Technology Publisher), 269–290.

Ichinose, T. K., O'Leary, D. S., and Scislo, T. J. (2009). Activation of NTS A2a adenosine receptors differentially resets baroreflex control of renal vs. adrenal sympathetic nerve activity. *Am. J. Physiol.* 296, H1058–H1068. doi: 10.1152/ajpheart.00906.2008

Jiang, M., Zhang, C., Wang, J., Chen, J., Xia, C., Du, D., et al. (2011). Adenosine A(2A)R modulates cardiovascular function by activating ERK1/2 signal in the rostral ventrolateral medulla of acute myocardial ischemic rats. *Life Sci.* 89, 182–187. doi: 10.1016/j.lfs.2011.06.003

Li, M., Tjen-A-Looi, S. C., Guo, Z. L., and Longhurst, J. C. (2012). Repetitive electroacupuncture causes prolonged increased met-enkephalin expression in the rVLM of conscious rats. *Auton. Neurosci.* 170, 30–35. doi: 10.1016/j.autneu.2012.07.001

Li, M., Tjen-A-Looi, S. C., Guo, Z. L., and Longhurst, J. C. (2013). Electroacupuncture modulation of reflex hypertension in rats: role of cholecystokinin octapeptide. *Am. J. Physiol.* 305, R404–R413. doi: 10.1152/ajpregu.00196.2013

Li, M., Tjen-A-Looi, S. C., Guo, Z. L., and Longhurst, J. C. (2016). Repetitive electroacupuncture attenuates cold-induced hypertension through enkephalin in the rostral ventral lateral medulla. *Sci. Rep* 6:35791. doi: 10.1038/srep35791

Li, M., Tjen-A-Looi, S. C., and Longhurst, J. C. (2010). Electroacupuncture enhances preproenkephalin mRNA expression in rostral ventrolateral medulla of rats. *Neurosci. Lett.* 477, 61–65. doi: 10.1016/j.neulet.2010.04.025

Li, P., and Longhurst, J. C. (2010). Neural mechanism of electroacupuncture's hypotensive effects. *Auton. Neurosci.* 157, 24–30. doi: 10.1016/j.autneu.2010.03.015

Li, P., Rowshan, K., Crisostomo, M., Tjen-A-Looi, S. C., and Longhurst, J. C. (2002). Effect of electroacupuncture on pressor reflex during gastric distention. *Am. J. Physiol.* 283, R1335–R1345.

Li, P., Tjen-A-Looi, S. C., Cheng, L., Lui, D., Painovich, J., Vinjanury, S., et al. (2015). Long-lasting reduction of blood pressure by electroacupuncture in patients with hypertension: randomized controlled trial. *Med. Acupunct.* 27, 253–266. doi: 10.1089/acu.2015.1106

Li, P., Tjen-A-Looi, S. C., Guo, Z. L., Fu, L.-W., and Longhurst, J. C. (2009). Long-loop pathways in cardiovascular electroacupuncture responses. *J. Appl. Physiol.* 106, 620–630. doi: 10.1152/japplphysiol.91277.2008

Li, P., Tjen-A-Looi, S. C., and Longhurst, J. C. (2001). Rostral ventrolateral medullary opioid receptor subtypes in the inhibitory effect of electroacupuncture on reflex autonomic response in cats. *Auton. Neurosci.* 89, 38–47. doi: 10.1016/s1566-0702(01)00247-8

Longhurst, J. C., and Tjen-A-Looi, S. C. (2013). Acupuncture regulation of blood pressure: two decades of research. *Int. Rev. Neurobiol.* 111, 257–271. doi: 10.1016/B978-0-12-411545-3.00013-4

Moazzami, A., Tjen-A-Looi, S. C., Guo, Z.-L., and Longhurst, J. C. (2010). Serotonergic projection from nucleus raphe pallidus to rostral ventrolateral medulla modulates cardiovascular reflex responses during acupuncture. *J. Appl. Physiol.* 108, 1336–1346. doi: 10.1152/japplphysiol.00477.2009

Nassar, N., and bdel-Rahman, A. A. (2008). Brainstem phosphorylated extracellular signal-regulated kinase 1/2-nitric-oxide synthase signaling mediates the adenosine A2A-dependent hypotensive action of clonidine in conscious aortic barodenervated rats. *J. Pharmacol. Exp. Ther.* 324, 79–85. doi: 10.1124/jpet.107.129692

Nassar, N., and bdel-Rahman, A. A. (2009). Brainstem adenosine A1 receptor signaling masks phosphorylated extracellular signal-regulated kinase 1/2-dependent hypotensive action of clonidine in conscious normotensive rats. *J. Pharmacol. Exp. Ther.* 328, 83–89. doi: 10.1124/jpet.108.143883

Noble, F., and Cox, B. M. (1995). Differential regulation of D1 dopamine receptor- and of A2a adenosine receptor-stimulated adenylyl cyclase by mu-, delta 1-, and delta 2-opioid agonists in rat caudate putamen. *J. Neurochem.* 65, 125–133. doi: 10.1046/j.1471-4159.1995.65010125.x

Paxinos, G., and Watson, C. (2005). *The Rat Brain in Stereotaxic Coordinates*, 5th Edn. Cambridge, MA: Academic Press.

Ribeiro, J. A., Sebastiao, A. M., and de Mendonça, A. (2002). Adenosine receptors in the nervous system: pathophysiological implications. *Prog. Neurobiol.* 68, 377–392. doi: 10.1016/s0301-0082(02)00155-7

Scislo, T. J., and O'Leary, D. S. (2006). Adenosine receptors located in the NTS contribute to renal sympathoinhibition during hypotensive phase of severe hemorrhage in anesthetized rats. *Am. J. Physiol.* 291, H2453–H2461.

Spyer, K. M., Lambert, J. H., and Thomas, T. (1997). Central nervous system control of cardiovascular function: neural mechanisms and novel modulators. *Clin. Exp. Pharmacol. Physiol.* 24, 743–747. doi: 10.1111/j.1440-1681.1997.tb02125.x

St Lambert, J. H., Dashwood, M. R., and Spyer, K. M. (1996). Role of brainstem adenosine A1 receptors in the cardiovascular response to hypothalamic defence area stimulation in the anaesthetized rat. *Br. J. Pharmacol.* 117, 277–282. doi: 10.1111/j.1476-5381.1996.tb15187.x

St Lambert, J. H., Thomas, T., Burnstock, G., and Spyer, K. M. (1997). A source of adenosine involved in cardiovascular responses to defense area stimulation. *Am. J. Physiol.* 272, R195–R200. doi: 10.1111/j.1476-5381.1996.tb15187.x

Thomas, T., and Spyer, K. M. (1996). The role of adenosine receptors in the rostral ventrolateral medulla in the cardiovascular response to defence area stimulation in the rat. *Exp. Physiol.* 81, 67–77. doi: 10.1113/expphysiol.1996.sp003919

Thomas, T., and Spyer, K. M. (1999). A novel influence of adenosine on ongoing activity in rat rostral ventrolateral medulla. *Neuroscience* 88, 1213–1223. doi: 10.1016/s0306-4522(98)00296-6

Tjen-A-Looi, S. C., Guo, Z. L., Fu, L. W., and Longhurst, J. C. (2016). Paraventricular Nucleus Modulates Excitatory Cardiovascular Reflexes during Electroacupuncture. *Sci. Rep.* 6:25910. doi: 10.1038/srep25910

Tjen-A-Looi, S. C., Guo, Z. L., Li, M., and Longhurst, J. C. (2013). Medullary GABAergic mechanisms contribute to electroacupuncture modulation of cardiovascular depressor responses during gastric distention in rats. *Am. J. Physiol.* 304, R321–R332. doi: 10.1152/ajpregu.00451.2012

Tjen-A-Looi, S. C., Li, P., and Longhurst, J. C. (2004). Medullary substrate and differential cardiovascular response during stimulation of specific acupoints. *Am. J. Physiol.* 287, R852–R862.

Tjen-A-Looi, S. C., Li, P., and Longhurst, J. C. (2007). Role of medullary GABA, opioids, and nociceptin in prolonged inhibition of cardiovascular sympathoexcitatory reflexes during electroacupuncture in cats. *Am. J. Physiol.* 293, H3627–H3635.

Zhou, W., Fu, L.-W., Guo, Z. L., and Longhurst, J. C. (2007). Role of glutamate in rostral ventrolateral medulla in acupuncture-related modulation of visceral reflex sympathoexcitation. *Am. J. Physiol.* 292, H1868–H1875.

Zhou, W., Fu, L.-W., Tjen-A-Looi, S. C., Li, P., and Longhurst, J. C. (2005a). Afferent mechanisms underlying stimulation modality-related modulation of acupuncture-related cardiovascular responses. *J. Appl. Physiol.* 98, 872–880. doi: 10.1152/japplphysiol.01079.2004

Zhou, W., Tjen-A-Looi, S., and Longhurst, J. C. (2005b). Brain stem mechanisms underlying acupuncture modality-related modulation of cardiovascular responses in rats. *J. Appl. Physiol.* 99, 851–860. doi: 10.1152/japplphysiol.01365.2004

Conflict of Interest: The authors declare that the research was conducted in the absence of any commercial or financial relationships that could be construed as a potential conflict of interest.

frontiers in Physiology

REVIEW
published: 18 October 2019
doi: 10.3389/fphys.2019.01311

Mechanisms Responsible for Genetic Hypertension in Schlager BPH/2 Mice

Kristy L. Jackson[1], Geoffrey A. Head[1], Cindy Gueguen[1], Emily R. Stevenson[1], Kyungjoon Lim[1,2] and Francine Z. Marques[1,3]*

[1] Neuropharmacology Laboratory, Baker Heart and Diabetes Institute, Melbourne, VIC, Australia, [2] Department of Physiology, Anatomy and Microbiology, School of Life Sciences, La Trobe University, Melbourne, VIC, Australia, [3] Hypertension Research Laboratory, School of Biological Sciences, Monash University, Clayton, VIC, Australia

It has been 45 years since Gunther Schlager used a cross breeding program in mice to develop inbred strains with high, normal, and low blood pressure (BPH/2, BPN/3, and BPL/1 respectively). Thus, it is timely to gather together the studies that have characterized and explored the mechanisms associated with the hypertension to take stock of exactly what is known and what remains to be determined. Growing evidence supports the notion that the mechanism of hypertension in BPH/2 mice is predominantly neurogenic with some of the early studies showing aberrant brain noradrenaline levels in BPH/2 compared with BPN/3. Analysis of the adrenal gland using microarray suggested an association with the activity of the sympathetic nervous system. Indeed, in support of this, there is a larger depressor response to ganglion blockade, which reduced blood pressure in BPH/2 mice to the same level as BPN/3 mice. Greater renal tyrosine hydroxylase staining and greater renal noradrenaline levels in BPH/2 mice suggest sympathetic hyperinnervation of the kidney. Renal denervation markedly reduced the blood pressure in BPH/2 but not BPN/3 mice, confirming the importance of renal sympathetic nervous activity contributing to the hypertension. Further, there is an important contribution to the hypertension from miR-181a and renal renin in this strain. BPH/2 mice also display greater neuronal activity of amygdalo-hypothalamic cardiovascular regulatory regions. Lesions of the medial nucleus of the amygdala reduced the hypertension in BPH/2 mice and abolished the strain difference in the effect of ganglion blockade, suggesting a sympathetic mechanism. Further studies suggest that aberrant GABAergic inhibition may play a role since BPH/2 mice have low $GABA_A$ receptor δ, α4 and β2 subunit mRNA expression in the hypothalamus, which are predominantly involved in promoting tonic neuronal inhibition. Allopregnanolone, an allosteric modulator of $GABA_A$ receptors, which increase the expression of these subunits in the amygdala and hypothalamus, is shown to reduce the hypertension and sympathetic nervous system contribution in BPH/2 mice. Thus far, evidence suggests that BPH/2 mice have aberrant GABAergic inhibition, which drives neuronal overactivity within amygdalo-hypothalamic brain regions. This overactivity is responsible for the greater sympathetic contribution to the hypertension in BPH/2 mice, thus making this an ideal model of neurogenic hypertension.

Keywords: neurogenic hypertension, allopregnanolone, orexin, GABA receptor A, amygdala, hypothalamus, Schlager mice, sympathetic nervous system

OPEN ACCESS

Edited by:
Ovidiu Constantin Baltatu, Anhembi Morumbi University, Brazil

Reviewed by:
Brian James Morris, University of Sydney, Australia
Olaf Grisk, University of Greifswald, Germany

***Correspondence:**
Geoffrey A. Head
geoff.head@baker.edu.au

Specialty section:
This article was submitted to Integrative Physiology, a section of the journal Frontiers in Physiology

Received: *30 August 2019*
Accepted: *30 September 2019*
Published: *18 October 2019*

Citation:
Jackson KL, Head GA, Gueguen C, Stevenson ER, Lim K and Marques FZ (2019) Mechanisms Responsible for Genetic Hypertension in Schlager BPH/2 Mice. Front. Physiol. 10:1311. doi: 10.3389/fphys.2019.01311

INTRODUCTION

Experimental models of hypertension have been developed over the last half century and have made a major contribution to our understanding of the mechanisms underlying the development and treatment of hypertension. Of particular note here is the spontaneously hypertensive rat (SHR), the stroke-prone SHR from Japan, and other inbred strains such as the Milan (Bianchi et al., 1986) and Lyon strains (Sassolas et al., 1981). There are also a number of transgenic hypertensive rats such as those that have been encoded with the mouse renin gene, which results in hypertension (Sander et al., 1992). By contrast, there have been relatively few hypertensive mouse strains available for hypertension research that have been crossbred from normotensive mice. A frequently studied model is that developed by Gunther Schlager and colleagues in the early 1970s (Schlager, 1974). They established an inbred hypertensive strain of mice (BPH/2, Blood Pressure High) that has subsequently been studied in a wide range of investigations. These have described the phenotype, including genetics (Schlager, 1994; Marques et al., 2011a), cardiovascular function (McGuire et al., 2007; Davern et al., 2009), renal function (Rosenberg et al., 1982), behavior (Elias et al., 1975a), as well as involvement of the sympathetic (Davern et al., 2009; Jackson et al., 2013) and central nervous system (Jackson et al., 2014d). Thus, we have reached a point where we know a great deal about the mechanisms involved in producing the higher blood pressure (BP) in this mouse strain. What has become clear is the important contribution of the sympathetic nervous system (SNS) as well as the renal contribution that appears to involve a specific microRNA regulation of renin (Jackson et al., 2013). Importantly, these revelations are paralleled in the human form of hypertension (Marques et al., 2011c, 2015). Nevertheless, there is still a great deal to discover about these intriguing hypertensive mice. The present review aims to provide an overview of the literature published on BPH/2 mice, with a particular focus on the evidence that these mice represent a unique model of neurogenic hypertension.

DEVELOPMENT AND CARDIOVASCULAR CHARACTERISTICS

Genetically hypertensive mice are one of three lines of mice, namely BPL/1 (Blood Pressure Low), BPH/2, and BPN/3 (Blood Pressure Normal), which were concurrently selectively bred based on their BP (Schlager, 1974). It is worth noting that measuring BP in the 1970s in mice involved the tail-cuff technique that required restraining and heating the animals to 37° to determine systolic blood pressure (SBP) (Schlager, 1974). Thus, the target BP for breeding was in effect the level of BP reached during restraint stress, which is known to elevate BP by 30–40 mmHg and is therefore unlikely to be resting BP (Chen et al., 2009). The stable hypertensive phenotype in BPH/2 and hypotensive phenotype in BPL/1 mice were derived through a breeding program applying a two-way selection for high and low SBP respectively, using tail-cuff BP measurements (Schlager, 1974). The third line was randomly selected for breeding from the same base population and resulted in a normotensive (BPN/3) strain of mice. The basis for the cross breeding were eight different inbred strains to produce maximum genetic heterogeneity (C57BL/6J, SJL/J, LP/J, BALB/cJ, RF/J, 129/J, CBA/J, and BDP/J) (Schlager, 1974).

Hypertensive BPH/2 mice display higher BP than control lines from as young as 6 weeks of age, based on tail-cuff measurements (Schlager and Sides, 1997). SBP in BPH/2 mice can range from approximately 100 to 150 mmHg depending on the method of BP measurement (tail-cuff versus radio-telemetry), age (6–23 weeks old), and time of day (light versus dark period) (Schlager and Sides, 1997; Davern et al., 2009). Furthermore, SBP in male and female BPH/2 were found to be similar (Leckie, 2001). Regardless, a statistically and physiologically important and genetically determined difference in BP between the BPN/3 normotensive control mice compared with BPH/2 mice is always apparent. These characteristics give BPH/2 mice an advantage over experimentally or pharmacologically induced hypertensive models, which require extra interventions to initiate the hypertensive phenotype. Further, there can be a large difference between the degree of hypertension in males and females as in the case of Angiotensin II-induced hypertension (Xue et al., 2007).

The introduction of radio-telemetry measurement for mice was developed in 2000 (Kramer et al., 2000; Butz and Davisson, 2001) nearly a decade after implants for rats (Brockway et al., 1991). Continuous 24-h telemetry measurements confirmed the hypertension in adult BPH/2 compared with BPN/3 mice but the technique was not suitable to measure BP in mice weighing less than 17 g (~6–8 weeks old for BPH/2). At 15 weeks of age, the SBP was 24% and at 23 weeks 18% higher than that observed in BPN/3 mice (Davern et al., 2009). This compares surprisingly well to 24% higher SBP at 14–21 weeks of age as measured 30 years earlier by tail-cuff (Schlager et al., 1979). The BP varies during the 24-h period in mice, following a nocturnal pattern with the highest BP, heart rate (HR), and locomotor activity during the night when the mice are active, and lowest during the day when the mice are less active (Davern et al., 2009). A major characteristic of the BPH/2 strain is a markedly exaggerated day-night difference in BP, HR, and activity compared to the normotensive BPN/3 (Jackson et al., 2014b), C57/Bl6 (Davern et al., 2009), and hypertensive BPH/ApoE mice (**Figure 1**; Al-Sharea et al., 2019). This day-night difference was small and did not reach statistical significance in the first telemetry study with BPH/2 mice (McGuire et al., 2007) but has been observed in most if not all subsequent studies (Palma-Rigo et al., 2011; Davern et al., 2014; Jackson et al., 2014b,d, 2016; Stevenson et al., 2017; Gueguen et al., 2019; Watson et al., 2019). Reports of HR measured by the tail-cuff technique are variable as to whether BPH/2 mice are tachycardic (Schlager and Sides, 1997) or not (Schlager, 1974) but radio-telemetric measurement of HR under non-stressed conditions consistently shows that BPH/2 mice have higher HR than the normotensive BPN/3 mice (McGuire et al., 2007; Davern et al., 2009).

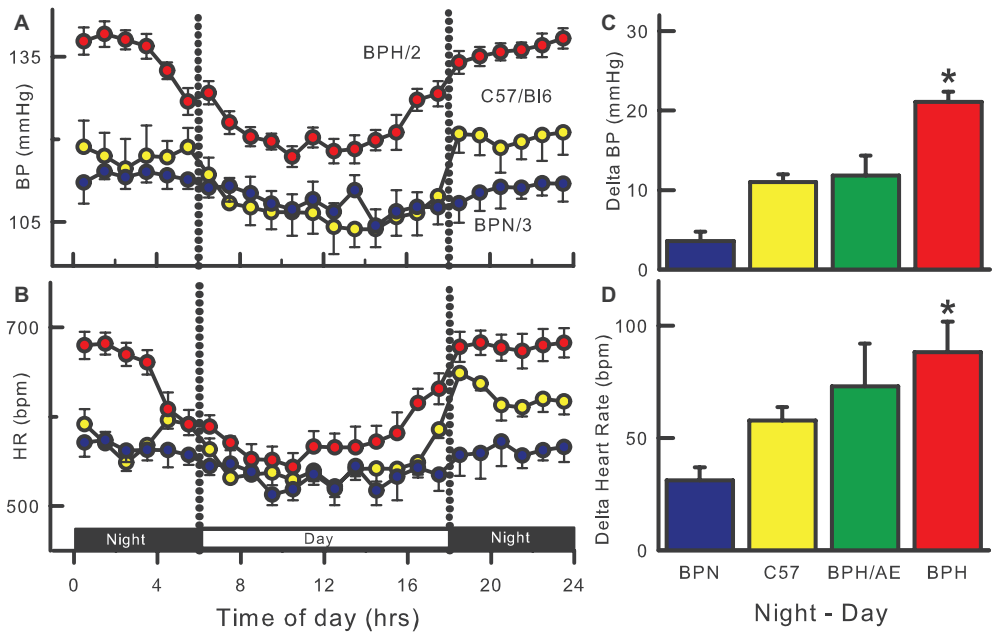

FIGURE 1 | Twenty-four-hour patterns of blood pressure (BP, **A**) and heart rate (HR, **B**) in BPH/2 (red), BPN/3 (blue), and C57/Bl6 (yellow) mice. Right histograms are the average day-night differences for each strain in BP **(C)** and HR **(D)** and also include a BPH/ApoE cross (green). Data adapted from Davern et al. (2009), Jackson et al. (2014b), Al-Sharea et al. (2019). *Indicates $p < 0.05$ between BPN/3 and BPH/2.

Response to Aversive or Non-aversive Stress

Davern and colleagues measured the cardiovascular response to a range of acute stressors in BPH/2 mice compared with BPN/3 mice (Davern et al., 2010b). These included aversive stressors of 5- or 60-min duration such as restraining mice in a plexi-glass tail-cuff restrainer and "shaker stress" which involved placing mice (in cages) on a rotating platform. Mice were also subject to the non-aversive "appetitive" stimulus of being presented with a piece of almond to eat, which produced a pressor response of approximately 20 mmHg, the same magnitude as aversive stressors in BPN/3 mice. The pressor response induced by appetitive stress was only 20% greater in BPH/2 mice whereas aversive stressors were 60–80% greater than in BPN/3 (Davern et al., 2010a,b). The exaggerated cardiovascular response to stress in BPH/2 mice may be due to greater perception of the stress or changes in the central pathways integrating the cardiovascular response. BPH/2 mice appear to be less anxious than controls, based on more frequent entry and greater duration spent in the open arms of an elevated plus/minus maze (Thifault et al., 2001). However, lower activity measurements in BPH/2 mice compared with BPN/3 mice in an open-field test suggest that under certain conditions, BPH/2 mice may be more anxious (Elias and Pentz, 1977). In behavioral terms, based on subjective observation of fighting, BPH/2 mice were reported to be more aggressive than control strains (Elias et al., 1975a). However, BPH/2 mice were shown to be less socially aggressive than control mice through a semi-quantitative assessment of social aggression based on time taken to attack and time spent in non-aggressive and aggressive social interaction toward other mice (Elias et al., 1975a). These inconsistencies in behavioral responses to environmental or socially stressful stimuli could further indicate abnormalities in anxiety and aggression which can be related to hypertension in humans (Perini et al., 1990). Yet the question still remains whether there are any environmental cues in the life of a laboratory mouse that contribute to development of hypertension in this model. This is likely to be a difficult question to answer given that hypertension is reportedly apparent at a very young age, when telemetric BP measurement is difficult to obtain. Furthermore, if stress is driving the hypertension, and since BPH/2 mice spontaneously develop hypertension without any deliberate external interventions such as chronic stress exposure, the stimuli that the BPH/2 mice may perceive as "stressful" would likely be those that are naturally occurring in the life of a laboratory mouse. Furthermore, since BPH/2 and BPN/3 mice are housed under comparable conditions, the same stimuli that lead to hypertension in BPH/2 mice could be considered relatively benign in BPN/3 mice, in that they would not usually lead to hypertension in BPN/3 mice.

SYMPATHETIC CONTRIBUTION TO THE HYPERTENSION IN BPH/2 MICE

The earliest indication that BPH/2 mice may have a neurogenic form of hypertension came from findings showing an inverse relationship between whole brain noradrenaline levels and BP in the three lines of mice (BPN/3, BPH/2, and BPL/1) (Schlager et al., 1979). However, dopamine levels in the brain were

similar between strains suggesting that the availability of this precursor of noradrenaline was not limiting the production of noradrenaline of BPH/2 mice (Buu et al., 1987). A more discrete assessment of central noradrenaline content revealed lower levels in the midbrain and cerebellum in BPH/2 compared with control mice, despite similar levels of noradrenaline in the hypothalamus and brainstem (Schlager et al., 1983; Buu et al., 1987). As such, strain differences in brain noradrenaline levels are unlikely to be caused by a global abnormality of noradrenaline metabolism because noradrenaline content was not consistently low throughout the whole brain. Further evidence of a central mechanism came from observations that higher brain cytochrome oxidase staining (an indicator of neuronal activity) and greater acute BP response to nicotine occurred in BPH/2 (Schlager and Freeman, 1983; Backer and Schlager, 1984; Denoroy et al., 1985; Strazielle et al., 2004). An important confirmation of the contribution of the SNS to hypertension in BPH/2 mice has only been demonstrated in the last decade, initiated by the finding that ganglion blockade abolished the hypertension in BPH/2 mice, ultimately reducing BP to levels comparable with normotensive BPN/3 control mice (Davern et al., 2009). Furthermore, even when the depressor response to ganglion blockade was represented as a percentage of baseline, the response was still greater in BPH/2 compared with BPN/3 normotensive controls (Davern et al., 2009), unlike findings in SHR where the percentage reduction by hexamethonium was the same as the control normotensive strain (Touw et al., 1980). A similar 23% reduction in BP was observed with the central sympatholytic drug α-methyldopa in both SHR and normotensive Wistar rats (Head and de Jong, 1986). Thus, the BPH/2 differs from the SHR in being more dependent on the SNS for hypertension. Greater SNS activity in BPH/2 was also supported by a greater mid-frequency BP power, which is an indirect indicator of vasomotor SNS activity, in BPH/2 compared with BPN/3 mice (Davern et al., 2009). Using ganglion blockade with prior angiotensin-converting-enzyme (ACE) inhibitor pretreatment, the SNS contribution to BP was 1.7-fold greater in BPH/2 mice compared with BPN/3 mice during both light (inactive) and dark (active) periods (Jackson et al., 2013). Importantly, the contribution of the SNS to BP did show typical circadian fluctuations, with the SNS excitation peaking during the active period in both strains. This suggests that the cause of the hypertension is likely to be 24-h overactivity of the SNS (tonic component) but there is still an overlying circadian pattern with the SNS activity being greatest (in all mice) during the active period (phasic component). Greater tyrosine hydroxylase staining in the kidney of BPH/2 mice also indicated sympathetic hyperinnervation (Jackson et al., 2013) which has been seen in other models of hypertension such as SHR (Cassis et al., 1985). More recently, renal noradrenaline levels were reported to be markedly greater in BPH/2 compared with BPN/3 mice and bilateral renal denervation was shown to reduce the hypertension by one-third in BPH/2 mice without affecting BP in BPN/3 mice (Gueguen et al., 2019). Interestingly, the hypotensive response may also involve the renin-angiotensin system (RAS) since the enhanced renin mRNA levels in BPH/2 mice were normalized following renal denervation (Gueguen et al., 2019). Overall, greater sympathetic drive to the kidneys and possibly more generally, contribute largely to the hypertension in BPH/2 mice.

BRAIN REGIONS INVOLVED IN MEDIATING THE HYPERTENSION IN BPH/2 MICE

Amygdalo-Hypothalamic Pathway Contribution to Hypertension in BPH/2 Mice

The amygdala integrates sensory (e.g., olfactory) and cognitive information to initiate behavioral responses to specific stimuli during aversive psychological and physiological stress as well as reproductive stimuli. In addition, a major pathway for sympathetic activation involves projections from the amygdala to the anterior hypothalamus, the dorsomedial hypothalamus (DMH), and the ventromedial hypothalamus (VMH) (Choi et al., 2005). These projections are glutamatergic and GABAergic (Choi et al., 2005). Davern and Head suggested that forebrain regions including the medial amygdala (MeAm) may be responsible for driving the hypertension in BPH/2 mice (Davern and Head, 2011). Indeed, marked differences in neuronal activity were observed between BPH/2 and BPN/3 mice in different brain regions before and after the surge in BP that occurs during the onset of the dark (active) period. In particular, Davern and colleagues showed that the number of neurons expressing c-Fos, a protein marker of recent neuronal activation (Li and Dampney, 1992), in the DMH, the paraventricular hypothalamus (PVN), the central amygdala, and the MeAm of BPH/2 mice was markedly greater compared with BPN/3 mice (Davern et al., 2009). Interestingly, the authors reported that the MeAm was the only region to display greater c-Fos stained neurons in both the light (inactive) and dark (active) periods in BPH/2 compared with BPN/3 mice. Furthermore, neuronal activity within the MeAm of BPN/3 and BPH/2 mice strongly correlated with BP and also with the decrease in BP caused by ganglion blockade (Davern et al., 2009). Taken together, these findings suggest that greater neuronal activity in the MeAm of BPH/2 mice may lead to elevations in BP *via* influences on the SNS.

The MeAm was also one of the brain regions with greater c-Fos containing neurons in BPH/2 mice compared with BPN/3 mice following exposure to 1 h of dirty cage switch stress (Davern et al., 2010a). This involved placing a mouse in a previously occupied cage and after an hour, greater c-Fos stained neurons were observed in the CeAm, DMH, PVN, and rostro-ventrolateral medulla (RVLM) (Davern et al., 2010a). Using c-Fos-immunohistochemistry, the MeAm can be readily observed as playing a major role in regulating stress (Cullinan et al., 1995; Beckett et al., 1997; Dayas et al., 2001; Dielenberg et al., 2001; Porter and Hayward, 2011). Moreover, this region is particularly important for integration of olfactory and chemosensory signaling involved in predator and territorial responses and reproduction

(Dielenberg et al., 2001; Samuelsen and Meredith, 2009). Although Dielenberg and colleagues identified that predominantly psychological stressors activated the MeAm, it was interesting to note that physiological stressors such as hemorrhage also selectively activated the CeAm (Dielenberg et al., 2001). However, greater levels of c-Fos-staining is not the only indication that the MeAm is involved in regulating the response to stress. Many studies using lesions, electrical or pharmacological stimulation or inhibition have supported the view that the MeAm plays a key role in mediating the cardiovascular, hormonal, and behavioral responses to stress (Han et al., 1996; Kubo et al., 2004; Herdade et al., 2006; Fortaleza et al., 2009, 2012; Solomon et al., 2010; Vinkers et al., 2010).

Effect of Lesions of the Medial Amygdala

The idea that the amygdala contributes to hypertension is not new and was shown to be important to the development of hypertension in SHR, based on the antihypertensive effect of electrolytic lesions of the amygdala (Folkow et al., 1982). Fukumori and colleagues showed that the MeAm region in particular influences hypertension in SHR as excitotoxic lesions created in the MeAm of SHR at 4 weeks of age attenuated the development of hypertension by 14–16 weeks of age (Fukumori et al., 2004). A normotensive strain was not included as a control in this study, and so drawing conclusions about the contribution of the MeAm to hypertension as opposed to BP maintenance is problematic.

Microinjections into the MeAm with ibotenic acid, which ablates cell bodies but not fibers of passage, resulted in a hypotensive effect that abolished 64% of the hypertension in BPH/2 but had no effect in BPN/3 (Jackson et al., 2014d). MeAm lesions also decreased the depressor response to ganglion blockade as well as the mid-frequency BP power in BPH/2 mice, suggesting the lesions had a sympatholytic effect. The hypotensive effect of the lesions was similar during the dark (active) and light (inactive) periods suggesting that the MeAm has a tonic influence on BP in BPH/2 but not in normotensive animals. Intriguingly, despite MeAm lesions lowering BP in BPH/2 mice, lesions had little effect on the exaggerated cardiovascular response to stressors in these mice, suggesting that established hypertension is independent of the exaggerated cardiovascular response to stress.

Rostro-Ventrolateral Medulla Contribution to Hypertension in BPH/2 Mice

Premotor sympathetic neurons within the RVLM are important for regulating sympathetic vasomotor tone (Dampney et al., 1982; Horiuchi and Dampney, 1998) and have been implicated in many models of hypertension including renovascular, Goldblatt, L-NAME–induced, and SHR models (Muratani et al., 1993; Bergamaschi et al., 1995, 1999; Matsuura et al., 2002). Intriguingly, assessment of two different markers of neuronal activity, c-Fos and cytochrome oxidase staining, indicated that RVLM neuronal activity was similar in BPN/3 and BPH/2 mice (Strazielle et al., 2004; Davern et al., 2009). SHRs are known to be responsive to centrally acting sympatholytic drugs such as rilmenidine, which act predominantly at the level of the RVLM (Sannajust et al., 1989; Mayorov et al., 2001; Zhang and Abdel-Rahman, 2002). A comprehensive study administering rilmenidine to BPH/2 mice *via* multiple routes (i.p., i.c.v., s.c., p.o.) and for a range of durations (30 min to 2 weeks) revealed that the sympathetic vasomotor inhibitory effect of rilmenidine is minimal and similar in hypertensive BPH/2 and normotensive BPN/3 mice (Jackson et al., 2014c). Rilmenidine administered acutely (i.p.) did cause a greater depressor and marked bradycardic effect in BPH/2 compared with BPN/3 mice. By contrast, pre-treatment with atropine (a muscarinic receptor antagonist) prior to rilmenidine actually abolished any difference between the two strains, ultimately revealing that the difference between them was due to vagal excitatory effects of rilmenidine, and the sympatholytic effects were comparable in BPH/2 and BPN/3 mice (Jackson et al., 2014c). Furthermore, chronic administration of rilmenidine, where the vagal excitatory effects are known to be less prominent (Godwin et al., 1998; Parkin et al., 2003), showed only minor and similar reductions in BP between the strains (Jackson et al., 2014c). Together, the lack of neuronal activity differences between strains and lack of responsiveness to rilmenidine suggest that the RVLM is not a major driver of the sympathetically mediated hypertension in BPH/2 mice. Thus, if the RVLM, which is a major premotor sympatho-regulatory brain region, is not playing a major role in hypertension, it is possible that the greater sympathetic outflow may be mediated *via* sympathetic premotor neurons other than those located in the RVLM. In this context, the PVN, which is a region that contains sympathetic premotor neurons that project directly to sympathetic preganglionic neurons in the spinal cord (Strack et al., 1989), could be a nucleus of interest as it has been shown to be highly activated during the dark active period in BPH/2 mice (Davern et al., 2009).

MOLECULAR CONTRIBUTIONS TO HYPERTENSION IN BPH/2 MICE

Wright and colleagues performed the first genome-wide scan in F2 intercrosses of BPH/2 and BPL/1 mice as well as backcrosses revealed significant linkage on chromosome 10 and 13 with suggestive linkages on chromosomes 2, 6, 8, and 18. Exactly what micro-satellite polymorphisms are distinguishing high- and low-BP mice has not as yet been discovered (Wright et al., 1999). The earliest examination using genome-wide microarray analysis from adrenal tissue was designed to identify genes whose difference in expression contributes to hypertension in the Schlager BPH/2 mice and used the BPL/1 strain for comparison rather than the normotensive strain (Fries et al., 2004). This may be an issue if the genes differently expressed in the low-BP strain compared to normotensive mice are different to those differentially expressed in the strain with high BP. It should also be remembered that 1) the differential expression of particular genes may contribute directly to the condition, or 2) that differential expression may be a secondary response to a primary difference in expression of other gene(s), or 3) the

differential expression may be a compensatory response to the BP elevation or another phenotypic difference between each mouse strain. Using a systems biology approach, Fries and colleagues found differences in pathways associated with the SNS activity, oxidative stress, and also carbohydrate metabolism (Fries et al., 2004). A later comparison of BPH/2 to SHR showed that the concentration of enzymes responsible for noradrenaline and adrenaline synthesis, tyrosine hydroxylase, and phenylethanolamine N-methyltransferase were greater in BPH/2 mice but normal in SHR. This suggests species differences in the contribution of the SNS to the hypertension. This is, however, consistent with the differential effects of ganglionic blockade mentioned earlier. Specifically, this treatment abolished the difference in BP between the BPH/2 and BPN/3, but in rats, the difference in BP between SHR and the normotensive rats remained after ganglion blockade. By contrast, the activity of oxidative stress pathways is elevated in both hypertensive strains of the two species (Friese et al., 2005). More recently, an integrated combination of transcriptomics, bioinformatics, and molecular biology of the BPH/2 compared to the BPL/1 strain led the investigators to suggest that from the differential expression analysis, *HOXA3*, *SRY,* and transcriptional factor *Yy1* might predict BP in humans. Further analysis of human population indicated that a single nucleotide polymorphism of *Yy1* was associated with BP, body mass index, and fasting glucose. They suggested this gene as the strongest candidate influencing hypertension and metabolic syndrome (Friese et al., 2012).

Puig and colleagues examined liver, heart, kidney, and vessels from all three of the Schlager strains using microarray analysis of 38,000 transcripts (Puig et al., 2010). A number of genes known to be involved in BP regulation were differentially expressed between the strains, one of these genes being the natriuretic peptide receptor gene *Npr1*. Since expression of *Npr1* is upregulated in hypertension, it is likely countering the effects of hypertension (Puig et al., 2010). The chemokine receptor gene *Ccr5* and the gene for arachidonic acid metabolic enzyme *Cyp2j2* were also found to be differentially expressed and have been implicated in hypertension (Puig et al., 2010). A later microarray analysis of kidney tissue by Chiu and colleagues compared expression in male and female BPH/2 with male and female normotensive BPN/3 (Chiu et al., 2014). Several genes were differentially expressed and associated with hypertension. One was angiopoietin-like 7, which may reflect increased vascular pressure in the kidney. Others were *Hdc* and *Cndp2,* which are associated with histamine metabolism and possibly sympathetic activity or inflammation (Chiu et al., 2014). A gene associated with vascular aging, *Edn3*, was also differentially expressed as were the DNA maintenance genes, *Mcm6 and Dna2*, which are involved in telomere length maintenance. A further analysis revealed that BPH/2 mice have shorter telomeres, but this occurs after hypertension is established and is a consequence rather than a cause of the hypertension (Chiu et al., 2016). Other bio-informatic analyses of the Chiu et al. dataset have been made by Gao et al. (2017) and further novel uses of meta-genome data have suggested transcriptome networks associated with hypertension, so providing scope for new therapeutic targets (Zubcevic et al., 2017). A more recent transcriptome analysis of cardiac endothelial cells suggested that differences between prehypertensive and hypertensive adult BPH/2 mice are related to fibrosis (Nelson et al., 2018). While endothelial dysfunction is known in the BPH/2 strain, no differences in the endothelial genes associated with the nitric oxide pathway were detected. However, expression of the PPARα pathway genes was reduced. These genes encode proteins thought to be protective against the damage from hypertension-induced oxidative stress (Nelson et al., 2018). Interestingly, the authors found that treating BPH/2 mice with antihypertensive drugs such as losartan or the calcium channel blocker amlodipine reversed the expression pattern of some genes but not others. Such interventions should help discriminate between the effect of hypertension itself on gene expression as opposed to effects arising from strain differences.

While the earlier microarray studies of Fries and colleagues suggested a contribution of the SNS to the hypertension in the BPH/2 mice, most other studies concentrated on peripheral organs such as adrenal, liver, blood vessels, heart, and kidney. While the kidney is well known to contribute to a number of forms of hypertension, it is surprising that there have been few studies examining the central nervous system (CNS). A major study by Marques and colleagues used microarray and quantitative real-time polymerase chain reaction (qPCR) of the hypothalamus of young and adult BPH/2 and BPN/3 mice (Marques et al., 2011a). This work revealed an elevation in the expression of genes implicated in oxidative stress and inflammation in BPH/2 mice as well as higher expression of hypocretin (Orexin) and the neuropeptide S receptor (Npsr1). Hypocretin neurons display synaptic plasticity in response to overnight fasting (Horvath and Gao, 2005) while Npsr1 administration can reduce the anxiety-like behavior in mice associated with open field, elevated plus maze, light-dark box, and marble burying (Okamura and Reinscheid, 2007). A further study of the genes that might contribute to the exaggerated nocturnal differences in BP in BPH/2 was conducted and revealed 212 differentially expressed genes including those for vasopressin, oxytocin, and thyrotropin-releasing hormone (Marques et al., 2011b). Although not highlighted in these analyses, there were also differences in expression of a number of type A gamma-aminobutyric acid (GABA) receptor ($GABA_AR$) subunits in the hypothalamus of BPH/2 compared to BPN/3 (Marques et al., 2011a,b). This has prompted further research into the possible contribution of $GABA_AR$ to neurogenic hypertension – in particular in the BPH/2 strain (Davern et al., 2014).

NEUROPEPTIDE AND NEUROSTEROID CONTRIBUTION TO HYPERTENSION IN BPH/2 MICE

Gamma-Aminobutyric Acid Receptors

The $GABA_AR$ is a heteromeric pentamer made up of five of 19 currently known subunits arranged in a combination of two α, two β, and a third (γ, δ, ϵ, ρ, or θ) subunit all

arranged around a chloride conducting central pore. The combination of subunits gives rise to the vast number of structurally unique $GABA_AR$, which contributes to its diverse functionality. The amygdalo-hypothalamic pathway contributes to hypertension in both BPH/2 mice and SHR and may involve a common mechanism leading to increased sympathetic vasomotor tone. Combining the microarray finding of altered $GABA_AR$ subunit expression in the hypothalamus with the lower levels of $GABA_AR$ in the hypothalamus and amygdala of SHR (Kunkler and Hwang, 1995), we suggested that inadequate GABAergic inhibitory signaling may contribute to the higher activity in the pre-sympathetic pathways leading to the hypertension in BPH/2 (Davern et al., 2014). A lack of GABAergic inhibition of the MeAm in BPH/2 mice would be expected to result in tonic hyperactivity of these neurons and activation of hypothalamic autonomic influences. Patterns of expression of the different subunits of $GABA_AR$ indicate that the δ, α4, β2 subunits are underexpressed in BPH/2 hypothalamus while α2, γ1, α5, θ and ε subunits are more highly expressed in BPH/2 compared to BPN/3 (**Figure 2**; Marques et al., 2011a).

Effect of the Benzodiazepine Diazepam

It is well known that benzodiazepines such as diazepam can modulate $GABA_AR$ activity by binding to an allosteric site on the receptor (Bormann, 1991). Chronic administration of diazepam in drinking water reduced BP of the BPN/3 mice but had no effect on the BP of BPH/2 mice (Davern et al., 2014). We used triple labeling immunohistochemistry to show that neurons in the hypothalamus and amygdala of diazepam-treated BPH/2 mice that had been activated by restraint stress (contained c-Fos protein in the nucleus) also contain $GABA_AR$. By contrast, neurons activated by restraint stress in the same regions of diazepam-treated BPN/3 mice did not label for $GABA_AR$. Presumably this is because they were inhibited by the diazepam treatment unlike those of BPH/2 mice, which did not respond to diazepam. The inability of diazepam to be effective in BPH/2 may have allowed greater activity within the neurons of the amygdala and the hypothalamus (Davern et al., 2014). Thus, there appears to be a fundamental difference between the $GABA_AR$ in the two strains that respond to benzodiazepines. The benzodiazepine binding socket in the $GABA_AR$ involves the α1, α2, α3, α5, and γ2 subunits (Benson et al., 1998) and, of these, only the α2 subunit was differentially expressed between BPH/2 (higher) and BPN/3 (lower expression).

Effect of the Neurosteroid Allopregnanolone on BPH Hypertension

The reduced expression of the δ, α4, and β2 subunits in the hypothalamus of the BPH/2 compared with BPN/3 mice (**Figure 2**) is a key finding as these are also the same combination of subunits common to extrasynaptic $GABA_AR$ (Smith et al., 2007) that are responsible for tonic GABAergic inhibition in the brain (Farrant and Nusser, 2005). In the rat thalamus, all δ subunits co-exist with an α4 subunit (Sur et al., 1999). The δ, α4, and β2-$GABA_AR$ have a high affinity for GABA, which means they sense its ambient levels of GABA in the extrasynaptic space and provide a background level of inhibition (Farrant and Nusser, 2005). These receptors are also more resistant to desensitization (Farrant and Nusser, 2005). The δ, α4, and β2-$GABA_AR$ are the most sensitive to modulation from allopregnanolone-like neurosteroids. Allopregnanolone can be synthesized in glia in the CNS from cholesterol *via* a pathway involving initial transport to the mitochondria and conversion by cytochrome P450 to pregnenolone, which is converted to progesterone and 5α-dihydroprogesterone and finally to allopregnanolone (**Figure 3**; Farrant and Nusser, 2005). The effect of allopregnanolone on δ-$GABA_AR$ is an allosteric modulation of chloride currents by enhancing chloride channel opening time and potentiating inhibition (Hosie et al., 2006). There is potentiation and direct activation (**Figure 3**). Most critically, treatment with allopregnanolone or its precursor, progesterone, can increase the expression of the exact subunits that are reduced in BPH/2, namely the α4 and δ subunits, through transcriptional and post-transcription effects (**Figure 3**; Gulinello et al., 2001). Thus, treatment with allopregnanolone may alter subunit composition of $GABA_AR$ in a manner that promotes GABAergic inhibition and thus increases tonic inhibition in the brain. Patients and animal models of chronic stress, anxiety disorders, or depression have lower levels of allopregnanolone than controls (Serra et al., 2000; Rasmusson et al., 2006).

Thus, we hypothesized that the lower levels of expression of the δ, β2, and α4 subunits of $GABA_AR$ in BPH/2 may provide insufficient tonic inhibition of sympatho-excitatory neurons in the amygdala and hypothalamus and therefore these hypertensive mice might respond to allopregnanolone. Treatment of adult Schlager mice with 200 μg/kg/h of allopregnanolone (s.c.) reduced BP by 40% in BPH/2 after 14 days with no effect in BPN/3 mice (Stevenson et al., 2017). Lower doses of allopregnanolone and shorter treatment duration (1 week) were ineffective on BPH/2 hypertension suggesting

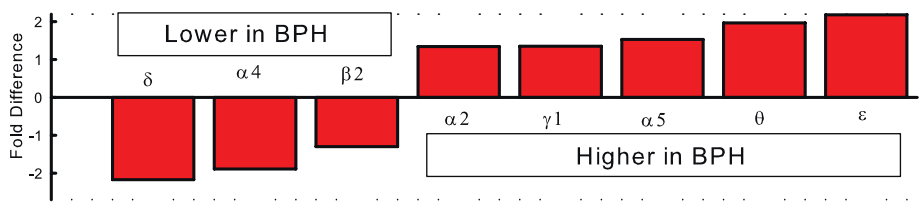

FIGURE 2 | Fold differences in $GABA_AR$ subunit expression in the hypothalamus of BPH/2 compared to BPN/3 mice (Marques et al., 2011a,b).

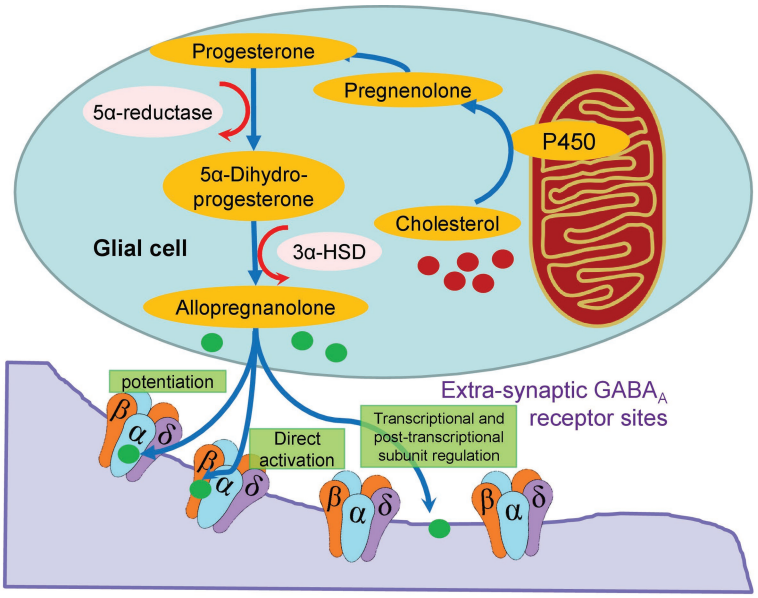

FIGURE 3 | Schema showing the intracellular synthesis of allopregnanolone in glia from cholesterol and the direct and indirect action of the neurosteroid on extracellular $GABA_AR$. The latter involves potentiation and transcription and post-transcriptional subunit regulation.

that transcriptional changes to subunit composition of $GABA_AR$ were required rather than a direct activation or potentiating of the neurosteroid (Stevenson et al., 2017). We also observed a reduction in the depressor response to pentolinium in BPH/2 and not in BPN/3, indicating less sympathetic contribution to BP. Allopregnanolone had no effect on mouse activity or anxiety levels suggesting that the BP changes are not secondary to behavioral effects (Stevenson et al., 2017). The low dose suggests that the particular $GABA_AR$ involved has a high affinity for allopregnanolone with effective doses well below those that induce sedation or even anxiolysis (Deo et al., 2010). This is consistent with the high affinity characteristics of the extra-synaptic δ-containing $GABA_AR$. Both the pressor response to dirty cage swap stress and the elevation in neuronal activity observed in the MeAm and PVN of BPH/2 mice were reduced or abolished following treatment with allopregnanolone (Stevenson et al., 2017). These findings suggest that the MeAm and the PVN are likely major sites of action of allopregnanolone. While we observed a substantial reduction in BP in the BPH/2 mice, the hypertension was not abolished, suggesting other mechanisms may also contribute to the elevated BP in these mice.

Orexin

Orexin is a neuropeptide known for its role in regulating feeding, stress, and arousal but importantly it is also able to regulate BP, HR, and sympathetic activity (Sakurai, 2005; Carrive, 2013; Inutsuka and Yamanaka, 2013). Orexin/hypocretin was initially identified as a potential contributor to the hypertension in BPH/2 mice based on a study showing that BPH/2 mice have at least 2-fold higher *hcrt* mRNA in the hypothalamus than BPN/3 mice (Marques et al., 2011a). Furthermore, BPH/2 mice were shown to have almost 30% more orexinergic neurons than BPN/3 mice (Jackson et al., 2016). To determine whether this augmented orexin level actually contributes to the hypertension in BPH/2 mice, almorexant, a dual orexin receptor antagonist, was administered to BPH/2 mice (Jackson et al., 2016). Almorexant caused a marked reduction in BP in BPH/2 mice during the dark (active) period but had no effect in the BPN/3 mice, whereas during the light (inactive) period, there was no reduction from baseline in either strain (Jackson et al., 2016). While a portion of the hypotensive effect of almorexant was due to a concurrent reduction in locomotor activity, part of the hypertension could still be attributed to an activity-independent reduction in BP (Jackson et al., 2016). Furthermore, the reduction in BP during the dark period in BPH/2 mice was associated with a reduction in depressor response to ganglion blockade and mid-frequency BP power, both suggesting almorexant reduced SNS activity. Orexin is known to contribute to hypertension in at least two other models of hypertension including SHR and stress-induced hypertension, but does not appear to regulate basal BP maintenance in normotensive animals (Lee et al., 2013; Li et al., 2013; Xiao et al., 2013).

Renin-Angiotensin System in BPH/2 Mice

The renin-angiotensin system (RAS) has been explored in a variety of ways in BPH/2 mice including genetic investigations, analysis of expression or activity of RAS components, and pharmacological assessment of the RAS contribution to BP. Yet, delineating the contribution of the RAS to the hypertension in BPH/2 mice has proven quite complex. Angiotensin II (AngII) is an important effector hormone, being part of the RAS, which is well known to contribute to BP regulation by

influencing dipsogenic and sodium appetitive responses, vasopressin release, and importantly sympathetic vasomotor tone (Keil et al., 1975; Head, 1996; Fitzsimons, 1998). In 2001, Leckie described a larger depressor effect of the ACE inhibitor captopril in BPH/2 mice (Leckie, 2001), but plasma renin levels and renin enzyme activity were reportedly similar among BPN/3, BPH/2, and BPL/1 mice (Iwao et al., 1984). However, there are conflicting findings with regard to renin activity in the submandibular glands of BPH/2 mice, regarding whether it is comparable with BPN/3 mice or greater in BPH/2 mice (Iwao et al., 1984; Uddin et al., 2003a; Uddin and Harris-Nelson, 2004). Additionally, lower angiotensin I in the submandibular gland is hypothesized to reflect a faster rate of conversion to AngII but this has not been verified (Uddin and Harris-Nelson, 2004). Gene array of the liver, heart, and aorta reveals no strain difference in expression of any major components of the RAS (Puig et al., 2010). However, there is a 1.3-fold greater expression of ACE specifically in the kidney of BPH/2 mice compared with BPN/3 mice, suggesting tissue-specific RAS differences may be apparent (Puig et al., 2010). The differences in expression or activity of the RAS could be due to differences in the state of the animal immediately prior to collection of tissue, as RAS activity is subject to changes in state such as sleep, wakefulness, and stress (Jindra and Kvetnansky, 1982; Brandenberger et al., 1994).

Using a large dose of losartan for 14 days [150 mg/kg/day, angiotensin II type 1 receptor (AT_1R) antagonist], Palma-Rigo and colleagues found little difference between the hypertension induced by the drug in both strains, which was in the order of 23–25 mmHg (Palma-Rigo et al., 2011). This study assessed potential interaction between the SNS and the RAS in BPH/2 mice, whereby the effect of ganglion blockade was assessed before and during chronic AT_1R inhibition (Palma-Rigo et al., 2011). The findings suggest that there was no interaction between the RAS and SNS in BPH/2 mice that might contribute to the hypertension. However, high doses of losartan were administered, which likely inhibited both the central and peripheral RAS. If the central and peripheral RAS contributions to hypertension of BPH/2 were in opposite directions, the high dose of losartan that blocked both would not necessarily reveal these subtle differences.

Contribution From Renal Renin-Angiotensin System and Influence of MicroRNA-181a

When an acute treatment with the ACE inhibitor enalaprilat was given in the active period, it produced a small hypotensive effect in BPH/2 but no effect in BPN/3 (Jackson et al., 2013). One limitation of using an ACE inhibitor to assess the contribution of AngII to hypertension in BPH/2 mice is that ACE inhibitors also reduce the degradation of bradykinin, which itself could have a vasodilatory effect. However, the vasorelaxation caused by bradykinin was previously shown to be markedly reduced in BPH/2 compared with BPN/3 mice (McGuire et al., 2007). During the active period when enalaprilat produced hypotension, there was also a 1.6-fold greater expression of the renin gene and lesser abundance of the microRNA microRNA-181a (miR-181a). Interestingly, the hypotension from enalaprilat and the difference in renin and miR-181a expression were not observed during the inactive period (Jackson et al., 2013). MiR-181a has been shown previously to bind to the 3′ untranslated region and to regulate renin mRNA in humans and is reciprocally expressed with respect to renin in kidneys of hypertensive subjects compared to normotensive mice (Marques et al., 2011c, 2015). Thus, when renin expression levels are high in hypertensive compared to normotensive mice, miR-181a levels are the opposite (Marques et al., 2015). Likewise, in BPH/2 mice, miR-181a was downregulated specifically during the active period in BPH/2 mice, corresponding to the time when RAS activity was greatest. While miR-181a negatively regulates renin mRNA levels, it is unknown what regulates miR-181a. The possibility that miR-181a might be regulated by the SNS was suggested by a correlation between the depressor response to ganglion blockade with renal abundance of miR-181a (Jackson et al., 2013). BPH/2 mice also have greater renal sympathetic innervation density as identified by tyrosine hydroxylase staining of cortical tubules (Jackson et al., 2013) which is where in human, miR-181a is expressed (Marques et al., 2015). Also, renal denervation reduced the higher renal expression of the renin gene and lowered renal renin levels but had no effect on plasma renin concentrations (Gueguen et al., 2019). In a preliminary abstract report, BPH/2 mice treated with a miR-181a mimic had a reduced level of hypertension and normalized levels of renal renin expression (Jackson et al., 2014a). Injection of such miR-181a mimetics *in vivo* has previously been effectively used to restore low levels of miR-181b in the vasculature of mice (Sun et al., 2012).

The mechanism by which peripheral AngII increases BP in BPH/2 mice has not been assessed and could be produced by anti-natriuretic or vasoconstrictive effects. Alternatively, circulating AngII could even potentially facilitate the augmented SNS in BPH/2 mice. However, the finding that pretreatment with an ACE inhibitor did not attenuate the exaggerated depressor response to ganglion blockade suggests that there is no overt facilitation of the SNS by the peripheral RAS in BPH/2 mice (Jackson et al., 2013). Direct vasoconstrictive effects of AngII are likely to contribute to elevated BP in BPH/2 mice. This is supported by a preliminary abstract report showing that AngII causes greater vasoconstriction in BPH/2 mice using myography (Jelinic et al., 2018). It is also possible that renal sympathetic hyperinnervation and increased AngII levels result in increased anti-natriuretic effects in BPH/2 mice. Rosenberg and colleagues measured glomerular filtration rate in mature BPH/2 mice and while it tended to be lower than in BPN/3 mice, this did not reach significance (Rosenberg et al., 1985). Furthermore, BPH/2 mice are reportedly not salt sensitive (Leckie, 2001). Total body water as a percentage of body weight is comparable in BPH/2 and BPN/3 mice, indicating that volume expansion due to greater retention of water was unlikely to contribute to the hypertension (Jackson et al., 2014b). Thus, greater anti-natriuretic effects of RSNA or AngII do not seem to be likely mechanisms causing hypertension in BPH/2 mice.

Central Renin-Angiotensin System Contribution to Hypertension in BPH/2

In addition to the peripheral RAS, a separate renin-angiotensin system within the CNS has been reported to contribute to the hypertension of animal models including SHR, phenol renal injury hypertension model, and cold-induced hypertension (Huang and Leenen, 1996; Ito et al., 2002; Sun et al., 2002; Ye et al., 2002). Circulating AngII can affect the CNS by acting on AT_1R in areas such as the circumventricular organs that do not have a blood-brain barrier. Since it has been suggested that there is an apparent overactivity of the peripheral RAS, which was based on the greater acute depressor response to ACE inhibition (Jackson et al., 2013), assessment of the role of the central RAS was pertinent. Gene array analysis of the hypothalamus in BPH/2 mice did not identify any major differences in the expression of components of the brain RAS, to suggest that there are inherent abnormalities in BPH/2 mice compared with BPN/3 controls (Marques et al., 2011a,b). However, this does not necessarily refute the possibility that central RAS signaling could contribute to hypertension in BPH/2 mice, as is the case in other models of hypertension (Muratani et al., 1993; Campese et al., 2000).

The suggestion that augmented central AngII stimulation of AT_1R may contribute to the hypertension in BPH/2 mice was recently examined. Surprisingly, the activity of central AT_1Rs appears to contribute equally or less to BP regulation in BPH/2 mice (Jackson et al., 2018). This was based on a study which administered AT_1R antagonists (i.c.v.) both acutely and chronically in BPH/2 and BPN/3 mice. Acute administration of candesartan actually produced a lesser depressor response in BPH/2 mice compared with BPN/3 mice during the dark (active) period, whereas the response was comparable between strains in the light (inactive) period (Jackson et al., 2018). Subcutaneously infused losartan for 2 weeks produced the same small hypotensive effect as centrally infused losartan, suggesting that the central AT_1R contribution to BP is not evident in BPH/2 mice. Reactive oxygen species (ROS) such as superoxide can be second messengers for AngII-mediated signaling in the brain (Zimmerman et al., 2002; Chan et al., 2005); therefore, the contribution of central ROS to hypertension in BPH/2 mice was also assessed. When the ROS scavenger tempol and the superoxide dismutase (SOD) mimetic resveratrol were administered (i.c.v.), the acute cardiovascular response was comparable between BPN/3 and BPH/2 mice, suggesting that central ROS is unlikely to play a role in the hypertension (Jackson et al., 2018). Taken together, these findings indicate that a generalized overactivity of the central AT_1R-ROS signaling is not driving the hypertension in BPH/2 mice. However, due to the intricacies of AngII signaling in the brain, this study cannot completely exclude a role for the central RAS in discrete regions, which would require a more targeted approach. It is interesting to note that the greater contribution of the peripheral RAS distinctly contrasts the lesser contribution of central AT_1R activity to hypertension in BPH/2 mice during this dark (active) period (Jackson et al., 2013, 2018). Exposure to high levels of circulating AngII in rabbits for longer than a few days has previously been shown to result in desensitization of neurons to AngII activation in circumventricular organs and sensitization in hypothalamic regions (Davern and Head, 2007). Furthermore, circulating AngII is also shown to influence brain AT_1R expression, in a site-specific manner (Thomas and Sernia, 1985). It would be interesting to investigate whether greater circulating AngII in BPH/2 mice could also potentially lead to downregulation of AT_1Rs centrally, which may account for the smaller depressor response induced by candesartan (i.c.v.) in BPH/2 mice. Nonetheless, it seems that in contrast to the peripheral RAS, overactivity of the central RAS does not contribute to the hypertension in BPH/2 mice.

HEART, VESSEL, AND KIDNEY STRUCTURE AND FUNCTION

Despite being hypertensive from a relatively young age, BPH/2 mice do not have greater absolute heart weight nor left ventricle weight compared with normotensive BPN/3 mice (Schlager et al., 1979; Schlager and Sides, 1997). However, the body weight of BPH/2 mice was lower than BPN/3 mice, so when expressed as HW:BW ratio, there was a tendency for this measure to be greater in BPH/2 mice (Schlager and Sides, 1997) and normotensive C57Bl/6 mice (Elias et al., 1975b). Thus, a degree of cardiac hypertrophy is apparent in BPH/2 mice but it appears to be mild. Interestingly, a later transcriptome analysis of cardiac endothelial cells revealed greater expression of fibrosis-related genes in BPH/2 mice, some of which could be reversed by antihypertensive treatment (Nelson et al., 2018).

To date, the impact of hypertension on the structure of the vasculature has only been assessed in cerebral arterioles. Baumbach and colleagues reported that BPH/2 mice exhibit cerebral arteriole hypertrophy but no reduction in external diameter (remodeling) such as that seen in other models of hypertension (Baumbach et al., 2003). This is supported by a preliminary abstract reporting hypertrophic inward remodeling in mesenteric arteries of BPH/2 mice (Jelinic et al., 2018). Recently, BPH/2 have been shown to develop retinal disease, with a thinner neural structure and complete loss by 21 weeks of age of the outer layers of the retina including the plexiform, nuclear, and photoreceptive layers (Herat et al., 2020). Functionally, BPH/2 mice are reported to have endothelial dysfunction in small caliber arteries, demonstrated by a 25–50% reduction in maximal vasorelaxation in response to acetylcholine and bradykinin (McGuire et al., 2007). Using Doppler ultrasound, BPH/2 have been shown to have impaired endothelium-dependent dilatation in femoral arteries (Nelson et al., 2018). A comprehensive myographical examination of arteries from different vascular beds of BPH/2 and BPN/3 found that the arteries from the hypertensive mice have greater myogenic tone and impaired relaxation despite having similar passive qualities (Tajada et al., 2012). In the same study using electrophysiology techniques, the authors found a decreased contribution of potassium ATP-dependent channels, which was also consistent with the findings of lower expression of some potassium channels including Kir2.1 and Kir4.1 (Tajada et al., 2012). Thus, there was a good correlation between the changes

in excitability, the electrophysiological/pharmacological assessment of the contribution of potassium channels, and the molecular expression of specific channels in this study (Tajada et al., 2012).

Hypertensive BPH/2 mice are reported to release double the amount of hydrogen peroxide from the aorta compared with BPN/3, which may indicate a greater level of oxidative stress (Uddin et al., 2003b). Measurement of oxidants and antioxidants in the aorta showed that this may be attributable to elevated SOD activity and reduced catalase activity leading to greater production of hydrogen peroxide and decreased catalase-mediated conversion of hydrogen peroxide to water (Uddin et al., 2003b). Different expression of canonical transient receptor potential (TRPC) 3 channels and of hetero-multimeric TRPC channels may also contribute to differences in vascular tone in the BPH/2 mice (Alvarez-Miguel et al., 2017).

Hypertensive BPH/2 mice have similar kidney-to-body weight ratio as BPN/3 (Schlager et al., 1979) but have fewer nephrons per kidney (Rosenberg et al., 1982). Morphometric analysis of kidneys from older BPH/2 mice showed none of the characteristic features of renal parenchymal pathology (Rosenberg et al., 1979) indicating that major morphological differences in the kidney are not likely driving the hypertension. However, the available filtration surface area in juxtamedullary glomeruli in BPH/2 mice is less than half that of BPN/3 mice while the superficial cortical glomeruli were comparable between strains (Rosenberg et al., 1982). By contrast, it is the superficial glomeruli in BPH/2 mice that show reduced permeability of the basement membrane compared with BPN/3 mice but not the juxtamedullary glomeruli. Theoretically, reduced filtration surface and permeability could lead to decreased glomerular filtration rate, volume expansion, and hypertension (Rosenberg, 1983). However, glomerular filtration rate was shown to be less in juvenile BPH/2 mice than in mature BPH/2 mice (Rosenberg et al., 1985). Yet, both normotensive and hypertensive mice have comparable glomerular number until about 7 weeks of age. Glomerular number then plateaus in BPH/2 mice, which have markedly fewer glomeruli in adulthood compared with BPN/3 mice. Total body water, used as a measure of volume expansion, was also greater in younger BPH/2 mice than BPN/3 but this trend reversed with age and resulted in a lower total body water in older mice (Rosenberg et al., 1985). When a comparison is made between glomerular number and total body volume, it is noticeable that total body volume only starts to decrease toward normal levels after glomerular number becomes lower in the BPH/2 mice. Additionally, BPH/2 mice are not salt sensitive, suggesting natriuresis is not impaired (Leckie, 2001).

METABOLIC ABNORMALITIES IN BPH/2 MICE

An important phenotypic difference observed in BPH/2 mice is that their body weight is lower compared with BPN/3 mice (Rosenberg et al., 1982; Buu et al., 1987). However, hypotensive BPL/1 mice also have lower body weight than BPN/3 mice suggesting that this attribute is not likely to be associated with the hypertension (Rosenberg et al., 1979). Early studies suggested that water intake of female BPH/2 mice was 20% greater than the normotensive strain but if offered a choice, they preferred solutions of lower NaCl or KCl concentration (Bachmanov et al., 1998). The higher water intake was not observed in a later metabolic study of male mice in which it was 11% higher in BPH/2 mice, but the difference was not significant due to the small n value (Jackson et al., 2014b). Hypertensive BPH/2 mice are also markedly more active compared with BPN/3 mice, particularly during the dark phase of the daily light cycle, as shown by radio-telemetric measurement of locomotor activity (McGuire et al., 2007; Davern et al., 2009). While locomotor activity is positively associated with BP, hyperactivity alone is unlikely to contribute to the elevated BP. This is because analysis of covariance showed that elevated BP in BPH/2 mice compared with BPN/3 mice was independent of locomotor activity (Davern et al., 2009). Furthermore, normotensive C57Bl6 mice also have a similar level of activity as BPH/2 mice, indicating hyperactivity is not only apparent in hypertensive mice (Davern et al., 2009). Metabolic rate was greater in young BPH/2 compared to the normotensive control strain BPN/3 mice but was similar to normotensive C57Bl6 strain. When the activity of the mice was considered, there were no differences in energy metabolism per se (Jackson et al., 2014b). Also percentage lean mass was similar in young and older BPH/2 and BPN/3 suggesting that differences in body weight were due to lower fat mass in the more active BHP/2 (Jackson et al., 2014b).

The lower fat mass may also contribute to why hypertensive BPH/2 mice are less capable of thermoregulation than BPN/3 mice, as indicated by a greater rate of rise of body temperature, higher end temperature, and shorter time until death following exposure to 43°C heat (Malo et al., 1989). These differences may also indicate that thermoregulation may be abnormal in BPH/2 mice. However, the validity of these findings is questionable owing to exposure to heat taking place while the mice were anesthetized, causing thermoregulatory impairment (Kurz, 2001). However, Malo and colleagues also found that long-term (40 days) acute (5 min per day) exposure to 40°C heat could reversibly reduce the BP in BPH/2 mice by 20 mmHg, which was not due to the direct vasodilatory effect of the heat (Malo et al., 1990). One hypothesized cause of abnormal thermoregulation in BPH/2 mice is greater production of heat shock protein 70 (HSP70), which is overexpressed in the kidney of BPH/2 compared with BPN/3 mice following heat stress (Hamet et al., 1990). This suggests that BPH/2 mice may have abnormal cellular response to stress. However, it is also possible that central thermoregulatory control mechanisms may be different in BPH/2 mice. Indeed orexin, a central hormone known to be involved in thermoregulatory control, is overexpressed in hypothalamic tissue of BPH/2 mice as mentioned earlier (Marques et al., 2011a,b). Moreover, orexin is also involved in BP control, stress, sympathetic activity, and energy metabolism (Shirasaka et al., 1999, 2002; Szekely et al., 2002; Furlong et al., 2009), making it a potential mediator of many of the phenotypic abnormalities in these mice. Taken together, there are numerous metabolic abnormalities in BPH/2 mice

and while some abnormalities such as thermoregulation appear to be related to BP, others such as locomotor activity appear to be independent of hypertension (Davern et al., 2009).

BPH/2 MICE AND PREGNANCY, ATHEROSCLEROSIS, AND DIABETES

An additional subline of mice produced by Schlager and colleagues is the BPH/5 strain. Compared with C57Bl6 mice, this strain has moderately elevated BP, which is increased further during pregnancy (Davisson et al., 2002). As such, the BPH/5 strain has been used extensively as a model of pre-eclampsia (Butz and Davisson, 2001; Davisson et al., 2002; Cross, 2003; Dokras et al., 2006; Hoffmann et al., 2008). Treatment with the superoxide scavenger tempol during gestation improved fetal outcome and offspring survival and reduced the level of BP rise during pregnancy (Hoffmann et al., 2008). BPH/5 mice normally have half the number of pups than normotensive mice due to reabsorption of placentas, which was reduced by half with tempol (Hoffmann et al., 2008). The higher oxidative stress in mothers is consistent with many of the microarray studies that showed elevated expression of oxidative-stress-related markers in the BPH/2 mice (see above). Additionally, BPH/5J mice have greater adiposity, greater circulating leptin levels and leptin resistance, as indicated by the blunted effect of leptin on food intake and body weight (Sutton et al., 2017). Leptin resistance is a phenomenon also associated with sympathetically mediated BP elevations in other animal models (Prior et al., 2010, 2014); so leptin resistance may also contribute to the hypertension in this strain.

A more recent cross of BPH/2 with the apolipoprotein E-deficient mouse (APoE) was developed to examine the interaction between hypertension associated with high SNS activity with an atherosclerotic-prone mouse (Al-Sharea et al., 2019). These mice when fed a western diet developed unstable atheromatous plaques, the formation of which was independent of endothelial dysfunction. There were reduced levels of key hematopoietic stem and progenitor cells as well as sinusoidal endothelial cells and osteoblasts (Al-Sharea et al., 2019). Interestingly, all these effects could be reversed by a non-selective β-blocker propranolol.

Watson and colleagues recently examined the effect of streptozotocin-induced diabetes in the BPH/2 and BPN/3 strains (Watson et al., 2019). While diabetes did not change the degree of hypertension, the albuminuria was 3-fold higher in diabetic BPH/2 mice. This was most likely due to the hypertensive mice having greater levels of renal noradrenaline and dopamine and when combined with diabetes-induced abnormalities in levels of metabolic enzymes and impairment in antioxidant systems, produced greater overall oxidative stress (Watson et al., 2019).

PERSPECTIVE

The development of the strains of hypertensive mice by Gunther Schlager and colleagues in the 1970s has led to a comprehensive examination of mechanisms of hypertension. This led to the discovery that the hypertension is principally related to chronic activation of the SNS and as such is one of the few true models of neurogenic hypertension (**Figure 4A**). Our own research has revealed that a major mechanism involves $GABA_AR$ dysfunction within the CNS and most likely within the amygdala and hypothalamus (**Figure 4C**). Neurosteroids such as allopregnanolone offer a possible new opportunity to treat the neurogenic contribution to human hypertension. Importantly, the site of action is quite distinct from that of benzodiazepines like diazepam (**Figure 4C**). Exciting new discoveries that orexin systems are also involved come from the selective antihypertensive effect of the orexin receptor antagonist almorexant (**Figure 4C**).

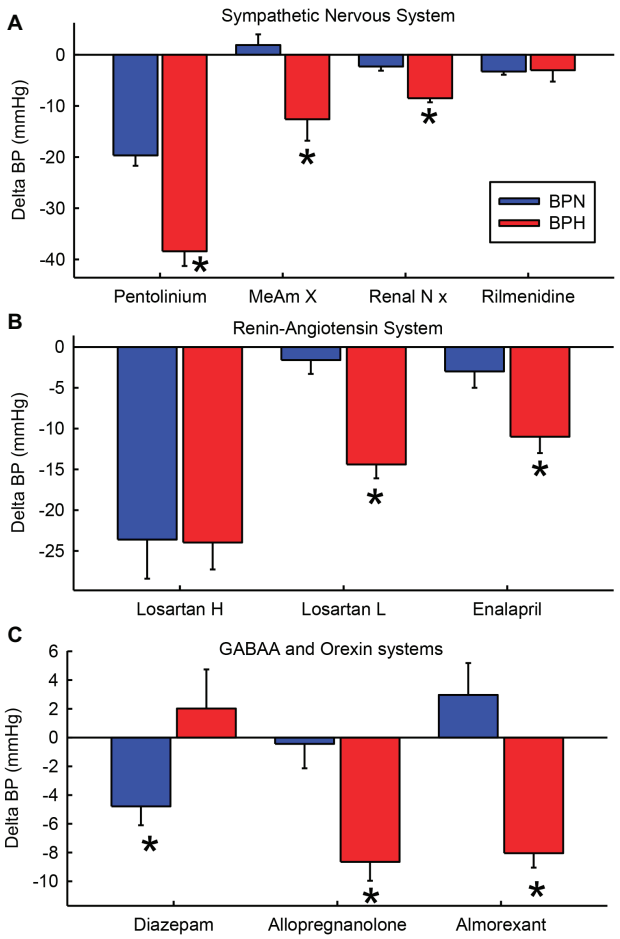

FIGURE 4 | Average change in blood pressure (BP) after treatments that affect the sympathetic nervous system **(A)**, the renin-angiotensin system and kidney **(B)** and GABAA and orexin systems **(C)** in BPN/3 (blue) and BPH/2 (red) mice. Treatments are pentolinium (Davern et al., 2009), medial amygdala lesions [MeAm X (Jackson et al., 2014d)], renal nerve denervation [Renal N x (Gueguen et al., 2019)], rilmenidine (Jackson et al., 2014c), high-dose Losartan [Losartan H 150 mg/kg/day (Palma-Rigo et al., 2011)], low-dose Losartan [Losartan L, 8 mg/kg/day (Jackson et al., 2018)], enalaprilat [1.5 mg/kg (Jackson et al., 2013)], diazepam [2.5 mg/kg/day orally for 7 days (Davern et al., 2014)], allopregnanolone [s.c. 5 mg/kg/day for 14 days (Stevenson et al., 2017)], almorexant [30 mg/kg i.p. (Jackson et al., 2016)]. *Indicates $p < 0.05$ between strains.

However, despite some evidence from animal models of hypertension, the role of limbic brain regions seems to be relatively unrecognized in human hypertension. The currently available centrally acting antihypertensive agents such as moxonidine or rilmenidine act predominantly in the brainstem and this is where interest seems to have remained in the clinical setting. However, these drugs are ineffective in BPH/2 (**Figure 4A**).

To date, the evidence for the involvement of limbic regions in human essential hypertension is limited to indirect associations. For instance, using blood-oxygen-level-dependent functional magnetic resonance imaging, greater amygdala activity is associated with greater BP reactivity to stress, which in turn is associated with greater risk of developing hypertension (Ming et al., 2004; Gianaros et al., 2008). Importantly, the Schlager strains have led us to understand that the SNS also influences mechanisms within the kidney, controlling renin, the vasculature and oxidative stress as well as other systems including the immune system and metabolic effects. Low doses of RAS blockers are much more effective in BPH/2 than in BPN/3 mice as is renal denervation, suggesting an important interaction between the brain and the kidney (**Figure 4B**). Thus, hypertension is one manifestation of SNS overactivity but the interactions of the SNS with other systems have far-reaching implications. The data may have implications for the effects of psychosocial stress on health generally.

AUTHOR CONTRIBUTIONS

All authors contributed to the drafting, editing and finalizing of the review.

FUNDING

This work was supported by grants from the National Health & Medical Research Council of Australia (NHMRC) (project grant 1065714) and in part by the Victorian Government's OIS Program. Investigators were supported by a NHMRC/National Heart Foundation Postdoctoral Fellowship (1052659 and PF12M6785 to FM), NHMRC Early Career Fellowship (1091688 to KJ, 1053928 to KL), and NHMRC Principal Research Fellowship (1002186 to GH).

ACKNOWLEDGMENTS

We acknowledge the contributions to the work described in this review of members of our laboratory Pamela Davern, Beza Abegaz, John-Louis Moretti, Thu-Phuc Nguyen-Huu, and Kesia Palma-Rigo.

REFERENCES

Al-Sharea, A., Lee, M., Whillas, A., Michell, D., Shihata, W., Nicholls, A. J., et al. (2019). Chronic sympathetic driven hypertension promotes atherosclerosis by enhancing hematopoiesis. *Haematologica* 104, 456–467. doi: 10.3324/haematol.2018.192898

Alvarez-Miguel, I., Cidad, P., Perez-Garcia, M. T., and Lopez-Lopez, J. R. (2017). Differences in TRPC3 and TRPC6 channels assembly in mesenteric vascular smooth muscle cells in essential hypertension. *J. Physiol.* 595, 1497–1513. doi: 10.1113/JP273327

Bachmanov, A. A., Schlager, G., Tordoff, M. G., and Beauchamp, G. K. (1998). Consumption of electrolytes and quinine by mouse strains with different blood pressures. *Physiol. Behav.* 64, 323–330. doi: 10.1016/S0031-9384(98)00069-9

Backer, L. C., and Schlager, G. (1984). The effect of nicotine on blood pressure in the genetically hypertensive mouse. *Experientia* 40, 1363–1364. doi: 10.1007/BF01951890

Baumbach, G. L., Sigmund, C. D., and Faraci, F. M. (2003). Cerebral arteriolar structure in mice overexpressing human renin and angiotensinogen. *Hypertension* 41, 50–55. doi: 10.1161/01.HYP.0000042427.05390.5C

Beckett, S. R., Duxon, M. S., Aspley, S., and Marsden, C. A. (1997). Central c-fos expression following 20kHz/ultrasound induced defence behaviour in the rat. *Brain Res. Bull.* 42, 421–426. doi: 10.1016/S0361-9230(96)00332-2

Benson, J. A., Low, K., Keist, R., Mohler, H., and Rudolph, U. (1998). Pharmacology of recombinant gamma-aminobutyric acidA receptors rendered diazepam-insensitive by point-mutated alpha-subunits. *FEBS Lett.* 431, 400–404. doi: 10.1016/S0014-5793(98)00803-5

Bergamaschi, C. T., Campos, R. R., and Lopes, O. U. (1999). Rostral ventrolateral medulla - a source of sympathetic activation in rats subjected to long-term treatment with L- NAME. *Hypertension* 34, 744–747. doi: 10.1161/01.HYP.34.4.744

Bergamaschi, C., Campos, R. R., Schor, N., and Lopes, O. U. (1995). Role of the rostral ventrolateral medulla in maintenance of blood pressure in rats with Goldblatt hypertension. *Hypertension* 26, 1117–1120. doi: 10.1161/01.HYP.26.6.1117

Bianchi, G., Ferrari, P., Salvati, P., Salardi, S., Parenti, P., Cusi, D., et al. (1986). A renal abnormality in the Milan hypertensive strain of rats and in humans predisposed to essential hypertension. *J. Hypertens. Suppl.* 4, S33–S36.

Bormann, J. (1991). Electrophysiological characterization of diazepam binding inhibitor (DBI) on GABAA receptors. *Neuropharmacology* 30, 1387–1389. doi: 10.1016/S0028-3908(11)80006-7

Brandenberger, G., Follenius, M., Goichot, B., Saini, J., Spiegel, K., Ehrhart, J., et al. (1994). Twenty-four-hour profiles of plasma renin activity in relation to the sleep-wake cycle. *J. Hypertens.* 12, 277–283

Brockway, B. P., Mills, P. A., and Azar, S. H. (1991). A new method for continuous chronic measurement and recording of blood pressure, heart rate and activity in the rat *via* radio-telemetry. *Clin. Exp. Hypertens.* 13, 885–895.

Butz, G. M., and Davisson, R. L. (2001). Long-term telemetric measurement of cardiovascular parameters in awake mice: a physiological genomics tool. *Physiol. Genomics* 5, 89–97. doi: 10.1152/physiolgenomics.2001.5.2.89

Buu, N. T., Duhaime, J., Racz, K., Kuchel, O., and Schlager, G. (1987). L-dopa metabolism in genetically hypertensive mice: effect of pargyline. *Can. J. Physiol. Pharmacol.* 65, 2390–2395. doi: 10.1139/y87-379

Campese, V. M., Ye, S., Truong, R. H., and Gamburd, M. (2000). Losartan reduces sympathetic nerve outflow from the brain of rats with chronic renal failure. *J. Renin-Angiotensin-Aldosterone Syst.* 1, 202–208. doi: 10.3317/jraas.2000.026

Carrive, P. (2013). Orexin, orexin receptor antagonists and central cardiovascular control. *Front. Neurosci.* 7:257. doi: 10.3389/fnins.2013.00257

Cassis, L. A., Stitzel, R. E., and Head, R. J. (1985). Hypernoradrenergic innervation of the caudal artery of the spontaneously hypertensive rat: an influence upon neuroeffector mechanisms. *J. Pharmacol. Exp. Ther.* 234, 792–803

Chan, S. H., Hsu, K. S., Huang, C. C., Wang, L. L., Ou, C. C., and Chan, J. Y. (2005). NADPH oxidase-derived superoxide anion mediates angiotensin II-induced pressor effect *via* activation of p38 mitogen-activated protein kinase in the rostral ventrolateral medulla. *Circ. Res.* 97, 772–780. doi: 10.1161/01.RES.0000185804.79157.C0

Chen, D., La Greca, L., Head, G. A., Walther, T., and Mayorov, D. (2009). Blood pressure reactivity to emotional stress is reduced in AT(1A)-receptor knockout mice on normal, but not high salt intake. *Hypertens. Res.* 32, 559–564. doi: 10.1038/hr.2009.59

Chiu, C. L., Hearn, N., Paine, D., Steiner, N., and Lind, J. (2016). Does telomere shortening precede the onset of hypertension in spontaneously hypertensive mice? *Twin Res. Hum. Genet.* 19, 422–429. doi: 10.1017/thg.2016.63

Chiu, C., Jackson, K., Hearn, N., Steiner, N., Head, G., and Lind, J. (2014). Identification of genes with altered expression in male and female Schlager hypertensive mice. *BMC Med. Genet.* 15, 101–107. doi: 10.1186/s12881-014-0101-x

Choi, G. B., Dong, H. W., Murphy, A. J., Valenzuela, D. M., Yancopoulos, G. D., Swanson, L. W., et al. (2005). Lhx6 delineates a pathway mediating innate reproductive behaviors from the amygdala to the hypothalamus. *Neuron* 46, 647–660. doi: 10.1016/j.neuron.2005.04.011

Cross, J. C. (2003). The genetics of pre-eclampsia: a feto-placental or maternal problem? *Clin. Genet.* 64, 96–103. doi: 10.1034/j.1399-0004.2003.00127.x

Cullinan, W. E., Herman, J. P., Battaglia, D. F., Akil, H., and Watson, S. J. (1995). Pattern and time course of immediate early gene expression in rat brain following acute stress. *Neuroscience* 64, 477–505. doi: 10.1016/0306-4522(94)00355-9

Dampney, R. A. L., Goodchild, A. K., Robertson, L. G., and Montgomery, W. (1982). Role of ventrolateral medulla in vasomotor regulation: a correlative anatomical and physiological study. *Brain Res.* 249, 223–235. doi: 10.1016/0006-8993(82)90056-7

Davern, P. J., Chowdhury, S., Jackson, K. L., Nguyen-Huu, T.-P., and Head, G. A. (2014). $GABA_A$ receptor dysfunction contributes to high blood pressure and exaggerated response to stress in schlager genetically hypertensive mice. *J. Hypertens.* 32, 352–362. doi: 10.1097/HJH.0000000000000015

Davern, P. J., and Head, G. A. (2007). Fos-related antigen immunoreactivity after acute and chronic angiotensin II-induced hypertension in the rabbit brain. *Hypertension* 49, 1170–1177. doi: 10.1161/HYPERTENSIONAHA.106.086322

Davern, P. J., and Head, G. A. (2011). Role of the medial amygdala in mediating responses to aversive stimuli leading to hypertension. *Clin. Exp. Pharmacol. Physiol.* 38, 136–143. doi: 10.1111/j.1440-1681.2010.05413.x

Davern, P. J., Jackson, K. L., Nguyen-Huu, T., La Greca, L., and Head, G. A. (2010a). Cardiovascular reactivity and neuronal activation to stress in Schlager genetically hypertensive mice. *Neuroscience* 170, 551–558. doi: 10.1016/j.neuroscience.2010.07.040

Davern, P. J., Jackson, K. L., Nguyen-Huu, T., La Greca, L., and Head, G. A. (2010b). Cardiovascular responses to aversive and non-aversive stressors in Schlager genetically hypertensive mice. *Am. J. Hypertens.* 23, 838–844. doi: 10.1038/ajh.2010.69

Davern, P. J., Nguyen-Huu, T., La Greca, L., and Head, G. A. (2009). Role of the sympathetic nervous system in Schlager genetically hypertensive mice. *Hypertension* 54, 852–859. doi: 10.1161/HYPERTENSIONAHA.109.136069

Davisson, R. L., Hoffmann, D. S., Butz, G. M., Aldape, G., Schlager, G., Merrill, D. C., et al. (2002). Discovery of a spontaneous genetic mouse model of preeclampsia. *Hypertension* 39, 337–342. doi: 10.1161/hy02t2.102904

Dayas, C. V., Buller, K. M., and Day, T. A. (2001). Medullary neurones regulate hypothalamic corticotropin- releasing factor cell responses to an emotional stressor. *Neuroscience* 105, 707–719. doi: 10.1016/S0306-4522(01)00213-5

Denoroy, L., Sautel, M., Schlager, G., Sacquet, J., and Sassard, J. (1985). Catecholamine concentrations in discrete brain nuclei and sympathetic tissues of genetically hypertensive mice. *Brain Res.* 340, 148–150. doi: 10.1016/0006-8993(85)90784-X

Deo, G. S., Dandekar, M. P., Upadhya, M. A., Kokare, D. M., and Subhedar, N. K. (2010). Neuropeptide Y Y1 receptors in the central nucleus of amygdala mediate the anxiolytic-like effect of allopregnanolone in mice: behavioral and immunocytochemical evidences. *Brain Res.* 1318, 77–86. doi: 10.1016/j.brainres.2009.12.088

Dielenberg, R. A., Hunt, G. E., and McGregor, I. S. (2001). "when a rat smells a cat": the distribution of Fos immunoreactivity in rat brain following exposure to a predatory odor. *Neuroscience* 104, 1085–1097. doi: 10.1016/S0306-4522(01)00150-6

Dokras, A., Hoffmann, D. S., Eastvold, J. S., Kienzle, M. F., Gruman, L. M., Kirby, P. A., et al. (2006). Severe feto-placental abnormalities precede the onset of hypertension and proteinuria in a mouse model of preeclampsia. *Biol. Reprod.* 75, 899–907. doi: 10.1095/biolreprod.106.053603

Elias, J. W., Elias, M. F., and Schlager, G. (1975a). Aggressive social interaction in mice genetically selected for blood pressure extremes. *Behav. Biol.* 13, 155–166.

Elias, M. F., and Pentz, C. A. III. (1977). Blood pressure extremes and activity in aging mice. *Physiol. Behav.* 19, 811–813. doi: 10.1016/0031-9384(77)90320-1

Elias, M. F., Sorrentino, R. N., Pentz, C. A. III., and Florini, J. R. (1975b). "Spontaneously" hypertensive mice: a potential genetic model for the study of the relationship between heart size and blood pressure. *Exp. Aging Res.* 1, 251–265.

Farrant, M., and Nusser, Z. (2005). Variations on an inhibitory theme: phasic and tonic activation of GABA(A) receptors. *Nat. Rev. Neurosci.* 6, 215–229. doi: 10.1038/nrn1625

Fitzsimons, J. T. (1998). Angiotensin, thirst, and sodium appetite. *Physiol. Rev.* 78, 583–686. doi: 10.1152/physrev.1998.78.3.583

Folkow, B., Hallback-Nordlander, M., Martner, J., and Nordborg, C. (1982). Influence of amygdala lesions on cardiovascular responses to alerting stimuli, on behaviour and on blood pressure development in spontaneously hypertensive rats. *Acta Physiol. Scand.* 116, 133–139. doi: 10.1111/j.1748-1716.1982.tb07121.x

Fortaleza, E. A., Scopinho, A. A., and de Aguiar Correa, F. M. (2012). Alpha1 and alpha2-adrenoceptors in the medial amygdaloid nucleus modulate differently the cardiovascular responses to restraint stress in rats. *Pharmacol. Res.* 66, 154–162. doi: 10.1016/j.phrs.2012.04.004

Fortaleza, E. A., Tavares, R. F., and Correa, F. M. (2009). The medial amygdaloid nucleus modulates cardiovascular responses to acute restraint in rats. *Neuroscience* 159, 717–726. doi: 10.1016/j.neuroscience.2009.01.003

Fries, R. S., Mahboubi, P., Mahapatra, N. R., Mahata, S. K., Schork, N. J., Schmid-Schoenbein, G. W., et al. (2004). Neuroendocrine transcriptome in genetic hypertension: multiple changes in diverse adrenal physiological systems. *Hypertension* 43, 1301–1311. doi: 10.1161/01.HYP.0000127708.96195.e6

Friese, R. S., Mahboubi, P., Mahapatra, N. R., Mahata, S. K., Schork, N. J., Schmid-Schonbein, G. W., et al. (2005). Common genetic mechanisms of blood pressure elevation in two independent rodent models of human essential hypertension. *Am. J. Hypertens.* 18, 633–652. doi: 10.1016/j.amjhyper.2004.11.037

Friese, R. S., Ye, C., Nievergelt, C. M., Schork, A. J., Mahapatra, N. R., Rao, F., et al. (2012). Integrated computational and experimental analysis of the neuroendocrine transcriptome in genetic hypertension identifies novel control points for the cardiometabolic syndrome. *Circ. Cardiovasc. Genet.* 5, 430–440. doi: 10.1161/CIRCGENETICS.111.962415

Fukumori, R., Nishigori, Y., Goshima, Y., and Kubo, T. (2004). Contribution of the medial amygdaloid nucleus to the development of hypertension in spontaneously hypertensive rats. *Neurosci. Lett.* 365, 128–131. doi: 10.1016/j.neulet.2004.04.066

Furlong, T. M., Vianna, D. M., Liu, L., and Carrive, P. (2009). Hypocretin/orexin contributes to the expression of some but not all forms of stress and arousal. *Eur. J. Neurosci.* 30, 1603–1614. doi: 10.1111/j.1460-9568.2009.06952.x

Gao, Y., Qi, G. X., Jia, Z. M., and Sun, Y. X. (2017). Prediction of marker genes associated with hypertension by bioinformatics analyses. *Int. J. Mol. Med.* 40, 137–145. doi: 10.3892/ijmm.2017.3000

Gianaros, P. J., Sheu, L. K., Matthews, K. A., Jennings, J. R., Manuck, S. B., and Hariri, A. R. (2008). Individual differences in stressor-evoked blood pressure reactivity vary with activation, volume, and functional connectivity of the amygdala. *J. Neurosci.* 28, 990–999. doi: 10.1523/JNEUROSCI.3606-07.2008

Godwin, S. J., Tortelli, C. F., Parkin, M. L., and Head, G. A. (1998). Comparison of the baroreceptor-heart rate reflex effects of rilmenidine, moxonidine and clonidine. *J. Auton. Nerv. Syst.* 72, 195–204.

Gueguen, C., Jackson, K. L., Marques, F. Z., Eikelis, N., Phillips, S., Stevenson, E. R., et al. (2019). Renal nerves contribute to hypertension in Schlager BPH/2J mice. *Hypertens. Res.* 42, 306–318. doi: 10.1038/s41440-018-0147-9

Gulinello, M., Gong, Q. H., Li, X., and Smith, S. S. (2001). Short-term exposure to a neuroactive steroid increases alpha4 GABA(A) receptor subunit levels in association with increased anxiety in the female rat. *Brain Res.* 910, 55–66. doi: 10.1016/S0006-8993(01)02565-3

Hamet, P., Malo, D., and Tremblay, J. (1990). Increased transcription of a major stress gene in spontaneously hypertensive mice. *Hypertension* 15, 904–908. doi: 10.1161/01.HYP.15.6.904

Han, Y., Shaikh, M. B., and Siegel, A. (1996). Medial amygdaloid suppression of predatory attack behavior in the cat: I role of a substance P pathway from the medial amygdala to the medial hypothalamus. *Brain Res.* 716, 59–71. doi: 10.1016/0006-8993(95)01586-8

Head, G. A. (1996). Role of AT1 receptors in the central control of sympathetic vasomotor function. *Clin. Exp. Pharmacol. Physiol.* 23, S93–S98.

Head, G. A., and de Jong, W. (1986). Differential blood pressure responses to intracisternal clonidine, a-methyldopa, and 6-hydroxydopamine in

conscious normotensive and spontaneously hypertensive rats. *J. Cardiovasc. Pharmacol.* 8, 735–742.

Herat, L. Y., Magno, A. L., Kiuchi, M. G., Jackson, K. L., Carnagarin, R., Head, G. A., et al. (2020). The Schlager mouse as a model of altered retinal phenotype. *Neural. Regen. Res.* 15, 512–518. doi: 10.4103/1673-5374.266069

Herdade, K. C., Strauss, C. V., Zangrossi Junior, H., and Viana, M. B. (2006). Effects of medial amygdala inactivation on a panic-related behavior. *Behav. Brain Res.* 172, 316–323. doi: 10.1016/j.bbr.2006.05.021

Hoffmann, D. S., Weydert, C. J., Lazartigues, E., Kutschke, W. J., Kienzle, M. F., Leach, J. E., et al. (2008). Chronic tempol prevents hypertension, proteinuria, and poor feto-placental outcomes in BPH/5 mouse model of preeclampsia. *Hypertension* 51, 1058–1065. doi: 10.1161/HYPERTENSIONAHA.107.107219

Horiuchi, J., and Dampney, R. A. L. (1998). Dependence of sympathetic vasomotor tone on bilateral inputs from the rostral ventrolateral medulla in the rabbit: role of baroreceptor reflexes. *Neurosci. Lett.* 248, 113–116. doi: 10.1016/S0304-3940(98)00349-8

Horvath, T. L., and Gao, X. B. (2005). Input organization and plasticity of hypocretin neurons: possible clues to obesity's association with insomnia. *Cell Metab.* 1, 279–286. doi: 10.1016/j.cmet.2005.03.003

Hosie, A. M., Wilkins, M. E., da Silva, H. M., and Smart, T. G. (2006). Endogenous neurosteroids regulate GABAA receptors through two discrete transmembrane sites. *Nature* 444, 486–489. doi: 10.1038/nature05324

Huang, B. S., and Leenen, F. H. (1996). Brain "ouabain" and angiotensin II in salt-sensitive hypertension in spontaneously hypertensive rats. *Hypertension* 28, 1005–1012. doi: 10.1161/01.HYP.28.6.1005

Inutsuka, A., and Yamanaka, A. (2013). The regulation of sleep and wakefulness by the hypothalamic neuropeptide orexin/hypocretin. *Nagoya J. Med. Sci.* 75, 29–36.

Ito, S., Komatsu, K., Tsukamoto, K., Kanmatsuse, K., and Sved, A. F. (2002). Ventrolateral medulla AT1 receptors support blood pressure in hypertensive rats. *Hypertension* 40, 552–559. doi: 10.1161/01.HYP.0000033812.99089.92

Iwao, H., Nakamura, N., Kim, S., Ikemoto, F., Yamamoto, K., and Schlager, G. (1984). Renin-angiotensin system in genetically hypertensive mice. *Jpn. Circ. J.* 48, 1270–1279. doi: 10.1253/jcj.48.1270

Jackson, K., Dampney, B., Moretti, J.-L., Stevenson, E., Davern, P., Carrive, P., et al. (2016). The contribution of orexin to the neurogenic hypertension in BPH/2J mice. *Hypertension* 67, 959–969. doi: 10.1161/HYPERTENSIONAHA.115.07053

Jackson, K., Marques, F., Lim, K., Davern, P., and Head, G. (2018). Circadian differences in the contribution of the brain renin angiotensin system in genetically hypertensive mice. *Front. Physiol.* 9, 1–15. doi: 10.3389/fphys.2018.00231

Jackson, K., Marques, F., Nguyen-Huu, T., Stevenson, E., Charchar, F., Davern, P., et al. (2014a). The role of microRNA-181a in mediating the greater renin-angiotensin system contribution to hypertension in BPH/2J hypertensive mice. Paper presented at the High Blood Pressure Research Council of Australia. Adelaide, Australia.

Jackson, K. L., Marques, F. Z., Watson, A. M. D., Palma Rigo, K., Nguyen-Huu, T.-P., Morris, B. J., et al. (2013). A novel interaction between sympathetic overactivity and aberrant regulation of renin by mir-181a in BPH/2J genetically hypertensive mice. *Hypertension* 62, 775–781. doi: 10.1161/HYPERTENSIONAHA.113.01701

Jackson, K. L., Nguyen-Huu, T.-P., Davern, P. J., and Head, G. A. (2014b). Energy metabolism in BPH/2J genetically hypertensive mice. *Hypertens. Res.* 37, 413–421. doi: 10.1038/hr.2013.156

Jackson, K. L., Palma-Rigo, K., Nguyen-Huu, T.-P., Davern, P. J., and Head, G. A. (2014c). Actions of rilmenidine on neurogenic hypertension in BPH/2J genetically hypertensive mice. *J. Hypertens.* 32, 575–586. doi: 10.1097/hjh.0000000000000036

Jackson, K. L., Palma-Rigo, K., Nguyen-Huu, T.-P., Davern, P. J., and Head, G. A. (2014d). Major contribution of the medial amygdala to hypertension in BPH/2J genetically hypertensive mice. *Hypertension* 63, 811–818. doi: 10.1161/hypertensionaha.113.02020

Jelinic, M., Leo, C., Jackson, K., Deo, M., Parry, L., Ritchie, R., et al. (2018). Renal fibrosis and vascular dysfunction in BPH/2J genetically hypertensive mice. Paper presented at the 27th Scientific Meeting of the International Society of Hypertension. Beijing.

Jindra, A. Jr., and Kvetnansky, R. (1982). Stress-induced activation of inactive renin. Molecular weight aspects. *J. Biol. Chem.* 257, 5997–5999.

Keil, L. C., Summy-Long, J., and Severs, W. B. (1975). Release of vasopressin by angiotensin II. *Endocrinology* 96, 1063–1065. doi: 10.1210/endo-96-4-1063

Kramer, K., Voss, H. P., Grimbergen, J. A., Mills, P. A., Huetteman, D., Zwiers, L., et al. (2000). Telemetric monitoring of blood pressure in freely moving mice: a preliminary study. *Lab. Anim.* 34, 272–280. doi: 10.1258/002367700780384663

Kubo, T., Okatani, H., Nishigori, Y., Hagiwara, Y., Fukumori, R., and Goshima, Y. (2004). Involvement of the medial amygdaloid nucleus in restraint stress-induced pressor responses in rats. *Neurosci. Lett.* 354, 84–86. doi: 10.1016/j.neulet.2003.09.061

Kunkler, P. E., and Hwang, B. H. (1995). Lower GABAA receptor binding in the amygdala and hypothalamus of spontaneously hypertensive rats. *Brain Res. Bull.* 36, 57–61. doi: 10.1016/0361-9230(94)00164-V

Kurz, A. (2001). Effects of anaesthesia on thermoregulation. *Curr. Anaesth. Crit. Care* 12, 72–78. doi: 10.1054/cacc.2001.0328

Leckie, B. J. (2001). The action of salt and captopril on blood pressure in mice with genetic hypertension. *J. Hypertens.* 19, 1607–1613. doi: 10.1097/00004872-200109000-00013

Lee, Y. H., Dai, Y. W., Huang, S. C., Li, T. L., and Hwang, L. L. (2013). Blockade of central orexin 2 receptors reduces arterial pressure in spontaneously hypertensive rats. *Exp. Physiol.* 98, 1145–1155. doi: 10.1113/expphysiol.2013.072298

Li, Y. W., and Dampney, R. A. L. (1992). Expression of c-fos protein in the medulla-oblongata of conscious rabbits in response to baroreceptor activation. *Neurosci. Lett.* 144, 70–74. doi: 10.1016/0304-3940(92)90718-M

Li, A., Hindmarch, C. C., Nattie, E. E., and Paton, J. F. (2013). Antagonism of orexin receptors significantly lowers blood pressure in spontaneously hypertensive rats. *J. Physiol.* 591, 4237–4248. doi: 10.1113/jphysiol.2013.256271

Malo, D., Pang, S. C., Schlager, G., Tremblay, J., and Hamet, P. (1990). Decrease of blood pressure in spontaneously hypertensive mice by heat treatment. *Am. J. Hypertens.* 3, 400–404. doi: 10.1093/ajh/3.5.400

Malo, D., Schlager, G., Tremblay, J., and Hamet, P. (1989). Thermosensitivity, a possible new locus involved in genetic hypertension. *Hypertension* 14, 121–128. doi: 10.1161/01.HYP.14.2.121

Marques, F. Z., Campain, A. E., Davern, P. J., Yang, Y. H., Head, G. A., and Morris, B. J. (2011a). Global identification of the genes and pathways differentially expressed in hypothalamus in early and established neurogenic hypertension. *Physiol. Genomics* 43, 766–771. doi: 10.1152/physiolgenomics.00009.2011

Marques, F. Z., Campain, A. E., Davern, P. J., Yang, Y. H. I., Head, G. A., and Morris, B. J. (2011b). Genes influencing circadian differences in blood pressure in hypertensive mice. *PLoS One* 6:e19203. 1–9. doi: 10.1371/journal.pone.0019203

Marques, F. Z., Campain, A. E., Tomaszewski, M., Zukowska-Szczechowska, E., Yang, Y. H., Charchar, F. J., et al. (2011c). Gene expression profiling reveals renin mRNA overexpression in human hypertensive kidneys and a role for microRNAs. *Hypertension* 58, 1093–1098. doi: 10.1161/hypertensionaha.111.180729

Marques, F. Z., Romaine, S. P., Denniff, M., Eales, J., Dormer, J., Garrelds, I. M., et al. (2015). Signatures of miR-181a on renal transcriptome and blood pressure. *Mol. Med.* 21, 739–748. doi: 10.2119/molmed.2015.00096

Matsuura, T., Kumagai, H., Kawai, A., Onimaru, H., Imai, M., Oshima, N., et al. (2002). Rostral ventrolateral medulla neurons of neonatal Wistar-Kyoto and spontaneously hypertensive rats. *Hypertension* 40, 560–565. doi: 10.1161/01.HYP.0000032043.64223.87

Mayorov, D. N., Burke, S. L., and Head, G. A. (2001). Relative importance of rostral ventrolateral medulla in sympathoinhibitory action of rilmenidine in conscious and anesthetized rabbits. *J. Cardiovasc. Pharmacol.* 37, 252–261. doi: 10.1097/00005344-200103000-00003

McGuire, J. J., Van Vliet, B. N., Gimenez, J., King, J. C., and Halfyard, S. J. (2007). Persistence of PAR-2 vasodilation despite endothelial dysfunction in BPH/2 hypertensive mice. *Pflugers Arch. - Eur. J. Physiol.* 454, 535–543. doi: 10.1007/s00424-007-0226-2

Ming, E. E., Adler, G. K., Kessler, R. C., Fogg, L. F., Matthews, K. A., Herd, J. A., et al. (2004). Cardiovascular reactivity to work stress predicts subsequent onset of hypertension: the air traffic controller health change study. *Psychosom. Med.* 66, 459–465. doi: 10.1097/01.psy.0000132872.71870.6d

Muratani, H., Ferrario, C. M., and Averill, D. B. (1993). Ventrolateral medulla in spontaneously hypertensive rats - role of angiotensin-II. *Am. J. Physiol. Regul. Integr. Comp. Physiol.* 264, R388–R395. doi: 10.1152/ajpregu.1993.264.2.R388

Nelson, J. W., Ferdaus, M. Z., McCormick, J. A., Minnier, J., Kaul, S., Ellison, D. H., et al. (2018). Endothelial transcriptomics reveals activation of fibrosis-

related pathways in hypertension. *Physiol. Genomics* 50, 104–116. doi: 10.1152/physiolgenomics.00111.2017

Okamura, N., and Reinscheid, R. K. (2007). Neuropeptide S: a novel modulator of stress and arousal. *Stress* 10, 221–226. doi: 10.1080/10253890701248673

Palma-Rigo, K., Jackson, K. L., Davern, P. J., Nguyen-Huu, T.-P., Elghozi, J.-L., and Head, G. A. (2011). Renin-angiotensin and sympathetic nervous system contribution to high blood pressure in Schlager mice. *J. Hypertens.* 29, 2156–2166. doi: 10.1097/HJH.0b013e32834bbb6b

Parkin, M. L., Godwin, S. J., and Head, G. A. (2003). Importance of imidazoline-preferring receptors in the cardiovascular actions of chronically administered moxonidine, rilmenidine and clonidine in conscious rabbits. *J. Hypertens.* 21, 167–178. doi: 10.1097/00004872-200301000-00027

Perini, C., Muller, F. B., Rauchfleisch, U., Battegay, R., Hobi, V., and Buhler, F. R. (1990). Psychosomatic factors in borderline hypertensive subjects and offspring of hypertensive parents. *Hypertension* 16, 627–634. doi: 10.1161/01.HYP.16.6.627

Porter, K., and Hayward, L. F. (2011). Stress-induced changes in c-Fos and corticotropin releasing hormone immunoreactivity in the amygdala of the spontaneously hypertensive rat. *Behav. Brain Res.* 216, 543–551. doi: 10.1016/j.bbr.2010.08.036

Prior, L., Davern, P., Burke, S., Lim, K., Armitage, J., and Head, G. (2014). Exposure to a high fat diet during development alters leptin and ghrelin sensitivity and elevates renal sympathetic nerve activity and arterial pressure in rabbits. *Hypertension* 63, 338–345. doi: 10.1161/HYPERTENSIONAHA.113.02498

Prior, L., Eikelis, N., Armitage, J., Davern, P., Burke, S., Montani, J.-P., et al. (2010). Exposure to a high-fat diet alters leptin sensitivity and elevates renal sympathetic nerve activity and arterial pressure in rabbits. *Hypertension* 55, 862–868. doi: 10.1161/HYPERTENSIONAHA.109.141119

Puig, O., Wang, I. M., Cheng, P., Zhou, P., Roy, S., Cully, D., et al. (2010). Transcriptome profiling and network analysis of genetically hypertensive mice identifies potential pharmacological targets of hypertension. *Physiol. Genomics* 42A, 24–32. doi: 10.1152/physiolgenomics.00010.2010

Rasmusson, A. M., Pinna, G., Paliwal, P., Weisman, D., Gottschalk, C., Charney, D., et al. (2006). Decreased cerebrospinal fluid allopregnanolone levels in women with posttraumatic stress disorder. *Biol. Psychiatry* 60, 704–713. doi: 10.1016/j.biopsych.2006.03.026

Rosenberg, W. L. (1983). The glomerular origin of essential hypertension. *Med. Hypotheses* 10, 167–171. doi: 10.1016/0306-9877(83)90019-1

Rosenberg, W., Palmieri, C., Schlager, G., and Gennaro, J. F. Jr. (1982). Quantitative structural aspects of the renal glomeruli of hypertensive mice. *Nephron* 30, 161–165.

Rosenberg, W., Schlager, G., and Gennaro, J. F. Jr. (1979). A morphometric analysis of the glomerular capillary wall of a new strain of genetically hypertensive mice. *Anat. Rec.* 195, 511–524. doi: 10.1002/ar.1091950310

Rosenberg, W. L., Schlager, G., and Gennaro, J. F. Jr. (1985). Glomerular filtration and fluid balance in genetically hypertensive mice. *Exp. Biol. Med.* 178, 629–634. doi: 10.3181/00379727-178-42053

Sakurai, T. (2005). Roles of orexin/hypocretin in regulation of sleep/wakefulness and energy homeostasis. *Sleep Med. Rev.* 9, 231–241. doi: 10.1016/j.smrv.2004.07.007

Samuelsen, C. L., and Meredith, M. (2009). Categorization of biologically relevant chemical signals in the medial amygdala. *Brain Res.* 1263, 33–42. doi: 10.1016/j.brainres.2009.01.048

Sander, M., Bader, M., Djavidani, B., Masergluth, C., Vecsel, P., Mullins, J., et al. (1992). The role of the adrenal gland in hypertensive transgenic rat TGR(mREN2)27. *Endocrinology* 131, 807–814. doi: 10.1210/endo.131.2.1322284

Sannajust, F., Julien, C., Barres, C., Cerutti, C., Koenig-Berard, E., and Sassard, J. (1989). Cardiovascular effects of rilmenidine, a new alpha 2-adrenoceptor agonist, and clonidine in conscious spontaneously hypertensive rats. *Clin. Exp. Pharmacol. Physiol.* 16, 837–848. doi: 10.1111/j.1440-1681.1989.tb01523.x

Sassolas, A., Vincent, M., Benzoni, D., and Sassard, J. (1981). Plasma lipids in gentically hypertensive rats of the Lyon strain. *J. Cardiovasc. Pharmacol.* 3, 1008–1014. doi: 10.1097/00005344-198109000-00011

Schlager, G. (1974). Selection for blood pressure levels in mice. *Genetics* 76, 537–549.

Schlager, G. (1994). Biometrical genetic analysis of blood pressure level in the genetically hypertensive mouse. *Clin. Exp. Hypertens.* 16, 809–824.

Schlager, G., and Freeman, R. (1983). Norepinephrine level in the hypothalamus of the genetically hypertensive mouse. *Experientia* 39, 793–794. doi: 10.1007/BF01990332

Schlager, G., Freeman, R., and El Seoudy, A. A. (1983). Genetic study of norepinephrine in brains of mice selected for differences in blood pressure. *J. Hered.* 74, 97–100. doi: 10.1093/oxfordjournals.jhered.a109749

Schlager, G., Freeman, R., and Sustarsic, S. S. (1979). Brain catecholamines and organ weight of mice genetically selected for high and low blood pressure. *Experientia* 35, 67–69. doi: 10.1007/BF01917881

Schlager, G., and Sides, J. (1997). Characterization of hypertensive and hypotensive inbred strains of mice. *Lab. Anim. Sci.* 47, 288–292.

Serra, M., Pisu, M. G., Littera, M., Papi, G., Sanna, E., Tuveri, F., et al. (2000). Social isolation-induced decreases in both the abundance of neuroactive steroids and GABA(A) receptor function in rat brain. *J. Neurochem.* 75, 732–740. doi: 10.1046/j.1471-4159.2000.0750732.x

Shirasaka, T., Kunitake, T., Takasaki, M., and Kannan, H. (2002). Neuronal effects of orexins: relevant to sympathetic and cardiovascular functions. *Regul. Pept.* 104, 91–95. doi: 10.1016/S0167-0115(01)00352-4

Shirasaka, T., Nakazato, M., Matsukura, S., Takasaki, M., and Kannan, H. (1999). Sympathetic and cardiovascular actions of orexins in conscious rats. *Am. J. Physiol. Regul. Integr. Comp. Physiol.* 277, R1780–R1785. doi: 10.1152/ajpregu.1999.277.6.R1780

Smith, S. S., Shen, H., Gong, Q. H., and Zhou, X. (2007). Neurosteroid regulation of GABA(A) receptors: focus on the alpha4 and delta subunits. *Pharmacol. Ther.* 116, 58–76. doi: 10.1016/j.pharmthera.2007.03.008

Solomon, M. B., Jones, K., Packard, B. A., and Herman, J. P. (2010). The medial amygdala modulates body weight but not neuroendocrine responses to chronic stress. *J. Neuroendocrinol.* 22, 13–23. doi: 10.1111/j.1365-2826.2009.01933.x

Stevenson, E., Johns, E., Marques, F., Jackson, K., Abegaz, B., Moretti, J.-L., et al. (2017). Positive allosteric modulation of GABAA receptors attenuates high blood pressure in Schlager hypertensive mice. *J. Hypertens.* 35, 546–557. doi: 10.1097/HJH.0000000000001210

Strack, A. M., Sawyer, W. B., Hughes, J. H., Platt, K. B., and Loewy, A. D. (1989). A general pattern of CNS innervation of the sympathetic outflow demonstrated by transneuronal pseudorabies viral infections. *Brain Res.* 491, 156–162. doi: 10.1016/0006-8993(89)90098-X

Strazielle, C., Lalonde, R., Thifault, S., and Hamet, P. (2004). Regional brain variations of cytochrome oxidase activity in spontaneously hypertensive mice. *Exp. Brain Res.* 157, 255–264. doi: 10.1007/s00221-004-1841-1

Sun, Z., Cade, R., and Morales, C. (2002). Role of central angiotensin II receptors in cold-induced hypertension. *Am. J. Hypertens.* 15, 85–92. doi: 10.1016/S0895-7061(01)02230-0

Sun, X., Icli, B., Wara, A. K., Belkin, N., He, S., Kobzik, L., et al. (2012). MicroRNA-181b regulates NF-kappaB-mediated vascular inflammation. *J. Clin. Invest.* 122, 1973–1990. doi: 10.1172/JCI61495

Sur, C., Farrar, S. J., Kerby, J., Whiting, P. J., Atack, J. R., and McKernan, R. M. (1999). Preferential coassembly of alpha4 and delta subunits of the gamma-aminobutyric acidA receptor in rat thalamus. *Mol. Pharmacol.* 56, 110–115. doi: 10.1124/mol.56.1.110

Sutton, E. F., Lob, H. E., Song, J., Xia, Y., Butler, S., Liu, C. C., et al. (2017). Adverse metabolic phenotype of female offspring exposed to preeclampsia in utero: a characterization of the BPH/5 mouse in postnatal life. *Am. J. Physiol. Regul. Integr. Comp. Physiol.* 312, R485–R491. doi: 10.1152/ajpregu.00512.2016

Szekely, M., Petervari, E., Balasko, M., Hernadi, I., and Uzsoki, B. (2002). Effects of orexins on energy balance and thermoregulation. *Regul. Pept.* 104, 47–53. doi: 10.1016/S0167-0115(01)00348-2

Tajada, S., Cidad, P., Moreno-Dominguez, A., Perez-Garcia, M. T., and Lopez-Lopez, J. R. (2012). High blood pressure associates with the remodelling of inward rectifier K+ channels in mice mesenteric vascular smooth muscle cells. *J. Physiol.* 590, 6075–6091. doi: 10.1113/jphysiol.2012.236190

Thifault, S., Lalonde, R., Sanon, N., and Hamet, P. (2001). Longitudinal analysis of motor activity and coordination, anxiety, and spatial learning in mice with altered blood pressure. *Brain Res.* 910, 99–105. doi: 10.1016/S0006-8993(01)02658-0

Thomas, W. G., and Sernia, C. (1985). Regulation of rat brain angiotensin II (AII) receptors by intravenous AII and low dietary Na+. *Brain Res.* 345, 54–61. doi: 10.1016/0006-8993(85)90835-2

Touw, K. B., Haywood, J. R., Shaffer, R. A., and Brody, M. J. (1980). Contribution of the sympathetic nervous system to vascular resistance in conscious young

and adult spontaneously hypertensive rats. *Hypertension* 2, 408–418. doi: 10.1161/01.HYP.2.4.408

Uddin, M., and Harris-Nelson, N. (2004). Renin activity and angiotensinI concentration in genetically selective inbred line of hypertensive mice. *Biochem. Biophys. Res. Commun.* 316, 842–844. doi: 10.1016/j.bbrc.2004.02.128

Uddin, M., Polley-Mandal, M., and Beg, O. U. (2003a). Kallikrein-like prorenin-converting enzymes in inbred hypertensive mice. *Biochem. Biophys. Res. Commun.* 304, 724–728. doi: 10.1016/s0006-291x(03)00645-4

Uddin, M., Yang, H., Shi, M., Polley-Mandal, M., and Guo, Z. (2003b). Elevation of oxidative stress in the aorta of genetically hypertensive mice. *Mech. Ageing Dev.* 124, 811–817. doi: 10.1016/s0047-6374(03)00135-0

Vinkers, C. H., Bijlsma, E. Y., Houtepen, L. C., Westphal, K. G., Veening, J. G., Groenink, L., et al. (2010). Medial amygdala lesions differentially influence stress responsivity and sensorimotor gating in rats. *Physiol. Behav.* 99, 395–401. doi: 10.1016/j.physbeh.2009.12.006

Watson, A. M. D., Gould, E., Penfold, S. A., Lambert, G. W., Pramata, P. R., Gray, S. P., et al. (2019). Diabetes and hypertension differentially affect renal catecholamines and renal reactive oxygen species. *Front. Physiol.* 10, 1–16. doi: 10.3389/fphys.2019.00309

Wright, F. A., O'Connor, D. T., Roberts, E., Kutey, G., Berry, C. C., Yoneda, L. U., et al. (1999). Genome scan for blood pressure loci in mice. *Hypertension* 34, 625–630. doi: 10.1161/01.HYP.34.4.625

Xiao, F., Jiang, M., Du, D., Xia, C., Wang, J., Cao, Y., et al. (2013). Orexin A regulates cardiovascular responses in stress-induced hypertensive rats. *Neuropharmacology* 67, 16–24. doi: 10.1016/j.neuropharm.2012.10.021

Xue, B., Johnson, A. K., and Hay, M. (2007). Sex differences in angiotensin II- induced hypertension. *Braz. J. Med. Biol. Res.* 40, 727–734. doi: 10.1590/S0100-879X2007000500018

Ye, S., Zhong, H., Duong, V. N., and Campese, V. M. (2002). Losartan reduces central and peripheral sympathetic nerve activity in a rat model of neurogenic hypertension. *Hypertension* 39, 1101–1106. doi: 10.1161/01.HYP.0000018590.26853.C7

Zhang, J., and Abdel-Rahman, A. A. (2002). The hypotensive action of rilmenidine is dependent on functional N-methyl-D-aspartate receptor in the rostral ventrolateral medulla of conscious spontaneously hypertensive rats. *J. Pharmacol. Exp. Ther.* 303, 204–210. doi: 10.1124/jpet.102.037333

Zimmerman, M. C., Lazartigues, E., Lang, J. A., Sinnayah, P., Ahmad, I. M., Spitz, D. R., et al. (2002). Superoxide mediates the actions of angiotensin II in the central nervous system. *Circ. Res.* 91, 1038–1045. doi: 10.1161/01.RES.0000043501.47934.FA

Zubcevic, J., Baker, A., and Martyniuk, C. J. (2017). Transcriptional networks in rodent models support a role for gut-brain communication in neurogenic hypertension: a review of the evidence. *Physiol. Genomics* 49, 327–338. doi: 10.1152/physiolgenomics.00010.2017

Conflict of Interest: The authors declare that the research was conducted in the absence of any commercial or financial relationships that could be construed as a potential conflict of interest.

frontiers in Physiology

ORIGINAL RESEARCH
published: 22 November 2019
doi: 10.3389/fphys.2019.01420

Impaired Baroreflex Function in an Ovine Model of Chronic Heart Failure Induced by Multiple Coronary Microembolizations

*Yonis Abukar[1], Nigel Lever[2], Mridula Pachen[1], Ian J. LeGrice[1] and Rohit Ramchandra[1]**

[1]Department of Physiology, University of Auckland, Auckland, New Zealand, [2]Department of Cardiology, Auckland District Health Board, Auckland, New Zealand

Testing new therapies in heart failure (HF) requires a chronic stable model of HF in large animals. Microembolization of the coronary arteries has been used to model HF previously; however, neural control has not been previously explored in this model. Thus the aim of this study was to further characterize neural control in this model of HF. HF was induced by infusion of microspheres (45 micron; 1.3 ml) into the proximal left coronary artery or left descending coronary arteries, with three sequential embolizations over 3 weeks. Twelve to 14 weeks after the final embolization, and when ejection fraction had decreased below 45%, animals were instrumented to record blood pressure and heart rate. Baroreflex control of heart rate was investigated in conscious animals. Additionally, pressure-volume loops were constructed under anesthesia. Embolization-induced HF was associated with a decrease in mean arterial pressure (67 ± 2 vs. 85 ± 4 mmHg, $p < 0.05$), an increase in heart rate (108 ± 4 vs. 94 ± 4 bpm, $p < 0.05$), and a significant increase in left ventricular end-diastolic pressure (11.4 ± 2 vs. 6.2 ± 1 mmHg, $p < 0.01$). Under conscious conditions, there was a significant decrease in the gain (–8.2 ± 2 vs. –4.1 ± 1 beats/min/mmHg, $p < 0.05$) as well as the lower plateau of the baroreflex in HF compared to control animals. HF was also associated with significantly increased respiratory rate (107 ± 4 vs. 87 ± 4 breaths/min, $p < 0.01$) and incidence of apneas (520 ± 24 vs. 191 ± 8 apnea periods >4 s, $p < 0.05$), compared to control sheep. The microembolization model of heart failure is associated with an increase in left ventricular end-diastolic pressure, impaired cardiac function, and altered baroreflex control of the heart. These findings suggest this chronic model of HF is appropriate to use for investigating interventions aimed at improving neural control in HF.

Keywords: heart failure, embolization, neural control, sheep, heart failure model

OPEN ACCESS

Edited by:
Geoffrey A. Head, Baker Heart and Diabetes Institute, Australia

Reviewed by:
Mark Butlin, Macquarie University, Australia
Maria Claudia Costa Irigoyen, University of São Paulo, Brazil
Luciana A. Campos, Anhembi Morumbi University, Brazil

****Correspondence:***
Rohit Ramchandra
r.ramchandra@auckland.ac.nz

Specialty section:
This article was submitted to Integrative Physiology, a section of the journal Frontiers in Physiology

Received: *28 August 2019*
Accepted: *04 November 2019*
Published: *22 November 2019*

Citation:
Abukar Y, Lever N, Pachen M, LeGrice IJ and Ramchandra R (2019) Impaired Baroreflex Function in an Ovine Model of Chronic Heart Failure Induced by Multiple Coronary Microembolizations. Front. Physiol. 10:1420. doi: 10.3389/fphys.2019.01420

INTRODUCTION

Heart failure with reduced ejection fraction (HFrEF) is characterized by progressive dysfunction of left ventricular muscle, myocyte remodeling, and activation of autonomic and hormonal systems (Jackson et al., 2000; Kemp and Conte, 2012). Despite the advances in therapies and prevention, patients with HF have high rates of morbidity and mortality (Falk et al., 2005;

Savarese and Lund, 2017). The balance between the sympathetic and parasympathetic systems, in relation to cardiovascular function, is altered in response to ventricular dysfunction (Amorim et al., 1981; Benedict et al., 1996; Floras, 2009). Specifically, it is recognized that there is abnormal hyperactivity of the sympathetic nervous system (Watson et al., 2007; Ramchandra et al., 2009b) and disinhibition of the parasympathetic nervous system that leads to worsening of the condition (Eckberg et al., 1971; Kinugawa and Dibner-Dunlap, 1995; Bibevski and Dunlap, 1999; Dunlap et al., 2003).

Numerous studies have been conducted on small animal models of HF and these have been instrumental in understanding the pathogenesis of HF. However, there are significant differences between small animal models of HF and human HF beyond scale. These include differences in baseline heart rate, oxygen consumption, and excitation-contraction coupling in cardiac tissue (Haghighi et al., 2003; Dixon and Spinale, 2009). Therefore, a clinically relevant large animal model of HF with similar anatomy and physiology of the heart is crucial. In this context, a number of different large animal models of HF have been studied.

The primary methods to induce HFrEF in large animals include high rate pacing, cardiotoxin infusion, and coronary ligation. The pacing-induced HF model has been used in sheep (Timek et al., 2003; Byrne et al., 2004), pigs (Tanaka et al., 1993; McMahon et al., 1996), and dogs (Prabhu and Freeman, 1995; O'Rourke et al., 1999). The technique of rapid supraphysiological pacing of either the atrium or the ventricle for approximately 4 weeks results in a reproducible model of HFrEF. This model shows similar hemodynamic and mechanical phenotypes as dilated cardiomyopathy seen in human patients with HF. However, one disadvantage of this model is the absence of tissue fibrosis if the pacing is not continued for a prolonged period of time. In addition, left ventricle dysfunction tends to reverse when pacing is terminated, especially if the pacing was performed for short durations (Spinale et al., 1991; McMahon et al., 1996).

Intracoronary or intravenous infusion of the cardiotoxin doxorubicin in dogs (Bristow et al., 1980; Toyoda et al., 1998) and sheep (Chekanov, 1999; Borenstein et al., 2006) leads to cardiac myocyte injury, cell loss, and HF. A major limitation of this method is the variable degree of LV dysfunction that can result, with no reliable dosing strategy to provide a stable model. A further drawback is the potential for systemic side effects and the management of these.

Finally, coronary ligation has been used to induce HF in large animals (Hood et al., 1967). Infarcts larger than 25% resulted in a significant increase in left ventricular end-diastolic pressure and a reduction in stroke volume index. However, mortality using this model can be more than 50%, often as a result of fatal arrhythmias, despite the use of anti-arrhythmic agents or due to severe symptomatic heart failure. Additionally, when the infarction is induced by external coronary ligation rather than percutaneously, post-operative adhesions and fibrosis may make further surgical dissection for subsequent experimental work more difficult with higher rates of complications (Oizumi et al., 1990; Yim et al., 1998; Getman et al., 2006). The combination of extent and impact of infarction with animal loss and surgical access limits the usefulness of this model in the research setting.

Recently, the microembolization model has been used in sheep to develop a chronic model of HF over a period of 3 months. The embolizations have been conducted using injection of either microspheres (Schmitto et al., 2009) or gelfoam (Devlin et al., 2000). The advantage of the microembolization model is that the changes are irreversible and the study with the infusion of microspheres has reported a high success rate of induction of HF; however, mortality rates were high in the gelfoam study. Until now, studies that have examined this model have focused on structural changes in the heart (Huang et al., 2004; Monreal et al., 2004) and putative alterations in neural control have not been examined. Thus, the aim of this study was to further characterize changes in heart function after repeated microembolizations in sheep and examine whether baroreflex control of heart rate is altered in the conscious state.

MATERIALS AND METHODS

Experiments were conducted on conscious, adult female Romney ewes weighing 50–80 kg, housed in individual crates, and acclimatized to laboratory conditions (18°C, 50% relative humidity, and 12-h light-dark cycle) and human contact before any experiments. All experiments and surgical procedures were approved by the Animal Ethics Committee of the University of Auckland. The sheep were fed 2 kg/day (Country harvest pellets) and had access to water *ad libitum*.

Embolization Surgical Procedure

Nine sheep (female, weight: 59 ± 3 kg) underwent three weekly sequential embolizations of either the proximal left coronary artery or left descending coronary arteries. Six control sheep (female, weight: 55 ± 5 kg) without microembolizations were also used in the study. Anesthesia was induced with 2% Diprivan (Propofol) (5 mg/kg IV, AstraZeneca, AUS) and maintained with a 2% isoflurane-air-O_2 mixture. Sheep were given antibiotic injections (6 ml i.m.; Oxytetra, Phenix, NZ) at the start of the surgery. Additionally, to provide analgesia, sheep were given Ketofen 10% (1 ml i.m.; Merial, Boehringer Ingelheim, NZ) at the start of surgery.

The methods employed have been described before (Schmitto et al., 2009). Once anesthetized and intubated, the sheep were placed in a supine cradled position and four electrodes were inserted into the left and right sides of the sternum and in the hind-limbs near the knee joint, subcutaneously, to record ECG. Recordings were obtained from lead II prior to the infusion of the microspheres and for a further 5 min after infusion. The recordings were made on a dual bio amp electrocardiograph switch box with power lab and LabChart (AD Instruments, NZ). A change in the ST segment (elevation or depression) and T wave (inversion) on one or more limb leads was taken as indication of successful embolization. The

left or right femoral artery was accessed percutaneously using an 8F (CORDIS®, USA) sheath. Using an 8F AL2 (CORDIS®, USA) guide catheter under fluoroscopic guidance, the left main coronary artery was then cannulated and the catheter was advanced either into the proximal left coronary artery or left descending coronary arteries. All sheep in the HF group underwent three sequential selective microembolizations to arterial supply of the left ventricle with polystyrene latex microspheres (45 μm; 1.4 ml, Polysciences, Warrington, PA, USA). The three embolizations were each performed 1 week apart, to ensure maximum left ventricle coverage. Prior to each embolization event, β-blocker (metoprolol up to 20 mg/kg, IV) and lignocaine (2 mg/kg, IV) were injected intravenously in order to prevent ventricular arrhythmias. Three sheep did not survive to the second embolization. These sheep showed signs of pulmonary edema but despite diuretics did not recover and were euthanized.

Echocardiography

Echocardiogram recordings were obtained and analyzed before embolizations and 3 months after the first embolization procedure. This was also done for the group of control sheep. The echocardiogram, using a Hewlett Packard Sonos 1,000, was performed while the sheep were conscious. In the long-axis M-wave echocardiography, diastole, systole, fractional shortening, and ejection fraction parameters were obtained and calculated for the left ventricle.

Instrumentation Sheep Surgery

After 3 months, once sheep were deemed to have sufficient left ventricle dysfunction (ejection fraction <45%), the animals were instrumented to measure mean arterial pressure (MAP), heart rate (HR), and diaphragmatic electromyography (dEMG) as an index of respiration. The instrumentation procedure was also conducted in a group of control sheep. The procedure for electrodes placement for dEMG has been described previously (Sieck and Fournier, 1990). Two strips of seven-stranded Cooner Wires (AS 633-7SSF, Cooner Wire, CA, USA) were implanted into the diaphragm and secured with silicone gel. To get an index of blood pressure and venous infusion, an incision was made in the neck and a single-tip pressure probe (Millar Inc., Texas, USA) was inserted into the carotid artery. A cannula was inserted into the jugular vein to have an entry point for venous infusion. dEMG measurement was recorded from the pair of electrodes inserted into the diaphragm, with the signal amplified (X10, 000), and filtered (band pass 0.3–3.0 kHz). All the parameters were recorded on a desktop computer with a CED micro 1,401 interface and a data acquisition program (Spike 2).

Hemodynamics Measurements and Analysis

All recordings were done at least 3 days after instrumentation surgery. Blood pressure was obtained from a pressure probe unit (Millar Inc., USA). Heart rate (HR) was calculated from blood pressure channel. In conscious, standing sheep, HR and MAP were obtained from a 2-h recording and averages were obtained for each animal. To determine the adrenergic effects on hemodynamic parameters and heart rate, β-adrenergic receptor blockade (propranolol, LKT chemicals, USA) was infused (30 mg bolus followed by 0.5 mg/kg/h infusion for 90 min).

Arterial Baroreflex Control of Heart Rate

In two groups of six conscious sheep, after a 5-min baseline recording of mean arterial pressure and heart rate, baroreflex curves were generated by measuring the responses of heart rate to increasing doses of phenylephrine hydrochloride (25, 50, 100, 200, and 400 mg/min) and sodium nitroprusside (25, 50, 100, 200, and 400 mg/min). For analysis, the baseline blood pressures were sorted from the lowest to the highest pressures and put into bins of 3 mmHg change each. The mean systolic blood pressure of each bin was plotted against the mean HR.

Plasma Brain Natriuretic Peptide, Epinephrine, and Norepinephrine Measurement

Venous blood samples (10 ml) were collected into an EDTA (BD Vacutainer, NJ, USA) tube. Plasma was rapidly separated with a centrifuge at 4°C at 3,000 rpm, within 5 min of blood collection, and snap-frozen at −80°C. The assays for brain natriuretic peptide (BNP) (Pemberton et al., 1997; Lewis et al., 2017), epinephrine, and norepinephrine (Justice et al., 2015) have previously been described. All samples from individual animals were measured in the same assay (BNP or epinephrine or norepinephrine) to avoid inter-assay variability.

Diaphragm Electromyogram Analysis

To assess diaphragmatic EMG parameters, resting breathing rate and apnea periods were measured in control and HF animals. Breathing rate average was obtained from dEMG activity in a 12-h baseline period in each animal. Apnea was defined as cessation of diaphragmatic activity. To be considered significant, apnea events had to persist for a minimum of 4 s. To quantify apnea incidence, we calculated an apnea index to indicate the number of apnea periods (>4 s) occurring in a 12-h period.

Pressure-Volume Loops

The acute pressure-volume loop experiments were conducted at the end of the protocol under anesthesia. To determine the left ventricle pressure-volume relationship, a conductance catheter was placed into the left ventricle through the left carotid artery. This method has been described previously in detail by Baan et al. (1984). Briefly, a 5 s (number 5, straight) seven-electrode conductance catheter that has a micromanometer tip was inserted into the left ventricle *via* a guide cannula, along the longitudinal axis. The catheter was connected to a Millar (Millar Inc., Texas, USA) and AD Instruments pressure-volume processing unit and signals were acquired using LabChart, a data acquisition and data

analysis software. Volume correction was done through an estimation, using a hypertonic saline solution (20% salt, 10 ml per infusion) infusion. A cardiac output transonic flow probe was also inserted around the aorta. Briefly, a thoracotomy was performed and fourth rib removed to access the heart. A flow probe was implanted on the aorta (28PS, Transonic Systems, USA) and connected to LabChart to measure cardiac output while performing pressure-volume loops.

Pressure-volume loops were analyzed offline using LabChart (AD Instruments). After volume correction, 10 cardiac cycles at baseline were analyzed. Also, cardiac output recordings from the animal were used for alpha calibrations. Stroke volume, ejection fraction, left ventricular end-diastolic and end-systolic pressure and volume, maximum rate of pressure generation (dP/dt max), peak rate of pressure decline (dP/dt min), and maximum conduction velocity (dV/dt max) were measured.

At the end of these experiments, the sheep were euthanized with an overdose of sodium pentobarbitone (0.5 ml/kg, intravenously) (Provet NZ Pty Ltd., New Zealand). Once respiration and cardiac function had ceased, cardiac tissue was collected for histological analysis.

Measurement of Cardiac Collagen

At the end of the terminal experiment, the hearts were collected and a portion of the left ventricle wall (specifically left ventricle free wall) was fixed in neutral buffered formalin (Shandon Glyo-Fixx, Thermo Scientific). Tissue blocks were then transferred to 30% sucrose solution. Heart blocks were then cut at 40-μm sections using a cryostat. To measure collagen deposition in the left ventricle wall of the sheep hearts, 12 sections (six control and six HF sheep hearts) were stained with Masson's Trichrome stain (MTS) solution (Biebrich Scarlet-Acid Fuchsin, PTA/PMA and Aniline Blue). Cardiac muscle fibers stain red and collagen stains blue. Sections were subjected to two washes and then three changes of 100% ethanol and finally one wash of xylene solution before cover slipping.

Statistical Analysis

All data are expressed as mean ± SEM, except where indicated. The effects of the microembolizations on the baseline levels of MAP, HR, ejection fraction, fractional shortening, respiratory rate, apnea incidence, heart and body weight, collagen fibers deposition, pressure-volume relationship parameters, and the arterial baroreceptor relationships of HR and sysBP were determined using unpaired Student's *t*-tests (two groups – control vs. heart failure). The effects of the individual microembolization procedures on the baseline levels of ECG (before and after each microembolization) and ejection fraction and fractional shortening (before and 12–14 weeks after microembolizations) were determined using paired Student's *t*-tests (within-animal). A one-way ANOVA test was used for changes in resting heart rate plotted in 3 mmHg change bins. Data were analyzed using the statistical package SigmaStat (Version 2, Access Softek Inc., 1995). Data were considered significant if $p < 0.05$.

RESULTS

Acute Changes After Embolization

Embolization of the coronary artery at the first time point resulted in a significant change in the lower S-T segment height and also the T-wave amplitude ($p < 0.05$; **Figure 1**). There were, however, no further decreases in this parameter after embolization procedures 2 and 3. The baseline height of the S-T segment was significantly lower after the second and third embolization procedure compared to the first ($p < 0.05$). These differences in embolization procedures 2 and 3 compared to embolization 1 were also observed in the T-wave amplitude.

Resting Hemodynamic Variables

The resting levels of hemodynamic variables in the control and HF sheep are shown in **Table 1** and **Figure 1**. Ejection fraction and fractional shortening data in **Figure 1** are within animal and the rest of the data is a comparison between instrumented control and HF sheep. Repeated microsphere infusions into the coronary vasculature resulted in significantly lower ejection fraction ($p < 0.001$) and fractional shortening ($p < 0.0001$) in HF sheep, after 12–14 weeks (**Figure 1**). HF was associated with a significant decrease in MAP (67 ± 2 vs. 85 ± 4 mmHg, $p < 0.01$), and an increase in heart rate (108 ± 4 vs. 94 ± 4 bpm, $p < 0.05$) compared to the control animals. Plasma levels of norepinephrine and brain natriuretic peptide were also significantly higher ($p < 0.05$) (**Table 1**). The respiratory rate was significantly higher in the HF sheep (109 ± 4 vs. 88 ± 5 breaths/min, $p < 0.01$) (**Figure 2**). The HF sheep showed more incidences of temporary cessation of breathing in a 12-h cycle (525 ± 123 vs. 179 ± 44 apnea periods longer than 4 s, $p < 0.05$, **Figure 2**). Infusion of propranolol reduced heart rate more in the HF group compared with control (9 ± 1 vs. 3 ± 1, bpm, change in HR before and after propranolol, $p < 0.001$) and there was no significant change in MAP between the groups after propranolol infusion.

To determine whether repeated micro-embolism induced any impairment in baroreflex control, we assessed arterial baroreflex function in both control and HF sheep. The baroreflex relationship showed a significant difference in the maximum gain (−8.2 ± 2 vs. −4.1 ± 1 beats/min/mmHg, $p < 0.05$), as well as the upper (152 ± 4 vs. 130 ± 8 beats min^{-1}, $p < 0.05$) and lower (70 ± 3 vs. 57 ± 4 beats min^{-1}, $p < 0.05$) plateaus of the HR baroreflex curve (**Figure 3A**). To determine the responses in HR over the operating range of the curve, we examined the differences in the mean resting HR values close to the resting MAP levels. HR changes from baseline, in response to phenylephrine and sodium nitroprusside infusions, plotted in 3-bpm bins highlight the significantly decreased response in the HF animals (**Figure 3B**) suggesting an impaired gain of the baroreflex curve at the operating ranges in these animals.

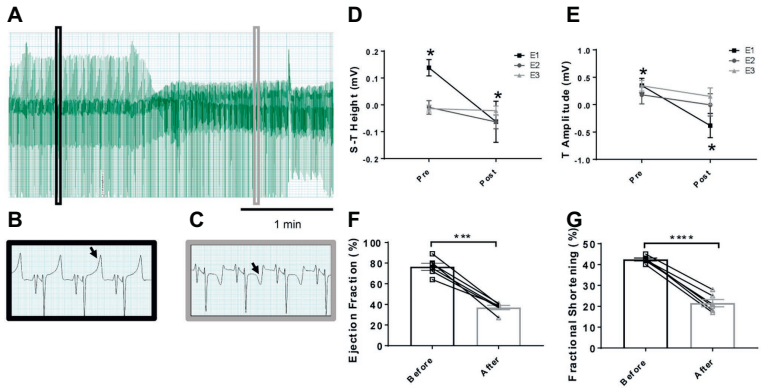

FIGURE 1 | Representative electrocardiogram traces in sheep before and after microembolizations and mean data on S-T and T-wave segments. **(A)** Lead II trace highlighting the changes over time in the ECG, with **(B)** highlighting magnified lead II activity before microembolization and **(C)** after microembolization. Arrows highlight the T-wave of the ECG, showing a depression after microembolization. **(D)** Mean data on the height of the S-T segment and **(E)** T-wave amplitude before and after the individual microembolization procedures. Pre- indicates before microembolization and post- after microembolization. Microembolization 1 (E1) represented by square, microembolization 2 (E2) by circle, and microembolization 3 (E3) by triangle. **(F)** Ejection fraction before (open square) and after (12–14 weeks after) embolizations (open triangle) in the same animals and **(G)** fractional shortening before (open square) and after (12–14 weeks after embolizations) (open triangle). *$p < 0.05$ in E1 only, $n = 6$, ***$p < 0.0001$ in ejection fraction, ****$p < 0.0001$ in fractional shortening, $n = 6$.

TABLE 1 | Resting values for hemodynamic parameters between conscious normal and heart failure sheep.

Parameter	Normal ($n = 6$)	Heart failure ($n = 6$)
Ejection fraction	79 ± 1	39 ± 2†
Fractional shortening	43 ± 1	20 ± 1†
Heart rate, beats/min	94 ± 4	108 ± 4*
Mean arterial pressure, mmHg	85 ± 4	67 ± 2**
Body weight (kg)	56 ± 2	70 ± 3**
Brain natriuretic peptide (pmol/L)	2.20 ± 0.12	3.79 ± 0.52*
Epinephrine (pmol/L)	380 ± 73	751 ± 188
Norepinephrine (pmol/L)	3,272 ± 901	10,628 ± 2509*

*$p < 0.05$; **$p < 0.01$; †$p < 0.0001$.

Pressure-Volume Loops Under Anesthesia

The ejection fractions calculated from the pressure-volume loops under anesthesia showed significantly lower ejection fraction compared to the conscious condition in both groups of sheep ($p < 0.01$); however, the difference between the groups remained intact. Interestingly, there was no change in baseline cardiac output between the normal and the HF sheep. The LV end-diastolic pressures and volumes in the HF sheep were significantly higher, similar to end-systolic volume (**Table 2**). The maximum rate of pressure generation tended to be higher in the control animals; however, this was not significant.

Collagen Deposition

Microscopically, there was a significant degree of ischemic damage seen in the hearts of the HF sheep. Left ventricular collagen deposition in the HF sheep was determined as an indicator of cardiac damage. The mean left ventricular collagen content in the HF sheep was significantly higher than in healthy control sheep (8.9 ± 1 vs. 1.3 ± 0.3% of LV wall area, $p < 0.001$). The wet heart weight of the sheep in HF was also significantly greater than that of the control sheep (426 ± 35 vs. 322 ± 15 g, $p < 0.05$, **Figure 4**).

DISCUSSION

We have established a reliable model of heart failure with reduced ejection fraction by repeated microembolizations of left ventricular coronary arteries. Our study has a number of new findings not reported previously: (1) there is a depression in the gain of the baroreflex in this model of HF; (2) diaphragmatic electromyography showed increased respiratory rate in the HF animals compared to the control animals, suggesting increased inspiratory effort; (3) in addition to an increase in respiratory rate, there was an increased incidence of apneas in this animal model. Taken together, our findings suggest that this model of HFrEF replicates the neural and respiratory instabilities seen in human HF.

One of the main clinical signs of a myocardial infarct is changes in the ECG, namely changes in the S-T segment and the T-wave. For the S-T segment, in most cases, patients that have had a suspected myocardial infarct present with an elevation in this segment (Members et al., 2012). In contrast to clinical findings, we observed a consistent depression in the S-T segment of the embolized animals. Clinically, patients exhibiting an S-T depression had adverse long-term outcomes (Schechtman et al., 1989; Krone et al., 1993; Hyde et al., 1999). This depression in our study may reflect the recordings being done in a supine cradled position for these sheep. In the absence of pre-cordial leads, it makes it difficult to draw conclusions as to which region of the left ventricle received most ischemic damage.

Several other studies, in patients, have shown collagen deposition in the myocardium, suggestive of ventricular remodeling (Weber et al., 1993; Martos et al., 2007; Mewton

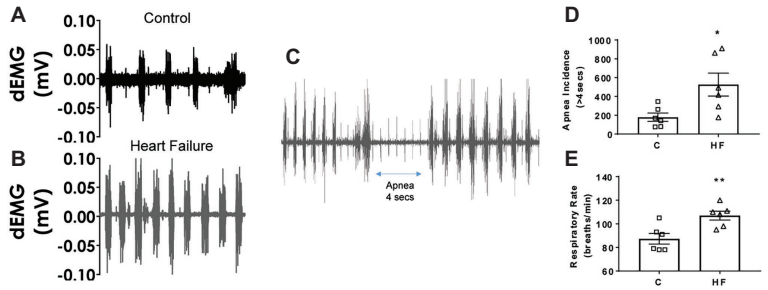

FIGURE 2 | Raw traces of sheep diaphragmatic electromyography and respiration rate in control and heart failure sheep. **(A)** Raw signal of dEMG in a control sheep and **(B)** raw signal of dEMG in a HF sheep, and **(C)** raw signal showing an apnea segment in a HF sheep 16 weeks after embolization. **(D)** Apnea incidence and **(E)** respiratory rate in control healthy sheep and in HF sheep 16 weeks after microembolization, control (square) and HF (triangle). *$p < 0.05$, **$p < 0.01$. Bars represent mean values ± SEM. Data from individual sheep are illustrated with symbols; dEMG, diaphragmatic electromyography.

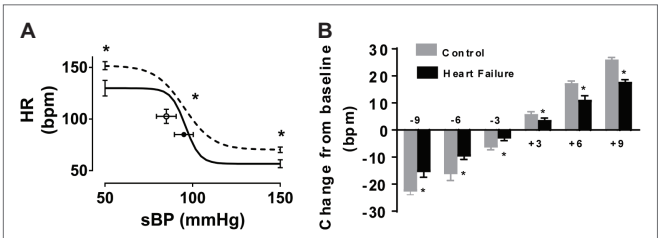

FIGURE 3 | Effect of microembolizations on the arterial baroreflex in conscious healthy and HF sheep. **(A)** Control animals (solid line) and HF animals (dashed line) (n = 6/group). Error bars at each end of the curves refer to ±SEM of the upper and lower heart rate (HR) plateaus. Circles and error bars represent mean ± SEM of resting systolic blood pressure (sBP) and heart rate (HR). **(B)** Changes in resting heart rate, due to phenylephrine and sodium nitroprusside infusions, plotted in 3 mmHg change bins. Gray bars represent control animals, black bars represent heart failure animals. *$p < 0.05$, n = 6/group.

TABLE 2 | Pressure-volume loops testing left ventricular function in anesthetized normal and heart failure sheep.

Parameter	Normal (n = 6)	Heart failure (n = 6)
Ejection fraction (%)	56 ± 7	25 ± 4**
Cardiac output (L/min)	2.8 ± 1	3.9 ± 1
Stroke volume (ml)	33 ± 6	42 ± 6
End-diastolic volume (ml/min)	74 ± 21	194 ± 36*
End-systolic volume (ml/min)	40 ± 20	154 ± 34*
End-diastolic pressure (mmHg)	6.2 ± 1	11.4 ± 2**
dP/dT max (mmHg/s)	1,745 ± 321	1,257 ± 154
dV/dT max (ml/s)	1,425 ± 155	3,361 ± 617**

*$p < 0.05$; **$p < 0.01$.

et al., 2011). The gross and microscopic changes of myocyte hypertrophy and increased collagen fibrosis have also been demonstrated in other models of HF (Falk et al., 2005). After an episode of myocardial infarction, there is structural remodeling that is initiated by an inflammatory response (Sun, 2008; Suthahar et al., 2017). Scarring then forms at the infarcted area. While the scarring and fibrosis at the site of infarct maintain the structure and integrity of the heart, this remodeling can have consequences for ventricular contractility (Brilla and Weber, 1992).

One of the ways to assess the degree of HF is the construction of pressure-volume loops. One of the advantages of constructing pressure-volume loops is the measurement of parameters independent of pre- and after load (Burkhoff, 2013). A hallmark of systolic dysfunction with reduced ejection is an increase in left ventricular end-diastolic pressure (LVEDP), which was observed in the present study (**Table 2**). Since LVEDP is a reflection of ventricular performance, the increases in LVEDP may be associated with the size of the infarct or the amount of damage to the left ventricle (Mielniczuk et al., 2007). Furthermore, we also see a significantly higher end-diastolic volume in the HF animals similar to findings in other studies (Sabbah et al., 2000; Morita et al., 2002; Falk et al., 2005). Additionally, there was a significant increase in both end-diastolic (EDV) and end-systolic volume (ESV) in the HF animals. In HF, the severity of an increase in both these volumes at time of referral is a prognostic indicator of mortality in patients (Diaz et al., 1987).

In the present study, we show significant increases in plasma levels of brain natriuretic peptide (BNP) and norepinephrine (**Table 1**). These increases in plasma levels of BNP (Sakurai et al., 2003) and norepinephrine (Cohn et al., 1984) have been shown previously to relate to the severity of HF. Our findings are in agreement with other models of HF, which have also found elevated plasma levels of norepinephrine and brain natriuretic peptide (Sabbah et al., 2000; Morita et al., 2002).

We report a significant decrease in the MAP of the animals with HF. One mechanism that serves to maintain BP is the arterial baroreflex and previous studies have reported a dampening of the sensitivity of the arterial baroreflex control of heart rate in HF (Eckberg et al., 1971; Ferguson et al., 1992; Grassi et al., 1995) as well as in clinical patients (Mortara et al., 1997). We hypothesized that this model would be associated with a blunted baroreflex and observed an impaired HR response to changes in MAP. This impaired baroreflex is similar to previous reports by us in a pacing-induced model of HF (Watson et al., 2007; Abukar et al., 2016) as well as other

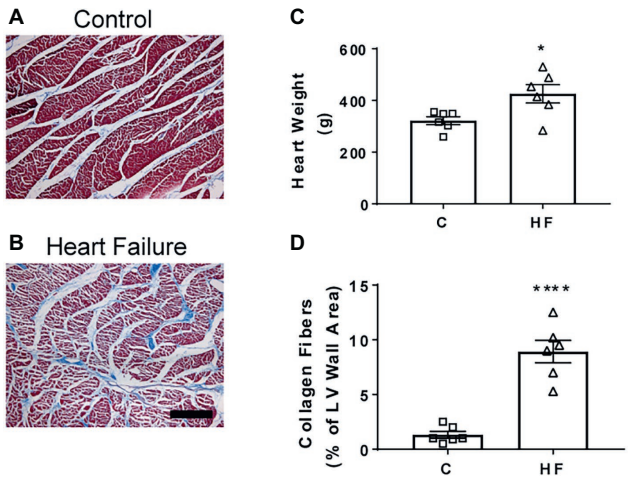

FIGURE 4 | Representative sheep cardiac tissue images and effect of microembolizations on collagen deposition and heart weight. **(A)** Top image shows section of left ventricle wall of the sheep heart in a control healthy animal and **(B)** bottom image shows section of left ventricle wall in a HF sheep 16 weeks after microembolization. **(C)** Heart weights of control (square) and HF (triangle) sheep. **(D)** Collagen content in control and HF sheep, $^{*}p < 0.05$, $^{****}p < 0.0001$. Bars represent mean values ± SEM. Data from individual sheep are illustrated with symbols. C, control (square); HF (triangle), heart failure; LV, left ventricle of heart. Scale bar = 100 μm.

models (Higgins et al., 1972; Greenberg et al., 1973; Zucker et al., 1977). In addition to depressed baroreflex function, we also examined sympathetic control of heart rate in this model. We observed a significant decrease in heart rate in the HF animals after beta blockade. This suggests there is a significant contribution in HF animals from the sympathetic nervous system, more so than the control animals in which no significant decrease in heart rate was observed after propranolol infusion. These findings are consistent with our previous studies suggesting low levels of cardiac sympathetic drive and cardiac norepinephrine spillover in normal animals. Both these variables are elevated in animals with pacing-induced HF (Ramchandra et al., 2009a, 2018).

In addition to changes in hemodynamic parameters, we also observed an increase in the breathing rate and an increase in the incidence of apneas. Chronic hyperventilation has been reported in HF patients (Sullivan et al., 1988) and pulmonary congestion is suspected to be the main cause of this hyperventilation (Sullivan et al., 1988). The animals in the HF group had significantly increased body weight compared to the control animals (**Figure 1**), which points toward fluid congestion. We also saw signs of fluid congestion in the heart and ascites in the HF group at the time of post-mortem although this was not systematically investigated. We speculate that this fluid congestion contributed to the hyperventilation in these animals. In addition to peripheral causes, central apneas are also common in heart failure, with around 40–50% of patients being affected (Javaheri et al., 1995; Vazir et al., 2007). Central sleep apnea can be a marker of HF severity, with central apnea patients showing more advanced symptoms (Oldenburg et al., 2007). Together, these results suggest that the microembolization model replicates the respiratory imbalance seen in HF.

We report successful induction of heart failure in sheep using repeated percutaneous injection of microspheres into the coronary arteries. This approach targets the coronary circulation and thereby circumvents potential systemic effects if a toxin is administered intravenously. Since the HF is induced by a durable ischemic insult, interventions with novel pacing paradigms can be undertaken in pacing naïve hearts, avoiding the potential confounder of pacing-induced changes. Practically, repeated access to the arterial circulation is an important consideration. Previous studies have constructed carotid artery loops to allow repeated access. We percutaneously accessed the femoral arteries and following embolization, digitally compressed the puncture site for hemostasis without the use of a closure device, returning the animal to the crate/pen without any indwelling cannulae retained for future access. This has a number of advantages over other methods of surgical approach to perform the microembolization. Cardiac catheterization using these techniques requires access to fluoroscopy to guide cannulation and confirm successful and stable engagement in the coronary vessels.

There are a few limitations to this approach as well. One important limitation of this approach is the diffuse pattern of blockage and fibrosis that is observed. As such, it is difficult to quantify the region of infarcted tissue adequately as would be possible with coronary ligation. We utilized ejection fraction and fractional shortening from the echocardiographic data to quantify the decline in heart function. In addition, three out of the nine sheep did not survive the first embolization as they developed pulmonary congestion that could be resolved using diuretics. In addition to these three animals, two of the animals studied also needed administration of diuretics after the embolization procedure, and in these two cases, the congestion was resolved and the animals continued in the protocol. While the presence of congestion makes this model clinically relevant, this does necessitate increased animal numbers to complete a cohort of animals for a study.

In conclusion, our study indicates that chronic heart failure can be successfully induced in sheep using repeated injection of microspheres into the coronary arteries. After 2 months, the animals develop clinical signs of heart failure. There is marked increase in heart weight with histological evidence of ventricular fibrosis. There is a decrease in mean arterial pressure and an increase in incidence of apneas. Furthermore, pressure-volume loops show altered left ventricle dynamics in the heart failure sheep and the baroreflex challenge under conscious conditions showed a significant decrease in the gain. We conclude that this is a good model of HF to test changes in either neural control or respiratory function after interventions.

DATA AVAILABILITY STATEMENT

The data gathered in this study are available upon request to the corresponding author.

ETHICS STATEMENT

The animal study was reviewed and approved by The University of Auckland Animal Ethics Committee.

AUTHOR CONTRIBUTIONS

YA, NL, MP, IL, and RR collected the ECG data for this study. All other data were collected by RR, MP, and YA. RR supervised the study. YA completed the data analysis and wrote initial manuscript. All authors contributed in revising the manuscript toward the final version.

FUNDING

The authors gratefully acknowledge granting support from the Health Research Council of New Zealand, the National Heart Foundation of New Zealand, the University of Auckland Faculty Research Development Fund, and the Maurice Phyllis Paykel Trust.

ACKNOWLEDGMENTS

The authors would like to thank Bindu George and Linley Nisbet for their expert technical assistance.

REFERENCES

Abukar, Y., May, C. N., and Ramchandra, R. (2016). Role of endothelin-1 in mediating changes in cardiac sympathetic nerve activity in heart failure. *Am. J. Phys. Regul. Integr. Comp. Phys.* 310, R94–R99. doi: 10.1152/ajpregu.00205.2015

Amorim, D., Heer, K., Jenner, D., Richardson, P., Dargie, H., Brown, M., et al. (1981). Is there autonomic impairment in congestive (dilated) cardiomyopathy? *Lancet* 317, 525–527. doi: 10.1016/S0140-6736(81)92863-4

Baan, J., Van Der Velde, E. T., De Bruin, H. G., Smeenk, G. J., Koops, J., Van Dijk, A. D., et al. (1984). Continuous measurement of left ventricular volume in animals and humans by conductance catheter. *Circulation* 70, 812–823. doi: 10.1161/01.CIR.70.5.812

Benedict, C. R., Shelton, B., Johnstone, D. E., Francis, G., Greenberg, B., Konstam, M., et al. (1996). Prognostic significance of plasma norepinephrine in patients with asymptomatic left ventricular dysfunction. *Circulation* 94, 690–697. doi: 10.1161/01.CIR.94.4.690

Bibevski, S., and Dunlap, M. E. (1999). Ganglionic mechanisms contribute to diminished vagal control in heart failure. *Circulation* 99, 2958–2963. doi: 10.1161/01.CIR.99.22.2958

Borenstein, N., Bruneval, P., Behr, L., Laborde, F., Montarras, D., Daurès, J. P., et al. (2006). An ovine model of chronic heart failure: echocardiographic and tissue Doppler imaging characterization. *J. Card. Surg.* 21, 50–56. doi: 10.1111/j.1540-8191.2006.00168.x

Brilla, C. G., and Weber, K. T. (1992). Reactive and reparative myocardial fibrosis in arterial hypertension in the rat. *Cardiovasc. Res.* 26, 671–677. doi: 10.1093/cvr/26.7.671

Bristow, M. R., Sageman, W. S., Scott, R. H., Billingham, M. E., Bowden, R. E., Kernoff, R. S., et al. (1980). Acute and chronic cardiovascular effects of doxorubicin in the dog: the cardiovascular pharmacology of drug-induced histamine release. *J. Cardiovasc. Pharmacol.* 2, 487–515. doi: 10.1097/00005344-198009000-00002

Burkhoff, D. (2013). Pressure-volume loops in clinical research: a contemporary view. *J. Am. Coll. Cardiol.* 62, 1173–1176. doi: 10.1016/j.jacc.2013.05.049

Byrne, M. J., Kaye, D. M., Mathis, M., Reuter, D. G., Alferness, C. A., and Power, J. M. (2004). Percutaneous mitral annular reduction provides continued benefit in an ovine model of dilated cardiomyopathy. *Circulation* 110, 3088–3092. doi: 10.1161/01.CIR.0000146904.13677.E4

Chekanov, V. S. (1999). A stable model of chronic bilateral ventricular insufficiency (dilated cardiomyopathy) induced by arteriovenous anastomosis and doxorubicin administration in sheep. *J. Thorac. Cardiovasc. Surg.* 117, 198–199. doi: 10.1016/s0022-5223(99)70494-0

Cohn, J. N., Levine, T. B., Olivari, M. T., Garberg, V., Lura, D., Francis, G. S., et al. (1984). Plasma norepinephrine as a guide to prognosis in patients with chronic congestive heart failure. *N. Engl. J. Med.* 311, 819–823. doi: 10.1056/NEJM198409273111303

Devlin, G., Matthews, K., McCracken, G., Stuart, S., Jensen, J., Conaglen, J., et al. (2000). An ovine model of chronic stable heart failure. *J. Card. Fail.* 6, 140–143. doi: 10.1016/S1071-9164(00)90016-2

Diaz, R. A., Obasohan, A., and Oakley, C. M. (1987). Prediction of outcome in dilated cardiomyopathy. *Heart* 58, 393–399. doi: 10.1136/hrt.58.4.393

Dixon, J. A., and Spinale, F. G. (2009). Large animal models of heart failure: a critical link in the translation of basic science to clinical practice. *Circ. Heart Fail.* 2, 262–271. doi: 10.1161/CIRCHEARTFAILURE.108.814459

Dunlap, M. E., Bibevski, S., Rosenberry, T. L., and Ernsberger, P. (2003). Mechanisms of altered vagal control in heart failure: influence of muscarinic receptors and acetylcholinesterase activity. *Am. J. Phys. Heart Circ. Phys.* 285, H1632–H1640. doi: 10.1152/ajpheart.01051.2002

Eckberg, D. L., Drabinsky, M., and Braunwald, E. (1971). Defective cardiac parasympathetic control in patients with heart disease. *N. Engl. J. Med.* 285, 877–883. doi: 10.1056/NEJM197110142851602

Falk, V., Garbade, J., and Walther, T. (2005). *Experimental models of heart failure practical methods in cardiovascular research*. Germany: Springer-Verlag, Berlin, Heidelberg, 83–110.

Ferguson, D. W., Berg, W. J., Roach, P. J., Oren, R. M., and Mark, A. L. (1992). Effects of heart failure on baroreflex control of sympathetic neural activity. *Am. J. Cardiol.* 69, 523–531. doi: 10.1016/0002-9149(92)90998-E

Floras, J. S. (2009). Sympathetic nervous system activation in human heart failure: clinical implications of an updated model. *J. Am. Coll. Cardiol.* 54, 375–385. doi: 10.1016/j.jacc.2009.03.061

Getman, V., Devyatko, E., Wolner, E., Aharinejad, S., and Mueller, M. R. (2006). Fleece bound sealing prevents pleural adhesions. *Interact. Cardiovasc. Thorac. Surg.* 5, 243–246. doi: 10.1510/icvts.2005.121129

Grassi, G., Seravalle, G., Cattaneo, B. M., Lanfranchi, A., Vailati, S., Giannattasio, C., et al. (1995). Sympathetic activation and loss of reflex sympathetic control in mild congestive heart failure. *Circulation* 92, 3206–3211. doi: 10.1161/01.CIR.92.11.3206

Greenberg, T. T., Richmond, W. H., Stocking, R. A., Gupta, P. D., Meehan, J. P., and Henry, J. P. (1973). Impaired atrial receptor responses in dogs with heart failure due to tricuspid insufficiency and pulmonary artery stenosis. *Circ. Res.* 32, 424–433.

Haghighi, K., Kolokathis, F., Pater, L., Lynch, R. A., Asahi, M., Gramolini, A. O., et al. (2003). Human phospholamban null results in lethal dilated cardiomyopathy revealing a critical difference between mouse and human. *J. Clin. Invest.* 111, 869–876. doi: 10.1172/JCI17892

Higgins, C. B., Vatner, S. F., Eckberg, D. L., and Braunwald, E. (1972). Alterations in the baroreceptor reflex in conscious dogs with heart failure. *J. Clin. Invest.* 51, 715–724. doi: 10.1172/JCI106865

Hood, W. B. Jr., McCarthy, B., and Lown, B. (1967). Myocardial infarction following coronary ligation in dogs: hemodynamic effects of isoproterenol and acetylstrophanthidin. *Circ. Res.* 21, 191–200. doi: 10.1161/01.RES.21.2.191

Huang, Y., Hunyor, S. N., Jiang, L., Kawaguchi, O., Shirota, K., Ikeda, Y., et al. (2004). Remodeling of the chronic severely failing ischemic sheep heart after coronary microembolization: functional, energetic, structural, and cellular responses. *Am. J. Phys. Heart Circ. Phys.* 286, H2141–H2150. doi: 10.1152/ajpheart.00829.2003

Hyde, T. A., French, J. K., Wong, C.-K., Straznicky, I. T., Whitlock, R. M., and White, H. D. (1999). Four-year survival of patients with acute coronary syndromes without ST-segment elevation and prognostic significance of 0.5-mm ST-segment depression. *Am. J. Cardiol.* 84, 379–385. doi: 10.1016/S0002-9149(99)00319-7

Jackson, G., Gibbs, C., Davies, M., and Lip, G. (2000). ABC of heart failure: pathophysiology. *BMJ* 320, 167–170. doi: 10.1136/bmj.320.7228.167

Javaheri, S., Parker, T. J., Wexler, L., Michaels, S. E., Stanberry, E., Nishyama, H., et al. (1995). Occult sleep-disordered breathing in stable congestive heart failure. *Ann. Intern. Med.* 122, 487–492. doi: 10.7326/0003-4819-122-7-199504010-00002

Justice, T. D., Hammer, G. L., Davey, R. J., Paramalingam, N., Guelfi, K. J., Lewis, L., et al. (2015). Effect of antecedent moderate-intensity exercise on the glycemia-increasing effect of a 30-sec maximal sprint: a sex comparison. *Physiol. Rep.* 3, E12386–E12406. doi: 10.14814/phy2.12386

Kemp, C. D., and Conte, J. V. (2012). The pathophysiology of heart failure. *Cardiovasc. Pathol.* 21, 365–371. doi: 10.1016/j.carpath.2011.11.007

Kinugawa, T., and Dibner-Dunlap, M. E. (1995). Altered vagal and sympathetic control of heart rate in left ventricular dysfunction and heart failure. *Am. J. Phys. Regul. Integr. Comp. Phys.* 268, R310–R316. doi: 10.1152/ajpregu.1995.268.2.R310

Krone, R. J., Greenberg, H., Dwyer, E. M. Jr., Kleiger, R. E., and Boden, W. E. Group, M. D. P. T. R (1993). Long-term prognostic significance of ST segment depression during acute myocardial infraction. *J. Am. Coll. Cardiol.* 22, 361–367. doi: 10.1016/0735-1097(93)90038-3

Lewis, L. K., Raudsepp, S. D., Yandle, T. G., Prickett, T. C., and Richards, A. M. (2017). Development of a BNP1-32 immunoassay that does not cross-react with proBNP. *Clin. Chem.* 63, 1110–1117. doi: 10.1373/clinchem.2016.269712

Martos, R., Baugh, J., Ledwidge, M., O'Loughlin, C., Conlon, C., Patle, A., et al. (2007). Diastolic heart failure: evidence of increased myocardial collagen turnover linked to diastolic dysfunction. *Circulation* 115, 888–895. doi: 10.1161/CIRCULATIONAHA.106.638569

McMahon, W. S., Mukherjee, R., Gillette, P. C., Crawford, F. A., and Spinale, F. G. (1996). Right and left ventricular geometry and myocyte contractile processes with dilated cardiomyopathy: myocyte growth and β-adrenergic responsiveness. *Cardiovasc. Res.* 31, 314–323. doi: 10.1016/0008-6363(95)00212-X

Members, A. T. F., Steg, P. G., James, S. K., Atar, D., Badano, L. P., Lundqvist, C. B., et al. (2012). ESC guidelines for the management of acute myocardial infarction in patients presenting with ST-segment elevation: the task force on the management of ST-segment elevation acute myocardial infarction of the European Society of Cardiology (ESC). *Eur. Heart J.* 33, 2569–2619. doi: 10.1093/eurheartj/ehs215

Mewton, N., Liu, C. Y., Croisille, P., Bluemke, D., and Lima, J. A. (2011). Assessment of myocardial fibrosis with cardiovascular magnetic resonance. *J. Am. Coll. Cardiol.* 57, 891–903. doi: 10.1016/j.jacc.2010.11.013

Mielniczuk, L. M., Lamas, G. A., Flaker, G. C., Mitchell, G., Smith, S. C., Gersh, B. J., et al. (2007). Left ventricular end-diastolic pressure and risk of subsequent heart failure in patients following an acute myocardial infarction. *Congest. Heart Fail.* 13, 209–214. doi: 10.1111/j.1527-5299.2007.06624.x

Monreal, G., Gerhardt, M. A., Kambara, A., Abrishamchian, A. R., Bauer, J. A., and Goldstein, A. H. (2004). Selective microembolization of the circumflex coronary artery in an ovine model: dilated, ischemic cardiomyopathy and left ventricular dysfunction. *J. Card. Fail.* 10, 174–183. doi: 10.1016/j.cardfail.2003.08.013

Morita, H., Suzuki, G., Mishima, T., Chaudhry, P. A., Anagnostopoulos, P. V., Tanhehco, E. J., et al. (2002). Effects of long-term monotherapy with metoprolol CR/XL on the progression of left ventricular dysfunction and remodeling in dogs with chronic heart failure. *Cardiovasc. Drugs Ther.* 16, 443–449. doi: 10.1023/A:1022142620189

Mortara, A., La Rovere, M. T., Pinna, G. D., Prpa, A., Maestri, R., Febo, O., et al. (1997). Arterial baroreflex modulation of heart rate in chronic heart failure: clinical and hemodynamic correlates and prognostic implications. *Circulation* 96, 3450–3458. doi: 10.1161/01.CIR.96.10.3450

O'Rourke, B., Kass, D. A., Tomaselli, G. F., Kääb, S., Tunin, R., and Marbán, E. (1999). Mechanisms of altered excitation-contraction coupling in canine tachycardia-induced heart failure, I: experimental studies. *Circ. Res.* 84, 562–570. doi: 10.1161/01.RES.84.5.562

Oizumi, H., Naruke, T., Watanabe, H., Sano, T., Kondo, H., Goya, T., et al. (1990). Completion pneumonectomy–a review of 29 cases. *Nihon Kyobu Geka Gakkai Zasshi* 38, 72–77.

Oldenburg, O., Lamp, B., Faber, L., Teschler, H., Horstkotte, D., and Töpfer, V. (2007). Sleep-disordered breathing in patients with symptomatic heart failure a contemporary study of prevalence in and characteristics of 700 patients. *Eur. J. Heart Fail.* 9, 251–257. doi: 10.1016/j.ejheart.2006.08.003

Pemberton, C., Yandle, T., Charles, C., Rademaker, M., Aitken, G., and Espiner, E. (1997). Ovine brain natriuretic peptide in cardiac tissues and plasma: effects of cardiac hypertrophy and heart failure on tissue concentration and molecular forms. *J. Endocrinol.* 155, 541–550. doi: 10.1677/joe.0.1550541

Prabhu, S. D., and Freeman, G. L. (1995). Effect of tachycardia heart failure on the restitution of left ventricular function in closed-chest dogs. *Circulation* 91, 176–185. doi: 10.1161/01.CIR.91.1.176

Ramchandra, R., Hood, S. G., Denton, D. A., Woods, R. L., McKinley, M. J., McAllen, R. M., et al. (2009a). Basis for the preferential activation of cardiac sympathetic nerve activity in heart failure. *Proc. Natl. Acad. Sci. USA* 106, 924–928. doi: 10.1073/pnas.0811929106

Ramchandra, R., Hood, S. G., Frithiof, R., and May, C. N. (2009b). Discharge properties of cardiac and renal sympathetic nerves and their impaired responses to changes in blood volume in heart failure. *Am. J. Phys. Regul. Integr. Comp. Phys.* 297, R665–R674. doi: 10.1152/ajpregu.00191.2009

Ramchandra, R., Hood, S. G., Xing, D., Lambert, G. W., and May, C. N. (2018). Mechanisms underlying the increased cardiac norepinephrine spillover in heart failure. *Am. J. Phys. Heart Circ. Phys.* 315, H340–H347. doi: 10.1152/ajpheart.00069.2018

Sabbah, H. N., Stanley, W. C., Sharov, V. G., Mishima, T., Tanimura, M., Benedict, C. R., et al. (2000). Effects of dopamine β-hydroxylase inhibition with nepicastat on the progression of left ventricular dysfunction and remodeling in dogs with chronic heart failure. *Circulation* 102, 1990–1995. doi: 10.1161/01.CIR.102.16.1990

Sakurai, S., Adachi, H., Hasegawa, A., Hoshizaki, H., Oshima, S., Taniguchi, K., et al. (2003). Brain natriuretic peptide facilitates severity classification of stable chronic heart failure with left ventricular dysfunction. *Heart* 89, 661–662. doi: 10.1136/heart.89.6.661

Savarese, G., and Lund, L. H. (2017). Global public health burden of heart failure. *Card. Fail. Rev.* 3, 7–11. doi: 10.15420/cfr.2016:25:2

Schechtman, K. B., Capone, R., Kleiger, R. E., Gibson, R. S., Schwartz, D. J., Roberts, R., et al. (1989). Risk stratification of patients with non-Q wave myocardial infarction. The critical role of ST segment depression. The Diltiazem Reinfarction Study Research Group. *Circulation* 80, 1148–1158. doi: 10.1161/01.CIR.80.5.1148

Schmitto, J. D., Coskun, K. O., Coskun, S. T., Ortmann, P., Vorkamp, T., Heidrich, F., et al. (2009). Hemodynamic changes in a model of chronic heart failure induced by multiple sequential coronary microembolization in sheep. *Artif. Organs* 33, 947–952. doi: 10.1111/j.1525-1594.2009.00921.x

Sieck, G. C., and Fournier, M. (1990). Changes in diaphragm motor unit EMG during fatigue. *J. Appl. Physiol.* 68, 1917–1926. doi: 10.1152/jappl.1990.68.5.1917

Spinale, F. G., Tomita, M., Zellner, J. L., Cook, J. C., Crawford, F. A., and Zile, M. R. (1991). Collagen remodeling and changes in LV function during development and recovery from supraventricular tachycardia. *Am. J. Phys. Heart Circ. Phys.* 261, H308–H318. doi: 10.1152/ajpheart.1991.261.2.H308

Sullivan, M., Higginbotham, M., and Cobb, F. (1988). Increased exercise ventilation in patients with chronic heart failure: intact ventilatory control despite hemodynamic and pulmonary abnormalities. *Circulation* 77, 552–559. doi: 10.1161/01.CIR.77.3.552

Sun, Y. (2008). Myocardial repair/remodelling following infarction: roles of local factors. *Cardiovasc. Res.* 81, 482–490. doi: 10.1093/cvr/cvn333

Suthahar, N., Meijers, W. C., Silljé, H. H., and de Boer, R. A. (2017). From inflammation to fibrosis—molecular and cellular mechanisms of myocardial tissue remodelling and perspectives on differential treatment opportunities. *Curr. Heart Fail. Rep.* 14, 235–250. doi: 10.1007/s11897-017-0343-y

Tanaka, R., Fulbright, B. M., Mukherjee, R., Burchell, S. A., Crawford, F. A., Zile, M. R., et al. (1993). The cellular basis for the blunted response to β-adrenergic stimulation in supraventricular tachycardia-induced cardiomyopathy. *J. Mol. Cell. Cardiol.* 25, 1215–1233. doi: 10.1006/jmcc.1993.1134

Timek, T. A., Dagum, P., Lai, D. T., Liang, D., Daughters, G. T., Tibayan, F., et al. (2003). Tachycardia-induced cardiomyopathy in the ovine heart: mitral annular dynamic three-dimensional geometry. *J. Thorac. Cardiovasc. Surg.* 125, 315–324. doi: 10.1067/mtc.2003.80

Toyoda, Y., Okada, M., and Kashem, M. A. (1998). A canine model of dilated cardiomyopathy induced by repetitive intracoronary doxorubicin administration. *J. Thorac. Cardiovasc. Surg.* 115, 1367–1373. doi: 10.1016/S0022-5223(98)70221-1

Vazir, A., Hastings, P., Dayer, M., McIntyre, H., Henein, M., Poole-Wilson, P., et al. (2007). A high prevalence of sleep disordered breathing in men with mild symptomatic chronic heart failure due to left ventricular systolic dysfunction. *Eur. J. Heart Fail.* 9, 243–250. doi: 10.1016/j.ejheart.2006.08.001

Watson, A. M., Hood, S. G., Ramchandra, R., McAllen, R. M., and May, C. N. (2007). Increased cardiac sympathetic nerve activity in heart failure is not due to desensitization of the arterial baroreflex. *Am. J. Phys. Heart Circ. Phys.* 293, H798–H804. doi: 10.1152/ajpheart.00147.2007

Weber, K. T., Brilla, C. G., and Janicki, J. S. (1993). Myocardial fibrosis: functional significance and regulatory factors. *Cardiovasc. Res.* 27, 341–348. doi: 10.1093/cvr/27.3.341

Yim, A. P., Liu, H.-P., Hazelrigg, S. R., Izzat, M. B., Fung, A. L., Boley, T. M., et al. (1998). Thoracoscopic operations on reoperated chests. *Ann. Thorac. Surg.* 65, 328–330. doi: 10.1016/S0003-4975(97)01341-6

Zucker, I. H., Earle, A. M., and Gilmore, J. P. (1977). The mechanism of adaptation of left atrial stretch receptors in dogs with chronic congestive heart failure. *J. Clin. Investig.* 60, 323–331. doi: 10.1172/JCI108780

Conflict of Interest: The authors declare that the research was conducted in the absence of any commercial or financial relationships that could be construed as a potential conflict of interest.

frontiers in Neuroscience

ORIGINAL RESEARCH
published: 13 December 2019
doi: 10.3389/fnins.2019.01343

Adaptation of Respiratory-Related Brain Regions to Long-Term Hypercapnia: Focus on Neuropeptides in the RTN

*Ayse Sumeyra Dereli[1], Zarwa Yaseen[1], Pascal Carrive[2] and Natasha N. Kumar[1]**

[1] Department of Pharmacology, School of Medical Sciences, University of New South Wales, Sydney, NSW, Australia,
[2] Department of Anatomy, School of Medical Sciences, University of New South Wales, Sydney, NSW, Australia

Long-term hypercapnia is associated with respiratory conditions including obstructive sleep apnea, chronic obstructive pulmonary disease and obesity hypoventilation syndrome. Animal studies have demonstrated an initial (within hours) increase in ventilatory drive followed by a decrease in this response over the long-term (days–weeks) in response hypercapnia. Little is known about whether changes in the central respiratory chemoreflex are involved. Here we investigated whether central respiratory chemoreceptor neurons of the retrotrapezoid nucleus (RTN), which project to the respiratory pattern generator within the ventral respiratory column (VRC) have a role in the mechanism of neuroplasticity associated with long-term hypercapnia. Adult male C57BL/6 mice (n = 5/group) were used. Our aims were (1) to determine if galanin, neuromedin B and gastrin-releasing peptide gene expression is altered in the RTN after long-term hypercapnia. This was achieved using qPCR to measure mRNA expression changes of neuropeptides in the RTN after short-term hypercapnia (6 or 8 h, 5 or 8% CO_2) or long-term hypercapnia exposure (10 day, 5 or 8% CO_2), (2) in the mouse brainstem, to determine the distribution of preprogalanin in chemoreceptors, and the co-occurrence of the galanin receptor 1 (GalR1:Gi-coupled receptor) with inhibitory GlyT2 ventral respiratory column neurons using *in situ* hybridization (ISH) to better characterize galaninergic RTN-VRC circuitry, (3) to investigate whether long-term hypercapnia causes changes to recruitment (detected by cFos immunohistochemistry) of respiratory related neural populations including the RTN neurons and their galaninergic subset, *in vivo*. Collectively, we found that hypercapnia decreases neuropeptide expression in the RTN in the short-term and has the opposite effect over the long-term. Following long term hypercapnia, the number of RTN galanin neurons remains unchanged, and their responsiveness to acute chemoreflex is sustained; in contrast, we identified multiple respiratory related sites that exhibit blunted chemoreflex activation. GalR1 was distributed in 11% of preBötC and 30% of BötC glycinergic neurons. Our working hypothesis is that during long-term hypercapnia, galanin co-release from RTN neurons may counterbalance glutamatergic inputs to respiratory centers to downscale energetically wasteful hyperventilation, thereby having a role in neuroplasticity by contributing to a decrease in ventilation, through the inhibitory effects of galanin.

Keywords: chemoreception, neuropeptide, hypercapnia, neuroplasticity, respiratory, retrotrapezoid nuclus, c-Fos

OPEN ACCESS

Edited by:
Vaughan G. Macefield, Baker Heart and Diabetes Institute, Australia

Reviewed by:
Ana Paula Abdala, University of Bristol, United Kingdom
Thiago S. Moreira, University of São Paulo, Brazil

***Correspondence:**
Natasha N. Kumar
natasha.kumar@unsw.edu.au

Specialty section:
This article was submitted to Autonomic Neuroscience, a section of the journal Frontiers in Neuroscience

Received: *27 September 2019*
Accepted: *28 November 2019*
Published: *13 December 2019*

Citation:
Dereli AS, Yaseen Z, Carrive P and Kumar NN (2019) Adaptation of Respiratory-Related Brain Regions to Long-Term Hypercapnia: Focus on Neuropeptides in the RTN. Front. Neurosci. 13:1343. doi: 10.3389/fnins.2019.01343

INTRODUCTION

Respiratory conditions including chronic obstructive pulmonary disease (COPD), obesity hypoventilation syndrome (OHS) and obstructive sleep apnea (OSA) are associated with long-term hypercapnia and hypoxia. Associated long-term detrimental effects include poor quality of life, poor cognitive function and increased mortality rate. While the changes in the respiratory chemoreflex mechanisms during long-term hypoxia are extensively investigated (Peng et al., 2001, 2003, 2006; Rey et al., 2004; Huang et al., 2009; Morgan et al., 2016; Barnett et al., 2017) little is known about long-term hypercapnia. Acute hypercapnia causes an increase in ventilatory drive by peripherally and centrally mediated chemoreflex mechanisms (Forster and Smith, 2010; Smith et al., 2010). Long-term hypercapnia shows a biphasic ventilatory response in humans, dogs, goats and rodents, consisting of an initial increase in ventilatory drive in the first 8 h (rodents), 24 h (goats and dogs), 5 days (human) followed by a sustained decrease in this response (21–44 days) (Schaefer, 1963; Schaefer et al., 1963; Clark et al., 1971; Pingree, 1977; Lai et al., 1981; Jennings and Davidson, 1984; Burgraff et al., 2018; Burgraff et al., 2019). The mechanism underlying physiological adaptation to long-term hypercapnia is not clearly understood. Many peripheral factors are suggested to contribute to this plasticity including metabolic compensation, muscle fiber transformation in the diaphragm and changes in lung hyaline membrane turnover (Schaefer et al., 1964; Lai et al., 1981; Kondo et al., 2000; Johnson, 2017; Burgraff et al., 2018). Lai et al. (1981) first suggested a contribution from central chemoreceptors to this adaptation; more recently, changes in glutamate receptor expression were observed in central chemoreceptors (Burgraff et al., 2019).

The retrotrapezoid nucleus (RTN) chemoreceptor neurons are intrinsically sensitive to brain pH/Pco_2 (Takakura et al., 2006; Wang S. et al., 2013) and are critical in mediating the central respiratory chemoreflex. RTN neurons send excitatory drive to the ventral respiratory column (VRC) via extensive projections (Mulkey et al., 2004; Abbott et al., 2009b; Bochorishvili et al., 2012). The VRC generates the rhythmic breathing pattern and regulates the depth and frequency of breathing through innervation of motor neurons that control the muscles of breathing (Feldman et al., 2003; Nattie and Li, 2012).

It is clear that glutamatergic neurotransmission from the RTN confers CO_2 stimulated breathing (Holloway et al., 2015), however, RTN neurons also express a distinctive peptidergic phenotype. All RTN neurons contain mRNA for neuromedin B (NMB) and pituitary adenylate-activating polypeptide (PACAP) (Shi et al., 2017), 50–70% express galanin (Stornetta et al., 2009; Shi et al., 2017), and a subset express gastrin-releasing peptide (GRP) (Li et al., 2016). Furthermore, the RTN has distinct functional subpopulations of neurons; for example, pre-inspiratory oscillatory neurons provide rhythmic excitatory drive (Onimaru et al., 1997; Smith et al., 2009), neurons lateral to the facial nucleus are involved in active expiration (Pagliardini et al., 2011) and ventral to parafacial neurons are chemosensitive (Huckstepp et al., 2015). The expression of specific neuropeptides by the RTN neurons might further elucidate the mechanism of these functionally distinct RTN subpopulations.

Various functional studies have indicated the role of inducible neuropeptides in the control of breathing. While NMB and GRP are excitatory (Moody and Merali, 2004; Dickson et al., 2006; Roesler and Schwartsmann, 2012), galanin is an inhibitory neuropeptide (Lang et al., 2015). Microinjection of galanin into the VRC induces apnea by inhibiting phrenic nerve activity and ventilatory chemoreflex responses (Abbott et al., 2009a) and injection of NMB and GRP into the VRC causes sighing (Li et al., 2016). Neuropeptides are known to have long-lasting effects since they act on G-protein coupled receptors (Salio et al., 2006; Nassel, 2009). Therefore, long term adjustments in neuropeptide co-release are likely important in fine-tuning the fast transmitter output of respiratory neuronal circuits in response to long-term changes in blood gas levels. Such long-term changes may occur during chronic respiratory disorders (such as hypercapnia and hypoxia related COPD, OHS, OSA, etc.) or following long-term exposure to altered environmental gas conditions (such as hypoxia at high altitudes, or hypercapnia in submarines, caves, space shuttles or mines).

The impact of long-term hypercapnia on the central respiratory chemoreflex and the contribution of neuropeptides has not been explored. Following chronic exposure (35 days) to elevated inspired CO_2 (1.5% CO_2), healthy human subjects show a significant depression of the respiratory response to 15 min inhalation of 5% CO_2 (Schaefer, 1963; Schaefer et al., 1963). Furthermore, there is a decreased ventilatory response of respiratory disease patients to acute inspired hypercapnia, suggesting a decline in their central CO_2/H^+ chemoreflex system (Kepron and Cherniack, 1973; Montes De Oca and Celli, 1998). The underlying mechanism for this blunted ventilatory response to acute hypercapnia following exposure to long-term hypercapnia is not clear. Altered chemosensory responsiveness, or adjusted peptidergic transmission by RTN neurons may explain this change in respiratory behavior following long-term hypercapnia.

In light of these gaps in knowledge, we hypothesize that neuropeptides have a role in adaptation of central respiratory chemoreception and may be involved in the pathophysiology

Abbreviations: 4V, 4th ventricle; AH, acute hypercapnic chemoreflex challenge; AP, area postrema; BötC, Bötzinger complex; CO_2, carbon dioxide; A1/C1, catecholaminergic populations of A1 and C1 area; c-, r-, caudal and rostral; cc, central canal; CL, CM, MHb, MDM, PC, PV, central lateral, central medial, medial mediodorsal, medial habenula, paracentral, paraventricular thalamic nuclei; ChAT, choline acetyltransferase; COPD, Chronic Obstructive Pulmonary Disease; comm-, m-, l-, commissural, medial, lateral NTS; DG, dentate gyrus; X, dorsal motor nucleus of vagus; VII, facial nucleus; FISH, fluorescent *in situ* hybridization; GalR1, galanin receptor 1; GRP, gastrin releasing peptide; GlyT2, glycine transporter 2; HKG, house-keeping gene; XII, hypoglossal nucleus; HPRT, hypoxanthine-guanine phosphoribosyltransferase; IHC, immunohistochemistry; ISH, *in situ* hybridization; KF, Kölliker Fuse; LC, locus coeruleus; LH, long-term hypercapnia; NMB, neuromedin b; N_2, Nitrogen; na, nucleus ambiguous; NTS, nucleus of the solitary tract; OHS, obesity hypoventilation syndrome; OSA, obstructive sleep apnea; O_2, oxygen; Phox2b, paired−like homeobox 2b; PbN, parabrachial nucleus; PFA, paraformaldehyde; preBötC, preBötzinger complex; pp-, prepro-; py, pyramids; qPCR, quantitative polymerase chain reaction; RPLPO, ribosomal protein lateral stalk subunit P0; RA, room air; SH, short-term hypercapnia; scp, superior cerebral peduncle; Sp5, trigeminal nucleus; TH, tyrosine hydroxylase; VRC, ventral respiratory column; VLM, ventrolateral medulla; VAChT, vesicular acetylcholine transporter.

of respiratory disorders associated with long-term hypercapnia. Our aims are (1) to determine if neuropeptide gene expression is altered in the RTN after long-term hypercapnia. This is achieved using quantitative polymerase chain reaction (qPCR) to determine mRNA expression changes in the RTN after short-term hypercapnia (6 or 8 h exposure to 5 or 8% CO_2) or long-term hypercapnia (10 days exposure to 5 or 8% CO_2), (2) to determine the distribution of preprogalanin in chemoreceptors in the mouse brainstem by *in situ* hybridization (ISH), and the co-occurrence of the galanin receptor 1 (GalR1:Gi-coupled receptor) in VRC neurons using multiplex fluorescent ISH (FISH) (RNAscope, ACD BioScience, Hayward, CA, United States) to better characterize galaninergic VRC circuitry, (3) to investigate whether long-term hypercapnia causes changes to recruitment of known respiratory related neuronal populations (detected by c-Fos immunohistochemistry) including RTN neurons and the galaninergic subset, *in vivo*.

Collectively, we found that hypercapnia (short-term and long-term) alters neuropeptide expression in the RTN; we decided to follow up the observed changes in preprogalanin expression. GalR1 was distributed throughout the VRC, including in 9% of glycinergic VRC neurons. We identified multiple respiratory-related populations that exhibit blunted chemoreflex activation following long-term hypercapnia. However, RTN neurons (pre-eminently galaninergic subset) retained their responsiveness to the chemoreflex following long-term hypercapnia.

MATERIALS AND METHODS

Animals

All experiments in this project were conducted in accordance with the National Health and Medical Research Council (Australia) with the approval by the University of New South Wales Animal Care and Ethics Committee. The animals used were male adult C57BL/6J mice (25–30 g). All animal experiments were conducted in the Biological Resources Centre (University of New South Wales, Sydney, Australia). They were maintained on 12 h:12 h light:dark cycle at 23°C with standard chow and tap water available *ad libitum* and housed in conventional caging.

Respiratory Paradigms

Short-Term and Long-Term Hypercapnia Paradigms

Mice were randomly assigned to either short-term hypercapnia (SH), long-term hypercapnia (LH) or room air (RA) (n = 5/group). Hypercapnia was achieved by placing the animals within their home cages in a sealed chamber measuring 9000 cm^3 (Biospherix, NY, United States). A CO_2 monitor was connected, that continuously flushed a designated amount of CO_2 into the chamber. Animals were acclimatized to the experimental room or the hypercapnia chamber for 1 h a day over 2 days in order to minimize stress and non-specific gene expression related to novel environment. Then, the CO_2 monitor was set to either 5 or 8% CO_2 (balanced with room air, 20 ± 0.5% O_2) at 15 psi. See **Figure 1** for the timeline. During all exposures, O_2 and CO_2 concentrations were continuously monitored by capnometry (Normocap oxy, Datex Engstrom, WI, United States) and CO_2 meter (GM70, Vaisala, Finland). Room air mice were left outside the chamber in the experimental room for the same period of time. At the end of the paradigm, animals were deeply anaesthetized with sodium pentobarbital (70 mg/kg, ip) followed by immediate isolation of the brain (qPCR) or transcardial perfusion with heparinised 0.1M phosphate buffered saline (PBS) and 4% paraformaldehyde (PFA, Sigma-Aldrich, NSW) in 0.1M sodium phosphate buffer (ISH/IHC).

c-Fos Studies: Acute Hypercapnic Chemoreflex Challenge (AH)

A subset of long-term hypercapnia or room air animals were exposed to 10% CO_2, 30–40% O_2 balanced with N_2 for 1 h then left in room air for 1 h (**Figure 1**) before being deeply anaesthetized followed by transcardial perfusion as described above. Hyperoxic conditions were used for the acute hypercapnic chemoreflex challenge because this silences the peripheral chemoreceptors (Lahiri et al., 1987), ensuring that the ventilatory response is mediated by central mechanisms.

Quantitative PCR

Following isolation of the brainstem, a cut was made separating the dorsal brainstem from the ventral brainstem. The rostral parafacial region containing rostral RTN (rRTN: 0.7 mm rostral, 0.5 mm caudal to the trapezoid line, Bregma −5.3 to −6.5, midline omitted), caudal parafacial region containing caudal RTN (cRTN: 1 mm immediately caudal to the rRTN, Bregma −6.5 to −7.5, midline omitted), left lateral cerebellum were excised, rapidly frozen in liquid nitrogen and stored at −80°C. Following RNA isolation (Promega SV Total RNA isolation kit, WI, United States), a cDNA library was generated by subjecting RNA (1000 ng) to SuperScriptTM III First Strand Synthesis System (Invitrogen, MA, United States), according to the manufacturer's instructions. qPCR was carried out using KAPA SYBR FAST kit (Kapa Biosystems, MA, United States) in a total reaction volume of 20 μl containing 1 μl cDNA, 10 μl of qPCR mastermix and 1 μl (10 nM) forward and reverse primer. Primer sequences for neuropeptide mRNA (ppGal, ppNMB and ppGRP) (**Table 1**) were designed using Primer3 (v.0.4.0, Whitehead Institute for Biomedical Research). qPCR reaction was performed with Eppendorf Mastercycler® ep realplex using initial denaturation (3 min 95°C), followed by 40 cycles of denaturation (95°C for 10 s), annealing (60–64°C for 20 s), and extension (72°C for 20 s). PCR products were verified by melt curve analysis and separation on a 2% agarose gel. We performed qPCR on samples in the absence of reverse transcriptase and non-template controls concurrently, to control for genomic DNA contamination. Sequencing analysis (Garvan Molecular Genetics, Sydney) confirmed that the DNA fragments generated by PCR were identical to the mRNA sequences reported in the GenBank database (**Table 1**). The cycle threshold (Ct) values were used to calculate mRNA expression of ppGal, ppNMB, and ppGRP relative to the expression of two house-keeping genes (HKG), hypoxanthine phosphoribosyltransferase (HPRT), and ribosomal protein lateral stalk subunit P0 (RPLPO) using the ΔΔCt method (Pfaffl, 2001). HKG mRNA was expressed at a similar

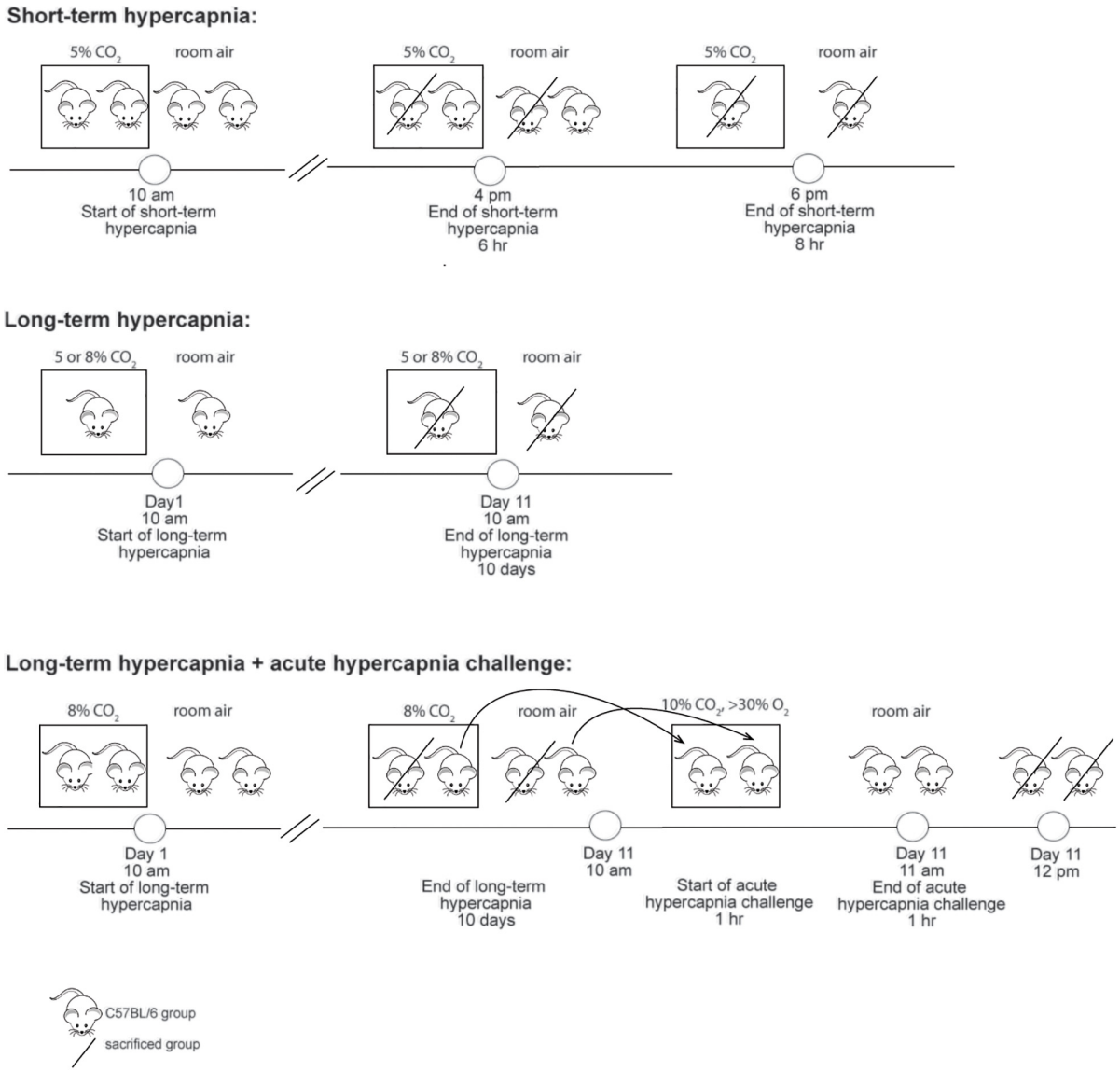

FIGURE 1 | Timeline summarizing different experimental paradigms.

abundance to the genes of interest and standard curve analysis was initially performed to assure their stability in the brain following hypercapnia used in this study. Lateral cerebellum does not have a function in the control of respiration (Xu and Frazier, 2000); therefore, it was used as a control tissue. Furthermore, to decrease bias in the experimental results, the person quantifying experimental outcomes was blinded to the experimental groups.

Non-radioactive Chromogenic *in situ* Hybridization Combined With Immunohistochemistry

Fixed brains were vibratome sectioned coronally (30 μm) (Leica VT1200S, Leica, Germany) and stored in cryoprotectant solution (30% RNase free sucrose, 30% ethylene glycol, 1% polyvinylpyrrolidone in 0.1M sodium phosphate buffer, pH 7.4) at −20°C.

A template cDNA library was generated by reverse transcription of total RNA isolated from mouse brain (Kumar et al., 2012). ISH riboprobes were synthesized from cDNA which was amplified by scaled-up PCR reaction. The list of PCR primers used (with either T7 or SP6 RNA polymerase promoter regions attached) can be found in **Table 1**. Following purification by gel extraction of the amplified cDNA templates, antisense and sense (control) riboprobes were prepared by *in vitro* transcription with digoxigenin-11-UTP (Roche Applied Science, Mannheim, Germany) using the AmpliScribe T7 FLASH transcription kit (Epicentre Biotechnologies, Madison, WI, United States) and SP6 RiboMAX large-scale RNA production system (Promega, Madison, WI, United States), respectively.

TABLE 1 | Details of primers used for qPCR and for generating non-radioactive ISH riboprobes.

	Species	Primer	Genebank ref no	Sequence (5′→3′)	Amplicon length (bp)	Annealing temp (°C)	Extension time (sec)
For qPCR	mouse	Galanin	NM_010253.4	F: CATGCCATTGACAACCACAG	331	61	20
				R: CGATTGGCTTGAGGAGTTGG			
	mouse	NMB	NM_026523.4	F: GGCGACCGGTCACTTCAT	191	61	20
				R: GCCTCCTGTACTGGATTGG			
	mouse	GRP	NM_175012.4	F: CACGGTCCTGGCTAAGATGTAT	418	61	20
				R: CCAGTAGAGTTGACGTTTGCAGA			
	mouse	HPRT	NM_013556.2	F: TCTTTGCTGACCTGCTGGATTACAT	228	61	20
				R: CCAGGGAAAGCAAAGTTTGCATT			
	mouse	RPLPO	NM_007475.5	F: CCCTGCACTCTCGCTTTCTGGA	212	61	20
				R: AGGGGCAGCAGCCGCAAATG			
For ISH riboprobes	mouse	Galanin	NM_010253.4	Fggatccatttaggtgacactatagaag**CACCGAGAGAGCCTTGATCCTG***	526	60	45
				R:gaattctaatacgactcactatagggaga**ACGATTGGCTTGAGGAGTTGG****			
	mouse	GalR1	NM_008082.2	F:ggatccatttaggtgacactatagaag**ATGTCTGTGGATCGCTACGT***	568	64	45
				R:gaattctaatacgactcactatagggaga**TGAACACTTGCTTGTACGCC****			

** Lowercase base sequences indicate the SP6 universal promoter. ** Lowercase base sequences indicate T7 universal promoter.*

For digoxigenin (DIG) labeled ISH assay, free floating brainstem sections were assayed as described previously (Kumar et al., 2012; Spirovski et al., 2012). Briefly, riboprobes were added to the hybridization solution (500–1000 ng/μl) for an overnight incubation at 58°C. The sections were then rinsed through a series of decreasing salt concentrations and blocked prior to primary antibody incubation (24–48 h at 4°C). The antibodies and concentrations used are summarized in **Table 2** and include sheep-anti DIG (1:1000, tagged with alkaline phosphatase, Roche). Sections were then rinsed with tris buffered saline (TBS) buffer and secondary antibodies were added at 1:400, diluted in TBS buffer containing 1% NHS and 0.1% Tween-20, and incubated at 4°C overnight. Following detection of cytoplasmic DIG labeling, sections were mounted and coverslipped with mounting medium with DAPI (Fluoroshield, Sigma, Australia) or without DAPI (Fluoromount Aqueous Mounting Medium, Sigma, Australia).

Fluorescent *in situ* Hybridization Combined With Immunohistochemistry

To label GalR1 on GlyT2 neurons in the brainstem, multiplex FISH (RNAscope, ACDBio, Hayward, CA, United States) was performed (n = 5). Briefly, animals were deeply anaesthetized with sodium pentobarbital (70 mg/kg, ip), brains were isolated following transcardial perfusion with 0.1M PBS and embedded in OCT. Coronal sections (14 μm thick) were cut on a cryostat, mounted on superfrost plus slides (Thermo Fisher Scientific, Waltham, MA, United States) and stored at −80°C. Sections were fixed in 4% PFA/0.1M phosphate buffer, dehydrated and subjected to the RNAscope multiplex fluorescent assay according to the manufacturer's instructions, in combination with fluorescence IHC. The riboprobes used were GalR1 (448821-C1) and GlyT2 (409741-C3). We also employed GalR2 (448831-C2) riboprobe, however, were unable to detect a signal anywhere in the brain using this probe. Positive and negative controls were incorporated into each procedure to verify RNA quality and specific staining. Slides were coverslipped with ProLong Gold Antifade Mountant with or without DAPI (Life technologies).

Cell Counts and Analysis

A 1 in 6 series of 14 μm coronal sections and a 1 in 3 series of 30 μm coronal sections through the brain was examined for FISH and non-radioactive chromogenic ISH respectively. Immunostaining was examined under brightfield and epifluorescence microscopy using an Olympus BX51 equipped with a motor driven microscope stage, a digital camera (2000R-F-CLR) and a mercury powered light burner (Olympus U-LH100HG 100w). Neuronal profiles were plotted with using StereoInvestigator software version 9 (Microbrightfield, United States). Sections were aligned with reference to Bregma level according to a mouse stereotaxic brain atlas (Paxinos and Franklin, 2004). Only neurons with DAPI-stained nuclei were considered for counting and mapped. Furthermore, to decrease bias in the experimental results, the person quantifying experimental outcomes was blinded to the experimental groups. For quantitative analysis, the total cell counts were obtained following Abercrombie correction (Abercrombie, 1946): for 30 μm thick sections, an average nuclear width of 7.2 ± 0.2 μm and average section thickness of 29.7 ± 1 μm was measured from 30 cells and 10 sections respectively in 10 animals; for 14 μm thick sections, an average nuclear width of 7.9 ± 0.3 μm and average section thickness of 14 ± 1 μm was measured from 30 cells and 10 sections respectively in 5 animals. All values are given with ± SEM values. For semi-quantitative analysis, 5 sections per animal were screened from 5 animals per group. Regions were graded for expression density; - (not expressed), + (scattered sparsely), ++ (expressed by 1/3 of the neurons in the area), +++ (expressed by > 1/3 of the neurons in the area). Representative images were first exported into Fiji (RRID:SCR_002285) as TIFF files for brightness/contrast adjustment to increase the clarity and to reflect true rendering. Images were not otherwise altered. TIFF images were then

TABLE 2 | Antibodies used for IHC.

Antibody	Host	Working dilution	Company (Cat no)	Specificity and related PMID	Associated figures
PRIMARY					
DIG	Sheep	1:1000	Roche (11093274910)		
Phox2b	Guinea pig	1:1500	Gift from Professor Hideki Enomoto (Nagashimada et al., 2012)	Confirmed by co-expression with rabbit anti-Phox2b (J.-F. Brunet, Ecole Normale Supeìrieure, Paris, France), for which there was complete absence of reactivity in Phox2b knockout mice (Lazarenko et al., 2009; Nagashimada et al., 2012)	**F 6A–D**
c-Fos	Rabbit	1:1000	Cell Signaling (2250S)	29888787	**F 6A–D**
c-Fos	Rabbit	1:4000	Santa Cruz (sc-253)	21800306, 30136719, 31423585	**F 7A–D**, **SF 3A–D**, **SF 4A–D**
TH (tyrosine hydroxylase)	Sheep	1:1000	Millipore (AB1542)	29888787	**SF 1F,L,N**, **SF 3A–D, SF 4A–D**
TH	Chicken	1:1000	Aves (TYH)	21858819, 21858821, 28472858, 30592042	N/A
VAChT (Vesicular acetylcholine transporter)	Goat	1:1000	Millipore Sigma (ABN100)	30926750	**F 4B1,2**, **SF 3A–D, SF 4A–D**
ChAT (Choline acetyltransferase)	Goat	1:1000	Millipore Sigma (AB144P)	26470751, 22237784, 16917846, 17111374, 22173709, 21618225	N/A
SECONDARY					
α-Guinea pig 488	Donkey	1:400	Jackson ImmunoResearch (706-545-148)		
α-Rabbit 594	Donkey	1:400	Jackson ImmunoResearch (711-585-152)		
α-Rabbit 488	Donkey	1:400	Jackson ImmunoResearch (711-545-152)		
α-Sheep Cy5	Donkey	1:400	Jackson ImmunoResearch (713-175-147)		
α-Sheep 488	Donkey	1:400	Abcam (ab150177)		
α-Chicken AMCA	Donkey	1:400	Jackson ImmunoResearch (703-155-155)		
α-Goat 594	Donkey	1:400	Jackson ImmunoResearch (705-585-147)		
α-Goat Cy5	Donkey	1:400	Jackson ImmunoResearch (705-175-147)		

F, Figure; SF, Supplementary Figure.

imported into CorelDraw Graphics Suite X7 (64-bit) or Adobe Illustrator CC (2019) for final presentation.

RESULTS

The Effect of Hypercapnia on Neuropeptide Expression in the Rostral RTN (rRTN)

As a result of short-term (6 h), exposure to 5% CO_2, ppGal expression significantly decreased in the rRTN (33%, $p < 0.01$) (**Figure 2B**). This decrease was no longer evident at the 8 h timepoint. In contrast, 10 days exposure to either 5 or 8% CO_2 increased ppGal expression by 60% ($p < 0.001$) and 40% ($p < 0.01$) respectively (**Figure 2B**). There was no change to ppGRP nor ppNMB expression during either short-term or long-term hypercapnia (**Figures 2C,D**). Neuropeptide expression did not change in the lateral cerebellum.

The Effect of Hypercapnia on Neuropeptide Expression in the Caudal RTN (cRTN)

Following a 6 h exposure to 5% CO_2, there was a significant decrease in the expression of ppGal in the cRTN (27%, $p < 0.01$) (**Figure 3B**). After 8 h, the expression of ppGRP decreased by 49% ($p < 0.01$) and ppNMB by 33% ($p < 0.01$) (**Figures 3C,D**) with no change in ppGal expression. On the other hand, after long-term exposure to hypercapnia (8% CO_2, 10 days), there was an increase in the expression of ppGal (40%, $p < 0.01$) and ppNMB (30%, $p < 0.05$) but not ppGRP.

ppGal Distribution in the Mouse Brainstem

In the dorsal brainstem, ppGal+ neurons were abundant in the non-catecholaminergic caudal NTS (cNTS); ppGal+ neurons lay immediately ventral to the TH+ A2 neurons, within the

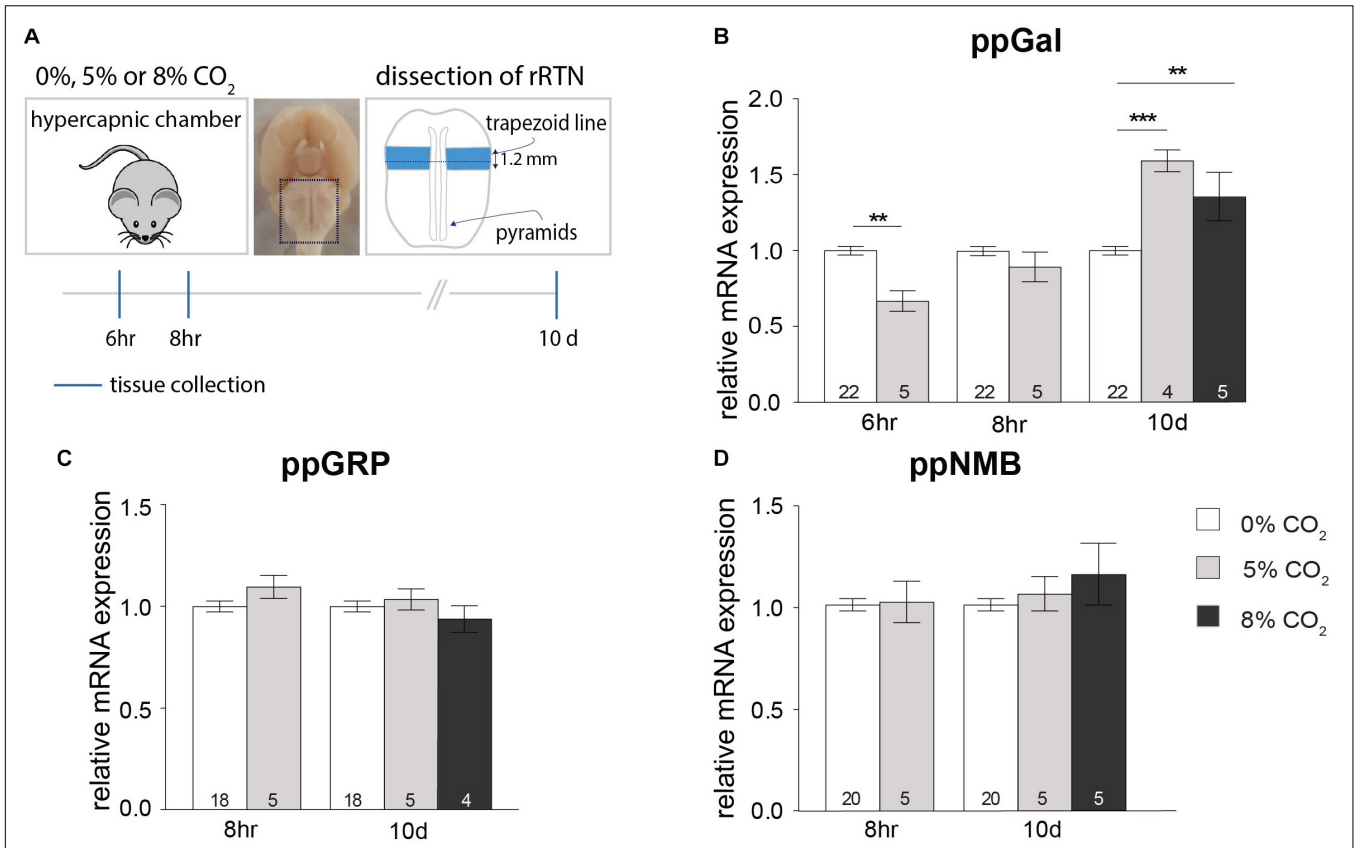

FIGURE 2 | Short-term hypercapnia downregulates and long-term hypercapnia upregulates ppGal but not ppGRP or ppNMB mRNA in rostral RTN (rRTN) measured by qPCR. **(A)** Strategy for hypercapnia exposure, tissue dissection and timeline for short-term and long-term hypercapnia paradigms. **(B–D)** ppGal, ppGRP and ppNMB mRNA expression levels following short-term (6 or 8 h) or long-term (10 days) elevated inspired CO_2 (5% or 8%). The qPCR results were normalized to the expression levels of two house-keeping genes: HPRT and RPLPO. $^{**}p < 0.01$, $^{***}p < 0.001$ (One-Way ANOVA, Multiple comparisons: Dunnet).

lateral cNTS. They were also abundant in vAChT+ neurons in the dorsal motor nucleus of the vagus (X), but absent in hypoglossal nucleus (XII) (**Supplementary Figure S3**). There was no ppGal mRNA labeling observed in the rostral NTS (rNTS, rostral to area postrema). In the ventral brainstem, ppGal mRNA labeling was present in the RTN, inferior olive (IO) and paragiganticellular reticular nucleus. There was no ppGal mRNA labeling observed in the mouse VRC, A1/C1 populations (**Supplementary Figure S4**) or caudal raphe nuclei. The quantitative profile for the distribution of the ppGal in the RTN is illustrated in **Supplementary Figures S2A,B**. The total number of ppGal+ RTN neurons counted between bregma levels −6.78 to −5.70 mm was 398 ± 19 neurons (n = 30) per animal which corresponded to 50.2% of total RTN neurons (Phox2b+ /TH-/ ChAT-) (**Supplementary Figure S2B**). Laterally, there was a moderate amount of ppGal+ neurons in the trigeminal nucleus (Sp5). In the rostral medulla, ppGal+ neurons were abundant in the locus coeruleus (LC) some of which were TH+. There was also a ppGal+/TH- population in proximity to A5 area, immediately lateral to the rostral pole of the facial nucleus (VII). In the context of respiratory populations in pons; parabrachial nucleus (PbN) and caudal Kölliker fuse (cKF) neurons did not contain ppGal mRNA. More rostrally in the pons, there was moderate amount of ppGal labeling in the area corresponding to rostral Kölliker fuse (rKF) and TH positive A4 population. Summary for semi-quantitative analysis of ppGal mRNA distribution in the brainstem is provided in **Table 3**.

GalR1 Distribution in the Mouse Brainstem

Both DIG-incorporated ISH and multiplex FISH approaches revealed high levels of GalR1 mRNA (GalR1+) in the PbN, cNTS and rNTS (**Supplementary Figure S1** and **Table 3**). GalR1+ neurons in the NTS were Phox2b- and TH- (**Supplementary Figures S1K,L**). Low to moderate GalR1 mRNA labeling was detected in the Sp5, XII, VRC, A1/C1, RTN, nucleus ambiguus (na), reticular nucleus, raphe nuclei, and LC. The GalR1+ neurons of the RTN were also Phox2b+ (**Supplementary Figures S1H,I**). Upon quantitation, GalR1 mRNA labeling in the VRC shows two peaks: at Bregma levels of approximately 7.38 and rostral to −6.6 which correspond to the preBötzinger complex (preBötC) and Bötzinger complex (BötC) respectively (**Figure 5D** and **Supplementary Figure S1O**). An average of 242 ± 23 (n = 3) TH+ neurons were positive for GalR1 mRNA in the C1 area

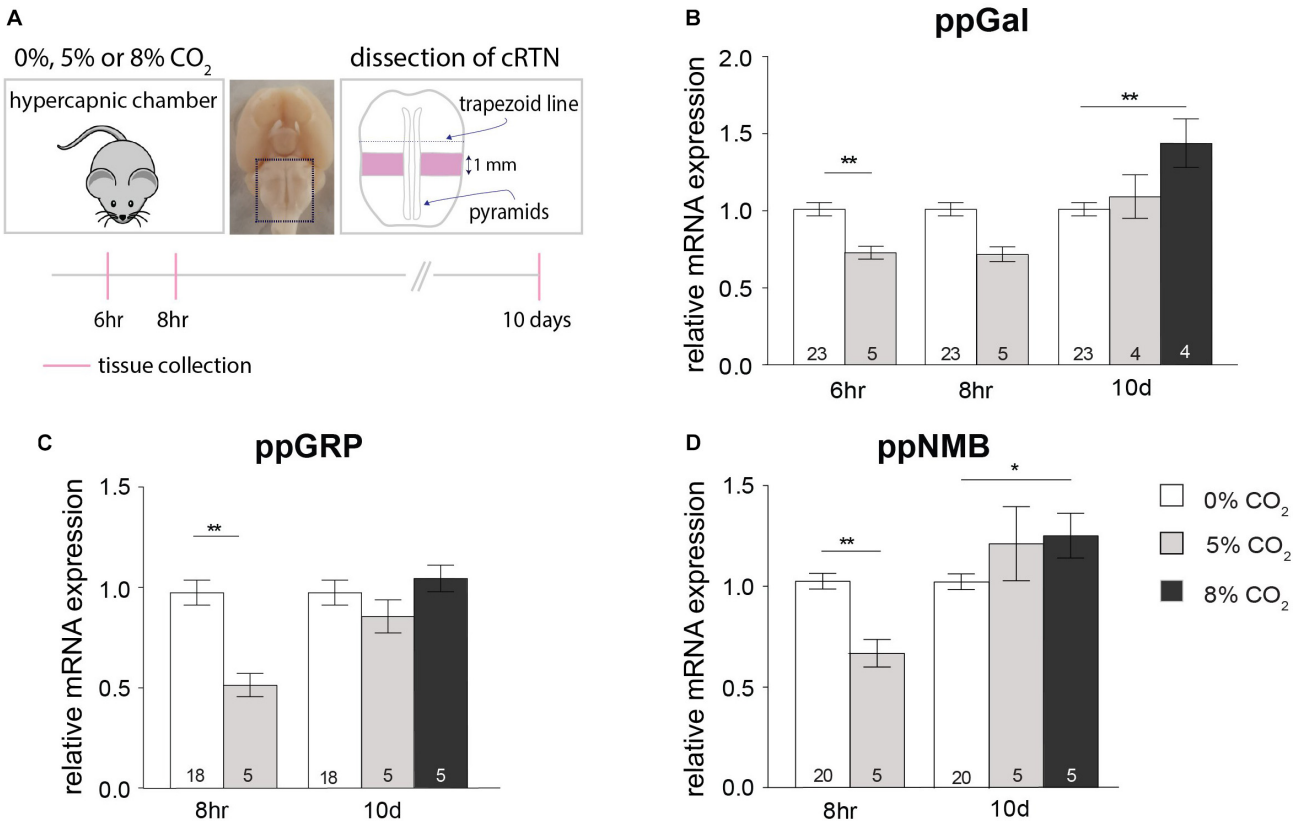

FIGURE 3 | Short-term hypercapnia downregulates and long-term hypercapnia upregulates ppGal, ppGRP or ppNMB mRNA in caudal RTN (cRTN) measured by qPCR. **(A)** Strategy for hypercapnia exposure, tissue dissection and timeline for short-term hypercapnia and long-term hypercapnia paradigms. **(B–D)** ppGal, ppGRP and ppNMB mRNA expression levels following short-term (6 or 8 h) or long-term (10 days) elevated inspired CO_2 (5% or 8%). The qPCR results were normalized to the expression levels of two house-keeping genes: HPRT and RPLPO. *$p < 0.05$, **$p < 0.01$ (One-Way ANOVA, Multiple comparisons: Dunnet).

(Bregma levels −7.47 to −6.66) which corresponds to an average of 34% of all TH+ neurons in the C1 (**Supplementary Figure S1P**). Summary for semi-quantitative analysis for the distribution of GalR1 mRNA labeling and representative microscopic images are provided in **Table 3** and **Supplementary Figure S1** respectively.

GalR1 Distribution in the Mouse Ventral Respiratory Column (VRC)

Inhibitory neurons in the VRC were identified by using a second riboprobe targeting GlyT2. Co-labeling of GalR1 with GlyT2 mRNA was apparent in the VRC (**Figure 4B**). Quantitative analysis for neurons containing both GalR1 and GlyT2 mRNA was performed in the ventral brainstem between Bregma levels −7.51 and −6.50. Based on previous studies (Abdala et al., 2015; Ausborn et al., 2018), preBötC and BötC correspond to Bregma levels −7.51 to 7.09 and −7.0 to −6.58 respectively. GalR1 distribution was not restricted to the VRC (**Figure 4C**). For this reason, cell counts were made from ventrolateral medulla (VLM) subdivisions (**Figures 5A–C**). The VRC was defined as a 400 μm^2 region immediately ventral to the nucleus ambiguus (Pagliardini et al., 2003; Stornetta et al., 2003; Bouvier et al., 2010; Le et al., 2016; **Figure 5A**) and there was an average of 840 ± 23 (n = 5) GalR1+ neurons between Bregma levels −7.51 and −6.50 out of which 198 ± 15 were glycinergic (23%). In the VRC, BötC contained more GalR1+ neurons 539 ± 20 compared to preBötC 301 ± 12 (n = 5) (**Figure 5G**). The percentage of GalR1+ neurons expressing GlyT2 was also higher in BötC (30%) compared to preBötC (11%) (**Figure 5J**).

Lateral to the VRC (750 μm × 250 μm) (**Figure 5B**), the distribution of GalR1+ neurons had a similar pattern to the VRC (**Figure 5E**). In total, there were 721 ± 35 (n = 5) GalR1+ neurons between Bregma levels −7.51 and −6.50 (**Figure 5H**). The percentage of GalR1+ neurons expressing GlyT2 was also similar in both preBötC and BötC (12 and 15% respectively) (**Figure 5J**).

In the region ventral to the VRC (250 μm × 500 μm) (**Figure 5C**), the distribution pattern of GalR1 was different to the other two regions (**Figure 5F**). There was a significantly greater number of GalR1+ neurons in the BötC (137 ± 29 neurons) compared to preBötC (22 ± 8 neurons) ($p < 0.005$) (n = 5) (**Figure 5I**). Very few GalR1+ neurons were positive for GlyT2 in preBötC or BötC (**Figure 5J**). This population of GalR1 neurons most likely corresponds to the bulbospinal presympathetic population of rostral ventrolateral medulla.

TABLE 3 | Distribution of ppGal and GalR1 mRNA in the mouse brainstem.

Brainstem region	GalR1	ppGal
Sp5	++	++
cNTS	+++	+++
rNTS	+++	−
XII	++	−
X	+	+++
IO	−	++
VRC	+	−
A1/C1	+	−
RTN	+	+++
na	+	−
Reticular nucleus	+	++
Caudal raphe nuclei	++	−
Lateral to A5	n/a	++
LC	+	+++
PbN	+++	−
cKF	+	−
rKF	+	+
A4	+	++

Adult male C57BL6/J mice (n = 5) were examined using DIG-incorporated riboprobes complementary to mouse ppGal and GalR1 mRNA by ISH. All anatomical areas listed are according to the atlas of Franklin and Paxinos (Paxinos and Franklin, 2004). −, not expressed; +, scattered sparsely; ++, expressed by 1/3 of the neurons in the area; +++, expressed by > 1/3 of the neurons in the area; n/a, not available.

Chemoreflex Activation of Brainstem Neuronal Populations After Long-Term Hypercapnia

A semi-quantitative analysis was performed to identify regions that are differentially affected by acute chemoreceptor stimulation following room air or long-term hypercapnia. c-Fos immunoreactivity in the caudal raphe nuclei, the reticular nuclei (corresponding to lateral and ventral to the VRC), PbN and KF and did not change with acute hypercapnia chemoreflex challenge with or without long-term hypercapnia (**Table 4**). ppGal+ neurons in the Sp5, IO, reticular nucleus, rKF and A4 were not activated by any conditions (**Table 4**).

As described previously, discrete neuronal populations were activated by acute chemoreflex challenge (10% CO_2-1 h). These included cNTS neurons, LC neurons, RTN neurons and A1/C1 neurons ($p < 0.001$). After 10 days of continuous 8% CO_2 (long-term hypercapnia), we observed that many fewer cNTS, LC and A1/C1 neurons were recruited in response to acute hypercapnia chemoreflex challenge (**Table 4** and **Supplementary Figures S3**, **S4**). The decreased activation of cNTS, LC, and C1 neurons suggests a blunting of the chemoresponsiveness of these regions after long-term hypercapnia.

RTN Neurons Retain Chemoresponsiveness Following Long-Term Hypercapnia

The rostrocaudal distribution of RTN neurons (Phox2b+ /TH-/ChAT-) in the parafacial region is shown in **Supplementary Figure S2A**. In total, we counted 793 ± 41 neurons ($n = 25$) per mouse (**Supplementary Figure S2B**).

Following control conditions of room air for 10 days, a baseline of 11.3% of RTN neurons displayed c-Fos immunoreactivity (84 ± 12, $n = 5$) (**Figures 6A,F** and **Supplementary Figure S2C**). By comparison, following the acute hypercapnia chemoreflex challenge, 39.5% of the RTN neurons were activated (275 ± 30 total cell counts) ($n = 5$) (**Figures 6B,F** and **Supplementary Figure S2C**), consistent with previous literature (Teppema et al., 1997; Kumar et al., 2015).

We observed a non-significant increase in c-Fos+ RTN neurons due to residual 8% CO_2 from the 10 days exposure (11.3% vs. 22.4%, 84 ± 12 vs. 161 ± 35 neurons, $n = 5$) (**Figures 6C,F** and **Supplementary Figure S2C**). When the acute hypercapnia challenge was administered following the long-term hypercapnia exposure, the responsiveness of RTN neurons was significantly higher compared to room air control (30.7% vs. 11.3%, 242 ± 31 vs. 84 ± 12 total cell counts, $n = 5$) (**Figures 6D,F** and **Supplementary Figure S2C**). In summary, the RTN was the only population assessed that retained its chemoresponsiveness following long-term hypercapnia.

ppGal+ RTN Neurons Retain Chemoresponsiveness Following Long-Term Hypercapnia

The ppGal+ subset of mouse RTN neurons displayed extensive c-Fos immunoreactivity in response to the acute hypercapnia challenge, consistent with previous descriptions in rat (Spirovski et al., 2012). Under control conditions (room air, 10 days), 26 ± 5 ($n = 5$) ppGal+ RTN neurons were activated (**Figure 7A** and **Supplementary Figure S2D**), representing 7.6% of the ppGal+ neurons (**Figure 7F**) which we infer to be 31% of the activated RTN neurons in the area. By comparison, following the acute hypercapnia challenge, 157 ± 33 ppGal+ RTN neurons were activated, representing 37.4% the ppGal+ neurons ($p < 0.01$) ($n = 5$) (**Supplementary Figure S2D** and **Figures 7B,F**) which we infer to be 57.1% of the activated RTN neurons in the area.

After long-term hypercapnia, there was no change in the number of ppGal+ RTN neurons activated by acute chemoreflex challenge (36.8% vs. 37.4% of ppGal+ RTN neurons, 167 ± 29 vs. 157 ± 33 total cell counts, $n = 5$) (**Figures 7D,F** and **Supplementary Figure S2D**). This was inferred to be 68.7% of the activated RTN neurons.

The qPCR results showed increased ppGal expression in both cRTN and rRTN following exposure to 8% CO_2 for 10 days (**Figures 2**, **3**). This could be explained by either an increase in the number of ppGal expressing neurons or increased expression of ppGal mRNA within each ppGal+ neuron. However, the number of ppGal+ RTN neurons did not change following long-term hypercapnia (**Figure 7E**). Furthermore, there was also no difference in the number of ppGal+ neurons when an analysis was conducted compartmentalizing RTN into rostral and caudal regions. Taken together, this suggests that whilst long-term hypercapnia does not induce more RTN neurons to

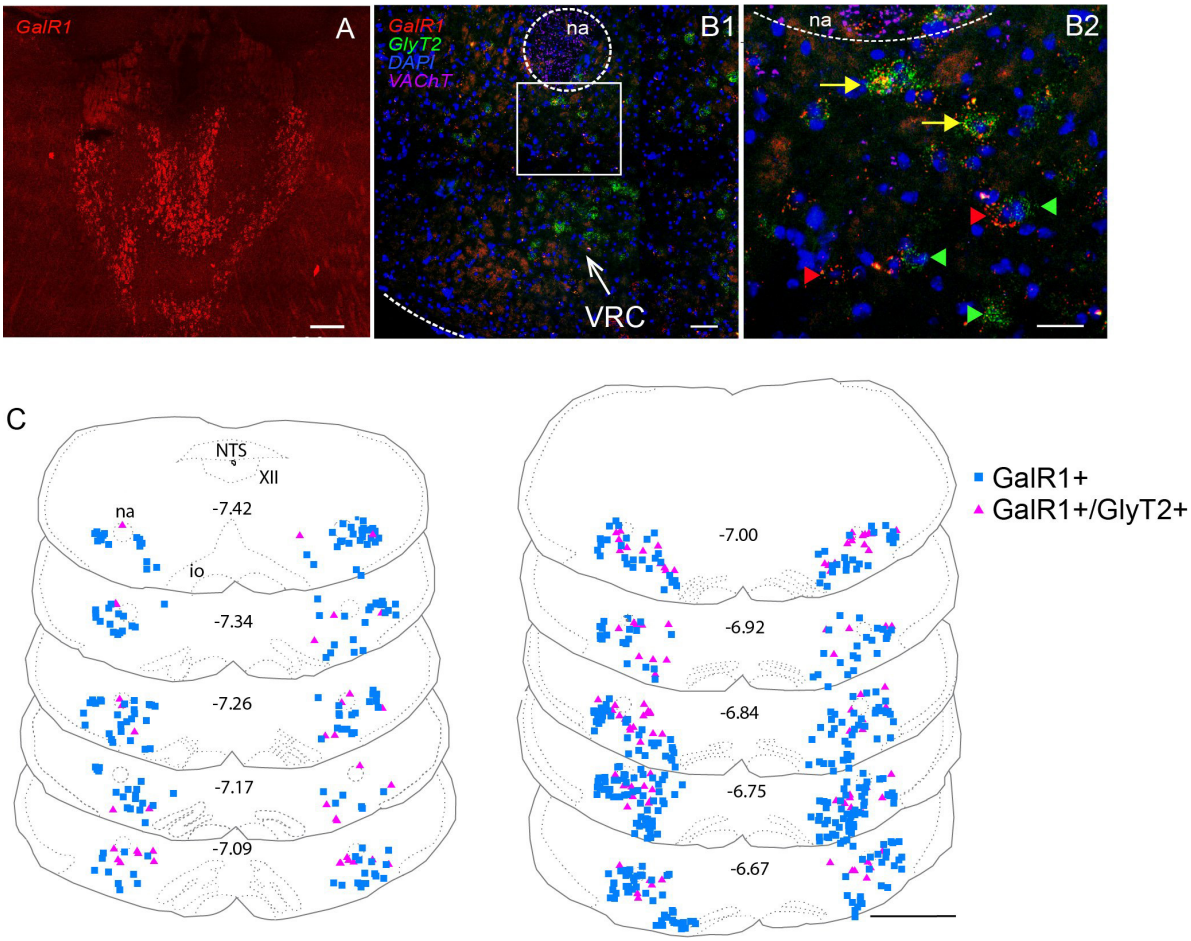

FIGURE 4 | Distribution of GalR1 mRNA expressing neurons in the VLM. **(A)** The GalR1 FISH riboprobe demonstrated labeling of specific thalamic nuclei as described previously [**Supplementary Figures S1A** (adapted from Kerr et al., 2015), **1B**]. **(B1)** GalR1 and GlyT2 mRNA labeling was observed ventral to nucleus ambiguus (na), in a region corresponding to the VRC. **(B2)** Inset in B1 enlarged, showing GalR1+ (red arrowhead), GlyT2+ (green arrowhead) and GalR1+/GlyT2+ double labeled (yellow arrow) neurons. **(C)** Representative mouse brainstem coronal sections, showing GalR1 and GlyT2 mRNA labeling from Bregma level −7.42 to −6.67. Scale bars are 200 μm **(A)**, 50 μm **(B1)**, 25 μm **(B2)** and 1 mm **(C)**.

express ppGal or alter the recruitment of ppGal+ neurons, it does increase the transcription of galanin mRNA.

DISCUSSION

The principal findings of this study are as follows: in the mouse, 50% of RTN neurons express galanin mRNA; gene expression for galanin was reduced by 30% following short-term hypercapnia and increased by 60% following long-term hypercapnia in both rostral and caudal RTN. In the mouse, galanin mRNA is distributed in brainstem regions important for cardiorespiratory regulation including cNTS and LC but in contrast to the rat, was absent in the VRC and A1 populations. Furthermore, the presence of GalR1 mRNA in the BötC and preBötC supports the existence of an RTN-VRC galaninergic circuit. Finally, our c-Fos studies showed that all brainstem galaninergic populations; RTN, NTS, LC, and some non-galaninergic populations such as A1 neurons were recruited by the acute hypercapnia chemoreflex challenge (indicated by increased c-Fos expression) which was consistent with previous literature (Spirovski et al., 2012). The CO_2 responsiveness of all populations recruited (including galaninergic subpopulations) was blunted after long-term hypercapnia, however, RTN neurons retained their CO_2 responsiveness. Taken together, there was both increased ppGal expression and sustained chemoresponsiveness of ppGal+ RTN neurons following long-term hypercapnia.

Neuroplasticity Underlying Adaptation to Long-Term Hypercapnia

While it is well established that acute hypercapnia causes an increase in the ventilatory drive by peripherally and centrally mediated chemoreflex systems (Forster and Smith, 2010; Smith et al., 2010), the ventilation pattern is altered during long-term hypercapnia. The most common trend during long-term hypercapnia is a biphasic response consisting of an initial increase in ventilatory drive followed by a reduced response

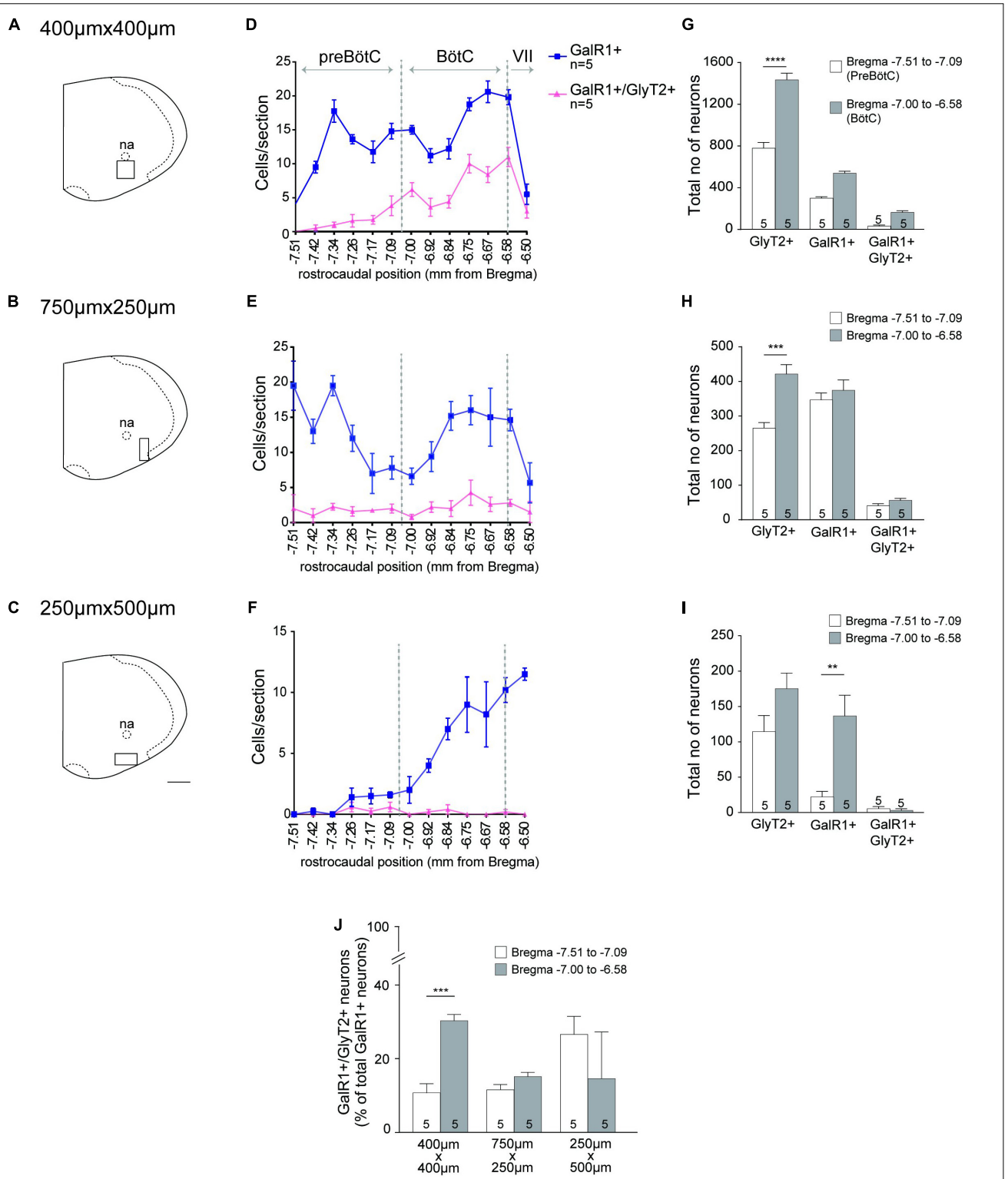

FIGURE 5 | GalR1 mRNA is expressed in the glycinergic subset of VRC neurons. **(A–C)** Representative coronal hemisection of mouse brainstem showing three distinct areas analyzed (VRC immediately ventral to nucleus ambiguus (na); 750 × 250 µm region immediately lateral to the VRC; 500 µm × 250 µm region immediately ventral to the VRC). **(D–F)** Rostrocaudal distribution of GalR1 and GlyT2 mRNA containing neurons counted within the regions depicted in **(A-C)** respectively. **(G–I)** Total number of neurons per region of interest per mouse. PreBötC was defined to correspond to Bregma level −7.51 to 7.09 and BötC was defined to correspond to Bregma level −7.00 to −6.58. **(J)** Percentage of GalR1 neurons that are glycinergic in the region depicted in **(A–C)**. ****$p < 0.0001$, ***$p < 0.001$, **$p < 0.01$, *$p < 0.05$ (Two-Way ANOVA, Multiple comparisons: Tukey). Scale bar is 500 µm.

TABLE 4 | c-Fos expression evoked by acute hypercapnia following room air or long-term hypercapnia conditions.

		c-Fos expression			
		RA*	**RA + AH***	**LH***	**LH + AH***
Brainstem region		**(0% CO_2)**	**(0% CO_2 + AH)**	**(8% CO_2)**	**(8% CO_2 + AH)**
ppGal+	Sp5	–	–	–	–
	cNTS	–	+++	–	–
	IO	–	–	–	–
	RTN	+	+++	+++	+++
	Reticular nucleus	–	–	–	–
	LC	–	+	–	–
	rKF	–	–	–	–
	A4	–	–	–	–
ppGal–	rNTS	–	–	–	–
	A1/C1	–	++	–	–
	Caudal raphe nuclei	++	++	++	++
	PbN	++	++	++	++
	KF	++	++	++	++

*Adult male C57BL6/J mice (n = 5) were examined using c-Fos by IHC for activation and DIG-incorporated riboprobes complementary to mouse ppGal mRNA by ISH. All anatomical areas listed are according to the atlas of Franklin and Paxinos (Paxinos and Franklin, 2004). –, not expressed; +, scattered sparsely; ++, expressed by 1/3 of the neurons in the ROI; +++, expressed by > 1/3 of the neurons in the ROI. *RA, Room air; AH, acute hypercapnic chemoreflex challenge; LH, long-term hypercapnia.*

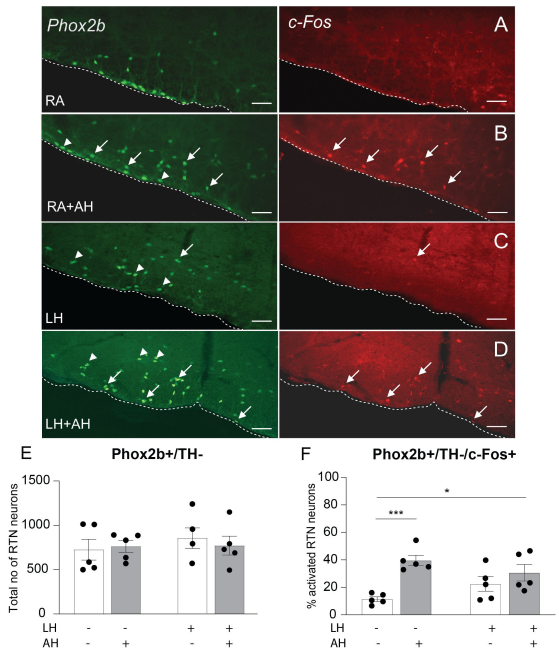

FIGURE 6 | RTN neurons retain their responsiveness to acute hypercapnia chemoreflex challenge following long-term hypercapnia. Representative image of a coronal brainstem section from the RTN region for each experimental group immunostained for Phox2b (green) and c-Fos (red), **(A)** room air (RA) control, **(B)** room air + acute hypercapnia chemoreflex challenge (RA + AH), **(C)** long-term hypercapnia (LH), **(D)** long-term hypercapnia + acute hypercapnia chemoreflex challenge (LH + AH). Arrowheads point to non-activated RTN neurons; arrows point to activated RTN neurons. Scalebars are 25 μm. **(E)** The total number of RTN neurons (Phox2b+ /TH–) per mouse. **(F)** The percentage of activated RTN neurons following different experimental conditions. *$p < 0.05$, ***$p < 0.001$ (Two-Way ANOVA, Multiple comparisons: Sidak).

over the long term (Schaefer, 1963; Schaefer et al., 1963; Clark et al., 1971; Guillerm and Radziszewski, 1979; Jennings and Davidson, 1984; Burgraff et al., 2018, 2019). This time-dependent physiologic change suggests an adaptation or acclimatization to long-term hypercapnia. Peripheral homeostatic mechanisms including metabolic compensation by the kidneys are partly responsible for maintaining body pH by increasing HCO_3^+ levels (Schaefer, 1963; Schaefer et al., 1963; Johnson, 2017; Burgraff et al., 2018). Recently central mechanisms contributing to adaptation to long-term hypercapnia, including central/neural resetting, have been purported (Burgraff et al., 2019; Chuang et al., 2019). These studies suggest that changes in synaptic expression or changes in the phosphorylation of glutamate receptors contribute to this neuroplasticity. Since glutamate is the primary transmitter responsible for CO_2 stimulated breathing (Bochorishvili et al., 2012; Holloway et al., 2015), glutamate receptors were good candidates for contributing to chronic hypercapnia-related neuroplasticity. Indeed, there are time dependent changes of glutamate receptor expression within cVLM, rRTN, rNTS, medullary raphe, rVRC and XII during chronic hypercapnia (Miller et al., 2014; Burgraff et al., 2019). These previous studies demonstrate that time and site-specific neuroplasticity occurs during long-term hypercapnia.

The data presented herein focuses on the RTN and proposes other neuromodulatory candidates that may contribute to neuroplasticity during long-term hypercapnia; neuropeptides galanin, NMB and GRP. Our qPCR results support the theory of a biphasic response to long-term hypercapnia; we found a decrease in neuropeptide mRNA expression in the first 6–8 h exposure, followed by an increase after 10 days. The decreased neuropeptide expression in the first phase aligns temporally with the initial hyperventilation and the increased neuropeptide mRNA expression in the second phase ultimately may reflect the neuroplastic change that underlies the decreased ventilation following long-term exposure to hypercapnia.

Neuropeptide mRNA Expression in the RTN Is Altered in Response to Long-Term Hypercapnia

Our ppGal *in situ* hybridization data revealed ppGal mRNA expression in mouse brainstem is restricted to the RTN, IO, medial reticular nucleus, NTS and LC. In contrast to the rat, ppGal mRNA is absent in the VRC and A1/C1 populations of the mouse. Since the dissections separated ventral brainstem from dorsal brainstem and the midline region was excluded, "RTN" dissections were free from IO, medial reticular nucleus, NTS and LC ppGal mRNA. Therefore, we can confirm specificity of ppGal from the RTN in our dissections.

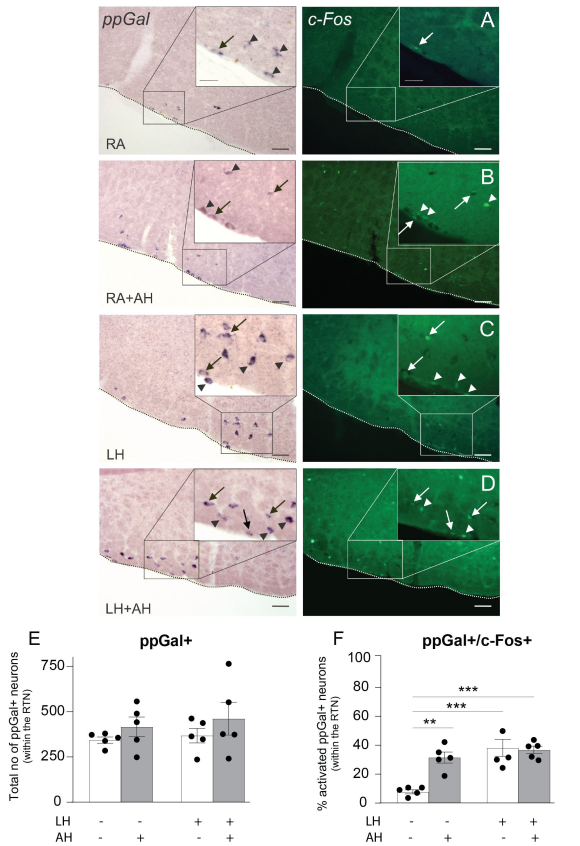

FIGURE 7 | The ppGal+ neurons in the RTN do not change their responsiveness to acute hypercapnic chemoreflex challenge after a long-term exposure to hypercapnia. Representative images of the coronal brainstem sections from the RTN region showing the activation of the galaninergic RTN neurons following **(A)** room air (RA), **(B)** room air + acute hypercapnia chemoreflex challenge (RA + AH), **(C)** long-term hypercapnia (LH), **(D)** long-term hypercapnia + acute hypercapnia chemoreflex challenge (LH + AH). ppGal+ neurons are purple (alkaline phosphatase ISH labeled neurons) and c-Fos+ neurons are in green (IHC). The box in each panel is enlarged for a higher magnification representation of the area. Arrowheads point to single labeled neurons; arrows point to activated ppGal+ RTN neurons. Scale bars are 50 μm in low magnification images and 25 μm in high magnification images. **(E)** The total number of ppGal+ RTN neurons per mouse. **(F)** The percentage of activated ppGal+ neurons of total ppGal+ neurons within the RTN following different challenge conditions. $^{**}p < 0.01$, $^{***}p < 0.001$ (Two-Way ANOVA, Multiple comparisons: Sidak).

Previous studies showed that galanin levels do not change in whole brainstem homogenate after 3 h exposure to hypercapnia (Wang W. et al., 2013), however, here we have demonstrated 30% reduction in galanin gene expression following precise excision of the RTN. Since, galanin exerts a powerful inhibitory effect on the phrenic motor output by depressing the activity of neurons in the BötC and preBötC (Abbott et al., 2009a), the downregulation of ppGal mRNA we observed after 6 h would be expected to cause a consequent increase in phrenic motor output, facilitating hyperventilation.

Long-term hypercapnia did not change ppGRP mRNA expression, whereas ppGal and ppNMB mRNA levels were upregulated in the cRTN, and ppGal mRNA in the rRTN. Sustained increased activity of glutamatergic transmission was observed in the RTN and VRC following 30 days exposure to hypercapnia (Burgraff et al., 2019). It was shown that during the first hour of 6% CO_2 exposure, there is an increase in minute ventilation by 355% of control (room air) levels, which decreases to 235% and was maintained over 30 days in goats (Burgraff et al., 2018). Upregulation of galanin mRNA expression in the RTN may contribute to the decrease in ventilation whereas increased NMB mRNA expression, an excitatory neuropeptide, may act as a counterbalancing mechanism to contribute to the sustained increased steady state minute ventilation after long-term hypercapnia compared to room air. In order to further support this hypothesis and establish a causal relationship, galanin co-release with glutamate and NMB can be investigated using electrophysiological and pharmacological approaches.

Neuropeptides are inducible and are known to have long-lasting effects since they act on G-protein coupled receptors (Salio et al., 2006; Nassel, 2009). Furthermore, they require progressively larger frequencies of stimulation for vesicular release (Fulop et al., 2005) and are released at synapses in response to higher frequencies of discharge than fast neurotransmitters (Balkowiec and Katz, 2000; Sauerstein et al., 2000). The increase in ppGal mRNA expression following exposure to long-term hypercapnia (5 and 8% CO_2) may reflect increased neurotransmission.

mRNA for Galanin Receptor 1 (GalR1) Is Distributed in the Mouse VRC

Since microinjection of galanin into the VRC results in an inhibitory effect on ventilation (Abbott et al., 2009a), we hypothesized that there would be GalR1 and 3 present in the VRC, because they are Gi/Go coupled and mediate inhibitory actions of galanin (Ogren et al., 2010). The present study demonstrates the presence of >840 GalR1+ neurons in the BötC and preBötC area.

A subpopulation (23%) of these GalR1+ neurons are glycinergic which may implicate a disinhibitory effect of galanin neurotransmission. However, photo- or pharmacological inhibition of the VRC is not obligatory for cessation of preBötC rhythmogenesis (Feldman and Smith, 1989; Sherman et al., 2015; Del Negro et al., 2018). Nevertheless, the inhibitory effect of galanin (Abbott et al., 2009a) following microinjection into the VRC might be through (1) indirect innervation of the phrenic motor nucleus by glycinergic VRC neurons (via XII, NTS, RTN, LC, PbN, KF, periaqueductal gray, colliculi nuclei, hypothalamus, thalamus, zona incerta, lateral preoptic area) (Yang and Feldman, 2018), or (2) GalR effects on other subtypes of VRC neurons since the phenotype of the remaining 77% of GalR1 neurons in VRC is unknown. The VRC also contains excitatory neurons (Del Negro et al., 2018). Therefore, there exists a complex circuitry between RTN galaninergic and target VRC neurons with the possibility of multiple combinations of galanin receptors and downstream excitatory or inhibitory VRC neurons which requires further elucidation.

The Responsiveness of ppGal+ RTN Neurons to Acute Hypercapnia Challenge Is Not Altered Following Long-Term Hypercapnia

This study is also the first to look at the effect of long-term hypercapnia on the activation and responsiveness of galaninergic and non-galaninergic respiratory nuclei. There are multiple studies that looked at the alterations in c-Fos expression within central respiratory populations following acute (1–2 h) exposure to hypercapnia (5–15% CO_2) or hypoxia (8–10% O_2) (Teppema et al., 1997; Takakura et al., 2006; Spirovski et al., 2012; Wakai et al., 2015). Here we wanted to see if there are alterations in the responsiveness to acute hypercapnia chemoreflex challenge following long-term hypercapnia.

All the RTN neurons are vesicular glutamate transporter 2+ (Stornetta et al., 2009) and glutamate is the neurotransmitter used by the RTN during CO_2-stimulated breathing (Holloway et al., 2015). Acute hypercapnia chemoreflex challenge activated ∼40% of ppGal+ RTN neurons which we inferred represents ∼60% of activated RTN neurons, in accordance with the previous literature (Stornetta et al., 2009). Our gene expression data shows a decrease in ppGal mRNA expression in the first 6 h of exposure to 5% CO_2. A reduction in ppGal neurotransmission within the RTN may potentiate glutamatergic transmission, possibly contributing to the hyperventilatory response of the first phase of long-term hypercapnia.

The activation state of RTN neurons including the ppGal+ subset was sustained by the continuous 10 days exposure to 8% CO_2. One limitation is that c-Fos is not an appropriate marker for long-term neuroplasticity because its protein expression peaks within 2 h of a stimulus challenge; it is a marker for transient neuronal activation and does not reflect long-term synaptic activity (Muller et al., 1984; Nestler et al., 2001). In future, ΔFosB, another member of the Fos family of transcription factors (Nestler et al., 2001), can be used to detect sustained changes in gene expression that persist long after exposure. ΔFosB accumulates during repeated activating stimuli thus whether RTN neurons are continuously responsive to the hypercapnia exposure over 10 days or not can be confirmed by the accumulation of the transcription factor ΔFosB.

Unlike RTN, the Responsiveness of NTS, LC, and A1/C1 Neurons to Acute Hypercapnia Challenge Is Blunted Following Long-Term Hypercapnia

Our data demonstrating recruitment of cNTS neurons during acute chemoreflex challenge is in concert with the previous experiments conducted in rats where there was 10% increase in activation of ppGal+ NTS neurons (Spirovski et al., 2012). This might be due to either second order activation or intrinsic acid sensing nature of the NTS neurons. Focal acidification by CO_2 dialysis with 25% CO_2 increased ventilation *in vivo* (Nattie and Li, 2002) and increased the firing rate of Phox2B+ NTS neurons *in vitro* (Fu et al., 2017). Lesions of Phox2b containing NTS neurons by injections of neurotoxin substance P-saporin reduced minute ventilation and tidal volume during exposures to 4–8% CO_2 (Fu et al., 2017). This transient activation of cNTS in response to acute hypercapnia chemoreflex challenge was lost following long-term hypercapnia.

The responsiveness to acute hypercapnia challenge of LC neurons was consistent with previous studies (Ritucci et al., 2005; Biancardi et al., 2008; Spirovski et al., 2012). This responsiveness is likely to be due to the intrinsic chemosensitive properties of the LC neurons. Indeed, local dialysis with acetazolamide increased ventilation (Biancardi et al., 2008), whereas focal deletion of these neurons decreased hypercapnic ventilatory response in unanesthetized rats (Biancardi et al., 2008). LC neurons are exclusively TH+ (Pickel et al., 1975); most ppGal+ neurons in the LC were TH+ as described previously (Dobbins and Feldman, 1994). Although not specifically characterized, these neurons may project to the VRC. Transsynaptic retrograde virus injections into the phrenic nucleus show third order LC afferents passing through the VRC (Holets et al., 1988). Similar to our findings with the NTS, LC neurons were responsive to acute hypercapnia chemoreflex challenge, and this responsiveness was blunted following long-term hypercapnia.

Similarly, the responsiveness of A1/C1 neurons to acute hypercapnia challenge following room air was consistent with the results reported by Spirovski et al. (2012) and Haxhiu et al. (1996). In rats, 52% of the ppGal+ neurons of the A1 population are activated by 2 h exposure to 10% CO_2 even following carotid denervation (Haxhiu et al., 1996). Although A1 neurons do not express ppGal in mice, they remain responsive to acute hypercapnia challenge. Our data demonstrates for the first time that like NTS and LC, the responsiveness of A1/C1 neurons to chemoreflex challenge is blunted following long-term hypercapnia.

The blunting of respiratory related populations in response to the acute chemoreflex suggests an adaptation of the chemoreflex circuitry under chronic hypercapnic conditions. Our working hypothesis is that this type of adaptation would be advantageous for people with chronic respiratory diseases like COPD, OHS, and OSA who normally live under chronic hypercapnic conditions. The RTN was the only brain region assessed that remained recruited following long-term hypercapnia; this sustained chemoresponsiveness attests to its crucial role in central regulation of breathing. The conservation of ppGal+ RTN neurons that retained chemoresponsiveness following long-term hypercapnia suggests that the ppGal+ subpopulation is likely to be modulated during the adaptation process.

CONCLUSION AND SIGNIFICANCE

Hypercapnia is a respiratory stressor that occurs in many disease (e.g., COPD, OHS, OSA, etc.) or non-disease conditions (e.g., miners, submarines, scuba divers, astronauts, hibernating animals, deep sea creatures, etc.). While the physiologic mechanism that underlies the central respiratory chemoreflex response to long term hypoxia is well established, the mechanisms underlying central neuroplastic changes that occur during long-term hypercapnia are yet to be clarified. This is the first study

assigning a role to the neuropeptides galanin, NMB and GRP in the RTN to adaptive changes during long-term hypercapnia. The major findings are as follows: (1) Neuropeptide gene expression decreased after short-term hypercapnia and increased after long-term hypercapnia with galanin showing the most prominent changes. This supports the concept of a biphasic neuroplastic contribution during adaptation to long-term hypercapnia. (2) For the first time, GalR1 mRNA was shown to be present in the BötC and preBötC supporting the existence of an RTN-VRC galaninergic circuitry. (3) Finally, c-Fos studies showed that after exposure to long-term hypercapnia, the responsiveness of the NTS, LC and A1 populations to acute hypercapnia chemoreflex challenge was blunted. In contrast RTN neurons including galaninergic subpopulation retained their responsiveness to acute hypercapnia. Co-release of galanin from RTN neurons may (1) counterbalance glutamatergic inputs to the respiratory centers in order to downscale energetically wasteful hyperventilation in the first phase of chronic respiratory stress (hypercapnia) (2) have a role in the second phase of adaptation to long-term hypercapnia, contributing to the observed decrease in ventilation through the inhibitory effects of galanin.

DATA AVAILABILITY STATEMENT

All datasets generated for this study are included in the article/**Supplementary Material**.

ETHICS STATEMENT

Experiments were performed on adult male wild type (C57BL6/J) mice, reviewed and approved by the University of New South Wales Animal Care and Ethics Committee and conducted in accordance with the Australian Code for the Care and Use of Animals for Scientific Purposes (National Health and Medical Research Council of Australia).

AUTHOR CONTRIBUTIONS

NK conceptualized the research and provided critical revisions. NK and AD designed the research, with the guidance of NK, AD, and ZY conducted all experiments and acquired data. NK, AD, ZY, and PC analyzed, interpreted results of experiments, and approved final version of the manuscript. AD prepared the figures and drafted the manuscript.

FUNDING

This work was supported by the Australian Research Council (NK, Grant No. ARC DP180101890), Rebecca Cooper Foundation (NK, Grant No. PG2018110), and Australian Government Research Training Program Scholarship (AD).

ACKNOWLEDGMENTS

We thank Prof. Hideki Enomoto for providing us with the guinea pig-anti-Phox2b antibody. We gratefully acknowledge the technical assistance of Evan Bailey.

SUPPLEMENTARY MATERIAL

The Supplementary Material for this article can be found online at: https://www.frontiersin.org/articles/10.3389/fnins.2019.01343/full#supplementary-material

REFERENCES

Abbott, S. B., Burke, P. G., and Pilowsky, P. M. (2009a). Galanin microinjection into the prebotzinger or the botzinger complex terminates central inspiratory activity and reduces responses to hypoxia and hypercapnia in rat. *Respir. Physiol. Neurobiol.* 167, 299–306. doi: 10.1016/j.resp.2009.06.003

Abbott, S. B., Stornetta, R. L., Fortuna, M. G., Depuy, S. D., West, G. H., Harris, T. E., et al. (2009b). Photostimulation of retrotrapezoid nucleus Phox2b-expressing neurons in vivo produces long-lasting activation of breathing in rats. *J. Neurosci.* 29, 5806–5819. doi: 10.1523/JNEUROSCI.1106-09.2009

Abdala, A. P., Paton, J. F., and Smith, J. C. (2015). Defining inhibitory neurone function in respiratory circuits: opportunities with optogenetics? *J. Physiol.* 593, 3033–3046. doi: 10.1113/jphysiol.2014.280610

Abercrombie, M. (1946). Estimation of nuclear population from microtome sections. *Anat. Rec.* 94, 239–247. doi: 10.1002/ar.1090940210

Ausborn, J., Koizumi, H., Barnett, W. H., John, T. T., Zhang, R., Molkov, Y. I., et al. (2018). Organization of the core respiratory network: insights from optogenetic and modeling studies. *PLoS Comput. Biol.* 14:E1006148. doi: 10.1371/journal.pcbi.1006148

Balkowiec, A., and Katz, D. M. (2000). Activity-dependent release of endogenous brain-derived neurotrophic factor from primary sensory neurons detected by elisa in situ. *J. Neurosci.* 20, 7417–7423. doi: 10.1523/jneurosci.20-19-07417.2000

Barnett, W. H., Abdala, A. P., Paton, J. F., Rybak, I. A., Zoccal, D. B., and Molkov, Y. I. (2017). Chemoreception and neuroplasticity in respiratory circuits. *Exp. Neurol.* 287, 153–164. doi: 10.1016/j.expneurol.2016.05.036

Biancardi, V., Bicego, K. C., Almeida, M. C., and Gargaglioni, L. H. (2008). Locus coeruleus noradrenergic neurons and Co2 drive to breathing. *Pflugers Arch.* 455, 1119–1128. doi: 10.1007/s00424-007-0338-8

Bochorishvili, G., Stornetta, R. L., Coates, M. B., and Guyenet, P. G. (2012). Pre-botzinger complex receives glutamatergic innervation from galaninergic and other retrotrapezoid nucleus neurons. *J. Comput. Neurol.* 520, 1047–1061. doi: 10.1002/cne.22769

Bouvier, J., Thoby-Brisson, M., Renier, N., Dubreuil, V., Ericson, J., Champagnat, J., et al. (2010). Hindbrain interneurons and axon guidance signaling critical for breathing. *Nat. Neurosci.* 13, 1066–1074. doi: 10.1038/nn.2622

Burgraff, N. J., Neumueller, S. E., Buchholz, K., Langer, T. M. III, Hodges, M. R., Pan, L., et al. (2018). Ventilatory and integrated physiological responses to chronic hypercapnia in goats. *J. Physiol.* 596, 5343–5363. doi: 10.1113/JP276666

Burgraff, N. J., Neumueller, S. E., Buchholz, K. J., Hodges, M. R., Pan, L., and Forster, H. V. (2019). Glutamate receptor plasticity in brainstem respiratory nuclei following chronic hypercapnia in goats. *Physiol. Rep.* 7:E14035. doi: 10.14814/phy2.14035

Chuang, S. Y., Teng, A., Butler, J., Gandevia, S., Narang, I., Briggs, N., et al. (2019). Quantitative assessment of nocturnal neural respiratory drive in children with and without obstructive sleep apnoea using surface Emg. *Exp. Physiol.* 104, 755–764. doi: 10.1113/EP087441

Clark, J. M., Sinclair, R. D., and Welch, B. E. (1971). *Rate Of Acclimatization To Chronic Hypercapnia in Man. Underwater Physiology*. Cambridge, MA: Academic Press.

Del Negro, C. A., Funk, G. D., and Feldman, J. L. (2018). Breathing Matters. *Nat. Rev. Neurosci.* 19, 351–367. doi: 10.1038/s41583-018-0003-6

Dickson, L., Aramori, I., Sharkey, J., and Finlayson, K. (2006). Vip and pacap receptor pharmacology: a comparison of intracellular signaling pathways. *Ann. N. Y. Acad. Sci.* 1070, 239–242. doi: 10.1196/annals.1317.021

Dobbins, E. G., and Feldman, J. L. (1994). Brainstem network controlling descending drive to phrenic motoneurons in rat. *J. Comput. Neurol.* 347, 64–86. doi: 10.1002/cne.903470106

Feldman, J. L., Mitchell, G. S., and Nattie, E. E. (2003). Breathing: rhythmicity, plasticity, chemosensitivity. *Annu. Rev. Neurosci.* 26, 239–266. doi: 10.1146/annurev.neuro.26.041002.131103

Feldman, J. L., and Smith, J. C. (1989). Cellular mechanisms underlying modulation of breathing pattern in mammals. *Ann. N. Y. Acad. Sci.* 563, 114–130. doi: 10.1111/j.1749-6632.1989.tb42194.x

Forster, H. V., and Smith, C. A. (2010). Contributions of central and peripheral chemoreceptors to the ventilatory response to Co2/H+. *J. Appl. Physiol.* 108, 989–994. doi: 10.1152/japplphysiol.01059.2009

Fu, C. R., Xue, J. Y., Wang, R., Chen, J. T., Ma, L., Liu, Y. X., et al. (2017). Chemosensitive Phox2b-expressing neurons are crucial for hypercapnic ventilatory response in the nucleus tractus solitarius. *J. Physiol. Lond.* 595, 4973–4989. doi: 10.1113/JP274437

Fulop, T., Radabaugh, S., and Smith, C. (2005). Activity-dependent differential transmitter release in mouse adrenal chromaffin cells. *J. Neurosci.* 25, 7324–7332. doi: 10.1523/jneurosci.2042-05.2005

Guillerm, R., and Radziszewski, E. (1979). Effects on man Of 30-day exposure to a pico2 Of 14 Torr (2 %): application to exposure limits. *Undersea Biomed. Res.* 6(Suppl.), S91–S114.

Haxhiu, M. A., Yung, K., Erokwu, B., and Cherniack, N. S. (1996). Co2-induced C-Fos expression in the CNS catecholaminergic neurons. *Respir. Physiol.* 105, 35–45. doi: 10.1016/0034-5687(96)00034-5

Holets, V. R., Hokfelt, T., Rokaeus, A., Terenius, L., and Goldstein, M. (1988). Locus coeruleus neurons in the rat containing neuropeptide y, tyrosine hydroxylase or galanin and their efferent projections to the spinal cord, cerebral cortex and hypothalamus. *Neuroscience* 24, 893–906. doi: 10.1016/0306-4522(88)90076-0

Holloway, B. B., Viar, K. E., Stornetta, R. L., and Guyenet, P. G. (2015). The retrotrapezoid nucleus stimulates breathing by releasing glutamate in adult conscious mice. *Eur. J. Neurosci.* 42, 2271–2282. doi: 10.1111/ejn.12996

Huang, J., Lusina, S., Xie, T., Ji, E., Xiang, S., Liu, Y., et al. (2009). Sympathetic response to chemostimulation in conscious rats exposed to chronic intermittent hypoxia. *Respir. Physiol. Neurobiol.* 166, 102–106. doi: 10.1016/j.resp.2009.02.010

Huckstepp, R. T., Cardoza, K. P., Henderson, L. E., and Feldman, J. L. (2015). Role of parafacial nuclei in control of breathing in adult rats. *J. Neurosci.* 35, 1052–1067. doi: 10.1523/JNEUROSCI.2953-14.2015

Jennings, D. B., and Davidson, J. S. (1984). Acid-base and ventilatory adaptation in conscious dogs during chronic hypercapnia. *Respir. Physiol.* 58, 377–393. doi: 10.1016/0034-5687(84)90013-6

Johnson, R. A. (2017). A quick reference on respiratory alkalosis. *Vet Clin. North Am. Small Anim. Pract.* 47, 181–184. doi: 10.1016/j.cvsm.2016.10.005

Kerr, N., Holmes, F. E., Hobson, S. A., Vanderplank, P., Leard, A., Balthasar, N., and Wynick, D. (2015). The generation of knock-in mice expressing fluorescently tagged galanin receptors 1 and 2. *Mol. Cell Neurosci.* 68, 258–271. doi: 10.1016/j.mcn.2015.08.006

Kepron, W., and Cherniack, R. M. (1973). The ventilatory response to hypercapnia and to hypoxemia in chronic obstructive lung disease. *Am. Rev. Respir. Dis.* 108, 843–850.

Kondo, T., Kumagai, M., Ohta, Y., and Bishop, B. (2000). Ventilatory responses to hypercapnia and hypoxia following chronic hypercapnia in the rat. *Respir. Physiol.* 122, 35–43. doi: 10.1016/s0034-5687(00)00134-1

Kumar, N., Bowman, B. R., and Goodchild, A. K. (2012). "Combined in situ hybridization and immunohistochemistry in rat brain tissue using Digoxigenin-labeled Riboprobes," in *Visualization Techniques. Neuromethods*, ed. E. Badoer, (Totowa, NJ: Humana Press).

Kumar, N. N., Velic, A., Soliz, J., Shi, Y., Li, K., Wang, S., et al. (2015). Physiology. regulation of breathing by Co(2) requires the proton-activated receptor Gpr4 in retrotrapezoid nucleus neurons. *Science* 348, 1255–1260. doi: 10.1126/science.aaa0922

Lahiri, S., Mulligan, E., Andronikou, S., Shirahata, M., and Mokashi, A. (1987). Carotid body chemosensory function in prolonged Normobaric Hyperoxia in the cat. *J. Appl. Physiol.* 62, 1924–1931.

Lai, Y. L., Lamm, J. E., and Hildebrandt, J. (1981). Ventilation during prolonged Hypercapnia in the rat. *J. Appl. Physiol. Respir. Environ. Exerc. Physiol.* 51, 78–83. doi: 10.1152/jappl.1981.51.1.78

Lang, R., Gundlach, A. L., Holmes, F. E., Hobson, S. A., Wynick, D., Hokfelt, T., et al. (2015). Physiology, signaling, and pharmacology of galanin peptides and receptors: three decades of emerging diversity. *Pharmacol. Rev.* 67, 118–175. doi: 10.1124/pr.112.006536

Lazarenko, R. M., Milner, T. A., Depuy, S. D., Stornetta, R. L., West, G. H., Kievits, J. A., et al. (2009). Acid sensitivity and ultrastructure of the retrotrapezoid nucleus in Phox2b-Egfp transgenic mice. *J. Comp. Neurol.* 517, 69–86. doi: 10.1002/cne.22136

Le, S., Turner, A. J., Parker, L. M., Burke, P. G., Kumar, N. N., Goodchild, A. K., et al. (2016). Somatostatin 2a receptors are not expressed on functionally identified respiratory neurons in the ventral respiratory column of the rat. *J. Comp. Neurol.* 524, 1384–1398. doi: 10.1002/cne.23912

Li, P., Janczewski, W. A., Yackle, K., Kam, K., Pagliardini, S., Krasnow, M. A., et al. (2016). The Peptidergic control circuit for sighing. *Nature* 530, 293–297. doi: 10.1038/nature16964

Miller, J. R., Neumueller, S., Muere, C., Olesiak, S., Pan, L., Bukowy, J. D., et al. (2014). Changes in glutamate receptor subunits within the medulla in goats after section of the carotid sinus nerves. *J. Appl. Physiol.* 116, 1531–1542. doi: 10.1152/japplphysiol.00216.2014

Montes De Oca, M., and Celli, B. R. (1998). Mouth occlusion pressure, Co_2 response and hypercapnia in severe chronic obstructive Pulmonary Disease. *Eur. Respir. J.* 12, 666–671. doi: 10.1183/09031936.98.12030666

Moody, T. W., and Merali, Z. (2004). Bombesin-like peptides and associated receptors within the brain: distribution and behavioral implications. *Peptides* 25, 511–520.

Morgan, B. J., Bates, M. L., Rio, R. D., Wang, Z., and Dopp, J. M. (2016). Oxidative stress augments chemoreflex sensitivity in rats exposed to chronic intermittent hypoxia. *Respir. Physiol. Neurobiol.* 234, 47–59. doi: 10.1016/j.resp.2016.09.001

Mulkey, D. K., Stornetta, R. L., Weston, M. C., Simmons, J. R., Parker, A., Bayliss, D. A., et al. (2004). Respiratory control by ventral surface chemoreceptor neurons in rats. *Nat. Neurosci.* 7, 1360–1369. doi: 10.1038/nn1357

Muller, R., Bravo, R., Burckhardt, J., and Curran, T. (1984). Induction Of C-Fos gene and protein by growth factors precedes activation of C-Myc. *Nature* 312, 716–720. doi: 10.1038/312716a0

Nagashimada, M., Ohta, H., Li, C., Nakao, K., Uesaka, T., Brunet, J. F., et al. (2012). Autonomic Neurocristopathy-associated mutations in Phox2b dysregulate Sox10 expression. *J. Clin. Invest.* 122, 3145–3158. doi: 10.1172/JCI63401

Nassel, D. R. (2009). Neuropeptide signaling near and far: how localized and timed is the action of neuropeptides in brain circuits? *Invert. Neurosci.* 9, 57–75. doi: 10.1007/s10158-009-0090-1

Nattie, E., and Li, A. (2012). Central chemoreceptors: locations and functions. *Compr. Physiol.* 2, 221–254. doi: 10.1002/cphy.c100083

Nattie, E. E., and Li, A. (2002). Co2 dialysis in nucleus tractus solitarius region of rat increases ventilation in sleep and wakefulness. *J. Appl. Physiol.* 92, 2119–2130. doi: 10.1152/japplphysiol.01128.2001

Nestler, E. J., Barrot, M., and Self, D. W. (2001). Deltafosb: a sustained molecular switch for addiction. *Proc. Natl. Acad. Sci. U.S.A.* 98, 11042–11046. doi: 10.1073/pnas.191352698

Ogren, S. O., Kuteeva, E., Elvander-Tottie, E., and Hokfelt, T. (2010). Neuropeptides in learning and memory processes with focus on galanin. *Eur. J. Pharmacol.* 626, 9–17. doi: 10.1016/j.ejphar.2009.09.070

Onimaru, H., Arata, A., and Homma, I. (1997). Neuronal mechanisms of respiratory rhythm generation: an approach using *in vitro* preparation. *JPN J. Physiol.* 47, 385–403. doi: 10.2170/jjphysiol.47.385

Pagliardini, S., Janczewski, W. A., Tan, W., Dickson, C. T., Deisseroth, K., and Feldman, J. L. (2011). Active expiration induced by excitation of ventral medulla in adult anesthetized rats. *J. Neurosci.* 31, 2895–2905. doi: 10.1523/JNEUROSCI.5338-10.2011

Pagliardini, S., Ren, J., and Greer, J. J. (2003). Ontogeny of the pre-botzinger complex in perinatal rats. *J. Neurosci.* 23, 9575–9584. doi: 10.1523/jneurosci.23-29-09575.2003

Paxinos, G., and Franklin, K. B. (2004). *The Mouse Brain In Stereotaxic Coordinates*. Gulf: Professional Publishing.

Peng, Y., Kline, D. D., Dick, T. E., and Prabhakar, N. R. (2001). Chronic intermittent hypoxia enhances carotid body chemoreceptor response to low oxygen. *Adv. Exp. Med. Biol.* 499, 33–38. doi: 10.1007/978-1-4615-1375-9_5

Peng, Y. J., Overholt, J. L., Kline, D., Kumar, G. K., and Prabhakar, N. R. (2003). Induction of sensory long-term facilitation in the carotid body by intermittent hypoxia: implications for recurrent apneas. *Proc. Natl. Acad. Sci. U.S.A.* 100, 10073–10078. doi: 10.1073/pnas.1734109100

Peng, Y. J., Yuan, G., Ramakrishnan, D., Sharma, S. D., Bosch-Marce, M., Kumar, G. K., et al. (2006). Heterozygous Hif-1alpha deficiency impairs carotid body-mediated systemic responses and reactive oxygen species generation in mice exposed to intermittent hypoxia. *J. Physiol.* 577, 705–716. doi: 10.1113/jphysiol.2006.114033

Pfaffl, M. W. (2001). A new mathematical model for relative quantification in real-time Rt-Pcr. *Nucleic Acids Res.* 29:E45.

Pickel, V. M., Joh, T. H., and Reis, D. J. (1975). Immunohistochemical localization of tyrosine hydroxylase in brain by light and electron microscopy. *Brain Res.* 85, 295–300. doi: 10.1016/0006-8993(75)90084-0

Pingree, B. J. (1977). Acid-base and respiratory changes after prolonged exposure to 1% carbon dioxide. *Clin. Sci. Mol. Med.* 52, 67–74. doi: 10.1042/cs0520067

Rey, S., Del Rio, R., Alcayaga, J., and Iturriaga, R. (2004). Chronic intermittent hypoxia enhances cat chemosensory and ventilatory responses to hypoxia. *J. Physiol.* 560, 577–586. doi: 10.1113/jphysiol.2004.072033

Ritucci, N. A., Dean, J. B., and Putnam, R. W. (2005). Somatic Vs. dendritic responses to hypercapnia in chemosensitive locus coeruleus neurons from neonatal rats. *Am. J. Physiol. Cell Physiol.* 289, C1094–C1104.

Roesler, R., and Schwartsmann, G. (2012). Gastrin-releasing peptide receptors in the central nervous system: role in brain function and as a drug target. *Front. Endocrinol.* 3:159. doi: 10.3389/fendo.2012.00159

Salio, C., Lossi, L., Ferrini, F., and Merighi, A. (2006). Neuropeptides as synaptic transmitters. *Cell Tissue Res.* 326, 583–598. doi: 10.1007/s00441-006-0268-3

Sauerstein, K., Klede, M., Hilliges, M., and Schmelz, M. (2000). Electrically evoked neuropeptide release and neurogenic inflammation differ between rat and human skin. *J. Physiol.* 529(Pt 3), 803–810. doi: 10.1111/j.1469-7793.2000.00803.x

Schaefer, K. E. (1963). Respiratory adaptation to chronic hypercapnia. *Ann. N. Y. Acad. Sci.* 109, 772–782. doi: 10.1111/j.1749-6632.1963.tb13505.x

Schaefer, K. E., Avery, M. E., and Bensch, K. (1964). Time course of changes in surface tension and morphology of alveolar epithelial cells in Co_2-induced hyaline membrane disease. *J. Clin. Invest.* 43, 2080–2093. doi: 10.1172/jci105082

Schaefer, K. E., Hastings, B. J., Carey, C. R., and Nichols, G. Jr. (1963). Respiratory acclimatization to carbon dioxide. *J. Appl. Physiol.* 18, 1071–1078. doi: 10.1152/jappl.1963.18.6.1071

Sherman, D., Worrell, J. W., Cui, Y., and Feldman, J. L. (2015). Optogenetic perturbation of prebotzinger complex inhibitory neurons modulates respiratory pattern. *Nat. Neurosci.* 18, 408–414. doi: 10.1038/nn.3938

Shi, Y., Stornetta, R. L., Stornetta, D. S., Onengut-Gumuscu, S., Farber, E. A., Turner, S. D., et al. (2017). Neuromedin B expression defines the mouse retrotrapezoid nucleus. *J. Neurosci.* 37, 11744–11757. doi: 10.1523/JNEUROSCI.2055-17.2017

Smith, C. A., Forster, H. V., Blain, G. M., and Dempsey, J. A. (2010). An interdependent model of central/peripheral chemoreception: evidence and implications for ventilatory control. *Respir. Physiol. Neurobiol.* 173, 288–297. doi: 10.1016/j.resp.2010.02.015

Smith, J. C., Abdala, A. P., Rybak, I. A., and Paton, J. F. (2009). Structural and functional architecture of respiratory networks in the mammalian brainstem. *Philos. Trans. R. Soc. Lond. B Biol. Sci.* 364, 2577–2587. doi: 10.1098/rstb.2009.0081

Spirovski, D., Li, Q., and Pilowsky, P. M. (2012). Brainstem galanin-synthesizing neurons are differentially activated by chemoreceptor stimuli and represent a subpopulation of respiratory neurons. *J. Comp. Neurol.* 520, 154–173. doi: 10.1002/cne.22723

Stornetta, R. L., Rosin, D. L., Wang, H., Sevigny, C. P., Weston, M. C., and Guyenet, P. G. (2003). A group of glutamatergic interneurons expressing high levels of both neurokinin-1 receptors and somatostatin identifies the region of the pre-botzinger complex. *J. Comp. Neurol.* 455, 499–512. doi: 10.1002/cne.10504

Stornetta, R. L., Spirovski, D., Moreira, T. S., Takakura, A. C., West, G. H., Gwilt, J. M., et al. (2009). Galanin is a selective marker of the retrotrapezoid nucleus in rats. *J. Comp. Neurol.* 512, 373–383. doi: 10.1002/cne.21897

Takakura, A. C., Moreira, T. S., Colombari, E., West, G. H., Stornetta, R. L., and Guyenet, P. G. (2006). Peripheral chemoreceptor inputs to retrotrapezoid nucleus (Rtn) Co2-sensitive neurons in rats. *J. Physiol.* 572, 503–523. doi: 10.1113/jphysiol.2005.103788

Teppema, L. J., Veening, J. G., Kranenburg, A., Dahan, A., Berkenbosch, A., and Olievier, C. (1997). Expression of C-Fos in the rat brainstem after exposure to hypoxia and to normoxic and hyperoxic hypercapnia. *J. Comp. Neurol.* 388, 169–190. doi: 10.1002/(sici)1096-9861(19971117)388:2<169::aid-cne1>3.0.co;2-#

Wakai, J., Takamura, D., Morinaga, R., Nakamuta, N., and Yamamoto, Y. (2015). Differences in respiratory changes and fos expression in the ventrolateral medulla of rats exposed to hypoxia, hypercapnia, and hypercapnic hypoxia. *Respir. Physiol. Neurobiol.* 215, 64–72. doi: 10.1016/j.resp.2015.05.008

Wang, S., Shi, Y., Shu, S., Guyenet, P. G., and Bayliss, D. A. (2013). Phox2b-expressing retrotrapezoid neurons are intrinsically responsive to H+ and Co2. *J. Neurosci.* 33, 7756–7761. doi: 10.1523/JNEUROSCI.5550-12.2013

Wang, W., Li, Q., Pan, Y., Zhu, D., and Wang, L. (2013). Influence of hypercapnia on the synthesis of neuropeptides and their receptors in murine brain. *Respirology* 18, 102–107. doi: 10.1111/j.1440-1843.2012.02245.x

Xu, F., and Frazier, D. T. (2000). Modulation of respiratory motor output by cerebellar deep nuclei in the rat. *J. Appl. Physiol.* 89, 996–1004. doi: 10.1152/jappl.2000.89.3.996

Yang, C. F., and Feldman, J. L. (2018). Efferent projections of excitatory and inhibitory prebotzinger complex neurons. *J. Comp. Neurol.* 526, 1389–1402. doi: 10.1002/cne.24415

Conflict of Interest: The authors declare that the research was conducted in the absence of any commercial or financial relationships that could be construed as a potential conflict of interest.

frontiers in Neuroscience

REVIEW
published: 21 January 2020
doi: 10.3389/fnins.2019.01369

Identifying Increases in Activity of the Human RVLM Through MSNA-Coupled fMRI

Vaughan G. Macefield[1,2]* *and Luke A. Henderson*[3,4]

[1] Human Autonomic Neurophysiology Laboratory, School of Medicine, Baker Heart and Diabetes Institute, Melbourne, VIC, Australia, [2] Department of Physiology, School of Biomedical Sciences, The University of Melbourne, Melbourne, VIC, Australia, [3] Discipline of Anatomy and Histology, School of Medical Sciences, The University of Sydney, Sydney, NSW, Australia, [4] Brain and Mind Centre, The University of Sydney, Sydney, NSW, Australia

Aim: We initially developed concurrent recording of muscle sympathetic nerve activity (MSNA) and functional magnetic resonance imaging (fMRI) of the brain to functionally identify the human homolog of the rostral ventrolateral medulla (RVLM). Here we summarize the cortical and subcortical connections to the RVLM, as identified using MSNA-coupled fMRI.

Methods: MSNA was recorded via tungsten microelectrodes inserted into the peroneal nerve. Gradient echo, echo-planar fMRI was performed at 3T (Philips Achieva). 200 volumes (46 axial slices (TR = 8 s, TE = 4 s, flip angle = 90°, raw voxel size = 1.5 × 1.5 × 2.75 mm) were collected in a 4 s-ON, 4 s-OFF sparse sampling protocol and MSNA measured in each 1 s epoch in the 4-s period between scans. Blood oxygen level dependent (BOLD) signal intensity was measured in the corresponding 1 s epoch 4 s later to account for peripheral neural conduction and central neurovascular coupling delays.

Results: BOLD signal intensity was positively related to bursts of MSNA in the RVLM, dorsomedial hypothalamus (DMH), ventromedial hypothalamus (VMH), insula, dorsolateral prefrontal cortex (dlPFC), posterior cingulate cortex (PCC), and precuneus, and negatively related in the caudal ventrolateral medulla (CVLM), nucleus tractus solitarius (NTS), and the midbrain periaqueductal gray (PAG). During physiological increases in MSNA (tonic muscle pain), MSNA-coupled BOLD signal intensity was greater in RVLM, NTS, PAG, DMH, dlPFC, medial prefrontal cortex (mPFC), precuneus, and anterior cingulate cortex (ACC) than at rest. During pathophysiological increases in MSNA [obstructive sleep apnoea (OSA)] signal intensity was also higher in dlPFC, mPFC, ACC, and precuneus than in controls. Conversely, signal intensity was lower in RVLM in OSA than in controls, which we interpret as reflecting a withdrawal of active inhibition of the RVLM.

Conclusion: These results suggest that multiple cortical and subcortical areas are functionally coupled to the RVLM, which in turn is functionally coupled to the generation of spontaneous bursts of MSNA and their augmentation during physiological and pathophysiological increase in vasoconstrictor drive.

Keywords: muscle sympathetic nerve activity, functional magnetic resonance imaging, rostral ventrolateral medulla, blood pressure, human

OPEN ACCESS

Edited by:
Elisabeth Lambert, Swinburne University of Technology, Australia

Reviewed by:
Stephanie Tjen-A-Looi, University of California, Irvine, United States
Thiago S. Moreira, University of São Paulo, Brazil
Simon McMullan, Macquarie University, Australia

***Correspondence:**
Vaughan G. Macefield
vaughan.macefield@baker.edu.au

Specialty section:
This article was submitted to Autonomic Neuroscience, a section of the journal Frontiers in Neuroscience

Received: *07 September 2019*
Accepted: *04 December 2019*
Published: *21 January 2020*

Citation:
Macefield VG and Henderson LA (2020) Identifying Increases in Activity of the Human RVLM Through MSNA-Coupled fMRI. Front. Neurosci. 13:1369. doi: 10.3389/fnins.2019.01369

THE ROLE OF THE RVLM IN THE REGULATION OF BLOOD PRESSURE

From classic studies of decerebrate animals, it has long been known that the control of blood pressure requires an intact brainstem, in particular the medulla oblongata; section of the spinal cord immediately below the medulla leads to a precipitous fall in blood pressure, while section of the brainstem at the pontomedullary junction does not. The maintenance of blood pressure within a relatively narrow range depends on the integrity of a simple reflex arc, the baroreflex. Baroreceptors – mechanoreceptors located within the carotid sinus and aortic arch that are sensitive to radial distension of the arterial wall and hence to intraluminal pressure – detect the pulsatile fluctuations in blood pressure and, via the glossopharyngeal and vagus nerves, send excitatory synaptic projections to the primary visceral sensory nucleus, the nucleus of the solitary tract (NTS). Second-order neurones within NTS then send excitatory projections to neurones of the caudal ventrolateral medulla (CVLM), which exerts tonic inhibitory control of the rostral ventrolateral medulla (RVLM) (Dampney et al., 2003a,b; Guyenet, 2006). It is well known that the RVLM plays a critical role in maintaining absolute levels of blood pressure, as well as being essential for the beat-to-beat control of blood pressure: almost all sympathetic vasoconstrictor neurones originate in the RVLM and electrolytic lesions of the RVLM result in precipitous falls in blood pressure (Kumada et al., 1979; Dampney and Moon, 1980). However, there is evidence suggesting that this view of the RVLM being critical to the maintenance of blood pressure is incorrect. Recently, Wenker et al. (2017) showed that laser-induced inhibition of archaerhodopsin-expressing RVLM neurones failed to drop blood pressure significantly in conscious rats. However, the authors do acknowledge that just over 50% of the neurones expressed archaerhodopsin, so it is possible that inadequate inhibition was produced during laser stimulation.

Given that the RVLM is the primary (albeit not exclusive) output nucleus for sympathetic vasoconstrictor drive to the muscle, splanchnic, and renal vascular beds (Dampney and McAllen, 1988; McAllen et al., 1995), and thereby plays an important role in the ongoing regulation of total peripheral resistance and blood pressure, measuring sympathetic vasoconstrictor nerve activity in the periphery can be used to infer the state of activity of the RVLM, as well as other nuclei with spinally projecting neurones – such as the paraventricular

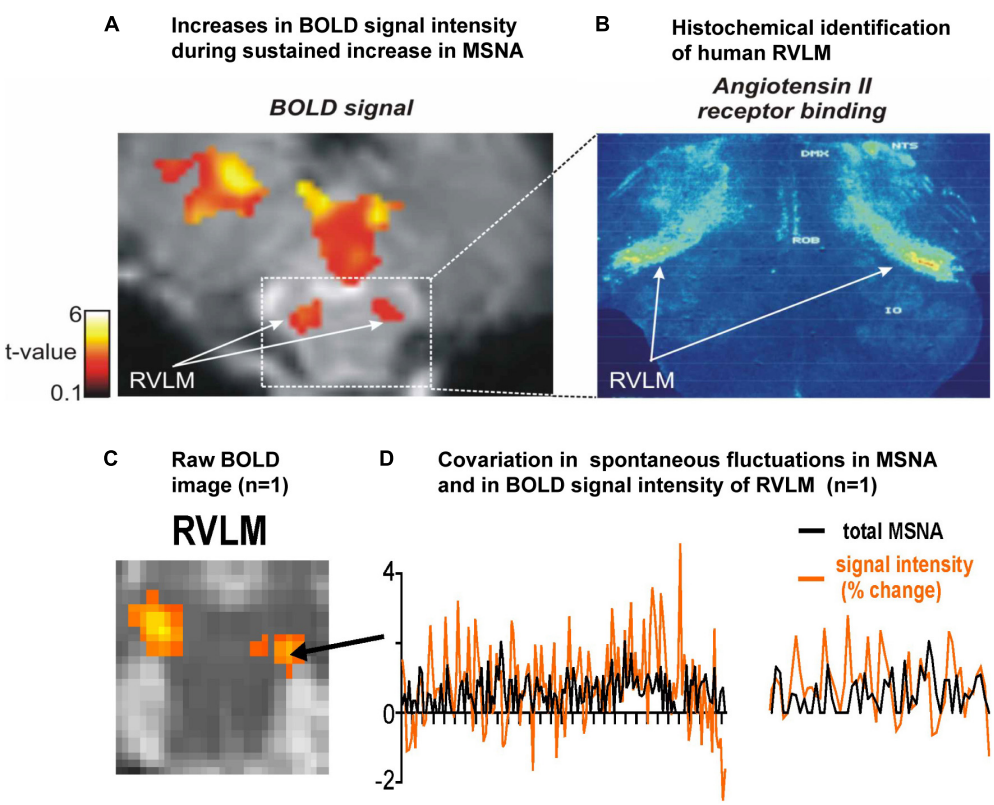

FIGURE 1 | (A) Axial section of the rostral medulla showing bilateral increases in BOLD signal intensity in the dorsolateral medulla – the region of the human rostral ventrolateral medulla (RVLM) – during sustained increases in MSNA during a set of three maximal inspiratory breath-holds in 15 participants. **(B)** Histochemical identification of the human RVLM based on the high density of Angiotensin II receptor binding (data reproduced with permission from Allen et al., 1998). **(C)** Bilateral increases in MSNA-coupled BOLD signal intensity in the region of the RVLM. **(D)** Covariation in total MSNA, shown as the total amplitude of MSNA measured in each 1 s epoch, and BOLD signal intensity in the corresponding 1 s epochs, measured over 30 s in the region indicated in panel **(C)** for the same participant; an expanded section is shown on the right. Reproduced, with permission, from Macefield and Henderson (2019).

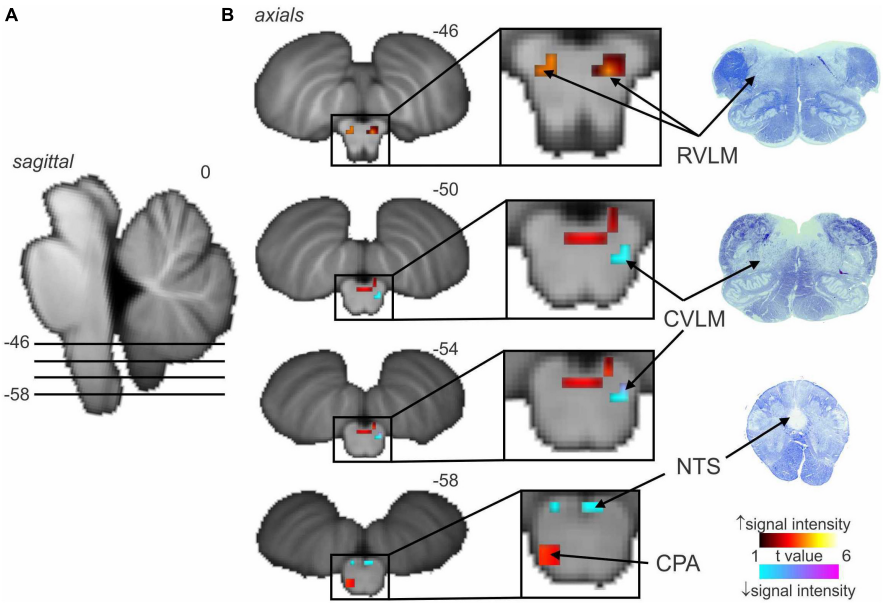

FIGURE 2 | Significant increases (warm color scale) and decreases (cool color scale) in functional magnetic resonance imaging (fMRI) signal intensity within the brainstem correlated with spontaneous muscle sympathetic nerve activity (MSNA; total burst activity) in the resting state; data from seven experiments. **(A)** Significant changes are overlaid onto sagittal and axial slices of a T1-weighted brainstem template, with slice locations in Montreal Neurological Institute space indicated at the top right of each slice. **(B)** Equivalent histological sections. Note that spontaneous bursts of MSNA are associated with increases in signal intensity in the regions of the rostral ventrolateral medulla (RVLM) and caudal pressor area (CPA) and decreases in the region of the caudal ventrolateral medulla (CVLM) and nucleus tractus solitarius (NTS). Reproduced, with permission, from Macefield and Henderson (2019).

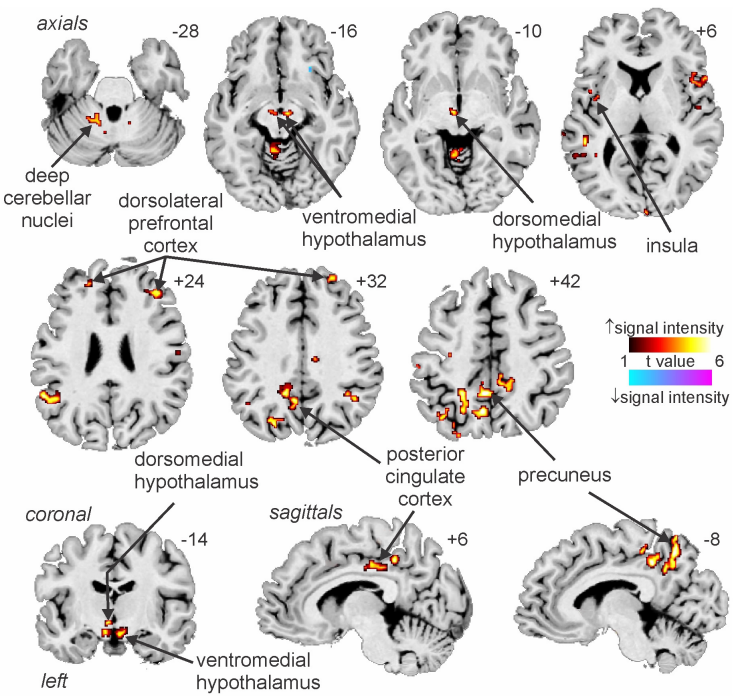

FIGURE 3 | Increases and decreases in functional magnetic resonance imaging (fMRI) signal intensity correlated with muscle sympathetic nerve activity (MSNA) in 14 healthy participants. The hot color scale indicates regions in which signal intensity was high during periods of high MSNA and low during low MSNA. Conversely, the cool color scale indicates regions where signal intensity was high during low MSNA and low during high MSNA. Clusters are overlaid onto axial, coronal and sagittal slices of an individual subject's T1-weighted anatomical and slice locations in Montreal Neurological Space are shown at the top right of each section. Reproduced, with permission, from James et al. (2013).

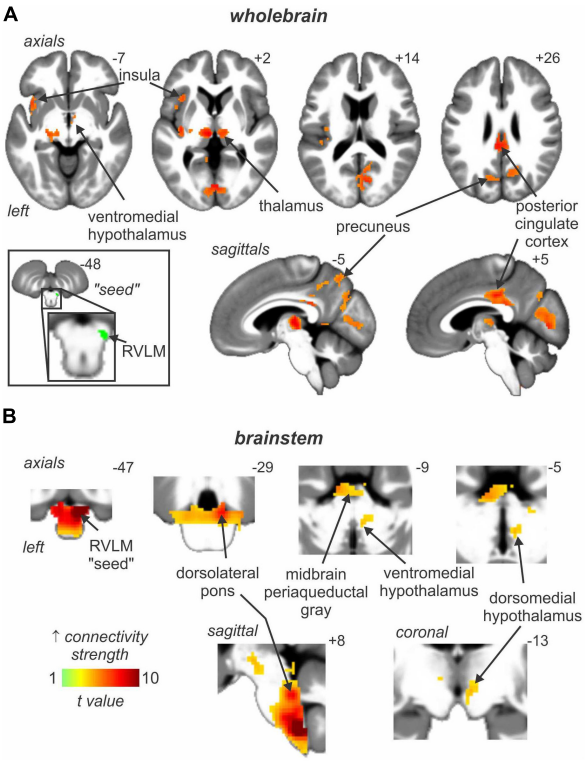

FIGURE 4 | Brain regions in which signal intensity fluctuations at rest are significantly positively coupled to those in the rostral ventrolateral medulla (RVLM) in 29 healthy participants. Results from an analysis focused on rostral brain sites are shown in panel **(A)** whereas panel **(B)** focusses on the brainstem only. Significant positive signal couplings with the RVLM are indicated with the hot color scale and overlaid onto and axial, coronal and sagittal slices of a mean T1-weighted anatomical image. Slice locations in Montreal Neurological Space are shown at the top right of each section. Reproduced, with permission, from Macefield and Henderson (2019).

nucleus of the hypothalamus (PVN), which sends direct projections to the spinal cord as well as to RVLM (Shafton et al., 1998; Pyner and Coote, 2000). However, given that spinally projecting PVN neurones do not respond to baroreceptor input in the conscious rabbit (Dampney et al., 2003b) it is likely that this nucleus contributes little to resting vasoconstrictor drive to vascular beds involved in regulating total peripheral resistance, such as those in skeletal muscle.

Sympathetic outflow to the muscle vascular bed can be recorded directly in humans via a tungsten microelectrode inserted percutaneously into an accessible peripheral nerve, an invasive technique known as microneurography. Muscle sympathetic nerve activity (MSNA) occurs as spontaneous bursts that show a strong temporal coupling to the heart beat; bursts occur in the intervals between heart beats, with longer cardiac intervals being associated with lower diastolic pressures and a greater incidence and amplitude of bursts of MSNA (Macefield, 2013). Although there is no association between resting MSNA and blood pressure in normotensive humans (Joyner et al., 2010), it is well established that elevated MSNA contributes to the development of neurogenic hypertension (Wallin et al., 1973; Grassi et al., 1998; Schlaich et al., 2004).

FUNCTIONAL IDENTIFICATION OF THE HUMAN RVLM USING MSNA-COUPLED fMRI

Nearly 10 years ago we published our first paper (Macefield and Henderson, 2010) on MSNA-coupled functional magnetic resonance imaging (fMRI), in which we combined direct recordings of MSNA with fMRI of the brainstem. Our approach, in which fluctuations in the incidence and amplitude of spontaneous bursts of MSNA recorded in the periphery are used to identify covarying fluctuations in BOLD (blood oxygen level dependent) signal intensity, was used to identify individual nuclei in the brainstem responsible for the generation of the signal. In other words, recording the output signal at the same time as imaging the brain allowed us to identify the central source of the output signal. Given the technical difficulties of recording small nerve signals in a large magnetic field (3 Tesla, and we are now doing this at 7T), this had never before been attempted. Details of our methodology can be found elsewhere (Macefield and Henderson, 2010, 2016, 2019), but briefly spontaneous bursts of MSNA were recorded via a tungsten microelectrode inserted percutaneously into a muscle fascicle of the right common peroneal nerve in supine participants, and neural activity amplified, filtered (2×10^4, 0.3–5.0 kHz; NeuroAmpEx, ADInstruments, Sydney, NSW, Australia) and sampled on computer at 10 kHz (PowerLab 16S and LabChart 7 software, ADInstruments). The head was enclosed in a 32-channel SENSE head coil and a sparse gradient-gradient echo sampling protocol was performed: 200 volumes (TR = 8 s, TE = 4 s, flip angle = 90°, raw voxel size = 1.5 × 1.5 × 2.75 mm) were acquired over 27 min, each volume comprising 46 axial slices collected in a caudal to rostral direction and extending from the top of the cervical spinal cord to the vertex. Each 8 s TR period was composed of an initial 4 s "ON" phase during which the entire fMRI volume was collected, followed by a non-scanning "OFF" phase of 4 s, in which bursts of MSNA were measured in each of the four 1-s epochs. BOLD signal intensity (SPM12, uncorrected $p < 0.001$) was measured in each of the four 1-s epochs in the subsequent 4-s period to account for the ∼1 s required for arrival of the sympathetic volley at the peripheral recording site (Fagius and Wallin, 1980) and the ∼5 s hemodynamic delay between the neuronal activity and generation of the BOLD signal (Logothetis et al., 2001). Importantly, we do not use a region-of-interest approach: rather, areas of the brain are identified as being involved in the regulation of MSNA because the spontaneous fluctuations in BOLD signal intensity covaried with the spontaneous fluctuations in burst amplitude of the MSNA signal. In other words, these areas "popped out" because of their temporal coupling to the bursts of MSNA.

Figure 1A shows a bilateral increase in BOLD signal intensity in the medulla during three sets of maximal inspiratory breath holds – a manoeuver that causes a sustained increase in MSNA – in 15 participants (Macefield et al., 2006). We believe

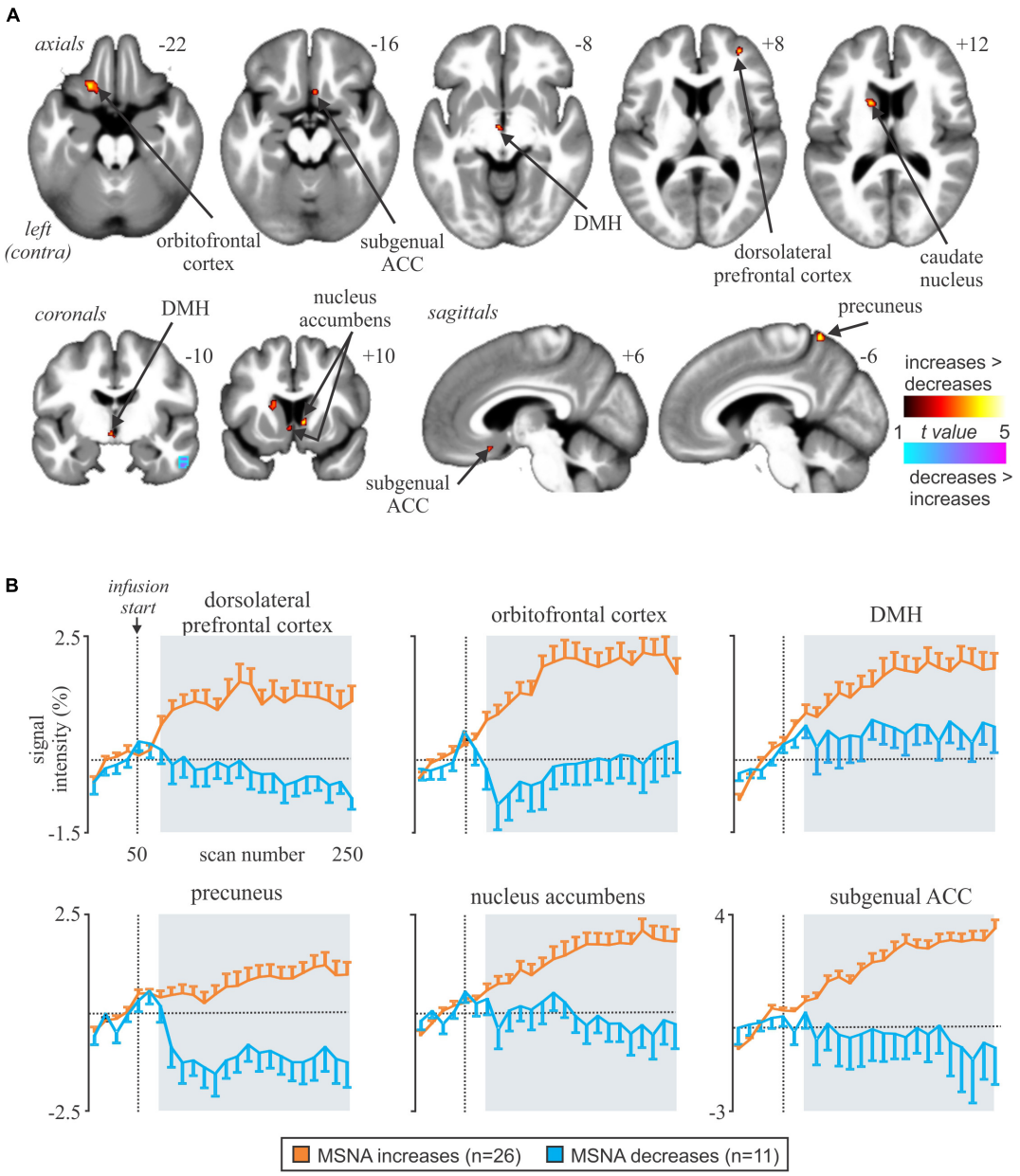

FIGURE 5 | (A) Brain regions in which increases in BOLD signal intensity were greater or lower during tonic muscle pain. Significant clusters are overlaid onto a mean T1-weighted anatomical image set created from all 37 subjects. Slice locations in MNI space are indicated in the upper right of each image. The left side of the image is the side contralateral to the noxious stimulus. **(B)** Plots of mean (±SEM) percentage changes, measured every 5 min, at baseline and during pain (gray shading) in the increasing (orange) and decreasing (blue) groups. Reproduced, with permission, from Kobuch et al. (2017).

these clusters represent the human homolog of the RVLM: the human RVLM is not located in the ventrolateral part of the medulla, where it was first identified in the rabbit, but in the *dorsolateral* aspect of the medulla (**Figure 1B**). This is because the human RVLM, identified as such because of its high density of angiotensin II type IA receptors (AT1AR), is displaced by the large inferior olives in humans (Allen et al., 1998). In **Figure 1C** we show for one participant bilateral increases in MSNA-coupled BOLD signal intensity in these same areas: it can be seen that the BOLD signal and MSNA signal covary over time, shown for a 30 s sample for this same participant in **Figure 1D**.

Figure 2 shows average data from eight participants. MSNA-coupled signal intensity was high in RVLM, yet low in the regions corresponding to NTS and CVLM. This makes sense, given that spontaneous bursts of MSNA only occur when diastolic blood pressure is low and hence the excitatory input to NTS from the arterial baroreceptors is also low. And, because NTS sends an excitatory projection to CVLM, BOLD signal intensity

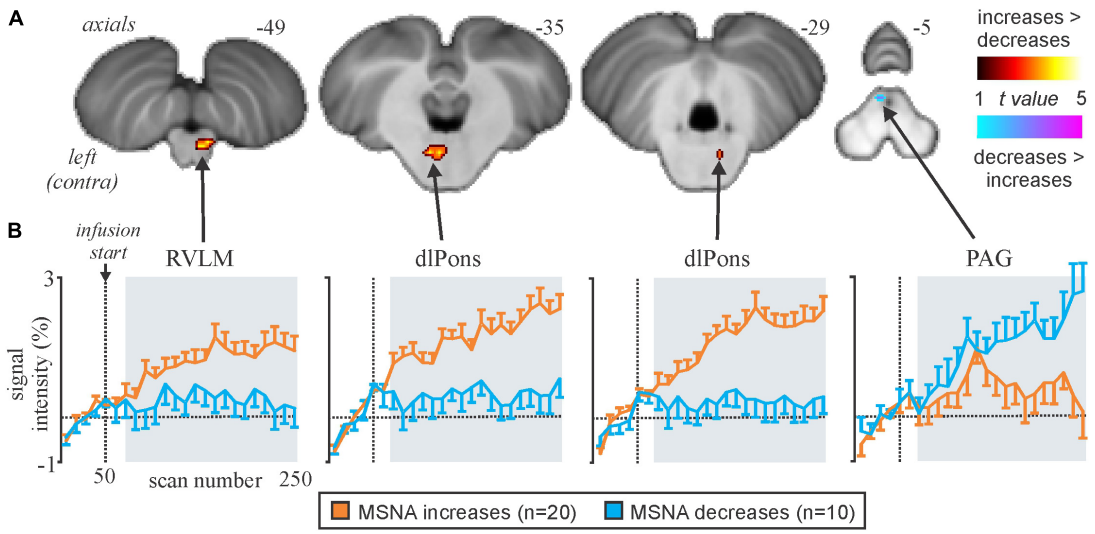

FIGURE 6 | (A) Brainstem regions in which signal intensity increases were greater (hot color scale) or lower (cool color scale) in the increasing MSNA (*n*=20) compared with the decreasing MSNA (*n*=10) group during tonic muscle pain. Significant clusters were overlaid onto a mean SUIT T1-weighted anatomical image set created from 30 subjects. **(B)** Plots of mean (±SEM) percentage signal intensity changes during pain relative to the baseline period for significant clusters in the increasing MSNA (orange) and decreasing MSNA groups (blue). RVLM, rostroventrolateral medulla; dlPons, dorsolateral pons; PAG, midbrain periaqueductal gray. Reproduced, with permission, from Kobuch et al. (2017).

in this nucleus is also low. The opposite occurs when bursts of MSNA are absent when diastolic pressure is high. As such, these findings demonstrate the existence in humans of the serial NTS-CVLM-RVLM baroreflex circuit identified in experimental animals referred to above (Macefield and Henderson, 2010). It can also be seen that there is a unilateral (left) caudal medullary site in which BOLD signal intensity is high when bursts of MSNA occur: we suggest that this cluster corresponds to the caudal pressor area (CPA), an area known to send excitatory projections to RVLM (Dampney et al., 2003a,b).

We have also used MSNA-coupled fMRI to identify structures above the brainstem. As shown in **Figure 3**, MSNA-coupled signal intensity was high in a number of discrete regions, including the left insula, left and right dorsolateral prefrontal cortex (dlPFC), posterior cingulate cortex (PCC), and precuneus. There was also significant MSNA-coupled signal intensity in the left dorsomedial hypothalamus (DMH) and both the left and right ventromedial hypothalamus (VMH). Neither DMH nor VMH send direct projections to the spinal cord, with DMH influencing sympathetic outflow via RVLM (DiMicco et al., 2002; Horiuchi et al., 2004; Wang et al., 2010) and VMH acting via DMH, midbrain periaqueductal gray (PAG), parabrachial nucleus, and NTS (ter Horst and Luiten, 1986; Canteras et al., 1994; Jansen et al., 1995). Note, however, that there was no signal in the PVN which – as noted above – is the one hypothalamic nucleus known to send direct projections to the spinal cord in parallel to those to RVLM (Shafton et al., 1998; Pyner and Coote, 2000).

In addition to these areas being functionally coupled to bursts of MSNA, as shown in **Figure 4** connectivity analysis revealed that the RVLM is functionally coupled to the anterior insula, PCC, precuneus, VMH and DMH, PAG, and dorsolateral pons (dlPons). This means that each of these areas are all functionally coupled to the generation of spontaneous bursts of MSNA and hence are likely to be involved in the generation of, and/or regulation of, MSNA at rest. We were surprised to find that changes in signal intensity in certain areas – including NTS, CVLM, CPA, DMH, and insula – were not symmetrical, although changes in RVLM, VMH, dlPFC, PCC, and precuneus were bilateral. We always recorded MSNA from the right common peroneal nerve, but given that both the incidence and amplitude of bursts of MSNA directed to the left and right legs are symmetrical, as demonstrated during bilateral recordings of MSNA (Sundlof and Wallin, 1977; El Sayed et al., 2012), any attempt to explain these side-to-side differences would be purely speculative. We direct the reader to our recent review in which we consider the functional significance of the sympathetic connectome we have identified (Macefield and Henderson, 2019).

CHANGES IN MSNA-COUPLED BOLD SIGNAL INTENSITY DURING PHYSIOLOGICAL INCREASES IN MSNA

We had already shown that BOLD signal intensity increases in RVLM during a maximal inspiratory breath-hold (see **Figure 1A**) while signal intensity in NTS and CVLM goes down (Macefield et al., 2006), and have shown that signal intensity increases in both NTS and RVLM during activation of metaboreceptors by inducing 6 min of post-exercise ischemia following 4 min of static handgrip exercise (Sander et al., 2010). Earlier studies had also shown that BOLD signal

intensity increased in the medulla and dorsal pons during a Valsalva maneuver (Harper et al., 2000; Henderson et al., 2002), with increases in signal intensity in NTS and the parabrachial nucleus (to which NTS projects) being reported during a maximal inspiratory effort, isometric handgrip exercise and the Valsalva maneuver (Topolovec et al., 2004). However, in none of these studies had MSNA been recorded at the same time.

We recently examined functional changes in the brain during experimental muscle pain, induced by a 40-min infusion of hypertonic saline into a leg muscle, which causes a sustained increase in MSNA in some participants but a sustained decrease in others; the pattern is reproducible in a given individual and we recently showed that those in whom MSNA increased during tonic muscle pain exhibited increases in BOLD signal intensity in several areas (Kobuch et al., 2017, 2018), including the anterior insula and anterior medial prefrontal cortex (mPFC) on the left, and dlPFC and anterior cingulate cortex (ACC) on the right, while signal intensity decreased in the mPFC and dlPFC on the left (**Figure 5**). We also saw an increase in signal intensity in the left DMH, which fits with the role of this nucleus in the generation of autonomic responses to stress (DiMicco et al., 2002; Fontes et al., 2017). A brainstem-specific analysis also showed differential responses, with increases in BOLD signal intensity in RVLM and dlPons, as well as NTS (not shown), in the group exhibiting an increase in MSNA, while activity in the midbrain PAG only showed a sustained increase in the group in whom MSNA fell (**Figure 6**).

Because MSNA was recorded at the same time as we scanned the brain we could then correlate BOLD signal intensity to the pain-evoked changes in amplitude of MSNA. At rest, BOLD signal intensity was strongly coupled to bursts of MSNA in the RVLM, insula, dlPFC, PCC, and precuneus, and decreased in the region of the midbrain PAG. During pain, MSNA-coupled BOLD signal intensity was significantly higher in the region of the NTS and ventrolateral PAG on the right, dlPFC and ACC on the right, and insula and mPFC on the left; conversely, MSNA-coupled signal intensity decreased during pain in parts of the left dlPFC and mPFC (Kobuch et al., 2018). Mean data, showing the correlations between the change in BOLD signal intensity and change in MSNA burst amplitude, from 37 participants are illustrated in **Figure 7**. These results indicate that several areas of the brain are engaged in a burst-to-burst manner, with the magnitudes of these changes in signal intensity being correlated to the overall change in MSNA amplitude during tonic muscle pain (Kobuch et al., 2018). Interestingly, some important brain regions did not display pain-related changes. For example, while we had found that the RVLM and precuneus displayed strong coupling to MSNA at rest, during tonic muscle pain neither of these regions showed changes in signal intensity as a function of MSNA burst intensity. However, as noted above both of these regions displayed sustained signal intensity increases in the increasing MSNA group, and decreases in the decreasing MSNA group, suggesting that both RVLM and precuneus may provide a tonic modulatory role rather than changing in a burst-to-burst fashion during muscle pain (Kobuch et al., 2018).

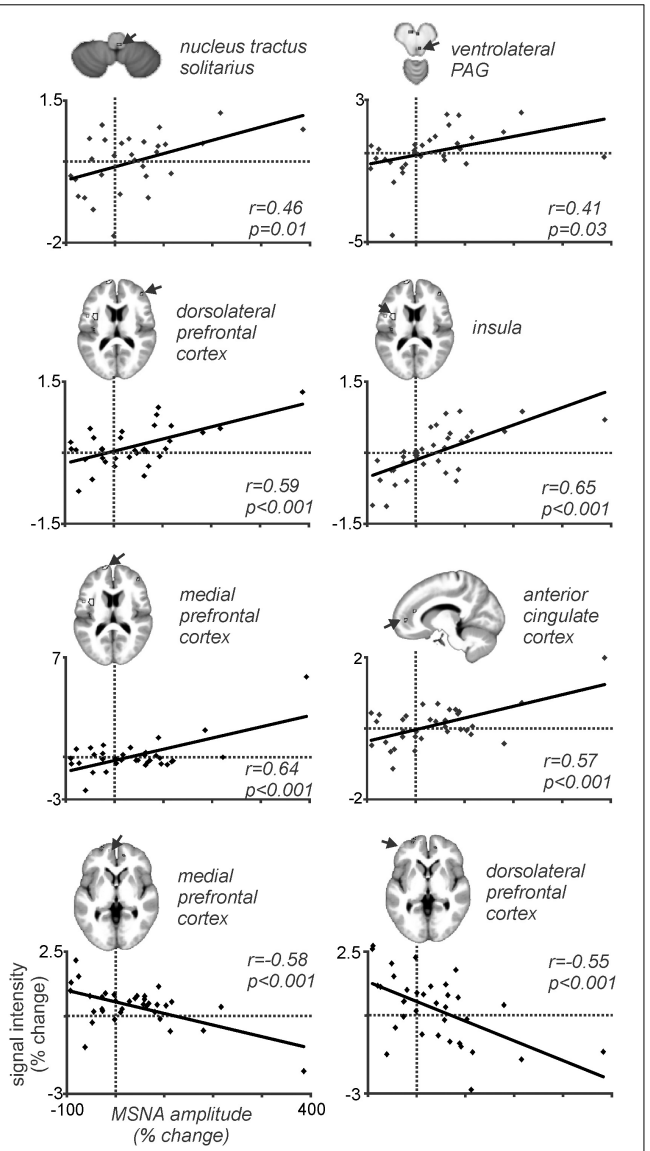

FIGURE 7 | Plots of MSNA-coupled BOLD signal intensity during tonic pain in all 37 participants. In all regions there is a significant linear relationship between the change in BOLD signal intensity and the change in burst amplitude of MSNA. Reproduced, with permission, from Kobuch et al. (2018).

CHANGES IN MSNA-COUPLED BOLD SIGNAL INTENSITY DURING PATHOPHYSIOLOGICAL INCREASES IN MSNA

Patients with obstructive sleep apnoea (OSA) have markedly elevated MSNA at rest, due to the repetitive episodes of nocturnal hypoxemia associated with collapse of the upper

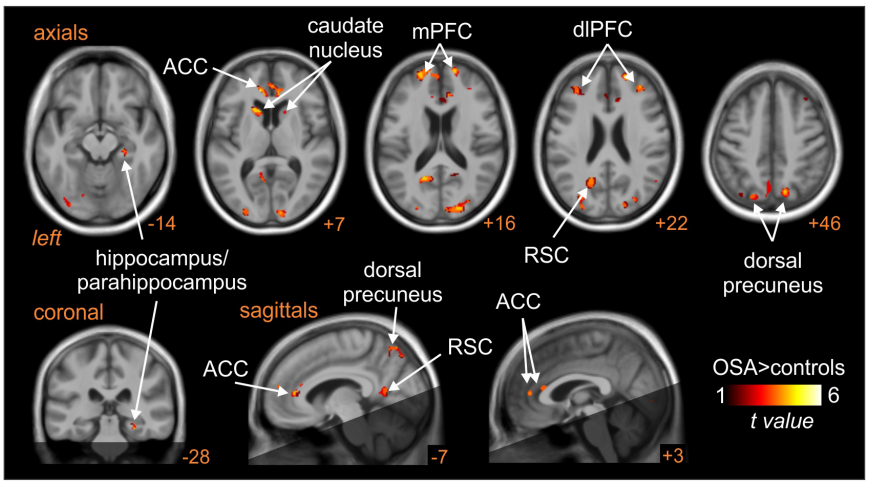

FIGURE 8 | Brain regions in which MSNA-coupled changes in BOLD signal intensity were significantly different in OSA than controls. The dark shading indicates brain regions not included in the analysis. ACC, anterior cingulate cortex; dlPFC, dorsolateral prefrontal cortex; mPFC, medial prefrontal cortex; RSC, retrosplenial cortex. Reproduced, with permission, from Fatouleh et al. (2014).

airways, which leads to neurogenic hypertension. This then is a pathophysiological model of high MSNA. As shown in **Figure 8**, MSNA-coupled BOLD signal intensity was higher in OSA than in controls in the following areas: dlPFC and mPFC bilaterally, dorsal precuneus, ACC, retrosplenial cortex (RSC), and caudate nucleus (Fatouleh et al., 2014). These data suggest that the elevated MSNA may be driven by changes in higher cortical regions, possibly through influences on brainstem nuclei.

Indeed, as shown in **Figure 9**, high-resolution scanning of the brainstem revealed significant coupling between spontaneous bursts of MSNA and BOLD signal intensity in a number of brainstem regions, including the medullary raphé, RVLM, dlPons, and midbrain, and significant increases in gray matter volume in the same areas (Lundblad et al., 2014). Although several mechanisms may lead to this increase in gray matter volume, it is possible that these changes are brought about by astrocytic activation and modulation of synaptic activity through altered gliotransmission. Indeed, it has been reported

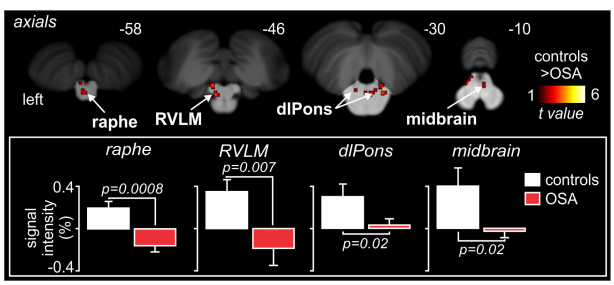

FIGURE 9 | Brainstem regions in which MSNA-coupled BOLD signal intensity was significantly different in OSA and controls. Signal intensity increased in controls but decreased in OSA. Reproduced, with permission, from Lundblad et al. (2014).

that chronic intermittent hypoxia is associated with activation of astrocytes in cortical regions such as the hippocampus (Aviles-Reyes et al., 2010). It is possible that repeated hypoxic events somehow evoke astrocyte activation in the raphe, dlPons and the RVLM which is consistent with increased gray matter density. Curiously, despite this increase in gray matter volume, MSNA-coupled BOLD signal intensity was actually *lower* in OSA than in controls, as shown in **Figure 9**. It is possible that reduced tonic inhibitory drive on rostral ventrolateral medullary premotor sympathetic neurones by the dlPons and medullary raphe leads to the increase in resting MSNA in OSA. Given that the BOLD signal is believed to reflect synaptic energy-dependent processes (Logothetis et al., 2001), a reduction in signal intensity within RVLM, despite an increase in output from this nucleus (MSNA was higher), may reflect a *reduction in active inhibition* onto the RVLM. Activation of astrocytes might then alter synaptic dynamics through the release of gliotransmitters such as glutamate, ATP or even GABA (Halassa et al., 2007; Ben Achour and Pascual, 2012). Regardless of the underlying mechanisms, our data show that there are changes in the brain that may be responsible for the increase in MSNA and blood pressure in OSA. In other words, *pathophysiological changes within the brain* lead to one of the clinical features of OSA – the hypertension. If this was true, we might expect that treatment of the condition would reverse these changes. Indeed, we showed that 6 months of continuous positive airway pressure (CPAP), which produced a significant fall in MSNA, caused reversal of the functional changes seen in OSA (Fatouleh et al., 2015; Lundblad et al., 2015).

CONCLUSION

Muscle sympathetic nerve activity-coupled fMRI has allowed us to functionally identify the human RVLM and shown that its

ongoing activity is coupled to several cortical and subcortical structures at rest. Moreover, the strength of this coupling can be modified by physiological or pathophysiological processes that lead to increases in MSNA. While physiological increases in MSNA may result in an increase in BOLD signal intensity of the RVLM, in the pathophysiological increase in MSNA seen in OSA it would appear that BOLD signal goes down, which we interpret as being due to a reduction in ongoing inhibition. Indeed, we suggest that the output of the human RVLM at rest is held in check by active inhibition, withdrawal of which can lead to increases in MSNA and blood pressure. Of course, we cannot exclude the possibility that other brainstem or hypothalamic areas contribute to the physiological or pathophysiological increases in MSNA, but the fact that we are seeing significant changes in RVLM, which receives inputs from many other brainstem and hypothalamic areas, leads us to conclude that much of what we see is indeed due to changes within RVLM.

AUTHOR CONTRIBUTIONS

This manuscript is a review of the authors' collaborative work on the technique of MSNA-coupled fMRI. VM wrote the draft review, with contributions by LH.

FUNDING

This work was supported by grants from the National Health and Medical Research Council of Australia (GTN1007557, GTN1100038, and GTN1100042).

ACKNOWLEDGMENTS

We are grateful to the contributions of Dr. Cheree James, Dr. Rania Fatouleh, Dr. Linda Lundblad, and Dr. Sophie Kobuch to the acquisition and analysis of the data reported herein.

REFERENCES

Allen, A. M., Moeller, I., Jenkins, T. A., Zhuo, J., Aldred, G. P., Chai, S. Y., et al. (1998). Angiotensin receptors in the nervous system. *Brain Res. Bull.* 47, 17–28.

Aviles-Reyes, R. X., Angelo, M. F., Villarreal, A., Rios, H., Lazarowski, A., and Ramos, A. J. (2010). Intermittent hypoxia during sleep induces reactive gliosis and limited neuronal death in rats: implications for sleep apnea. *J. Neurochem.* 112, 854–869. doi: 10.1111/j.1471-4159.2009.06535.x

Ben Achour, S., and Pascual, O. (2012). Astrocyte-neuron communication: functional consequences. *Neurochem. Res.* 37, 2464–2673. doi: 10.1007/s11064-012-0807-0

Canteras, N. S., Simerly, R. B., and Swanson, L. W. (1994). Organization of projections from the ventromedial nucleus of the hypothalamus: a Phaseolus vulgaris-leucoagglutinin study in the rat. *J. Comp. Neurol.* 348, 41–79. doi: 10.1002/cne.903480103

Dampney, R. A., Horiuchi, J., Tagawa, T., Fontes, M. A., Potts, P. D., and Polson, J. W. (2003a). Medullary and supramedullary mechanisms regulating sympathetic vasomotor tone. *Acta Physiol. Scand.* 177, 209–218. doi: 10.1046/j.1365-201x.2003.01070.x

Dampney, R. A., Polson, J. W., Potts, P. D., Hirooka, Y., and Horiuchi, J. (2003b). Functional organization of brain pathways subserving the baroreceptor reflex: studies in conscious animals using immediate early gene expression. *Cell Mol. Neurobiol.* 23, 597–616.

Dampney, R. A., and McAllen, R. M. (1988). Differential control of sympathetic fibres supplying hindlimb skin and muscle by subretrofacial neurones in the cat. *J. Physiol.* 395, 41–56. doi: 10.1113/jphysiol.1988.sp016907

Dampney, R. A., and Moon, E. A. (1980). Role of ventrolateral medulla in vasomotor response to cerebral ischemia. *Am. J. Physiol.* 239, H349–H358.

DiMicco, J. A., Samuels, B. C., Zaretskaia, M. V., and Zaretsky, D. V. (2002). The dorsomedial hypothalamus and the response to stress: part renaissance, part revolution. *Pharmacol. Biochem. Behav.* 71, 469–480. doi: 10.1016/s0091-3057(01)00689-x

El Sayed, K., Dawood, T., Hammam, E., and Macefield, V. G. (2012). Evidence from bilateral recordings of sympathetic nerve activity for lateralization of vestibular contributions to cardiovascular control. *Exp. Brain Res.* 221, 427–436. doi: 10.1007/s00221-012-3185-6

Fagius, J., and Wallin, B. G. (1980). Sympathetic reflex latencies and conduction velocities in normal man. *J. Neurol. Sci.* 47, 433–448. doi: 10.1016/0022-510x(80)90098-2

Fatouleh, R. H., Hammam, E., Lundblad, L. C., Macey, P. M., McKenzie, D. K., Henderson, L. A., et al. (2014). Functional and structural changes in the brain associated with the increase in muscle sympathetic nerve activity in obstructive sleep apnea. *NeuroImage* 6, 275–283. doi: 10.1016/j.nicl.2014.08.021

Fatouleh, R. H., Lundblad, L. C., Macey, P. M., McKenzie, D. K., Henderson, L. A., and Macefield, V. G. (2015). Reversal of functional changes in the brain associated with obstructive sleep apnea following 6 months of CPAP. *NeuroImage* 7, 799–806. doi: 10.1016/j.nicl.2015.02.010

Fontes, M. A. P., Filho, M. L., Machado, N. L. S., de Paula, C. A., Cordeiro, L. M. S., Xavier, C. H., et al. (2017). Asymmetric sympathetic output: the dorsomedial hypothalamus as a potential link between emotional stress and cardiac arrhythmias. *Auton. Neurosci.* 207, 22–27. doi: 10.1016/j.autneu.2017.01.001

Grassi, G., Colombo, M., Seravalle, G., Spaziani, D., and Mancia, G. (1998). Dissociation between muscle and skin sympathetic nerve activity in essential hypertension, obesity, and congestive heart failure. *Hypertension* 31, 64–67. doi: 10.1161/01.hyp.31.1.64

Guyenet, P. G. (2006). The sympathetic control of blood pressure. *Nat. Rev. Neurosci.* 7, 335–346. doi: 10.1038/nrn1902

Halassa, M. M., Fellin, T., and Haydon, P. G. (2007). The tripartite synapse: roles for gliotransmission in health and disease. *Trends Mol. Med.* 13, 54–63. doi: 10.1016/j.molmed.2006.12.005

Harper, R. M., Bandler, R., Spriggs, D., and Alger, J. R. (2000). Lateralized and widespread brain activation during transient blood pressure elevation revealed by magnetic resonance imaging. *J. Comp. Neurol.* 417, 195–204. doi: 10.1002/(sici)1096-9861(20000207)417:2<195::aid-cne5>3.0.co;2-v

Henderson, L. A., Macey, P. M., Macey, K. E., Frysinger, R. C., Woo, M. A., Harper, R. K., et al. (2002). Brain responses associated with the Valsalva maneuver revealed by functional magnetic resonance imaging. *J. Neurophysiol.* 88, 3477–3486. doi: 10.1152/jn.00107.2002

Horiuchi, J., McAllen, R. M., Allen, A. M., Killinger, S., Fontes, M. A., and Dampney, R. A. (2004). Descending vasomotor pathways from the dorsomedial hypothalamic nucleus: role of medullary raphe and RVLM. *Am. J. Physiol. Regul. Integr. Comp. Physiol.* 287, R824–R832.

James, C., Macefield, V. G., and Henderson, L. A. (2013). Real-time imaging of cortical and subcortical control of muscle sympathetic nerve activity in awake human subjects. *NeuroImage* 70, 59–65. doi: 10.1016/j.neuroimage.2012.12.047

Jansen, A. S., Wessendorf, M. W., and Loewy, A. D. (1995). Transneuronal labeling of CNS neuropeptide and monoamine neurons after pseudorabies virus injections into the stellate ganglion. *Brain Res.* 683, 1–24. doi: 10.1016/0006-8993(95)00276-v

Joyner, M. J., Charkoudian, N., and Wallin, B. G. (2010). The sympathetic nervous system and blood pressure in humans: individualized patterns of regulation and their implications. *Hypertension* 56, 10–16. doi: 10.1161/hypertensionaha.109.140186

Kobuch, S., Fazalbhoy, A., Brown, R., Henderson, L. A., and Macefield, V. G. (2017). Central circuitry responsible for the divergent sympathetic responses

to tonic muscle pain in humans. *Hum. Brain Mapp.* 38, 869–881. doi: 10.1002/hbm.23424

Kobuch, S., Fazalbhoy, A., Brown, R., Macefield, V. G., and Henderson, L. A. (2018). Muscle sympathetic nerve activity-coupled changes in brain activity during sustained muscle pain. *Brain Behav.* 8:e00888. doi: 10.1002/brb3.888

Kumada, M., Dampney, R. A., and Reis, D. J. (1979). Profound hypotension and abolition of the vasomotor component of the cerebral ischemic response produced by restricted lesions of medulla oblongata in rabbit. Relationship to the so-called tonic vasomotor center. *Circ. Res.* 1979, 63–70. doi: 10.1161/01.res.45.1.63

Logothetis, N. K., Pauls, J., Augath, M., Trinath, T., and Oeltermann, A. (2001). Neurophysiological investigation of the basis of the fMRI signal. *Nature* 412, 150–157. doi: 10.1038/35084005

Lundblad, L. C., Fatouleh, R. H., Hammam, E., McKenzie, D. K., Macefield, V. G., and Henderson, L. A. (2014). Brainstem changes associated with increased muscle sympathetic drive in obstructive sleep apnea. *NeuroImage* 103, 258–266. doi: 10.1016/j.neuroimage.2014.09.031

Lundblad, L. C., Fatouleh, R. H., McKenzie, D. K., Macefield, V. G., and Henderson, L. A. (2015). Brainstem activity changes associated with restored sympathetic drive following CPAP treatment in OSA subjects; a longitudinal investigation. *J. Neurophysiol.* 114, 893–901. doi: 10.1152/jn.00092.2015

Macefield, V. G. (2013). "Sympathetic microneurography," in *Handbook of Clinical Neurology, Vol. 117 (3rd Series). Autonomic Nervous System*, eds M. Ruud Buijs, and F. Dick Swaab, (Amsterdam: Elsevier), 353–364. doi: 10.1016/b978-0-444-53491-0.00028-6

Macefield, V. G., Gandevia, S. C., and Henderson, L. A. (2006). Neural sites involved in the sustained increase in muscle sympathetic nerve activity induced by inspiratory-capacity apnea - a fMRI study. *J. Appl. Physiol.* 100, 266–273. doi: 10.1152/japplphysiol.00588.2005

Macefield, V. G., and Henderson, L. A. (2010). Real-time imaging of the medullary circuitry involved in the generation of spontaneous muscle sympathetic nerve activity in awake subjects. *Hum. Brain Map.* 31, 539–549. doi: 10.1002/hbm.20885

Macefield, V. G., and Henderson, L. A. (2016). 'Real-time' imaging of cortical and subcortical sites of cardiovascular control: concurrent recordings of sympathetic nerve activity and fMRI in awake subjects. *J. Neurophysiol.* 116, 1199–1207. doi: 10.1152/jn.00783.2015

Macefield, V. G., and Henderson, L. A. (2019). Identification of the human sympathetic connectome involved in blood pressure regulation. *NeuroImage* 202:116119. doi: 10.1016/j.neuroimage.2019.116119

McAllen, R. M., May, C. N., and Shafton, A. D. (1995). Functional anatomy of sympathetic premotor cell groups in the medulla. *Clin. Exp. Hypertens.* 17, 209–221. doi: 10.3109/10641969509087066

Pyner, S., and Coote, J. H. (2000). Identification of branching paraventricular neurons of the hypothalamus that project to the rostroventrolateral medulla and spinal cord. *Neuroscience* 100, 549–556. doi: 10.1016/s0306-4522(00)00283-9

Sander, M., Macefield, V. G., and Henderson, L. A. (2010). Cortical and brainstem changes in neural activity during static handgrip and post-exercise ischemia in humans. *J. Appl. Physiol.* 108, 1691–1700. doi: 10.1152/japplphysiol.91539.2008

Schlaich, M. P., Lambert, E., Kaye, D. M., Krozowski, Z., Campbell, D. J., Lambert, G., et al. (2004). Sympathetic augmentation in hypertension: role of nerve firing, norephinephrine reuptake, and angiotensin neuromodulation. *Hypertension* 43, 169–175. doi: 10.1161/01.hyp.0000103160.35395.9e

Shafton, A. D., Ryan, A., and Badoer, E. (1998). Neurons in the hypothalamic paraventricular nucleus send collaterals to the spinal cord and to the rostral ventrolateral medulla in the rat. *Brain Res.* 801, 239–243. doi: 10.1016/s0006-8993(98)00587-3

Sundlof, G., and Wallin, B. G. (1977). The variability of muscle nerve sympathetic activity in resting recumbent man. *J. Physiol.* 272, 383–397. doi: 10.1113/jphysiol.1977.sp012050

ter Horst, G. J., and Luiten, P. G. (1986). The projections of the dorsomedial hypothalamic nucleus in the rat. *Brain Res. Bull.* 16, 231–248. doi: 10.1016/0361-9230(86)90038-9

Topolovec, J. C., Gati, J. S., Menon, R. S., Shoemaker, J. K., and Cechetto, D. F. (2004). Human cardiovascular and gustatory brainstem sites observed by functional magnetic resonance imaging. *J. Comp. Neurol.* 471, 446–461. doi: 10.1002/cne.20033

Wallin, B. G., Delius, W., and Hagbarth, K. E. (1973). Comparison of sympathetic nerve activity in normotensive and hypertensive subjects. *Circ. Res.* 33, 9–21. doi: 10.1161/01.res.33.1.9

Wang, R., Koganezawa, T., and Terui, N. (2010). Differential responses of sympathetic premotor neurons in the rostral ventrolateral medulla to stimulation of the dorsomedial hypothalamus in rabbits. *Brain Res.* 1356, 44–53. doi: 10.1016/j.brainres.2010.08.024

Wenker, I. C., Abe, C., Viar, K. E., Stornetta, D. S., Stornetta, R. L., and Guyenet, P. G. (2017). Blood pressure regulation by the rostral ventrolateral medulla in conscious rats: effects of hypoxia, hypercapnia, baroreceptor denervation, and anesthesia. *J. Neurosci.* 37, 4565–4583. doi: 10.1523/JNEUROSCI.3922-16.2017

Conflict of Interest: The authors declare that the research was conducted in the absence of any commercial or financial relationships that could be construed as a potential conflict of interest.

frontiers in Physiology

ORIGINAL RESEARCH
published: 14 May 2020
doi: 10.3389/fphys.2020.00375

Impact of Bilateral Sympathetic Stellate Ganglionectomy on TGF-β1 Signaling Pathway in Rats With Chronic Volume Overload

*Mingjing Zhang†, Xiaogang Liu†, Jie Wu, Yijun Yu, Yuting Wang and Ye Gu**

Department of Cardiology, Wuhan Fourth Hospital, Puai Hospital, Tongji Medical College, Huazhong University of Science and Technology, Wuhan, China

OPEN ACCESS

Edited by:
Vaughan G. Macefield, Baker Heart and Diabetes Institute, Australia

Reviewed by:
De-Pei Li, University of Missouri, United States
Clive May, The University of Melbourne, Australia

***Correspondence:**
Ye Gu
yegu2003cn@163.com

† These authors have contributed equally to this work and share first authorship

Specialty section:
This article was submitted to Autonomic Neuroscience, a section of the journal Frontiers in Physiology

Received: *22 September 2019*
Accepted: *30 March 2020*
Published: *14 May 2020*

Citation:
Zhang M, Liu X, Wu J, Yu Y, Wang Y and Gu Y (2020) Impact of Bilateral Sympathetic Stellate Ganglionectomy on TGF-β1 Signaling Pathway in Rats With Chronic Volume Overload. Front. Physiol. 11:375. doi: 10.3389/fphys.2020.00375

Background: We previously reported that bilateral sympathetic stellate ganglionectomy attenuated cardiac remodeling and fibrosis in rats with chronic volume overload. Transforming growth factor beta 1 (TGF-β1) is a polypeptide member of the transforming growth factor beta superfamily of cytokines and actively involved in many pathological processes of cardiovascular diseases. The present study explored the impact of bilateral sympathetic stellate ganglionectomy on the TGF-β1 pathway in this model.

Methods and Results: Male Sprague–Dawley rats were randomly divided into sham (S) group, abdominal aorta-cava fistula (AV) group, and bilateral sympathetic stellate ganglionectomy after abdominal aorta-cava fistula (AD) group. Twelve weeks after the abdominal aorta-cava fistula surgery, the myocardial expressions of norepinephrine (NE) and hydroxyproline were significantly higher, while acetylcholine was downregulated in the AV group compared to the S group; the above changes were partly reversed in the AD group. The myocardial expression of TGF-β1 and activity of Smad2/3 phosphorylation were also upregulated in the AV group compared to the S group, which could be reversed by bilateral sympathetic stellate ganglionectomy. *In vitro*, the TGF-β1 expression in cultured myocardial fibroblasts and the proliferation of myocardial fibroblasts were significantly increased post-stimulation with NE in a dose-dependent manner, and these effects could be blunted by co-treatment with a TGF-β1 inhibitor.

Conclusion: Our study results indicate that stellate ganglionectomy decreases cardiac norepinephrine release, which leads to decreased TGF-β1 release and reduced fibrosis in rats with chronic volume overload.

Keywords: transforming growth factor beta 1, bilateral sympathetic stellate ganglionectomy, sympathetic neurohormone, cardiac fibrosis, chronic volume overload

Abbreviations: ACF, abdominal aorta-cava fistula; ACh, acetylcholine; ECM, extracellular matrix; IPP, Image ProPlus; LV, left ventricle; NE, norepinephrine; RV, right ventricle; SGX, sympathetic stellate ganglionectomy; TGF-β1, transforming growth factor beta 1.

INTRODUCTION

Heart failure is a process of progressively pathological disorder, cardiac remodeling and secondary injury after compensatory adaptations, belong to the pathological features of heart failure (Mann and Bristow, 2005). Neurohormone compensation plays an important role in the process of cardiac remodeling, which manifests as sympathetic/parasympathetic imbalance, i.e., an activated sympathetic nervous system accompanied with withdrawal of parasympathetic activity (Packer, 1992; Louridas and Lourida, 2012; Fukuda et al., 2015). Restoring the sympathetic/parasympathetic balance serves as one of the emerging therapy options for heart failure (De Ferrari and Schwartz, 2014; Schrodl et al., 2014; Floras and Ponikowski, 2015). A clinical study of cardiac sympathetic denervation is ongoing for patients of heart failure with reduced ejection fraction (HFrEF), aiming to test whether this strategy could delay the progression of heart failure (Chin et al., 2017). Our previous study found that bilateral sympathetic stellate ganglionectomy (SGX; inferior cervical and T1 ganglia) attenuated cardiac remodeling and fibrosis in rats with chronic volume overload (Zhang et al., 2019). However, the signaling mechanism remains elusive.

Cardiac remodeling is characterized by changes in myocardial mass, size, shape, and accumulation of fibrosis in cardiac ECM in the failing heart (Dhalla et al., 2009). Cardiac fibroblasts are major components of the ECM, which play an important role in cardiac remodeling (Porter and Turner, 2009). Cardiac fibroblasts respond to hormones (such as norepinephrine, NE) and cytokines (such as TGF-β), and the levels of NE and TGF-β are further increased in the myocardial remodeling process. Many of the functional effects of cardiac fibroblasts are mediated through the differentiation of cardiac fibroblasts to myofibroblasts (Yuan et al., 2019). Myofibroblasts play an important role in cardiac ECM remodeling. A previous study showed that a reduction of myofibroblasts could delay the process of cardiac ECM remodeling (Liguori et al., 2019).

Transforming growth factor betas (TGF-βs) are a widely expressed fibrosis regulator factor. TGF-βs include three mammalian isoforms (TGF-β1, TGF-β2, and TGF-β3). The TGF-β subtypes demonstrate sequence homology and have similar mechanisms for processing and activation. TGF-β1 signaling pathways play critical roles in cardiovascular diseases, which might be a potential therapeutic target (Doetschman et al., 2012). TGF-β1 binds to their receptors and related protein and induces cardiac fibroblasts to activate and differentiate into myofibroblasts. Canonical TGF-β signaling promotes cardiac fibrosis by activating Smad2/3 transcription factors through upregulating gene expression (Khalil et al., 2017). The impact of bilateral SGX on the TGF-β1 signaling pathway in the setting of chronic volume overload in a rat model is not fully understood. The aim of this study was therefore to investigate the impact of bilateral SGX on the TGF-β1 signaling pathway and the levels of sympathetic/vagal neurohormones in rats with chronic volume overload.

MATERIALS AND METHODS

Experimental Animal Preparation

Male Sprague–Dawley rats (180–200 g) were subjected to either sham or ACF surgery as described previously in our laboratory (Wu et al., 2015, 2016; Zhang M. J. et al., 2016). "Partial cardiac denervation" was performed by bilateral SGX. That was to say, 7 days after ACF operation, some rats underwent right stellate ganglion and branching resection. After being anesthetized, the rats were intubated endotracheally and connected to an ALCOTT rodent ventilator (model ALC-V8S, China), and then the second rib was cut off on the right to expose the inferior cervical and T1 sympathetic ganglia, known as the stellate ganglion. The stellate ganglion and its nerve branches running into the ganglion were separated from the tissue and cut by micro-forceps. The chest was closed in three separate layers by suturing and a negative intrathoracic pressure was reestablished after surgery. The same group of rats underwent left stellate ganglion and branch resection by the same method after another 7 days (Yoshimoto et al., 2008; Zhang et al., 2019). All procedures were approved and performed according to the Animal Care Committee of Wuhan Fourth Hospital. Animals were kept according to the Guide for the Care and Use of Laboratory Animals published by the United States National Institutes of Health (NIH Publication, 8th edition, 2011). One moribund rat in the aortocaval fistula with bilateral SGX group (AD group) died due to cardiac dysfunction. Data from seven rats in the sham group (S group) and aortocaval fistula group (AV group) and eight rats in the AD group were analyzed.

Plasma and Myocardial Tissue Biochemistry Examination and Enzyme-Linked Immunosorbent Assay

Twelve weeks after ACF, the rats were sacrificed under deep anesthesia (70 mg/kg sodium pentobarbital, intraperitoneally) after vena cava blood collection. Three rat hearts were randomly selected from each group and longitudinally divided into two portions, then embedded in paraffin for histological examinations. The remaining hearts of each group were divided in their anatomical parts (atria, right and left ventricles with the septum). All samples and tissues were frozen and stored at −80°C for future examinations. The blood was centrifuged at 3,000 × *g* and plasma drawn up into some tubes by pipette for future examinations. Three hundred fifty milligrams

TABLE 1 | RT-PCR forward/reverse (F/R) primer sequences.

Forward/Reverse	Sequence (5′–3′)
GAPDH	F: 5′-CGCTAACATCAAATGGGGTG-3′ R: 5′-TTGCTGACAATCTTGAGGGAG-3′
TGF-β1	F: 5′-AAGGAGACGGAATACAGGGCT-3′ R: 5′-ACCTCGACGTTTGGGACTGA-3′

GAPDH, glyceraldehyde-3-phosphate-dehydrogenase; TGF-β1, transforming growth factor beta 1.

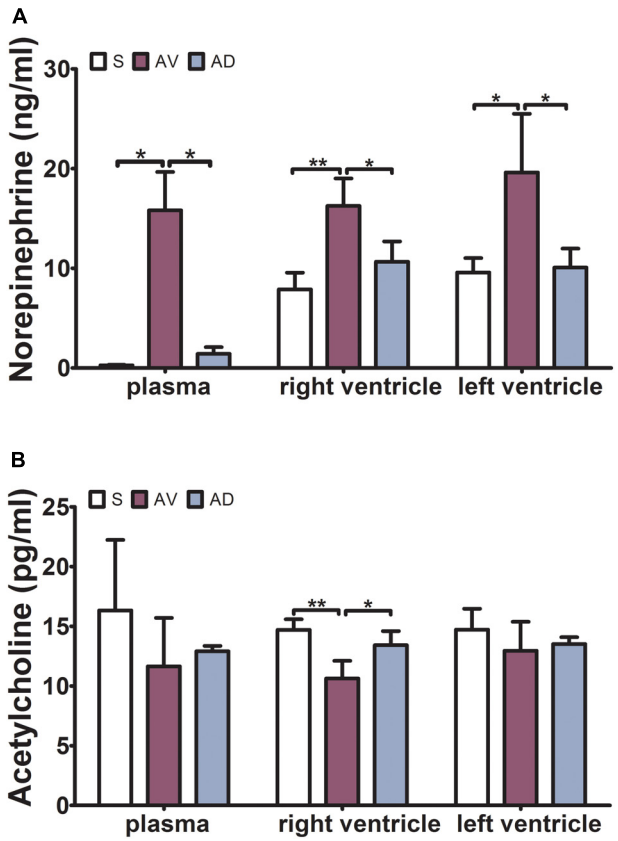

FIGURE 1 | Expressions of norepinephrine (NE) and acetylcholine (ACh) in the plasma, right ventricle (RV), and left ventricle (LV) by ELISA. **(A)** The expression of NE was significantly increased in the abdominal aorta-cava fistula (AV) group and decreased in the bilateral sympathetic stellate ganglionectomy after abdominal aorta-cava fistula (AD) group in the plasma, RV, and LV. **(B)** The expression of ACh was significantly decreased in the AV group and increased in the AD group in the RV (*$P < 0.05$, **$P < 0.01$) (three replicate experiments were performed).

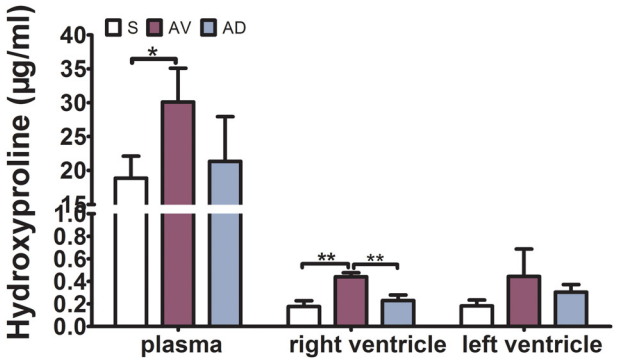

FIGURE 2 | Expression of hydroxyproline in the plasma, RV, and LV by ELISA. The expression of hydroxyproline was significantly increased in the abdominal aorta-cava fistula (AV) group in the plasma and RV (*$P < 0.05$, **$P < 0.01$) and significantly reduced in the bilateral sympathetic stellate ganglionectomy after abdominal aorta-cava fistula (AD) group in the RV (**$P < 0.01$) (three replicate experiments were performed).

of myocardial tissues of the LV and RV, respectively, were placed into a centrifuge tube and added with 700 μl sterile PBS (pH 7.4), the myocardial tissues homogenated, centrifuged at 3,000 × *g*, and the supernatant drawn up by pipette into some tubes for future examinations. Homogenate samples of the plasma, RV, and LV were extracted and acylated using the NE ELISA kit (Abnova, KA1891, Taiwan, China) following the manufacturer's instructions. NE concentrations of the plasma, RV, and LV were determined with the ELISA kit following the manufacturer's instructions. The absorbance was recorded at 450 nm. Acetylcholine (ACh) concentrations of the plasma, RV, and LV were determined with the ELISA kit (BioVision, E4454-100, Milpitas, CA, United States) following the manufacturer's instructions. The absorbance was recorded at 450 nm. We drew up 100 μl plasma into a centrifuge tube and added 200 μl hydrolysate. Twenty micrograms of myocardial tissues of the RV and LV, respectively, was added with 200 μl hydrolysate into a centrifuge tube. Bathed plasma and myocardial tissue with hydrolysate were placed into a centrifuge tube at 95°C for 20 min and the hydrolysis mixture tube mixed once every 10 min to make sure it hydrolyzes sufficiently. The hydroxyproline of the plasma and myocardial tissue was measured following the manufacturer's instructions (njjcbio, A030-2, Nanjing, China). The absorbance was recorded at 550 nm.

Quantitation of mRNA Levels

Total RNA was extracted from the LV and RV with the RNeasy Mini Kit (Qiagen, 74104, Hilden, Germany), following the manufacturer's instructions. PrimeScript RT Master Mix Perfect Real Time (Takara, RR036A, Kusatsu, Shiga, Japan) was used for reverse transcription and cDNA synthesis. Expression of TGF-β1 was detected by QuantiFast SYBR Green PCR Kit (Qiagen, 204057, Hilden, Germany) and Bio-Rad CFX96 (Bio-Rad, C1000, Hercules, CA, United States), following the manufacturer's instructions. Computation of fold changes in the messenger RNA (mRNA) levels from C_T values was done using $2^{-\Delta\Delta CT}$ methods. GAPDH mRNA levels were used as an internal reference standard. Primer sequences are provided in **Table 1**.

Western Blotting

Total proteins were extracted from the LV and RV and protein concentrations were determined through the bicinchoninic acid method. The primary antibodies were as follows: anti-TGF-β1 monoclonal antibody (1:500; Abcam, ab190503, Cambridge, United Kingdom), anti-Smad2/3 monoclonal antibody (1:1,000; Abcam, ab202445, Cambridge, United Kingdom), and anti-pSmad2/3 polyclonal antibody (1:500; Abcam, ab63399, Cambridge, United Kingdom). Secondary antibodies were goat anti-rabbit and goat anti-mouse (KPL, Milford, MA, United States). The images were captured and semi-quantitatively analyzed by the ChemiDoc XRS + System (Bio-Rad, Hercules, CA, United States).

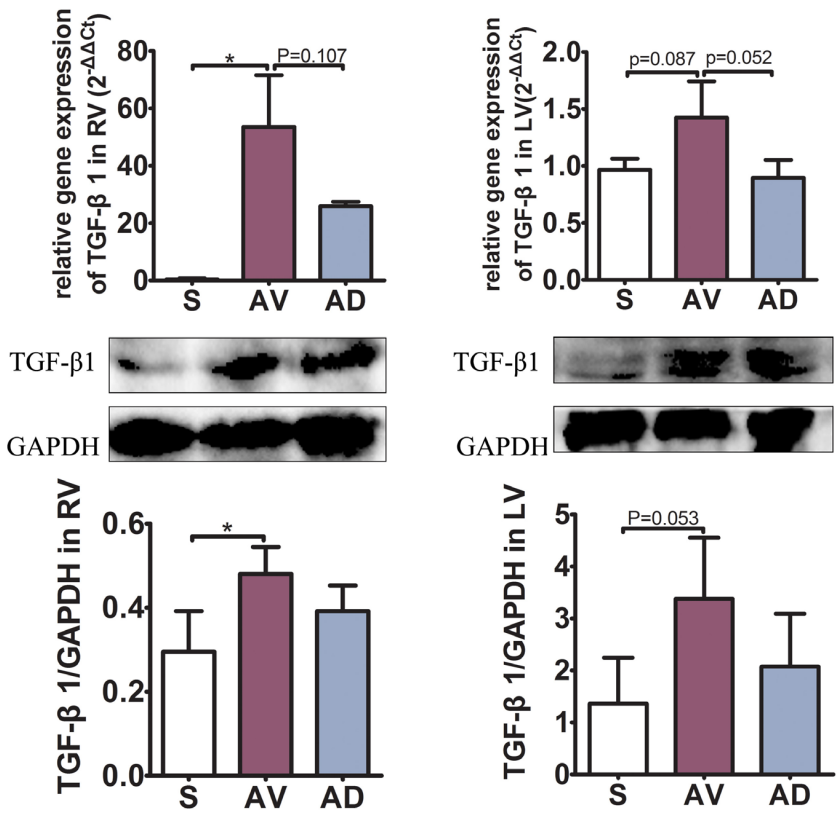

FIGURE 3 | mRNA and protein expressions of TGF-β1 of the myocardial tissue in the right (RV) and left (LV) ventricles. The mRNA and protein expression of TGF-β1 in the RV were significantly increased in the abdominal aorta-cava fistula (AV) group compared to the sham (S) group ($P < 0.05$) and tended to be higher in the LV ($P = 0.087$). The mRNA expression of TGF-β1 tended to be downregulated in the bilateral sympathetic stellate ganglionectomy after abdominal aorta-cava fistula (AD) group compared to the AV group in both the RV and LV ($P = 0.107$ and $P = 0.052$, respectively) (three replicate experiments were performed). *$P < 0.05$.

Cultured Cardiac Fibroblasts *in vitro*, WST-8 Assay, and Cellular Immunofluorescence

Cardiac fibroblasts purchased from iCell Bioscience (RAT-iCell-c002, Shanghai, China) were cultured in PriMed-iCELL-003 (Shanghai, China) supplemented with 10% fetal bovine serum, 10% fibroblast growth factor, 100 U/ml penicillin, and 100 mg/ml streptomycin in a humidified atmosphere of 5% CO_2 at 37°C. The cells were treated with NE (TargetMol, T7044-1, United States) 0, 5, 10, and 20 μM, respectively, and cultured for 6, 12, and 24 h, respectively, in order to choose the most appropriate concentration and time of NE stimulation.

NE-treated cells were co-cultured with 5 ng/ml TGF-β1 inhibitors (MCE, HY-N0158, China). The cells were seeded at a density of 5×10^3 cells in a 96-well plate and then treated with NE or co-cultured with NE and a TGF-β1 inhibitor to quantify cell proliferation. The water-soluble tetrazolium (WST)-8 assay using a sulfonated tetrazolium salt (Cell Counting Kit-8, Biosharp, China) was performed as recommended in the manufacturer's instructions. The absorbance was recorded at 450 nm.

Cells were seeded in a 12-well plate with the slides of cells and then treated with NE or co-cultured with NE and a TGF-β1 inhibitor for 12 h. After the supernatant was discarded, the cells were fixed with paraformaldehyde, then treated with Triton X-100, and blocked with serum. After incubation with the first antibody (TGF-β1, 1:200; Abcam, ab190503, United Kingdom) and the second antibody, the cells were then treated with DAPI and observed using a fluorescence microscope.

Statistical Analysis

Data were shown as the mean ± SD. All data were evaluated for normal distribution using the Shapiro–Wilk test. A non-parametric test was used to analyze non-normal distribution of the data. One-way ANOVA, Tukey's *post hoc* test, or Games–Howell test was performed to test for differences among the means of various groups. $P < 0.05$ was considered as statistically significant (SPSS Statistics 21.0).

RESULTS

Effect of Bilateral SGX on the Expression of Neurohormones in Rats With Chronic Volume Overload

The expression of NE was significantly upregulated in the AV group compared to the S group in the plasma, RV, and

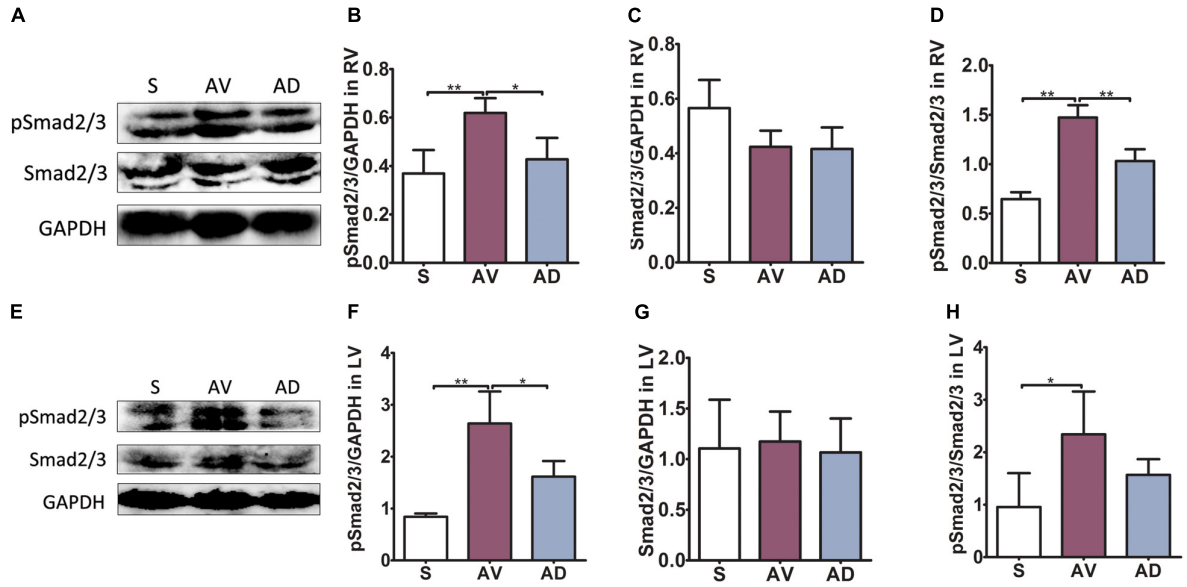

FIGURE 4 | Protein expression of Smad2/3 phosphorylation in cardiac extracellular matrix (ECM) remodeling. In the RV **(A–D)**, the protein expression of pSmad2/3 and the ratio of pSmad2/3 to Smad2/3 were significantly upregulated in the abdominal aorta-cava fistula (AV) group compared to the sham (S) group (both $P < 0.01$) and significantly downregulated in the bilateral sympathetic stellate ganglionectomy after abdominal aorta-cava fistula (AD) group compared to the AV group ($P < 0.05$ and $P < 0.01$, respectively). The protein expression of Smad2/3 was similar among groups in the RV. In the LV **(E–H)**, the protein expression of pSmad2/3 and the ratio of pSmad2/3 to Smad2/3 were significantly upregulated in the AV group ($P < 0.01$ and $P < 0.05$, respectively) and pSmad2/3 was significantly reduced in the AD group ($P < 0.05$). The protein expression of Smad2/3 in the LV was similar among groups (six replicate experiments were performed). *$P < 0.05$, **$P < 0.01$.

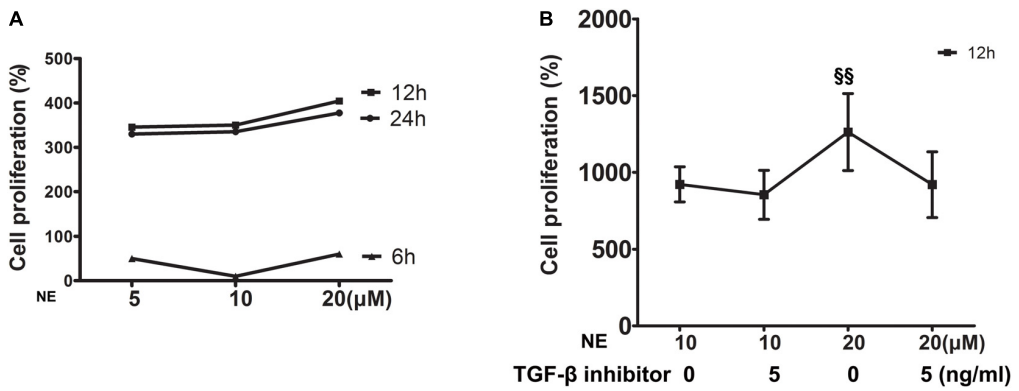

FIGURE 5 | Proliferation of cardiac fibroblasts *in vitro*. **(A)** Cardiac fibroblasts were stimulated with different concentrations of norepinephrine (NE) for 6, 12, and 24 h. The strongest cell proliferation was induced by 20 μM NE at 12 h (four replicate experiments were performed). **(B)** The proliferation of cardiac fibroblasts was higher with 20 μM NE than that of 10 μM NE at 12 h ($P < 0.01$), and this effect could be blunted by co-treatment with a TGF-β1 inhibitor. (§§ $P < 0.01$, NE 10 μM vs. 20 μM) (four replicate experiments were performed).

LV ($P < 0.05$, $P < 0.01$, and $P < 0.05$, respectively) and downregulated in the AD group compared to the AV group in both RV and LV ($P < 0.05$). The expression of ACh was significantly downregulated in the AV group ($P < 0.01$) and upregulated in the AD group ($P < 0.05$) in the RV (**Figure 1**).

Impact of Bilateral SGX on Hydroxyproline and TGF-β1 Expression

The expression of hydroxyproline was significantly increased in the AV group compared to the S group in the plasma and RV ($P < 0.05$ and $P < 0.01$, respectively) and tended to be increased in the LV. It was significantly reduced in the AD group compared to the AV group in the RV ($P < 0.01$) and tended to be reduced in the plasma and LV (**Figure 2**). The mRNA and protein expression of TGF-β1 in the RV were significantly increased in the AV group compared to the S group ($P < 0.05$) and tended to be higher in the LV ($P = 0.087$). The mRNA expression of TGF-β1 tended to be downregulated in the AD group compared to the AV group in both the RV and LV ($P = 0.107$ and $P = 0.052$, respectively) (**Figure 3**).

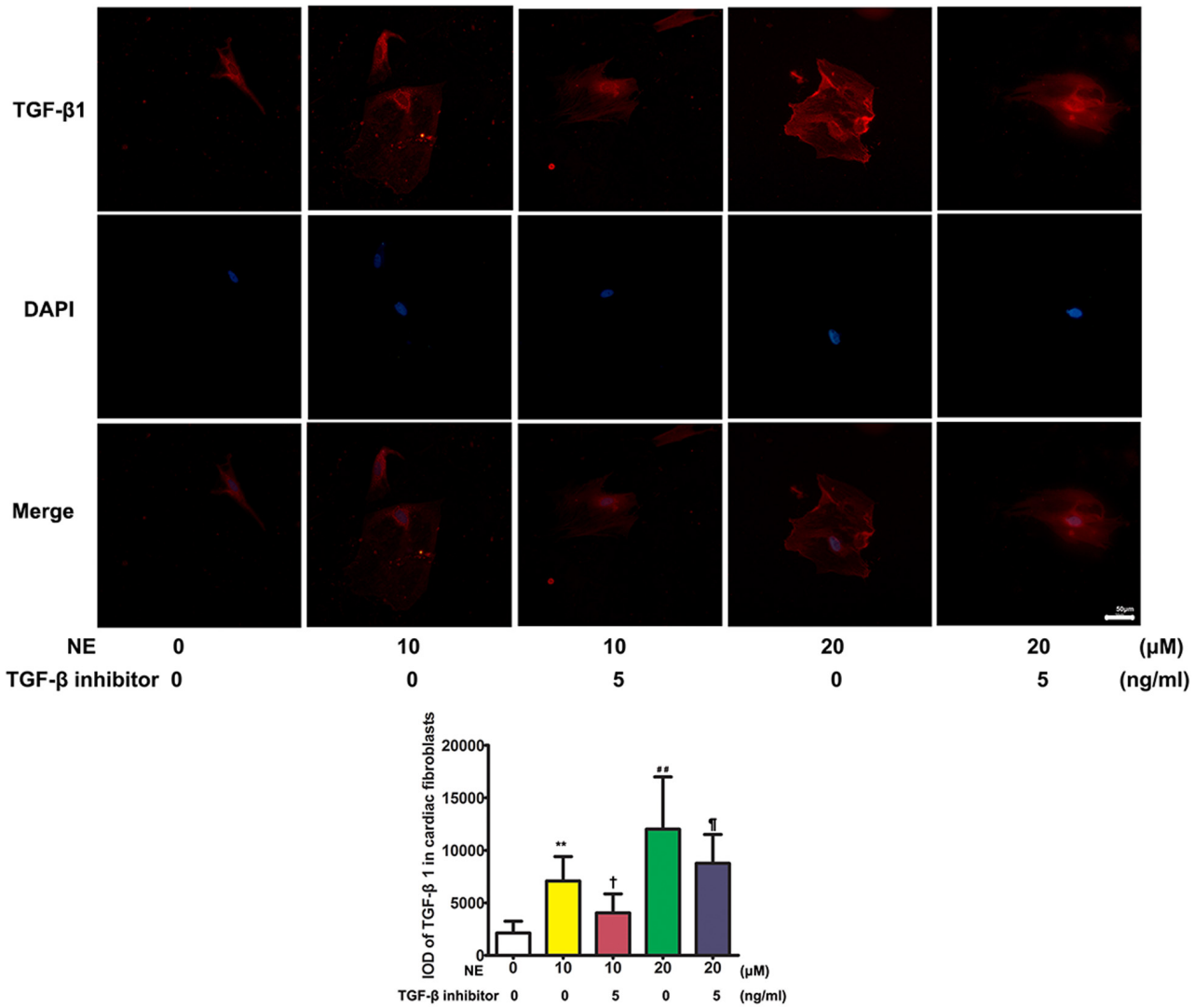

FIGURE 6 | Expression of TGF-β1 in cardiac fibroblasts *in vitro*. The integrated option density (IOD) of TGF-β1 was significantly higher in the norepinephrine (NE) 20 μM group than in the NE 10 μM group ($P < 0.01$), and the IOD of TGF-β1 was reduced after co-treatment with a TGF-β1 inhibitor ($P < 0.05$) *in vitro* (NE 0 vs. 10 μM: $^{**}P < 0.01$; NE 0 vs. 20 μM: $^{\#\#}P < 0.01$; NE 10 μM vs. NE 10 μM + TGF-β1 inhibitor: $^{\dagger}P < 0.05$; NE 10 μM + TGF-β1 inhibitor vs. NE 20 μM + TGF-β1 inhibitor: $^{¶}P < 0.05$) (four replicate experiments were performed).

Myocardial Protein Expression of Smad2/3 Phosphorylation

In the RV, the protein expression of pSmad2/3 and the ratio of pSmad2/3 to Smad2/3 were significantly upregulated in the AV group compared to the S group (both $P < 0.01$) and significantly downregulated in the AD group compared to the AV group ($P < 0.05$ and $P < 0.01$, respectively). The protein expression of Smad2/3 was similar among groups in the RV. In the LV, the protein expression of pSmad2/3 and the ratio of pSmad2/3 to Smad2/3 was significantly upregulated in the AV group ($P < 0.01$ and $P < 0.05$, respectively). pSmad2/3 was significantly reduced in the AD group ($P < 0.05$). The protein expression of Smad2/3 in the LV was similar among groups (**Figure 4**).

Proliferation of Cardiac Fibroblasts and Expression of TGF-β1 *in vitro*

In vitro, cardiac fibroblasts were stimulated with different concentrations of NE at various time intervals and the cell proliferation capacity was detected by the WST-8 assay. The results showed that the strongest cell proliferation was induced by 20 μM NE at 12 h (**Figure 5A**). This effect could be blunted by co-treatment with a TGF-β1 inhibitor (**Figure 5B**).

The immunofluorescence results showed that TGF-β1 was significantly upregulated after stimulation with NE in cardiac fibroblasts *in vitro*. The integrated option density (IOD) of TGF-β1 was significantly higher in the NE 20 μM group than in the NE 10 μM group ($P < 0.01$), and the IOD of TGF-β1 was reduced after co-treatment with a TGF-β1 inhibitor ($P < 0.05$) (**Figure 6**).

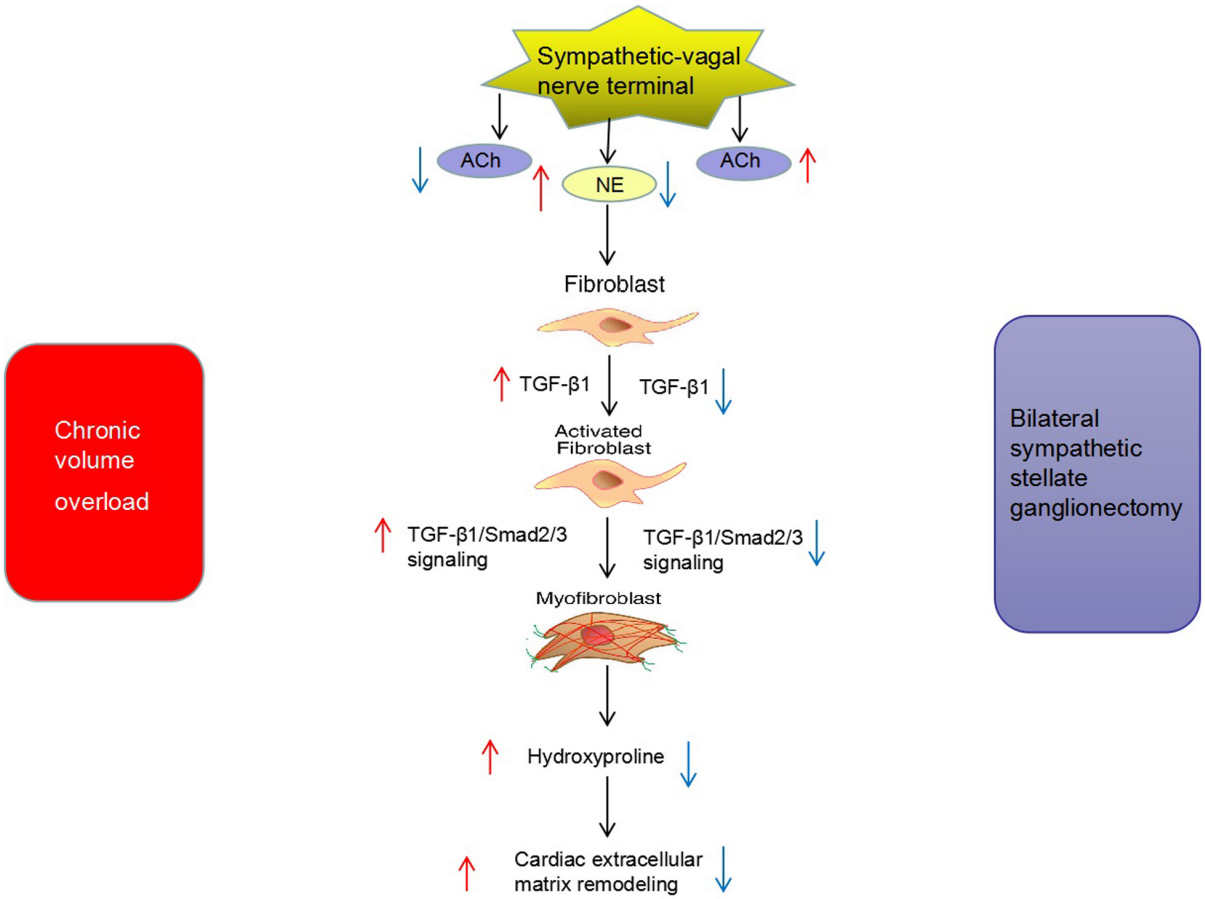

FIGURE 7 | Potential mechanism of bilateral sympathetic stellate ganglionectomy (SGX) on cardiac ECM remodeling in rats with chronic volume overload.

DISCUSSION

The major findings of the present study were as follows. (1) The secretion of sympathetic neurohormone was increased and vagal neurohormone was decreased in the hearts of rats with chronic volume overload, indicating sympathetic activation in this model. TGF-β1 signaling was also activated in this model. (2) The above changes could be partly reversed by bilateral SGX, suggesting that the previously observed beneficial effects of bilateral SGX in this model (Zhang et al., 2019) were at least partly mediated by downregulating TGF-β1 signaling. (3) *In vitro* results further evidenced the positive causal relationship among NE, TGF-β1, and myocardial fibroblast proliferation. To the best of our knowledge, this is the first report on the impact of bilateral SGX on the TGF-β1 signaling pathway in rats with chronic volume overload (**Figure 7**).

Effect of Bilateral SGX on Cardiac ECM Remodeling-Related Signaling Under Chronic Volume Overload

The level of sympathetic neurohormone was closely related to ECM. Briest et al. (2003) showed that NE injection resulted in ECM remodeling in the LV. A previous study also found that sympathetic nerve activity was increased in rats post-myocardial infarction and that dexamethasone could reduce sympathetic innervation and myocardial reactive fibrosis in the myocardial infarction area (El-Helou et al., 2008). We previously showed that bilateral SGX attenuated cardiac remodeling and fibrosis under chronic volume overload. Our previous results showed that the weights of the left and right ventricles and the heart-to-body ratio were increased under chronic volume overload, which were decreased by bilateral stellate ganglionectomy (Zhang et al., 2019). The collagen of heart tissue sections was detected by Sirius red staining. The results showed that the collagen deposition was obviously increased under chronic volume overload and decreased after bilateral stellate ganglionectomy (Zhang et al., 2019). The efferent sympathetic nerve that controls the heart includes the superior cervical ganglia, middle cervical ganglia, stellate ganglion (inferior cervical ganglia and the T1 ganglion fusion), and thoracic sympathetic ganglion II to IV, known as the cardiac sympathetic nerve (Schwartz, 2014). To our surprise, bilateral stellate ganglion denervation resulted in a large decrease in the plasma norepinephrine levels compared to the levels measured in normal rats in this study. The potential reason might be that bilateral stellate ganglion

resection induced not only the decrease of norepinephrine secretion but also the decrease of sympathetic activity due to the influence on other vascular beds (such as kidneys) in the setting of volume expansion. The results of the present study evidenced the sympathetic activation in this model, in which sympathetic neurohormone was upregulated and vagal neurohormone was downregulated. These changes were joined by increased hydroxyproline, a characteristic component of collagen (Meng et al., 2019), while bilateral SGX could partly reverse the above changes. Our results thus hinted that the direct anti-sympathetic effects of bilateral SGX could lead to a reduced ECM remodeling. The sympathetic nerve and vagus nerve in the autonomic nerve are a pair of equilibrium bodies. Cerati et al. showed that left stellectomy is accompanied by a reflex increase in cardiac vagal efferent nerve activity and pulse synchronous activity (Cerati and Schwartz, 1991). Li et al. demonstrated that increased vagal activity with chronic electrical stimulation of the vagus nerve could reduce the expression of NE and attenuate cardiac remodeling in heart failure rats (Li et al., 2004). Taken together, strategies aiming to upregulate vagal activity and/or downregulate sympathetic tone, as in the case of bilateral SGX, could effectively reduce cardiac ECM remodeling.

Impact of Bilateral SGX on TGF-β1 Signaling Pathways in the Setting of Chronic Volume Overload

Transforming growth factor betas were a multifunctional cytokine secreted by a variety of cells with multiple physiological and pathological functions (Doetschman et al., 2012). The close relationship between TGF-β activity and sympathetic activity serves as a focus in recent research. Vega et al. (2009) showed that superior cervical ganglionectomy (SCGX) could downregulate TGF-β and reduce ocular sympathetic nerve activity. TGF-β receptors are widely distributed on the membrane of myofibroblasts and could bind to TGF-β, mediating the downstream signaling pathways involved in cardiac ECM remodeling and fibrosis (Fix et al., 2019). Smad2/3 is one of the signaling pathways regulated by TGF-β1, and TGF-β1 could mediate the phosphorylated activity of Smad2/3 and participate in ECM remodeling (Zhang F. et al., 2016; Han et al., 2018). Our study demonstrated the upregulated expression of TGF-β1 and Smad2/3 phosphorylation in this chronic volume overload model. It is known that activated Smad2/3 phosphorylation signaling pathway could promote collagen synthesis (Khalil et al., 2017). After bilateral SGX, the expression levels of both TGF-β1 and phosphorylated Smad2/3 were significantly downregulated in this chronic volume overload model. The above results suggested that the beneficial effects of bilateral SGX in this model are partly mediated by downregulating the upregulated TGF-β1 expression and Smad2/3 phosphorylation.

Changes of Cardiac Fibroblasts Stimulated by NE

To verify the causal relationship between NE stimulation and TGF-β1 signaling, we stimulated the cardiac fibroblasts *in vitro* with NE of various concentrations at different time intervals. The results showed that the proliferation capacity of cardiac fibroblasts and TGF-β1 expression in these cells were increased after being cultured with NE, while the TGF-β1 inhibitor could blunt the above changes *in vitro*, indicating the causal relationship between NE, TGF-β1, and cardiac fibroblast proliferation. A previous study by Akiyama-Uchida et al. (2002) demonstrated that NE enhanced cardiac fibrosis through TGF-β1 post-receptor signaling, predominantly *via* the p38 MAP kinase pathway. NE enhances fibrosis mediated by TGF-β in cardiac fibroblasts (Akiyama-Uchida et al., 2002).

Study Limitations

There were some study limitations in this study. Firstly, bilateral sympathetic stellate ganglionectomy was not performed in sham animals as the control group because the members of the Ethics Committee of our hospital did not approve this operation in normal animals. They argued that this adds extra harm to animals without clinical significance. Therefore, we had to focus on the impact of bilateral sympathetic stellate ganglionectomy on the TGF-β1 signaling pathway of rats with volume overload. Secondly, it is important to measure the hemodynamics data to show the effects of stellate ganglionectomy. Future study is warranted to clarify this issue. Thirdly, TGF-β1 knockout rats were not used due to technical limitations. The expression of TGF-β1 was inhibited only by the chemical reagent in this study. Future study is warranted to use genetic methods such as miRNA, siRNA, etc., to inhibit TGF-β1 gene expression and protein synthesis to define the related mechanisms.

CONCLUSION

In conclusion, our study indicates that the activation of the sympathetic nervous system is one of the mechanisms in a failing heart induced by chronic volume overload. Bilateral SGX could reduce the expression of sympathetic neurohormone. This effect is partly mediated by downregulating TGF-β1 as well as Smad2/3 phosphorylation in rats with chronic volume overload. Our findings provide experimental and molecular evidence for the treatment of heart failure by bilateral SGX.

DATA AVAILABILITY STATEMENT

The datasets generated for this study are available on request to the corresponding author.

ETHICS STATEMENT

This study was carried out in accordance with the principles of the Guide for the Care and Use of Laboratory Animals of the

United States National Institutes of Health (NIH Publication, 8th Edition, 2011). The protocol was approved by the Animal Care Committee of Wuhan Fourth Hospital.

AUTHOR CONTRIBUTIONS

MZ and YG contributed to the conception and design of research. MZ and YY analyzed the data. MZ and XL interpreted the results of experiments. MZ drafted the manuscript. YG edited and revised the manuscript. MZ, XL, and JW performed the experiments. All authors approved the submitted version of the manuscript.

FUNDING

This work was supported by the Health and Family Planning Commission of Wuhan Municipality, China (Grant No. WX18Q43).

REFERENCES

Akiyama-Uchida, Y., Ashizawa, N., Ohtsuru, A., Seto, S., Tsukazaki, T., Kikuchi, H., et al. (2002). Norepinephrine enhances fibrosis mediated by TGF-beta in cardiac fibroblasts. *Hypertension* 40, 148–154. doi: 10.1161/01.hyp.0000025443.61926.12

Briest, W., Holzl, A., Rassler, B., Deten, A., Baba, H. A., and Zimmer, H. G. (2003). Significance of matrix metalloproteinases in norepinephrine-induced remodelling of rat hearts. *Cardiovasc. Res.* 57, 379–387. doi: 10.1016/s0008-6363(02)00700-9

Cerati, D., and Schwartz, P. J. (1991). Single cardiac vagal fiber activity, acute myocardial ischemia, and risk for sudden death. *Circ. Res.* 69, 1389–1401. doi: 10.1161/01.res.69.5.1389

Chin, A., Ntsekhe, M., Viljoen, C., Rossouw, J., Pennel, T., and Schwartz, P. J. (2017). Rationale and design of a prospective study to assess the effect of left cardiac sympathetic denervation in chronic heart failure. *Int. J. Cardiol.* 248, 227–231. doi: 10.1016/j.ijcard.2017.08.012

De Ferrari, G. M., and Schwartz, P. J. (2014). Left cardiac sympathetic denervation in patients with heart failure: a new indication for an old intervention? *J. Cardiovasc. Transl. Res.* 7, 338–346. doi: 10.1007/s12265-014-9541-0

Dhalla, N. S., Rodriguez-Leyva, D., Elimban, V., Dent, M. R., and Tappia, P. S. (2009). Subcellular remodelling may induce cardiac dysfunction in congestive heart failure. *Cardiovasc. Res.* 81, 429–438. doi: 10.1093/cvr/cvn281

Doetschman, T., Barnett, J. V., Runyan, R. B., Camenisch, T. D., Heimark, R. L., Granzier, H. L., et al. (2012). Transforming growth factor beta signaling in adult cardiovascular diseases and repair. *Cell Tissue Res.* 347, 203–223. doi: 10.1007/s00441-011-1241-1243

El-Helou, V., Proulx, C., Gosselin, H., Clement, R., Mimee, A., Villeneuve, L., et al. (2008). Dexamethasone treatment of post-MI rats attenuates sympathetic innervation of the infarct region. *J. Appl. Physiol.* 104, 150–156. doi: 10.1152/japplphysiol.00663.2007

Fix, C., Carver-Molina, A., Chakrabarti, M., Azhar, M., and Carver, W. (2019). Effects of the isothiocyanate sulforaphane on TGF-beta1-induced rat cardiac fibroblast activation and extracellular matrix interactions. *J. Cell Physiol.* 234, 13931–13941. doi: 10.1002/jcp.28075

Floras, J. S., and Ponikowski, P. (2015). The sympathetic/parasympathetic imbalance in heart failure with reduced ejection fraction. *Eur. Heart J.* 36, 1974–1982. doi: 10.1093/eurheartj/ehv087

Fukuda, K., Kanazawa, H., Aizawa, Y., Ardell, J. L., and Shivkumar, K. (2015). Cardiac innervation and sudden cardiac death. *Circ. Res.* 116, 2005–2019. doi: 10.1161/CIRCRESAHA.116.304679

Han, A., Lu, Y., Zheng, Q., Zhang, J., Zhao, Y., Zhao, M., et al. (2018). Qiliqiangxin attenuates cardiac remodeling via inhibition of TGF-beta1/Smad3 and NF-kappaB signaling pathways in a rat model of myocardial infarction. *Cell Physiol. Biochem.* 45, 1797–1806. doi: 10.1159/000487871

Khalil, H., Kanisicak, O., Prasad, V., Correll, R. N., Fu, X., Schips, T., et al. (2017). Fibroblast-specific TGF-beta-Smad2/3 signaling underlies cardiac fibrosis. *J. Clin. Invest.* 127, 3770–3783. doi: 10.1172/JCI94753

Li, M., Zheng, C., Sato, T., Kawada, T., Sugimachi, M., and Sunagawa, K. (2004). Vagal nerve stimulation markedly improves long-term survival after chronic heart failure in rats. *Circulation* 109, 120–124. doi: 10.1161/01.CIR.0000105721.71640.DA

Liguori, T. T. A., Liguori, G. R., Moreira, L. F. P., and Harmsen, M. C. (2019). Adipose tissue–derived stromal cells'conditioned medium modulates endothelial-mesenchymal transition induced by IL-1β/TGF-β2 but does not restore endothelial function. *Cell Prolif.* 52:e12629. doi: 10.1111/cpr.12629

Louridas, G. E., and Lourida, K. G. (2012). Systems biology and biomechanical model of heart failure. *Curr. Cardiol. Rev.* 8, 220–230. doi: 10.2174/157340312803217238

Mann, D. L., and Bristow, M. R. (2005). Mechanisms and models in heart failure: the biomechanical model and beyond. *Circulation* 111, 2837–2849. doi: 10.1161/circulationaha.104.500546

Meng, Q., Guo, Y., Zhang, D., Zhang, Q., Li, Y., and Bian, H. (2019). Tongsaimai reverses the hypertension and left ventricular remolding caused by abdominal aortic constriction in rats. *J. Ethnopharmacol.* 246:112154. doi: 10.1016/j.jep.2019.112154

Packer, M. (1992). The neurohormonal hypothesis: a theory to explain the mechanism of disease progression in heart failure. *J. Am. Coll. Cardiol.* 20, 248–254. doi: 10.1016/0735-1097 (92)90167-l

Porter, K. E., and Turner, N. A. (2009). Cardiac fibroblasts: at the heart of myocardial remodeling. *Pharmacol. Ther.* 123, 255–278. doi: 10.1016/j.pharmthera.2009.05.002

Schrodl, F., Trost, A., Strohmaier, C., Bogner, B., Runge, C., Kaser-Eichberger, A., et al. (2014). Rat choroidal pericytes as a target of the autonomic nervous system. *Cell Tissue Res.* 356, 1–8. doi: 10.1007/s00441-013-1769-1765

Schwartz, P. J. (2014). Cardiac sympathetic denervation to prevent life-threatening arrhythmias. *Nat. Rev. Cardiol.* 11, 346–353. doi: 10.1038/nrcardio.2014.19

Vega, J. L., Keino, H., and Masli, S. (2009). Surgical denervation of ocular sympathetic afferents decreases local transforming growth factor-beta and abolishes immune privilege. *Am. J. Pathol.* 175, 1218–1225. doi: 10.2353/ajpath.2009.090264

Wu, J., Cheng, Z., Gu, Y., Zou, W., Zhang, M., Zhu, P., et al. (2015). Aggravated cardiac remodeling post aortocaval fistula in unilateral nephrectomized rats. *PLoS One* 10:e0134579. doi: 10.1371/journal.pone.0134579

Wu, J., Cheng, Z., Zhang, M., Zhu, P., and Gu, Y. (2016). Impact of aortocaval shunt flow on cardiac and renal function in unilateral nephrectomized rats. *Sci. Rep.* 6:27493. doi: 10.1038/srep27493

Yoshimoto, M. W. E., Novotny, M., Swain, G. M., Kreulen, D. L., and Osborn, J. W. (2008). Effect of stellate ganglionectomy on basal cardiovascular function and responses to beta1-adrenoceptor blockade in the rat. *Am. J. Physiol. Heart Circ. Physiol.* 295, H2447–H2454. doi: 10.1152/ajpheart.00958.2008

Yuan, Q., Cao, S., Dong, Q., Wang, Z., Xu, Y., Han, Q., et al. (2019). ALDH2 activation inhibited cardiac fibroblast-to-myofibroblast transformation via the TGF-beta1/Smad signaling pathway. *J. Cardiovasc. Pharmacol.* 73, 248–256. doi: 10.1097/FJC.0000000000000655

Zhang, F., Dang, Y., Li, Y., Hao, Q., Li, R., and Qi, X. (2016). Cardiac contractility modulation attenuate myocardial fibrosis by inhibiting tgf-beta1/smad3 signaling pathway in a rabbit model of chronic

heart failure. *Cell Physiol. Biochem.* 39, 294–302. doi: 10.1159/000445624

Zhang, M. J., Gu, Y., Wang, H., Zhu, P. F., Liu, X. Y., and Wu, J. (2016). Valsartan attenuates cardiac and renal hypertrophy in rats with experimental cardiorenal syndrome possibly through down-regulating galectin-3 signaling. *Eur. Rev. Med. Pharmacol. Sci.* 20, 345–354.

Zhang, M., Zhu, P., Wang, Y., Wu, J., Yu, Y., Wu, X., et al. (2019). Bilateral sympathetic stellate ganglionectomy attenuates myocardial remodelling and fibrosis in a rat model of chronic volume overload. *J. Cell. Mol. Med.* 23, 1001–1013. doi: 10.1111/jcmm.14000

Conflict of Interest: The authors declare that the research was conducted in the absence of any commercial or financial relationships that could be construed as a potential conflict of interest.

frontiers in Physiology

REVIEW
published: 25 August 2020
doi: 10.3389/fphys.2020.01069

The Carotid Body a Common Denominator for Cardiovascular and Metabolic Dysfunction?

*Emilio Badoer**

School of Health and Biomedical Sciences, Royal Melbourne Institute of Technology (RMIT) University, Melbourne, VIC, Australia

The carotid body is a highly vascularized organ designed to monitor oxygen levels. Reducing oxygen levels in blood results in increased activity of the carotid body cells and reflex increases in sympathetic nerve activity. A key contributor to elevated sympathetic nerve activity in neurogenic forms of hypertension is enhanced peripheral chemoreceptor activity. Hypertension commonly occurs in metabolic disorders, like obesity. Such metabolic diseases are serious global health problems. Yet, the mechanisms contributing to increased sympathetic nerve activity and hypertension in obesity are not fully understood and a better understanding is urgently required. In this review, we examine the literature that suggests that overactivity of the carotid body may also contribute to metabolic disturbances. The purine ATP is an important chemical mediator influencing the activity of the carotid body and the role of purines in the overactivity of the carotid body is explored. We will conclude with the suggestion that tonic overactivity of the carotid body may be a common denominator that contributes to the hypertension and metabolic dysfunction seen in conditions in which metabolic disease exists such as obesity or insulin resistance induced by high caloric intake. Therapeutic treatment targeting the carotid bodies may be a viable treatment since translation to the clinic could be more easily performed than expected via repurposing antagonists of purinergic receptors currently in clinical practice, and the use of other minimally invasive techniques that reduce the overactivity of the carotid bodies which may be developed for such clinical use.

Keywords: carotid body, chemoreceptors, hypoxia, hypertension, ventilation, glucose utilization

OPEN ACCESS

Edited by:
Vaughan G. Macefield, Baker Heart and Diabetes Institute, Australia

Reviewed by:
Harold D. Schultz, University of Nebraska Medical Center, United States
David D. Kline, University of Missouri, United States
Davi J. A. Moraes, Faculty of Medicine of Ribeirão Preto, University of São Paulo, Brazil

***Correspondence:**
Emilio Badoer
emilio.badoer@rmit.edu.au

Specialty section:
This article was submitted to Integrative Physiology, a section of the journal Frontiers in Physiology

Received: *31 January 2020*
Accepted: *04 August 2020*
Published: *25 August 2020*

Citation:
Badoer E (2020) The Carotid Body a Common Denominator for Cardiovascular and Metabolic Dysfunction? Front. Physiol. 11:1069. doi: 10.3389/fphys.2020.01069

INTRODUCTION

The carotid body was primarily regarded as a chemoreceptor organ that regulated oxygen levels in the blood. Recent evidence is now showing that in addition to respiratory regulatory functions, the carotid bodies also contribute to hypertension both essential and that associated with chronic hypoxia. Even more recently, evidence is accumulating to suggest that carotid bodies are contributing to glucose utilization and insulin resistance. This review discusses the evidence that the carotid bodies may be a common denominator that contributes to the dysregulation of cardiovascular, respiratory and glucose homeostasis in conditions of metabolic dysfunction such as obesity. We also hypothesize that purinergic receptors of the $P2X_3$ subtype may be novel targets that could redress the impaired regulation of the cardiovascular and respiratory systems and glucose utilization in such conditions.

CAROTID BODY ANATOMY

The carotid body is an oxygen-sensing organ of sympatho-adrenal lineage. It is located near the carotid sinus and the bifurcation of the common carotid artery, but may vary between species (Clarke and de Burgh Daly, 1981). It is a small organ (in humans it is approximately 4 mm in diameter and weighing just over 10 gm) that is highly vascularized and receives its blood supply from a branch of nearby arteries (Clarke and de Burgh Daly, 1981). Sensory fibers, originating from cell bodies in the petrosal ganglion, innervate the oxygen sensing cells in the carotid body.

The carotid body consists primarily of two types of cells known as the glomus or Type I cells and the sustentacular or Type II cells (Biscoe, 1971). Glomus cells are the oxygen sensing cells and are activated by hypoxia through inhibition of oxygen-sensitive potassium channels. Sustentacular cells are glia-like cells that wrap around glomus cells. The functions of the sustentacular cells were believed to be primarily related to supporting glomus cells but recent evidence is appearing to suggest that sustentacular cells can form synaptic-like specializations with glomus cells (Platero-Luengo et al., 2014) which suggests these cells may be playing a key role in the sensory signaling process (Tse et al., 2012; Nurse, 2014). There is also evidence that sustentacular cells are stem cells that can replace/increase the pool of glomus cells in the carotid body (Pardal et al., 2007). These new glomus cells show all the characteristics, and respond, just like glomus cells already present in the carotid body.

PRIMARY FUNCTION OF THE CAROTID BODIES: PROTECTION FROM HYPOXIA

The primary function of the carotid body is in sensing oxygen levels in the blood. In addition to this sensory stimulus, hypercapnia, pH, hypoglycemia, inflammatory mediators, and circulating hormones can influence the afferent information arising from the carotid body through activation of the glomus cells (see later sections for further discussion) (Gonzalez et al., 1994; Nurse, 2005, 2014; Garcia-Fernandez et al., 2007; Zhang M. et al., 2007; Zhang X.J. et al., 2007; Del Rio et al., 2011, 2012; Kumar and Prabhakar, 2012). The mechanisms involved in transmitting low oxygen levels and the activation of the glomus cell are still unclear. Most likely the mitochondrial electron transport chain plays a key part since inhibitors of the mitochondrial electron transport chain mimic the actions of hypoxia. The likely mechanism involves reduced oxygen levels eliciting increased levels of the reduced form of the mitochondrial complex IV which causes a build-up of reactive oxygen species and NADH resulting in a reduction in background K-channel conductance and depolarization of the cell membrane (Buckler, 2015; Fernandez-Aguera et al., 2015; Lopez-Barneo et al., 2016; Prabhakar and Semenza, 2016). An excellent review on the physiology of the carotid body deals with this in much more detail (Ortega-Saenz and Lopez-Barneo, 2019).

What is not in doubt, however, is the essential role of ion channels, particularly potassium channels, of which several have been identified on glomus cells and it is likely that many of these potassium channels contribute to the depolarization of the glomus cells that occurs when oxygen levels fall. Depolarization of the glomus cells induces the opening of calcium channels and the resultant increase in intracellular calcium elicits the exocytotic release of neurotransmitters from granules within the glomus cells.

THE CHEMORECEPTOR REFLEX RESPONSE TO ACUTE HYPOXIA

When the body is subjected to a stimulus that reduces oxygen levels, the chemoreceptors in the carotid body and aortic arch are activated, although, other regions of the body may also contain oxygen sensors (Deane et al., 1975). The most well-studied, of course, are those that emanate from the carotid body and activate afferents in the carotid sinus nerve that relay information to the nucleus tractus solitarius in the medulla oblongata in the brainstem (Finley and Katz, 1992; Finley et al., 1992).

The efferent responses to an acute hypoxic stimulus result in increases in blood pressure and ventilation, responses designed to counteract the initial stimulus. The elevated blood pressure results from rapid increases in sympathetic nerve discharge to the majority of vascular tissues including the renal, adrenal, splanchnic, muscle and cardiac beds (Marshall, 1994; Cao and Morrison, 2001). By contrast, sympathetic discharge to brown adipose tissue is reduced in response to acute hypoxia (Madden and Morrison, 2005).

CHRONIC INTERMITTENT HYPOXIA

The cardiovascular and ventilatory responses to acute hypoxia are augmented by prior exposure to chronic episodes of intermittent hypoxia (Greenberg et al., 1999; Dick et al., 2007; Marcus et al., 2010; Del Rio et al., 2014). In patients with newly diagnosed obstructive sleep apnea, augmented cardiovascular and respiratory responses to hypoxia are also observed (Narkiewicz et al., 1999). These findings suggest that chronic intermittent hypoxia-induced activation of the chemoreceptor reflex could potentially contribute to pathological cardiovascular and respiratory complications.

Intermittent hypoxia is associated with transient interruption to breathing resulting in transient cycles of oxygen desaturation and re-oxygenation, and can result from obstruction of airway passages and altered respiratory rhythm. Continued intermittent hypoxia chronically over time has deleterious effects as shown by the population cohort that suffers from obstructive sleep apnea (Neubauer, 2001; Wszedybyl-Winklewska et al., 2018). This cohort has been estimated to be 13% of the adult population (Peppard et al., 2013) and the resultant co-morbidities, including cardiovascular dysregulation and hypertension, contribute to poor prognosis and increased mortality (Lavie and Lavie, 2008).

Obstructive sleep apnea is associated with hypertension such that at least 30% of people diagnosed with hypertension suffer from obstructive sleep apnea and this proportion almost triples

in those with drug-resistant hypertension (Muxfeldt et al., 2015). Furthermore, the degree of hypertension correlates with the severity of obstructive sleep apnea and male caucasians appear to be most prevalent within the cohort (Hou et al., 2018).

Activation of the carotid bodies during hypoxia induces increased sympathetic nerve activity, and elevated sympathetic outflow is known to contribute to hypertension. Cutting the carotid sinus nerve has been found to reduce blood pressure in spontaneously hypertensive rats suggesting that activated carotid body activity contributes to essential hypertension (McBryde et al., 2017; Niewinski et al., 2017; Paton, 2017). More recently, selective resection of the carotid bodies, and sparing arterial baroreceptor function, also lowered blood pressure in the spontaneously hypertensive rat, strongly implicating overactivity of the carotid bodies as a key contributor to chronic high blood pressure (Pijacka et al., 2018).

Increased sympathetic nerve activity is a contributing cause of the hypertension seen in patients with obstructive sleep apnea (Grassi, 2010; Shell et al., 2016), and in animal models of chronic intermittent hypoxia which develop hypertension (Peng et al., 2014; Takahashi et al., 2018). Overactivity of the carotid bodies may play a key role in the development of hypertension in response to chronic intermittent hypoxia as evidenced by studies showing that ablation of the carotid bodies reduce chronic intermittent hypoxia-induced hypertension (Del Rio et al., 2016).

The overactivation of the carotid bodies induced by chronic intermittent hypoxia and the resultant hypertension may result from increased production of reactive oxygen species (ROS). Following chronic intermittent hypoxia, overexpression of pro-oxidant enzymes like NADPH Oxidase-2 and reduced expression of anti-oxidant enzymes like superoxide dismutase have been detected in the glomus cells and in the brain medullary regions that form part of the central pathways mediating the chemoreceptor reflex [i.e., the nucleus tractus solitarii (NTS) and the rostral ventrolateral medulla (RVLM)] (Peng et al., 2009, 2014). Furthermore, the adrenal gland showed similar changes in the expression of those enzymes suggesting that increased oxidative stress may also occur in the efferent sympathetic outflow and eliciting increased blood pressure. This is supported by the findings that show that scavengers of ROS can reduce the increased blood pressure elicited by chronic intermittent hypoxia in rodents (Iturriaga et al., 2016), and reduce the overexpression of pro-oxidant enzymes and restores the expression of anti-oxidant enzymes in the glomus cells, brainstem, and adrenal gland suggesting a key link between hyperactive carotid bodies, excessive ROS production and elevated sympathetic nerve activity. Strong support for this link has been shown by studies from Prabhakar's laboratory where the mechanism mediating the increase in ROS and carotid body overactivity has been investigated. Following chronic intermittent hypoxia, that resulted in oxygen levels that simulated sleep apnea, the increased ROS production correlated with DNA methylation that repressed anti-oxidant enzyme genes (Nanduri et al., 2018). Treatment with ROS scavengers prevented the DNA methylation, and ablation of the carotid body prevented the DNA methylation in the NTS and RVLM (Nanduri et al., 2018). Finally, treatment of rats that prevented DNA methylation resulted in normalization of plasma catecholamines and hypertension that occurred following chronic intermittent hypoxia (Nanduri et al., 2018). Taken together the data suggest that DNA methylation and ROS production may be critical in the dysfunction that results from overactivation of the carotid bodies following chronic intermittent hypoxia. Whether the role of DNA methylation contributes to the metabolic disturbances in addition to cardiovascular dysfunction that can accompany carotid body over-activation will be an interesting avenue of research.

CHRONIC INTERMITTENT HYPOXIA, OBESITY, AND METABOLIC DYSFUNCTION

With chronic intermittent hypoxia, evidence suggests that the effects on glucose homeostasis are detrimental. This is evidenced by increased fasting blood glucose, increased insulin resistance and reduced glucose tolerance as well as impaired pancreatic beta cell function (Polak et al., 2013). The duration of the hypoxia may be correlated to the reduction in insulin sensitivity (Sacramento et al., 2016). Furthermore, although blood glucose may return to normal following cessation of the intermittent hypoxia, continued impairment of glucose tolerance, insulin resistance, and beta cell function can still be observed (Polak et al., 2013), and this may contribute to the detrimental long-term metabolic effects induced by chronic intermittent hypoxia.

Patients suffering from obstructive sleep apnea also show dysfunctional metabolism, including reduced glucose tolerance and elevated risk of type 2 diabetes. Since chronic intermittent hypoxia is a characteristic of obstructive sleep apnea, it would suggest that the chronic intermittent hypoxia may contribute to the detrimental glucose regulation observed in obstructive sleep apnea. There is a close association between obesity and obstructive sleep apnea which may complicate the relationship between dysfunctional glucose metabolism and obstructive sleep apnea. However, even accounting for obesity, obstructive sleep apnea is still an independent risk factor for impaired glucose utilization and type 2 diabetes (Drager et al., 2013). It has also been demonstrated that obese patients with obstructive sleep apnea may have an increased risk of developing metabolic syndrome and higher levels of serum lipids, fasting glucose, and insulin resistance than obese subjects who did not suffer from sleep apnea (Basoglu et al., 2011).

Taken together, the evidence suggests that chronic activation of the carotid bodies may contribute to impaired glucose utilization and thus may be a key factor that links metabolic dysfunction and chronic intermittent hypoxia?

THE CAROTID BODIES AND METABOLIC DYSFUNCTION

Emerging evidence supports the hypothesis that overactivation of the carotid bodies contributes to metabolic dysfunction including the elevated fasting blood glucose and insulin resistance. The mechanisms that link overactivation of the carotid bodies and

insulin resistance are not clear but the increase in sympathetic nerve activity and the resultant lipolysis and increased levels of free fatty acids are likely contributors to the insulin resistance (Boden, 2011; Conde et al., 2017).

Denervation of the carotid bodies by cutting the carotid sinus nerve improved insulin sensitivity in mice subjected to chronic intermittent hypoxia suggesting that activity of the carotid bodies can influence glucose homeostasis (Shin et al., 2014). Furthermore, in animal models of diet-induced insulin resistance, there is over activation of the carotid bodies, and when the carotid sinus nerves were cut the sensitivity to insulin was improved and fasting blood glucose was reduced (Ribeiro et al., 2013; Sacramento et al., 2017). More recently, bioelectric modulation to reversibly reduce carotid sinus nerve activity in rats fed a high fat plus high sucrose diet restored insulin sensitivity whilst carotid sinus nerve activity was reduced. However, the impaired insulin sensitivity returned when carotid sinus nerve activity was allowed to return to its abnormally elevated level (Sacramento et al., 2018).

Thus, elevated carotid sinus nerve activity may be an important contributor to the development of insulin resistance and impaired glucose utilization, characteristics of type 2 diabetes. This does not preclude other causes of insulin resistance and impaired glucose tolerance such as the view that hyperinsulinemia is the product of obesity and excess food intake and the concomitant development of insulin resistance (Landsberg and Young, 1978; Reaven, 2004), or the view that increased sympathetic nerve activity decreases glucose uptake and utilization in skeletal muscle resulting in hyperinsulinemia (Masuo et al., 1997; Flaa et al., 2008).

Nonetheless, given the evidence, together with the studies showing that elevated carotid body activity may contribute to the increased sympathetic nerve activity in hypertension; could over-activation of the carotid body be a common factor in dysfunction of glucose utilization and hypertension in conditions in which chronic intermittent hypoxia is a feature?

CAROTID BODIES AND GLUCOSE SENSING

Although oxygen sensing is a key function of the carotid bodies, there is evidence indicating that the carotid bodies have additional monitoring capabilities, including responding to glucose levels, which further supports a role of the carotid bodies in glucose homeostasis. In contrast to the pancreatic beta cells in which elevated glucose depolarizes the cells, glomus cells are depolarized by low glucose (Lopez-Barneo, 2003). The mechanisms involved still need to be clarified, however, activation of TRPC3/6 channel subtypes appear to be involved (Garcia-Fernandez et al., 2007). Furthermore, glucose sensing by the glomus cells does not appear to depend on GLUT-2 mediated membrane transport and evidence suggests that metabolites of glucose, independent of hexokinase since this enzyme does not appear to be required in glomus cells, are sensed by the glomus cells (Garcia-Fernandez et al., 2007). Ultimately, the glucose-sensing mechanisms involved in glomus cells involve opening of voltage-dependent calcium channels mediated via the closing of voltage dependent potassium channels and opening of sodium channels (Pardal and Lopez-Barneo, 2002; Lopez-Barneo, 2003).

Activation of the carotid body increases sympathetic nerve activity resulting in increased hepatic glucose release as a counter-regulatory mechanism to counteract hypoglycemia. Such a mechanism also appears to explain the increase in plasma glucose induced in response to intermittent hypoxia seen in animals and humans (Wehrwein et al., 2015; Newhouse et al., 2017). Hypoxia and hypoglycemia have additive effects on the activity of the glomus cells (Pardal and Lopez-Barneo, 2002). Conversely, one would expect that hypoxia and hyperglycemia would have antagonistic actions on glomus cell activity. Since hypoxia and hypoglycemia appear to mediate their excitatory action on glomus cells via independent mechanisms (Garcia-Fernandez et al., 2007), an opportunity may exist to reduce overactivity of the carotid bodies by selectively reducing the influence of hypoxia in conditions in which hypoxia and hyperglycemia are prevalent (i.e., metabolic syndrome and sleep apnea).

WHAT ARE THE POTENTIAL TRANSMITTERS THAT CAN REGULATE CAROTID BODY SENSORY ACTIVITY

As mentioned earlier, the carotid body is made up of type I glomus cells, sustentacular (type II cells) and the afferent terminals of the petrosal ganglion sensory neurons. Each of these structures are closely apposed to each other and can produce and release potential transmitters and/or express receptors that can be activated. In the following paragraphs we briefly highlight the potentially rich microenvironment that is capable of regulating the afferent sensory responses to hypoxic stimuli. The reader is referred to reviews on this topic for detailed information (Nurse, 2005, 2014; Kumar and Prabhakar, 2012; Nurse and Piskuric, 2013; Zera et al., 2019).

Glomus cells contain many potential chemical transmitters. Acetylcholine, dopamine, histamine, serotonin, adenosine triphosphate (ATP) are amongst the most concentrated within the glomus cells. Acetylcholine and ATP are candidates that appear to be the primary neurotransmitters activating afferent sensory nerves in the carotid body and inhibition of both nicotinic and purinergic receptors, in combination, can prevent the hypoxia-induced responses (Zhang et al., 2000; Zhou et al., 2016). There are species differences, for example, in humans, ACh and ATP also appear to be main mediators of the hypoxic signaling response (Kahlin et al., 2014), just as in rodents and rabbits (Iturriaga and Alcayaga, 2004). However, in the cat dopamine may also play an important role (Iturriaga and Alcayaga, 2004). It should also be noted ACh is inhibitory via muscarinic receptors but excitatory via nicotinic ACh receptors in the rabbit carotid body (Iturriaga and Alcayaga, 2004; Jonsson et al., 2004). Furthermore, transcriptomic studies have compared the human and mouse carotid body transcriptome and shown marked similarities but there were also striking differences in the expression of genes involved in oxygen sensing and

cytokine production in the carotid body (Mkrtchian et al., 2012; Kahlin et al., 2014).

Neuropeptides like Substance P, enkephalins, endothelin, and angiotensin II are also present in glomus cells, and so are gaseous neurotransmitters. The glomus cells contain the enzymes required for the synthesis of H_2S and CO (Peng et al., 2010, 2017, 2019). The generation of H_2S in glomus cells appears to be a very important mediator in the chemosensory function of the carotid body as highlighted by studies in which the prevention of the generation of H_2S resulted in the impairment of the respiratory responses induced by hypoxia (Peng et al., 2010, 2017). It has been hypothesized that hypoxia induces a reduction of CO production within the glomus cells and this enables increased production of H_2S. This appears to contribute to the activation of glomus cells following hypoxic but not anoxic conditions (Peng et al., 2019).

Clearly, such a diverse grouping of neurochemicals involved in influencing the glomus cells and/or the afferent nerve terminals of the sensory fibers, raises the possibility that they have neuromodulatory roles and may contribute to the afferent information depending upon the physiological stimulus.

The activity of glomus cells also may be influenced by the activation of the receptors expressed by the cells. Single cell RNA sequencing techniques have identified several G-protein coupled receptors that are highly expressed on glomus cells (Zhou et al., 2016). These receptors include the olfactory receptor 78, adenosine A2A, purinergic P2Y12, cannabinoid type 1, and pituitary adenylate cyclase-activating peptide type 1. Less frequently found receptors were the angiotensin type, dopamine D2, endothelin A and glutamatergic AMPA and NMDA subtypes. Inhibitory ligand-gated ion channel receptors activated by glycine and GABA were also identified (Zhou et al., 2016).

Afferent sensory terminals in the carotid body are also known to express a broad variety of receptors. These include purinergic P2X, A2A and nicotinic ACh receptors, dopaminergic receptors, serotonergic receptors, neurotrophic receptors (TRK), and TRPV1 receptors, which upon activation can influence afferent activity (Nurse, 2014; Leonard et al., 2018). In addition to potential transmitters produced within the carotid bodies, circulating hormones may also influence carotid body activity, including hormones involved in glucose homeostasis such as insulin and leptin, the renin-angiotensin system and inflammatory mediators.

Insulin receptors have been identified in rat carotid bodies and are functional since insulin increases carotid body activity resulting in increased reflex ventilatory responses and increased blood pressure (Ribeiro et al., 2013). Furthermore, in rats that were insulin resistant due to a high caloric diet, the increase in circulating catecholamines normally observed, was attenuated by denervation of the carotid bodies. The insulin sensitivity was restored to normal and the hypertension seen in rats on the hypercaloric diet was also reduced following the denervation of the carotid bodies (Ribeiro et al., 2013). These experiments provide strong support for a physiological role of the carotid bodies in glucose homeostasis and suggest that circulating insulin can activate the carotid bodies. In humans, the physiological role of insulin on carotid body function still needs to be clarified, Infusions of insulin have been shown to increase muscle sympathetic nerve activity, but this could not be attenuated by low dose dopamine and/or hyperoxia suggesting acute insulin infusion does not affect carotid body function (Limberg et al., 2020). However, in chronic conditions like diabetes, insulin may well have an important role in glucose homeostasis mediated by the carotid bodies (Vera-Cruz et al., 2015).

Leptin receptors have also been identified on glomus cells and their activation by leptin results in increased glomus cell activity (Porzionato et al., 2011; Messenger and Ciriello, 2013). Interestingly, leptin is expressed within glomus cells suggesting that both locally produced and systemic leptin may influence carotid body activity. Furthermore, the leptin receptors are downregulated by intermittent hypoxia but the expression of leptin itself in the carotid body is upregulated by intermittent hypoxia (Messenger and Ciriello, 2013), suggesting a complex inter-relationship between intermittent hypoxia and leptin on carotid body activity. This issue has been addressed by an interesting recent study that found up to 74% of glomus cells in mice expressed the leptin receptor and that the hypoxia-induced increase in the activity of the carotid sinus nerve was enhanced by leptin administration (Caballero-Eraso et al., 2019). Furthermore, this study also showed that in mice deficient in the leptin receptor (i.e., *db/db* mice), re-introduction of the leptin receptor in the carotid bodies of these mice increased minute volume and the ventilatory response to hypoxia (Caballero-Eraso et al., 2019), confirming that leptin is playing a key physiological role in carotid body function.

Leptin's role in carotid body function does not appear to be restricted to respiratory regulation. Leptin administration is well-known to induce increases in blood pressure, and in hypertension associated with obesity, it has been long recognized that the cardiovascular responses to leptin are not reduced which is in stark contrast to the effects on dietary intake which were diminished compared to lean controls. Such observations led to the concept of "selective leptin resistance" (Prior et al., 2010; Mark, 2013).

A recent exciting study has now highlighted a key role for leptin in the carotid body (Shin et al., 2019). In that study, peripheral leptin administration induced increases in blood pressure in lean mice and the effect was prevented by carotid body denervation. The hypertensive response initiated by the activation of leptin receptors was mediated by TRPM7 calcium channels. Furthermore, overexpression of the leptin receptor selectively in the carotid body of leptin receptor-deficient mice enhanced TRPM7 gene expression and induced hypertension (Shin et al., 2019). Thus, taken together, the findings suggest that leptin acting within the carotid body is playing a major role in the cardiovascular and respiratory function. The contribution of leptin within the carotid body to glucose homeostasis clearly needs investigation and potentially would support the hypothesis linking the carotid body activity as a common mediator regulating cardiovascular, respiratory and glucose homeostasis. The role of TRPM7 channels would be an exciting focus.

The peptide hormone, angiotensin, can also influence carotid body activity. The angiotensin II type I receptor (ATIR) is

found on glomus cells in the carotid body and angiotensin II predominantly stimulates the carotid body as determined from electrophysiological recordings of the carotid sinus nerve (Allen, 1998). The expression of AT1R in the carotid body is increased by chronic intermittent hypoxia and this may contribute to the increase in sympathetic nerve activity elicited by chronic intermittent hypoxia (Marcus et al., 2010; Takahashi et al., 2018). Furthermore, the enhanced activation of lumbar sympathetic nerve activity in rats following chronic intermittent hypoxia was prevented with treatment using the ATIR antagonist, losartan, suggesting angiotensin II activation of the carotid body played an important role in sympathetic nerve activity responses induced by chronic intermittent hypoxia (Marcus et al., 2010).

In obesity, the renin-angiotensin-aldosterone system may take on more importance since adipose cells can produce angiotensinogen (Cassis et al., 1988), and overexpression of angiotensinogen in adipose tissue can contribute to hypertension and adipose tissue development (Massiera et al., 2001). In humans, obstructive sleep apnea has been reported to increase the activity of the renin-angiotensin-aldosterone system (Goodfriend and Calhoun, 2004). Thus, angiotensin II may be an important link between obesity and chronic intermittent hypoxia and overactivity of the carotid body.

Evidence also suggests that inflammatory mediators within the chemosensory pathways are key mediators of cardiorespiratory dysfunction. Studies using human carotid bodies (taken from patients undergoing surgical procedures for head and neck tumors) show that hypoxia can induce the release of cytokines (Kahlin et al., 2014). Furthermore, chronic intermittent hypoxia in rats induces increased production of pro-inflammatory cytokines in the carotid body and in the nucleus tractus solitarii (Del Rio et al., 2011). This increased production of pro-inflammatory cytokines and the resultant cardiorespiratory responses can be prevented by pretreatment with the non-steroidal anti-inflammatory drug, ibuprofen (Del Rio et al., 2012). Since obesity is associated with abnormally elevated sympathetic nerve activity, elevated levels of cytokines, adipokines and obstructive sleep apnea (Lambert et al., 2010; Armitage et al., 2012), and the observation that intermittent hypoxia has been reported to induce inflammation in adipose tissue (Poulain et al., 2017), the evidence suggests that increased levels of pro-inflammatory cytokines within the peripheral and central components of the chemosensory pathways contribute to the cardiovascular and respiratory dysfunction seen in conditions like obesity that involve chronic intermittent hypoxia.

IS THERE A ROLE FOR PURINES IN THE CAROTID BODY IN THE REGULATION OF GLUCOSE HOMEOSTASIS?

To date, there have been no reports directly investigating whether inhibition of purinergic function can influence glucose homeostasis. However, the following evidence provides circumstantial evidence in support of such a hypothesis.

The release of ATP in response to hypoxia is well-recognized. ATP and adenosine (which can be produced through the metabolism of ATP) activate sensory afferent neurons in the carotid body through P2X and A2A purinergic receptors (Zhang and Nurse, 2004; Conde et al., 2006), which results in increased activity of the carotid sinus nerve. Inhibition of P2X2/3 and A2A purinergic receptors can reduce carotid sinus nerve activity, and the resultant reflex ventilatory responses (Zhang et al., 2000, 2018; Conde et al., 2006). Thus, activation of the carotid body in response to hypoxia involves purinergic receptor activation.

In addition to mediating reflex respiratory function, the increased carotid sinus nerve activity induced by carotid body activation also results in increased sympathetic nerve activity and blood pressure, as indicated earlier. There is good evidence indicating a role of $P2X_3$ receptors in mediating this cardiovascular reflex response. In an extensive study by Pijacka and colleagues, they showed that spontaneously hypertensive rats have a hyper-reflexive response to acute stimulation of the carotid body chemoreceptors and this is associated with upregulation of the $P2X_3$ receptors in the carotid body (note P2X2 and $P2X_3$ receptors can heterodimerize to form functional purinergic P2X2/3 receptors). Furthermore, antagonism of $P2X_3$ receptors with a selective antagonist reduced sympathetic nerve activity and blood pressure in the spontaneously hypertensive rat (Pijacka et al., 2016). There was no effect in the normotensive control rats. This led the authors to suggest that using the $P2X_3$ receptor antagonist may reduce overactivity of the carotid body and this was supported by the finding that petrosal ganglion neurons (cell bodies of the carotid body afferent fibers) from Spontaneously Hypertensive rats were sensitized to purinergic receptor activation but this was not observed in normotensive Wistar rats. Furthermore, the activity of the petrosal ganglion neurons from Spontaneously Hypertensive rats was normalized by $P2X_3$ receptor antagonism (Pijacka et al., 2016). Taken together, the findings suggest that normal function of the carotid body chemoreceptors may not be markedly affected by administration of purinergic $P2X_3$ receptor antagonists but overactivity of those chemoreceptors may be attenuated.

Thus, respiratory and cardiovascular function can be influenced by purinergic $P2X_3$ receptor antagonism, whether regulation of glucose homeostasis can be added to this action has not been reported to date. However, the circumstantial evidence available points to such a possibility. Very interesting work emanating from Conde and colleagues has shown that there is increased sympathetic nerve activity in rats fed high caloric diets that have hypertension, hyperinsulinemia and hyperglycemia. In these rats, carotid body denervation reduced sympathetic nerve activity, blood pressure and restored insulin sensitivity and glucose utilization (Ribeiro et al., 2013). Externally applied, bioelectric modulation has recently been used to reversibly reduce carotid sinus nerve activity in rats fed high caloric diets and restore insulin sensitivity (Sacramento et al., 2018). Whether purinergic $P2X_3$ receptor antagonism could induce similar positive effects on insulin sensitivity needs to be investigated. Interestingly, a positive finding may be readily translatable to clinical situations since $P2X_3$ receptor antagonists have been developed and one is currently in phase III trials for persistent

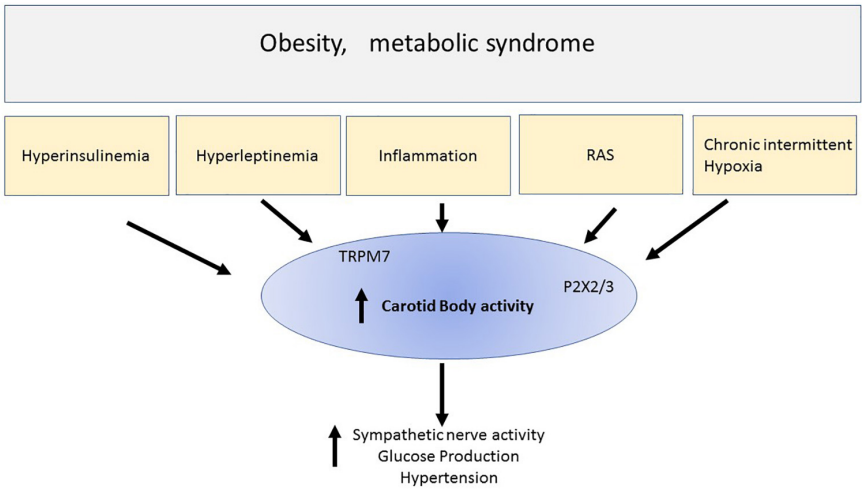

FIGURE 1 | This simple schematic highlights the possibility that chronic intermittent hypoxia and hyper-insulinemia and hyperleptinemia inflammation and elevated renin -angiotensin aldosterone system (RAS) that may be observed in metabolic conditions like obesity or metabolic syndrome, activate the carotid bodies. The result includes increase sympathetic nerve activity, hyperglycemia, and hypertension. Activation of the carotid body can result from many chemicals and receptors that were discussed in the text. The schematic highlights ATP released from glomus cells and acting on purinergic receptors ($P2X_3$) which we suggest is particularly important in contributing to the activation of the afferent pathways initiated by chronic intermittent hypoxia. We also highlight new findings suggesting that stimulation of leptin receptors activates TRPM7 ion channels. Thus, overactivity of the carotid body may be a common denominator involved in the cardiovascular and metabolic disturbances seen in metabolic disorders. Reducing the overactivity of carotid bodies, for example using P2X2/3 antagonists which are in clinical practice, may prove to be a novel therapeutic treatment regime, or developing non-invasive bioelectric modulation techniques may prove useful therapeutic strategies.

cough (ClinicalTrials.gov Identifier: NCT03449134) and may be useful in other hyper-reflexive states (Richards et al., 2019).

CLINICAL TRANSLATION

Unilateral and bilateral carotid body removal have been utilized in small clinical studies of patients with drug-resistant hypertension and in patients with low ejection fraction heart failure. In about half of the hypertensive patients, blood pressure was reduced even up to 12 months post-unilateral carotid body resection. The responders were those that had enhanced ventilatory responses to chemoreceptor stimulation prior to the procedure (Narkiewicz et al., 2016). In the heart failure patients, the quality of life was improved but given the size of the cohort, much more work is needed, particularly since bilateral carotid body resection was often associated with poorer nocturnal oxygen saturation content suggesting an increase in sleep apnea (Niewinski et al., 2017). Therefore, bilateral carotid body resection may not be an entirely safe viable therapeutic option for most patients. However, modulating the activity of the carotid sinus nerve by targeting specific receptors (e.g., purinergic $P2X_3$) or ion channels (e.g., TRPM7) could prove to be a useful therapeutic intervention. Bioelectric modulation of neuronal activity is another relatively non-invasive mechanism that could be explored (Iturriaga et al., 2016).

SUMMARY AND CONCLUSION

The carotid bodies are small organs that are exquisitely sensitive to the level of oxygen in the blood and initiate a response to hypoxia that includes increased sympathetic nerve activity, increased blood pressure and increased ventilation and increased glucose production due to catecholaminergic actions on the liver. Chronic intermittent hypoxia is associated with obesity and overactivity of the carotid bodies has been described in this metabolic condition (**Figure 1**). Thus, reducing this overactivity may be beneficial for the cardiovascular, respiratory and hyperglycemia present in obesity and other conditions of metabolic dysfunction. There is evidence supporting this. Therefore, the carotid bodies may be a common link and thus an attractive potential target to tackle the cardiorespiratory and metabolic dysfunction that are observed in obesity and metabolic syndrome. Potential approaches to therapy include the development of antagonists to TRPM7 channels and $P2X_3$ receptors which may contribute to the increase in sympathetic nerve activity in response to hypoxia (**Figure 1**). Antagonists to $P2X_3$ receptors are already in late clinical trials (for persistent cough) which may make translation to other clinical conditions more practicable. Bioelectric modulation, which is a relatively non-invasive technique to lower carotid sinus nerve activity, may also find translation into the clinical setting more readily.

AUTHOR CONTRIBUTIONS

EB wrote the review and designed the figure.

ACKNOWLEDGMENTS

I thank Prof. J. F. Paton for critically reading the manuscript.

REFERENCES

Allen, A. M. (1998). Angiotensin AT1 receptor-mediated excitation of rat carotid body chemoreceptor afferent activity. *J. Physiol.* 510(Pt 3), 773–781. doi: 10.1111/j.1469-7793.1998.773bj.x

Armitage, J. A., Burke, S. L., Prior, L. J., Barzel, B., Eikelis, N., Lim, K., et al. (2012). Rapid onset of renal sympathetic nerve activation in rabbits fed a high-fat diet. *Hypertension* 60, 163–171. doi: 10.1161/hypertensionaha.111.190413

Basoglu, O. K., Sarac, F., Sarac, S., Uluer, H., and Yilmaz, C. (2011). Metabolic syndrome, insulin resistance, fibrinogen, homocysteine, leptin, and C-reactive protein in obese patients with obstructive sleep apnea syndrome. *Ann. Thorac. Med.* 6, 120–125.

Biscoe, T. J. (1971). Carotid body: structure and function. *Physiol. Rev.* 51, 437–495. doi: 10.1152/physrev.1971.51.3.437

Boden, G. (2011). Obesity, insulin resistance and free fatty acids. *Curr. Opin. Endocrinol. Diabetes Obes.* 18, 139–143. doi: 10.1097/med.0b013e3283444b09

Buckler, K. J. (2015). TASK channels in arterial chemoreceptors and their role in oxygen and acid sensing. *Pflugers Arch.* 467, 1013–1025. doi: 10.1007/s00424-015-1689-1

Caballero-Eraso, C., Shin, M. K., Pho, H., Kim, L. J., Pichard, L. E., Wu, Z. J., et al. (2019). Leptin acts in the carotid bodies to increase minute ventilation during wakefulness and sleep and augment the hypoxic ventilatory response. *J. Physiol.* 597, 151–172. doi: 10.1113/jp276900

Cao, W. H., and Morrison, S. F. (2001). Differential chemoreceptor reflex responses of adrenal preganglionic neurons. *Am. J. Physiol. Regul. Integr. Comp. Physiol.* 281, R1825–R1832.

Cassis, L. A., Saye, J., and Peach, M. J. (1988). Location and regulation of rat angiotensinogen messenger RNA. *Hypertension* 11, 591–596. doi: 10.1161/01.hyp.11.6.591

Clarke, J. A., and de Burgh Daly, M. (1981). A comparative study of the distribution of carotid body type-I cells and periadventitial type-I cells in the carotid bifurcation regions of the rabbit, rat, guinea-pig and mouse. *Cell Tissue Res.* 220, 753–772. doi: 10.1007/bf00210459

Conde, S. V., Obeso, A., Vicario, I., Rigual, R., Rocher, A., and Gonzalez, C. (2006). Caffeine inhibition of rat carotid body chemoreceptors is mediated by A2A and A2B adenosine receptors. *J. Neurochem.* 98, 616–628. doi: 10.1111/j.1471-4159.2006.03912.x

Conde, S. V., Ribeiro, M. J., Melo, B. F., Guarino, M. P., and Sacramento, J. F. (2017). Insulin resistance: a new consequence of altered carotid body chemoreflex? *J. Physiol.* 595, 31–41. doi: 10.1113/jp271684

Deane, B. M., Howe, A., and Morgan, M. (1975). Abdominal vagal paraganglia: distribution and comparison with carotid body, in the rat. *Acta Anat.* 93, 19–28. doi: 10.1159/000144493

Del Rio, R., Andrade, D. C., Lucero, C., Arias, P., and Iturriaga, R. (2016). Carotid Body Ablation Abrogates Hypertension and Autonomic Alterations Induced by Intermittent Hypoxia in Rats. *Hypertension* 68, 436–445. doi: 10.1161/hypertensionaha.116.07255

Del Rio, R., Moya, E. A., and Iturriaga, R. (2011). Differential expression of pro-inflammatory cytokines, endothelin-1 and nitric oxide synthases in the rat carotid body exposed to intermittent hypoxia. *Brain Res.* 13, 74–85. doi: 10.1016/j.brainres.2011.04.028

Del Rio, R., Moya, E. A., and Iturriaga, R. (2014). Carotid body potentiation during chronic intermittent hypoxia: implication for hypertension. *Front. Physiol.* 5:434. doi: 10.3389/fphys.2014.00434

Del Rio, R., Moya, E. A., Parga, M. J., Madrid, C., and Iturriaga, R. (2012). Carotid body inflammation and cardiorespiratory alterations in intermittent hypoxia. *Eur. Respir. J.* 39, 1492–1500. doi: 10.1183/09031936.00141511

Dick, T. E., Hsieh, Y. H., Wang, N., and Prabhakar, N. (2007). Acute intermittent hypoxia increases both phrenic and sympathetic nerve activities in the rat. *Exp. Physiol.* 92, 87–97. doi: 10.1113/expphysiol.2006.035758

Drager, L. F., Togeiro, S. M., Polotsky, V. Y., and Lorenzi-Filho, G. (2013). Obstructive sleep apnea: a cardiometabolic risk in obesity and the metabolic syndrome. *J. Am. Coll. Cardiol.* 569–576.

Fernandez-Aguera, M. C., Gao, L., Gonzalez-Rodriguez, P., Pintado, C. O., Arias-Mayenco, I., Garcia-Flores, P., et al. (2015). Oxygen sensing by arterial chemoreceptors depends on mitochondrial complex I signaling. *Cell Metab.* 22, 825–837. doi: 10.1016/j.cmet.2015.09.004

Finley, J. C., and Katz, D. M. (1992). The central organization of carotid body afferent projections to the brainstem of the rat. *Brain Res.* 572, 108–116. doi: 10.1016/0006-8993(92)90458-l

Finley, J. C., Polak, J., and Katz, D. M. (1992). Transmitter diversity in carotid body afferent neurons: dopaminergic and peptidergic phenotypes. *Neuroscience* 51, 973–987. doi: 10.1016/0306-4522(92)90534-9

Flaa, A., Aksnes, T. A., Kjeldsen, S. E., Eide, I., and Rostrup, M. (2008). Increased sympathetic reactivity may predict insulin resistance: an 18-year follow-up study. *Metabolism* 57, 1422–1427. doi: 10.1016/j.metabol.2008.05.012

Garcia-Fernandez, M., Ortega-Saenz, P., Castellano, A., and Lopez-Barneo, J. (2007). Mechanisms of low-glucose sensitivity in carotid body glomus cells. *Diabetes* 56, 2893–2900. doi: 10.2337/db07-0122

Gonzalez, C., Almaraz, L., Obeso, A., and Rigual, R. (1994). Carotid body chemoreceptors: from natural stimuli to sensory discharges. *Physiol. Rev.* 74, 829–898. doi: 10.1152/physrev.1994.74.4.829

Goodfriend, T. L., and Calhoun, D. A. (2004). Resistant hypertension, obesity, sleep apnea, and aldosterone: theory and therapy. *Hypertension* 43, 518–524. doi: 10.1161/01.hyp.0000116223.97436.e5

Grassi, G. (2010). Sympathetic neural activity in hypertension and related diseases. *Am. J. Hypertens.* 23, 1052–1060. doi: 10.1038/ajh.2010.154

Greenberg, H. E., Sica, A., Batson, D., and Scharf, S. M. (1999). Chronic intermittent hypoxia increases sympathetic responsiveness to hypoxia and hypercapnia. *J. Appl. Physiol.* 86, 298–305. doi: 10.1152/jappl.1999.86.1.298

Hou, H., Zhao, Y., Yu, W., Dong, H., Xue, X., Ding, J., et al. (2018). Association of obstructive sleep apnea with hypertension: a systematic review and meta-analysis. *J. Glob. Health* 8:010405.

Iturriaga, R., and Alcayaga, J. (2004). Neurotransmission in the carotid body: transmitters and modulators between glomus cells and petrosal ganglion nerve terminals. *Brain Res. Brain Res. Rev.* 47, 46–53. doi: 10.1016/j.brainresrev.2004.05.007

Iturriaga, R., Del Rio, R., Idiaquez, J., and Somers, V. K. (2016). Carotid body chemoreceptors, sympathetic neural activation, and cardiometabolic disease. *Biol. Res.* 49:13.

Jonsson, M., Wyon, N., Lindahl, S. G., Fredholm, B. B., and Eriksson, L. I. (2004). Neuromuscular blocking agents block carotid body neuronal nicotinic acetylcholine receptors. *Eur. J. Pharmacol.* 497, 173–180. doi: 10.1016/j.ejphar.2004.06.052

Kahlin, J., Mkrtchian, S., Ebberyd, A., Hammarstedt-Nordenvall, L., Nordlander, B., Yoshitake, T., et al. (2014). The human carotid body releases acetylcholine, ATP and cytokines during hypoxia. *Exp. Physiol.* 99, 1089–1098. doi: 10.1113/expphysiol.2014.078873

Kumar, P., and Prabhakar, N. R. (2012). Peripheral chemoreceptors: function and plasticity of the carotid body. *Compr. Physiol.* 2, 141–219.

Lambert, G. W., Straznicky, N. E., Lambert, E. A., Dixon, J. B., and Schlaich, M. P. (2010). Sympathetic nervous activation in obesity and the metabolic syndrome–causes, consequences and therapeutic implications. *Pharmacol. Ther.* 126, 159–172. doi: 10.1016/j.pharmthera.2010.02.002

Landsberg, L., and Young, J. B. (1978). Fasting, feeding and regulation of the sympathetic nervous system. *N. Engl. J. Med.* 298, 1295–1301. doi: 10.1056/nejm197806082982306

Lavie, P., and Lavie, L. (2008). Cardiovascular morbidity and mortality in obstructive sleep apnea. *Curr. Pharm. Des* 14, 3466–3473. doi: 10.2174/138161208786549317

Leonard, E. M., Salman, S., and Nurse, C. A. (2018). Sensory processing and integration at the carotid body tripartite synapse: neurotransmitter functions and effects of chronic hypoxia. *Front. Physiol.* 9:225. doi: 10.3389/fphys.2018.00225

Limberg, J. K., Johnson, B. D., Mozer, M. T., Holbein, W. W., Curry, T. B., Prabhakar, N. R., et al. (2020). Role of the carotid chemoreceptors in insulin-mediated sympathoexcitation in humans. *Am. J. Physiol. Regul. Integr. Comp. Physiol.* 318, R173–R181. doi: 10.1152/ajpregu.00257.2019

Lopez-Barneo, J. (2003). Oxygen and glucose sensing by carotid body glomus cells. *Curr. Opin. Neurobiol.* 13, 493–499. doi: 10.1016/s0959-4388(03)00093-x

Lopez-Barneo, J., Macias, D., Platero-Luengo, A., Ortega-Saenz, P., and Pardal, R. (2016). Carotid body oxygen sensing and adaptation to hypoxia. *Pflugers Arch.* 468, 59–70.

Madden, C. J., and Morrison, S. F. (2005). Hypoxic activation of arterial chemoreceptors inhibits sympathetic outflow to brown adipose tissue in rats. *J. Physiol.* 566, 559–573. doi: 10.1113/jphysiol.2005.086322

Marcus, N. J., Li, Y. L., Bird, C. E., Schultz, H. D., and Morgan, B. J. (2010). Chronic intermittent hypoxia augments chemoreflex control of sympathetic activity: role of the angiotensin II type 1 receptor. *Respir. Physiol. Neurobiol.* 171, 36–45. doi: 10.1016/j.resp.2010.02.003

Mark, A. L. (2013). Selective leptin resistance revisited. *Am. J. Physiol. Regul. Integr. Comp. Physiol.* 305, R566–R581.

Marshall, J. M. (1994). Peripheral chemoreceptors and cardiovascular regulation. *Physiol. Rev.* 74, 543–594. doi: 10.1152/physrev.1994.74.3.543

Massiera, F., Bloch-Faure, M., Ceiler, D., Murakami, K., Fukamizu, A., Gasc, J. M., et al. (2001). Adipose angiotensinogen is involved in adipose tissue growth and blood pressure regulation. *FASEB J.* 15, 2727–2729.

Masuo, K., Mikami, H., Ogihara, T., and Tuck, M. L. (1997). Sympathetic nerve hyperactivity precedes hyperinsulinemia and blood pressure elevation in a young, nonobese Japanese population. *Am. J. Hypertens.* 10, 77–83. doi: 10.1016/s0895-7061(96)00303-2

McBryde, F. D., Hart, E. C., Ramchandra, R., and Paton, J. F. (2017). Evaluating the carotid bodies and renal nerves as therapeutic targets for hypertension. *Auton. Neurosci.* 204, 126–130. doi: 10.1016/j.autneu.2016.08.002

Messenger, S. A., and Ciriello, J. (2013). Effects of intermittent hypoxia on leptin signalling in the carotid body. *Neuroscience* 232, 216–225. doi: 10.1016/j.neuroscience.2012.11.018

Mkrtchian, S., Kahlin, J., Ebberyd, A., Gonzalez, C., Sanchez, D., Balbir, A., et al. (2012). The human carotid body transcriptome with focus on oxygen sensing and inflammation–a comparative analysis. *J. Physiol.* 590, 3807–3819. doi: 10.1113/jphysiol.2012.231084

Muxfeldt, E. S., Margallo, V., Costa, L. M., Guimaraes, G., Cavalcante, A. H., Azevedo, J. C., et al. (2015). Effects of continuous positive airway pressure treatment on clinic and ambulatory blood pressures in patients with obstructive sleep apnea and resistant hypertension: a randomized controlled trial. *Hypertension* 65, 736–742. doi: 10.1161/hypertensionaha.114.04852

Nanduri, J., Peng, Y. J., Wang, N., Khan, S. A., Semenza, G. L., and Prabhakar, N. R. (2018). DNA methylation in the central and efferent limbs of the chemoreflex requires carotid body neural activity. *J. Physiol.* 596, 3087–3100. doi: 10.1113/jp274833

Narkiewicz, K., Ratcliffe, L. E., Hart, E. C., Briant, L. J., Chrostowska, M., Wolf, J., et al. (2016). Unilateral carotid body resection in resistant hypertension: a safety and feasibility trial. *JACC Basic Transl. Sci.* 1, 313–324. doi: 10.1016/j.jacbts.2016.06.004

Narkiewicz, K., van de Borne, P. J., Pesek, C. A., Dyken, M. E., Montano, N., and Somers, V. K. (1999). Selective potentiation of peripheral chemoreflex sensitivity in obstructive sleep apnea. *Circulation* 99, 1183–1189. doi: 10.1161/01.cir.99.9.1183

Neubauer, J. A. (2001). Invited review: physiological and pathophysiological responses to intermittent hypoxia. *J. Appl. Physiol.* 90, 1593–1599. doi: 10.1152/jappl.2001.90.4.1593

Newhouse, L. P., Joyner, M. J., Curry, T. B., Laurenti, M. C., Man, C. D., Cobelli, C., et al. (2017). Three hours of intermittent hypoxia increases circulating glucose levels in healthy adults. *Physiol. Rep.* 5:e13106. doi: 10.14814/phy2.13106

Niewinski, P., Janczak, D., Rucinski, A., Tubek, S., Engelman, Z. J., Piesiak, P., et al. (2017). Carotid body resection for sympathetic modulation in systolic heart failure: results from first-in-man study. *Eur. J. Heart Fail.* 19, 391–400. doi: 10.1002/ejhf.641

Nurse, C. A. (2005). Neurotransmission and neuromodulation in the chemosensory carotid body. *Auton. Neurosci.* 120, 1–9. doi: 10.1016/j.autneu.2005.04.008

Nurse, C. A. (2014). Synaptic and paracrine mechanisms at carotid body arterial chemoreceptors. *J. Physiol.* 592(Pt 16), 3419–3426. doi: 10.1113/jphysiol.2013.269829

Nurse, C. A., and Piskuric, N. A. (2013). Signal processing at mammalian carotid body chemoreceptors. *Semin. Cell Dev. Biol.* 24, 22–30. doi: 10.1016/j.semcdb.2012.09.006

Ortega-Saenz, P., and Lopez-Barneo, J. (2019). Physiology of the carotid body: from molecules to disease. *Annu. Rev. Physiol.* 82, 127–149. doi: 10.1146/annurev-physiol-020518-114427

Pardal, R., and Lopez-Barneo, J. (2002). Low glucose-sensing cells in the carotid body. *Nat. Neurosci.* 5, 197–198. doi: 10.1038/nn812

Pardal, R., Ortega-Saenz, P., Duran, R., and Lopez-Barneo, J. (2007). Glia-like stem cells sustain physiologic neurogenesis in the adult mammalian carotid body. *Cell* 131, 364–377. doi: 10.1016/j.cell.2007.07.043

Paton, J. F. (2017). Targeting autonomic imbalance in pathophysiology: is the carotid body the new nirvana? *J. Physiol.* 595, 29–30. doi: 10.1113/jp273604

Peng, Y.-J., Makarenko, V. V., Gridina, A., Chupikova, I., Zhang, X., Kumar, G. K., et al. (2019). H_2S mediates carotid body response to hypoxia but not anoxia. *Respir. Physiol. Neurobiol.* 259, 75–85. doi: 10.1016/j.resp.2018.08.001

Peng, Y.-J., Nanduri, J., Raghuraman, G., Souvannakitti, D., Gadalla, M. M., Kumar, G. K., et al. (2010). H_2S mediates O_2 sensing in the carotid body. *Proc. Natl. Acad. Sci. U.S.A.* 107, 10719–10724. doi: 10.1073/pnas.1005866107

Peng, Y.-J., Nanduri, J., Yuan, G., Wang, N., Deneris, E., Pendyala, S., et al. (2009). NADPH oxidase is required for the sensory plasticity of the carotid body by chronic intermittent hypoxia. *J. Neurosci.* 29, 4903–4910. doi: 10.1523/jneurosci.4768-08.2009

Peng, Y.-J., Yuan, G., Khan, S., Nanduri, J., Makarenko, V. V., Reddy, V. D., et al. (2014). Regulation of hypoxia-inducible factor-alpha isoforms and redox state by carotid body neural activity in rats. *J. Physiol.* 592, 3841–3858. doi: 10.1113/jphysiol.2014.273789

Peng, Y.-J., Zhang, X., Gridina, A., Chupikova, I., McCormick, D. L., Thomas, R. J., et al. (2017). Complementary roles of gasotransmitters CO and H_2S in sleep apnea. *Proc. Natl. Acad. Sci. U.S.A.* 114, 1413–1418. doi: 10.1073/pnas.1620717114

Peppard, P. E., Young, T., Barnet, J. H., Palta, M., Hagen, E. W., and Hla, K. M. (2013). Increased prevalence of sleep-disordered breathing in adults. *Am. J. Epidemiol.* 177, 1006–1014.

Pijacka, W., Katayama, P. L., Salgado, H. C., Lincevicius, G. S., Campos, R. R., McBryde, F. D., et al. (2018). Variable role of carotid bodies in cardiovascular responses to exercise, hypoxia and hypercapnia in spontaneously hypertensive rats. *J. Physiol.* 596, 3201–3216. doi: 10.1113/jp275487

Pijacka, W., Moraes, D. J., Ratcliffe, L. E., Nightingale, A. K., Hart, E. C., da Silva, M. P., et al. (2016). Purinergic receptors in the carotid body as a new drug target for controlling hypertension. *Nat. Med.* 22, 1151–1159. doi: 10.1038/nm.4173

Platero-Luengo, A., Gonzalez-Granero, S., Duran, R., Diaz-Castro, B., Piruat, J. I., Garcia-Verdugo, J. M., et al. (2014). An O2-sensitive glomus cell-stem cell synapse induces carotid body growth in chronic hypoxia. *Cell* 156, 291–303. doi: 10.1016/j.cell.2013.12.013

Polak, J., Shimoda, L. A., Drager, L. F., Undem, C., McHugh, H., Polotsky, V. Y., et al. (2013). Intermittent hypoxia impairs glucose homeostasis in C57BL6/J mice: partial improvement with cessation of the exposure. *Sleep* 36, 1483–1490. doi: 10.5665/sleep.3040

Porzionato, A., Rucinski, M., Macchi, V., Stecco, C., Castagliuolo, I., Malendowicz, L. K., et al. (2011). Expression of leptin and leptin receptor isoforms in the rat and human carotid body. *Brain Res.* 1385, 56–67. doi: 10.1016/j.brainres.2011.02.028

Poulain, L., Mathieu, H., Thomas, A., Borel, A. L., Remy, C., Levy, P., et al. (2017). Intermittent hypoxia-induced insulin resistance is associated with alterations in white fat distribution. *Sci. Rep.* 7:11180.

Prabhakar, N. R., and Semenza, G. L. (2016). Regulation of carotid body oxygen sensing by hypoxia-inducible factors. *Pflugers Arch.* 468, 71–75. doi: 10.1007/s00424-015-1719-z

Prior, L. J., Eikelis, N., Armitage, J. A., Davern, P. J., Burke, S. L., Montani, J. P., et al. (2010). Exposure to a high-fat diet alters leptin sensitivity and elevates renal sympathetic nerve activity and arterial pressure in rabbits. *Hypertension* 55, 862–868. doi: 10.1161/hypertensionaha.109.141119

Reaven, G. (2004). The metabolic syndrome or the insulin resistance syndrome? Different names, different concepts, and different goals. *Endocrinol. Metab. Clin. North Am.* 33, 283–303. doi: 10.1016/j.ecl.2004.03.002

Ribeiro, M. J., Sacramento, J. F., Gonzalez, C., Guarino, M. P., Monteiro, E. C., and Conde, S. V. (2013). Carotid body denervation prevents the development of insulin resistance and hypertension induced by hypercaloric diets. *Diabetes* 62, 2905–2916. doi: 10.2337/db12-1463

Richards, D., Gever, J. R., Ford, A. P., and Fountain, S. J. (2019). Action of MK-7264 (gefapixant) at human P2X3 and P2X2/3 receptors and in vivo efficacy in models of sensitisation. *Br. J. Pharmacol.* 176, 2279–2291.

Sacramento, J. F., Chew, D. J., Melo, B. F., Donega, M., Dopson, W., Guarino, M. P., et al. (2018). Bioelectronic modulation of carotid sinus nerve activity in the rat: a potential therapeutic approach for type 2 diabetes. *Diabetologia* 61, 700–710. doi: 10.1007/s00125-017-4533-7

Sacramento, J. F., Ribeiro, M. J., Rodrigues, T., Guarino, M. P., Diogo, L. N., Seica, R., et al. (2016). Insulin resistance is associated with tissue-specific regulation of HIF-1alpha and HIF-2alpha during mild chronic intermittent hypoxia. *Respir. Physiol. Neurobiol.* 228, 30–38. doi: 10.1016/j.resp.2016.03.007

Sacramento, J. F., Ribeiro, M. J., Rodrigues, T., Olea, E., Melo, B. F., Guarino, M. P., et al. (2017). Functional abolition of carotid body activity restores insulin action and glucose homeostasis in rats: key roles for visceral adipose tissue and the liver. *Diabetologia* 60, 158–168. doi: 10.1007/s00125-016-4133-y

Shell, B., Faulk, K., and Cunningham, J. T. (2016). Neural control of blood pressure in chronic intermittent hypoxia. *Curr. Hypertens. Rep.* 18:19.

Shin, M. K., Caballero-Eraso, C., Mu, Y. P., Gu, C., Hyeung, B. H., Kim, L. J., et al. (2019). Leptin induces hypertension acting on transient receptor potential melastatin 7 channel in the carotid body. *Circ. Res.* 125, 989–1002. doi: 10.1161/circresaha.119.315338

Shin, M. K., Yao, Q., Jun, J. C., Bevans-Fonti, S., Yoo, D. Y., Han, W., et al. (2014). Carotid body denervation prevents fasting hyperglycemia during chronic intermittent hypoxia. *J. Appl. Physiol.* 117, 765–776. doi: 10.1152/japplphysiol.01133.2013

Takahashi, K., Ueda, S., Kobayashi, T., Nishiyama, A., Fujisawa, Y., Sugaya, T., et al. (2018). Chronic intermittent hypoxia-mediated renal sympathetic nerve activation in hypertension and cardiovascular disease. *Sci. Rep.* 8, 17926.

Tse, A., Yan, L., Lee, A. K., and Tse, F. W. (2012). Autocrine and paracrine actions of ATP in rat carotid body. *Can. J. Physiol. Pharmacol.* 90, 705–711. doi: 10.1139/y2012-054

Vera-Cruz, P., Guerreiro, F., Ribeiro, M. J., Guarino, M. P., and Conde, S. V. (2015). Hyperbaric oxygen therapy improves glucose homeostasis in type 2 diabetes patients: a likely involvement of the carotid bodies. *Adv. Exp. Med. Biol.* 860, 221–225. doi: 10.1007/978-3-319-18440-1_24

Wehrwein, E. A., Limberg, J. K., Taylor, J. L., Dube, S., Basu, A., Basu, R., et al. (2015). Effect of bilateral carotid body resection on the counterregulatory response to hypoglycaemia in humans. *Exp. Physiol.* 100, 69–78. doi: 10.1113/expphysiol.2014.083154

Wszedybyl-Winklewska, M., Wolf, J., Szarmach, A., Winklewski, P. J., Szurowska, E., and Narkiewicz, K. (2018). Central sympathetic nervous system reinforcement in obstructive sleep apnoea. *Sleep Med. Rev.* 39, 143–154. doi: 10.1016/j.smrv.2017.08.006

Zera, T., Moraes, D. J. A., da Silva, M. P., Fisher, J. P., and Paton, J. F. R. (2019). The logic of carotid body connectivity to the brain. *Physiology* 34, 264–282. doi: 10.1152/physiol.00057.2018

Zhang, M., Buttigieg, J., and Nurse, C. A. (2007). Neurotransmitter mechanisms mediating low-glucose signalling in cocultures and fresh tissue slices of rat carotid body. *J. Physiol.* 578, 735–750. doi: 10.1113/jphysiol.2006.121871

Zhang, M., and Nurse, C. A. (2004). CO2/pH chemosensory signaling in co-cultures of rat carotid body receptors and petrosal neurons: role of ATP and ACh. *J. Neurophysiol.* 92, 3433–3445. doi: 10.1152/jn.01099.2003

Zhang, M., Vollmer, C., and Nurse, C. A. (2018). Adenosine and dopamine oppositely modulate a hyperpolarization-activated current Ih in chemosensory neurons of the rat carotid body in co-culture. *J. Physiol.* 596, 3101–3117. doi: 10.1113/jp274743

Zhang, M., Zhong, H., Vollmer, C., and Nurse, C. A. (2000). Co-release of ATP and ACh mediates hypoxic signalling at rat carotid body chemoreceptors. *J. Physiol.* 525(Pt 1), 143–158. doi: 10.1111/j.1469-7793.2000.t01-1-00143.x

Zhang, X. J., Wang, X., Xiong, L. Z., Fan, J., Duan, X. L., and Wang, B. R. (2007). Up-regulation of IL-1 receptor type I and tyrosine hydroxylase in the rat carotid body following intraperitoneal injection of IL-1beta. *Histochem. Cell. Biol.* 128, 533–540. doi: 10.1007/s00418-007-0346-y

Zhou, T., Chien, M. S., Kaleem, S., and Matsunami, H. (2016). Single cell transcriptome analysis of mouse carotid body glomus cells. *J. Physiol.* 594, 4225–4251. doi: 10.1113/jp271936

Conflict of Interest: The author declares that the research was conducted in the absence of any commercial or financial relationships that could be construed as a potential conflict of interest.

Advantages of publishing in Frontiers

OPEN ACCESS
Articles are free to read for greatest visibility and readership

FAST PUBLICATION
Around 90 days from submission to decision

HIGH QUALITY PEER-REVIEW
Rigorous, collaborative, and constructive peer-review

TRANSPARENT PEER-REVIEW
Editors and reviewers acknowledged by name on published articles

Frontiers
Avenue du Tribunal-Fédéral 34
1005 Lausanne | Switzerland

Visit us: www.frontiersin.org
Contact us: info@frontiersin.org | +41 21 510 17 00

REPRODUCIBILITY OF RESEARCH
Support open data and methods to enhance research reproducibility

DIGITAL PUBLISHING
Articles designed for optimal readership across devices

FOLLOW US
@frontiersin

IMPACT METRICS
Advanced article metrics track visibility across digital media

EXTENSIVE PROMOTION
Marketing and promotion of impactful research

LOOP RESEARCH NETWORK
Our network increases your article's readership